

Membrane Technology and Applications

Membrane Technology and Applications

Third Edition

RICHARD W. BAKER

*Membrane Technology and Research, Inc.
Newark, California*



A John Wiley & Sons, Ltd., Publication

This edition first published 2012
© 2012 John Wiley and Sons Ltd

Registered office

John Wiley & Sons Ltd, The Atrium, Southern Gate, Chichester, West Sussex, PO19 8SQ, United Kingdom

For details of our global editorial offices, for customer services and for information about how to apply for permission to reuse the copyright material in this book please see our website at www.wiley.com.

The right of the author to be identified as the author of this work has been asserted in accordance with the Copyright, Designs and Patents Act 1988.

All rights reserved. No part of this publication may be reproduced, stored in a retrieval system, or transmitted, in any form or by any means, electronic, mechanical, photocopying, recording or otherwise, except as permitted by the UK Copyright, Designs and Patents Act 1988, without the prior permission of the publisher.

Wiley also publishes its books in a variety of electronic formats. Some content that appears in print may not be available in electronic books.

Designations used by companies to distinguish their products are often claimed as trademarks. All brand names and product names used in this book are trade names, service marks, trademarks or registered trademarks of their respective owners. The publisher is not associated with any product or vendor mentioned in this book. This publication is designed to provide accurate and authoritative information in regard to the subject matter covered. It is sold on the understanding that the publisher is not engaged in rendering professional services. If professional advice or other expert assistance is required, the services of a competent professional should be sought.

The publisher and the author make no representations or warranties with respect to the accuracy or completeness of the contents of this work and specifically disclaim all warranties, including without limitation any implied warranties of fitness for a particular purpose. This work is sold with the understanding that the publisher is not engaged in rendering professional services. The advice and strategies contained herein may not be suitable for every situation. In view of ongoing research, equipment modifications, changes in governmental regulations, and the constant flow of information relating to the use of experimental reagents, equipment, and devices, the reader is urged to review and evaluate the information provided in the package insert or instructions for each chemical, piece of equipment, reagent, or device for, among other things, any changes in the instructions or indication of usage and for added warnings and precautions. The fact that an organization or Website is referred to in this work as a citation and/or a potential source of further information does not mean that the author or the publisher endorses the information the organization or Website may provide or recommendations it may make. Further, readers should be aware that Internet Websites listed in this work may have changed or disappeared between when this work was written and when it is read. No warranty may be created or extended by any promotional statements for this work. Neither the publisher nor the author shall be liable for any damages arising herefrom.

Library of Congress Cataloging-in-Publication Data

Baker, Richard W. (Richard William), 1941-
Membrane technology and applications / Richard W. Baker. – 3rd ed.
p. cm.

Includes bibliographical references and index.

ISBN 978-0-470-74372-0 (cloth)

1. Membranes (Technology) 2. Membrane separation. I. Title.

TP159.M4B35 2012

660'.28424–dc23

2012008854

A catalogue record for this book is available from the British Library.

ISBN: 9780470743720

Typeset in 10/12pt Times-Roman by Laserwords Private Limited, Chennai, India

Contents

<i>Preface</i>	xi
<i>Acknowledgments</i>	xiii
1. Overview of Membrane Science and Technology	1
1.1 Introduction	1
1.2 Historical Development of Membranes	1
1.3 Types of Membranes	4
1.3.1 Isotropic Membranes	4
1.3.2 Anisotropic Membranes	6
1.3.3 Ceramic, Metal, and Liquid Membranes	6
1.4 Membrane Processes	6
References	13
2. Membrane Transport Theory	15
2.1 Introduction	15
2.2 The Solution-Diffusion Model	18
2.2.1 Molecular Dynamics Simulations	18
2.2.2 Concentration and Pressure Gradients in Membranes	22
2.2.3 Application of the Solution-Diffusion Model to Specific Processes	27
2.2.4 A Unified View	50
2.3 Structure-Permeability Relationships in Solution-Diffusion Membranes	53
2.3.1 Diffusion Coefficients	55
2.3.2 Sorption Coefficients in Polymers	64
2.4 Pore-Flow Membranes	72
2.4.1 Permeation in Ultrafiltration and Microfiltration Membranes	73
2.4.2 Knudsen Diffusion and Surface Diffusion in Microporous Membranes	79
2.4.3 Polymers with Intrinsic Microporosity (PIMs)	86
2.4.4 The Transition Region	89
2.5 Conclusions and Future Directions	90
References	92

3. Membranes and Modules	97
3.1 Introduction	97
3.2 Isotropic Membranes	98
3.2.1 Isotropic Nonporous Membranes	98
3.2.2 Isotropic Microporous Membranes	100
3.3 Anisotropic Membranes	102
3.3.1 Phase separation membranes	104
3.3.2 Interfacial Polymerization Membranes	121
3.3.3 Solution-Coated Composite Membranes	125
3.3.4 Other Anisotropic Membranes	128
3.3.5 Repairing Membrane Defects	132
3.4 Metal, Ceramic, Zeolite, Carbon, and Glass Membranes	134
3.4.1 Metal Membranes	134
3.4.2 Ceramic Membranes	135
3.4.3 Zeolite Membranes	139
3.4.4 Mixed-Matrix Membranes	141
3.4.5 Carbon Membranes	145
3.4.6 Microporous Glass Membranes	148
3.5 Liquid Membranes	148
3.6 Hollow Fiber Membranes	148
3.7 Membrane Modules	154
3.7.1 Plate-and-Frame Modules	155
3.7.2 Tubular Modules	157
3.7.3 Spiral-Wound Modules	158
3.7.4 Hollow Fiber Modules	162
3.7.5 Other Module Types	165
3.8 Module Selection	167
3.9 Conclusions and Future Directions	169
References	170
4. Concentration Polarization	179
4.1 Introduction	179
4.2 Boundary Layer Film Model	182
4.3 Determination of the Peclet Number	191
4.4 Concentration Polarization in Liquid Separation Processes	193
4.5 Concentration Polarization in Gas Separation Processes	196
4.6 Cross-Flow, Co-Flow, and Counter-Flow	197
4.7 Conclusions and Future Directions	204
References	205
5. Reverse Osmosis	207
5.1 Introduction and History	207
5.2 Theoretical Background	208
5.3 Membranes and Materials	213
5.3.1 Cellulosic Membranes	213

5.3.2	Noncellulosic Polymer Membranes	216
5.3.3	Interfacial Composite Membranes	217
5.3.4	Other Membrane Materials	219
5.4	Reverse Osmosis Membrane Categories	220
5.4.1	Seawater and Brackish Water Desalination Membranes	221
5.4.2	Nanofiltration Membranes	222
5.4.3	Hyperfiltration Organic Solvent Separating Membranes	224
5.5	Membrane Selectivity	227
5.6	Membrane Modules	228
5.7	Membrane Fouling Control	231
5.7.1	Scale	231
5.7.2	Silt	233
5.7.3	Biofouling	233
5.7.4	Organic Fouling	235
5.7.5	Membrane Cleaning	236
5.8	Applications	237
5.8.1	Brackish Water Desalination	238
5.8.2	Seawater Desalination	240
5.8.3	Ultrapure Water	241
5.8.4	Wastewater Treatment	242
5.8.5	Nanofiltration	244
5.8.6	Organic Solvent Separation	245
5.9	Conclusions and Future Directions	246
	References	247
6.	Ultrafiltration	253
6.1	Introduction and History	253
6.2	Characterization of Ultrafiltration Membranes	254
6.3	Membrane Fouling	257
6.3.1	Constant Pressure/Constant Flux Operation	257
6.3.2	Concentration Polarization	261
6.3.3	Fouling Control	271
6.4	Membranes	274
6.5	Constant Pressure Modules, System Design, and Applications	274
6.5.1	Cross-Flow Ultrafiltration Modules	275
6.5.2	Constant Pressure (Cross-Flow) System Design	278
6.5.3	Applications of Cross-Flow Membrane Modules	282
6.6	Constant Flux Modules, System Design, and Applications	292
6.6.1	Constant Flux/Variable Pressure Modules	292
6.6.2	Submerged Membrane Modules and System Design	293
6.6.3	Submerged Membrane Applications	296
6.7	Conclusions and Future Directions	299
	References	300

7. Microfiltration	303
7.1 Introduction and History	303
7.2 Background	305
7.2.1 Types of Membrane	305
7.2.2 Membrane Characterization	306
7.2.3 Microfiltration Membranes and Modules	313
7.2.4 Process Design	316
7.3 Applications	320
7.3.1 Sterile Filtration of Pharmaceuticals	322
7.3.2 Sterilization of Wine and Beer	322
7.3.3 Microfiltration in the Electronics Industry	323
7.4 Conclusions and Future Directions	323
References	324
8. Gas Separation	325
8.1 Introduction and History	325
8.2 Theoretical Background	326
8.2.1 Polymer Membranes	328
8.2.2 Metal Membranes	337
8.2.3 Ceramic and Zeolite Membranes	337
8.2.4 Thermally Rearranged/Microporous Carbon Membranes	338
8.2.5 Mixed-Matrix Membranes	338
8.3 Membrane Modules	338
8.4 Process Design	339
8.4.1 Pressure Ratio	340
8.4.2 Stage-Cut	343
8.4.3 Multistep and Multistage System Designs	345
8.4.4 Recycle Designs	347
8.5 Applications	349
8.5.1 Hydrogen Separations	350
8.5.2 Oxygen/Nitrogen Separation	352
8.5.3 Natural Gas Separations	359
8.5.4 Carbon Dioxide Separation	361
8.5.5 Vapor/Gas Separations	368
8.5.6 Dehydration of Air	369
8.5.7 Carbon Dioxide/Hydrogen and Carbon Dioxide/ Nitrogen Separations	370
8.5.8 Vapor/Vapor Separations	372
8.6 Conclusions and Future Directions	373
References	375
9. Pervaporation	379
9.1 Introduction and History	379
9.2 Theoretical Background	381
9.3 Membrane Materials and Modules	389
9.3.1 Membrane Materials	389
9.3.2 Dehydration Membranes	392

9.3.3	Organic/Water Separation Membranes	393
9.3.4	Organic/Organic Separation Membranes	394
9.3.5	Membrane Modules	395
9.4	System Design	398
9.5	Applications	400
9.5.1	Solvent Dehydration	401
9.5.2	Separation of Dissolved Organics from Water	406
9.5.3	Separation of Organic Mixtures	409
9.6	Conclusions and Future Directions	412
	References	412
10.	Ion Exchange Membrane Processes – Electrodialysis	417
10.1	Introduction/History	417
10.2	Theoretical Background	421
10.2.1	Transport through Ion Exchange Membranes	421
10.3	Chemistry of Ion Exchange Membranes	423
10.3.1	Homogeneous Membranes	425
10.3.2	Heterogeneous Membranes	426
10.4	Electrodialysis	428
10.4.1	Concentration Polarization and Limiting Current Density	428
10.4.2	Current Efficiency and Power Consumption	433
10.4.3	System Design	435
10.5	Electrodialysis Applications	438
10.5.1	Brackish Water Desalination	438
10.5.2	Salt Recovery from Seawater	438
10.5.3	Other Electrodialysis Separation Applications	440
10.5.4	Continuous Electrodeionization and Ultrapure Water	442
10.5.5	Bipolar Membranes	443
10.6	Fuel Cells	444
10.7	Membranes in Chlor-Alkali Processes	448
10.8	Conclusions and Future Directions	449
	References	449
11.	Carrier Facilitated Transport	453
11.1	Introduction/History	453
11.2	Coupled Transport	459
11.2.1	Background	459
11.2.2	Characteristics of Coupled Transport Membranes	463
11.2.3	Coupled Transport Membranes	468
11.2.4	Applications	472
11.3	Facilitated Transport	473
11.3.1	Background	473
11.3.2	Process Designs	476
11.3.3	Applications	481
11.4	Conclusions and Future Directions	486
	References	487

12. Medical Applications of Membranes	493
12.1 Introduction	493
12.2 Hemodialysis	493
12.3 Blood Oxygenators	498
12.4 Plasma Fractionation	500
12.5 Controlled Drug Delivery	501
12.5.1 Membrane Diffusion-Controlled Systems	502
12.5.2 Biodegradable Systems	510
12.5.3 Osmotic Systems	512
References	518
13. Other Membrane Processes	521
13.1 Introduction	521
13.2 Dialysis	521
13.3 Donnan Dialysis (Diffusion Dialysis)	522
13.4 Charge Mosaic Membranes and Piezodialysis	526
13.5 Membrane Contactors and Membrane Distillation	529
13.5.1 Applications of Membrane Contactors	532
13.6 Membrane Reactors	538
13.6.1 Applications of Membrane Reactors	541
13.7 Ion-Conducting Membrane Reactors	544
13.8 Pressure-Retarded Osmosis (PRO) and Reverse Electrodialysis (RED)	547
13.9 Chiral Drug Separation	551
13.10 Conclusions and Future Directions	552
References	553
Appendix	559
Index	571

Preface

My introduction to membranes was as a graduate student in 1963. At that time membrane permeation was a sub-study of materials science. What is now called membrane technology did not exist, nor did any large industrial applications of membranes. Since then, sales of membranes and membrane equipment have increased more than 100-fold and several tens of millions of square meters of membrane are produced each year – a membrane industry has been created.

This membrane industry is very fragmented. Industrial applications are divided into six main sub-groups: reverse osmosis, ultrafiltration, microfiltration, gas separation, pervaporation, and electrodialysis. Medical applications are divided into three more: artificial kidneys, blood oxygenators, and controlled release pharmaceuticals. Few companies are involved in more than one sub-group of the industry. Because of these divisions it is difficult to obtain an overview of membrane science and technology; this book is an attempt to give such an overview.

The book starts with a series of general chapters on membrane preparation, transport theory, and concentration polarization. Thereafter, each major membrane application is treated in a single 20- to 50-page chapter. In a book of this size it is impossible to describe every membrane process in detail, but the major processes are covered. However, medical applications were short-changed somewhat and some applications – battery separators and membrane sensors, for example – are not covered at all.

Each application chapter starts with a short historical background to acknowledge the developers of the technology. I am conscious that my views of what was important in the past differ from those of many of my academic colleagues. In this book I have given more credit than is usual to the engineers who actually made the processes work.

Membrane technology continues to expand and change. For this reason, some change has been made to every chapter in this edition of the book to reflect these new developments. The use of bioreactors fitted with submerged-air scrubbed membranes – barely touched on in the second edition – is now a significant industry and so the ultrafiltration chapter has been completely rewritten. I also took this opportunity to rework the chapter on pervaporation and the section on membrane contactors, and included new sections on the use of membranes in fuel cells and the chlor-alkali industry. These updates and additions have added new figures and references, so the page count has increased more than 10% over the second edition.

Readers of the Theory section (Chapter 2) and elsewhere in the book will see that membrane permeation is described using simple phenomenological equations, most commonly, Fick's law. There is no mention of irreversible thermodynamics. The irreversible thermodynamic approach to permeation was very fashionable when I began to work

with membranes in the 1960s. This approach has the appearance of rigor but hides the physical reality of even simple processes behind a fog of tough equations. As a student and young researcher, I struggled with irreversible thermodynamics for more than 15 years before finally giving up in the 1970s. I have lived happily ever after.

Finally, a few words on units. Because a great deal of modern membrane technology originated in the United States, the US engineering units – gallons, cubic feet, and pounds per square inch – are widely used in the membrane industry. Unlike the creators of the Pascal, I am not a worshipper of mindless uniformity. Nonetheless, in this edition, I have used metric units to describe most of the processes covered in this book. British/US units are now only used when they are the industry standard and metric units would lead to confusion.

Acknowledgments

Acknowledgments for the First Edition

As a school boy I once received a mark of 1/2 out of a possible 20 in an end-of-term spelling test. My spelling is still weak, and the only punctuation I every really mastered was the period. This made the preparation of a polished final book draft from my yellow notepads a major undertaking. This effort was headed by Tessa Ennals and Cindi Wieselman. Cindi typed and retyped the manuscript with amazing speed, through its numerous revisions, without complaint. Tessa corrected my English, clarified my language, unsplit my infinitives, and added every semicolon found in this book. She also chased down a source for all of the illustrations used and worked with David Lehmann, our graphics artist, to prepare the figures. It is a pleasure to acknowledge my debt to these people. This book would have been far weaker without the many hours they spent working on it. I also received help from other friends and colleagues at MTR. Hans Wijmans read, corrected, and made numerous suggestions on the theoretical section of the book (Chapter 2). Ingo Pinnau also provided data, references, and many valuable suggestions in the area of membrane preparation and membrane material sciences. I am also grateful to Kenji Matsumoto, who read the section on Reverse Osmosis and made corrections, and to Heiner Strathmann, who did the same for Electrodialysis. The assistance of Marcia Patten, who proofed the manuscript, and Vivian Tran, who checked many of the references, is also appreciated.

Acknowledgments for the Second Edition

Eighteen months after the first edition of this book appeared, it was out of print. Fortunately, John Wiley and Sons agreed to publish a second edition, and I have taken the opportunity to update and revise a number of sections. Tessa Ennals, long-time editor at Membrane Technology and Research, postponed her retirement to help me finish the new edition. Tessa has the standards of an earlier time, and here, as in the past, she gave the task nothing but her best effort. I am indebted to her, and wish her a long and happy retirement. Marcia Patten, Eric Peterson, David Lehmann, Cindy Dunnegan, and Janet Farrant assisted Tessa by typing new sections, revising and adding figures, and checking references, as well as helping with proofing the manuscript. I am grateful to all of these colleagues for their help.

Acknowledgements for the Third Edition

As with the earlier editions of this book, I would not have been able to produce this manuscript without the support of my co-workers at Membrane Technology and Research, Inc. I work with a group of scientist-engineers interested in many aspects of membrane technology. This has kept me informed on new developments affecting our own company's interests and on developments across the membrane field. I also had the assistance of Sara Soder, our company's technical editor, who by mastering my spelling and handwriting was able to provide me with a polished manuscript draft, and who then had the patience to allow me to change and re-change the draft as I clarified my thoughts. Crystal Min and David Lehmann added to and revised the nearly 400 figures, and Beth Godfrey, Jenny Valcov, and Linda Szkoropad pitched in to assist with the figure permissions and final manuscript preparation. I am grateful to all of these colleagues for their help.

1

Overview of Membrane Science and Technology

1.1 Introduction

Membranes have gained an important place in chemical technology and are used in a broad range of applications. The key property that is exploited is the ability of a membrane to control the permeation rate of a chemical species through the membrane. In controlled drug delivery, the goal is to moderate the permeation rate of a drug from a reservoir to the body. In separation applications, the goal is to allow one component of a mixture to permeate the membrane freely, while hindering permeation of other components.

This book provides a general introduction to membrane science and technology. Chapters 2–4 cover membrane science, that is, topics that are basic to all membrane processes, such as transport mechanisms, membrane preparation, and boundary layer effects. The next six chapters cover the industrial membrane separation processes that represent the heart of current membrane technology. Carrier facilitated transport is covered next, followed by a chapter reviewing the medical applications of membranes. The book closes with a chapter that describes various minor or yet-to-be-developed membrane processes, including membrane reactors, membrane contactors, and piezodialysis.

1.2 Historical Development of Membranes

Systematic studies of membrane phenomena can be traced to the eighteenth century philosopher scientists. For example, Abbé Nolet coined the word “osmosis” to describe permeation of water through a diaphragm in 1748. Through the nineteenth and early twentieth centuries, membranes had no industrial or commercial uses, but were used as laboratory tools to develop physical/chemical theories. For example, the measurements of solution osmotic pressure made with membranes by Traube and Pfeffer were used by van’t Hoff in 1887 to develop his limit law, which explains the behavior of ideal dilute

2 Membrane Technology and Applications

solutions; this work led directly to the van't Hoff equation. At about the same time, the concept of a perfectly selective semipermeable membrane was used by Maxwell and others in developing the kinetic theory of gases.

Early membrane investigators experimented with every type of diaphragm available to them, such as bladders of pigs, cattle or fish, and sausage casings made of animal gut. Later, collodion (nitrocellulose) membranes were preferred, because they could be made reproducibly. In 1907, Bechhold devised a technique to prepare nitrocellulose membranes of graded pore size, which he determined by a bubble test [1]. Other early workers, particularly Elford [2], Zsigmondy and Bachmann [3], and Ferry [4] improved on Bechhold's technique, and by the early 1930s microporous collodion membranes were commercially available. During the next 20 years, this early microfiltration membrane technology was expanded to other polymers, notably cellulose acetate.

Membranes found their first significant application in the testing of drinking water at the end of World War II. Drinking water supplies serving large communities in Germany and elsewhere in Europe had broken down, and filters to test for water safety were needed urgently. The research effort to develop these filters, sponsored by the US Army, was later exploited by the Millipore Corporation, the first and still the largest US microfiltration membrane producer.

By 1960, the elements of modern membrane science had been developed, but membranes were used in only a few laboratory and small, specialized industrial applications. No significant membrane industry existed, and total annual sales of membranes for all industrial applications probably did not exceed US\$20 million in 2012 dollars. Membranes suffered from four problems that prohibited their widespread use as a separation process: they were too unreliable, too slow, too unselective, and too expensive. Solutions to each of these problems have been developed during the last 40 years, and membrane-based separation processes are now commonplace.

The seminal discovery that transformed membrane separation from a laboratory to an industrial process was the development, in the early 1960s, of the Loeb–Sourirajan process for making defect-free, high-flux, anisotropic reverse osmosis membranes [5]. These membranes consist of an ultrathin, selective surface film on a much thicker but much more permeable microporous support, which provides the mechanical strength. The flux of the first Loeb–Sourirajan reverse osmosis membrane was 10 times higher than that of any membrane then available and made reverse osmosis a potentially practical method of desalting water. The work of Loeb and Sourirajan, and the timely infusion of large sums of research and development dollars from the US Department of Interior, Office of Saline Water (OSW), resulted in the commercialization of reverse osmosis and was a major factor in the development of ultrafiltration and microfiltration. The development of electrodialysis was also aided by OSW funding.

Concurrent with the development of these industrial applications of membranes was the independent development of membranes for medical separation processes, in particular, the artificial kidney. Kolf and Berk [6] had demonstrated the first successful artificial kidney in The Netherlands in 1945. It took almost 20 years to refine the technology for use on a large scale, but these developments were complete by the early 1960s. Since then, the use of membranes in artificial organs has become a major life-saving procedure. More than 800 000 people are now sustained by artificial kidneys and a further million people undergo open-heart surgery each year, a procedure made possible by development

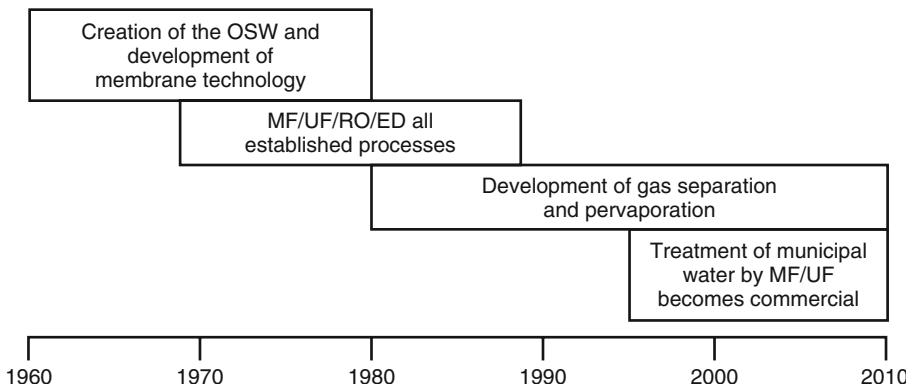


Figure 1.1 The development of the membrane separation industry, 1960–2010

of the membrane blood oxygenator. The sales of these devices comfortably exceed the total industrial membrane separation market. Another important medical application of membranes is for controlled drug delivery systems. A key figure in this area was Alex Zaffaroni, who founded Alza, a company dedicated to developing these products, in 1966. The membrane techniques developed by Alza and its competitors are widely used in the pharmaceutical industry to improve the efficiency and safety of drug delivery.

The modern membrane separation industry began in the 1960s. The creation of this industry can be divided into the four phases shown in Figure 1.1. In the first phase, building on the original Loeb–Sourirajan technique, other membrane formation processes, including interfacial polymerization and multilayer composite casting and coating, were developed for making high-performance membranes. Using these processes, membranes with selective layers as thin as $0.1\text{ }\mu\text{m}$ or less are now being produced by a number of companies. Methods of packaging membranes into large-membrane-area spiral-wound, hollow-fine-fiber, capillary, and plate-and-frame modules were also developed, and advances were made in improving membrane stability. The support of the OSW was key to these developments.

In the second phase, beginning in the early 1970s, the developments that came out of the OSW program began to appear in commercial membrane units; by the 1980s, microfiltration, ultrafiltration, reverse osmosis, and electrodialysis were all established processes. The third phase, which began in the 1980s, was the emergence of industrial membrane gas separation processes. The first major product was the Monsanto Prism® membrane for hydrogen separation, introduced in 1980 [7]. Within a few years, Dow was producing systems to separate nitrogen from air, and Cynara and Separex were producing systems to separate carbon dioxide from natural gas. Gas separation technology is continuing to evolve and expand; further growth will be seen in the coming years. Another development of the 1980s was the introduction by GFT, a small German engineering company, of the first commercial pervaporation systems for dehydration of alcohol and other solvents. Pervaporation has been slow to take off and 2010 sales were still not more than \$20 million. However, the development of bioethanol from biomass has produced a new, very large potential market for the technology, which may lead to future growth.

The final development phase, which began in the mid-1990s, was the development of reliable, economical microfiltration/ultrafiltration systems for the treatment of municipal water sources and for use in membrane bioreactors in sewage treatment plants. These applications were targets for membrane developers as early as the 1960s, but membrane fouling leading to low fluxes could not be overcome. In the late 1980s, Dr. Kazuo Yamamoto began to develop low-pressure, submerged air-sparged membranes [8]. It took another 10 years for companies like Kubota, Mitsubishi Rayon, and Zenon to scale up and bring these ideas to the commercial stage, and by the late 1990s, commercial systems began to be installed. Since then, treatment of municipal water has become one of the most rapidly growing areas of membrane technology. Membrane systems are competitive with conventional biological treatment in terms of price and cost, and produce a far superior treated water product.

1.3 Types of Membranes

This book is limited to synthetic membranes, excluding all biological structures, but the topic is still large enough to include a wide variety of membranes that differ in chemical and physical composition and in the way they operate. In essence, a membrane is nothing more than a discrete, thin interface that moderates the permeation of chemical species in contact with it. This interface may be molecularly homogeneous – that is, completely uniform in composition and structure – or it may be chemically or physically heterogeneous – for example, containing holes or pores of finite dimensions or consisting of some form of layered structure. A normal filter meets this definition of a membrane, but, by convention, the term filter is usually limited to structures that separate particulate suspensions larger than $1\text{--}10\,\mu\text{m}$. The principal types of membrane are shown schematically in Figure 1.2 and are described briefly below.

1.3.1 Isotropic Membranes

1.3.1.1 Microporous Membranes

A microporous membrane is very similar in structure and function to a conventional filter. It has a rigid, highly voided structure with randomly distributed, interconnected pores. However, these pores differ from those in a conventional filter by being extremely small, on the order of $0.01\text{--}10\,\mu\text{m}$ in diameter. All particles larger than the largest pores are completely rejected by the membrane. Particles smaller than the largest pores but larger than the smallest pores are partially rejected, according to the pore size distribution of the membrane. Particles much smaller than the smallest pores will pass through the membrane. Thus, separation of solutes by microporous membranes is mainly a function of molecular size and pore size distribution. In general, only molecules that differ considerably in size can be separated effectively by microporous membranes, for example, in ultrafiltration and microfiltration.

1.3.1.2 Nonporous, Dense Membranes

Nonporous, dense membranes consist of a dense film through which permeants are transported by diffusion under the driving force of a pressure, concentration, or electrical

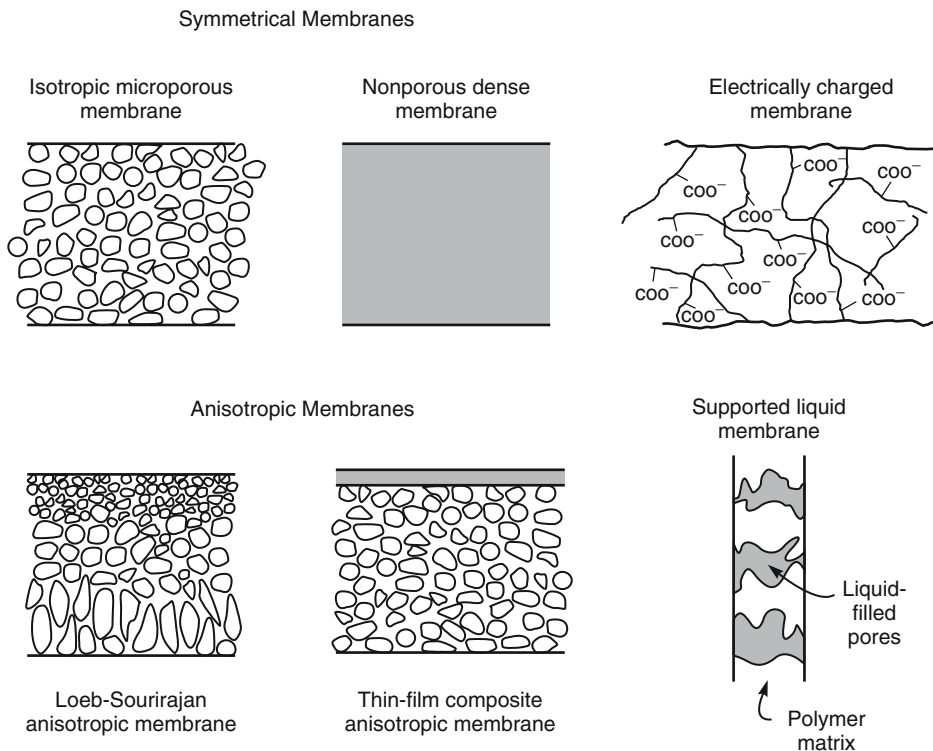


Figure 1.2 Schematic diagrams of the principal types of membranes

potential gradient. The separation of various components of a mixture is related directly to their relative transport rate within the membrane, which is determined by their diffusivity and solubility in the membrane material. Thus, nonporous, dense membranes can separate permeants of similar size if the permeant concentrations in the membrane material (that is, their solubilities) differ significantly. Most gas separation, pervaporation, and reverse osmosis membranes use dense membranes to perform the separation. Usually these membranes have an anisotropic structure to improve the flux.

1.3.1.3 Electrically Charged Membranes

Electrically charged membranes can be dense or microporous, but are most commonly very finely microporous, with the pore walls carrying fixed positively or negatively charged ions. A membrane with fixed positively charged ions is referred to as an anion exchange membrane because it binds anions in the surrounding fluid. Similarly, a membrane containing fixed negatively charged ions is called a cation exchange membrane. Separation with charged membranes is achieved mainly by exclusion of ions of the same charge as the fixed ions of the membrane structure, and to a much lesser extent by the pore size. The separation is affected by the charge and concentration of the ions in solution. For example, monovalent ions are excluded less effectively than divalent

ions and, in solutions of high ionic strength, selectivity decreases. Electrically charged membranes are used for processing electrolyte solutions in electrodialysis.

1.3.2 Anisotropic Membranes

The transport rate of a species through a membrane is inversely proportional to the membrane thickness. High transport rates are desirable in membrane separation processes for economic reasons; therefore, the membrane should be as thin as possible. Conventional film fabrication technology limits manufacture of mechanically strong, defect-free films to thicknesses of about $20\text{ }\mu\text{m}$. The development of novel membrane fabrication techniques to produce anisotropic membrane structures was one of the major breakthroughs of membrane technology during the past 40 years. Anisotropic membranes consist of an extremely thin surface layer supported on a much thicker, porous substructure. The surface layer and its substructure may be formed in a single operation or separately. In composite membranes, the layers are usually made from different polymers. The separation properties and permeation rates of the membrane are determined exclusively by the surface layer; the substructure functions as a mechanical support. The advantages of the higher fluxes provided by anisotropic membranes are so great that almost all commercial processes use such membranes.

1.3.3 Ceramic, Metal, and Liquid Membranes

The discussion so far implies that membrane materials are organic polymers and, in fact, the vast majority of membranes used commercially are polymer based. However, in recent years, interest in membranes formed from less conventional materials has increased. Ceramic membranes, a special class of microporous membranes, are being used in ultrafiltration and microfiltration applications for which solvent resistance and thermal stability are required. Dense metal membranes, particularly palladium membranes, are being considered for the separation of hydrogen from gas mixtures, and supported liquid films are being developed for carrier facilitated transport processes.

1.4 Membrane Processes

Six developed and developing industrial membrane technologies, plus a number of yet-to-be-developed technologies, are discussed in this book. In addition, sections are included describing the use of membranes in medical applications such as the artificial kidney, blood oxygenation, and controlled drug delivery devices. The status of all of these processes is summarized in Table 1.1.

The developed industrial membrane separation processes are microfiltration, ultrafiltration, reverse osmosis, and electrodialysis. These processes are all well established, and the market is served by a number of experienced companies.

The range of application of the three pressure-driven membrane water separation processes – reverse osmosis, ultrafiltration, and microfiltration – is illustrated in Figure 1.3. Ultrafiltration (Chapter 6) and microfiltration (Chapter 7) are basically similar in that the mode of separation is molecular sieving through increasingly fine pores. Microfiltration membranes filter colloidal particles and bacteria from 0.1 to $10\text{ }\mu\text{m}$

Table 1.1 Membrane technologies addressed in this book

Category	Process	Status
Developed industrial membrane separation technologies	Microfiltration Ultrafiltration Reverse osmosis Electrodialysis	Well established unit operations. No major breakthroughs seem imminent
Developing industrial membrane separation technologies	Gas separation Pervaporation	A number of plants have been installed. Market size and number of applications served are expanding
To-be-developed industrial membrane separation technologies	Carrier-facilitated transport Membrane contactors Piezodialysis, and so on	Major problems remain to be solved before industrial systems will be installed on a large scale
Medical applications of membranes	Artificial kidneys Artificial lungs Controlled drug delivery	Well-established processes. Still the focus of research to improve performance, for example, improving biocompatibility

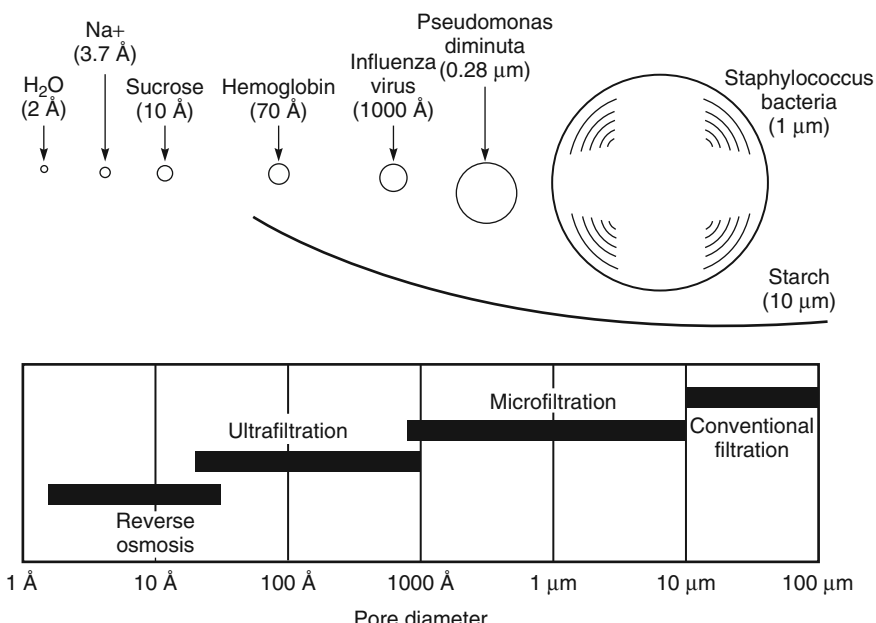


Figure 1.3 Reverse osmosis, ultrafiltration, microfiltration, and conventional filtration are related processes differing principally in the average pore diameter of the membrane filter. Reverse osmosis membranes are so dense that discrete pores do not exist; transport occurs via statistically distributed free volume areas. The relative size of different solutes removed by each class of membrane is illustrated in this schematic

in diameter. Ultrafiltration membranes can be used to filter dissolved macromolecules, such as proteins, from solutions. The mechanism of separation by reverse osmosis membranes is quite different. In reverse osmosis membranes (Chapter 5), the membrane pores are so small, from 3 to 5 Å in diameter, that they are within the range of thermal motion of the polymer chains that form the membrane. The accepted mechanism of transport through these membranes is called the solution-diffusion model. According to this model, solutes permeate the membrane by dissolving in the membrane material and diffusing down a concentration gradient. Separation occurs because of the difference in solubilities and mobilities of different solutes in the membrane. The principal application of reverse osmosis is desalination of brackish groundwater or seawater.

Although reverse osmosis, ultrafiltration, and microfiltration are conceptually similar processes, the difference in pore diameter (or apparent pore diameter) produces dramatic differences in the way the membranes are used. A simple model of liquid flow through these membranes describes the membranes as a series of cylindrical capillary pores of diameter d . The liquid flow through a pore (q) is given by Poiseuille's Law as:

$$q = \frac{\pi d^4}{128 \mu \ell} \times \Delta p \quad (1.1)$$

where Δp is the pressure difference across the pore, μ is the liquid viscosity, and ℓ is the pore length. The flux, or flow per unit membrane area, is the sum of all the flows through the individual pores and so is given by:

$$J = N \times \frac{\pi d^4}{128 \mu \ell} \times \Delta p \quad (1.2)$$

where N is the number of pores per square centimeter of membrane.

For membranes of equal pore area and porosity (ε), the number of pores per square centimeter is proportional to the inverse square of the pore diameter. That is,

$$N = \varepsilon \times \frac{4}{\pi d^2} \quad (1.3)$$

It follows that the flux through membranes of equal porosity, given by combining Equations 1.2 and 1.3, is

$$J = \frac{\Delta p \varepsilon}{32 \mu \ell} \times d^2 \quad (1.4)$$

From Figure 1.3, the typical pore diameter of a microfiltration membrane is 10 000 Å. This is 100-fold larger than the average ultrafiltration pore and 1000-fold larger than the (nominal) diameter of pores in reverse osmosis membranes. Because flux is proportional to the square of the pore diameter, the permeance (that is, flux per unit pressure difference ($J/\Delta p$)) of microfiltration membranes is enormously higher than that of ultrafiltration membranes, which in turn is much higher than that of reverse osmosis membranes. These differences significantly impact the operating pressure and the way that these membranes are used industrially.

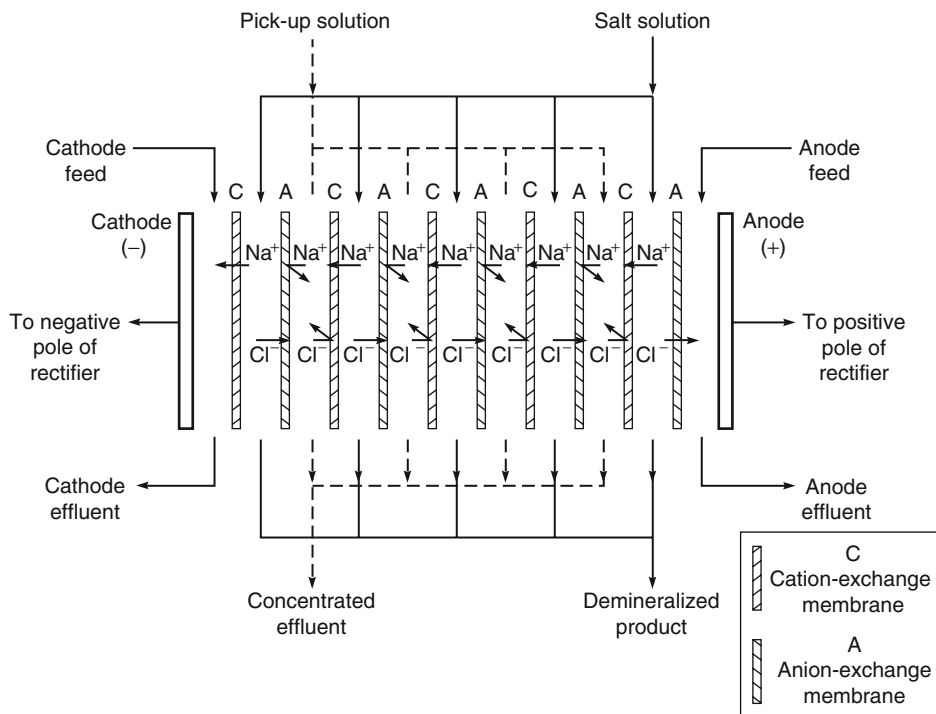


Figure 1.4 Schematic diagram of an electrodialysis process

The fourth fully developed membrane process is electrodialysis (Chapter 10), in which charged membranes are used to separate ions from aqueous solutions under the driving force of an electrical potential difference. The process utilizes an electrodialysis stack, built on the filter-press principle, and containing several hundred individual cells, each formed by a pair of anion- and cation-exchange membranes. The principal application of electrodialysis is the desalting of brackish groundwater. However, industrial use of the process in the food industry, for example, to deionize cheese whey, is growing, as is its use in pollution control applications. A schematic of the process is shown in Figure 1.4.

Table 1.1 shows two developing industrial membrane separation processes: gas separation with polymer membranes (Chapter 8) and pervaporation (Chapter 9). Gas separation with membranes is the more advanced of the two techniques; at least 20 companies worldwide offer industrial, membrane-based gas separation systems for a variety of applications. Only a handful of companies currently offer industrial pervaporation systems. In gas separation, a gas mixture at an elevated pressure is passed across the surface of a membrane that is selectively permeable to one component of the feed mixture; the membrane permeate is enriched in this species. The basic process is illustrated in Figure 1.5. Major current applications of gas separation membranes are the separation of hydrogen from nitrogen, argon, and methane in ammonia plants; the production of

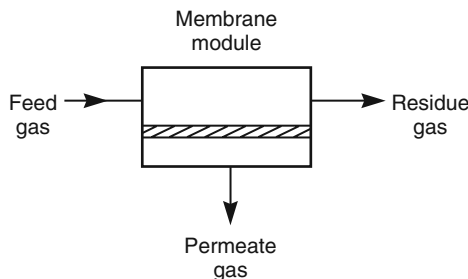


Figure 1.5 Schematic diagram of the basic membrane gas separation process

nitrogen from air; and the separation of carbon dioxide from methane in natural gas operations. Membrane gas separation is an area of considerable current research interest, and the number of applications is expanding rapidly.

Pervaporation is a relatively new process that has elements in common with reverse osmosis and gas separation. In pervaporation, a liquid mixture contacts one side of a membrane, and the permeate is removed as a vapor from the other. The driving force for the process is the low vapor pressure on the permeate side of the membrane generated by cooling and condensing the permeate vapor. The attraction of pervaporation is that the separation obtained is proportional to the rate of permeation of the components of the liquid mixture through the selective membrane. Therefore, pervaporation offers the possibility of separating closely boiling mixtures or azeotropes that are difficult to separate by distillation or other means. A schematic of a simple pervaporation process using a condenser to generate the permeate vacuum is shown in Figure 1.6. Currently,

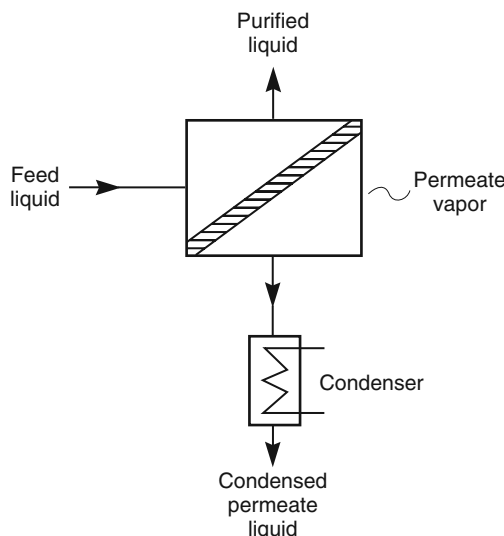


Figure 1.6 Schematic diagram of the basic pervaporation process

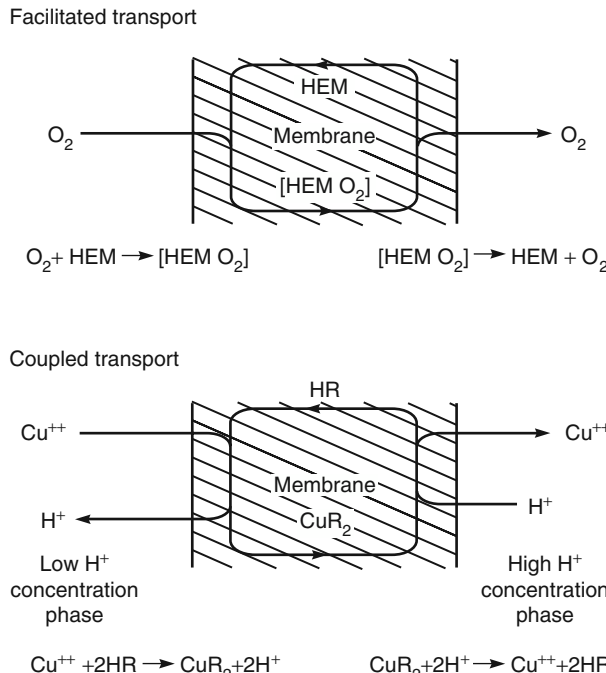


Figure 1.7 Schematic examples of carrier facilitated transport of gas and ions. The gas transport example shows the transport of oxygen across a membrane using hemoglobin dissolved in water as the carrier agent. The ion transport example shows the transport of copper ions across a membrane using a liquid ion exchange reagent dissolved in a water immiscible solvent as the carrier agent

the main industrial application of pervaporation is the dehydration of organic solvents, in particular, the dehydration of 90–95% ethanol solutions, a difficult separation problem because of the ethanol/water azeotrope at 95% ethanol. Pervaporation membranes that selectively permeate water can produce more than 99.9% ethanol from these solutions. Pervaporation processes are also being developed for the removal of dissolved organics from water and for the separation of organic mixtures.

A number of other industrial membrane processes are placed in the category of to-be-developed technologies in Table 1.1. Perhaps the most important of these is carrier facilitated transport (Chapter 11), which often employs liquid membranes containing a complexing or carrier agent. The carrier agent reacts with one component of a mixture on the feed side of the membrane and then diffuses across the membrane to release the permeant on the product side of the membrane. The reformed carrier agent then diffuses back to the feed side of the membrane. Thus, the carrier agent acts as a shuttle to selectively transport one component from the feed to the product side of the membrane.

Facilitated transport membranes can be used to separate gases; membrane transport is then driven by a difference in the gas partial pressure across the membrane. Metal ions can also be selectively transported across a membrane, driven by a flow of hydrogen or

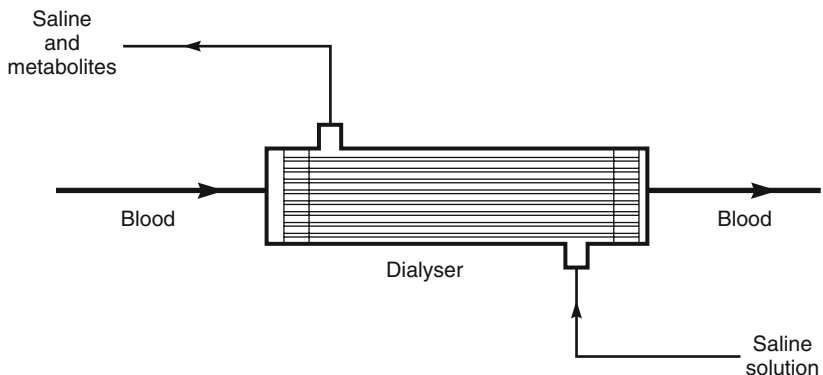


Figure 1.8 Schematic of a hollow fiber artificial kidney dialyzer used to remove urea and other toxic metabolites from blood. About 100 million of these devices are used every year

hydroxyl ions in the other direction. This process is sometimes called coupled transport. Examples of carrier facilitated transport processes for gas and ion transport are shown in Figure 1.7.

Because the carrier facilitated transport process employs a reactive carrier species, very high membrane selectivities can be achieved. These selectivities are often far larger than the selectivities achieved by other membrane processes. This one fact has maintained interest in facilitated transport for the past 40 years, but no commercial applications have developed. The principal problem is the physical instability of the liquid membrane and the chemical instability of the carrier agent. In recent years, a number of potential solutions to this problem have been developed, which may yet make carrier facilitated transport a viable process.

The membrane separation processes described above represent the bulk of the industrial membrane separation industry. Another process, dialysis, is not used industrially but is used on a large scale in medicine to remove toxic metabolites from blood in patients suffering from kidney failure. The first successful artificial kidney was based on cellophane (regenerated cellulose) dialysis membranes and was developed in 1945. Over the past 60 years, many changes have been made. Currently, most artificial kidneys are based on hollow-fiber membranes formed into modules having a membrane area of about 1 m^2 ; the process is illustrated in Figure 1.8. Blood is circulated through the center of the fiber, while isotonic saline, the dialysate, is pumped countercurrently around the outside of the fibers. Urea, creatinine, and other low-molecular-weight metabolites in the blood diffuse across the fiber wall and are removed with the saline solution. The process is quite slow, usually requiring several hours to remove the required amount of the metabolite from the patient, and must be repeated one or two times per week. In terms of membrane area used and dollar value of the membrane produced, artificial kidneys are the single largest application of membranes.

Following the success of the artificial kidney, similar devices were developed to remove carbon dioxide and deliver oxygen to the blood. These so-called artificial lungs are used in surgical procedures during which the patient's lungs cannot function.

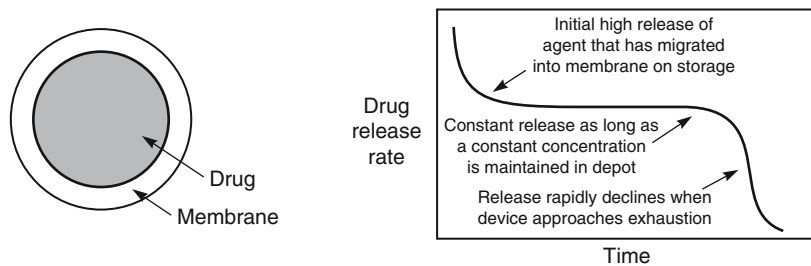


Diagram and release curve for a simple reservoir system

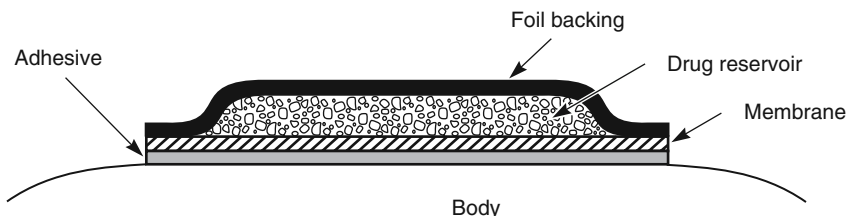


Figure 1.9 Schematic of transdermal patch in which the rate of delivery of drug to the body is controlled by a polymer membrane. Such patches are used to deliver many drugs including nitroglycerine, estradiol, nicotine, and scopolamine

The dialysate fluid shown in Figure 1.8 is replaced with a carefully controlled sweep gas containing oxygen, which is delivered to the blood, and carbon dioxide, which is removed. These two medical applications of membranes are described in Chapter 12.

Another major medical use of membranes is in controlled drug delivery (Chapter 12). Controlled drug delivery can be achieved by a wide range of techniques, most of which involve membranes; a simple example is illustrated in Figure 1.9. In this device, designed to deliver drugs through the skin, drug is contained in a reservoir surrounded by a membrane. With such a system, the release of drug is constant as long as a constant concentration of drug is maintained within the device. A constant concentration is maintained if the reservoir contains a saturated solution and sufficient excess of solid drug. Systems that operate using this principle are used to moderate delivery of drugs such as nitroglycerine (for angina), nicotine (for smoking cessation), and estradiol (for hormone replacement therapy) through the skin. Other devices using osmosis or biodegradation as the rate-controlling mechanism are also produced as implants and tablets. The total market of controlled release pharmaceuticals is comfortably above US\$3 billion per year.

References

1. Bechhold, H. (1907) Kolloidstudien mit der Filtrationsmethode. *Z. Phys. Chem.*, **60**, 257.

14 Membrane Technology and Applications

2. Elford, W.J. (1937) Principles governing the preparation of membranes having graded porosities. The properties of 'Gradocol' membranes as ultrafilters. *Trans. Faraday Soc.*, **33**, 1094.
3. Zsigmondy, R. and Bachmann, W. (1918) Über neue filter. *Z. Anorg. Chem.*, **103**, 119.
4. Ferry, J.D. (1936) Ultrafilter membranes and ultrafiltration. *Chem. Rev.*, **18**, 373.
5. Loeb, S. and Sourirajan, S. (1963) Sea water demineralization by means of an osmotic membrane, in *Saline Water Conversion II*, Advances in Chemistry Series Number, Vol. **38** (ed. R.F. Gould), American Chemical Society, Washington, DC, pp. 117–132.
6. Kolf, W.J. and Berk, H.T. (1944) The artificial kidney: a dialyzer with great area. *Acta Med. Scand.*, **117**, 121.
7. Henis, J.M.S. and Tripodi, M.K. (1980) A novel approach to gas separation using composite hollow fiber membranes. *Sep. Sci. Technol.*, **15**, 1059.
8. Yamamoto, K., Hiasa, M., and Mahmood, T. (1989) Direct solid-liquid separation using hollow fiber membrane in an activated sludge aeration tank. *Water Sci. Technol.*, **21**, 43.

2

Membrane Transport Theory

2.1 Introduction

The most important property of membranes is their ability to control the rate of permeation of different species. The two models used to describe the mechanism of permeation are illustrated in Figure 2.1. One is the pore-flow model, in which permeants are transported by pressure-driven convective flow through tiny pores. Separation occurs because one of the permeants is excluded (filtered) from some of the pores in the membrane through which other permeants move. The other model is the solution-diffusion model, in which permeants dissolve in the membrane material and then diffuse through the membrane down a concentration gradient. Permeants are separated because of differences in their solubilities in the membrane and differences in the rates at which they diffuse through the membrane. Both models were proposed in the nineteenth century, but the pore-flow model, because it was closer to normal physical experience, was more popular until the mid-1940s. However, during the 1940s, the solution-diffusion model was used to explain transport of gases through polymeric films. This use of the solution-diffusion model was uncontroversial, but the transport mechanism in reverse osmosis membranes was a hotly debated issue in the 1960s and early 1970s [1–6]. By 1980, however, the proponents of solution-diffusion had carried the day; currently only a few die-hard pore-flow modelers use this approach to rationalize reverse osmosis.

Diffusion, the basis of the solution-diffusion model, is the process by which permeants are transported from one part of a system to another by a concentration gradient. The individual permeant molecules in the membrane medium are in constant random molecular motion, but in an isotropic medium, individual molecules have no preferred direction of motion. Although the average displacement of a molecule from its starting point can be calculated after a period of time, nothing can be said about the direction in which any individual molecule will move. However, if a concentration gradient of permeate molecules is formed in the medium, simple statistics show that a net transport of matter will occur from the high concentration to the low concentration region. For example, when two adjacent volume elements with slightly different permeant concentrations

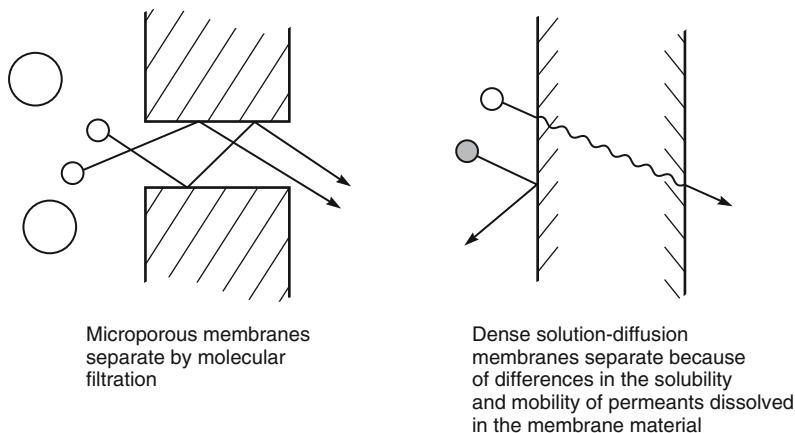


Figure 2.1 Molecular transport through membranes can be described by a flow through permanent pores or by the solution-diffusion mechanism

are separated by an interface, then simply because of the difference in the number of molecules in each volume element, more molecules will move from the concentrated side to the less concentrated side of the interface than will move in the other direction. This concept was first recognized by Fick theoretically and experimentally in 1855 [7]. Fick formulated his results as the equation now called Fick's law of diffusion, which states

$$J_i = -D_i \frac{dc_i}{dx} \quad (2.1)$$

where J_i is the rate of transfer of component i or flux ($\text{g}/\text{cm}^2 \cdot \text{s}$) and dc_i/dx is the concentration gradient of component i ($\text{g}/\text{cm}^3 \cdot \text{cm}$). The term D_i is called the diffusion coefficient ($\text{cm}^2 \cdot \text{s}$) and is a measure of the mobility of the individual molecules. The minus sign shows that the direction of diffusion is down the concentration gradient. Diffusion is an inherently slow process. In practical diffusion-controlled separation processes, useful fluxes across the membrane are achieved by making the membranes very thin and creating large concentration gradients in the membrane.

Pressure-driven convective flow, the basis of the pore-flow model, is most commonly used to describe flow in a capillary or porous medium. The basic equation covering this type of transport is Darcy's law, which can be written as

$$J_i = K' c_i \frac{dp}{dx} \quad (2.2)$$

where dp/dx is the pressure gradient existing in the porous medium, c_i is the concentration of component i in the medium, and K' is a coefficient reflecting the nature of the medium. In general, pore-flow pressure-driven membrane fluxes are high compared with those obtained by simple diffusion.

The difference between the solution-diffusion and pore-flow mechanisms lies in the relative size and permanence of the pores. For membranes in which transport is best

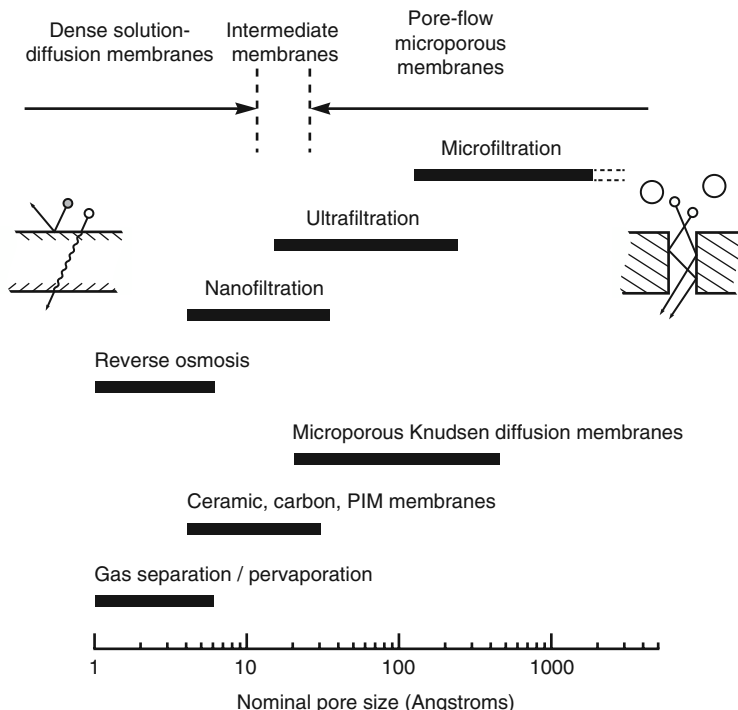


Figure 2.2 Schematic representation of the nominal pore size and best theoretical model for the principal membrane separation processes

described by the solution-diffusion model and Fick's law, the free volume elements (pores) in the membrane are tiny spaces between polymer chains caused by thermal motion of the polymer molecules. These volume elements appear and disappear on about the same time scale as the motions of the permeants traversing the membrane. On the other hand, for a membrane in which transport is best described by a pore-flow model and Darcy's law, the free volume elements (pores) are relatively large and fixed, and do not fluctuate in position or volume on the time scale of permeant motion. These pores are usually connected to one another. The larger the individual free volume elements (pores), the more likely they are to be present long enough to produce pore-flow characteristics in the membrane. As a rough rule of thumb, the transition between transient (solution-diffusion) and permanent (pore-flow) pores is a diameter in the range of 5–10 Å.

The average pore diameter in a membrane is difficult to measure directly and must often be inferred from the size of the molecules that permeate the membrane or by some other indirect technique. With this caveat in mind, membranes can be organized into the three general groups shown in Figure 2.2:

- Ultrafiltration, microfiltration, and microporous Knudsen diffusion gas separation membranes are all clearly microporous. They all contain pores larger than 10–15 Å in diameter and transport occurs by pore flow.

- Reverse osmosis, pervaporation, and polymeric gas separation membranes contain a dense selective polymer layer with no visible pores. These membranes show different transport rates for molecules as small as 2–5 Å in diameter. The fluxes of permeants through these membranes are also much lower than through microporous membranes. Transport in these membranes is best described by the solution-diffusion model. The spaces between polymer chains in these membranes are less than 5–10 Å in diameter and so are within the normal range of thermal motion of the polymer chains that make up the membrane matrix. Molecules permeate the membrane through free volume elements between polymer chains that are transient on the time scale of the diffusion processes occurring.
- Membranes in the third group contain pores with diameters between 5 and 15 Å and are intermediate between truly microporous and truly solution-diffusion membranes. For example, nanofiltration membranes are intermediate between ultrafiltration membranes – clearly microporous – and reverse osmosis membranes – clearly dense films. Nanofiltration membranes have high rejections for the di- and trisaccharides, sucrose and raffinose, with molecular diameters of 10–13 Å, but freely pass the monosaccharide fructose with a molecular diameter of about 5–6 Å. Some gas separation membranes also fall into this intermediate category. If gas separation membranes are made from polymers with extremely stiff polymer chains, the molecular motion of the polymer can be so restricted that semi-permanent microcavities form. These cavities or free volume elements have diameters of 5–15 Å and appear to be connected, forming relatively long continuous pathways through the membranes. These polymers are called polymers with intrinsic microporosity (PIM) [8–10]. Some finely porous ceramic membranes or carbonized polymer membranes also fall into this intermediate range.

In this chapter, permeation through dense nonporous membranes is covered first; this includes permeation in reverse osmosis, pervaporation, and gas separation membranes. Transport occurs by molecular diffusion and is described by the solution-diffusion model. The predictions of this model are in good agreement with experimental data, and a number of simple equations that usefully rationalize the properties of these membranes result. In the second part of the chapter, transport in microporous ultrafiltration and microfiltration membranes is covered more briefly. Transport through these membranes occurs by convective flow with some form of sieving mechanism producing the separation. However, the ability of theory to rationalize transport in these membranes is poor. A number of factors concurrently affect permeation, so a simple quantitative description of the process is not possible. Finally, a brief discussion of membranes that fall into the “intermediate” category is given.

2.2 The Solution-Diffusion Model

2.2.1 Molecular Dynamics Simulations

The solution-diffusion model applies to reverse osmosis, pervaporation, and gas permeation in polymer films. At first glance, these processes appear to be very different. Reverse osmosis uses a large pressure difference across the membrane to separate water

from salt solutions. In pervaporation, the membrane separates a liquid feed solution from a permeate vapor. The pressure difference across the membrane is small, and the process is driven by the vapor pressure difference between the feed liquid and the low partial pressure of the permeate vapor. Gas permeation involves transport of gases down a pressure or concentration gradient. However, all three processes involve diffusion of molecules in a dense polymer. The pressure, temperature, and composition of the fluids on either side of the membrane determine the concentration of the diffusing species at the membrane surface in equilibrium with the fluid. Once dissolved in the membrane, individual permeating molecules move by the same process of random molecular diffusion, no matter whether the membrane is being used in reverse osmosis, pervaporation, or gas permeation. Often, similar membranes are used in very different processes. For example, cellulose acetate membranes were developed for desalination of water by reverse osmosis, but essentially identical membranes have been used in pervaporation to dehydrate alcohol and are widely used in gas permeation to separate carbon dioxide from natural gas. Similarly, silicone rubber membranes are too hydrophobic to be useful in reverse osmosis, but are used to separate volatile organics from water by pervaporation and organic vapors from air in gas permeation.

The advent of powerful computers has allowed the fluctuations in the volumes between polymer chains due to thermal motion to be calculated. Figure 2.3 shows the results of a

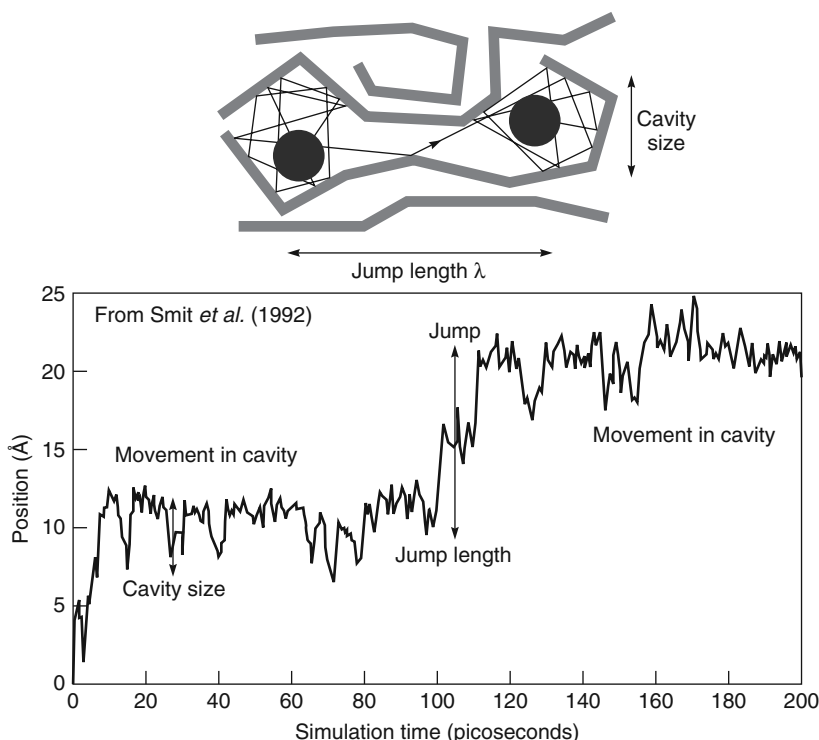


Figure 2.3 Motion of a carbon dioxide molecule in a 6FDA-4PDA polymer matrix. Reprinted with permission from [11]. Copyright (1992) Elsevier.

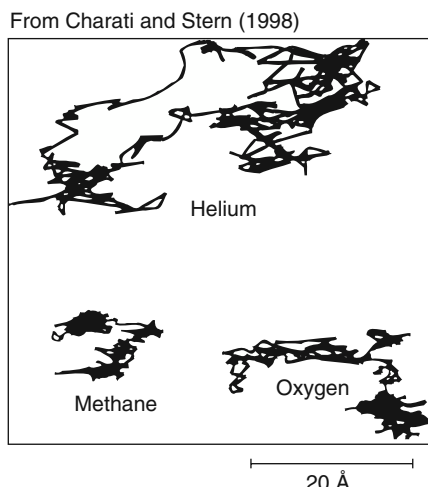


Figure 2.4 Simulated trajectories of helium, oxygen, and methane molecules during a 200-ps time period in a poly(dimethylsiloxane) matrix. Reprinted with permission from [12] Copyright (1998) American Chemical Society.

molecular dynamics simulation for a small-volume element of a polymer. The change in position of individual polymer molecules in a small-volume element can be calculated at short enough time intervals to represent the normal thermal motion occurring in a polymeric matrix. If a penetrant molecule is placed in one of the small free volume microcavities between polymer chains, its motion can also be calculated. The simulated motion of a carbon dioxide molecule in a 6FDA-4PDA polyimide matrix is shown in Figure 2.3 [11]. During the first 100 ps of the simulation, the carbon dioxide molecule bounces around in the cavity where it has been placed, never moving more than about 5 Å, the diameter of the microcavity. After 100 ps, however, a chance thermal motion moves a segment of the polymer chain sufficiently for the carbon dioxide molecule to jump approximately 10 Å to an adjacent cavity, where it remains until another movement of the polymer chain allows it to jump to another cavity. By repeating these calculations many times and averaging the distance moved by the gas molecule, its diffusion coefficient can be calculated.

An alternative method of representing the movement of an individual molecule by computational techniques is shown in Figure 2.4 [12]. This figure shows the movements of three different permeate molecules over a period of 200 ps in a silicone rubber polymer matrix. The smaller helium molecule moves more frequently and makes larger jumps than the larger methane molecule. This is because helium, with a molecular diameter of 2.6 Å, has many more opportunities to move from one position to another than methane, with a molecular diameter of 3.7 Å. Oxygen, with a molecular diameter of 3.5 Å, has intermediate mobility.

The effect of polymer structure on diffusion can be seen by comparing the distance moved by the gas molecules in the same 200-ps period in Figures 2.3 and 2.4. Figure 2.3 simulates diffusion in a glassy rigid-backbone polyimide. In 200 ps, the

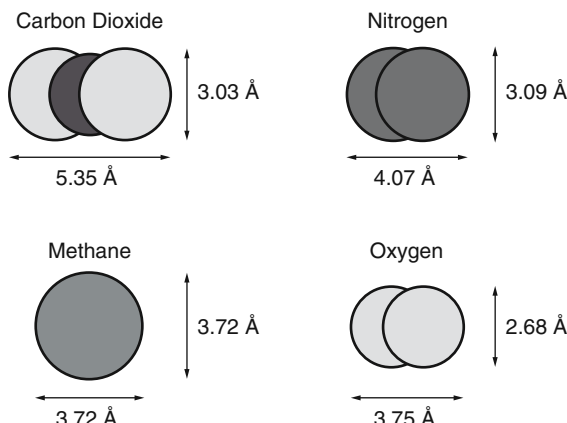


Figure 2.5 Illustration showing the approximate molecular dimensions of CO_2 , CH_4 , N_2 , and O_2 . Shape and size both influence permeant diffusion

permeate molecule has made only one large jump. Figure 2.4 simulates diffusion in silicone rubber, a material with a very flexible polymer backbone. In 200 ps, all the permeants in silicone rubber have made a number of large jumps from one microcavity to another.

This type of calculation also explains the anomalously high diffusion coefficient of carbon dioxide compared to methane. Carbon dioxide has a molar volume of $18.7 \text{ cm}^3/\text{mol}$. The molar volume of methane is a little lower, at $17.1 \text{ cm}^3/\text{mol}$, so methane is a slightly smaller molecule. However, as shown in Figure 2.5, methane is spherical with a kinetic diameter of 3.72 \AA , while carbon dioxide is an oblate ellipsoid. Viewed from the top, the carbon dioxide molecule is 5.25 \AA long, but seen end-on, the molecule's diameter is only 3.03 \AA . This means that as carbon dioxide molecules bounce around in their microcavities, they occasionally become oriented so they can slide through transient gaps between the polymer chains that are as small as 3.03 \AA , which completely reject methane molecules. The result is that the diffusion coefficient of carbon dioxide calculated by molecular dynamics simulation of glassy polymers is two to six times larger than methane. This result is also obtained experimentally.

Similarly, nitrogen, another oblate spheroid, although it has almost the same molar volume as methane, usually has a diffusion coefficient two to four times larger in most polymers.

Molecular dynamics simulations also allow the transition from the solution-diffusion to the pore-flow transport mechanism to be seen. As the microcavities become larger, the transport mechanism changes from the diffusion process simulated in Figures 2.3 and 2.4 to a pore-flow mechanism. Permanent pores form when the microcavities are larger than about $5\text{--}10 \text{ \AA}$ in diameter.

However, molecular dynamics calculations are at an early stage of development. Current estimates of diffusion coefficients from these simulations are generally far from matching the experimental values, and a better understanding of the interactions between

the molecules of polymer chains will be required to produce accurate predictions. Moreover, these simulations require the use of very large computers, and the longest times that can be simulated are a few hundred picoseconds. Unfortunately, relaxation times required for polymer chains in glassy polymers to approach an equilibrium state can be months or years. Extrapolation techniques are used to cover the gap, but the results are questionable. Several reviews of the development of molecular simulation techniques are available [13]. Despite their lack of quantitative success, molecular dynamic calculations demonstrate the qualitative basis of the solution-diffusion model in a very graphic way. However, the best quantitative description of permeation uses phenomenological equations, particularly Fick's law. This description is given in the section that follows, which outlines the mathematical basis of the solution-diffusion model. Much of this section is adapted from two review papers written with my colleague, Hans Wijmans [14, 15].

2.2.2 Concentration and Pressure Gradients in Membranes

The starting point for the mathematical description of diffusion in membranes is the proposition, solidly based in thermodynamics, that the driving forces of pressure, temperature, concentration, and electrical potential are interrelated and that the overall driving force producing movement of a permeant is a gradient in its chemical potential. Thus, the flux, J_i (g/cm²·s), of a component, i , is described by the simple equation

$$J_i = -L_i \frac{d\mu_i}{dx} \quad (2.3)$$

where $\frac{d\mu_i}{dx}$ is the chemical potential gradient of component i and L_i is a coefficient of proportionality (not necessarily constant) linking this chemical potential driving force to flux. Driving forces, such as gradients in concentration, pressure, temperature, and electrical potential, can be expressed as chemical potential gradients, and their effect on flux expressed by this equation. This approach is extremely useful, because many processes involve more than one driving force, for example, both pressure and concentration in reverse osmosis. Restricting the approach to driving forces generated by concentration and pressure gradients, the chemical potential is written as

$$d\mu_i = RT d \ln (\gamma_i n_i) + v_i dp \quad (2.4)$$

where n_i is the mole fraction (mol/mol) of component i , γ_i is the activity coefficient (mol/mol) linking mole fraction with activity, p is the pressure, and v_i is the molar volume of component i .

In incompressible phases, such as in a liquid or a solid membrane, volume does not change with pressure. In this case, integrating Equation 2.4 with respect to concentration and pressure gives

$$\mu_i = \mu_i^o + RT \ln (\gamma_i n_i) + v_i (p - p_i^o) \quad (2.5)$$

where μ_i^o is the chemical potential of pure i at a reference pressure, p_i^o .

In compressible gases, the molar volume changes with pressure. Using the ideal gas laws in integrating Equation 2.4 gives

$$\mu_i = \mu_i^o + RT \ln(\gamma_i n_i) + RT \ln \frac{p}{p_i^o} \quad (2.6)$$

To ensure that the reference chemical potential μ_i^o is identical in Equations 2.5 and 2.6, the reference pressure p_i^o is defined as the saturation vapor pressure of i , $p_{i,sat}$. Equations 2.5 and 2.6 can then be rewritten as

$$\mu_i = \mu_i^o + RT \ln(\gamma_i n_i) + v_i(p - p_{i,sat}) \quad (2.7)$$

for incompressible liquids and the membrane phase, and as

$$\mu_i = \mu_i^o + RT \ln(\gamma_i n_i) + RT \ln \frac{p}{p_{i,sat}} \quad (2.8)$$

for compressible gases.

Several assumptions must be made to define any permeation model. Usually, the first assumption governing transport through membranes is that the fluids on either side of the membrane are in equilibrium with the membrane material at the interface. This assumption means that the gradient in chemical potential from one side of the membrane to the other is continuous. Implicit in this assumption is that the rates of absorption and desorption at the membrane interface are much higher than the rate of diffusion through the membrane. This appears to be the case in almost all membrane processes, but may fail in transport processes involving chemical reactions, such as facilitated transport, or in diffusion of gases through metals, where interfacial absorption can be slow.

The second assumption concerns the way this chemical potential across the membrane is expressed within the membrane:

- The solution-diffusion model assumes that the pressure within a membrane is uniform and that the chemical potential gradient of a permeant across the membrane is represented only as a concentration gradient.
- The pore-flow model assumes that the permeant concentration within a membrane is uniform and that the chemical potential gradient across the membrane is represented only as a pressure gradient.

The consequences of these two assumptions are illustrated in Figure 2.6, which compares pressure-driven permeation of a one-component solution by solution-diffusion and by pore-flow. In both models, the difference in pressure across the membrane ($p_o - p_e$) produces a gradient in chemical potential (Equations 2.7 and 2.8). In the pore-flow model, the pressure difference produces a smooth gradient in pressure through the membrane, but the solvent concentration remains constant within the membrane. The solution-diffusion model on the other hand assumes that when a pressure is applied across a dense membrane, the pressure everywhere within the membrane is constant at the high-pressure value. This assumes, in effect, that solution-diffusion membranes transmit pressure in the same way as liquids. Consequently, the chemical potential difference

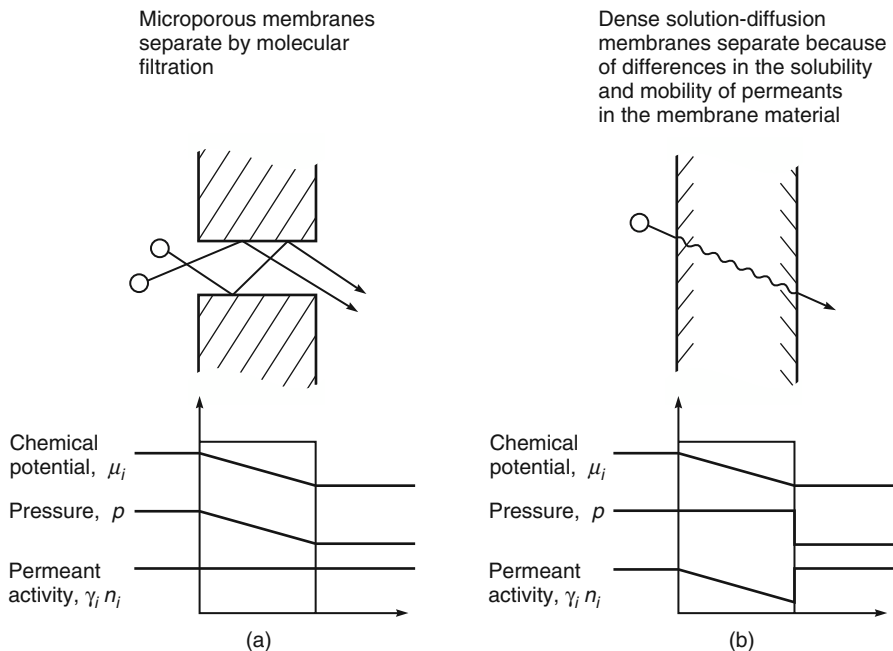


Figure 2.6 A comparison of the driving force gradients acting on a one-component solution permeating (a) a pore-flow and (b) a solution-diffusion membrane

across the membranes is represented as a concentration gradient within the membrane, with Equations 2.7 and 2.8 providing the mathematical link between pressure and concentration.

Consider the pore-flow model first. Combining Equations 2.3 and 2.4 in the absence of a concentration gradient in the membrane gives:

$$J_i = -L_i v_i \frac{dp}{dx} \quad (2.9)$$

This equation can be integrated across the membrane to give Darcy's law:

$$J_i = \frac{K' c_i (p_o - p_\ell)}{\ell} \quad (2.10)$$

where K' is the Darcy's law coefficient, equal to $L_i v_i$, and ℓ is the membrane thickness.

In the solution-diffusion model, the pressure within the membrane is constant at the high pressure value (p_o), and the gradient in chemical potential across the membrane is expressed as a smooth gradient in solvent activity ($\gamma_i n_i$). The flow that occurs down this gradient is expressed by Equation 2.3, but because no pressure gradient exists within the membrane, Equation 2.3 can be rewritten by combining Equations 2.3 and 2.4 as

$$J_i = -\frac{RT L_i}{n_i} \cdot \frac{dn_i}{dx} \quad (2.11)$$

In Equation 2.11, the gradient of component i across the membrane is expressed as a gradient in mole fraction of component i . Using the more practical term concentration (g/cm^3) defined as

$$c_i = m_i \rho n_i \quad (2.12)$$

where m_i is the molecular weight of i (g/mol) and ρ is the molar density (mol/cm^3), Equation 2.11 can be written as

$$J_i = -\frac{RTL_i}{c_i} \cdot \frac{dc_i}{dx} \quad (2.13)$$

Equation 2.13 has the same form as Fick's law, in which the term RTL_i/c_i can be replaced by the diffusion coefficient D_i . Thus,

$$J_i = -\frac{D_i dc_i}{dx} \quad (2.14)$$

Integrating over the thickness of the membrane then gives¹

$$J_i = \frac{D_i (c_{i_o(m)} - c_{i_\ell(m)})}{\ell} \quad (2.15)$$

By using osmosis as an example, concentration and pressure gradients according to the solution-diffusion model can be discussed in a somewhat more complex situation. The activity, pressure, and chemical potential gradients within this type of membrane are illustrated in Figure 2.7.

Figure 2.7a shows a semipermeable membrane separating a salt solution from pure solvent (water). The pressure is the same on both sides of the membrane. For simplicity, the gradient of salt (component j) is not shown in this figure, but the membrane is assumed to be very selective, so the concentration of salt within the membrane is small. The difference in concentration across the membrane results in a continuous, smooth gradient in the chemical potential of the water (component i) across the membrane, from μ_{i_ℓ} on the water side to a slightly lower value μ_{i_o} on the salt side. The pressure within and across the membrane is constant (that is, $p_o = p_m = p_\ell$) and the solvent activity gradient ($\gamma_{i(m)} n_{i(m)}$) falls continuously from the pure water (solvent) side to the saline (solution) side of the membrane. Consequently, water passes across the membrane from right to left.

Figure 2.7b shows the situation at the point of osmotic equilibrium, when sufficient pressure has been applied to the saline side of the membrane to bring the flow across the membrane to zero. As shown in Figure 2.7b, the pressure within the membrane is assumed to be constant at the high-pressure value (p_o). There is a discontinuity in pressure at the permeate side of the membrane, where the pressure falls abruptly from p_o to p_ℓ , the pressure on the solvent side of the membrane. This pressure difference

¹ In the equations that follow, the terms i and j represent components of a solution, and the terms o and ℓ represent the positions of the feed and permeate interfaces, respectively, of the membrane. Thus the term c_{i_o} represents the concentration of component i in the fluid (gas or liquid) in contact with the membrane at the feed interface. The subscript m is used to represent the membrane phase. Thus, $c_{i_o(m)}$ is the concentration of component i in the membrane at the feed interface (point o).

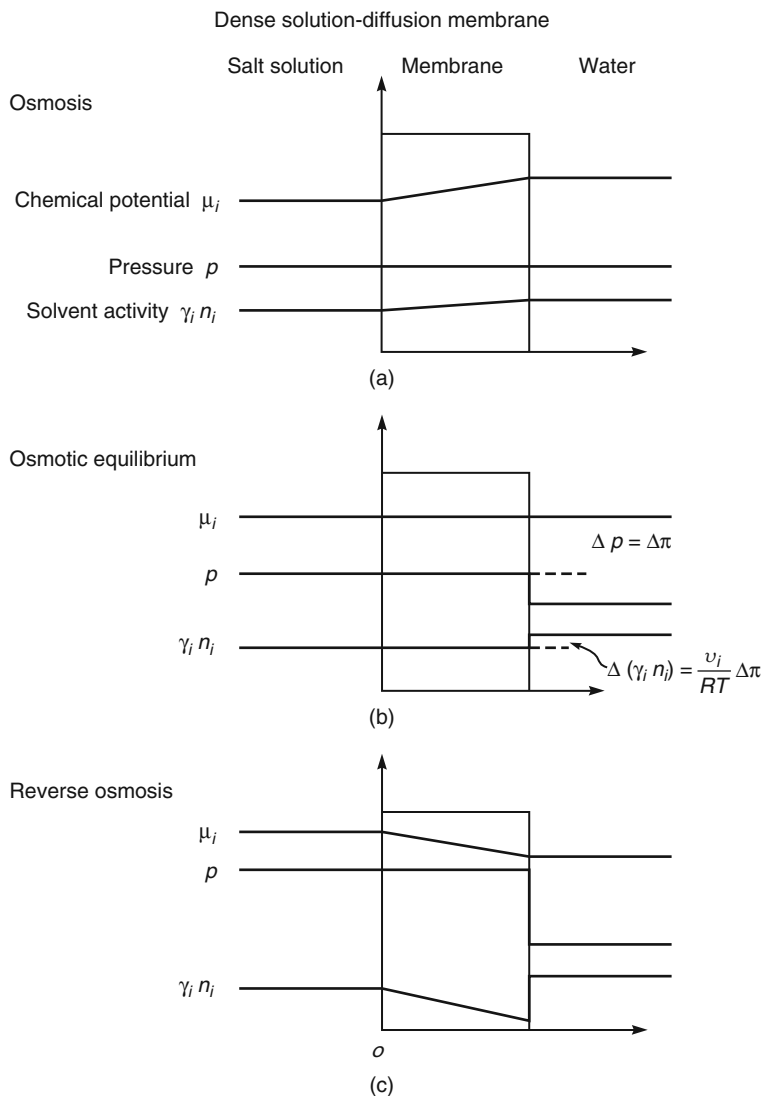


Figure 2.7 Chemical potential, pressure, and solvent gradients in an osmotic membrane following the solution-diffusion model for (a) osmosis, (b) osmotic equilibrium and (c) reverse osmosis. The pressure in the membrane is uniform and equal to the high-pressure value, so the chemical potential gradient within the membrane is expressed as a concentration gradient

$(p_o - p_\ell)$ can be expressed in terms of the concentration difference between the feed and permeate solutions.

The membrane in contact with the permeate-side solution is in equilibrium with this solution. Thus, Equation 2.7 can be used to link the two phases in terms of their chemical potentials, that is,

$$\mu_{i_{\ell(m)}} = \mu_{i_\ell} \quad (2.16)$$

and so

$$RT \ln (\gamma_{i_{\ell(m)}} n_{i_{\ell(m)}}) + v_i p_o = RT \ln (\gamma_{i_\ell} n_{i_\ell}) + v_i p_\ell \quad (2.17)$$

On rearranging, this gives

$$RT \ln (\gamma_{i_{\ell(m)}} n_{i_{\ell(m)}}) - RT \ln (\gamma_{i_\ell} n_{i_\ell}) = -v_i (p_o - p_\ell) \quad (2.18)$$

At osmotic equilibrium, $\Delta (\gamma_i n_i)$ can also be defined by

$$\Delta (\gamma_i n_i) = \gamma_{i_\ell} n_{i_\ell} - \gamma_{i_{\ell(m)}} n_{i_{\ell(m)}} \quad (2.19)$$

Since the permeate fluid is pure water, $\gamma_{i_\ell} n_{i_\ell} \approx 1$, and it follows, on substituting Equation 2.19 into 2.18, that

$$RT \ln [1 - \Delta (\gamma_i n_i)] = -v_i (p_o - p_\ell) \quad (2.20)$$

Since $\Delta (\gamma_i n_i)$ is small, $\ln[1 - \Delta (\gamma_i n_i)] \approx \Delta (\gamma_i n_i)$, and Equation 2.20 reduces to

$$\Delta (\gamma_i n_i) = \frac{-v_i (p_o - p_\ell)}{RT} = \frac{-v_i \Delta \pi}{RT} \quad (2.21)$$

Thus, the pressure difference, $(p_o - p_\ell) = \Delta \pi$, across the membrane balances the solvent activity difference $\Delta (\gamma_i n_i)$ across the membrane, and the flow is zero.

If a pressure higher than the osmotic pressure is applied to the feed side of the membrane, as shown in Figure 2.7c, then the solvent activity difference across the membrane increases further, resulting in a flow from left to right. This is the process of reverse osmosis.

The important conclusion illustrated by Figures 2.6 and 2.7 is that, although the fluids on either side of a membrane may be at different pressures and concentrations, within a perfect solution-diffusion membrane, there is no pressure gradient – only a concentration gradient. Flow through this type of membrane is expressed by Fick's law, Equation 2.15.

2.2.3 Application of the Solution-Diffusion Model to Specific Processes

In this section, the solution-diffusion model is used to describe transport in dialysis, reverse osmosis, gas permeation, and pervaporation membranes. The resulting equations, linking the driving forces of pressure and concentration with flow, are then shown to be consistent with experimental observations.

The general approach is to use the first assumption of the solution-diffusion model, namely, that the chemical potential of the feed and permeate fluids are in equilibrium with the adjacent membrane surfaces. From this assumption, the chemical potential in the fluid and membrane phases can be equated using the appropriate expressions for chemical potential given in Equations 2.7 and 2.8. By rearranging these equations, the concentrations of the different species in the membrane at the fluids interface ($c_{i_{o(m)}}$ and $c_{i_{\ell(m)}}$) can be obtained in terms of the pressure and composition of the feed and permeate fluids. These values for $c_{i_{o(m)}}$ and $c_{i_{\ell(m)}}$ can then be substituted into the Fick's law expression, Equation 2.15, to give the transport equation for the particular process.

2.2.3.1 Dialysis

Dialysis is the simplest application of the solution-diffusion model because only concentration gradients are involved. In dialysis, a membrane separates two solutions of different compositions. The concentration gradient across the membrane causes a flow of solute and solvent from one side of the membrane to the other.

Following the general procedure described above, equating the chemical potentials in the solution and membrane phase at the feed-side interface of the membrane gives

$$\mu_{i_o} = \mu_{i_{o(m)}} \quad (2.22)$$

Substituting the expression for the chemical potential of incompressible fluids from Equation 2.7 gives

$$\mu_i^o + RT \ln(\gamma_{i_o}^L n_{i_o}) + v_i (p_o - p_{i_{sat}}) = \mu_i^o + RT \ln(\gamma_{i_{o(m)}} n_{i_{o(m)}}) + v_i (p_o - p_{i_{sat}}) \quad (2.23)$$

which leads to²

$$\ln(\gamma_{i_o}^L n_{i_o}) = \ln(\gamma_{i_{o(m)}} n_{i_{o(m)}}) \quad (2.24)$$

and thus

$$n_{i_{o(m)}} = \frac{\gamma_{i_o}^L}{\gamma_{i_{o(m)}}} \cdot n_{i_o} \quad (2.25)$$

or from Equation 2.12

$$c_{i_{o(m)}} = \frac{\gamma_{i_o}^L \rho_m}{\gamma_{i_{o(m)}} \rho_o} \cdot c_{i_o} \quad (2.26)$$

Hence, defining a sorption coefficient K_i^L as

$$K_i^L = \frac{\gamma_{i_o}^L \rho_m}{\gamma_{i_{o(m)}} \rho_o} \quad (2.27)$$

Equation 2.26 becomes

$$c_{i_{o(m)}} = K_i^L \cdot c_{i_o} \quad (2.28)$$

That is, the concentration in the membrane at the feed-side surface $c_{i_{o(m)}}$ is proportional to the concentration of the feed solution, c_{i_o} .

On the permeate side of the membrane, the same procedure can be followed, leading to an equivalent expression

$$c_{i_{\ell(m)}} = K_i^L \cdot c_{i_\ell} \quad (2.29)$$

² The superscripts G and L are used here and later to distinguish between gas phase and liquid phase activity coefficients, sorption coefficients, and permeability coefficients.

The concentrations of permeant within the membrane phase at the two interfaces can then be substituted from Equations 2.28 and 2.29 into the Fick's law expression, Equation 2.15, to give the familiar expression describing permeation through dialysis membranes

$$J_i = \frac{D_i K_i^L}{\ell} (c_{i_o} - c_{i_\ell}) = \frac{P_i^L}{\ell} (c_{i_o} - c_{i_\ell}) \quad (2.30)$$

The product $D_i K_i^L$ is normally referred to as the permeability coefficient, P_i^L . For many systems, D_i , K_i^L , and thus P_i^L are concentration-dependent. Thus, Equation 2.30 implies the use of values for D_i , K_i^L , and P_i^L that are averaged over the membrane thickness.

The permeability coefficient P_i^L is often treated as a pure materials constant, depending only on the permeant and the membrane material, but the nature of the solvent used in the liquid phase is also important. From Equations 2.30 and 2.27, P_i^L can be written as

$$P_i^L = D_i \cdot \gamma_i^L / \gamma_{i(m)} \cdot \frac{\rho_m}{\rho_o} \quad (2.31)$$

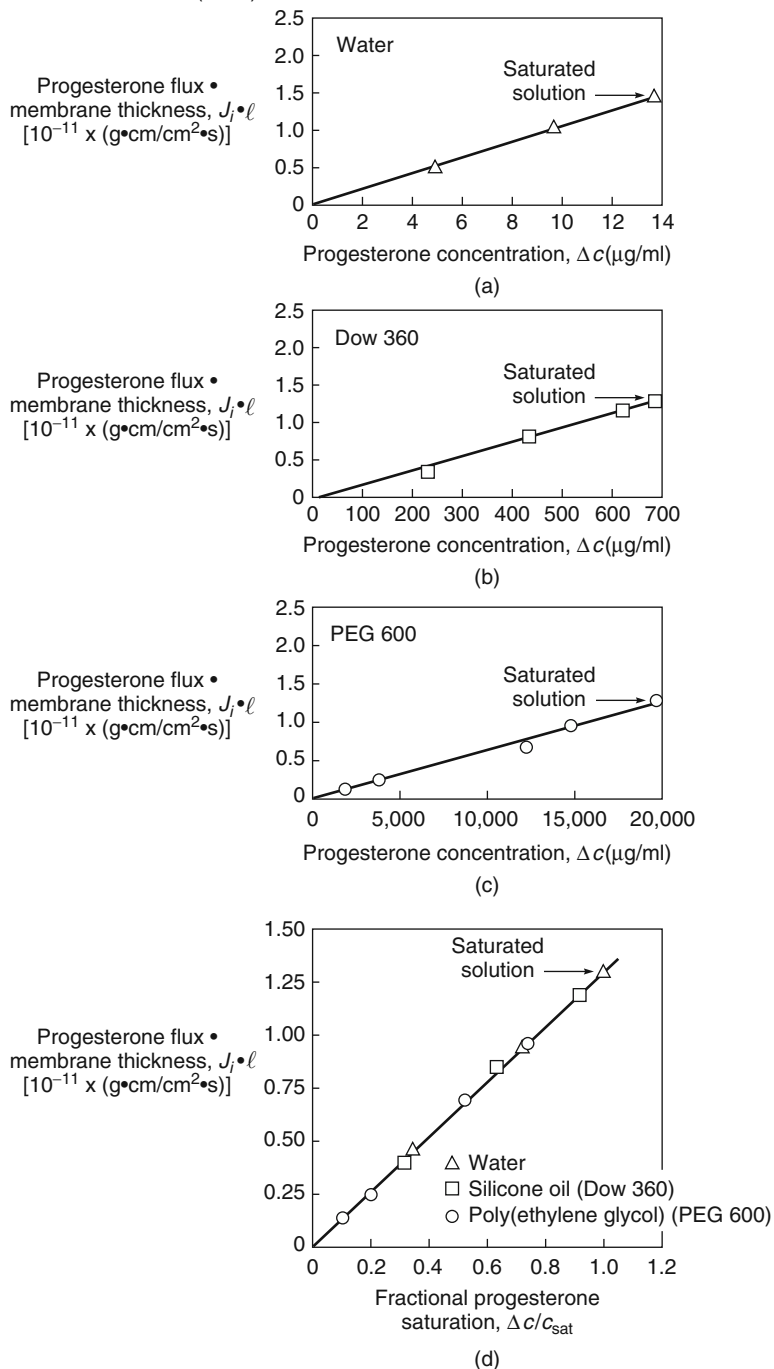
The presence of the term γ_i^L makes the permeability coefficient a function of the solvent in which the permeant is dissolved. Some measurements of the flux of the drug progesterone through the same membrane when dissolved in different solvents illustrate this effect, as shown in Figure 2.8 [16]. The figure is a plot of the product of the progesterone flux and the membrane thickness, $J_i \ell$, against the concentration difference across the membrane, $(c_{i_o} - c_{i_\ell})$. From Equation 2.30, the slope of this line is the permeability, P_i^L . Three sets of dialysis permeation experiments are reported, in which the solvent used to dissolve the progesterone is water, silicone oil, and polyethylene glycol MW 600 (PEG 600), respectively. The permeability calculated from these plots varies from 9.5×10^{-7} cm²/s for water to 6.5×10^{-10} cm²/s for PEG 600. This difference reflects the activity term γ_i^L in Equation 2.31. However, when the driving force across the membrane is represented not as a difference in concentration but as a difference in fractional saturation between the feed and permeate solution, all the data fall on a single line as shown in Figure 2.8d. The slope of this line is the term $P_i^L c_{i_{sat}}$. This result is also in agreement with Equation 2.31; when combined with the approximation that, for dilute solutions, the activity of component i can be written as

$$\gamma_i^L = \frac{1}{n_{i_{sat}}} = \frac{m_i \rho_o}{c_{i_{sat}}} \quad (2.32)$$

the result is

$$P_i^L c_{i_{sat}} = \frac{D_i m_i \rho_m}{\gamma_{i(m)}} \quad (2.33)$$

The terms $D_i m_i \rho_m / \gamma_{i(m)}$ and, therefore, $P_i^L c_{i_{sat}}$ are determined solely by the permeant and the membrane material and are thus independent of the liquid phase surrounding the membrane.

From Theeuwes *et al.* (1978)

2.2.3.2 Reverse Osmosis

Reverse osmosis and normal osmosis (dialysis) are directly related processes. In simple terms, if a selective membrane (i.e., a membrane freely permeable to water, but much less permeable to salt) separates a salt solution from pure water, water will pass through the membrane from the pure water side of the membrane into the side less concentrated in water (salt side) as shown in Figure 2.9. This process is called normal osmosis. If a hydrostatic pressure is applied to the salt side of the membrane, the flow of water can be retarded and, when the applied pressure is sufficient, the flow ceases. The hydrostatic pressure required to stop the water flow is called the osmotic pressure ($\Delta\pi$). If pressures greater than the osmotic pressure are applied to the salt side of the membrane, then the flow of water is reversed, and water begins to flow from the salt solution to the pure water side of the membrane. This process is called reverse osmosis, which is an important method of producing pure water from salt solutions.

Reverse osmosis usually involves two components, water (i) and salt (j). Following the general procedure for application of the solution-diffusion model, the chemical potentials at both sides of the membrane are first equated. At the feed interface, the pressures in the feed solution and within the membrane are identical (as shown in Figure 2.7c). Equating the chemical potentials at this interface gives the same expression as in dialysis (cf. Equation 2.28)

$$c_{i_{o(m)}} = K_i^L \cdot c_{i_o} \quad (2.34)$$

At the permeate interface, a pressure difference exists from p_o within the membrane to p_ℓ in the permeate solution (as shown in Figure 2.7c). Equating the chemical potentials across this interface gives

$$\mu_{i_\ell} = \mu_{i_{\ell(m)}} \quad (2.35)$$

Substituting the appropriate expression for the chemical potential of an incompressible fluid to the liquid and membrane phases (Equation 2.7) yields

$$\mu_i^o + RT \ln(\gamma_{i_\ell}^L n_{i_\ell}) + v_i(p_\ell - p_{isat}) = \mu_i^o + RT \ln(\gamma_{i_{\ell(m)}}^L n_{i_{\ell(m)}}) + v_i(p_o - p_{isat}) \quad (2.36)$$

which leads to

$$\ln(\gamma_{i_\ell}^L n_{i_\ell}) = \ln(\gamma_{i_{\ell(m)}}^L n_{i_{\ell(m)}}) + \frac{v_i(p_o - p_\ell)}{RT} \quad (2.37)$$

Figure 2.8 Permeation of progesterone through polyethylene vinyl acetate films. The thickness-normalized progesterone flux ($J_i \cdot \ell$) is plotted against the progesterone concentration across the membrane, Δc . [16] The solvents for the progesterone are (a) water, (b) silicone oil (Dow 360), and (c) polyethylene glycol (PEG 600). Because of the different solubilities of progesterone in these solvents, the permeabilities calculated from these data using Equation 2.28 vary 1000-fold. All the data can be rationalized onto a single curve by plotting the thickness-normalized flux against fractional progesterone saturation as described in the text and shown in (d). The slope of this line, $P_i^L c_{sat}$ or $D_i m_i \rho_i / \gamma_{i(m)}$, is a materials property, dependent only on the membrane material and the permeant, and independent of the solvent

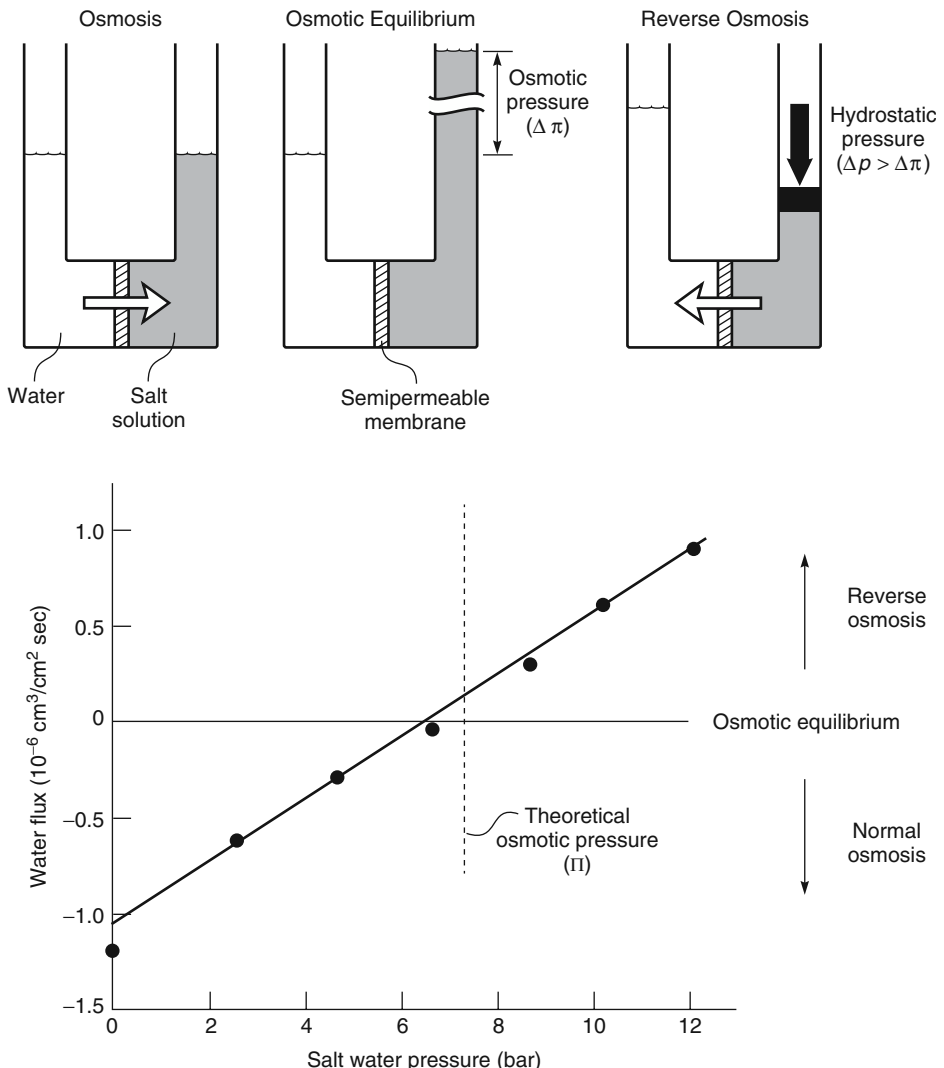


Figure 2.9 An illustration of the relationship between osmosis, osmotic equilibrium, and reverse osmosis. The data shown are from a paper by Thorsen and Holt [17] using a cellulose acetate membrane. Because the membrane is not perfectly selective for salt, the point of osmotic equilibrium (no flow across the membrane) is slightly below the theoretical osmotic pressure

Rearranging and substituting for the sorption coefficient, K_i^L (Equations 2.12 and 2.27), gives the expression

$$c_{i_{\ell(m)}} = K_i^L \cdot c_{i_\ell} \cdot \exp \left[\frac{-v_i (p_o - p_\ell)}{RT} \right] \quad (2.38)$$

The expressions for the concentrations within the membrane at the interface in Equations 2.34 and 2.38 can now be substituted into the Fick's law expression, Equation 2.15, to yield

$$J_i = \frac{D_i K_i^L}{\ell} \left\{ c_{i_o} - c_{i_\ell} \exp \left[\frac{-v_i (p_o - p_\ell)}{RT} \right] \right\} \quad (2.39)$$

The term $D_i K_i^L$ can also be written as a permeability and so Equation 2.39 becomes

$$J_i = \frac{P_i^L}{\ell} \left\{ c_{i_o} - c_{i_\ell} \exp \left[\frac{-v_i (p_o - p_\ell)}{RT} \right] \right\} \quad (2.40)$$

Equation 2.40 and the equivalent expression for component j give the water flux and the salt flux across the reverse osmosis membrane in terms of the pressure and concentration difference across the membrane.

One result of Equation 2.40 and the solution-diffusion model illustrated in Figure 2.7c is that the action of an applied pressure on the feed side of the membrane is to *decrease* the concentration of the permeant on the *low-pressure* side of the membrane. A number of workers have verified this prediction experimentally with a variety of membrane/permeant combinations, ranging from diffusion of water in glassy cellulose acetate membranes to diffusion of organics in swollen rubbers [18–20]. Convincing examples include the results of Rosenbaum and Cotton shown in Figure 2.10 [18]. In these experiments, four thin cellulose acetate films were laminated together, placed in a high-pressure reverse osmosis cell, and subjected to feed pressures of 69 or 138 bar. The permeate was maintained at atmospheric pressure. After the membrane laminate had reached a steady state, the membrane was quickly removed from the cell, and the water concentration in each laminate measured. As predicted by the solution-diffusion model and shown in Figure 2.7, the applied pressure decreases the concentration of water on the permeate side of the membrane. Also, the concentration difference across the membrane at 138 bar applied pressure is about twice that observed at 69 bar, and the measured concentration on the permeate side is within 20% of the expected value calculated from Equation 2.38.

Equation 2.40 predicts that as the pressure difference ($p_o - p_\ell$) across the membrane increases, the concentration gradient formed in the membrane will also increase, causing the membrane flux to increase. At small pressure differences, the concentration gradient and flux will increase almost linearly, but at higher pressure differences, Equation 2.40 predicts the concentration gradient and hence flux will plateau and approach a limiting value. The concentration on the permeate side of the membrane, $c_{i_\ell(m)}$, will approach zero, and the flux will approach $P_i^L c_{i_o} / \ell$. As Figure 2.10 shows, even at pressure differences of 69–138 bar, water sorption into the membrane, and hence water flux, is still in the linear part of the curve predicted by Equation 2.40 and shown in Figure 2.11. This result is because the molar volume (v_i) of water is small – 18 cm³/mol – and this reduces the effect of increasing pressure in Equation 2.40. Solvents of larger molar volume, for example, isoctane (molar volume 162 cm³/mol) have proportionally larger concentration gradients at comparable pressures. Figure 2.11 shows the flux of isoctane as a function of applied pressure, calculated using Equation 2.40. At transmembrane pressure differences of 500 bar and above, the concentration on the permeate side of the

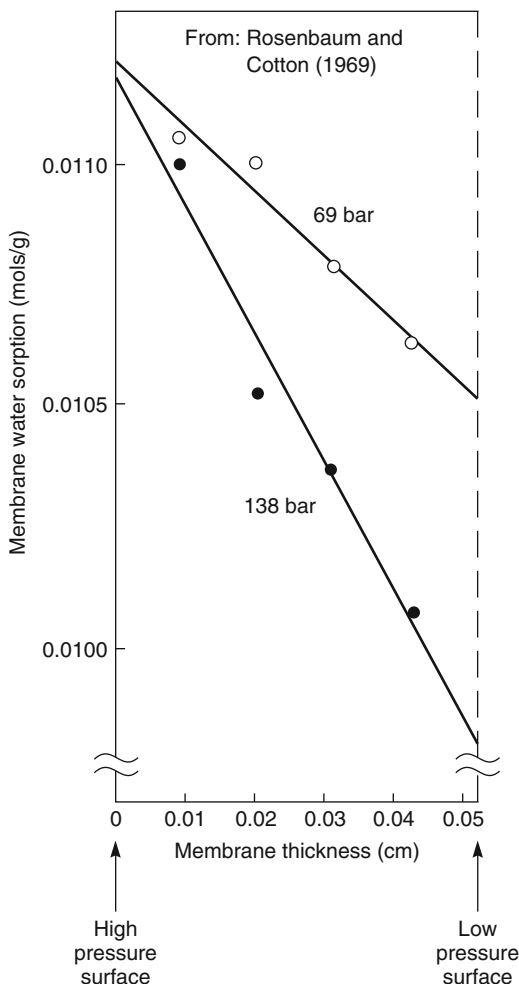


Figure 2.10 Measurements of Rosenbaum and Cotton of the water concentration gradients in a laminated reverse osmosis cellulose acetate membrane under applied pressures of 69 and 138 bar. Reprinted with permission from [18]. Copyright (1969) John Wiley & Sons, Inc.

membrane tends to zero and flux levels off to a limiting value, $J_{i\max}$. This plateauing of flux with applied pressure takes place at very high pressures in reverse osmosis and is not usually seen, but plateauing has been observed in hyperfiltration of organic liquids [20].

The above derivation of Equation 2.40 relies on the simplifying assumption that the molar volumes of the permeant in the membrane phase and in the liquid phase in contact with the membrane are equal. This assumption is not always valid. Transport equations can be derived for the case when the molar volumes in the membrane phase and liquid phase are different [21]. The resulting equations differ by a term called the “molar volume correction factor.” This correction factor is absent in the gas transport equation, and is

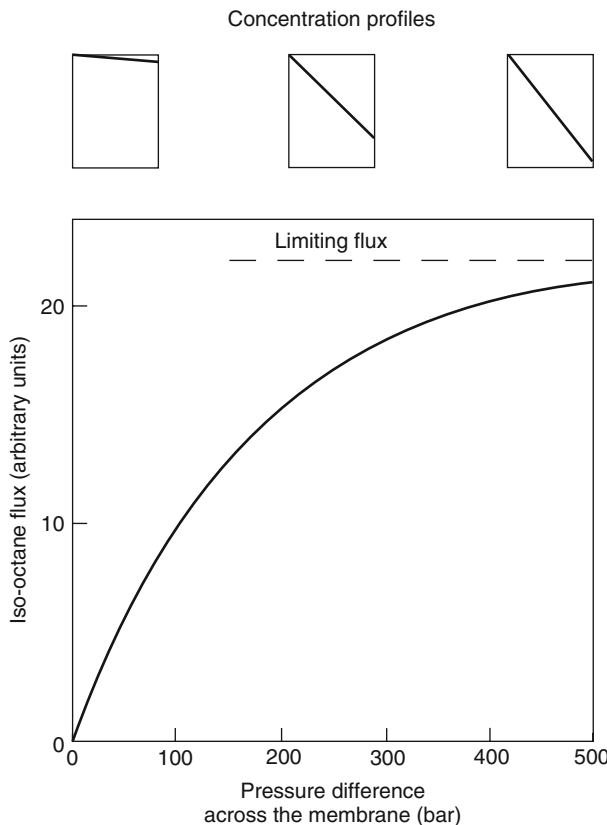


Figure 2.11 Calculated flux (arbitrary units) of liquid iso-octane as a function of applied pressure on the feed side of a hyperfiltration membrane (Equation 2.39). The change in concentration profile through the membrane as the pressure difference is increased is shown in the small boxes above the flux graph

insignificant for dialysis and pervaporation. For high-pressure hyperfiltration of organic mixtures containing relatively large molecules, the molar volume correction factor can be large enough to affect the dependence of flux on pressure.

2.2.3.3 Characterization of Reverse Osmosis and Hyperfiltration Membranes

Equation 2.39 allows the performance of a membrane to be calculated for known permeances, $D_i K_i^L / \ell$ and $D_j K_j^L / \ell$, and feed concentrations, c_{i_o} and c_{j_o} . More commonly, however, Equation 2.39 is simplified by assuming that the membrane selectivity is high, and the permeance of water is much higher than the permeance of salt; that is, $D_i K_i^L / \ell \gg D_j K_j^L / \ell$. This is a good assumption for most of the reverse osmosis membranes used to separate salts from water. Consider the water flux first. When the applied hydrostatic pressure balances the water activity gradient, that is, the point of osmotic

equilibrium in Figure 2.7b, the flux of water across the membrane is zero. Equation 2.39 then becomes

$$J_i = 0 = \frac{D_i K_i^L}{\ell} \left\{ c_{i_o} - c_{i_\ell} \exp \left[\frac{-v_i (\Delta\pi)}{RT} \right] \right\} \quad (2.41)$$

and, on rearranging

$$c_{i_\ell} = c_{i_o} \exp \left[\frac{v_i (\Delta\pi)}{RT} \right] \quad (2.42)$$

At hydrostatic pressures higher than $\Delta\pi$, Equations 2.39 and 2.42 can be combined to yield

$$J_i = \frac{D_i K_i^L c_{i_o}}{\ell} \left(1 - \exp \left\{ \frac{-v_i [(p_o - p_\ell) - \Delta\pi]}{RT} \right\} \right) \quad (2.43)$$

or

$$J_i = \frac{D_i K_i^L c_{i_o}}{\ell} \left\{ 1 - \exp \left[\frac{-v_i (\Delta p - \Delta\pi)}{RT} \right] \right\} \quad (2.44)$$

where Δp is the difference in hydrostatic pressure across the membrane ($p_o - p_\ell$). A trial calculation shows that the term $-v_i (\Delta p - \Delta\pi)/RT$ is small under the normal conditions of reverse osmosis. For example, in water desalination, when $\Delta p = 100$ bar, $\Delta\pi = 10$ bar, and $v_i = 18 \text{ cm}^3/\text{mol}$, the term $v_i (\Delta p - \Delta\pi)/RT$ is about 0.06.

Under these conditions, the simplification $1 - \exp(x) \rightarrow x$ as $x \rightarrow 0$ can be used, and Equation 2.44 can be written to a very good approximation as

$$J_i = \frac{D_i K_i^L c_{i_o} v_i (\Delta p - \Delta\pi)}{\ell RT} \quad (2.45)$$

This equation can be simplified to

$$J_i = A (\Delta p - \Delta\pi) \quad (2.46)$$

where A is a constant equal to the term $D_i K_i^L c_{i_o} v_i / \ell RT$. In the reverse osmosis literature, the constant A is usually called the *water permeability constant*.

Similarly, a simplified expression for the salt flux, J_j , through the membrane can be derived, starting with the salt equivalent to Equation 2.39

$$J_j = \frac{D_j K_j^L}{\ell} \left\{ c_{j_o} - c_{j_\ell} \exp \left[\frac{-v_i (p_o - p_\ell)}{RT} \right] \right\} \quad (2.47)$$

Because the term $-v_i (p_o - p_\ell) / RT$ is small, the exponential term in Equation 2.47 is close to one, and Equation 2.47 can then be written as

$$J_j = \frac{D_j K_j^L}{\ell} (c_{j_o} - c_{j_\ell}) \quad (2.48)$$

or

$$J_j = B(c_{j_o} - c_{j_e}) \quad (2.49)$$

where B is usually called the *salt permeability constant* and has the value

$$B = \frac{D_j K_j^L}{\ell} \quad (2.50)$$

Predictions of salt and water transport can be made from this application of the solution-diffusion model to reverse osmosis (first derived by Merten and coworkers) [22, 23]. According to Equation 2.46, the water flux through a reverse osmosis membrane remains small up to the osmotic pressure of the salt solution and then increases with applied pressure, whereas according to Equation 2.49, the salt flux is essentially independent of pressure. Some typical results are shown in Figure 2.12. This ability of reverse osmosis membranes to separate permeants can be expressed in several ways. Industrially, a term called the rejection coefficient, \mathbb{R} , is used, which is defined as

$$\mathbb{R} = \left(1 - \frac{c_{j_e}}{c_{j_o}}\right) \times 100\% \quad (2.51)$$

The rejection coefficient is a measure of the ability of the membrane to separate salt from the feed solution.

For a perfectly selective membrane the permeate salt concentration $c_{j_e} = 0$ and $\mathbb{R} = 100\%$, and for a completely unselective membrane the permeate salt concentration is the same as the feed salt concentration, $c_{j_e} = c_{j_o}$ and $\mathbb{R} = 0\%$. The rejection coefficient increases with applied pressure as shown Figure 2.12, because the water flux increases with pressure, but the salt flux does not.

Characterizing membrane properties in terms of the salt and water permeability constants, A and B , is widely used in the reverse osmosis industry. This is because these membranes have been developed for one application – desalination of sea water – and so the benefits of more fundamental measures of performance do not outweigh their greater complexity. As reverse osmosis begins to be applied to a wider range of applications, especially in the related process of hyperfiltration of organic mixtures, the use of permeabilities (P_i, P_j), permeances ($P_i/\ell, P_j/\ell$), and selectivities (α_{ij}) is becoming more common.

Membrane selectivity is best defined as the ratio of the permeability or permeances of components through the membrane. Thus

$$\alpha_{ij} = \frac{P_i}{P_j} \quad (2.52)$$

This can then be written

$$\alpha_{ij} = \left(\frac{D_i}{D_j}\right) \left(\frac{K_i}{K_j}\right) \quad (2.53)$$

This equation is useful because it illustrates the factors that determine membrane selectivity. The ratio (D_i/D_j) is the ratio of the diffusion coefficients and can be viewed as

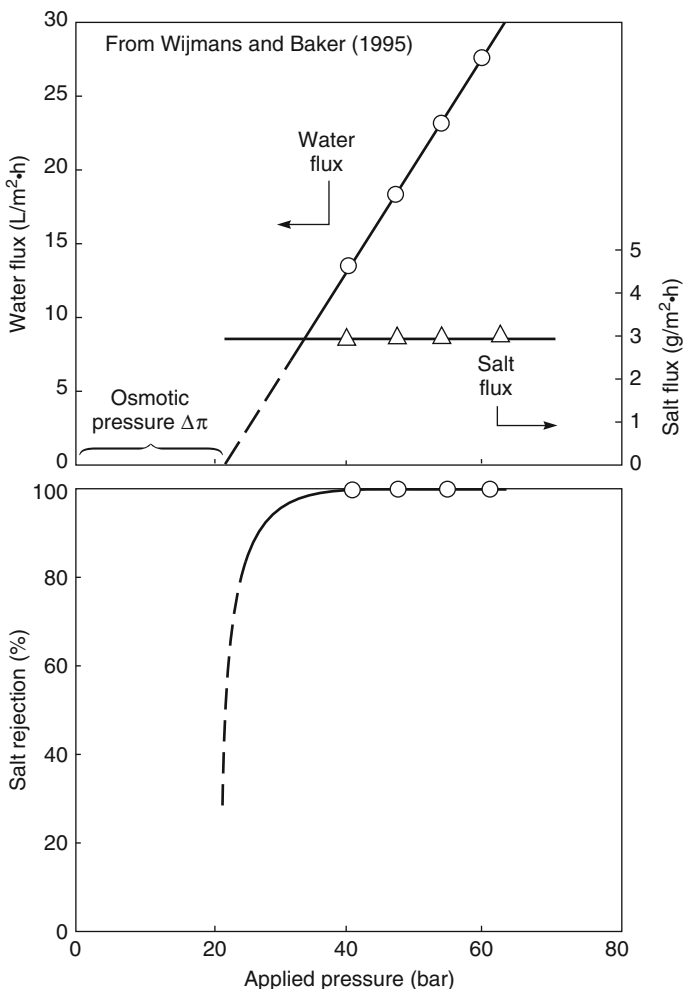


Figure 2.12 Flux and rejection data for a model seawater solution (3.5% sodium chloride) in a good quality reverse osmosis membrane (FilmTec Corp. FT 30 membrane) as a function of pressure [14]. The salt flux, in accordance with Equation 2.49, is essentially constant and independent of pressure. The water flux, in accordance with Equation 2.46, increases with pressure, and, at zero flux, meets the pressure axis at the osmotic pressure of seawater (~ 23 bar)

mobility selectivity, reflecting the relative size of the two permeants. Diffusion coefficients decrease with increasing molecular size because large molecules (or ions) interact with more segments of the polymer than small molecules. Hence, the ratio D_i/D_j always favors the permeation of water (*i*) over large hydrated ions such as Na^+ or Cl^- (*j*).

The ratio K_i/K_j is the ratio of the sorption coefficients. The magnitude of this term will depend on the nature of the permeants and the membrane. For water and salt diffusing in hydrophilic neutral polymers, this ratio also favors sorption of water over salt.

Table 2.1 Water (*w*) and sodium chloride (*s*) diffusion and partition data measured for a series of cellulose acetate films [22]

Properties			Membrane acetate content (wt%)			
			33.6	37.6	39.8	43.2
Water	Permeability	$D_w K_w$ (10^{-7} cm/s)	16	5.7	2.6	1.5
	Diffusion coefficient	D_w (10^{-6} cm 2 /s)	5.7	2.9	1.6	1.3
	Sorption coefficient	K_w (-)	0.29	0.20	0.16	0.12
Salt	Permeability	$D_s K_s$ (10^{-11} cm/s)	500	27	0.33	0.059
	Diffusion coefficient	D_s (10^{-10} cm 2 /s)	290	43	9.4	0.39
	Sorption coefficient	K_s (-)	0.17	0.062	0.035	0.015
Mobility selectivity		D_w/D_s	200	670	1700	3300
Solubility selectivity		K_w/K_s	1.6	3.2	4.6	8.0
Overall selectivity		$\alpha_{w/s}$	320	2100	7900	25000

A membrane acetate content of 33.6% acetate is close to cellulose diacetate; 43.2% acetate is close to cellulose triacetate.

The membrane selectivity can be calculated from Equations 2.39 and 2.47, but for very selective membranes, the approximate forms of these equations can be used. The membrane selectivity can then be written in terms of the water and salt permeability coefficients (Equations 2.46 and 2.50) as

$$\alpha = \frac{A}{B} \cdot \frac{RT}{c_{i_0} v_i} \quad (2.54)$$

The data in Figure 2.12 show that this good quality sea water desalination membrane has a selectivity for water over salt of more than 10 000.

For the past 20 years, the bulk of the reverse osmosis membrane data have been measured with interfacial composite membranes, where measurement of diffusion coefficient and partition coefficient data is not possible. However, data for the earlier first generation membrane materials (cellulose acetate) are available as shown in Table 2.1 [22].

Some trends are immediately clear. First, the bulk of the selectivity of these membranes is due to very large mobility selectivity in favor of water. The membrane's sorption selectivity, although it also favors permeation of water, is small in comparison. Second, as the acetate content of the cellulose ester membranes increases, making the membrane more hydrophobic, water sorption (K_w) decreases and the membrane sorption selectivity and mobility selectivity both increase. As a consequence, the overall selectivity of the membrane ($\alpha_{w/s}$) increases almost 100-fold. Concurrently, the membrane's water permeability ($D_w K_w$) decreases 10-fold. This tradeoff between permeation and selectivity is observed with many other separation membranes.

The very high overall selectivities shown in Table 2.1 suggest that membranes with rejection coefficients of 99.9% or more can be made from these materials. In fact, commercial reverse osmosis membranes almost always contain small imperfections, so the theoretical rejection can only be obtained with small membrane samples prepared in an ultraclean environment [24]. Typical water/NaCl selectivities of today's reverse osmosis membranes are about 10 000.

By convention, the term reverse osmosis is used to describe the separation of an aqueous salt solution by pressure-driven flow through a semipermeable membrane. Recently, the same type of process has been applied to the separation of organic mixtures. For example, Mobil Oil has installed a large plant to separate methyl ethyl ketone (MEK) from MEK/oil mixtures created in the production of lubricating oil [25], as described in Chapter 5. Separation of this type of mixture is best called hyperfiltration.

The mathematical description of this process is identical to that for reverse osmosis given in Equation 2.39, and leads to expressions for the solute and solvent fluxes

$$J_i = \frac{D_i K_i^L}{\ell} \left\{ c_{i_o} - c_{i_\ell} \exp \left[\frac{-v_i (p_o - p_\ell)}{RT} \right] \right\} \quad (2.55)$$

and

$$J_j = \frac{D_j K_j^L}{\ell} \left\{ c_{j_o} - c_{j_\ell} \exp \left[\frac{-v_j (p_o - p_\ell)}{RT} \right] \right\} \quad (2.56)$$

With currently available personal computing power, the numerical solution to these equations is straightforward even for multicomponent mixtures. Figure 2.13 shows a calculation example for the separation of a 20 wt% solution of *n*-decane in MEK. In these calculations, the selectivity of the membranes, that is, the ratio of the permeabilities of MEK and *n*-decane, $D_i K_i / D_j K_j$, is set at 10. The curves have essentially the same form as the salt solution flux data in Figure 2.12. At high pressures, the rejection approaches a limiting value of 90%, and the limiting equations for the solvent (MEK) flux (Equation 2.46) and for the solute flux (Equation 2.50) apply.

2.2.3.4 Gas Separation

In gas separation, a high-pressure gas mixture at a pressure p_o is applied to the feed side of the membrane, and the permeate gas at a lower pressure p_ℓ is removed from the downstream side of the membrane.

The concentration and pressure gradients through a dense polymer gas separation membrane are shown graphically in Figure 2.14. The figure has the features previously illustrated for reverse osmosis as shown in Figure 2.7. The pressure within the membrane is constant at the feed pressure and the chemical potential gradient is expressed as a gradient in concentration across the membrane. The gradient in concentration can be changed by changing the feed or permeate pressure. As the pressure is increased on the feed side of the membrane, the concentration in the membrane at the feed interface ($c_{i_{o(m)}}$) increases, reaching a maximum value when the vapor pressure of component i , p_{i_o} , reaches the saturation vapor pressure, $p_{i_{sat}}$. Similarly, the concentration in the membrane at the permeate side interface decreases with decreasing permeate pressure, reaching zero when a hard vacuum is created on the permeate side of the membrane. In gas separation therefore, the pressures on either side of the membrane can be linked by the expression

$$p_{i_{sat}} \geq p_{i_o} \geq p_{i_\ell} \quad (2.57)$$

As before, the starting point for the derivation of the gas separation transport equation is to equate the chemical potentials on either side of the gas/membrane interface. This

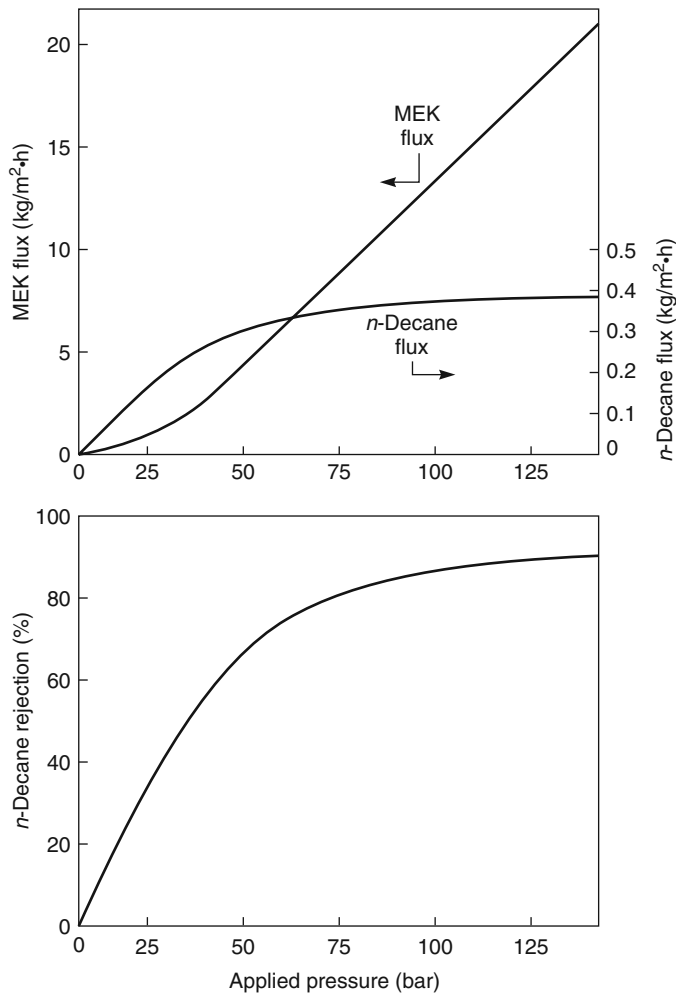


Figure 2.13 Flux and rejection curves calculated using Equations 2.55 and 2.56 for a 20 wt% n-decane solution in methyl ethyl ketone (MEK). MEK is assumed to be 10 times more permeable than n-decane

time, however, the chemical potential for the gas phase is given by Equation 2.8 for a compressible gas, and Equation 2.7 for an incompressible medium is applied to the membrane phase. Substitution of these equations into Equation 2.22 at the gas/membrane feed interface yields³

$$\mu_i^o + RT \ln (\gamma_{i_o}^G n_{i_o}) + RT \ln \frac{p_o}{p_{i_{sat}}} = \mu_i^o + RT \ln (\gamma_{i_o(m)} n_{i_o(m)}) + v_i (p_o - p_{i_{sat}}) \quad (2.58)$$

³ At this point the superscript *G* is introduced to denote the gas phase. For example, $\gamma_{i_o}^G$ is the activity of component *i* in the gas phase, and K_i^G is the sorption coefficient of component *i* between the gas and membrane phases (Equation 2.61).

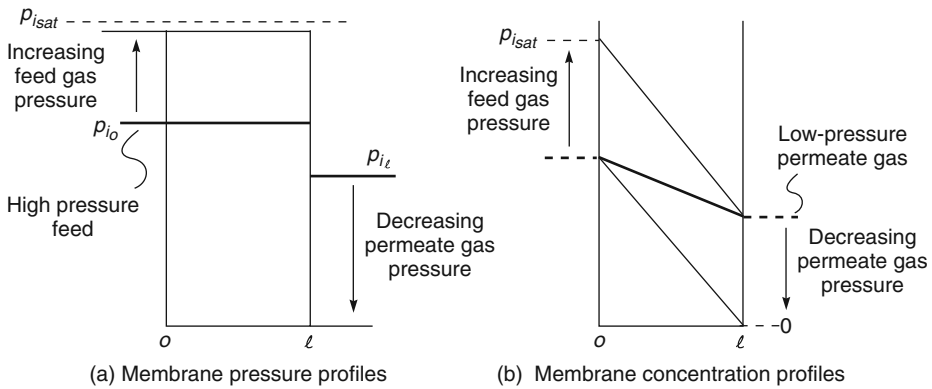


Figure 2.14 Changes in (a) the pressure and (b) the concentration profiles through a gas permeation membrane, according to the solution-diffusion model, as the high-pressure feed and low-pressure permeate pressure change

which rearranges to

$$n_{i_o(m)} = \frac{\gamma_{i_o}^G}{\gamma_{i_o(m)}} \cdot \frac{p_o}{p_{i_{sat}}} \cdot n_{i_o} \exp \left[\frac{-v_i (p_o - p_{i_{sat}})}{RT} \right] \quad (2.59)$$

Substituting concentration for mole fraction using Equation 2.12 and expressing $p_o n_{i_o}$ as the partial pressure p_{i_o} , Equation 2.59 can be rewritten as

$$c_{i_o(m)} = \frac{m_i \rho_m \gamma_{i_o}^G}{\gamma_{i_o(m)} p_{isat}} \cdot p_{i_o} \exp \left[\frac{-v_j (p_o - p_{isat})}{RT} \right] \quad (2.60)$$

Defining a gas phase sorption coefficient K_i^G in a similar way to the liquid phase coefficient K_i^L gives

$$K_i^G = \frac{m_i \rho_m \gamma_{l_o}^G}{\gamma_{l_o(m)} p_{sat}} \quad (2.61)$$

and so Equation 2.60 becomes

$$c_{i_o(m)} = K_i^G \cdot p_{i_o} \cdot \exp\left[\frac{-v_i(p_o - p_{i_{sat}})}{RT}\right] \quad (2.62)$$

In exactly the same way, the process represented by Equations 2.58–2.60 can be repeated at the membrane/permeate interface and the concentration of component i in the membrane at the membrane/permeate interface can be shown to be

$$c_{i_{\ell(m)}} = K_i^G \cdot p_{i_\ell} \cdot \exp \left[\frac{-v_i (p_o - p_{i_{sat}})}{RT} \right] \quad (2.63)$$

Combining Equations 2.62 and 2.63 with the Fick's law expression, Equation 2.15, then gives

$$J_i = \frac{D_i K_i^G (p_{i_o} - p_{i_\ell})}{\ell} \cdot \exp \left[\frac{-v_i (p_o - p_{i_{sat}})}{RT} \right] \quad (2.64)$$

Equation 2.64 shows the permeation of gas through a membrane is the product of two terms. The first term contains the partial pressure difference of component i across the membrane. The second exponential term contains the total gas pressure p_o of all gas components $p_o = (p_i + p_j + \dots)$ on the feed side of the membrane. Gas mixtures can have the same partial pressures for one of the components (i), but very different total pressures, so the exponential term is a measure of how much the total gas pressure produced by the presence of other components affects the partial pressure driving force for component i . It should be noted that the term v_i in Equation 2.64 is not the molar volume of i in the gas phase, but the partial molar volume of i dissolved in the membrane material, which is approximately equal to the molar volume of liquid i . As a result, the exponential term (known as the Poynting correction) usually is very close to 1 for permanent gases and only becomes significant for vapors with larger molar volumes at high pressures. For most gas permeation processes, Equation 2.64 reduces to

$$J_i = \frac{D_i K_i^G (p_{i_o} - p_{i_\ell})}{\ell} \quad (2.65)$$

The product $D_i K_i^G$ is often abbreviated to a permeability coefficient P_i^G , leading to the familiar expression

$$J_i = \frac{P_i^G (p_{i_o} - p_{i_\ell})}{\ell} \quad (2.66)$$

Equation 2.66 is widely used to accurately and predictably rationalize the properties of gas permeation membranes.

The derivation of Equation 2.66 might be seen as a long-winded way of arriving at a trivial result. However, this derivation explicitly clarifies the assumptions behind the equation. First, a gradient in concentration occurs within the dense polymer membrane, but there is no gradient in pressure. Second, absorption of a component into the membrane is proportional to its activity (partial pressure) in the adjacent gas, but is independent of the total gas pressure. This is related to the approximation made following Equation 2.64, in which the Poynting correction was assumed to be 1.

The permeability coefficient, P_i , equal to the product $D_i K_i^G$, can be expressed from the definition of K_i^G in Equation 2.61 as

$$P_i^G = \frac{\gamma_i^G D_i m_i \rho_m}{\gamma_{i(m)} \cdot p_{i_{sat}}} \quad (2.67)$$

In Equation 2.66 the membrane flux, J_i , is a mass flux ($\text{g}/\text{cm}^2/\text{s}$), whereas the gas separation literature predominantly uses a molar flux, typically expressed in the

units $\text{cm}^3(\text{STP}) \cdot \text{cm}^2 \cdot \text{s}$. The molar flux, j_i , can be linked to the mass flux, J_i , by the expression

$$j_i = J_i \frac{v_i^G}{m_i} \quad (2.68)$$

where v_i^G is the molar volume of gas i (22.4 l(STP/mol)). Similarly, the mass permeability unit P_i^G , defined in Equation 2.66, can be linked to the molar gas permeability \mathcal{P}_i^G , usually in the units $\text{cm}^3(\text{STP}) \cdot \text{cm/cm}^2 \cdot \text{s} \cdot \text{cmHg}$, as

$$\mathcal{P}_i^G = \frac{P_i^G v_i^G}{m_i} \quad (2.69)$$

Equation 2.66 can then be written as

$$j_i = \frac{\mathcal{P}_i^G}{\ell} (p_{i_o} - p_{i_\ell}) \quad (2.70)$$

The ability of a membrane to separate two gases can then be measured by the membrane selectivity term

$$\alpha_{ij} = \frac{P_i^G}{P_j^G} = \left(\frac{D_i}{D_j} \right) \left(\frac{K_i^G}{K_j^G} \right) \quad (2.71)$$

The effect of polymer chemistry and morphology on membrane permeabilities and selectivities is covered later in this chapter and in the Gas Separation chapter (Chapter 8).

2.2.3.5 Pervaporation

Pervaporation is a process intermediate between gas separation and hyperfiltration. The feed membrane interface is contacted with a feed fluid in the liquid phase at a pressure greater than the saturation vapor pressure; the permeate interface is in contact with a permeate fluid in the gas phase at a pressure below the saturation vapor pressure.

The selective layer of almost all pervaporation membranes is a dense polymer film and the pressure and concentration profiles that form across the membrane in pervaporation are shown in Figure 2.15. The pressure within the membrane is the same as the feed pressure. At the permeate side interface, the pressure then drops to a value below the saturation vapor pressure. The pressures on either side of the membrane can be linked by the expression

$$p_{i_o} \geq p_{i_{sat}} \geq p_{i_\ell} \quad (2.72)$$

As before, the flux through the membrane can be determined by calculating the concentration in the membrane at the two interfaces.

At the liquid solution/membrane feed interface, the chemical potential of the feed liquid is equilibrated with the chemical potential in the membrane at the same pressure. Equation 2.7 then gives

$$\mu_i^o + RT \ln (\gamma_{i_o}^L n_{i_o}) + v_i (p_o - p_{i_{sat}}) = \mu_i^o + RT \ln (\gamma_{i_{o(m)}} n_{i_{o(m)}}) + v_i (p_o - p_{i_{sat}}) \quad (2.73)$$

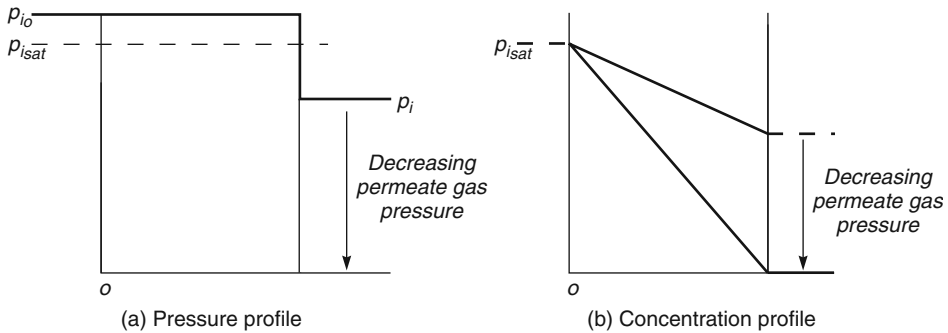


Figure 2.15 Changes in (a) the pressure and (b) the concentration profiles through a pervaporation membrane as the permeate pressure changes, according to the solution-diffusion model. In pervaporation, the feed is a liquid; therefore, the feed pressure p_{i_0} exceeds the saturated pressure p_{isat}

which leads to an expression for the concentration at the feed-side interface

$$c_{i_0(m)} = \frac{\gamma_{i_0}^L \rho_m}{\gamma_{i_0(m)} \rho_o} \cdot c_{i_0} = K_i^L \cdot c_{i_0} \quad (2.74)$$

where K_i^L is the liquid phase sorption coefficient defined in Equation 2.27.

At the permeate gas/membrane interface, the pressure drops from p_o in the membrane to p_ℓ in the permeate vapor. The equivalent expression for the chemical potentials in each phase is then

$$\mu_i^o + RT \ln (\gamma_{i_\ell}^G n_{i_0}) + RT \ln \left(\frac{p_\ell}{p_{isat}} \right) = \mu_i^o + RT \ln \left(\gamma_{i_\ell(m)} n_{i_\ell(m)} \right) + v_i (p_o - p_{isat}) \quad (2.75)$$

Rearranging Equation 2.75 gives

$$n_{i_\ell(m)} = \frac{\gamma_{i_\ell}^G}{\gamma_{i_\ell(m)}} \cdot \frac{p_\ell}{p_{isat}} \cdot n_{i_\ell} \cdot \exp \left[\frac{-v_i (p_o - p_{isat})}{RT} \right] \quad (2.76)$$

As before, the exponential term is close to unity; thus, the concentration at the permeate-side interface is

$$n_{i_\ell(m)} = \frac{\gamma_{i_\ell}^G}{\gamma_{i_\ell(m)}} \cdot n_{i_\ell} \cdot \frac{p_\ell}{p_{isat}} \quad (2.77)$$

The product $n_{i_\ell} p_\ell$ can be replaced by the partial pressure term p_{i_ℓ} , thus

$$n_{i_\ell(m)} = \frac{\gamma_{i_\ell}^G}{\gamma_{i_\ell(m)}} \cdot \frac{p_{i_\ell}}{p_{isat}} \quad (2.78)$$

and substituting concentration for mole fraction from Equation 2.12,

$$c_{i_{\ell(m)}} = m_i \rho_m \times \frac{\gamma_i^G p_{i_\ell}}{\gamma_{i_{\ell(m)}} p_{i_{sat}}} = K_i^G p_{i_\ell} \quad (2.79)$$

where K_i^G is the gas phase sorption coefficient defined in Equation 2.61.

The concentration terms in Equations 2.74 and 2.79 can be substituted into Equation 2.15 (Fick's law) to obtain an expression for the membrane flux:

$$J_i = \frac{D_i (K_i^L c_{i_o} - K_i^G p_{i_\ell})}{\ell} \quad (2.80)$$

Equation 2.80 contains two different sorption coefficients, deriving from Equations 2.27 and 2.61. The sorption coefficient in Equation 2.27 is a liquid phase coefficient, whereas the sorption coefficient in Equation 2.61 is a gas phase coefficient. The interconversion of these two coefficients can be handled by considering a hypothetical vapor in equilibrium with the feed solution. The vapor–liquid equilibrium can then be written

$$\mu_i^o + RT \ln (\gamma_i^L n_i^L) + v_i (p - p_{i_{sat}}) = \mu_i^o + RT \ln (\gamma_i^G \cdot n_i^G) + RT \ln \left(\frac{p_o}{p_{i_{sat}}} \right) \quad (2.81)$$

Following the same steps as were taken from Equations 2.75 to 2.79, Equation 2.81 becomes Equation 2.82

$$n_i^L = \frac{\gamma_i^G p_i}{\gamma_i^L p_{i_{sat}}} \quad (2.82)$$

Converting from mole fraction to concentration using Equation 2.12 gives

$$c_i^L = m_i \rho \left(\frac{\gamma_i^G p_i}{\gamma_i^L p_{i_{sat}}} \right) \quad (2.83)$$

and so

$$c_i^L = \left(\frac{K_i^G}{K_i^L} \right) p_i \quad (2.84)$$

This expression links the concentration of component i in the liquid phase, c_i^L with p_i , the partial vapor pressure of i in equilibrium with the liquid. Substitution of Equation 2.84 into Equation 2.80 yields

$$J_i = \frac{D_i K_i^G (p_{i_o} - p_{i_\ell})}{\ell} \quad (2.85)$$

where p_{i_o} and p_{i_ℓ} are the partial vapor pressures of component i on either side of the membrane. Equation 2.85 can also be written as

$$J_i = \left(\frac{P_i^G}{\ell} \right) (p_{i_o} - p_{i_\ell}) \quad (2.86)$$

where P_i^G is the gas permeation permeability coefficient. Equation 2.86 explicitly expresses the driving force in pervaporation as the vapor pressure difference across the membrane, a form of the pervaporation transport equation derived first by Kataoka *et al.* [26] and later, independently by Wijmans and Baker [27].

In the derivations given above, Equation 2.84 links the concentration of a vapor in the liquid phase (c_i^L) with the equilibrium partial pressure of the vapor. This relationship is more familiarly known as Henry's law, written as

$$H_i \cdot c_i^L = p_i \quad (2.87)$$

where H_i is the Henry's law coefficient.

From Equations 2.83 and 2.87, it follows that H_i can be written as

$$H_i = \frac{K_i^L}{K_i^G} = \frac{\gamma_i^L p_{i_{sat}}}{m_i \rho \gamma_i^G} \quad (2.88)$$

These expressions can be used to rewrite Equation 2.80 as

$$J_i = \frac{P_i^G}{\ell} (c_{i_o} H_i - p_{i_\ell}) \quad (2.89)$$

where P_i^G is the gas permeability coefficient, or

$$J_i = \frac{P_i^L}{\ell} (c_{i_o} - p_{i_\ell}/H_i) \quad (2.90)$$

where P_i^L is the liquid (hyperfiltration) permeability coefficient.

At low permeate side vapor pressure, the two alternative ways of describing the pervaporation flux reduce to

$$J_i = \frac{P_i^G}{\ell} p_{i_o} = \frac{P_i^L}{\ell} c_{i_o} \quad (2.91)$$

This equation shows that in pervaporation, the dependence of vapor pressure (driving force) on temperature in Equation 2.90 is hidden in the term P_i^L . This coefficient will increase exponentially with temperature as the vapor pressure term imbedded in P_i^L increases. In contrast, the gas phase permeability coefficient P_i^G is only a modest function of temperature.

The benefit of using the gas permeability constant P_i^G and Equation 2.86 to describe pervaporation has been amply demonstrated experimentally [26, 27]. For example, Figure 2.16 shows data for the pervaporation water flux through a silicone rubber membrane as a function of permeate pressure. As the permeate pressure (p_{i_ℓ}) increases, the water flux falls in accordance with Equation 2.86, reaching zero flux when the permeate pressure is equal to the vapor pressure (p_{i_o}) of the feed liquid at the temperature of the experiment. The straight lines in Figure 2.16 indicate that the permeability coefficient of water in silicone rubber is constant. This can be expected in systems in which the membrane material is a rubbery polymer and the permeant swells the polymer only moderately.

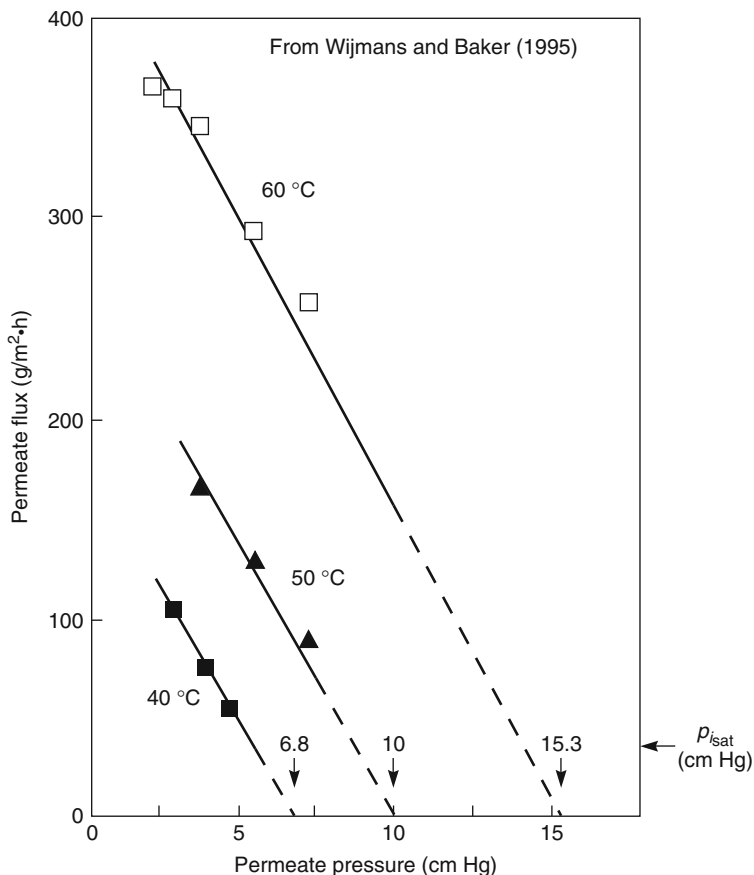


Figure 2.16 The effect of permeate pressure on the water flux through a silicone rubber membrane during pervaporation. The arrows on the horizontal axis represent the saturation vapor pressure of the feed solution at the experiment temperatures. Reprinted with permission from [14]. Copyright (1995), Elsevier.

Thompson and coworkers [28] have studied the effects of feed and permeate pressure on pervaporation flux in some detail. Some illustrative results are shown in Figure 2.17. As Figure 2.17a shows, the dependence of flux on permeate pressure is in accordance with Equation 2.86. At very low permeate pressures, $p_{i\ell}$ approaches zero ($p_{i\ell} \rightarrow 0$), and the membrane flux has its maximum value $J_{i\text{max}}$ equal to $P_i^G p_{i_0} / \ell$. As the permeate pressure increases, the flux decreases, reaching a zero flux when the permeate pressure equals the saturation vapor pressure of the feed ($p_{i\ell} = p_{i_0}$).

The line linking flux and permeate pressure in Figure 2.17a is curved. This curvature shows that the permeability coefficient decreases with decreasing permeate pressure, that is, P_{hexane} decreases with a decrease in hexane concentration in the membrane. This

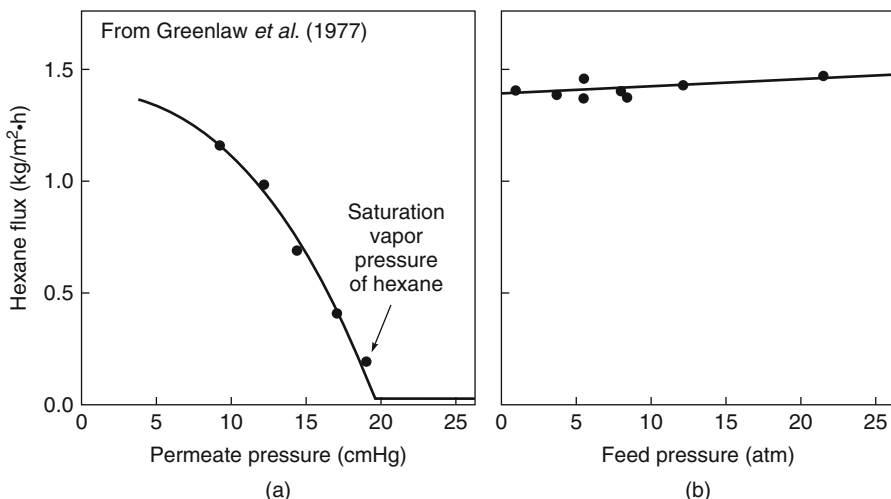


Figure 2.17 The effect of (a) permeate pressure and (b) feed pressure on the flux of hexane through a rubbery pervaporation membrane. The flux is essentially independent of feed pressure up to 20 bar, but is extremely sensitive to permeate pressure. Equations 2.85 and 2.86 explain this behavior. Reprinted with permission from [28]. Copyright (1977) Elsevier.

behavior is typical of membranes that are swollen significantly by the permeant. If on the other hand, as shown in Figure 2.17b, the permeate pressure is fixed at a low value, the hydrostatic pressure of the feed liquid can be increased to as much as 20 bar without any significant change in the flux. This is because the vapor pressure of a liquid (p_{i_o}) increases very little with increased hydrostatic pressure. Equation 2.86 shows that the feed vapor pressure is the true measure of the driving force for transport through the membrane. Thus, the properties of pervaporation membranes illustrated in Figures 2.16 and 2.17 are easily rationalized by the solution-diffusion model as given above but are much more difficult to explain by a pore-flow mechanism, although this has been tried.

A majority of the papers on pervaporation report membrane separation performance as raw data; that is, as fluxes J_i and J_j and separation factors β_{ij} defined as

$$\beta_{ij} = \frac{c_{i_\ell}/c_{j_\ell}}{c_{i_o}/c_{j_o}} \quad (2.92)$$

These values are a function of the intrinsic properties of the membrane and the operating conditions of the experiments (feed concentration, permeate pressure, feed temperatures); change the operating conditions and all the numbers change. A preferred way of measuring separation performance is to report data in a normalized form; that is, as permeabilities (P_i), permeances (P_i/ℓ), and selectivities (α_{ij}). The connection between these parameters and flux and separation factors is described in Chapter 9.

2.2.4 A Unified View

In the preceding section, the solution-diffusion model was used to calculate the concentration gradients formed through gas separation, pervaporation, and reverse osmosis membranes. The equations describing the flux through the membranes contain the same coefficients D_i , K_i , and P_i irrespective of the actual process. This happens because the driving force affecting the permeating component is the same for each process – a concentration gradient within the membrane. The fluid on either side of the membrane can change from a gas to a pressurized liquid, but the only effect of these changes on permeation within the membrane is to alter the concentration gradient driving force.

The pressure and concentration profiles within a solution-diffusion membrane for gas separation, pervaporation, and hyperfiltration (reverse osmosis), are compared in Figure 2.18. Considering gas separation first, the feed and permeate sides of the membrane are both below the saturation vapor pressure and we can write

$$p_{i_{sat}} > p_{i_o} > p_{i_\ell} \quad (\text{Gas separation})$$

The concentration in the membrane at the interfaces is proportional to the adjacent gas phase pressure as described in Equations 2.62 and 2.63.

If the feed gas pressure, p_{i_o} , is raised until it exceeds the saturation vapor pressure, then the membrane enters the pervaporation region, liquid forms on the feed side of the membrane and

$$p_{i_o} > p_{i_{sat}} > p_{i_\ell} \quad (\text{Pervaporation})$$

At this point, the concentrations in the membrane at the interfaces are described by Equations 2.74 and 2.79.

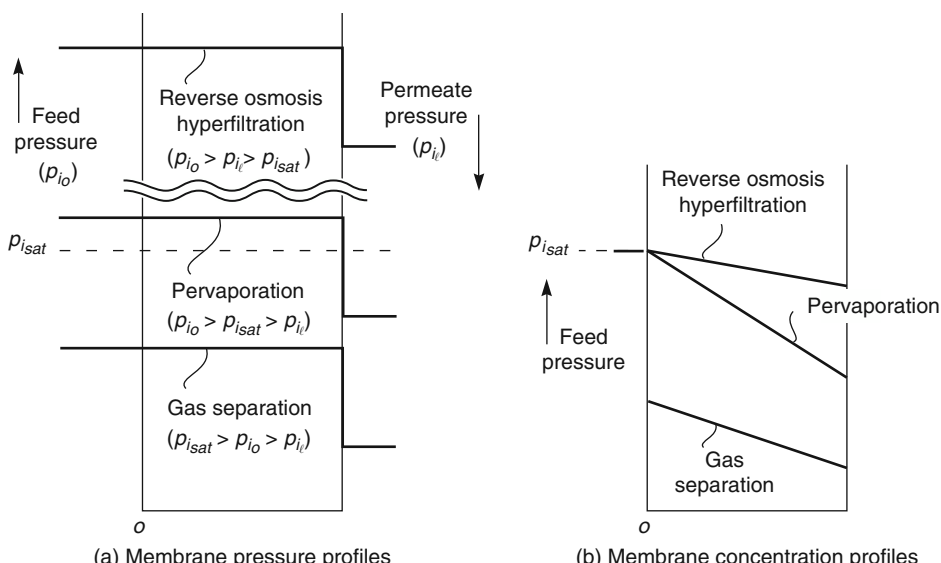


Figure 2.18 (a) Pressure profiles in gas separation, pervaporation and hyperfiltration membranes, relative to the saturation vapor pressure ($p_{i_{sat}}$). (b) Concentration profile created within the same membranes created by the pressure profiles shown in (a)

If the permeate side pressure, $p_{i\ell}$, is then increased, so that the saturation vapor pressure is exceeded on both sides of the membrane, liquid forms at both membrane interfaces. The membrane then enters the hyperfiltration (reverse osmosis) region and

$$p_{i_0} > p_{i\ell} > p_{i\text{sat}} \quad (\text{Hyperfiltration (reverse osmosis)})$$

At this point the concentrations in the membrane at the interfaces are described by Equations 2.34 and 2.38.

The connection between the three permeation processes can be represented in graphical form, as shown in Figure 2.19 [15]. This figure shows the transitions between the different operating regions as the feed and permeate pressures change. Three regions are shown in the figure: the gas separation region where the feed and permeate are both gases; the pervaporation region where the feed is a liquid and the permeate a gas; and the hyperfiltration (reverse osmosis) region where the feed and permeate are both liquids. The permeate flux through the membrane is plotted as a function of the normalized driving force, measured by the ratio of the feed pressure to saturation vapor pressure ($p_{i_0}/p_{i\text{sat}}$). A linear scale is used for feed pressure below the saturation vapor pressure, corresponding to the linear dependence of gas flux on feed pressure shown in Equation 2.65. Above the saturation vapor pressure an exponential scale is used, because the hyperfiltration equation (Equation 2.40) shows the membrane flux to be an exponential function of feed

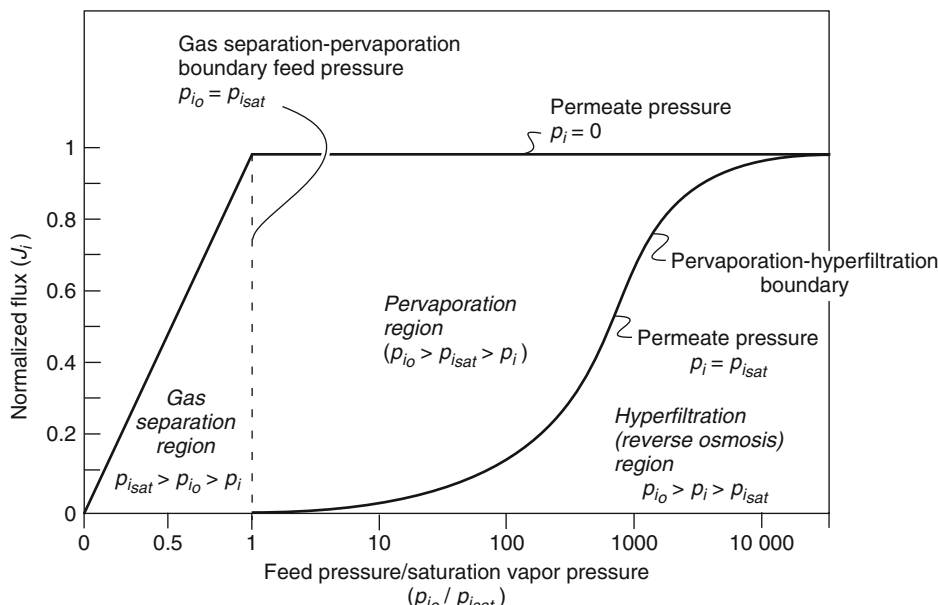


Figure 2.19 Permeation through a membrane, expressed as normalized flux, as a function of normalized feed pressure ($p_{i_0}/p_{i\text{sat}}$). The figure shows the smooth transition from gas separation, to pervaporation, to hyperfiltration. The curves shown are calculated using Equations 2.40, 2.65 and 2.86) in the gas separation, hyperfiltration, and pervaporation regions, respectively [15]

pressure. The flux axis of Figure 2.19 has also been normalized by setting $J_{i_{\max}}$ to 1 according to the equation:

$$J_{i_{\max}} = \frac{P_i^G p_{i_{\text{sat}}}}{\ell} = \frac{P_i^L c_{i_o}}{\ell} = 1 \quad (2.93)$$

Two lines separate the regions of the figure. A vertical line labeled the gas separation-pervaporation boundary feed pressure is set at the point where the feed pressure (p_{i_o}) equals the saturation vapor pressure ($p_{i_{\text{sat}}}$). This line represents the point at which the feed changes from a gas to a liquid. A second line labeled the pervaporation-hyperfiltration boundary is set at the point at which the permeate pressure $p_{i_\ell} = p_{i_{\text{sat}}}$. This line represents the point where the permeate changes from a gas to a liquid.

A third line shows the maximum achievable flux through the membrane. This corresponds to the point at which the permeate pressure p_{i_ℓ} is set to zero. This line represents gas separation and pervaporation with a hard vacuum on the permeate side. In these cases, at low feed pressures, the membrane is in the gas separation region and as the normalized feed pressure ($p_{i_o}/p_{i_{\text{sat}}}$) increases, the gas flux also increases. The gas flux reaches its maximum value (arbitrarily set to 1) when the feed pressure reaches the saturation vapor pressure ($p_{i_o}/p_{i_{\text{sat}}} = 1$). The gas flux at this point is $P_i^G p_{i_{\text{sat}}}/\ell$. When the feed pressure is increased further, the feed pressure exceeds the saturation vapor pressure and the feed gas liquefies. The process then enters the pervaporation region. At this point, further increases in feed pressure do not increase the flux. This is consistent with the pervaporation flux (Equation 2.86), in which the feed pressure p_{i_o} is set at the saturation vapor pressure $p_{i_{\text{sat}}}$, and the permeate pressure p_{i_ℓ} is set to zero. That is,

$$J_i = \frac{P_i^G}{\ell} (p_{i_o} - p_{i_\ell}) = \frac{P_i^G}{\ell} (p_{i_{\text{sat}}} - 0) = \frac{P_i^G \cdot p_{i_{\text{sat}}}}{\ell} \quad (2.94)$$

The pervaporation-hyperfiltration boundary line in Figure 2.19 represents the membrane flux at a permeate pressure just above the saturation vapor pressure. Under these conditions, liquid forms on both sides of the membrane and Equation 2.40 for hyperfiltration (reverse osmosis), repeated below as Equation 2.95, can be used to calculate the membrane flux.

$$J_i = \frac{P_i^L}{\ell} \left\{ c_{i_o} - c_{i_\ell} \exp \left[\frac{-v_i (p_o - p_\ell)}{RT} \right] \right\} \quad (2.95)$$

Initially, the flux increases linearly with increasing feed pressure, but then asymptotically approaches a maximum value $J_{i_{\max}}$ of $P_i^L c_{i_o}/\ell$ at very high feed pressures. This is consistent with Equation 2.95, because as $(p_o - p_\ell) \rightarrow \infty$, then

$$J_i \rightarrow \frac{P_i^L}{\ell} \cdot c_{i_o} \quad (2.96)$$

and following Equation 2.93, the maximum value of J_i is arbitrarily normalized to 1.

The ability of the solution-diffusion model to demonstrate the connection between the processes of gas separation, pervaporation, and hyperfiltration is one of its great

strengths. The performance of a membrane at any feed and permeate pressure can be represented as a point within this figure.

2.3 Structure-Permeability Relationships in Solution-Diffusion Membranes

In the preceding section, the effects of concentration and pressure gradient driving forces on permeation through membranes were described in terms of the solution-diffusion model and Fick's law. The resulting equations all contain a permeability term, P , which must be determined experimentally. This section describes how the nature of the membrane material affects permeant diffusion and sorption coefficients, which in turn determine membrane permeability. By analyzing the factors that determine membrane permeability, useful correlations and rules of thumb can be derived to guide the selection of membrane materials with the optimum flux and selectivity properties for a given separation. Most of the experimental data in this area have been obtained with gas-permeable membranes. However, the same general principles apply to all polymeric solution-diffusion membranes.

The problem of predicting membrane permeability can be divided into two parts because permeability is the product of the diffusion coefficient and the sorption coefficient:

$$P = D \cdot K \quad (2.97)$$

The sorption coefficient (K) in Equation 2.97 is the term linking the concentration of a component in the fluid phase with its concentration in the membrane polymer phase. Because sorption is an equilibrium term, conventional thermodynamics can be used to calculate the sorption coefficients of many components in polymers to within a factor of 2 or 3 of the experimental value. However, diffusion coefficients (D) are kinetic terms that reflect the effect of the surrounding environment on the molecular motion of permeating components. Calculation of diffusion coefficients in liquids and gases is possible, but calculation of diffusion coefficients in polymers is much more difficult. In the long term, the best hope for accurate predictions of diffusion in polymers are the molecular dynamics calculations described in an earlier section. However, this technique is still under development and is currently limited to calculations of the diffusion of small gas molecules in amorphous polymers; the agreement between theory and experiment is modest. In the meantime, simple correlations based on polymer-free volume must be used.

As a general rule, membrane material changes affect the diffusion coefficient of a permeant much more than the sorption coefficient. For example, Figure 2.20 shows some typical gas permeation data taken from a paper of Tanaka *et al.* [29]. The diffusion and sorption coefficients of four gases in a family of 18 related polyimides are plotted against each other. Both sorption and diffusion coefficients are fairly well grouped for each gas. However, for any one gas, the difference in diffusion coefficient from the highest to lowest value is approximately 100-fold, whereas the spread in sorption coefficients is only two- to four-fold. Changes in polymer chemistry affect both the sorption and diffusion coefficients, but the effect on the diffusion coefficient is much more profound.

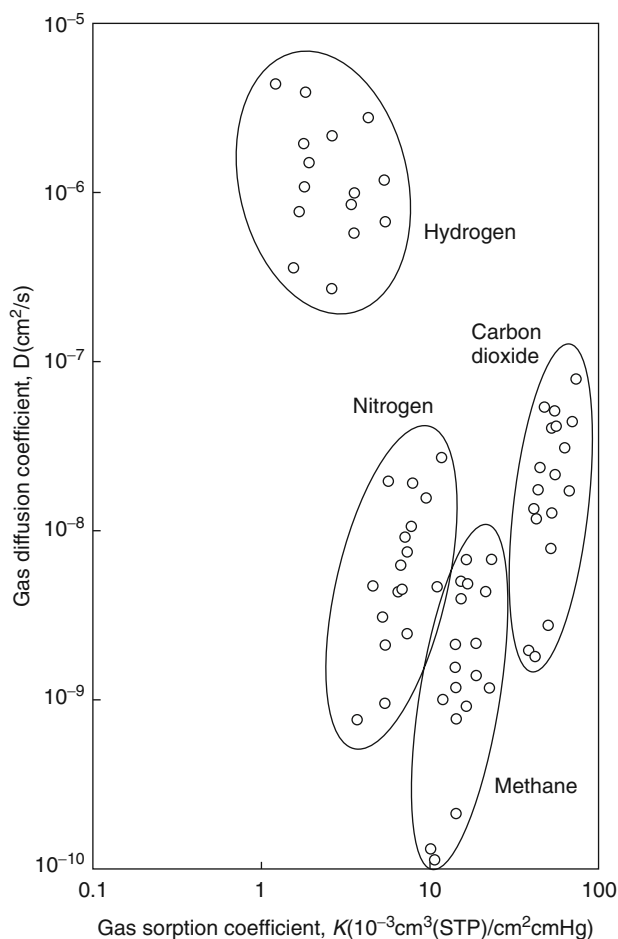


Figure 2.20 Diffusion and sorption coefficients plotted for gases in a family of 18 related polyimides. (Data of Tanaka *et al.* [29].)

This same effect was apparent in the discussion of the reverse osmosis data shown in Table 2.1. In that set of data, changing the membrane material chemistry changed the membrane sorption coefficients 10-fold, but the diffusion coefficients changed almost 1000-fold.

More detailed examination of the data shown in Figure 2.20 shows that the relative position of each polymer within the group of 18 is approximately the same for all gases. That is, the polymer with the highest diffusion coefficient for methane also has the highest diffusion coefficient for nitrogen, carbon dioxide, and hydrogen. The trend for the solubility coefficients is similar. As a general rule, changes in polymer chemistry and structure that change the diffusion coefficient or sorption coefficient of one gas change the properties of other gases in the same way. This is why membrane permeabilities can be varied by several orders of magnitude by changing the membrane material, whereas

Table 2.2 Diffusion and sorption selectivities for carbon dioxide/methane for a variety of polymers [29–31]

Polymer	P_{CO_2} (Barrer)	D_{CO_2} ($10^{-8} \text{ cm}^2/\text{s}$)	K_{CO_2} ($\text{cm}^3(\text{STP})/\text{cm}^3 \cdot \text{atm}$)	α_{CO_2/CH_4}	D_{CO_2}/D_{CH_4}	K_{CO_2}/K_{CH_4}
Rubbery polymers						
Silicone rubber	3800	2200	1.29	3.2	1.1	3.1
Polyisoprene	150	1350	3.83	5.0	1.5	3.4
Glassy polymers						
Polyethylene terephthalate	17.2	4.46	2.9	27.3	7.8	3.5
Polystyrene	12.4	8.50	1.1	15.8	5.5	2.9
Polycarbonate	6.8	3.20	1.6	19	4.7	4.0
Polysulfone	5.6	2.00	2.1	22	5.9	3.7
PMDA-ODA polyimide	2.7	0.56	3.6	46	11.9	3.8

changing membrane selectivities (proportional to the ratio of permeabilities) by more than a factor of 10 is difficult.

Some data shown in Table 2.2 showing data for the permeation of carbon dioxide and methane in several very different membrane materials illustrate the same effect. The permeabilities of carbon dioxide change by more than 1000-fold. Most of this difference is due to the membrane diffusion coefficients which vary by a factor of 5000, but the membrane sorption coefficients only vary by a factor of 3. Almost all of the difference in CO_2/CH_4 membrane selectivity is due to the mobility selectivity term, which varies from 1.1 for a soft, rubbery material (silicone rubber) to 11.9 for the most selective and lowest permeability polymer (PMDA-ODA polyimide). As with most membrane separation applications, there is a tradeoff between high permeability, low selectivity materials and low permeability, high selectivity materials.

In the following sections, factors that determine the magnitude of diffusion and solubility coefficients in polymers are discussed.

2.3.1 Diffusion Coefficients

The Fick's law diffusion coefficient of a permeating molecule is a measure of the frequency with which the molecule moves and the size of each movement. Therefore, the magnitude of the diffusion coefficient is governed by the restraining forces of the medium on the diffusing species. Isotopically labeled carbon in a diamond lattice has a very small diffusion coefficient. The carbon atoms of diamond move infrequently, and each movement is very small – only 1–2 Å. On the other hand, isotopically labeled carbon dioxide in a gas has an extremely large diffusion coefficient. The gas molecules are in constant motion and each jump is on the order of 1000 Å or more. Table 2.3 lists some representative values of diffusion coefficients in different media.

The main observation from Table 2.3 is the enormous range of values of diffusion coefficients – from 10^{-1} to $10^{-30} \text{ cm}^2/\text{s}$. Diffusion in gases is well understood and is

Table 2.3 Typical diffusion coefficients in various media (25°C)

Permeant/material	Diffusion coefficient, D (cm ² /s)
Oxygen in air (atmospheric pressure)	1×10^{-1}
Oxygen in water	3×10^{-5}
Oxygen in silicone rubber	3×10^{-5}
Oxygen in polysulfone	4×10^{-8}
Oxygen in polyester	5×10^{-9}
Sodium atoms in sodium chloride crystals	1×10^{-20}
Aluminum atoms in metallic copper	1×10^{-30}

treated in standard textbooks dealing with the kinetic theory of gases [32, 33]. Diffusion in metals and crystals is a topic of considerable interest to the semiconductor industry, but not in membrane permeation. This book focuses principally on diffusion in liquids and polymers in which the diffusion coefficients vary from about 10^{-5} to about 10^{-10} cm²/s.

2.3.1.1 Diffusion in Liquids

Liquids are simple, well-defined systems, and provide the starting point for modern theories of diffusion. An early and still fundamentally sound equation was derived by Einstein who applied simple macroscopic hydrodynamics to diffusion at the molecular level. He assumed the diffusing solute to be a sphere moving in a continuous fluid of solvent, in which case it can be shown that

$$D = \frac{kT}{6\pi a\eta} \quad (2.98)$$

where k is Boltzmann's constant, a is the radius of the solute, and η is the solution viscosity. This is known as the Stokes-Einstein equation. The equation is a good approximation for large solutes with radii greater than 5–10 Å. But, as the solute becomes smaller, the approximation of the solvent as a continuous fluid becomes less valid. In this case, there may be a slip of solvent at the solute molecule's surface. A second limiting case assumes complete slip at the surface of the solute sphere; in this case

$$D = \frac{kT}{4\pi a\eta} \quad (2.99)$$

Thus, the Stokes-Einstein equation is perhaps best expressed as

$$D = \frac{kT}{n\pi a\eta} \quad 4 \leq n \leq 6 \quad (2.100)$$

An important conclusion to be drawn from the Stokes-Einstein equation is that the diffusion coefficient of solutes in a liquid only changes slowly with molecular weight, because the diffusion coefficient is proportional to the reciprocal of the radius, which in turn is approximately proportional to the cube root of the molecular weight.

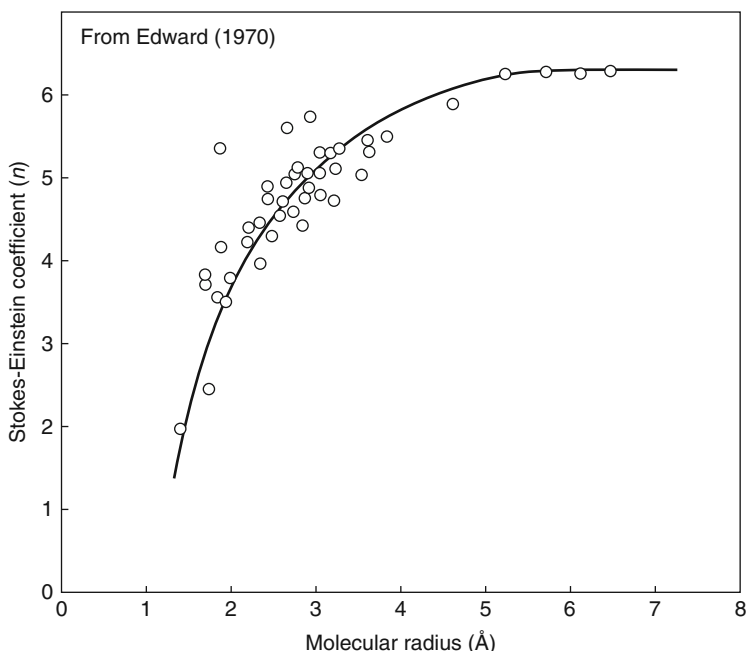


Figure 2.21 Value of the coefficient n in the Stokes-Einstein equation (Equation 2.98) required to achieve agreement between calculation and experimental solute diffusion coefficients in water. Reprinted with permission from [35]. Copyright (1970) American Chemical Society.

Application of the Stokes-Einstein equation requires a value for the solute radius. A simple approach is to assume the molecule is spherical, and calculate the solute radius from the molar volume of the chemical groups making up the molecule. Using values for the solute radius calculated this way, together with measured and known diffusion coefficients of solutes in water, Edward [34] constructed a graph of the coefficient n in the Stokes-Einstein Equation 2.100 as a function of solute radius as shown in Figure 2.21. With large solutes, n approaches 6; that is, Einstein's application of normal macroscopic fluid dynamics at the molecular level is a good approximation. However, when the solute radius falls below about 4 Å, water can no longer be regarded as a continuous fluid, and n falls below 6. Nonetheless, that an equation based on macroscopic hydrodynamic theory applies to molecules to the 4 Å level is an interesting result.

The Stokes-Einstein equation works well for diffusion of solutes in simple liquids, but fails in more complex fluids, such as a solution containing a high molecular weight polymer. Dissolving a polymer in a liquid increases the solvent viscosity, but the solute diffusion coefficient is not significantly affected. For example, as the concentration of poly(vinyl pyrrolidone) dissolved in water changes from 0 to 20 wt%, the viscosity of the solution increases by several orders of magnitude. However, the diffusion coefficient of sucrose in these solutions only changes by a factor of 4 [35]. The long polymer chains of dissolved poly(vinyl pyrrolidone) molecules link distant parts of the aqueous solution and change the macroscopic viscosity of the fluid substantially, but, in the fluid immediately

surrounding the diffusing sucrose molecule, the effect of polymer chain length is much less noticeable. This result illustrates the difference between the microscopic environment of the diffusing solute and the macroscopic environment measured by conventional viscometers. In simple liquids the macroscopic and microscopic environments are the same, but in liquids containing dissolved macromolecules, or in gels and polymer films, the microscopic environment and the macroscopic environment can be very different.

2.3.1.2 Diffusion in Polymers

The concept that the local environment around the permeating molecule determines the diffusion coefficient of the permeate is key to understanding diffusion in polymer membranes. Polymers can be divided into two broad categories – rubbers and glasses. In a rubbery polymer, portions of the polymer chains can freely move because of thermal motion, and segments of the polymer backbone can also rotate around their axis; this makes the polymer soft and elastic. Thermal motion of these segments also leads to high permeant diffusion coefficients. In a glassy polymer, steric hindrance along the polymer backbone inhibits rotation and free motion of segments of the polymer. The result is a rigid, tough polymer. Thermal motion in this type of material is limited, so permeant diffusion coefficients are also low. If the temperature of a glassy polymer is raised, the increase in thermal energy at some point becomes sufficient to overcome the steric hindrance restricting motion of the polymer backbone segments. At this temperature, called the *glass transition temperature* (T_g), the polymer changes from a glass to a rubber.

Figure 2.22 shows a plot of diffusion coefficient as a function of permeant molecular weight for permeants diffusing through a liquid (water), two soft rubbery polymers (natural rubber and silicone rubber), and a hard, stiff glassy polymer (polystyrene) [36]. For very small molecules, such as helium and hydrogen, the diffusion coefficients in all of the media are comparable, differing by no more than a factor of 2 or 3. These very small molecules only interact with one or two atoms in their immediate proximity. The local environment for these small solutes in the three polymers is not radically different to that in a liquid such as water. On the other hand, larger diffusing solutes with molecular weights of 200–300 and above have molecular diameters of 6–10 Å. Such solutes are in quite different local environments in the different media. In water, the Stokes-Einstein equation applies, and the resistance to movement of the solute is not much larger than that of a very small solute. In polymer membranes, however, several segments of the polymer chain are involved in each movement of the diffusing species. This type of cooperative movement is statistically unlikely; consequently, diffusion coefficients are much smaller than in liquid water. Moreover, the differences between the motion of polymer segments in the flexible rubbery membranes and in the stiff polystyrene membrane are large. The polymer chains in rubbers are considerably more flexible and rotate more easily than those in polystyrene. One manifestation of this difference in chain flexibility is the difference in elastic properties; another is the difference in diffusion coefficient.

An example of the change in diffusion coefficient as the matrix material changes is illustrated by Figure 2.23. In this example, the polymer matrix material is changed by plasticization of the polymer, ethyl cellulose, by the permeant, dichloroethane [37]. The resulting change in the diffusion coefficient is shown in the figure. The concentration of dichloroethane in the polymer matrix increases from very low levels (<1%

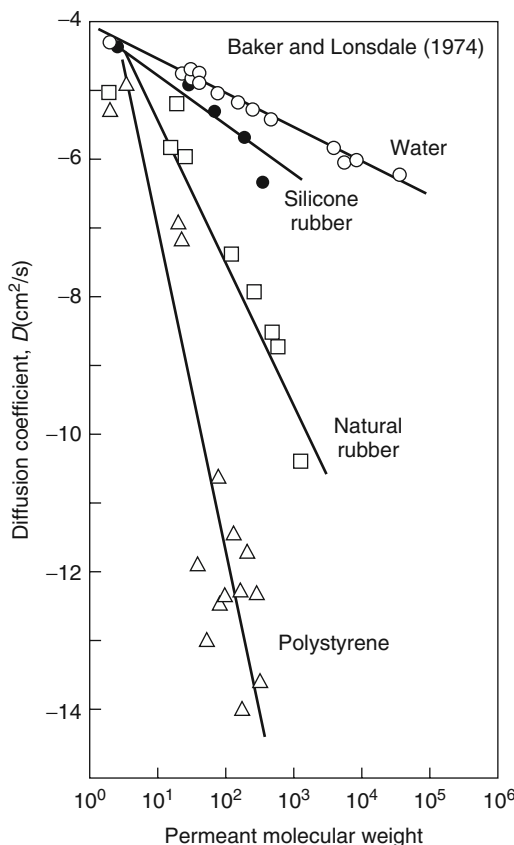


Figure 2.22 Permeant diffusion coefficient as a function of permeant molecular weight in water, natural rubber, silicone rubber, and polystyrene. Diffusion coefficients of solutes in polymers usually lie between the value in silicone rubber, an extremely permeable polymer, and the value in polystyrene, an extremely impermeable material [36]

dichloroethane) to very high levels (>90% dichloroethane). As the concentration of dichloroethane increases, the polymer changes from a glassy polymer to a rubbery polymer, to a solvent-swollen gel, and finally to a dilute polymer solution. Ethyl cellulose is a glassy polymer with a glass transition of about 45–50°C. At low concentrations of dichloroethane (below about 5 vol%) in the polymer, the ethyl cellulose matrix is glassy, and the dichloroethane diffusion coefficient is in the range of $1\text{--}5 \times 10^{-9}$ cm 2 /s. As the dichloroethane concentration increases to above 5 vol%, enough solvent has dissolved in the polymer to reduce the glass transition temperature to below the temperature of the experiment. The polymer chains then have sufficient freedom to rotate, and the polymer becomes rubbery. As the dichloroethane concentration increases further, the polymer chain mobility also increases as does the diffusion coefficient of dichloroethane. At 20% dichloroethane, the diffusion coefficient is 1×10^{-7} cm 2 /s, 100 times greater than the diffusion coefficient in the glassy polymer. Above 20 vol% dichloroethane, sufficient

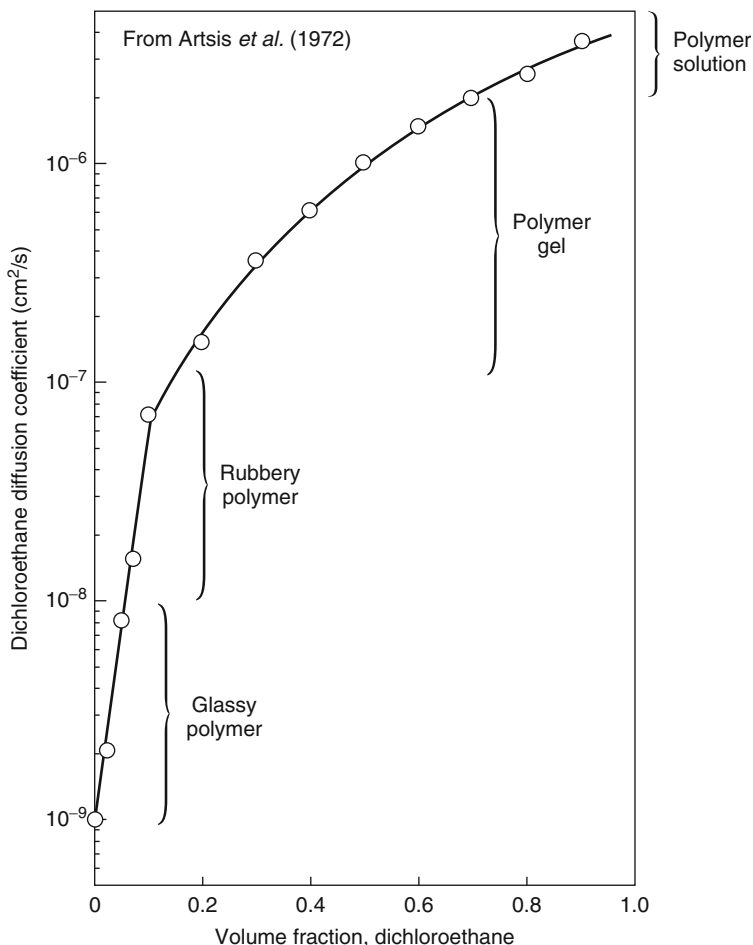


Figure 2.23 Changes in the diffusion coefficient of dichloroethane in ethyl cellulose as a function of the volume fraction of dichloroethane dissolved in the polymer matrix (Data of Artsis et al. [37].)

solvent is present to allow relatively large segments of the polymer chain to move. In this range, between 20 and 70 vol% dichloroethane, the matrix is best characterized as a solvent-swollen gel, and the diffusion coefficient of dichloroethane increases from 1×10^{-7} to 2×10^{-6} cm^2/s . Finally, at dichloroethane concentrations above 70 vol%, sufficient solvent is present for the matrix to be characterized as a polymer solution. In this final solvent concentration range, the increase in diffusion coefficient with further increases in dichloroethane concentration is relatively small.

Figures 2.22 and 2.23 show the significant difference between diffusion in liquids and in rubbery and glassy polymers. A great deal of work has been performed over the last two decades to achieve a quantitative link between the structure of polymers and their permeation properties. No such quantitative structure-property relationship is at hand or

even in sight. What has been achieved is a set of semi-empirical rules that allow the permeation properties of related families of polymers to be correlated based on small changes in their chemical structures. The correlating tool most generally used is the polymer's *fractional free volume* v_f (cm^3/cm^3). This free volume is the fraction of the space filled by the polymer that is not occupied by the atoms that make up the polymer chains. The fractional free volume is usually defined as

$$v_f = \frac{v - v_o}{v} \quad (2.101)$$

where v is the specific volume of the polymer (cm^3/g), that is, the reciprocal of the polymer density, and v_o is the volume occupied by the molecules themselves (cm^3/g). The free volume of a polymer is the sum of the many small spaces between the polymer chains in these amorphous, non-crystalline materials.

The free volume of a polymer can be determined by measuring the polymer's specific volume, then calculating the occupied volume (v_o) of the groups that form the polymer. Tables of the molar volume of different chemical groups have been prepared by Bondi [38] and van Krevelen [39]. By summing the molar volume of all the groups in the polymer repeat unit, the occupied molar volume of the polymer can be calculated. The occupied volume obtained in this way is about 1.3 times larger than the Van der Waals volume of the groups. The factor of 1.3 occurs because some unoccupied space is inevitably present even in crystals at 0 K. The fractional free volumes of a number of important membrane materials are given in Table 2.4.

The concept of polymer free volume is illustrated in Figure 2.24, which shows polymer specific volume (cm^3/g) as a function of temperature. At high temperatures the polymer is in the rubbery state. Even in the rubbery state, the polymer chains cannot pack perfectly, and some unoccupied space – free volume – exists between the polymer chains. This free volume is over and above the space normally present between molecules in a crystal lattice. Although this free volume is only a small percentage of the total volume, it is sufficient to allow motion of segments of the polymer backbone. In this sense a rubbery polymer, although solid at the macroscopic level, has some of the characteristics of a liquid. As the temperature of the polymer decreases, the free volume also

Table 2.4 Calculated fractional free volume for representative membrane materials at ambient temperatures (Bondi method)

Polymer	Polymer type	Glass transition temperature, T_g ($^\circ\text{C}$)	Fractional free volume (cm^3/cm^3)
Silicone rubber	Rubber	-129	0.16
Natural rubber	Rubber	-73	0.16
Polycarbonate	Glass	150	0.16
Poly(phenylene oxide)	Glass	167	0.20
Polysulfone	Glass	186	0.16
6FDA-ODA polyimide	Glass	300	0.16
Poly(4-methyl-2-pentyne) (PMP)	Glass	>250	0.28
Poly(1-trimethylsilyl-1-propyne) (PTMSP)	Glass	>250	0.34

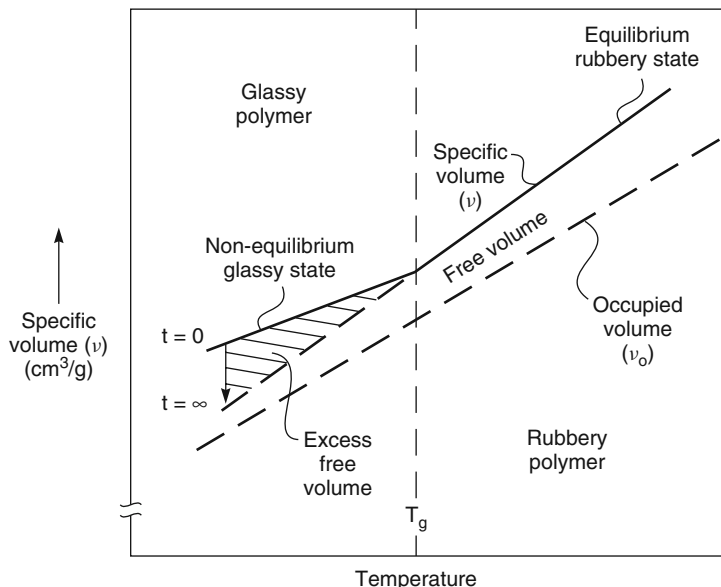


Figure 2.24 The change in specific volume as a function of temperature for a typical polymer

decreases. At the glass transition temperature (T_g), the free volume is reduced to a point at which the polymer chains can no longer move freely. This transition is quite sharp, usually over a temperature range of 3–5°C. Segmental motion is then reduced by several orders of magnitude. If the specific volume upon cooling the polymer to below the glass transition temperature remained on the equilibrium line (labeled $t = \infty$ in Figure 2.24), the diffusion coefficient of permeants in glassy polymers would be very low indeed. Normally, however, when the glass transition temperature is traversed, extra free volume elements between the polymer chains are frozen into the polymer matrix. As the polymer temperature is reduced further, its occupied volume will continue to decrease as the vibration energy of the groups forming the polymer decreases, but the free volume that is the difference between the occupied volume and the actual volume remains essentially constant. Therefore, a glassy polymer contains both the normal free volume elements caused by the incomplete packing of the groups making up the polymer chains and excess free volume elements frozen into the polymer matrix because motion of the polymer chains is very restricted. These free volume elements are only very slowly eliminated by movement of the glassy polymer chains. It is the existence of these tiny, frozen-in-place, excess free volume elements that contributes to the relatively high permeability of glassy polymers, and their ability to selectively permeate different-sized permeants at different rates.

The fractional free volume of most materials is quite small. For rubbers, the fractional free volume calculated by the Bondi method is generally about 10–15%. For glassy polymers, the fractional free volume is higher, generally in the range of 15–20% because of the excess free volume contribution. Recently, a number of polymers with extraordinarily rigid polymer backbones have been prepared, and their free volumes

are correspondingly unusually high – as much as 25–35% of the polymers' volume is unoccupied space [8–10]. Permeation through these polymers is described later in this chapter.

Diffusivity and hence permeability of a polymer can be linked to the fractional free volume by the empirical equation

$$D = A \cdot \exp\left(\frac{B}{v_f}\right) \quad (2.102)$$

where A and B are adjustable parameters. When applied within a single class of materials, the correlation between the free volume and gas diffusivity or permeability suggested by this equation is often good; an example is shown in Figure 2.25 [40]. When the correlation is broadened out to include more diverse types of polymer, there is much more scatter. The relationship between the free volume and the sorption and diffusion coefficients of gases in polymers, particularly glassy polymers, has been an area of a great deal of experimental and theoretical work, but a predictive model has yet to emerge. The subject has been reviewed recently [41–44].

A factor that complicates understanding the effect of free volume on permeation is that the excess free volume is not permanent and decreases slowly over time as the polymer moves from its initial ($t = 0$) non-equilibrium state to a final ($t = \infty$) equilibrium state. It appears that even in a glassy polymer, some motion of the polymer chains occurs. This

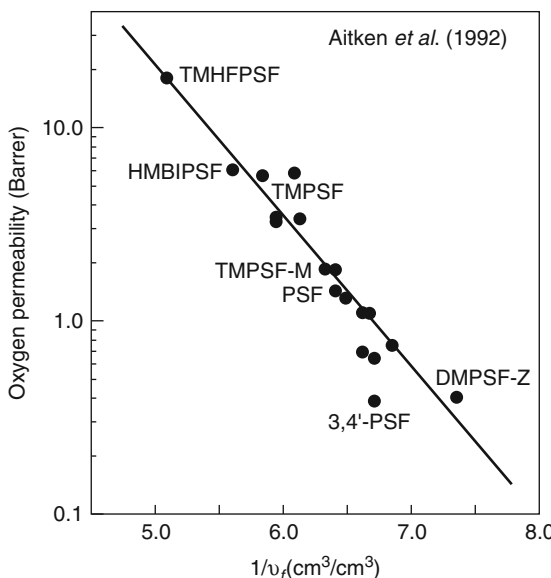


Figure 2.25 Correlation of the oxygen permeability coefficient for a family of related polysulfones with inverse fractional free volume (calculated using the Bondi method) [41]. Reprinted with permission from C.L. Aitken, W.J. Koros and D.R. Paul, Effect of Structural Symmetry on Gas Transport Properties of Polysulfones, *Macromolecules* **25**, 3424. Copyright 1992, American Chemical Society.

allows the polymer to slowly change to a lower excess free volume, higher density state. The loss of free volume is usually very slow in thick polymer films. This is because, to eliminate its space, a free volume element must move to the surface of the polymer like a bubble leaving a liquid. In a thick film, the volume element must move a considerable distance to escape and so densification of the polymer is very slow. However, in thin membranes a micron or so thick, the distance the free volume element must diffuse to escape is much less. In these thin membrane films, polymers can lose a large fraction of their excess free volume over a period of a few months to a few years. This loss of excess free volume has a significant effect on the permeation properties of these membranes.

Huang and Paul have measured the effects of loss of excess free volume on gas permeation with a number of polymers [45, 46]. Some of these data for polyphenylene oxide (PPO) are shown in Figure 2.26. The oxygen permeability of thick PPO films is 20 Barrers, and the film's oxygen/nitrogen selectivity is 4.4. The permeability of PPO films stored for long periods of time at 30°C steadily decreases and the rate of loss of permeability is inversely proportional to film thickness. The permeability of a 25 µm-thick film is reduced by only about 20% after one year of storage, but a 0.4 µm thick film loses almost two-thirds of its permeability in the same time. The oxygen/nitrogen selectivity of the thin membrane increases from 4.4 to about 5.1 as the permeability falls. Refractive index measurements show that these changes in permeation are accompanied by an increase in polymer density.

Producers of gas separation membranes made from glassy polymers usually see a decrease in the permeation rate over time. In the past, this decrease was ascribed to membrane substructure compaction or fouling, but some of the decrease is probably due to slow loss of free volume. To make a more stable and reproducible product, some producers anneal their membranes by storing them in an oven for a period prior to use. This treatment eliminates a portion of the initial rapid decline in permeation shown in Figure 2.26.

2.3.2 Sorption Coefficients in Polymers

The second key factor determining permeability in polymers is the sorption coefficient. The data in Figure 2.20 show that sorption coefficients for a particular gas are relatively constant within a single family of related materials. In fact, sorption coefficients of gases in polymers are relatively constant for a wide range of chemically different polymers. Figure 2.27 plots sorption and diffusion coefficients of methane in Tanaka's fluorinated polyimides [29], carboxylated polyvinyl trimethylsiloxane [47], and substituted polyacetylenes [48] (all amorphous glassy polymers) and a variety of substituted siloxanes [49] (all rubbers). The diffusion coefficients of methane in the different polymers vary by more than 100 000, showing the extraordinary sensitivity of the permeant diffusion coefficients to changes in the packing of the polymer chains and to their flexibility. In contrast, sorption coefficients vary by only a factor of 10 around a mean value of about $15 \times 10^{-3} \text{ cm}^3(\text{STP})/\text{cm}^3\cdot\text{cmHg}$. The ratio of sorption selectivities, that is, the sorption selectivity term for a gas pair (K_i/K_j) is even more constant, even for very different polymers, as the data in Table 2.2 show.

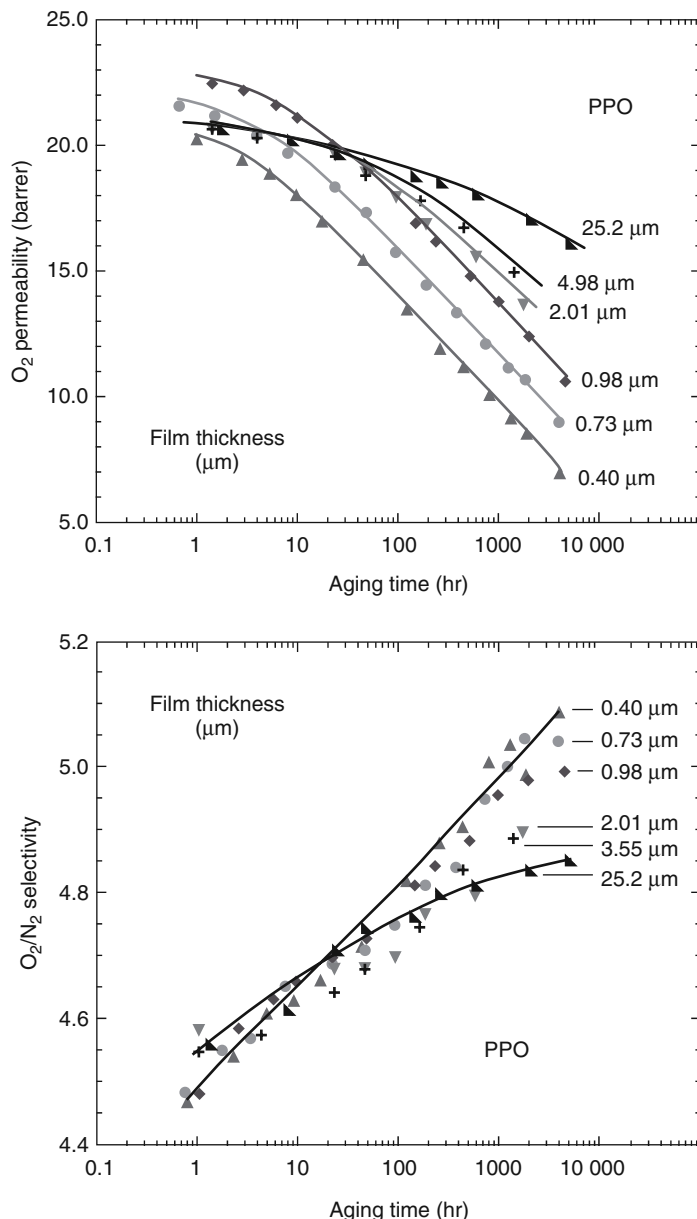


Figure 2.26 Effect of long-term storage on the permeability of thin polyphenylene oxide (PPO) films. Reprinted with permission from [46]. Copyright (2004) Elsevier.

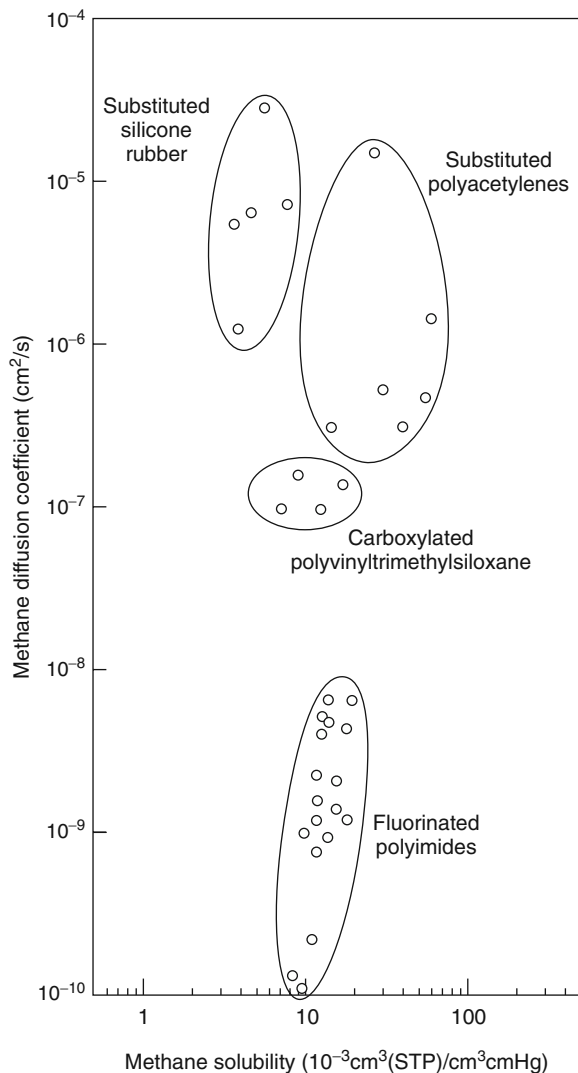


Figure 2.27 Diffusion and sorption coefficients of methane in different families of polymer materials. Diffusion coefficients change over a wide range but sorption coefficients are relatively constant (Data from Refs. [29, 41, 42, 47].)

The sorption coefficients of gases in polymers remain relatively constant because to a fair approximation, sorption in polymers behaves as though the polymers were ideal fluids. Gas sorption in a polymer is expressed from Equation 2.62 as

$$c_{i(m)} = K_i^G p_i \quad (2.103)$$

By substituting for the sorption coefficient K_i^G from Equation 2.61, Equation 2.103 can be written as

$$c_{i(m)} = m_i \rho_m \frac{\gamma_i^G p_i}{\gamma_{i(m)} p_{i_{sat}}} \quad (2.104)$$

Converting from concentration to mole fraction using

$$c_{i(m)} = m_i \rho_m n_{i(m)} \quad (2.105)$$

it follows that Equation 2.104 can be written as

$$\frac{c_{i(m)}}{\rho_m m_i} = n_{i(m)} = \frac{\gamma_i^G p_i}{\gamma_{i(m)} p_{i_{sat}}} \quad (2.106)$$

For an ideal gas dissolving in an ideal liquid, γ_i^G and $\gamma_{i(m)}$ are both unity, so Equation 2.106 can be written as

$$n_{i(m)} = \frac{p_i}{p_{i_{sat}}} \quad (2.107)$$

where $n_{i(m)}$ is the mole fraction of the gas sorbed in the liquid, p_i is the partial pressure of the gas, and $p_{i_{sat}}$ is the saturation vapor pressure at the pressure and temperature of the liquid. To apply Equation 2.107, the gas saturation vapor pressure must be determined. This can be done by extrapolating from available vapor pressure data to the ambient range using the Clausius-Clapeyron equation. For some gases, the vapor pressure obtained does not correspond to a stable gas-liquid equilibrium because the gas is supercritical at ambient temperatures. However, the calculated value is adequate to calculate the sorption coefficient using Equation 2.107 [50]. At 25°C, the saturation vapor pressure of methane extrapolated in this way is 289 atm. From Equation 2.107, the mole fraction of methane dissolved in an ideal liquid is then 1/289 or 0.0035. The ideal solubility and measured solubilities of methane in a number of common liquids are given in Table 2.5. Although there is some spread in the data, particularly for polar solvents such as water or methanol,

Table 2.5 Mole fraction of methane in various solvents at 25°C and 1 atm

Liquid	Methane solubility (mole fraction)
Ethyl ether	0.0045
Cyclohexane	0.0028
Carbon tetrachloride	0.0029
Acetone	0.0022
Benzene	0.0021
Methanol	0.0007
Water	0.00002

The solubility of methane in an ideal liquid under these conditions is 0.0035 [50].

the overall agreement is remarkably good. A more detailed discussion of the solubility of gases in polymers is given by Petropoulos [43] and Doghieri *et al.* [51].

To apply the procedure outlined above to a polymer, it is necessary to use the Flory-Huggins theory of polymer solution, which takes into account the entropy of mixing of solutes in polymers caused by the large difference in molecular size between the two components. The Flory-Huggins expression for the free energy of mixing of a gas in polymer solution can be written [52]

$$\Delta G = RT \ln \frac{p_i}{p_{i_{sat}}} = RT \left[\ln V_i + \left(1 - \frac{v_i}{v_j}\right) (1 - V_i) \right] \quad (2.108)$$

where v_i and v_j are the molar volumes of the gas (i) and the polymer (j) respectively, and V_i is the volume fraction of the polymer (j) occupied by the sorbed gas (i). When v_i/v_j , that is, the gas and polymer molecules are approximately the same size, Equation 2.108 reduces to Equation 2.107, the ideal liquid case. When the molar volume of a gas (v_i) is much smaller than the molar volume of the polymer (v_j), then $v_i/v_j \rightarrow 0$ and Equation 2.108 becomes

$$\ln \frac{p_i}{p_{i_{sat}}} = \ln V_i + (1 - V_i) \quad (2.109)$$

Equation 2.109 can be rearranged to

$$V_i = \frac{p_i/p_{i_{sat}}}{\exp(1 - V_i)} \quad (2.110)$$

and since V_i is small, $\exp(1 - V_i)$ is approximately $\exp(1) \approx 2.72$. Equation 2.109 then becomes

$$V_i = \frac{p_i/p_{i_{sat}}}{2.72} \quad (2.111)$$

Comparing Equations 2.107 and 2.111, we see that the volume fraction of gas sorbed by an ideal polymer is 1/2.72 of the mole fraction of the same gas sorbed in an ideal liquid.⁴

The results of such a calculation are shown in Table 2.6. In Figure 2.28, the calculated sorption coefficients in an ideal polymer from Table 2.6 are plotted against the average sorption coefficients of the same gases in Tanaka's polyimides [29]. The calculated values are within a factor of 2 of the experimental values, which is extremely good agreement considering the simplicity of Equation 2.111.

As shown above, thermodynamics can qualitatively predict the sorption of simple gases in polymers to within a factor of 2 or 3. Moreover, Equation 2.111 predicts that all polymers should have about the same sorption for the same gas and that sorption of different gases is inversely proportional to their saturation vapor pressures.

Another way of showing the same effect is to plot gas sorption against some convenient measure of saturation vapor pressure, such as the gas boiling point or critical temperature.

⁴ V_i is the volume fraction of the gas sorbed in the polymer. To calculate the amount of gas sorbed in cm³(STP)/cm³, the molar density of the sorbed gas must be known. We assume this density is 1/MW (mol/cm³).

Table 2.6 Solubility of gases in an ideal liquid and an ideal polymer (35°C)

Gas	Calculated saturation vapor pressure, $p_{i\text{sat}}$ (atm)	Ideal solubility in a liquid at 1 atm (mole fraction) (Equation 2.107)	Ideal solubility in a polymer ($10^{-3} \text{ cm}^3(\text{STP})/\text{cm}^3 \cdot \text{cmHg}$) (Equation 2.111)
N ₂	1400	0.0007	2.8
O ₂	700	0.0014	4.8
CH ₄	366	0.0027	18.5
CO ₂	79.5	0.0126	31.0

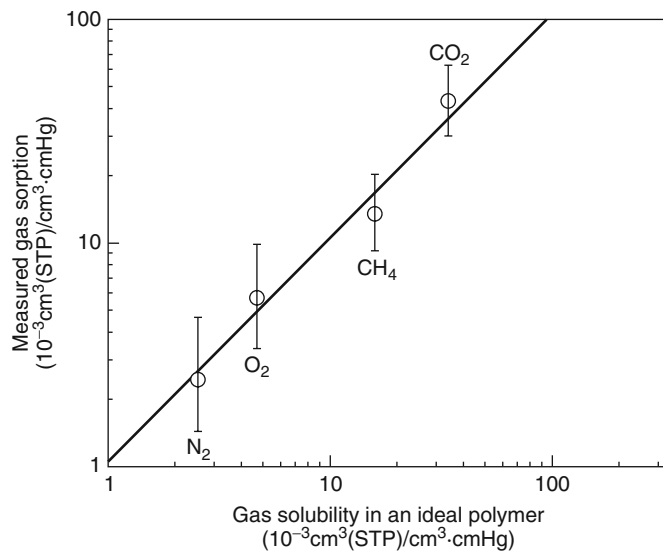


Figure 2.28 Average sorption coefficients of simple gases in a family of 18 related polyimides plotted against the expected sorption in an ideal polymer calculated using Equation 2.111 (Data from Tanaka *et al.* [29].)

Figure 2.29 shows a plot of this type for a typical glassy polymer (polysulfone), a typical rubber (silicone rubber), and the values for the ideal solubility of a gas in a polymer calculated using Equation 2.111 [53]. The figure shows that the difference in gas sorption values of polymers is relatively small and the values are grouped around the calculated value.

Although all of these predictions are qualitatively correct, the relatively small differences between the behavior of an ideal polymer and an actual polymer are important in selecting the optimum material for a particular separation. The usual starting point for this fine tuning is the dual-sorption model originally proposed by Barrer *et al.* [54]. This model has since been extended by Michaels *et al.* [55], Paul and coworkers [56], Koros *et al.* [57] and many others.

According to the dual-sorption model, gas sorption in a polymer (c_m) occurs in two types of sites. The first type is filled by gas molecules dissolved in the equilibrium free volume portion of a material (concentration c_H). In rubbery polymers, this is the only

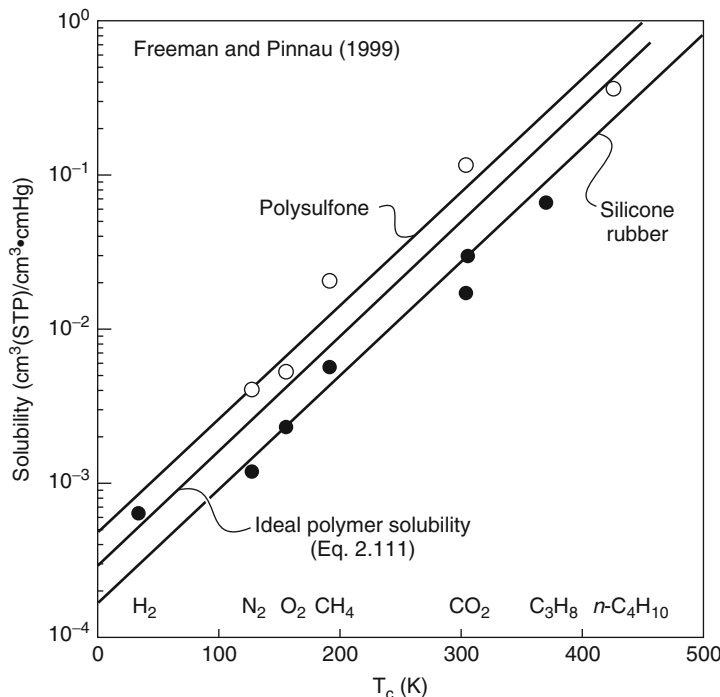


Figure 2.29 Solubilities as a function of critical temperature (T_c) for a typical glassy polymer (polysulfone) and a typical rubbery polymer (silicone rubber) compared with values for the ideal solubility calculated from Equation 2.111 [53]

population of dissolved gas molecules, but in glassy polymers a second type of site exists. This population of dissolved molecules (concentration c_D) is dissolved in the excess free volume of the glassy polymer. The total sorption in a glassy polymer is then

$$c_m = c_D + c_H \quad (2.112)$$

The number of molecules (c_D) dissolved in the equilibrium free volume portion of the polymer will behave as in normal sorption in a liquid and can be related to the pressure in the surrounding gas by a linear expression equivalent to Equation 2.103

$$c_D = K_D p \quad (2.113)$$

This fraction of the total sorption is equivalent to the value calculated in Equation 2.111. The other fraction (c_H) is assumed to be sorbed into the excess free volume elements, which are limited, so sorption will cease when all the sites are filled. Sorption in these sites is best approximated by a Langmuir-type absorption isotherm

$$c_H = \frac{c'_H bp}{1 + bp} \quad (2.114)$$

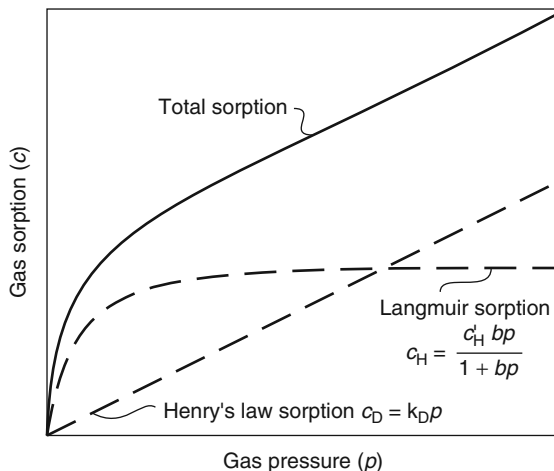


Figure 2.30 An illustration of the two components that contribute to gas sorption in a glassy polymer according to the dual-sorption model. Henry's law sorption occurs in the equilibrium free volume portion of the polymer. Langmuir sorption occurs in the excess free volume between polymer chains that exists in glassy polymers

At high pressures $c_H \rightarrow c'_H$, where c'_H is the saturation sorption concentration at which all excess free volume sites are filled.

From Equations 2.113 and 2.114, it follows that the total sorption can be written as

$$c_m = K_D p + \frac{c'_H bp}{1 + bp} \quad (2.115)$$

The form of the sorption isotherm predicted from the dual sorption model is shown in Figure 2.30. Because the expressions for sorption contain three adjustable parameters, good agreement between theory and experiment is usually obtained.

Sometimes, much is made of the particular values of the constants b and K . However, these constants should be treated with caution because they depend totally on the starting point of the curve-fitting exercise. That is, starting with an arbitrary value of c'_H , the other constants b and K can usually be adjusted to obtain good agreement of Equation 2.115 with experiment. If the starting value for c'_H is changed, then equally good agreement between theory and experiment can still be obtained, but with different values of b and K [58].

Permeation of gases in glassy polymers can also be described in terms of the dual sorption model. One diffusion coefficient (D_D) is used for the portion of the gas dissolved in the polymer according to the Henry's law expression and a second, somewhat larger, diffusion coefficient (D_H) for the portion of the gas contained in the excess free volume. The Fick's law expression for flux through the membrane has the form

$$J = -D_D \frac{dc_D}{dx} - D_H \frac{dc_H}{dx} \quad (2.116)$$

2.4 Pore-Flow Membranes

The creation of a unified theory able to rationalize transport in the dense membranes used in reverse osmosis, pervaporation, and gas separation occurred over a 20-year period from about 1960 to 1980. Development of this theory was one of the successes of membrane science. The theory did not form overnight as the result of one single breakthrough, but rather as the result of a series of incremental steps. The paper of Lonsdale *et al.* [22], applying the solution-diffusion model to reverse osmosis for the first time was very important.⁵ Also important was the series of papers by Paul and coworkers showing the connection between hydraulic permeation (reverse osmosis) and pervaporation [2–4, 20], and providing the experimental support for the solution-diffusion model as applied to these processes. Unfortunately, no equivalent unified theory to describe transport in microporous membranes has been developed. Figure 2.31 illustrates part of the problem, namely the extremely heterogeneous nature of microporous membranes. All of the microporous membranes shown in this figure perform approximately the same separation, but their porous structure and the mechanism of the separation differ significantly. The nucleation track membrane (Figure 2.31a) and the asymmetric Loeb-Sourirajan membrane (Figure 2.31d) both separate particles by molecular sieving. The cellulose acetate/cellulose nitrate membrane (Figure 2.31c) is a depth filter which captures particles within the interior of the membrane by adsorption. The expanded film membrane (Figure 2.31b) captures particles by both methods. The materials from which these membranes are made also differ, ranging from polyethylene and polysulfone, both hydrophobic, low-surface-energy materials, to cellulose acetate, a hydrophilic material that often carries charged surface groups.

The parameters available to characterize the complexity of microporous membranes are also imperfect. Some widely used parameters are illustrated in Figure 2.32. The membrane porosity (ε) is the fraction of the total membrane volume that is porous. Typical microporous membranes have average porosities in the range 0.3–0.7. This number can be obtained easily by weighing the membrane before and after filling the pores with an inert liquid. The average porosity obtained this way must be treated with caution, however, because the porosity of a membrane can vary from place to place. For example, anisotropic membranes, such as the Loeb-Sourirajan phase separation membrane shown in Figure 2.31d, often have an average porosity of 0.7–0.8, but the porosity of the skin layer that performs the actual separation may be as low as 0.05.

The membrane tortuosity (τ) reflects the length of the average pore compared to the membrane thickness. Simple cylindrical pores at right angles to the membrane surface have a tortuosity of 1, that is, the average length of the pore is the membrane thickness. Usually pores take a more meandering path through the membrane, so typical tortuosities are in the range 1.5–2.5.

The most important property characterizing a microporous membrane is the pore diameter (illustrated in the bottom half of Figure 2.32). Some of the methods of measuring pore diameters are described in Chapter 7. Although microporous membranes are usually characterized by a single pore diameter value, most membranes actually contain a range

⁵ This very readable paper was initially submitted by its three industrial authors for publication in the *Journal of Physical Chemistry* and was rejected as insufficiently fundamental. More than 40 years after it was finally published in the *Journal of Applied Polymer Science*, it remains a one of the most frequently cited papers on membrane transport theory.

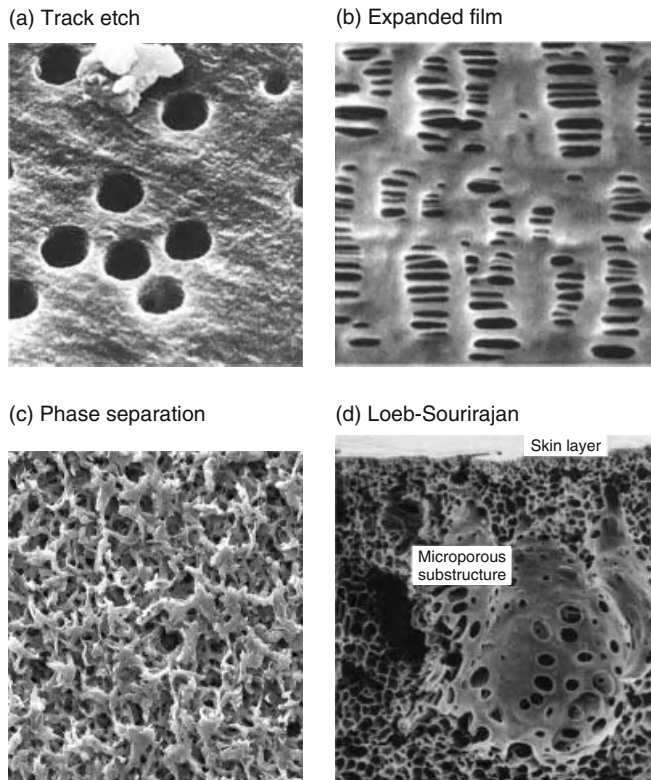


Figure 2.31 Scanning electron micrographs at approximately the same magnification of four microporous membranes having approximately the same particle retention. (a) Nucleopore (polycarbonate) nucleation track membrane. (b) Celgard® (polyethylene) expanded film membrane. (c) Millipore cellulose acetate/cellulose nitrate phase separation membrane made by water vapor imbibition. (d) Anisotropic symmetric polysulfone membrane made by the Loeb-Sourirajan phase separation process. Reprinted with permission of Millipore Corporation, Billerica, MA

of pore sizes. In ultrafiltration, the pore diameter quoted is usually an average value, but to confuse the issue, the pore diameter in microfiltration is usually defined in terms of the largest particle able to penetrate the membrane. This nominal pore diameter can be 5–10 times smaller than the apparent pore diameter based on direct microscopic examination of the membrane.

2.4.1 Permeation in Ultrafiltration and Microfiltration Membranes

Microporous ultrafiltration and microfiltration membranes used to filter particulates from liquids fall into the two general categories illustrated in Figure 2.33. The first category (a) is the surface or screen filter; such membranes contain surface pores smaller than the particles to be removed. These membranes are usually anisotropic, with a relatively finely microporous surface layer on a more open microporous support. Particles in the

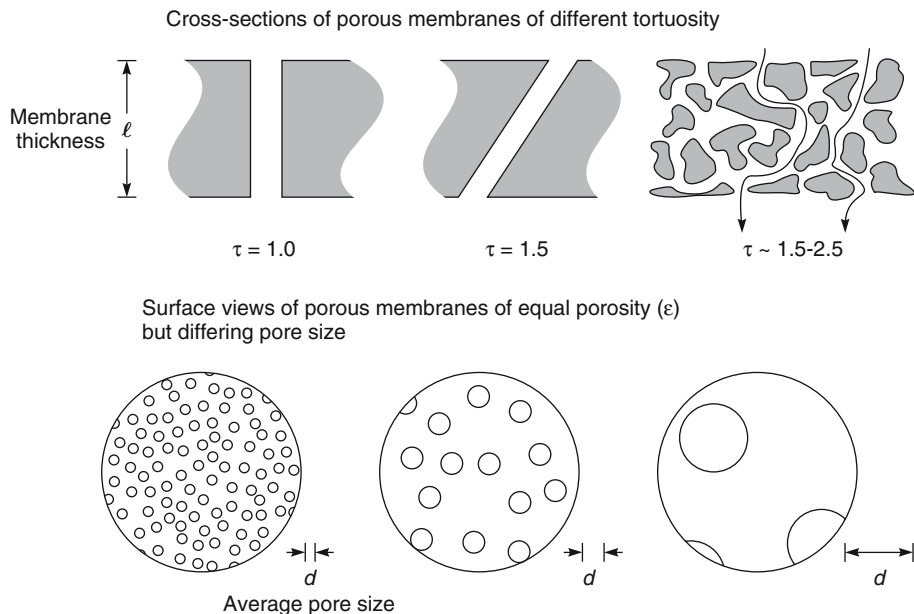


Figure 2.32 Microporous membranes are characterized by their tortuosity (τ), their porosity (ε), and their average pore diameter (d)

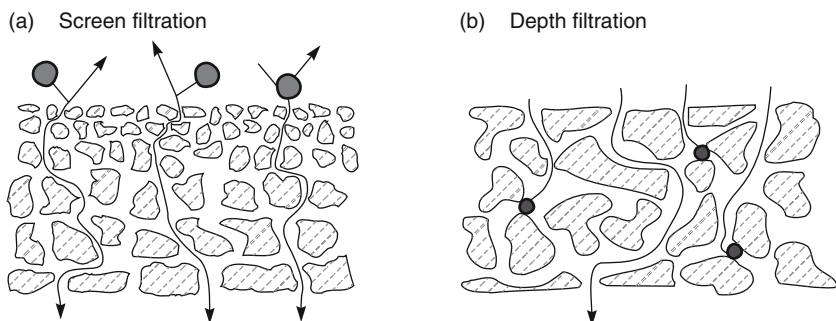


Figure 2.33 Separation of particulates can take place (a) at the membrane surface according to a screen filtration mechanism or (b) in the interior of the membrane by a capture mechanism as in depth filtration

permeating fluid are captured and accumulate on the surface of the membrane. Particles small enough to pass through the surface pores are not normally captured in the interior of the membrane. Most ultrafiltration membranes are screen filters.

The second category of microporous membranes is the depth filter (b), which captures the particles to be removed in the interior of the membrane. The average pore diameter of a depth filter is often 10 times the diameter of the smallest particle able to permeate the membrane. Some particles are captured at small constrictions within the membrane, others by adsorption as they permeate the membrane by a tortuous path.

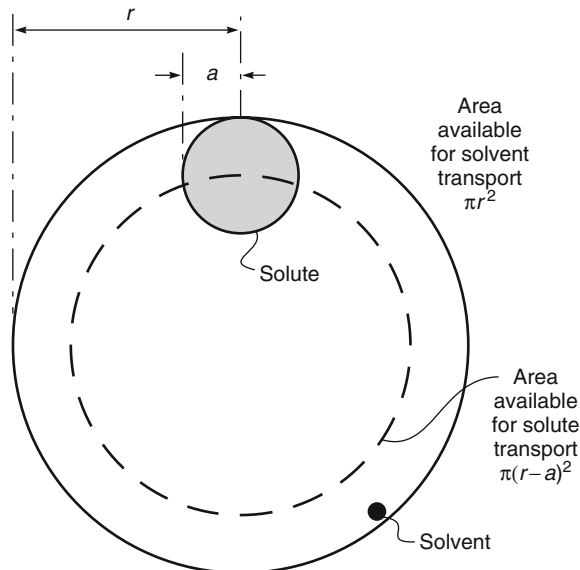


Figure 2.34 Illustration of the Ferry mechanical exclusion model of solute transport in small pores

Depth filters are usually isotropic, with a similar pore structure throughout the membrane. Most microfiltration membranes are depth filters.

2.4.1.1 Screen Filters

The mechanism of particle filtration by screen filters has been the subject of many studies because it is relatively easily described mathematically; Bungay has published a review of this work [59]. Ferry [60] was the first to model membrane retention by a screen filter; in his model, pores were assumed to be equal circular capillaries with a large radius, r , compared to the solvent molecule radius. Therefore, the total area of the pore is available for transport of solvent. A solute molecule whose radius, a , is an appreciable fraction of the pore radius cannot approach nearer than one molecular radius of the pore overall. The model is illustrated in Figure 2.34.

The area, A , of the pore available for solute transport is given by the equation

$$\frac{A}{A_o} = \frac{(r - a)^2}{r^2} \quad (2.117)$$

where A_o is the area of the pore available for solvent molecules. Later, Renkin [61] showed that Equation 2.117 has to be modified to account for the parabolic velocity profile of the fluid as it passes through the pore. The effective fractional pore area available for solutes in this case is

$$\left(\frac{A}{A_o} \right)' = 2 \left(1 - \frac{a}{r} \right)^2 - \left(1 - \frac{a}{r} \right)^4 \quad (2.118)$$

where $(A/A_o)'$ is equal to the ratio of the solute concentration in the filtrate (c_ℓ) to the concentration in the feed (c_o), that is,

$$\left(\frac{A}{A_o}\right)' = \left(\frac{c_\ell}{c_o}\right) \quad (2.119)$$

It follows from Equation 2.119 and the definition of solution rejection (Equation 2.51) that the rejection of an ultrafiltration membrane is

$$R = \left[1 - 2 \left(1 - \frac{a}{r} \right)^2 + \left(1 - \frac{a}{r} \right)^4 \right] \times 100\% \quad (2.120)$$

The Ferry-Renkin equation can be used to estimate the pore size of ultrafiltration membranes from the membrane's rejection of a solute of known radius. The rejections of globular proteins by four typical ultrafiltration membranes plotted against the cube root of the protein molecular weight (an approximate measure of the molecular radius) are shown in Figure 2.35a. The theoretical curves calculated from Equation 2.120 are shown directly in Figure 2.35b [62]. The abscissae of both figures have been made comparable because the radius of gyration of albumin is approximately 30 Å. A pore size that appears to be reasonable can then be obtained by comparing the two graphs. This procedure for obtaining an approximate pore size from membrane retention measurements shown in Figure 2.35 has been widely used. Globular proteins are usually the basis for this work because their molecular weights and molecular diameters can be calculated precisely. A list of some commonly used marker molecules is given in Table 2.7.

2.4.1.2 Depth Filters

The mechanism of particle capture by depth filtration is more complex than for screen filtration. Simple capture of particles by sieving at pore constrictions in the interior of the membrane occurs, but adsorption of particles on the interior surface of the membrane is usually at least as important. Figure 2.36 shows four mechanisms that contribute to particle capture in depth membrane filters. The most obvious mechanism, simple sieving and capture of particles at constrictions in the membrane, is often a minor contributor to the total separation. The three other mechanisms, which capture particles by adsorption, are inertial capture, Brownian diffusion, and electrostatic adsorption [63, 64]. In all cases, particles smaller than the diameter of the pore are captured by adsorption onto the internal surface of the membrane.

In inertial capture, relatively large particles in the flowing liquid cannot follow the fluid flow lines through the membrane's tortuous pores. As a result, such particles are captured as they impact the pore wall. This capture mechanism is more frequent for larger diameter particles. In experiments with colloidal gold particles and depth filtration membranes with tortuous pores approximately 5 µm in diameter, Davis showed that 60% of 0.05 µm diameter particles were captured [65]. Nucleation track membranes with 5 µm, almost straight-through pores and no tortuosity retained less than 1% of the particles. The retention of the small particles by the depth filter was caused by the greater tortuosity, which led to inertial capture.

The second mechanism is capture by Brownian diffusion, which is more of a factor for smaller particles. Small particles are easily carried along by the moving fluid.

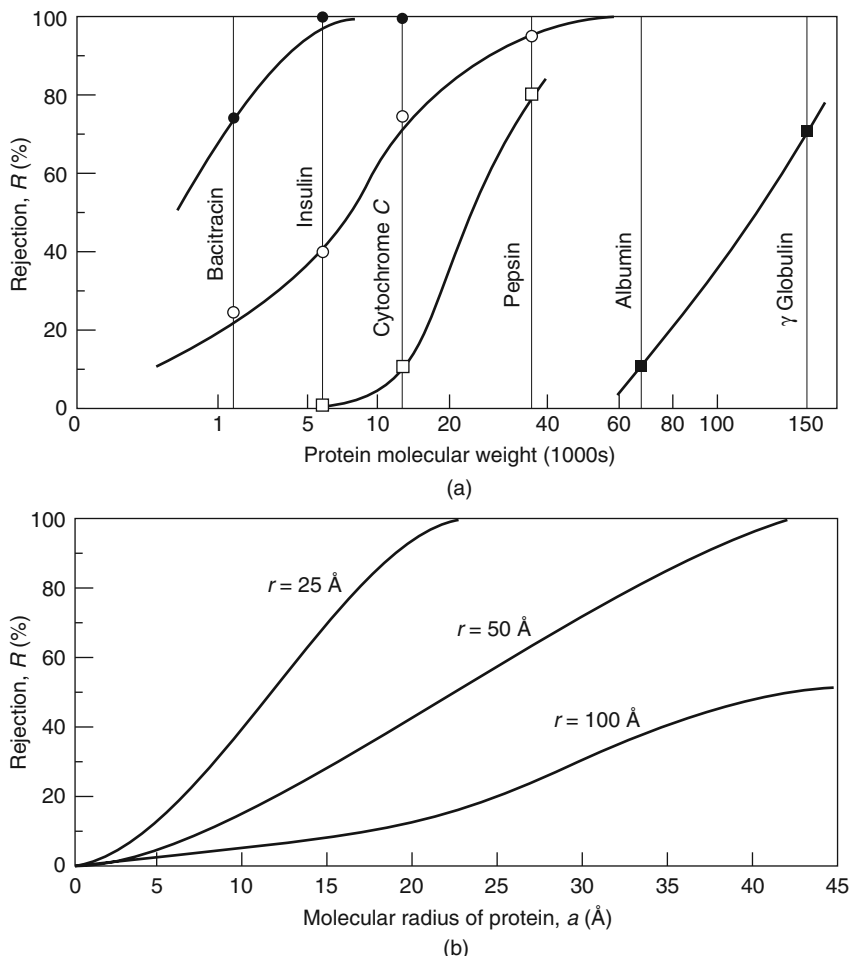


Figure 2.35 (a) Rejection of globular proteins by ultrafiltration membranes of increasing pore size and (b) calculated rejection curves from the Ferry-Renkin Equation 2.120 plotted on the same scale [62]

However, because the particles are small, they are subject to random Brownian motion that periodically brings them into contact with the pore walls. When this happens, capture by surface adsorption occurs.

The third mechanism is capture of charged particles by membranes having surface-charged groups. Many common colloidal materials carry a slight negative charge, so membranes containing an excess of positive groups can provide enhanced removal. Several microfiltration membrane manufacturers produce this type of charged membrane. One problem is that the adsorption capacity of the charged group is exhausted as filtration proceeds, and the retention then falls.

In the filtration of gas-borne aerosol particles by microfiltration membranes, capture by adsorption is usually far more important than capture by sieving. This leads to the

Table 2.7 Marker molecules used to characterize ultrafiltration membranes

Species	Molecular weight ($\times 1000$)	Estimated molecular diameter (\AA)
Sucrose	0.34	11
Raffinose	0.59	13
Vitamin B ₁₂	1.36	17
Bacitracin	1.41	17
Insulin	5.7	27
Cytochrome C	13.4	38
Myoglobin	17	40
α -Chymotrypsinogen	25	46
Pepsin	35	50
Ovalbumin	43	56
Bovine albumin	67	64
Aldolase	142	82
γ -Globulin	150	84

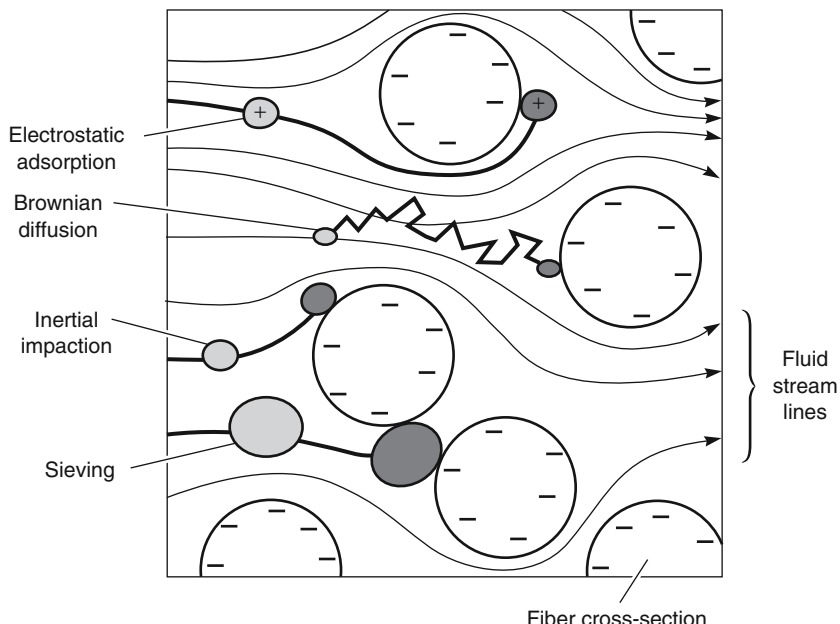


Figure 2.36 Particle capture mechanism in filtration of liquid solutions by depth microfilters. Four capture mechanisms are shown: simple sieving; electrostatic adsorption; inertial impaction; and Brownian diffusion

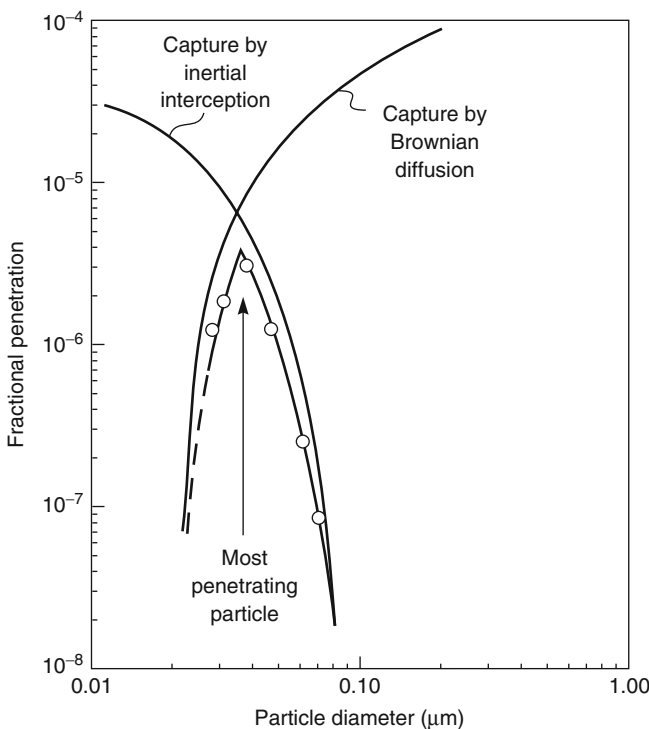


Figure 2.37 Gas-borne particle penetration through an ultrathin PVDF (poly(vinylidene fluoride)) membrane [65, 66]

paradoxical result that the most penetrating particle may not be the smallest one. This is because capture by inertial interception is most efficient for larger particles, whereas capture by Brownian motion is most efficient for smaller particles. As a result the most penetrating particle has an intermediate diameter, as shown in Figure 2.37 [65, 66].

2.4.2 Knudsen Diffusion and Surface Diffusion in Microporous Membranes

Essentially all industrial gas separation membranes involve permeation through dense polymeric membranes. But the study of gas permeation through finely microporous membranes has a long history dating back to Graham's work in the 1850s. If the pores of a microporous membrane are $0.1 \mu\text{m}$ (1000 \AA) or larger, gas permeation will take place by normal convective flow described by Poiseuille's law. As the pore radius (r) decreases, it can become smaller than the mean free path (λ) of the gas. (At atmospheric pressure the mean free path of common gases is in the range $500\text{--}2000 \text{ \AA}$.) When this occurs, the ratio of the pore radius to the gas mean free path (r/λ) is less than one. Diffusing gas molecules then have more collisions with the pore walls than with other gas molecules. Gas permeation in this region is called Knudsen diffusion. At every collision with the pore walls, the gas molecules are momentarily adsorbed and then reflected in a random direction. Molecule-molecule collisions are rare, so each gas molecule moves

independently of all others. Hence with gas mixtures in which the different species move at different average velocities, a separation is possible. The gas flow in a membrane made of cylindrical right capillaries for Knudsen diffusion is given by Equation 2.121

$$j = \frac{4r\varepsilon}{3} \cdot \left(\frac{2RT}{\pi m} \right)^{1/2} \cdot \frac{p_o - p_\ell}{\ell \cdot RT} \quad (2.121)$$

where m is the molecular weight of the gas, j is the flux in g mol/cm²/s, ε is the porosity of the membrane, r is the pore radius, ℓ is the pore length, and p_o and p_ℓ are the absolute pressures of the gas species at the beginning of the pore ($x = 0$) and at the end ($x = \ell$).

The equivalent equation for permeation by Poiseuille flow is

$$j = \frac{r^2\varepsilon}{8\eta} \times \frac{[p_o - p_\ell][p_o + p_\ell]}{\ell \cdot RT} \quad (2.122)$$

where η is the viscosity of the gas. Equation 2.122 differs from the more familiar Poiseuille equation for liquids by the additional term $[p_o + p_\ell]$ which arises from the expansion of a gas as it moves down the pressure gradient.

Figure 2.38 shows the effect of the ratio r/λ on the relative proportions of Knudsen to Poiseuille flow in a cylindrical capillary [67]. When r/λ is greater than 1, Poiseuille flow predominates. Because the mean free path of gases at atmospheric pressure is in the range of 500–2000 Å, for Knudsen flow to predominate and a separation to be obtained, the membrane pore radius must be less than 500 Å.

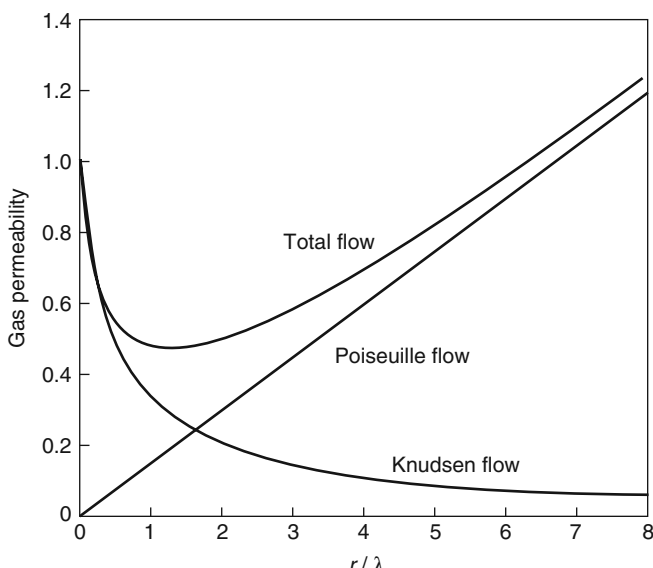


Figure 2.38 Illustration of the properties of Knudsen to Poiseuille flow in a finely microporous membrane as a function of the pore radius (r) divided by the mean pore path (λ) of the gas (after Barrer) [67]

It follows from Equation 2.121 that the permeability of a gas (i) through a Knudsen diffusion membrane is proportional to $1/\sqrt{m_i}$. The selectivity of this membrane (α_{ij}), proportional to the ratio of gas permeabilities, is given by the expression

$$\alpha_{ij} = \sqrt{\frac{m_j}{m_i}} \quad (2.123)$$

This result was first observed experimentally by Graham and is called Graham's law of diffusion. Knudsen diffusion membranes have been used to separate gas isotopes that are difficult to separate by other methods; for example, tritium from hydrogen, C^{12}H_4 from C^{14}H_4 , and most importantly U^{235}F_6 from U^{238}F_6 . The membrane selectivity for $\text{U}^{235}\text{F}_6/\text{U}^{238}\text{F}_6$ mixtures is only 1.0043, so hundreds of separation stages are required to produce a complete separation. Nevertheless, at the height of the Cold War, the U.S. Atomic Energy Commission operated three plants fitted with microporous metal membranes that processed almost 20 000 tons/year of uranium.

When the pore diameter of a microporous membrane decreases to the 5–10 Å range, the pores begin to separate gases by a molecular sieving effect. Production of these membranes is now a subject of considerable research interest. Zeolite and ceramic membranes can be made by a number of techniques described in Chapter 3. Microporous carbon membranes can be made by heating thin polymer films *in vacuo* to 500–1000°C. Under these conditions, most polymers partially or completely carbonize and the resulting films are very finely microporous. To date, none of these membranes has reached the commercial stage. However, in the laboratory, spectacular separations have been reported for gases that differ in size by only 0.1 Å. Figure 2.39 shows some data for permeation

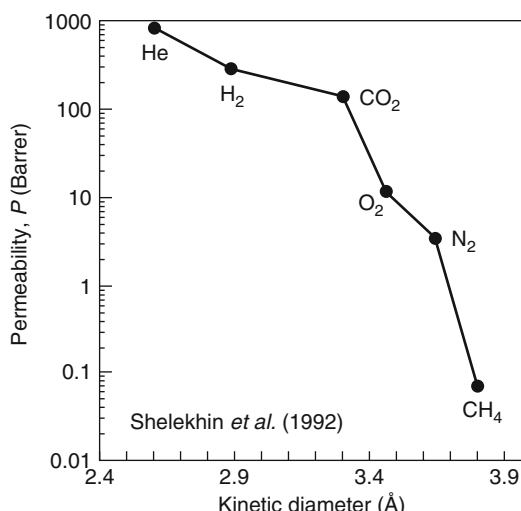


Figure 2.39 Permeability coefficients as a function of the gas kinetic diameter in microporous silica hollow fine fibers. Reprinted with permission from [69]. Copyright (1992) Elsevier.

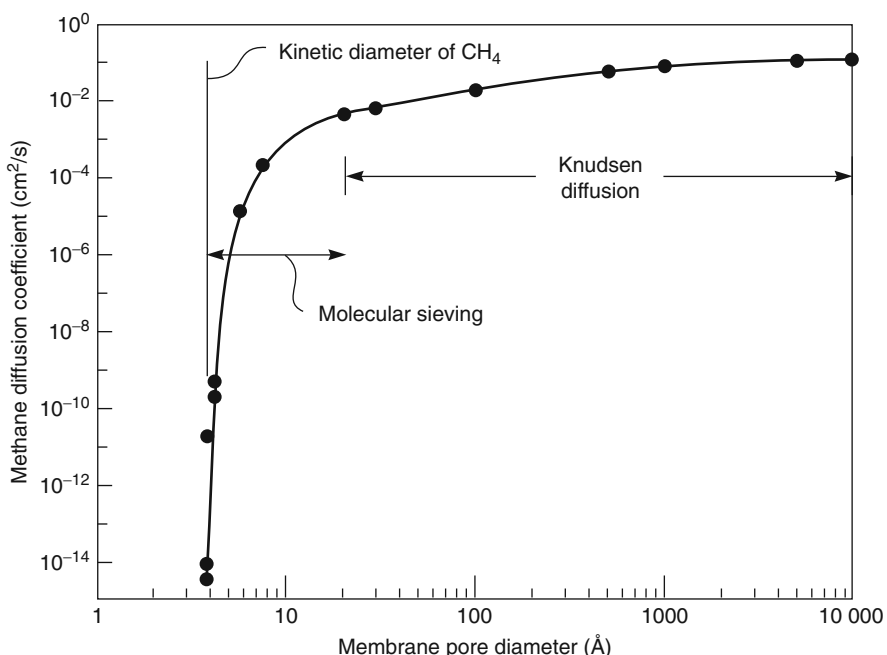


Figure 2.40 Diffusion coefficient of methane through zeolite and ceramic membranes of known pore diameter [69]

through microporous silica membranes [68]. No polymeric membranes can match this separation.

The very large decrease in permeation with increasing gas size shown in Figure 2.39 is characteristic of many of these finely microporous membranes. Small changes of less than 0.2 Å in permeant diameter can change permeance by orders of magnitude. Figure 2.40 shows the reason for this result [69]. The diffusion coefficient of methane through microporous membranes with different pore diameters is plotted. The diffusion coefficients for membranes with pore diameters below 10 Å are measured values obtained with different zeolite membranes. The diffusion coefficients shown for membranes with pore diameters of greater than 20 Å were estimated from their permeation properties. The diffusion coefficient of methane, kinetic diameter 3.8 Å, decreases almost 6 orders of magnitude as the pore diameter decreases from 5 to 4 Å.

Surface adsorption and diffusion are additional contributors to gas permeation that can occur in small-pore-diameter membranes. This phenomenon is illustrated in Figure 2.41. Adsorption onto the walls of the small pores becomes noticeable when the pore diameter drops below about 50–100 Å. At this pore diameter, the total surface area of the pore walls is in the range $100 \text{ m}^2/\text{cm}^3$ of material. Significant amounts of gas then adsorb onto the pore walls, particularly if the gas is condensable. Often the amount of gas sorbed onto the pore walls is greater than the amount of nonsorbed gas. Sorbed gas molecules are

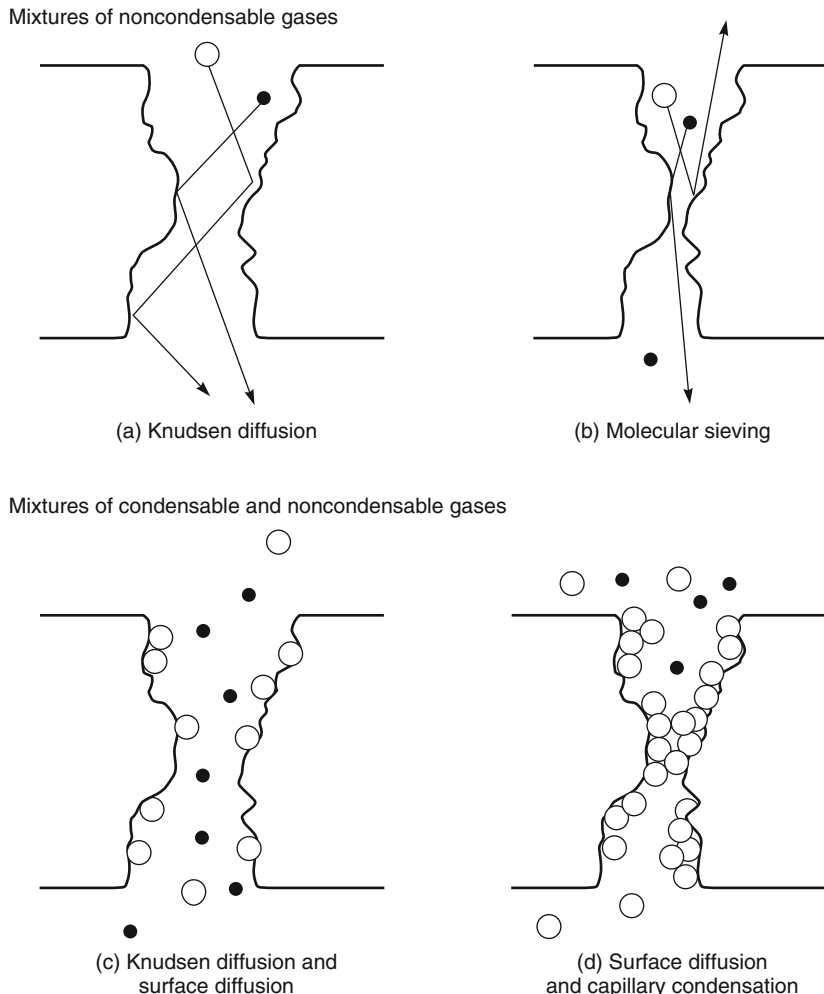


Figure 2.41 Permeation of noncondensable and condensable gas mixtures through finely microporous membranes. With noncondensable gases, molecular sieving occurs when the pore wall reaches the 5- to 10-Å diameter range. With gas mixtures containing condensable gases, surface diffusion increases as the pore diameter decreases and the temperature decreases (increasing adsorption)

mobile and can move by a process of surface diffusion through the membrane according to a Fick's law type of expression

$$J_s = -D_s \frac{dc_s}{dx} \quad (2.124)$$

where J_s is the contribution to permeation by surface diffusion of the sorbed gas c_s and D_s is a surface diffusion coefficient. At room temperature, typical surface diffusion

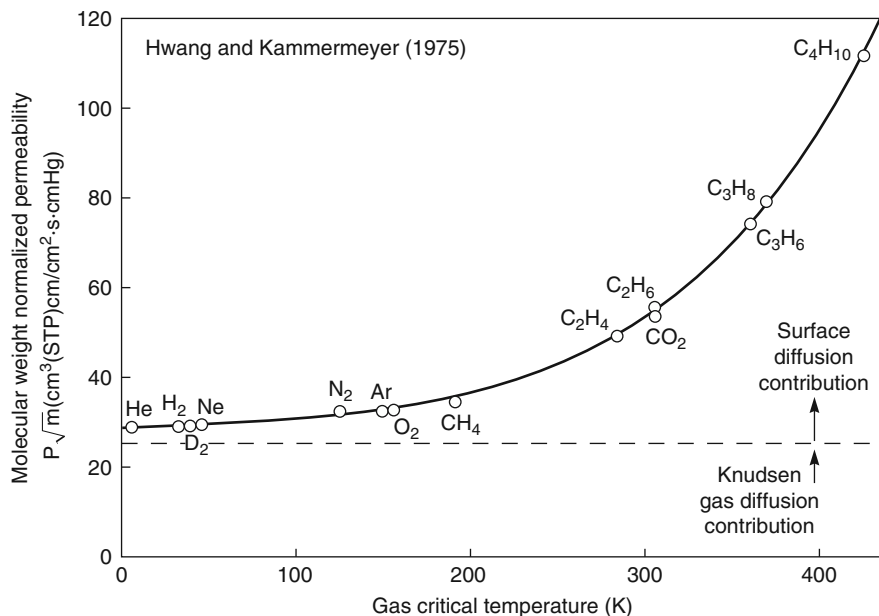


Figure 2.42 Molecular-weight-normalized permeability of gases through Vycor microporous glass membranes. Reprinted with permission from [72]. Copyright (1975) John Wiley & Sons, Inc.

coefficients are in the range 1×10^{-3} to 1×10^{-4} cm^2/s , intermediate between the diffusion coefficients of molecules in gases and liquids [70]. Although these coefficients are less than the diffusion coefficients for nonsorbed gas, surface diffusion still makes a significant contribution to total permeation.

Some typical results illustrating the effect of surface diffusion are shown in Figure 2.42 for permeation of gases through microporous glass [71]. The expected permeability normalized for gas molecular weight, $P\sqrt{m}$, is constant, but only the very low boiling gases, helium, hydrogen, and neon, approach this value. As the condensability of the gas increases (as measured by boiling point or critical temperature), the amount of surface adsorption increases and the contribution of surface diffusion to gas permeation increases. For butane, for example, 80% of the total gas permeation is due to surface diffusion.

In experiments with mixtures of condensable and noncondensable gases, adsorption of the condensable gas onto the pore walls can restrict or even completely block permeation of the noncondensable gas [72, 73]. This effect was first noticed by Ash, Barrer, and Pope in experiments with sulfur dioxide/hydrogen mixtures [74]; some of the data are shown in Figure 2.43. Sorption of sulfur dioxide on the pore walls of the microporous carbon membrane inhibits the flow of hydrogen. If adsorption is increased by increasing the sulfur dioxide partial pressure or by lowering the temperature, the amount of sulfur dioxide adsorbed increases until at some point the membrane pores are completely

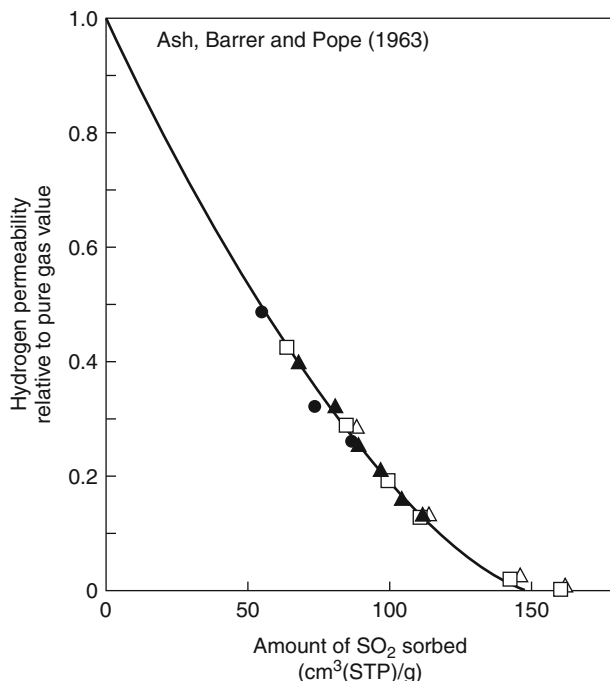


Figure 2.43 Blocking of hydrogen in hydrogen/sulfur dioxide gas mixture permeation experiments with finely microporous carbon membranes [74] as a function of the amount of sulfur dioxide sorbed by the membrane. As sulfur dioxide sorption increases the hydrogen permeability is reduced until at about $140 \text{ cm}^3 (\text{SO}_2)(\text{STP})/\text{g}$, the membrane is completely blocked and only sulfur dioxide permeates. Data obtained at several temperatures fall on the same master curve (\bullet , 0°C ; \blacktriangle , -10°C ; \square , -20.7°C ; \triangle , -33.6°C). Reprinted with permission from R. Ash, R.M. Barrer, and C.G. Pope, *Flow of Adsorbable Gases and Vapours in Microporous Medium*, Proc. R. Soc. London, Ser. A, **271**, 19. Copyright (1963) The Royal Society.

filled, blocking permeation of hydrogen. At this point, the membrane only permeates sulfur dioxide.

This blocking phenomenon described above is commonly seen when finely microporous carbon or ceramic membranes are used to separate condensable gas mixtures. In the 1990s, Rao, Sirkar, and others at Air Products tried to use surface diffusion of adsorbed permeants in microporous membranes to separate hydrogen/light hydrocarbon gas mixtures found in refinery fuel gas streams [69, 75, 76]. They used microporous carbon membranes, formed by vacuum carbonization of polymer films cast onto microporous ceramic supports. The adsorbed hydrocarbons permeate the membranes by surface diffusion while permeation of hydrogen and methane in the gas phase is blocked by capillary condensation in the membrane pores. Pure-gas and mixed-gas permeation data measured with these membranes are shown in Table 2.8 [76]. The membranes have very modest selectivities for pure gases, with the hydrocarbons being slightly more permeable than

Table 2.8 Permeabilities of hydrogen and hydrocarbons through a microporous carbon membrane at 295 K

Components	Pure-gas permeabilities (P_i^o in Barrers)	Mixture permeabilities ^a (P_i in Barrers)	Selectivity($P_{\text{hydrocarbon}}/P_{\text{H}_2}$)	
			Pure gas	Mixture
H ₂	130	1.2	1.0	1.0
CH ₄	660	1.3	5.1	1.1
C ₂ H ₆	850	7.7	6.6	6.4
C ₃ H ₈	290	25.4	2.3	21.2
C ₄ H ₁₀	155	112.3	1.2	93.6

^aGas composition of feed: 41.0% H₂, 20.2% CH₄, 9.5% C₂H₆, 9.4% C₃H₈, and 19.9% C₄H₁₀. Feed pressure: 4.4 bar; permeate pressure: 1 bar.
Data are from Sircar and Rao [76].

hydrogen, probably because of the surface diffusion contribution to diffusion. When used with a gas mixture, the results are very different. Propane and butane readily permeate the membrane, but permeation of hydrogen and methane are significantly reduced. This is because of blocking of the membrane pores to hydrogen and methane by adsorbed propane and butane. Processes using these membranes were tried at the pilot-plant scale, but eventually abandoned, in part because small amounts of C₆⁺ hydrocarbons also present in the feed gas slowly adsorbed in the pores and gradually blocked permeation of the lighter hydrocarbons as well as methane and hydrogen.

2.4.3 Polymers with Intrinsic Microporosity (PIMs)

The bulk of the literature data on the use of microporous membranes to separate gas mixtures involves ceramic, zeolite, or carbon membranes. However, in the last 10–15 years, a number of polymeric materials have been found that also appear to be finely microporous. The first material of this type was poly (1-trimethylsilyl-1-propyne) (PTMSP). The double bonds in the main chain of this polymer, together with severe steric hindrance from the bulky trimethylsilyl group, almost prohibit segmental rotation in the polymer. As a consequence, the polymer backbone is very rigid, the glass transition temperature (T_g) is very high and the fractional free volume is exceptionally high at 0.34. One-third of the polymer is unoccupied space, and PTMSP has the lowest density of any known polymer. Not unexpectedly, the gas permeation properties of PTMSP and similar exceptionally high fractional free volume polymers are anomalous.

The structures of three of the most-studied polymers of this class are shown in Figure 2.44. As a group, these materials are called polymers with intrinsic microporosity or sometimes superglassy polymers. Because of their exceptional free volume, these polymers are all extremely permeable materials. Some representative data are shown in Table 2.9. The permeation properties of polysulfone, a conventional glassy polymer, are included for comparison.

Gas permeabilities in PIM membranes are orders of magnitude higher than those of conventional, low free volume glassy polymers, and are also substantially higher than high permeability rubbery polymers such as poly(dimethyl siloxane), for many years the most permeable polymer known. The extremely high free volume provides a sorption

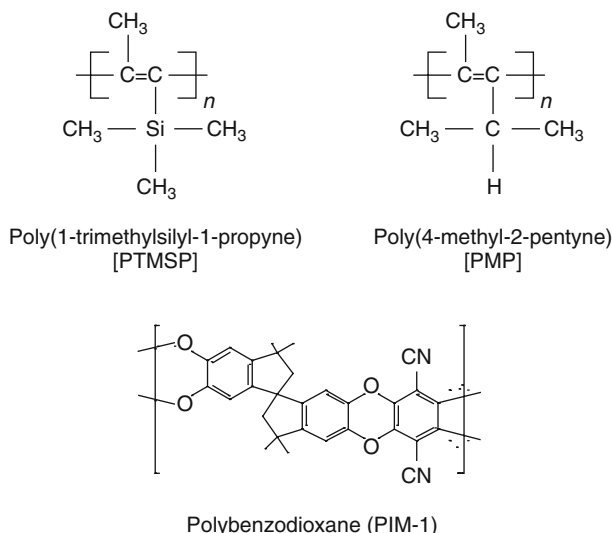


Figure 2.44 Structure of three exceptionally high free volume polymers. Extremely stiff-backed, rigid polymer chains pack poorly, leading to high fractional free volumes

Table 2.9 A comparison of the properties of two polymers with intrinsic microporosity (PTMSP and PIM-1) with a high free volume conventional glassy polymer (polysulfone) [77–79]

Polymer	Free volume (%)	BET surface area (m ² /g)	N ₂ permeability (Barrer)	Selectivity O ₂ /N ₂
PTMSP	29	550	6300	1.5
PIM-1	25	830	340	3.8
Polysulfone	18	<1	0.25	5.6

capacity as much as 10 times that of a conventional glassy polymer. More importantly, diffusion coefficients are 10³–10⁶ times greater than those observed in conventional glassy polymers. This combination of extraordinarily high permeabilities, together with the very high free volume, hints at a pore-flow transport contribution.

The finely nanoporous nature of PIM-type polymers is also demonstrated by the BET surface area measurements listed in Table 2.9. A conventional glassy polymer like polysulfone shows no evidence of any internal nanoporous structure; the BET surface area is very small. In contrast, PTMSP and PIM-1 have BET surface areas of 500–1000 m²/g of polymer. This surface area is comparable to that of carbon black, suggesting the internal structure of these polymers and adsorbent microporous solids such as carbon black are similar.

These high free volume polymers also have the pore blocking characteristics seen with finely microporous ceramic membranes when mixtures of condensable and noncondensable gases are being separated. For example, in the presence of as little as 1200 ppm of

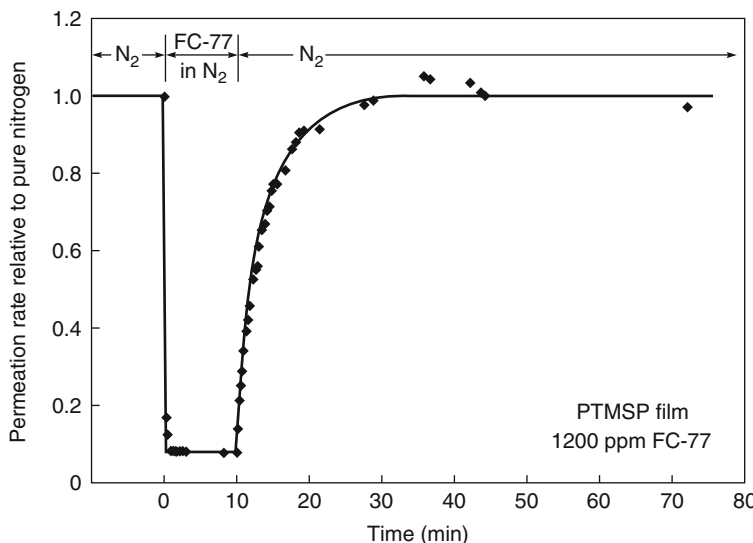


Figure 2.45 The change in nitrogen flux through a PTMSP membrane caused by the presence of a condensable vapor in the feed gas. This behavior is characteristic of extremely finely porous microporous ceramic or ultrahigh free volume polymeric membranes such as PTMSP. The condensable vapor adsorbs in the 5- to 15-Å-diameter pores of the membrane, blocking the flow of the noncondensable nitrogen gas

a condensable vapor such as the perfluorocarbon FC-77 (a perfluoro octane–perfluoro decane mixture), the nitrogen permeability of PTMSP is 20 times lower than the polymer pure nitrogen permeability [9], as the data in Figure 2.45 show. When the condensable vapor is removed from the feed gas, the nitrogen permeability rapidly returns to its original value. The best explanation for these unusual vapor permeation properties is that the PIMs polymers, because of their very high free volume, are ultra-microporous membranes in which pore-flow transport occurs. The FC-77 vapor causes capillary condensation in which the pores are partially or completely blocked by the adsorbed vapor, preventing the flow of noncondensed gases (nitrogen) through the membrane.

Another example of the effect of pore blocking by the adsorbed permeating component is shown in Figure 2.46 [77]. The pure-gas permeabilities of propane and hydrogen in PTMSP are very similar, so the membrane appears to have almost no selectivity for propane/hydrogen mixtures. The results when tested with gas mixtures are very different. As the fraction of propane in the propane/hydrogen feed gas is increased, the hydrogen permeability falls and the membrane becomes increasingly propane selective, reaching a propane/hydrogen selectivity of 25 at high propane partial pressures.

Although PIM membranes have been widely studied in the laboratory, they have found no industrial application. The reason is film densification and loss of free volume, resulting in drastically reduced permeability over time, of the type illustrated in Figure 2.26. This densification is more rapid than with conventional amorphous glassy polymers. PIMs membranes, for example, lose much of their permeability within days and weeks

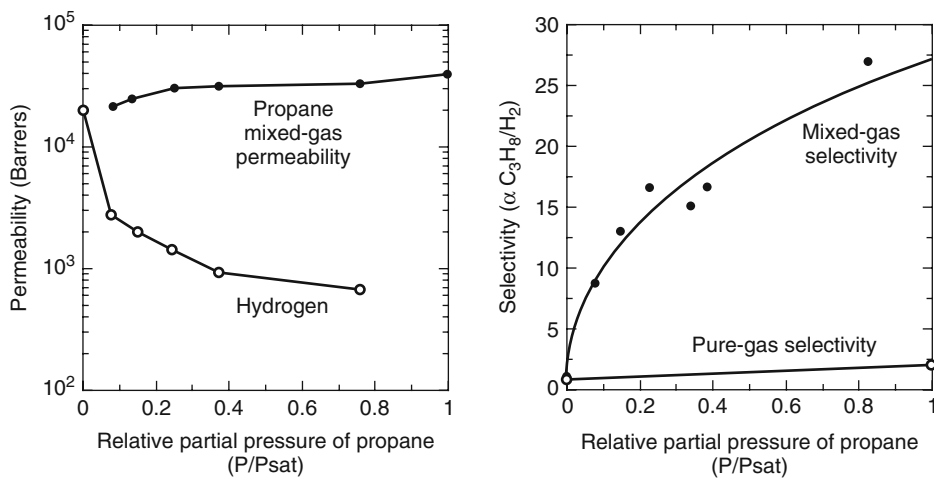


Figure 2.46 Permeation of propane/hydrogen gas mixtures through PTMSP membranes. The pure-gas permeabilities of propane and hydrogen are similar, but in gas mixtures, propane adsorption in the finely microporous PTMSP membrane blocks permeation of hydrogen. The membranes then permeate propane over hydrogen [77]

Table 2.10 Rejection of microsolute by nanofiltration membranes (FilmTec data) [79]

Solute	Solute rejection (%)		
	FT-30	XP-45	XP-20
NaCl	99.5	50	20
MgCl ₂	>99.5	83	—
MgSO ₄	>99.5	97.5	85
NaNO ₃	90	<20	0
Ethylene glycol	70	24	11
Glycerol	96	44	15
Glucose	99	95	60
Sucrose	100	100	89

Reprinted from *Desalination*, 70, J. Cadotte, R. Forester, M. Kim, R. Petersen, and T. Stocker, "Nanofiltration membranes broaden the use of membrane separation technology," p. 77, Copyright 1988, with permission from Elsevier.

of being made. To date, all attempts to stabilize these polymers in their initial high free volume state have failed.

2.4.4 The Transition Region

The transition between pore-flow and solution-diffusion transport, described above for gas permeation membranes, also occurs with ultrafiltration/reverse osmosis membranes. Ultrafiltration membranes that reject sucrose and raffinose but pass all micro-ions are

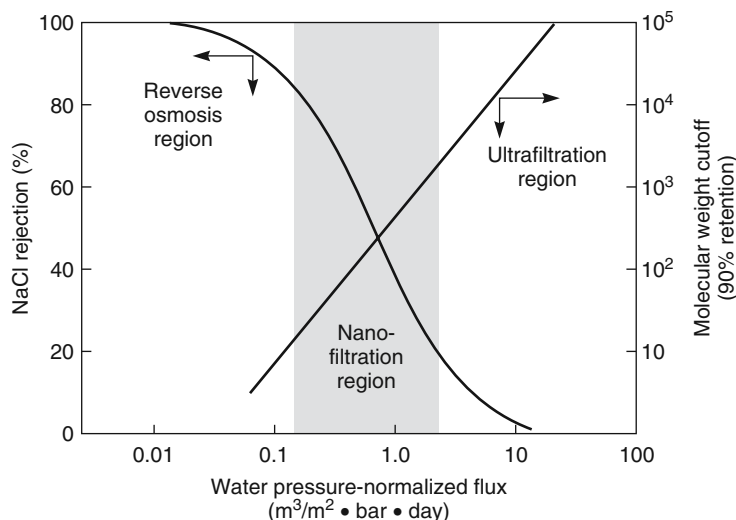


Figure 2.47 Diagram of the region of nanofiltration membrane performance relative to reverse osmosis and ultrafiltration membranes [81]

clearly pore-flow membranes, whereas desalination-grade sodium chloride-rejecting reverse osmosis membranes clearly follow the solution-diffusion model. The transition is in the nanofiltration range, with membranes having good rejections to divalent ions and most organic solutes, but rejection of monovalent ions in the 20–70% range. The performance of a family of nanofiltration membranes of this type is illustrated in Table 2.10 [80]. The FT30 membrane is clearly a good reverse osmosis membrane, whereas the XP-20 is a small pore-flow ultrafiltration membrane. The XP-45 membrane is intermediate in character.

The transition between reverse osmosis membranes with a salt rejection of more than 95% and molecular weight cut-offs below 50, and ultrafiltration membranes with a salt rejection of less than 10% and a molecular weight cut-off of more than 1000 is shown in Figure 2.47 [81]. The very large change in the pressure-normalized flux of water that occurs as the membranes become more retentive is noteworthy. Because these are anisotropic membranes, the thickness of the separating layer is difficult to measure, but clearly the permeability of water through the pores of ultrafiltration membranes is orders of magnitude higher than permeability through dense solution-diffusion reverse osmosis membranes.

2.5 Conclusions and Future Directions

During the last 30 years, the basis of permeation through membranes has become much clearer. This is particularly true for reverse osmosis, gas permeation, and pervaporation, for which the solution-diffusion model is now almost universally accepted and well-supported by a body of experimental evidence. The model is popular because it provides

simple equations that accurately link the driving forces of concentration and pressure with flux and selectivity. Also, the same set of assumptions can be used to describe permeation in a variety of seemingly different processes. This unity was illustrated in Figure 2.19, and in the equations used to draw this figure.

The solution-diffusion model uses Fick's law of diffusion (Equation 2.1) as its basis. However, Fick's law in the strictest sense is only valid for a two-component system comprised of a membrane and one diffusing component. Also, membranes highly swollen by the permeant require a "frame-of-reference correction" because the difference in velocity between the stationary membrane material and the permeating components is not accounted for. Fortunately for all of us, the deviations from Fick's law are minor when the permeant concentrations in the membrane are small, and the equations presented in this chapter are applicable to the majority of membrane applications without significant error.

The application of Fick's law to the diffusion part of the solution-diffusion model has to be re-examined, however, when the membrane is highly swollen by the permeants. The frame-of-reference correction to Fick's law, described in papers by Paul [82, 83] and Kamaruddin and Koros [84], can be applied, but this does not extend the description to more than two components, and a membrane separation process has a minimum of three components: the membrane material and at least two permeants which are being separated. An alternative approach is to replace Fick's law in the solution-diffusion model by the Maxwell-Stefan diffusive transport equation. This equation is based on the relative velocities of the components of the system to one another. The frame-of-reference problem is then "sidestepped." Those with a mathematical bent will find a readable introduction to the Maxwell-Stefan equation and its application to membrane processes is given in the book by Wesselingh and Krishna [85]. A recent paper by Paul [86] discusses the use of the Maxwell-Stefan equation for organic hyperfiltration processes.

Most readers are likely to find the Maxwell-Stefan approach heavy going. It is doubtful if the advantage of Maxwell-Stefan formalism will ever persuade the average membrane researcher to switch from the relative simplicity of Fick's law. Nonetheless, the Maxwell-Stefan approach has its supporters, particularly for use in fundamental investigations of membrane transport behavior.

The solution-diffusion model has been less successful at providing a link between the nature of membrane materials and their membrane permeation properties. This link requires an ability to calculate membrane diffusion and sorption coefficients. These calculations require knowledge of the molecular level of interactions of permeant molecules and their motion in the polymer matrix that is not yet available. Only semiempirical correlations such as the dual sorption model or free volume correlations are available. The best hope for future progress toward *a priori* methods of calculating permeant sorption and diffusion coefficients lies in computer-aided simulations of molecular dynamics, but accurate predictions using this technique are years – perhaps decades – away.

The theory of permeation through microporous membranes in ultrafiltration and microfiltration is even less developed and it is difficult to see a clear path forward to that end. Permeation through these membranes is affected by a variety of hard-to-compute effects and is also very much a function of membrane structure and composition. Measurements of permeation through ideal uniform-pore-diameter membranes made by the

nucleation track method are in good agreement with theory. Unfortunately, industrially useful membranes have non-uniform tortuous pores and are often anisotropic as well. Current theories cannot predict the permeation properties of these membranes.

References

1. Meares, P. (1966) On the mechanism of desalination by reversed osmotic flow through cellulose acetate membrane. *Eur. Polym. J.*, **2**, 241.
2. Paul, D.R. (1974) Diffusive transport in swollen polymer membranes, in *Permeability of Plastic Films and Coatings* (ed. H.B. Hopfenberg), Plenum Press, New York, pp. 35–48.
3. Paul, D.R. (1976) The solution-diffusion model for swollen membranes. *Sep. Purif. Methods*, **5**, 33.
4. Paul, D.R. and Ebra-Lima, O.M. (1970) Pressure-induced diffusion of organic liquids through highly swollen polymer membranes. *J. Appl. Polym. Sci.*, **14**, 2201.
5. Yasuda, H. and Peterlin, A. (1973) Diffusive and bulk flow transport in polymers. *J. Appl. Polym. Sci.*, **17**, 433.
6. Sourirajan, S. (1970) *Reverse Osmosis*, Academic Press, New York.
7. Fick, A. (1855) Über diffusion. *Poggendorff's Ann. Phys. Chem.*, **94**, 59.
8. Budd, P.M., McKeown, N.B., Ghanem, B.S. *et al.* (2008) Gas permeation parameters and other physicochemical properties of a polymer of intrinsic microporosity: polybenzodioxane PIM-1. *J. Membr. Sci.*, **325**, 851.
9. Pinna, I. and Toy, L.G. (1996) Transport of organic vapors through poly[1-(trimethylsilyl)-1-propyne]. *J. Membr. Sci.*, **116**, 199.
10. Srinivasan, R., Auvil, S.R., and Burban, P.M. (1994) Elucidating the mechanism(s) of gas transport in poly[1-(trimethylsilyl)-1-propyne] (PTMSP) membranes. *J. Membr. Sci.*, **86**, 67.
11. Smit, E., Mulder, M.H.V., Smolders, C.A., Karrenbeld, H., van Eerden, J. and Feil, D. (1992) Modeling of the diffusion of carbon dioxide in polyimide matrices by computer simulation. *J. Membr. Sci.*, **73**, 247.
12. Charati, S.G. and Stern, S.A. (1998) Diffusion of gases in silicone polymers: molecular dynamic simulations. *Macromolecules*, **31**, 5529.
13. Theodorou, D.N. (2006) Principles of molecular simulation of gas transport in polymers, in *Materials Science of Membranes for Gas and Vapor Separations* (eds Y. Yampolskii, I. Pinna, and B.D. Freeman), John Wiley & Sons Ltd, Chichester, pp. 49–89.
14. Wijmans, J.G. and Baker, R.W. (1995) The solution-diffusion model: a review. *J. Membr. Sci.*, **107**, 1.
15. Wijmans, J.G. and Baker, R.W. (2006) The solution-diffusion model: a unified approach to membrane permeation, in *Materials Science of Membranes for Gas and Vapor Separation* (eds Y. Yampolskii, I. Pinna, and B.D. Freeman), John Wiley & Sons Ltd, Chichester, pp. 159–188.
16. Theeuwes, F., Gale, R.M., and Baker, R.W. (1976) Transference: a comprehensive parameter governing permeation of solutes through membranes. *J. Membr. Sci.*, **1**, 3.
17. Thorsen, T. and Holt, T. (2009) The potential for power production from salinity gradients by pressure retarded osmosis. *J. Membr. Sci.*, **335**, 103–110.

18. Rosenbaum, S. and Cotton, O. (1969) Steady-state distribution of water in cellulose acetate membrane. *J. Polym. Sci.*, **7**, 101.
19. Kim, S.N. and Kammermeyer, K. (1970) Actual concentration profiles in membrane permeation. *Sep. Sci.*, **5**, 679.
20. Paul, D.R. and Paciotti, D.J. (1975) Driving force for hydraulic and pervaporation transport in homogeneous membranes. *J. Polym. Sci. Part B: Polym. Phys. Ed.*, **13**, 1201.
21. Wijmans, J.G. (2004) The role of permeant molar volume in the solution-diffusion model transport equations. *J. Membr. Sci.*, **237**, 39.
22. Lonsdale, H.K., Merten, U., and Riley, R.L. (1965) Transport properties of cellulose acetate osmotic membranes. *J. Appl. Polym. Sci.*, **9**, 1341.
23. Merten, U. (1966) Transport properties of osmotic membranes, in *Desalination by Reverse Osmosis* (ed. U. Merten), MIT Press, Cambridge, MA, pp. 15–54.
24. Riley, R.L., Lonsdale, H.K., Lyons, C.R., and Merten, U. (1967) Preparation of ultrathin reverse osmosis membranes and the attainment of theoretical salt rejection. *J. Appl. Polym. Sci.*, **11**, 2143.
25. Bhore, N., Gould, R.M., Jacob, S.M., Staffeld, P.O., McNally, D., Smiley, P.H. and Wildemuth, C.R. (1999) New membrane process Debottlenecks solvent Dewaxing unit. *Oil Gas J.*, **97**, 67.
26. Kataoka, T., Tsuro, T., Nakao, S-I., and Kimura, S. (1991) Permeation equations developed for prediction of membrane performance in pervaporation, vapor permeation and reverse osmosis based on the solution-diffusion model. *J. Chem. Eng. Jpn.*, **24**, 326–333.
27. Wijmans, J.G. and Baker, R.W. (1993) A simple predictive treatment of the permeation process in pervaporation. *J. Membr. Sci.*, **79**, 101.
28. Greenlaw, F.W., Prince, W.D., Shelden, R.A., and Thompson, E.V. (1977) Dependence of diffusive permeation rates by upstream and downstream pressures. *J. Membr. Sci.*, **2**, 141.
29. Tanaka, K., Kita, H., Okano, M., and Okamoto, K. (1992) Permeability and permselectivity of gases in fluorinated and non-fluorinated polyimides. *Polymer*, **33**, 585.
30. Koros, W.J., Coleman, M.R., and Walker, D.R.B. (1992) Controlled permeability polymer membranes. *Annu. Rev. Mater. Sci.*, **22**, 47.
31. Merkel, T.C., Bondar, V.I., Nagai, K., Freeman, B.D. and Pinnau, I. (2000) Gas sorption, diffusion, and permeation in poly(dimethylsiloxane). *J. Poly. Sci. Part B: Polym. Phys.*, **38**, 415.
32. Hirschfelder, J.O., Curtis, C.F., and Bird, B.B. (1954) *Molecular Theory of Gases and Liquids*, John Wiley & Sons, Inc., New York.
33. Reid, R.C., Prausnitz, J.M., and Poling, B.E. (1987) *The Properties of Gases and Liquids*, 4th edn, McGraw-Hill, New York.
34. Edward, J.T. (1970) Molecular volumes and the stokes-Einstein equation. *J. Chem. Ed.*, **47**, 261.
35. Nishijima, Y. and Oster, G. (1956) Diffusion in concentrated polymer solutions. *J. Polym. Sci.*, **19**, 337.

36. Baker, R.W. and Lonsdale, H.K. (1974) Controlled release: mechanisms and rates, in *Controlled Release of Biological Active Agents* (eds A.C. Tanquary and R.E. Lacey), Plenum Press, New York, pp. 15–72.
37. Artsis, M., Chalykh, A.E., Khalturinskii, N.A., Moiseev, W. and Zaikov, G.E. (1972) Diffusion of organic diluents into ethyl cellulose. *Eur. Polym. J.*, **8**, 613.
38. Bondi, A. (1968) *Physical Properties of Molecular Crystals, Liquids, and Glasses*, John Wiley & Sons, Inc., New York.
39. van Krevelen, D.W. (1990) *Properties of Polymers*, Elsevier Science B.V., Amsterdam.
40. Aitken, C.L., Koros, W.J., and Paul, D.R. (1992) Effect of structural symmetry on gas transport properties of polysulfones. *Macromolecules*, **25**, 3424.
41. Park, J.Y. and Paul, D.R. (1997) Correlation and prediction of gas permeability in glassy polymer membrane materials via a modified free volume based group contribution method. *J. Membr. Sci.*, **125**, 29.
42. Paxton, M.R. and Paul, D.R. (1994) Relationship between structure and transport properties for polymers with aromatic backbones, in *Polymeric Gas Separation Membranes* (eds D.R. Paul and Y.P. Yampolskii), CRC Press, Boca Raton, FL, pp. 83–154.
43. Petropoulos, J.H. (1994) Mechanisms and theories for sorption and diffusion of gases in polymers, in *Polymeric Gas Separation Membranes* (eds D.R. Paul and Y.P. Yampolskii), CRC Press, Boca Raton, FL, pp. 17–82.
44. Matteucci, S., Yampolskii, Y., Freeman, B.D., and Pinna, I. (2006) Transport of gases and vapors in glassy and rubbery polymers, in *Materials Science of Membranes for Gas and Vapor Separation* (eds Y. Yampolskii, I. Pinna, and B.D. Freeman), John Wiley & Sons, Ltd, Chichester, pp. 1–47.
45. Huang, Y. and Paul, D.R. (2004) Physical aging of thin glassy polymer films monitored by gas permeability. *Polymer*, **45**, 8377.
46. Huang, Y. and Paul, D.R. (2007) Effect of film thickness on the gas-permeation characteristics of glassy polymer membranes. *Ind. Eng. Chem. Res.*, **46**, 2342.
47. Platé, N.A. and Yampol'skii, Y.P. (1994) Relationship between structure and transport properties for high free volume polymeric materials, in *Polymeric Gas Separation Membranes* (eds D.R. Paul and Y.P. Yampolskii), CRC Press, Boca Raton, FL, pp. 155–208.
48. Masuda, T., Iguchi, Y., Tang, B-Z., and Higashimura, T. (1988) Diffusion and solution of gases in substituted polyacetylene membranes. *Polymer*, **29**, 2041.
49. Stern, S.A., Shah, V.M., and Hardy, B.J. (1987) Structure-permeability relationships in silicone polymers. *J. Polym. Sci. Polym. Phys. Ed.*, **25**, 1263.
50. Denbigh, K. (1961) *The Principles of Chemical Equilibrium*, Cambridge University Press, Cambridge.
51. Doghieri, F., Quinzi, M., Rethwisch, D.G., and Sarti, G.C. (2006) Predicting gas solubility in membranes through non-equilibrium thermodynamics for glassy polymers, in *Materials Science of Membranes for Gas and Vapor Separation* (eds B.D. Freeman, Y. Yampolskii, and I. Pinna), John Wiley & Sons, Ltd, Chichester, pp. 137–158.
52. Flory, P.J. (1953) *Principles of Polymer Chemistry*, Cornell University Press, Ithaca, NY, p. 511.

53. Freeman, B.D. and Pinna, I. (1999) Polymer membranes for gas separation. *ACS Symp. Ser.*, **733**, 6.
54. Barrer, R.M., Barrie, J.A., and Slater, J. (1958) Sorption and diffusion in ethyl cellulose. *J. Polym. Sci.*, **27**, 177.
55. Michaels, A.S., Vieth, W.R., and Barrie, J.A. (1963) Solution of gases in polyethylene terephthalate. *J. Appl. Phys.*, **34**, 1.
56. Toi, K., Morel, G., and Paul, D.R. (1982) Gas sorption in poly(phenylene oxide) and comparisons with other glassy polymers. *J. Appl. Sci.*, **27**, 2997.
57. Koros, W.J., Chan, A.H., and Paul, D.R. (1977) Sorption and transport of various gases in polycarbonate. *J. Membr. Sci.*, **2**, 165.
58. Morisato, A., Freeman, B.D., Pinna, I., and Casillas, C.G. (1996) Pure hydrocarbon sorption properties of poly(1-trimethylsilyl-1-propyne) [PTMSP] and poly(1-phenyl-1-propyne) [PPP] and PTMSP/PPP Blends. *J. Polym. Sci. Polym. Phys. Ed.*, **34**, 1925.
59. Bungay, P.M. (1986) Transport principles-porous membranes, in *Synthetic Membranes: Science Engineering and Applications* (eds P.M. Bungay, H.K. Lonsdale, and M.N. de Pinto), D. Reidel Publishing Company, Dordrecht, pp. 109–154.
60. Ferry, J.D. (1936) Ultrafilter membranes and ultrafiltration. *Chem. Rev.*, **18**, 373.
61. Renkin, E.M. (1955) Filtration, diffusion and molecular sieving through porous cellulose membranes. *J. Gen. Physiol.*, **38**, 225.
62. Baker, R.W. and Strathmann, H. (1970) Ultrafiltration of macromolecular solutions with high-flux membranes. *J. Appl. Polym. Sci.*, **14**, 1197.
63. Lukaszewicz, R.C., Tanny, G.B., and Meltzer, T.H. (1978) Membrane-filter characterizations and their implications for particle retention. *Pharm. Tech.*, **2**, 77.
64. Meltzer, T.H. (1987) *Filtration in the Pharmaceutical Industry*, Marcel Dekker, New York.
65. Davis, R.H. and Grant, D.C. (1992) Theory for dead end microfiltration, in *Membrane Handbook* (eds W.S.W. Ho and K.K. Sirkar), Van Nostrand Reinhold, New York, pp. 461–479.
66. Grant, D.C., Liu, B.Y.H., Fischer, W.G., and Bowling, R.A. (1989) Particle capture mechanisms in gases and liquids: an analysis of operative mechanisms. *J. Environ. Sci.*, **42**, 43.
67. Barrer, R.M. (1963) Diffusion in porous media. *Appl. Mater. Res.*, **2**, 129.
68. Shelekhin, A.B., Dixon, A.G., and Ma, Y.H. (1992) Adsorption, permeation, and diffusion of gases in microporous membranes. *J. Membr. Sci.*, **75**, 233.
69. Rao, M.B. and Sirkar, S. (1996) Performance and pore characterization of nanoporous carbon membranes for gas separation. *J. Membr. Sci.*, **110**, 109.
70. Ash, R., Barrer, R.M., and Sharma, P. (1976) Sorption and flow of carbon dioxide and some hydrocarbons in a microporous carbon membrane. *J. Membr. Sci.*, **1**, 17.
71. Hwang, S.T. and Kammermeyer, K. (1975) *Techniques of Chemistry*, Membranes in Separations, Vol. VII, John Wiley & Sons, Inc., New York.
72. Hassan, M.H., Way, J.D., Thoen, P.M., and Dillon, A.C. (1995) Single component and mixed gas transport in a silica fiber membrane. *J. Membr. Sci.*, **104**, 27.
73. Keizer, K., Burggraaf, A.J., Vroon, Z.A.E.P., and Verweij, H. (1998) Two component permeation through thin zeolite MFI membranes. *J. Membr. Sci.*, **147**, 159.

74. Ash, R., Barrer, R.M., and Pope, C.G. (1963) Flow of adsorbable gases and vapours in microporous medium. *Proc. R. Soc. Lond., Ser. A*, **271**, 19.
75. Rao, M.B. and Sirkar, S. (1993) Nanoporous carbon membranes for separation of gas mixtures by selective surface flow. *J. Membr. Sci.*, **85** (3), 253–264.
76. Sircar, S. and Rao, M.B. (2000) Nanoporous carbon membranes for gas separation, in *Recent Advances in Gas Separation by Microporous Ceramic Membranes* (ed. N.K. Kanellopoulos), Elsevier Science B.V., Amsterdam, pp. 473–496.
77. Pinna, I., Casillas, C.G., Morisato, A., and Freeman, B.D. (1996) Hydrocarbon/hydrogen mixed gas permeation in poly(1-trimethylsilyl-1-propyne) (PTMSP), poly(1-phenyl-1-propyne) (PPP), and PTMSP/PPP blends. *J. Polym. Sci. Part B: Polym. Phys.*, **34** (15), 2613–2621.
78. Budd, P.M., Ghanem, B.S., Makhseed, S. et al. (2004) Polymers of intrinsic micro-porosity (PIMs): robust, solution-processable, organic nanoporous materials. *Chem. Commun.*, (2), 230–231.
79. Thomas, S., Pinna, I., Du, N., and Guiver, M.D. (2009) Pure- and mixed-gas permeation properties of a microporous spirobisindane-based ladder polymer (PIM-1). *J. Membr. Sci.*, **333**, 125–131.
80. Cadotte, J., Forester, R., Kim, M. et al. (1988) Nanofiltration membranes broaden the use of membrane separation technology. *Desalination*, **70**, 77.
81. Egli, S., Ruf, A., and Wildmer, F. (1989) Entwicklung und charakterisierung von kompositmembranen für die nano- und ultrafiltration. *Swiss Chem.*, **11** (9), 53.
82. Paul, D.R. (1973) Relation between hydraulic permeation and diffusion in homogeneous swollen membranes. *J. Poly. Sci. Part B: Polym. Phys.*, **11**, 289.
83. Paul, D.R. (1974) Further comments on the relation between hydraulic permeation and diffusion. *J. Poly. Sci. Part B: Polym. Phys.*, **12**, 1221.
84. Kamaruddin, H.D. and Koros, W.J. (1997) Some observations about the application of Fick's first law for membrane separation of multicomponent mixtures. *J. Membr. Sci.*, **135**, 147.
85. Wesselingh, J.A. and Krishna, R. (2000) *Mass Transfer in Multi-Component Mixtures*, Delft University Press, Delft.
86. Paul, D.R. (2004) Reformulation of the solution-diffusion theory of reverse osmosis. *J. Membr. Sci.*, **241**, 371.
87. Teplyakov, V. and Meares, P. (1990) Correlation aspects of the selective gas permeabilities of polymeric materials and membranes. *Gas Sep. Purif.*, **4**, 66.

3

Membranes and Modules

3.1 Introduction

The surge of interest in membrane separation processes that began in the late 1960s was prompted by two developments: first, the ability to produce selective, high flux, essentially defect-free membranes on a large scale, and second, the ability to form these membranes into compact, high-surface-area, economical membrane modules. These breakthroughs in membrane technology took place in the 1960s to early 1970s, as part of the development of reverse osmosis and ultrafiltration. Adaptation of the technology to other membrane processes took place in the 1980s.

Several factors contribute to the successful fabrication of a high-performance membrane module. First, membrane materials with the appropriate chemical, mechanical, and permeation properties must be selected; this choice is very process specific. However, once the membrane material has been selected, the technology required to fabricate this material into a robust, thin, defect-free membrane, and then to package the membrane into an efficient, economical, high-surface-area module is similar for all membrane processes. Therefore, this chapter focuses on methods of forming membranes and membrane modules. The criteria used to select membrane materials for specific processes are described in the chapters covering each application.

In this chapter, membrane preparation techniques are organized by membrane structure: isotropic membranes; anisotropic membranes; metal, ceramic, zeolite, carbon, and glass membranes; and liquid membranes. Isotropic membranes have a uniform composition and structure throughout; such membranes can be porous or dense. Anisotropic (or asymmetric) membranes, on the other hand, consist of a number of layers, each with different structures and permeabilities. A typical anisotropic membrane has a relatively dense, thin surface layer supported on an open, much thicker microporous substrate. The surface layer performs the separation and is the principal barrier to flow through the membrane. The open support layer provides mechanical strength. Ceramic and metal membranes can be either isotropic or anisotropic. However, these membranes are grouped separately from polymeric membranes because their preparation methods are so different.

Liquid membranes are the final membrane category. The selective barrier in these membranes is a liquid phase, usually containing a dissolved carrier that selectively reacts with a specific permeant to enhance its transport rate through the membrane. Liquid membranes are used almost exclusively in carrier facilitated transport processes, so preparation of these membranes is covered in that chapter (Chapter 11).

The membrane classification scheme described above works fairly well. However, a major membrane preparation technique, phase separation, also known as phase inversion, is used to make both isotropic and anisotropic membranes. This technique is covered under anisotropic membranes.

3.2 Isotropic Membranes

3.2.1 Isotropic Nonporous Membranes

Dense nonporous isotropic membranes are not commonly used in membrane separation processes because the transmembrane flux through these relatively thick membranes is too low for practical separation processes. However, they are widely used in laboratory work to characterize membrane properties. In the laboratory, isotropic (dense) membranes are prepared by solution casting or thermal melt-pressing. The same techniques can be used on a larger scale to produce, for example, packaging materials.

3.2.1.1 Solution Casting

Solution casting is often used to prepare small samples of membrane for laboratory characterization experiments. An even film of an appropriate polymer solution is spread across a flat plate with a casting knife. The casting knife consists of a steel blade, resting on two runners, arranged to form a precise gap between the blade and the plate onto which the film is cast. A typical hand-held knife is shown in Figure 3.1. After casting, the solution is left to stand, and the solvent evaporates to leave a thin, uniform polymer film. A detailed description of many types of hand casting knives and simple casting machines is given in the book of Gardner and Sward [1].

The polymer solution used for solution casting should be sufficiently viscous to prevent it from running over the casting plate, so typical polymer concentrations are in the range 15–20 wt%. Preferred solvents are moderately volatile liquids such as acetone, ethyl acetate, and cyclohexane. Films cast from these solutions are dry within a few hours. When the solvent has completely evaporated, the dry film can be lifted from the glass plate. If the film adheres to the plate, soaking in a swelling nonsolvent such as water or alcohol will usually loosen the film.

Solvents with high boiling points such as dimethyl formamide or *N*-methyl pyrrolidone are unsuitable for solution casting, because their low volatility requires long evaporation times. During an extended solvent evaporation time, the cast film can absorb sufficient atmospheric water to precipitate the polymer, producing a mottled, hazy surface. Very volatile solvents such as methylene chloride can also cause problems. Rapid evaporation of the solvent cools the casting solution, causing gelation of the polymer. The result is a film with a mottled, orange-peel-like surface. Smooth films can be obtained with rapidly evaporating solvents by covering the cast film with a glass plate raised 1–2 cm above the film to slow evaporation. Solution-cast film is produced on a larger scale for medical applications, battery separators, or other specialty uses with machinery of the

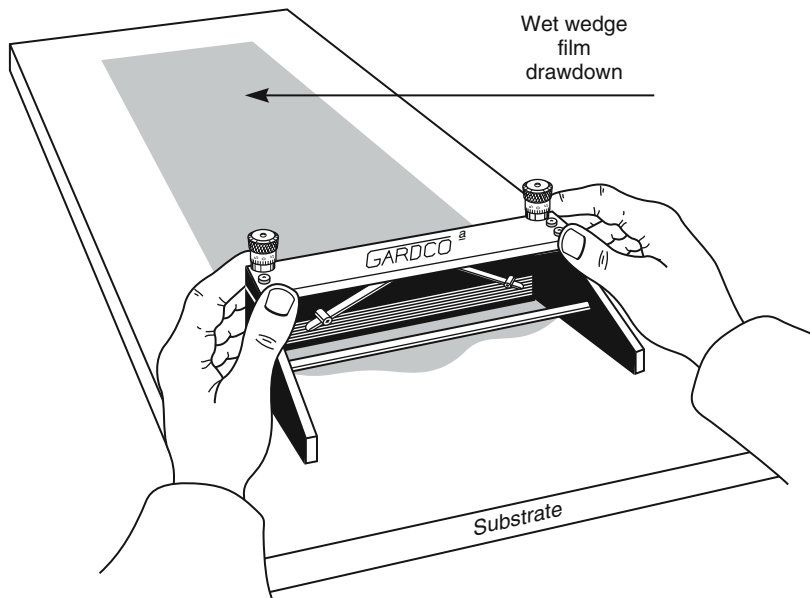


Figure 3.1 A typical hand-casting knife. (Courtesy of Paul N. Gardner Company, Inc., Pompano Beach, FL.)

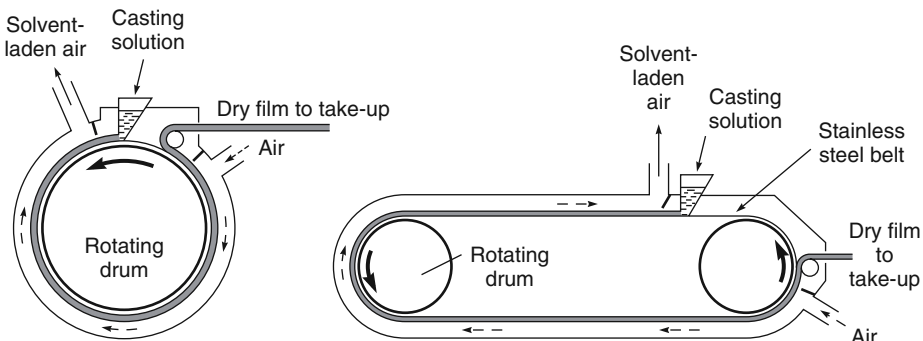


Figure 3.2 Machinery used to make solution-cast film on a commercial scale

type shown in Figure 3.2 [2]. Viscous film is made by this technique. The solution is cast onto the surface of a rotating drum or a continuous polished stainless steel belt. These machines are generally enclosed to control water vapor pickup by the film as it dries and to minimize solvent vapor losses to the atmosphere.

3.2.1.2 Melt Extruded Film

Many polymers, including polyethylene, polypropylene, and nylons, do not dissolve in appropriate solvents at room temperature, so membranes cannot be made by solution casting. To prepare small pieces of film, a laboratory press as shown in Figure 3.3 can be

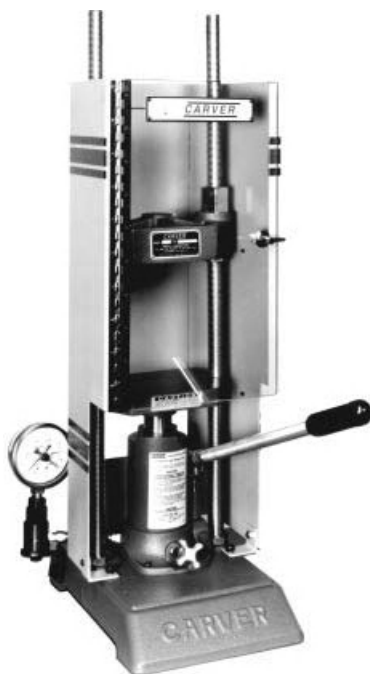


Figure 3.3 A typical laboratory press used to form melt-pressed membranes. (Courtesy of Carver, Inc., Wabash, IN.)

used. The polymer is compressed between two heated plates. Typically, a pressure of 2000–5000 psi is applied for 1–5 minutes, at a plate temperature just below the melting point of the polymer. Melt extrusion is also used on a very large scale to make dense films for packaging applications, either by extrusion as a sheet from a die or as blown film. Detailed descriptions of this equipment can be found in specialized monographs. A good overview is given in the article by Mackenzie in the *Encyclopedia of Chemical Technology* [2].

3.2.2 Isotropic Microporous Membranes

Isotropic microporous membranes have much higher fluxes than isotropic dense membranes and are widely used as microfiltration membranes. Other significant uses are as inert spacers in battery and fuel cell applications and as the rate-controlling element in controlled drug delivery devices.

The most important type of microporous membrane is formed by one of the phase separation techniques discussed in the next section; about half of the isotropic microporous membrane used is made in this way. The remaining types are made by various proprietary techniques, the more important of which are described below.

3.2.2.1 Track-Etch Membranes

Track-etch membranes were developed by the General Electric Corporation Schenectady Laboratory [3]. The two-step preparation process is illustrated in Figure 3.4. A thin

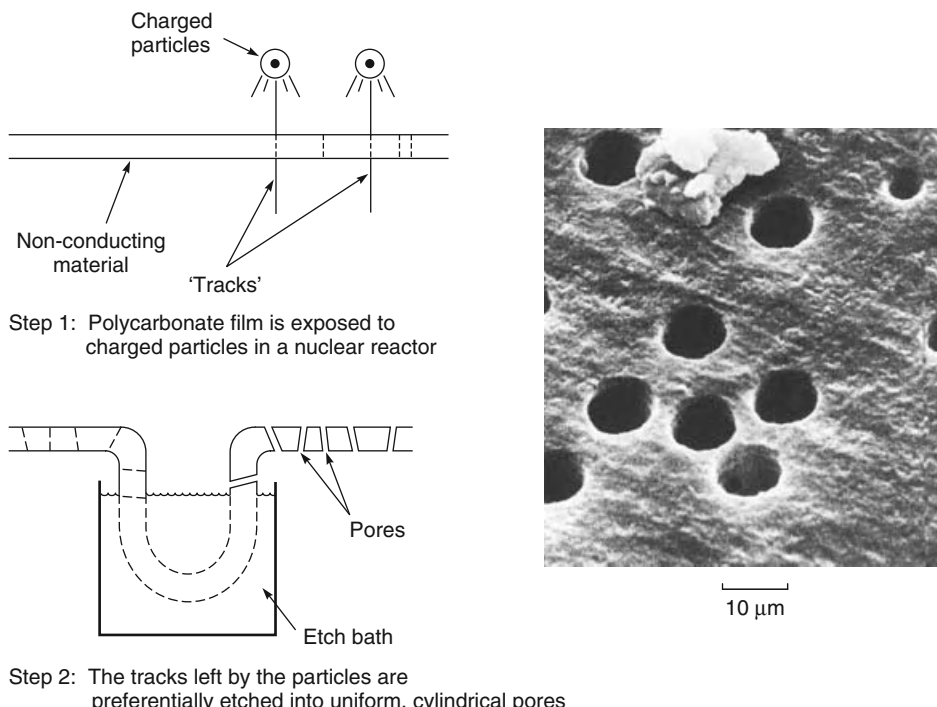


Figure 3.4 Diagram of the two-step process to manufacture nucleation track membranes [4] and photograph of resulting structure. Reprinted with permission from Whatman Ltd. Copyright (2012) Whatman Ltd, part of GE Healthcare.

polymer film is first irradiated with fission particles from a nuclear reactor or other radiation source. The massive particles pass through the film, breaking polymer chains, and leaving behind a sensitized track of damaged polymer molecules. These tracks are much more susceptible to chemical attack than the base polymer material. So when the film is passed through a solution that etches the polymer, the film is preferentially etched along the sensitized nucleation tracks, thereby forming pores. The exposure time of the film to radiation determines the number of membrane pores; the etch time determines the pore diameter [4]. A feature of the track-etch preparation technique is that the pores are uniform cylinders traversing the membrane at right angles. The membrane tortuosity is, therefore, close to one, and all pores have the same diameter. These membranes are an almost perfect screen filter; therefore, they are widely used to measure the number and type of suspended particles in air or water. A known volume of fluid is filtered through the membrane, and all particles larger than the pore diameter are captured on the surface of the membrane so they can be easily identified and counted under a microscope. To minimize the formation of doublet holes produced when two nucleation tracks are close together, the membrane porosity is usually kept relatively low, about 5% or less. This low porosity results in low fluxes. General Electric, the original developers of these membranes, assigned the technology to a spin-off company, the Nuclepore Corporation, in 1972 [5]. Nuclepore® membranes remain the principal commercially available

track-etch membranes. Polycarbonate or polyester films are usually used as the base membrane material and sodium hydroxide as the etching solution. Other materials can also be used; for example, etched mica has been used in research studies.

3.2.2.2 *Expanded-Film Membranes*

Expanded-film membranes are made from crystalline polymers by an orientation and annealing process. A number of manufacturers produce porous membranes by this technique. The original development began with a group at Celanese, which made microporous polypropylene membranes by this process under the trade name Celgard® [6]. In the first step of the process, a highly oriented film is produced by extruding polypropylene at close to its melting point coupled with a very rapid drawdown. The crystallites in the semi-crystalline polymer are then aligned in the direction of orientation. After cooling and annealing, the film is stretched at right angles a second time, up to 300%. During this second elongation the amorphous regions between the crystallites are deformed, forming slit-like voids, 250–2500 Å wide, between the polymer crystallites. The pore size of the membrane is controlled by the rate and extent of the second elongation step. The formation process is illustrated in Figure 3.5. This type of membrane is also made from poly(tetrafluoroethylene) film by W. L. Gore and sold under the trade name Gore-Tex® [7]. Expanded-film membrane was originally produced as rolled flat sheets. More recently, the process has also been adapted to the production of hollow fibers [8, 9]; Membrana produces this type of fiber on a large scale for use in blood oxygenator equipment (Chapter 12) and membrane contactors (Chapter 13). Gore-Tex® poly(tetrafluoroethylene) film is widely used as a water vapor permeable (that is, breathable) but liquid water impermeable fabric. These membranes are also used as separators in batteries. The commercial success of these products has motivated a number of other companies to produce similar materials [10, 11].

3.2.2.3 *Template Leaching*

Template leaching is another method of producing isotropic microporous membranes from insoluble polymers such as polyethylene, polypropylene, and poly(tetrafluoroethylene). In this process, a homogeneous melt is prepared from a mixture of the polymeric membrane matrix material and a leachable component. To finely disperse the leachable component in the polymer matrix, the mixture is often homogenized, extruded, and pelletized several times before final extrusion as a thin film. After formation of the film, the leachable component is removed with a suitable solvent, and a microporous membrane is formed [12–14]. The leachable component can be a soluble, low molecular weight solid, a liquid such as liquid paraffin, or even a polymeric material such as polystyrene. A drawing of a template leaching membrane production machine is shown in Figure 3.6.

3.3 Anisotropic Membranes

Anisotropic membranes are layered structures in which the porosity, pore size, or even membrane composition change from the top to the bottom surface of the membrane. Usually anisotropic membranes have a thin, selective layer supported on a much thicker,

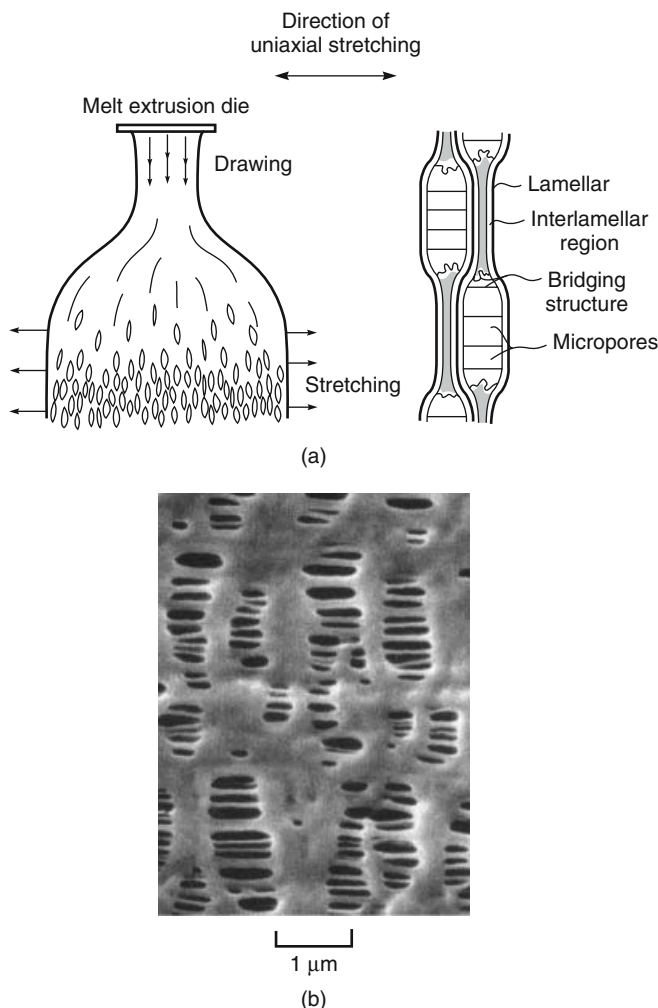


Figure 3.5 (a) Preparation method of a typical expanded polypropylene film membrane, in this case Celgard®. (b) Scanning electron micrograph of the microdefects formed on uniaxial stretching of films. Reprinted with permission from [6]. Copyright (1974) American Chemical Society.

highly permeable microporous substrate. Because the selective layer is very thin, membrane fluxes are high. The microporous substrate provides the strength required for handling the membrane. The importance of anisotropic membranes was not recognized until Loeb and Sourirajan prepared the first high-flux, anisotropic reverse osmosis membranes around 1960, by what is now known as the Loeb–Sourirajan technique [15]. Hindsight makes it clear that some of the membranes produced in the 1930s and 1940s were also anisotropic. Loeb and Sourirajan's discovery was a critical breakthrough in membrane technology. Their anisotropic reverse osmosis membranes were an order

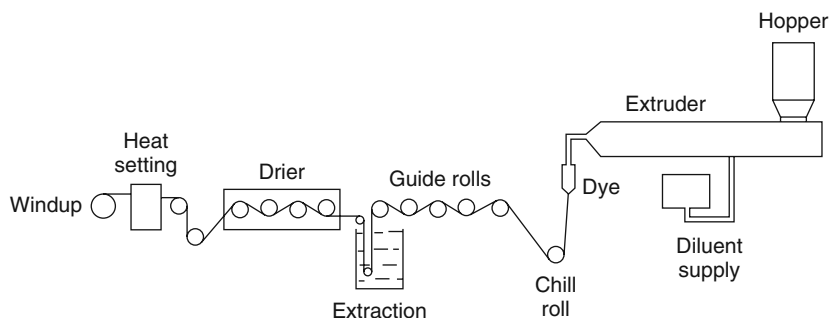


Figure 3.6 Flow schematic of a melt extruder system used to make polypropylene membranes by template leaching [14]

of magnitude more permeable than the isotropic membranes produced previously from the same materials. For a number of years the Loeb–Sourirajan technique was the only method of making anisotropic membranes, but the demonstrated benefits of the anisotropic structure encouraged the development of other methods. Improvements in anisotropic membrane preparation methods and properties were accelerated by the availability in the 1960s of the scanning electron microscope (SEM), which allowed the effects on structure of changes in the membrane formation process to be assessed easily.

Membranes made by the Loeb–Sourirajan process consist of a single membrane material, but the porosity and pore size change in different layers of the membrane. Anisotropic membranes made by other techniques often consist of layers of different materials which serve different functions. Important examples are reverse osmosis membranes made by the interfacial polymerization process discovered by Cadotte [16] and gas separation membranes made by the solution-coating processes developed by Ward *et al.* [17], Francis [18], and Riley *et al.* [19]. The following sections cover four types of anisotropic membranes:

- **Phase separation membranes:** This category includes membranes made by the Loeb–Sourirajan technique involving precipitation of a casting solution by immersion in a nonsolvent (water) bath. Also covered are a variety of related techniques such as precipitation by solvent evaporation, precipitation by absorption of water from the vapor phase, and precipitation by cooling.
- **Interfacial composite membranes:** This type of anisotropic membrane is made by polymerizing an extremely thin layer of polymer at the surface of a microporous support polymer.
- **Solution-coated composite membranes:** To prepare these membranes, one or more thin, dense polymer layers are solution coated onto the surface of a microporous support.
- **Other anisotropic membranes:** This category covers membranes made by a variety of specialized processes, such as plasma deposition, in the laboratory or on a small industrial scale, to prepare anisotropic membranes for specific applications.

3.3.1 Phase separation membranes

The Loeb–Sourirajan technique is now recognized as a special case of a more general class of membrane preparation, best called the phase separation process, but sometimes

called the phase inversion process or the polymer precipitation process. The term phase separation describes the process most clearly, namely, changing a one-phase casting solution into two separate phases. In all phase separation processes, a liquid polymer solution is precipitated into two phases: a solid, polymer-rich phase that forms the matrix of the membrane and a liquid, polymer-poor phase that forms the membrane pores.

Precipitation of the cast liquid polymer solution to form the anisotropic membrane can be achieved in several ways, as summarized in Table 3.1. Precipitation by immersion in a bath of water was the technique discovered by Loeb and Sourirajan, but precipitation can also be caused by absorption of water from a humid atmosphere. A third method is to cast the film as a hot solution. As the cast film cools, a point is reached at which precipitation occurs to form a microporous structure; this method is sometimes called thermally induced phase separation (TIPS). Finally, evaporation of one of the solvents in the casting solution can be used to cause precipitation. In this technique, the casting solution consists of a polymer dissolved in a mixture of a volatile good solvent and a less volatile nonsolvent (typically water or alcohol). When a film of the solution is cast and allowed to evaporate, the volatile good solvent evaporates first, the film then becomes enriched in the nonvolatile nonsolvent, and finally precipitates. Many combinations of these processes have also been developed. For example, a cast film placed in a humid atmosphere can precipitate partly because of water vapor absorption but also because of evaporation of one of the more volatile components.

3.3.1.1 Polymer Precipitation by Water (the Loeb–Sourirajan Process)

The first phase separation membrane was developed at UCLA from 1958 to 1960 by Sidney Loeb, then working on his Master's degree, and Srinivasa Sourirajan, then a post-doctoral researcher [15]. In their process, now called the Loeb–Sourirajan technique, precipitation is induced by immersing the cast film of polymer solution in a water bath. In the original Loeb–Sourirajan process, a solution containing 20–25 wt% cellulose acetate dissolved in a water-miscible solvent was cast as a thin film on a glass plate. The film was left to stand for 10–100 seconds to allow some of the solvent to evaporate, after which the film was immersed in a water bath to precipitate the film and form the membrane. The membrane was usually post-treated by annealing in a bath of hot water. The steps of the process are illustrated in Figure 3.7.

Table 3.1 Phase separation membrane preparation procedures

Procedure	Process
Water precipitation (the Loeb–Sourirajan process)	The cast polymer solution is immersed in a nonsolvent bath (typically water). Absorption of water and loss of solvent cause the film to rapidly precipitate from the top surface down
Water vapor absorption	The cast polymer solution is placed in a humid atmosphere. Water vapor absorption causes the film to precipitate
Thermal gelation	The polymeric solution is cast hot. Cooling causes precipitation
Solvent evaporation	A mixture of solvents is used to form the polymer casting solution. Evaporation of one of the solvents after casting changes the solution composition and causes precipitation

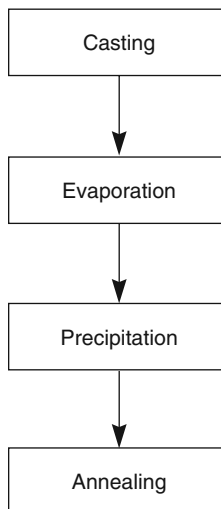
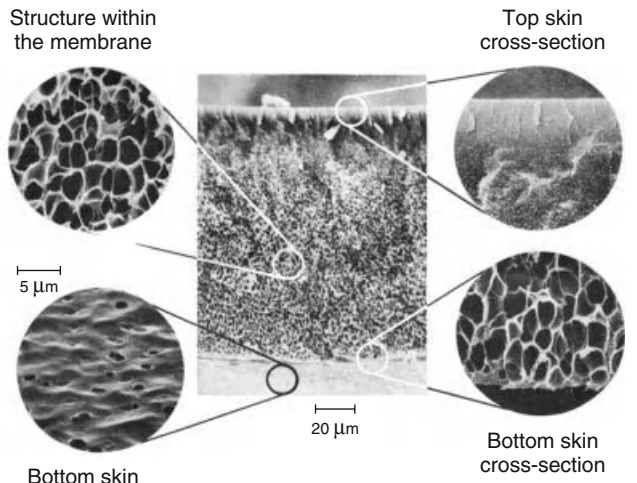


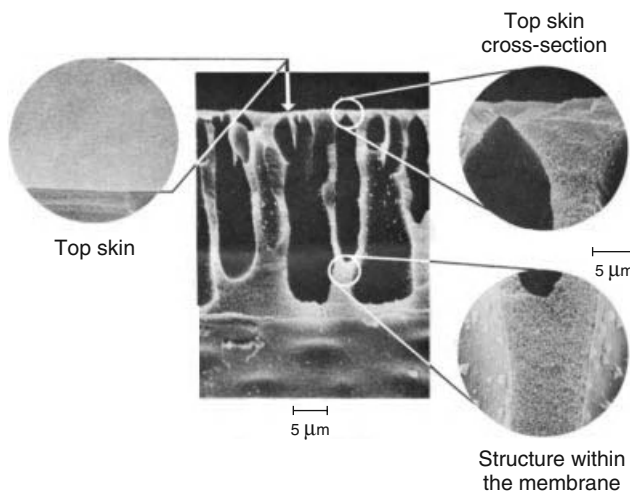
Figure 3.7 Process scheme used to form Loeb–Sourirajan water precipitation phase separation membranes [15]

The Loeb–Sourirajan process remains by far the most important membrane preparation technique. The process is part of the overall membrane preparation procedure for almost all reverse osmosis and ultrafiltration membranes, and many gas separation membranes. Reverse osmosis and gas separation membranes made by this technique consist of a completely dense top surface layer (the skin) on top of a microporous support structure. Ultrafiltration membranes, membranes used as supports for solution coating, and interfacial polymerization membranes have the same general anisotropic structure, but the skin layer is very finely microporous, typically with pores in the 10–200 Å diameter range. Also, the porous substrate of ultrafiltration membranes is usually more open, often consisting of large finger-like cavities extending from just under the selective skin layer to the bottom surface of the membrane. Scanning electron micrographs of typical sponge-structure reverse osmosis type and finger-structure ultrafiltration type membranes are shown in Figure 3.8 [20]. These photographs show how small changes in the casting solution can produce major differences in membrane properties. Both membranes are prepared from an aromatic polyamide-dimethylacetamide casting solution (Nomex® from DuPont (Wilmington, DE)), but the polymer concentration in the solutions is different.

The Loeb–Sourirajan water precipitation membranes shown in Figure 3.8 were made by casting the membranes onto glass plates. This procedure is still used in the laboratory, but for commercial production, large casting machines produce rolls of membrane up to 5000 m long and 1–2 m wide. A simplified diagram of a casting machine is shown in Figure 3.9. The polymer solution is cast onto a moving nonwoven paper web. The nonwoven paper provides mechanical strength so the membrane can be easily handled. The cast film is precipitated by immersion in a water bath. The water precipitates the top surface of the cast film rapidly, forming the dense, selective skin. This skin slows entry of water into the underlying polymer solution, which precipitates much more slowly and forms a more porous substructure. Depending on the polymer, the casting solution,



(a) Sponge structure cast from 22 wt% Nomex in dimethylacetamide



(b) Finger structure cast from 18 wt% Nomex in dimethylacetamide

Figure 3.8 Scanning electron micrographs of aromatic polyamide (Nomex®, Du Pont) Loeb–Sourirajan membranes cast from 22 and 18 wt% polymer in dimethylacetamide. Reprinted from Desalination, 16, H. Strathmann, K. Kock, P. Amar and R.W. Baker, The formation mechanism of anisotropic membranes, p. 179, Copyright 1975. Reprinted from [20]. Copyright (1975) Elsevier.

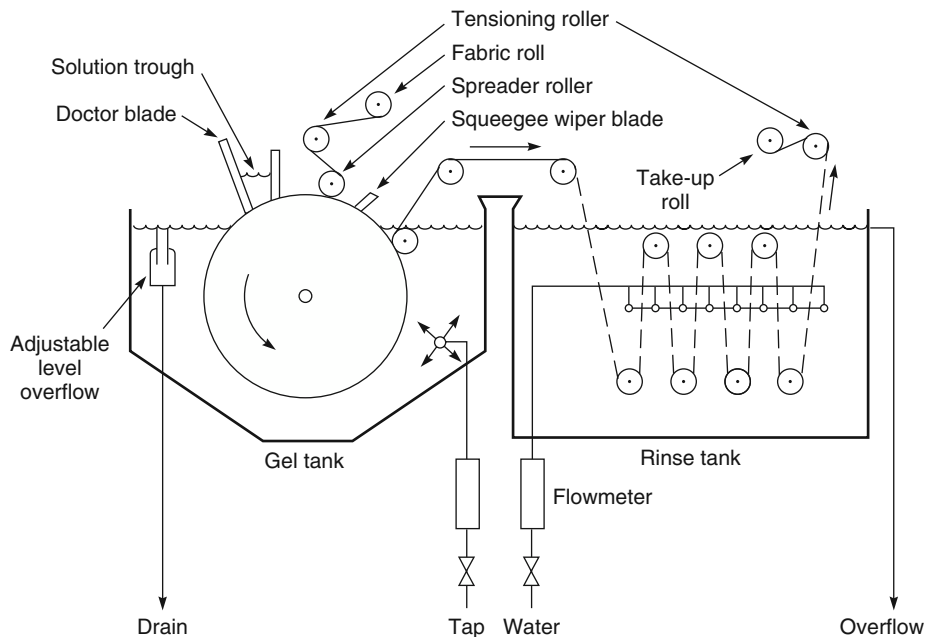


Figure 3.9 Schematic of Loeb–Sourirajan membrane casting machine used to prepare reverse osmosis or ultrafiltration membranes. A knife and trough are used to coat the casting solution onto a nonwoven paper web. The coated web then enters the water-filled gel tank, where the casting solution precipitates. After the membrane has formed, it is washed thoroughly to remove residual solvent before being wound up on the take-up roll

and other parameters, the thickness of the dense skin varies from 0.1 to 1.0 μm . Casting machine speeds vary from as low as 1–2 m/min for slowly precipitating casting solutions, such as cellulose acetate, to 10 m/min for rapidly precipitating casting solutions, such as polysulfone. A listing of some typical casting solutions and precipitation conditions for membranes made by the Loeb–Sourirajan technique is given in Table 3.2 [15, 21–24].

Small casting machines often apply the casting solution with a doctor blade as shown in Figure 3.10a. Large industrial machines use a curtain coating technique of the type shown in Figure 3.10b. The membrane made with this coating procedure is less sensitive to defects in the paper support or variations in the support paper thickness.

Since the discovery of the Loeb–Sourirajan technique in the 1960s, development of the technology has proceeded on two fronts. Industrial users of the technology have generally taken an empirical approach, making improvements in the technique based on trial and error experience. Concurrently, theories of membrane formation based on fundamental studies of the precipitation process have been developed. These theories originated with the early industrial developers of membranes at Amicon [20, 23, 25] and were then taken up at a number of academic centers. Much of the recent academic work is so complex that many industrial producers of phase separation membranes no longer follow these developments regularly.

Table 3.2 Historically important examples of conditions for preparation of solution-precipitation (Loeb–Sourirajan) membranes

Casting solution composition	Precipitation conditions	Application and comments
22.2 wt% cellulose acetate (39.8 wt% acetyl polymer)	3 min evaporation, precipitate into 0°C water, anneal for 5 min at 65–85°C	The first Loeb–Sourirajan reverse osmosis membrane [15]
66.7 wt% acetone		
10.0 wt% water		
1.1 wt% magnesium perchlorate		
25 wt% cellulose acetate (39.8 wt% acetyl polymer)	0.5–2 min evaporation, cast into 0°C water, anneal for 5 min at 65–85°C	The Manjikian formulation widely used in early 1970s for reverse osmosis membranes [21]
45 wt% acetone		
30 wt% formamide		
8.2 wt% cellulose acetate (39.8 wt% acetyl polymer)	Up to 3 min evaporation at 10°C, precipitation into an ice bath, anneal at 85–90°C for 3 min	A high-performance reverse osmosis cellulose acetate blend membrane [22]
8.2 wt% cellulose triacetate (43.2 wt% acetyl polymer)		
45.1 wt% dioxane		
28.7 wt% acetone		
7.4 wt% methanol		
2.5 wt% maleic acid		
15 wt% polysulfone (Udell P 1700)	Cast into 25°C water bath. No evaporation or annealing step necessary	An early ultrafiltration membrane formulation [23]. Similar polysulfone-based casting solutions are still widely used
85 wt% N-methyl-2- pyrrolidone		
20.9 wt% polysulfone		
33.2 wt% dimethyl formamide		
33.2 wt% tetrahydrofuran		
12.6 wt% ethanol	Forced evaporation with humid air 10–15 s. Precipitate into 20°C water	A high-performance gas separation membrane with a completely dense nonporous skin ~1000 Å thick [24]

3.3.1.2 Empirical Approach to Membrane Formation by Water Precipitation

Over the years, several rules of thumb have developed to guide producers of solution precipitation membranes. These rules can be summarized as follows:

- **Choice of polymer.** The ideal polymer is a tough, amorphous, but not brittle, thermoplastic with a glass transition temperature more than 50°C above the expected use temperature. A high molecular weight is important. Commercial polymers made for injection molding have molecular weights in the 30 000–40 000 Da range, but, for solution precipitation, polymers with higher molecular weights are usually preferable. If the polymer is crystalline or a rigid glass, the resulting membrane may be too brittle and will break if bent during later handling. The polymer must also be soluble in a suitable

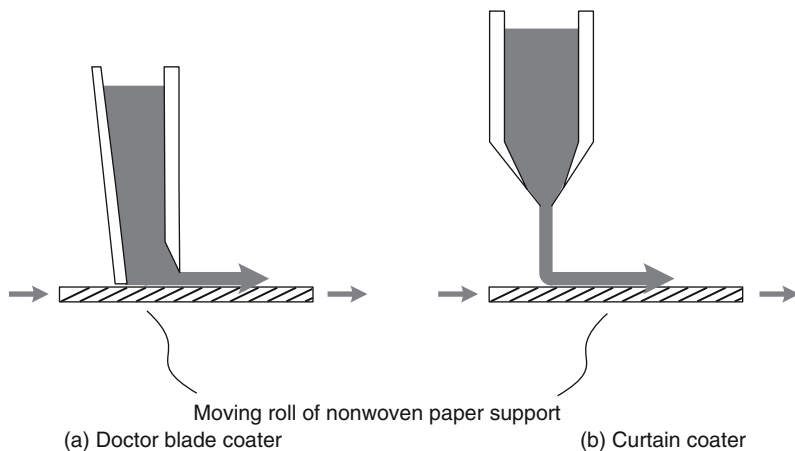


Figure 3.10 Doctor blade coating of casting solution onto a moving paper web is simple and easy, but curtain coaters give a better product with large scale production equipment

water-miscible solvent. Polymers that meet these specifications include cellulose acetate, polysulfone, poly(vinylidene fluoride), polyetherimide, and aromatic polyamides.

- **Choice of casting solution solvent.** Generally the best casting solution solvents are aprotic solvents such as dimethyl formamide, *N*-methyl pyrrolidone, and dimethyl acetamide. These solvents dissolve a wide variety of polymers, and casting solutions based on these solvents precipitate rapidly when immersed in water to give porous, anisotropic membranes. Casting solutions using low-solubility-parameter solvents, such as tetrahydrofuran, acetone, dioxane, and ethyl formate, are generally not appropriate. Such casting solutions precipitate slowly and give relatively nonporous membranes. However, small amounts of these solvents may be added as casting solution modifiers (see below). Figure 3.11 illustrates the apparent correlation between solvent solubility parameter and membrane porosity as demonstrated by So *et al.* [26].

Increasing the polymer casting solution concentration always reduces the porosity and flux of the membrane. Typical concentrations for porous ultrafiltration membranes are in the range of 15–20 wt%. Polymer casting solution concentrations for reverse osmosis or gas separation membranes are higher, generally about 25 wt%, and casting solutions used to make hollow fiber membranes by spinning a hot solution at 60–80°C may contain as much as 35 wt% polymer.

- **Precipitation medium.** Water is almost always the casting solution precipitation medium. Some work has been done with organic solvents, particularly to form hollow fiber membranes for which the mechanical and safety problems of handling an organic solvent precipitation bath and limiting atmospheric emissions are more easily controlled than in flat sheet casting. In general, the results obtained with nonaqueous precipitation baths have not justified the increased complexity of the process. Organic-based solvent precipitation media such as methanol or isopropanol almost always precipitate the casting solution more slowly than water, and the resulting membranes are usually denser, less anisotropic, and lower flux than membranes precipitated with water.

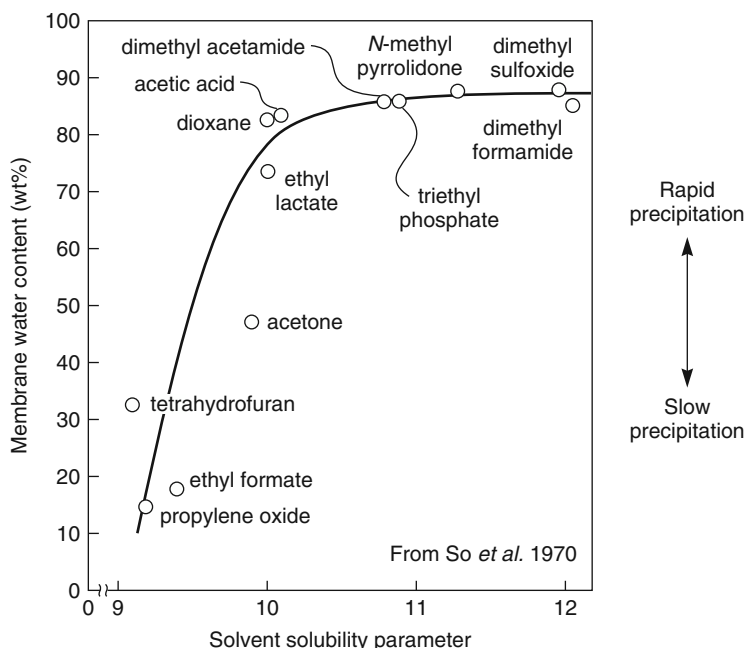


Figure 3.11 The porosity of cellulose acetate membranes cast from 15 wt% solutions with various solvents. The same trend of high porosity and rapid precipitation with high solubility-parameter solvents was seen with a number of other membrane materials [26]

The temperature of the water used to precipitate the casting solution is important; this temperature is controlled in commercial membrane plants. Generally low-temperature precipitation produces lower flux, more retentive membranes. For this reason, chilled water is sometimes used to prepare cellulose acetate reverse osmosis membranes.

- **Casting solution modifiers.** Membrane properties are often tailored by adding small amounts of modifiers to the casting solution. The casting solutions shown in Table 3.2 contain two to four components, but modern commercial casting solutions may be more complex. Even though the solution may contain only 5–10 wt% modifiers, these modifiers can change the membrane performance significantly. This aspect of membrane preparation is a black art, and most practitioners have their preferred ingredients. Addition of low-solubility-parameter solvents such as acetone, tetrahydrofuran, or dioxane will normally produce denser, more retentive membranes. Increasing the polymer concentration of the casting solution will also make the membrane more dense. Addition of salts such as zinc chloride and lithium chloride usually gives more open membranes. Polymeric additives – commonly poly(vinyl pyrrolidone) or poly(ethylene glycol) – may also be used; by making the casting solution more viscous, these polymers can eliminate the large finger pores shown in Figure 3.8. Also, although most of these water-soluble polymers and salts are removed during precipitation and washing of the membrane, a portion remains trapped, making the final membrane more hydrophilic and often less brittle.

The nature of the nonwoven support paper can be an important variable. Polyester paper is the most commonly used material, but nonwoven polypropylene and polyphenylene sulfide papers are also used. If the paper is too coarse, membrane pinholes can result; if the paper is too fine, adhesion between the paper and the microporous membrane layer will be poor.

When developing membranes from a new polymer, practitioners of the empirical approach usually prepare a series of trial casting solutions based on past experience with similar polymers. Membrane films are made by casting onto glass plates, followed by precipitation in a water bath. The casting solutions most likely to yield good membranes are often immediately apparent. The rate of precipitation is important. Slow precipitation produces dense, more isotropic membranes; rapid precipitation produces porous, anisotropic membranes. The appearance and mechanical properties of the membrane surface – shine, brittleness, and thickness – compared to casting solution thickness also provide clues to the membrane structure. Based on these trials, one or more casting solutions will be selected for systematic parametric development.

3.3.1.3 Theoretical Approach to Membrane Formation by Water Precipitation

Over the years, several approaches have been used to rationalize the formation of Loeb–Sourirajan (solution precipitation) and other phase inversion membranes. Most have involved the polymer-solvent-precipitation medium phase diagrams popularized by Michaels [23], Strathmann [20, 25, 27], and Smolders [28–30]. In this approach, the change in composition of the casting solution as membrane formation takes place is tracked as a path through the phase diagram. The path starts at a point representing the original casting solution and finishes at a point representing the composition of the final membrane. The casting solution composition moves to the final membrane composition by losing solvent and gaining water.

A typical three-component phase diagram for the components used to prepare Loeb–Sourirajan membranes is shown in Figure 3.12. The corners of the triangle represent the three pure components – polymer, solvent, and nonsolvent (water); points within the triangle represent mixtures of the three components. The diagram has two principal regions: a one-phase region, in which all components are miscible, and a two-phase region, in which the system separates into a solid (polymer-rich) phase and a liquid (polymer-poor) phase. During precipitation of the membrane casting solution, the solution loses solvent and gains water. The casting solution moves from a composition in the one-phase region to a composition in the two-phase region.

Although the one-phase region in the phase diagram is thermodynamically continuous, for practical purposes it can be conveniently subdivided into a liquid polymer solution region, a polymer gel region, and a glassy solid polymer region. Thus, in the low-polymer-concentration region, typical of the original casting solution, the compositions are viscous liquids. But, if the concentration of polymer is increased, the viscosity of compositions in the one-phase region increases rapidly, reaching such high values that the system can be regarded as a solid gel. The transition between the fluid and gel regions is arbitrary, but generally can be placed at a polymer concentration of 30–40 wt%. If the one-phase solution contains more than 90 wt% polymer, the swollen polymer gel may become so rigid that the polymer chains can no longer rotate. The polymer gel then becomes a solid polymer glass.

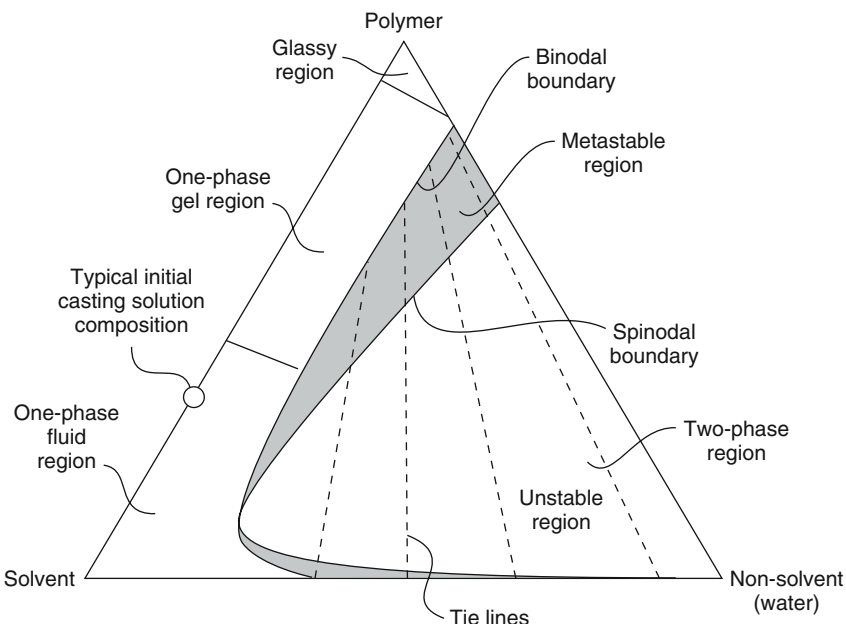


Figure 3.12 Schematic of the three-component phase diagram often used to rationalize the formation of water-precipitation phase separation membranes. In the two-phase region of the diagram, tie lines link the precipitated polymer-rich phase with its equilibrium polymer-poor phase

During the precipitation process, the casting solution enters the two-phase region of the phase diagram by crossing the so-called binodal boundary. This brings the casting solution into a metastable two-phase region. Polymer solution compositions in this region are thermodynamically unstable, but will not normally precipitate unless well nucleated. The metastable region in the phase diagrams of low-molecular weight materials is very small, but can be large for high molecular weight materials. As more solvent leaves the casting solution and water enters the solution, the composition crosses into another region of the phase diagram in which a one-phase solution is always thermodynamically unstable. In this region, polymer solutions spontaneously separate into two phases with compositions linked by tie lines. The boundary between the metastable and unstable regions is called the spinodal boundary.

Thus, the membrane precipitation process is a series of steps. First, solvent exchange with the precipitation medium occurs. Then, as the composition enters the two-phase region of the phase diagram, phase separation or precipitation begins. The time taken for solvent–water exchange before precipitation occurs can be measured because the membrane turns opaque as soon as precipitation begins. Depending on the casting solution composition, the time to first precipitation may be almost instantaneous to as long as 30–60 seconds. Initially, the polymer phase that separates on precipitation may be a viscous liquid. Portions of the precipitated polymer are then able to flow and agglomerate. Later, the precipitated polymer phase will be a semi-solid gel; further desolvation of the

polymer phase converts the polymer to a relatively solid gel phase, but the membrane structure does not change. The solid polymer phase forms the matrix of the final membrane, and the liquid solvent–nonsolvent phase forms the pores. Precipitation of polymer–solvent mixtures is further complicated by slow kinetics caused by the viscosity of polymer solutions and by thermodynamic effects that allow metastable solutions to exist for a prolonged time without precipitating. Much has been made of these effects in a number of theoretical papers, but application to concretely predict membrane permeation properties has proven difficult.

The original approach of Strathmann *et al.* [25] was to present the process of membrane formation as a line through the phase diagram. This approach is shown in Figure 3.13. During membrane formation, the composition changes from a composition A, which represents the initial casting solution composition, to a composition D, which represents the final membrane composition. At composition D, the two phases are in equilibrium: a solid (polymer-rich) phase, which forms the matrix of the final membrane, represented by point S, and a liquid (polymer-poor) phase, which constitutes the membrane pores filled with precipitant, represented by point L. The position of composition D on the line S–L determines the overall porosity of the membrane. The entire precipitation process is represented by the path A–D, along which the solvent is exchanged by the precipitant. The point B along the path is the concentration at which the polymer initially precipitates. As precipitation proceeds, more solvent is lost, and precipitant is imbibed by the polymer-rich phase, raising the viscosity. At some point, the viscosity is high enough for the precipitated polymer to be regarded as a solid. This

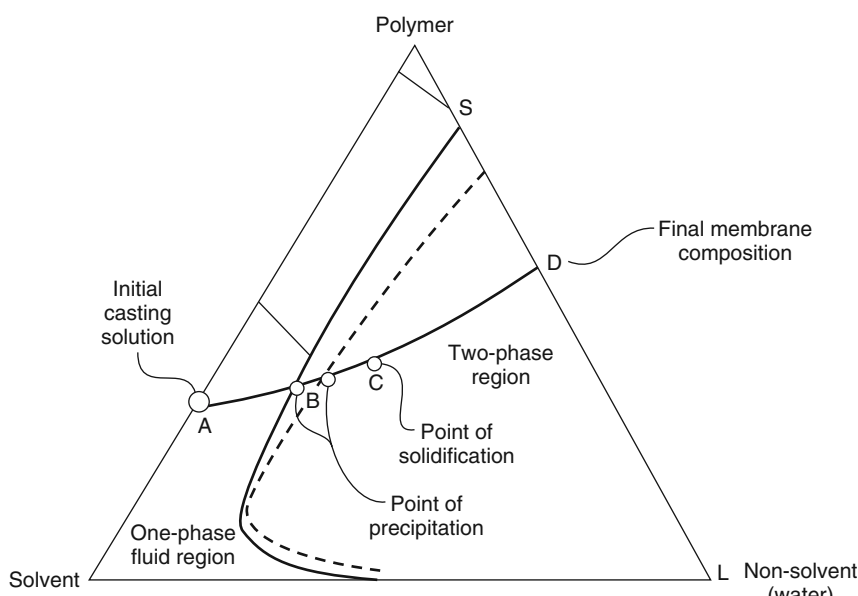


Figure 3.13 Membrane formation in water-precipitation membranes was first rationalized as a path through the three-component phase diagram from the initial polymer casting solution (A) to the final membrane (D) [25]

composition is at C in Figure 3.13. Once the precipitated polymer solidifies, further bulk movement of the polymer is hindered.

The precipitation path in Figure 3.13 is shown as a single line representing the average composition of the whole membrane. In fact, the rate of precipitation and the precipitation path through the phase diagram differ at different points in the membrane. When the cast film of polymer solution is exposed to the precipitation medium, the top surface begins to precipitate. This surface layer precipitates rapidly, so the two phases formed on precipitation do not have time to agglomerate. The resulting structure is finely micro-porous. However, the precipitated surface layer then becomes a barrier that slows further loss of solvent and imbibition of nonsolvent by the cast film. The result is increasingly slow precipitation from the top surface to the bottom surface of the film. As precipitation slows, the average pore size increases because the two phases formed on precipitation have more time to separate before the polymer phase gels. The differences between the precipitation rates and the pathway taken at different places in the casting solution mean that the precipitation process is best represented by the movement of a line through the phase diagram rather than a single point. This concept was developed in a series of papers on phase-separation membranes by Smolders and coworkers at Twente University [28–30]. The movement of this line is illustrated in Figure 3.14 [28]. At time t_2 , for example, a few seconds after the precipitation process has begun, the top surface of the polymer film has almost completely precipitated, and the composition of this surface layer is close to the polymer nonsolvent axis. On the other hand, at the bottom surface

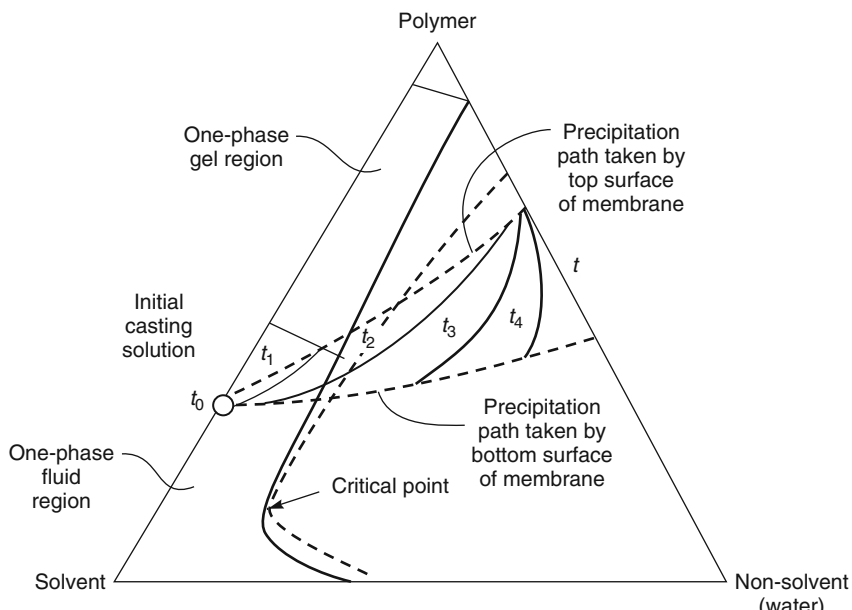


Figure 3.14 The surface layer of water-precipitation membranes precipitates faster than the underlying substrate. The precipitation pathway is best represented by the movement of a line through the three-component phase diagram [28]

of the film where precipitation has only just begun, the composition is still close to that of the original casting solution composition.

The precipitation pathways taken by the solutions at the top and bottom surfaces of the membrane are shown in Figure 3.14. The solution at the top surface of the membrane enters the gel region of the phase diagram before the precipitation boundary is reached. On precipitation, the polymer gel densifies, but no micropores are formed. The solution at the bottom surface of the membrane remains in the one-phase fluid solution region of the phase diagram until the precipitation boundary is reached. When precipitation occurs, the solution is fluid and can be separated into a polymer-rich phase and a polymer-poor phase. The polymer-poor phase eventually forms the pores in the final microporous membrane.

In Figure 3.14, the precipitation pathway enters the two-phase region of the phase diagram above the critical point at which the binodal and spinodal lines intersect. This is important because it means that precipitation will occur as a liquid droplet in a continuous polymer-rich phase. If dilute casting solutions are used, in which the precipitation pathway enters the two-phase region of the phase diagram below the critical point, precipitation produces polymer gel particles in a continuous liquid phase. The membrane that forms is then weak and powdery.

The simplified treatment of membrane formation using the three-component phase diagram given above is about as far as this approach can be usefully taken. Experimental measurement of the path taken by the membrane during the formation process is difficult. Recently, much effort has been made to calculate these pathways through the phase diagrams and to use the results to predict the effect of membrane formation variables on the fine membrane structure. As a quantitative predictor of membrane performance, this approach has failed. However, as a tool to qualitatively rationalize the complex interplay of factors determining membrane performance, the phase diagram approach has proven useful. Many of the recent papers describing the application of the phase diagram approach to membrane formation are a heavy read for industrial membrane producers faced with real-world problems. This literature is reviewed in detail elsewhere [28, 31–34].

3.3.1.4 *Polymer Precipitation by Cooling*

Perhaps the simplest solution-precipitation membrane preparation technique is thermal gelation, often called thermally induced phase separation, in which a film is cast from a hot, one-phase polymer/solvent solution. As the cast film cools, the polymer precipitates, and the solution separates into a polymer matrix phase containing dispersed pores filled with solvent. Because cooling is usually uniform throughout the cast film, the resulting membranes are relatively isotropic microporous structures with pores that can be controlled to within 0.1–10 µm. Macrovoids that often occur in Loeb–Sourirajan-type membranes are usually avoided.

The precipitation process that forms thermal gelation membranes can be represented by the phase diagram shown in Figure 3.15 and described in an early Akzo patent to Castro [35]. This is a simplified drawing of the actual phase diagram, described later in papers by Lloyd *et al.* [36] and others [34, 37–39]. The phase diagram shows the metastable region between the binodal and spinodal phase boundaries discussed in reference to Figure 3.12, with additional complications caused by the crystalline nature of many of the polymers used

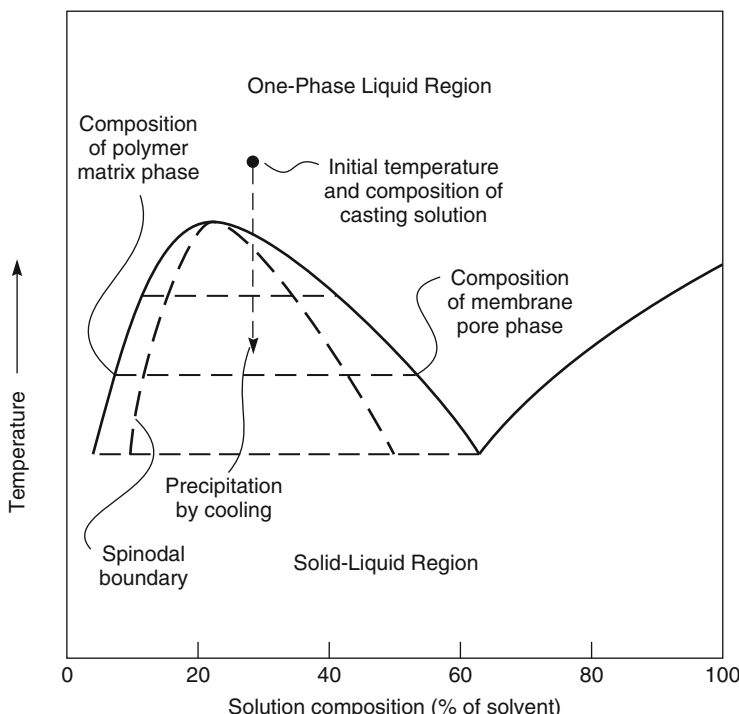


Figure 3.15 Phase diagram showing the composition pathway traveled by the casting solution during precipitation by cooling (thermal gelation)

to form thermal phase-separation membranes. The pore volume in the final membrane is determined mainly by the initial composition of the solution, because this determines the ratio of the polymer to liquid phase in the cooled film. However, the spatial distribution and size of the pores are determined largely by the rate of cooling and, hence, precipitation of the film. In general, more rapid cooling produces smaller membrane pores and greater membrane anisotropy [40, 41]. Membrane preparation by thermal gelation is possible with many polymers, but the technique is used mainly to make membranes from polyethylene, polypropylene, and poly(vinylidene fluoride).

Polymer precipitation by cooling to produce microporous membranes was first developed and commercialized by Akzo [35, 40], which produced microfiltration polypropylene and poly(vinylidene fluoride) membranes marketed under the trade name Accurel®. Flat sheet and hollow fiber membranes were made. Polypropylene membranes are prepared from a solution of polypropylene in *N,N*-bis(2-hydroxyethyl)tallow amine. The amine and polypropylene form a clear solution at temperatures above 100–150°C. Upon cooling, the solvent and polymer phases separate to form a microporous structure. If the solution is cooled slowly, an open cell structure of the type shown in Figure 3.16a results. The interconnecting passageways between cells are generally in the micrometer size range. If the solution is cooled and precipitated rapidly, a much finer structure is formed, as shown in Figure 3.16b. The rate of cooling is, therefore, a key parameter

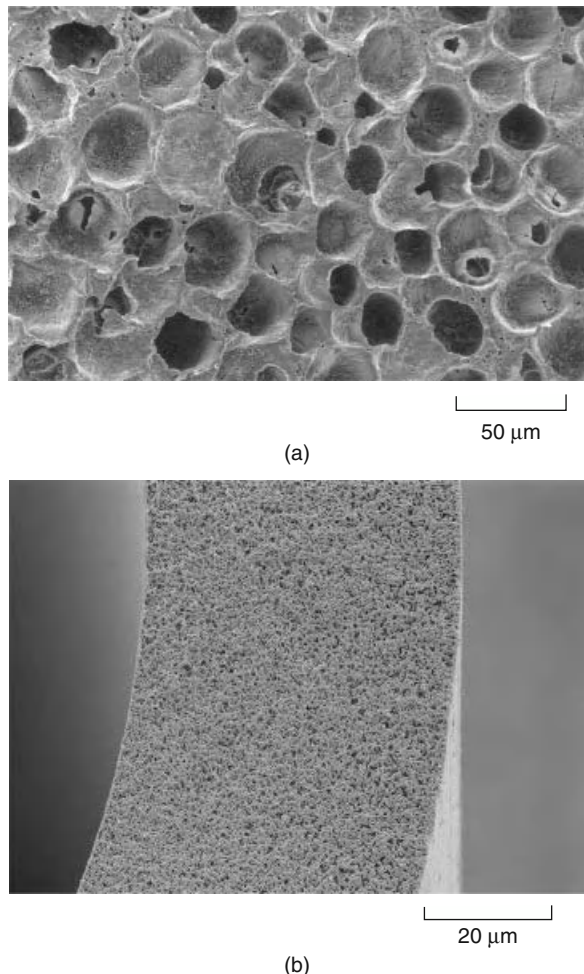


Figure 3.16 Polypropylene structures (a) type I: open cell structure formed at low cooling rates and (b) type II: fine structure formed at high cooling rates. Reprinted with permission from [40]. Copyright (1985) American Chemical Society.

determining the final structure of the membrane. The anisotropy of the membranes can be increased by cooling the top and bottom surface of the cast film at different rates.

A schematic diagram of a commercial-scale thermal gelation polymer precipitation process is shown in Figure 3.17. The hot polymer solution is cast onto a water-cooled chill roll, which cools the solution, causing the polymer to precipitate. The precipitated film is passed through an extraction tank containing methanol, ethanol, or isopropanol to remove the solvent. Finally, the membrane is dried, sent to a laser inspection station, trimmed and rolled up.

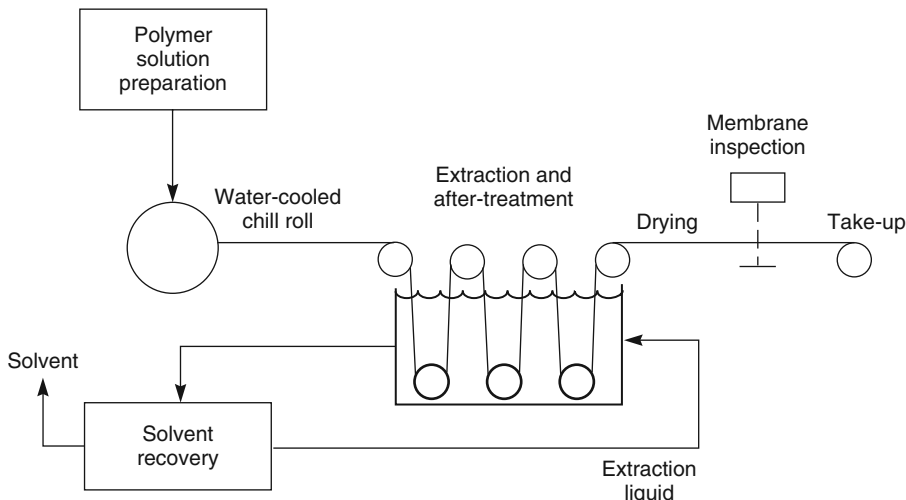


Figure 3.17 Equipment to prepare microporous membranes using the polymer precipitation by cooling technique. Reprinted with permission from [40]. Copyright (1985) American Chemical Society.

3.3.1.5 Polymer Precipitation by Solvent Evaporation

This technique, one of the earliest methods of making microporous membranes, was used by Bechhold, Elford, Pierce, Ferry, and others in the 1920s and 1930s [42–46]. In the simplest form of the method, a polymer is dissolved in a two-component solvent mixture consisting of a volatile solvent, such as methylene chloride or acetone, in which the polymer is readily soluble, and a less volatile nonsolvent, typically water or an alcohol. The polymer solution is cast onto a glass plate. As the volatile solvent evaporates, the casting solution is enriched in the nonvolatile solvent, so the polymer precipitates, forming the membrane structure. The process can be continued until the membrane has completely formed, or it can be stopped, and the membrane structure fixed, by immersing the cast film in a precipitation bath of water or other nonsolvent. The precipitation process used to form these membranes is much slower than precipitation by immersion into liquid water (the Loeb–Sourirajan process). As a result, membranes formed by solvent evaporation are only modestly anisotropic and have large pores. Scanning electron micrographs of some membranes made by this process are shown in Figure 3.18 [47].

Many factors determine the porosity and pore size of membranes formed by the solvent evaporation method. As Figure 3.18 shows, if the membrane is immersed in a nonsolvent after a short evaporation time, the resulting structure will be finely microporous. If the evaporation step is prolonged before fixing the structure by immersion in water, the average pore size will be larger. In general, increasing the nonsolvent content of the casting solution or decreasing the polymer concentration, increases porosity. It is important for the nonsolvent to be completely incompatible with the polymer. If partially compatible

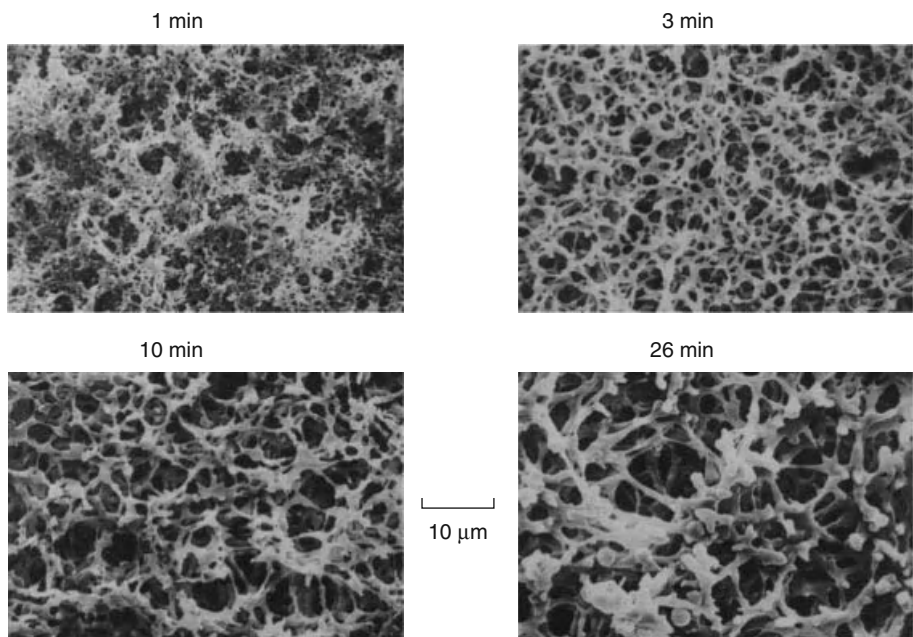


Figure 3.18 SEM photomicrographs of the bottom surface of cellulose acetate membranes cast from a solution of acetone (volatile solvent) and 2-methyl-2,4-pentanediol (nonvolatile nonsolvent). The evaporation time before the structure is fixed by immersion in water is shown. Reprinted with permission from [47]. Copyright (1994) Elsevier.

nonsolvents are used, the precipitating polymer phase contains sufficient residual solvent to allow it to flow, and the pores will collapse as the solvent evaporates. The result is a dense rather than a microporous film.

3.3.1.6 Polymer Precipitation by Absorption of Water Vapor

Preparation of microporous membranes by solvent evaporation alone is not widely practiced. However, a combination of solvent evaporation and absorption of water vapor from a humid atmosphere is an important method of making microfiltration membranes. The processes involve proprietary casting formulations not normally disclosed by membrane developers. However, during the development of composite membranes at Gulf General Atomic, Riley *et al.* prepared this type of membrane and described the technology in some detail in a series of Office of Saline Water Reports [48]. These reports remain the best published description of the technique. Casting solutions used to prepare these membranes are complex and often contain 5–10 components. For example, a typical casting solution composition taken from Riley's report [48] comprises 8.1 wt% cellulose nitrate, 1.3 wt% cellulose acetate, 49.5 wt% acetone (a volatile good solvent), 22.3 wt% ethanol and 14.7 wt% *n*-butanol (nonvolatile poor solvents), 2.6 wt% water (a nonsolvent), 0.5 wt% Triton X-100 (a surfactant solution modifier), and 1.2 wt% glycerin (a polymer plasticizer).

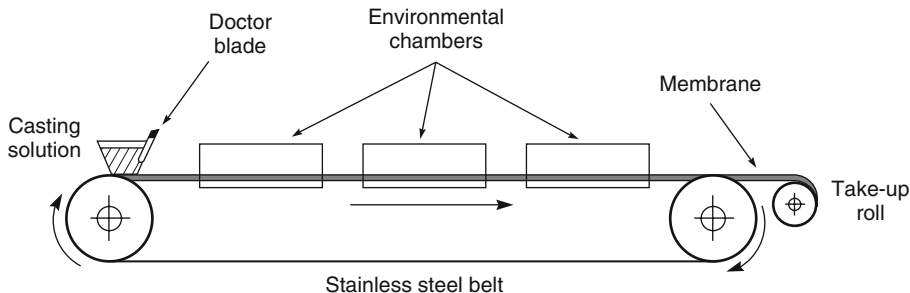


Figure 3.19 Schematic of casting machine used to make microporous membranes by water vapor absorption. A casting solution is deposited as a thin film on a moving stainless steel belt moving at about 0.3 m/min. The film passes through a series of humid and dry chambers, where the solvent evaporates from the solution, and water vapor is absorbed. This precipitates the polymer, forming a microporous membrane that is taken up on a collection roll. Reprinted with permission from [48]. Copyright (1969) Office of Saline Water Research and Development.

The type of equipment used by Riley *et al.* is shown in Figure 3.19. The casting solution is cast onto a moving stainless steel belt. The cast film then passes through a series of environmental chambers. Warm, humid air is usually circulated through the first chamber, where the film loses the volatile solvent by evaporation and simultaneously absorbs water. A key issue is to avoid formation of a dense surface skin on the air side of the membrane. Dense skin formation is generally prevented by incorporating sufficient polymer nonsolvent in the casting solution. Polymer precipitation and formation of two phases then occur when even a small portion of the volatile solvent component in the mixture evaporates. The total precipitation process is slow, taking about 10–30 minutes to complete. Typical casting speeds are on the order of 1–5 ft/min. To allow higher casting speeds the casting machine must be very long – commercial machines can be up to 100 ft. The resulting membrane structure is more isotropic and more microporous than membranes precipitated by immersion in water. After precipitation in the environmental chambers, the membrane passes to a second oven, through which hot, dry air is circulated, to evaporate the remaining solvent and dry the film. The formed membrane is then wound onto a take-up roll. This type of membrane is widely used in microfiltration. Membranes made by the water vapor absorption–solvent evaporation precipitation process often have the characteristic nodular form shown in Figure 3.20. A discussion of some of the practical considerations involved in making this type of membrane is given in a book by Zeman and Zydny [49].

3.3.2 Interfacial Polymerization Membranes

The production by Loeb and Sourirajan of the first anisotropic membrane stimulated the development of numerous other techniques for making the same type of structure. One of the most important of these new techniques was interfacial polymerization, an entirely new method of making anisotropic membranes developed by John Cadotte, then at North Star Research. Reverse osmosis membranes produced by this technique

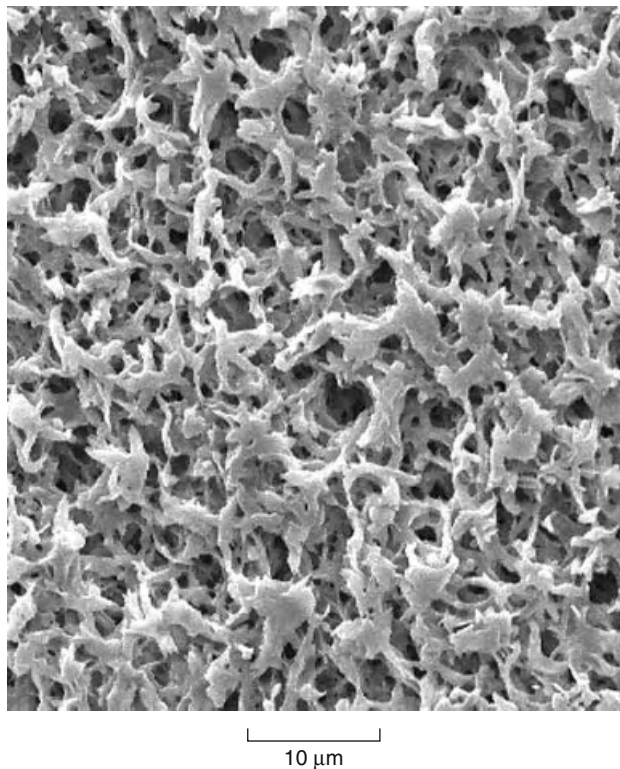


Figure 3.20 Characteristic structure of a phase-separation membrane made by water vapor absorption and solvent evaporation. Reprinted with permission of Millipore Corporation, Billerica, MA

had much improved salt rejections and water fluxes, compared to those prepared by the Loeb–Sourirajan process. Almost all reverse osmosis membranes are now made by the interfacial polymerization process, illustrated in Figure 3.21. In this technique, an aqueous solution of a reactive prepolymer, such as a polyamine, is first deposited in the pores of a microporous support membrane, typically a polysulfone ultrafiltration membrane. The amine-loaded support is then immersed in a water-immiscible solvent solution containing a reactant, such as a diacid or triacid chloride in hexane. The amine and acid chloride react at the interface of the two immiscible solutions to form a densely crosslinked, extremely thin membrane layer. The first membrane made by Cadotte was based on poly(ethyleneimine) crosslinked with toluene-2,4-diisocyanate, to form the structure shown in Figure 3.22 [50]. The process was later refined by Cadotte *et al.* at FilmTec Corp. [16, 51], Riley *et al.* at UOP [52], and Kamiyama *et al.* [53] at Nitto in Japan.

Membranes made by interfacial polymerization have a dense, highly crosslinked polymer layer formed on the surface of the support membrane at the interface of the two solutions. A less crosslinked, more permeable hydrogel layer forms under this surface layer and fills the pores of the support membrane. The dense, crosslinked polymer layer, which can only form at the interface, is extremely thin, on the order of 0.1 μm or less,

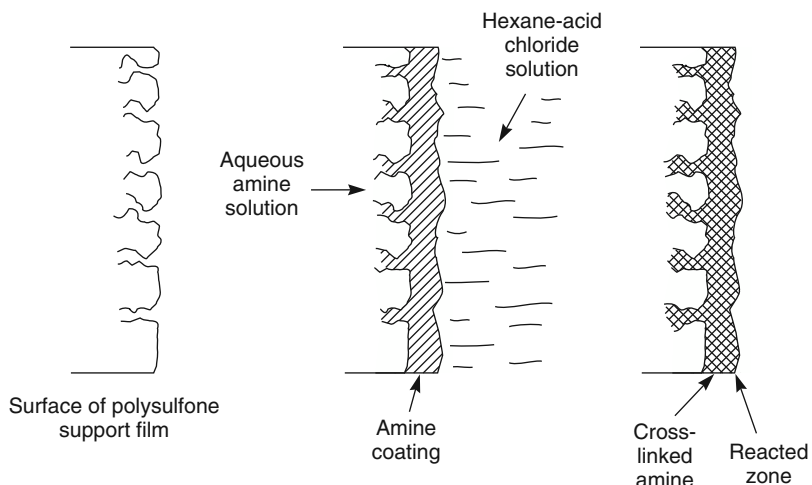


Figure 3.21 Schematic of the interfacial polymerization process. The microporous film is first impregnated with an aqueous amine solution. The film is then treated with a multivalent crosslinking agent dissolved in a water-immiscible organic fluid, such as hexane or Freon-113. An extremely thin polymer film forms at the interface of the two solutions [50]. Reprinted from L.T. Rozelle, J.E. Cadotte, K.E. Cobian, and C.V. Knopp, Jr., Nonpolysaccharide Membranes for Reverse Osmosis: NS-100 Membranes, in Reverse Osmosis and Synthetic Membranes, S. Sourirajan, (ed.), National Research Council Canada, Ottawa, Canada (1977) by permission from NRC Research Press

so the membrane permeance is high. Because the polymer is highly crosslinked, its selectivity is also high. Although the crosslinked interfacial polymer layer determines membrane selectivity, the nature of the microporous support film affects membrane flux significantly. The film has to be very finely porous to withstand the high pressures applied but must also have a high surface porosity so it is not a barrier to flow. The first reverse osmosis membranes made by the interfacial polymerization method were five times less salt permeable than the best cellulose acetate Loeb–Sourirajan membranes and had better water fluxes. Since then, interfacial polymerization chemistry has been refined. The first membrane produced by this method (and shown in Figure 3.22) was based on the reaction of a poly(ethyleneimine) (in water) and toluene-2,4-diisocyanate or isophthaloyl chloride (in hexane). These NS-100 membranes, first produced by Cadotte at North Star Research, had very good permeation properties but were very sensitive to even trace amounts (ppb levels) of chlorine commonly used as an antibacterial agent in water. The chlorine caused chain cleavage of the polymer at the amide bonds, resulting in loss of salt rejection properties. A number of other chemistries have been developed over the years; the FT-30 membrane produced by reaction of phenylenediamine with trimesoyl chloride, also developed by Cadotte when at FilmTec (now a division of Dow Chemical), is particularly important. This membrane, which has a high water flux and consistent salt rejections of greater than 99.5% with seawater [54, 55], made single-pass seawater desalination with anisotropic membranes possible. A more detailed description

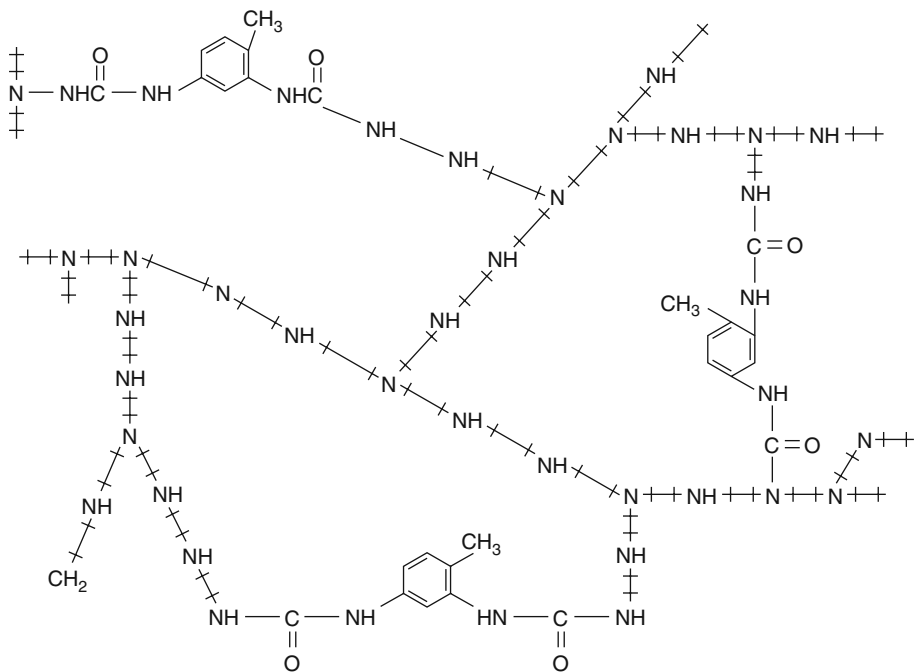


Figure 3.22 Idealized structure of polyethylenimine crosslinked with toluene 2,4-diisocyanate. This was called the NS-100 membrane. The chemistry was first developed by Cadotte to make interfacial reverse osmosis membranes with almost twice the water flux and 1/5th the salt leakage of the best reverse osmosis membranes then available. Even better membranes have since been developed by Cadotte and others [50]. Reprinted from L.T. Rozelle, J.E. Cadotte, K.E. Cobian, and C.V. Knopp, Jr., Nonpolysaccharide Membranes for Reverse Osmosis: NS-100 Membranes, in Reverse Osmosis and Synthetic Membranes, S. Sourirajan, (ed.), National Research Council Canada, Ottawa, Canada (1977) by permission from NRC Research Press

of the chemistry of interfacial composite membranes is given in the discussion of reverse osmosis membranes in Chapter 5 and in a review by Petersen [51].

Production of interfacial polymerization membranes in the laboratory is relatively easy, but development of equipment to produce these membranes on a large scale required some ingenuity. The problem is the fragility of the interfacial surface film, which cannot be handled once formed. One early solution to this problem is illustrated in Figure 3.23. The polysulfone or other material used as the support film is first immersed in an aqueous amine bath. On leaving this bath the membrane passes to a second organic acid chloride bath and then through a drying/curing oven. The transfer rollers are arranged so that the surface layer of the polymer on which the membrane forms never contacts a roller. On leaving the oven, the interfacial membrane is completely formed. This membrane is then coated with a protective solution of a water-soluble polymer such as poly(vinyl alcohol).

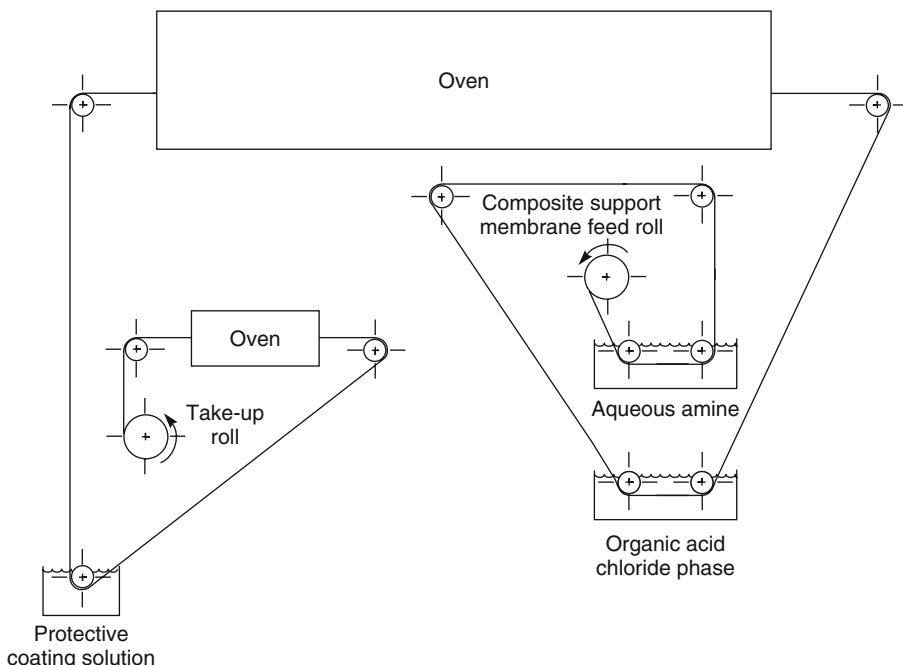


Figure 3.23 Schematic of the type of machinery used to make interfacial composite membranes

When this solution is dried, the membrane is wound onto a take-up roll. The poly(vinyl alcohol) layer protects the membrane from damage during subsequent handling as it is formed into spiral-wound modules. When the module is used for the first time, the feed water washes off the water-soluble poly(vinyl alcohol) layer to expose the interfacial polymerized membrane, and the module is ready for use. At the present time, very large machines – sometimes 50–100 m long – are used to make 5000 m rolls of membrane at speeds of 10–20 m/min.

Interfacial polymerization membranes are widely used in reverse osmosis and nanofiltration, but not in gas separation, because of the water-swollen hydrogel that fills the pores of the support membrane. In reverse osmosis, this layer is hydrated and offers little resistance to water flow, but when the membrane is dried for use in gas separation, the gel becomes a rigid glass with a low gas permeability. This glassy polymer fills the membrane pores, and as a result, defect-free interfacial composite membranes usually have low gas fluxes, although their selectivities can be good.

3.3.3 Solution-Coated Composite Membranes

Another important group of anisotropic composite membranes is formed by solution-coating a thin (0.5–2.0 μm) selective layer on a suitable microporous support. Membranes of this type were first prepared by Ward, Browell, and others at General Electric [17] and by Forester and Francis at North Star Research [18, 56] using a type

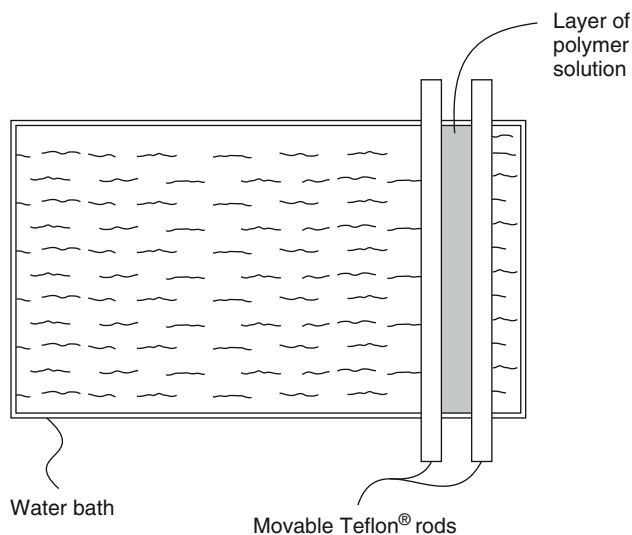


Figure 3.24 Schematic of the apparatus developed by Ward et al. to prepare water-cast composite membranes. Reprinted with permission from [17]. Copyright (1976) Elsevier.

of Langmuir trough system. In this system, a dilute polymer solution in a volatile water-insoluble solvent is spread over the surface of a water-filled trough.

The apparatus used to make small sections of water-cast composite membranes is shown in Figure 3.24. The dilute polymer solution is cast on the surface between two Teflon® rods. The rods are then moved apart to spread the film. The thin polymer film formed on the water surface is picked up on a microporous support. The main problem with this method is the transfer of the fragile, ultrathin film onto the microporous support. This is usually done by sliding the support membrane under the spread film. With care, small pieces of membrane as thin as 200 Å can be made.

Currently, most solution-coated composite membranes are prepared by the method developed by Riley and others [48, 57, 58]. In this technique, a polymer solution is coated directly onto the microporous support. The support must be clean, defect-free and very finely microporous, to prevent penetration of the coating solution into the pores. If these conditions are met, the support can be coated with a liquid layer 50–100 µm thick, which after evaporation leaves a thin selective polymer layer 0.5–2 µm thick. A schematic drawing of the meniscus-coating technique is shown in Figure 3.25 [59]. Obtaining defect-free films by this technique requires considerable attention to the preparation procedure and the coating solution. The nature of the microporous support is also critical. Some of the membrane support properties that affect the selective layer are shown in Figure 3.26.

The selective layer in composite membranes is extremely thin, so resistance to transport in the support layer can contribute to the total resistance to transport through the membrane. Not only does the resistance of the support decrease the flux through the membrane, but it can affect the separation [33, 61]. To achieve the intrinsic selectivity of the selective membrane layer, the flux of the uncoated support material must be at least 10 times that of

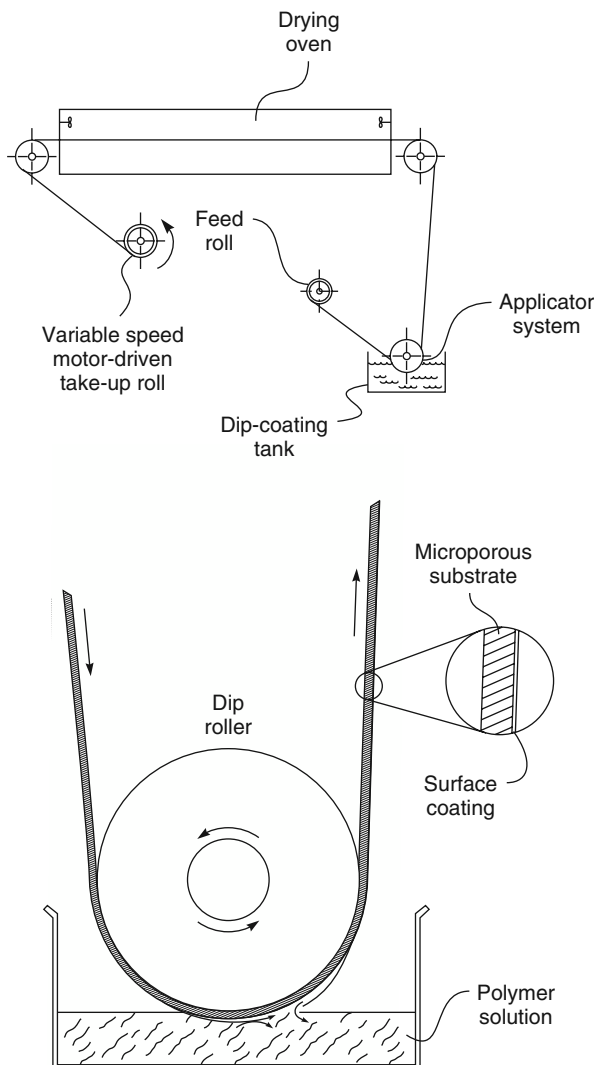
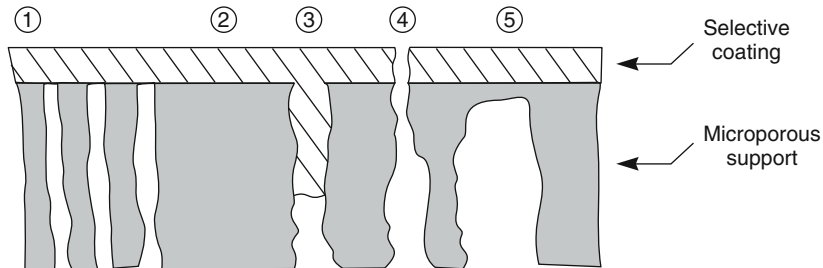


Figure 3.25 Schematic diagram of a film coating apparatus [59]

the coated support. This ensures that more than 90% of the resistance to flow lies within the selective coating layer. As well as having a high flux, the surface layer of the microporous support material must also be very finely microporous. The pores must be small enough to support the thin selective layer under high pressure, and must also be close together so the permeating components do not take a long tortuous path to reach the pore. When the selective layer is only a few tenths of a μm thick, this requirement may be difficult to meet. One solution to the problem is an intermediate gutter layer of a highly permeable polymer between the microporous support and the selective layer. The gutter layer material is much more permeable than the thin selective layer and acts as a conduit to transport material to the



- ① The ideal situation: No penetration, high pore density
- ② Low pore density: Low flux
- ③ Pore penetration: Low flux
- ④ Incomplete coating, pin holes: Low selectivity, high flux
- ⑤ Support with thin, dense skin layer: Support affects membrane selectivity; low flux and anomalous selectivity

Figure 3.26 Support membrane properties that affect composite membrane performance. Reprinted with permission from [60]. Copyright (1991) Bakish Materials Corporation.

support membrane pores. Finally, because the selective layer of the composite membrane is often very thin and correspondingly delicate, such membranes are often protected by a sealing layer, also formed from a highly permeable material, to protect the membrane from damage during handling. A schematic of a multilayer composite membrane of this type is shown in Figure 3.27a, and a scanning electron micrograph is presented in Figure 3.27b. A discussion of the issues involved in preparing this type of membrane is found in the review by Koros and Pinna [33].

3.3.4 Other Anisotropic Membranes

Most anisotropic membranes are produced by solution precipitation, interfacial polymerization, or solution coating. A number of other techniques developed in the laboratory are reviewed briefly below; none are used on a large scale.

3.3.4.1 Plasma Polymerization Membranes

Plasma polymerization of films was first used to form electrical insulation and protective coatings, but a number of workers have also prepared selective membranes by this method [62–65]. A simple plasma polymerization apparatus is shown in Figure 3.28. Most workers used RF fields at frequencies of 2–50 MHz to generate the plasma. In a typical plasma experiment helium, argon, or another inert gas is introduced at a pressure of 50–100 mTorr and a plasma is initiated. Monomer vapor is then introduced to bring the total pressure to 200–300 mTorr. These conditions are maintained for a period of 1–10 minutes, during which a thin polymer film is deposited on the membrane sample held in the plasma field.

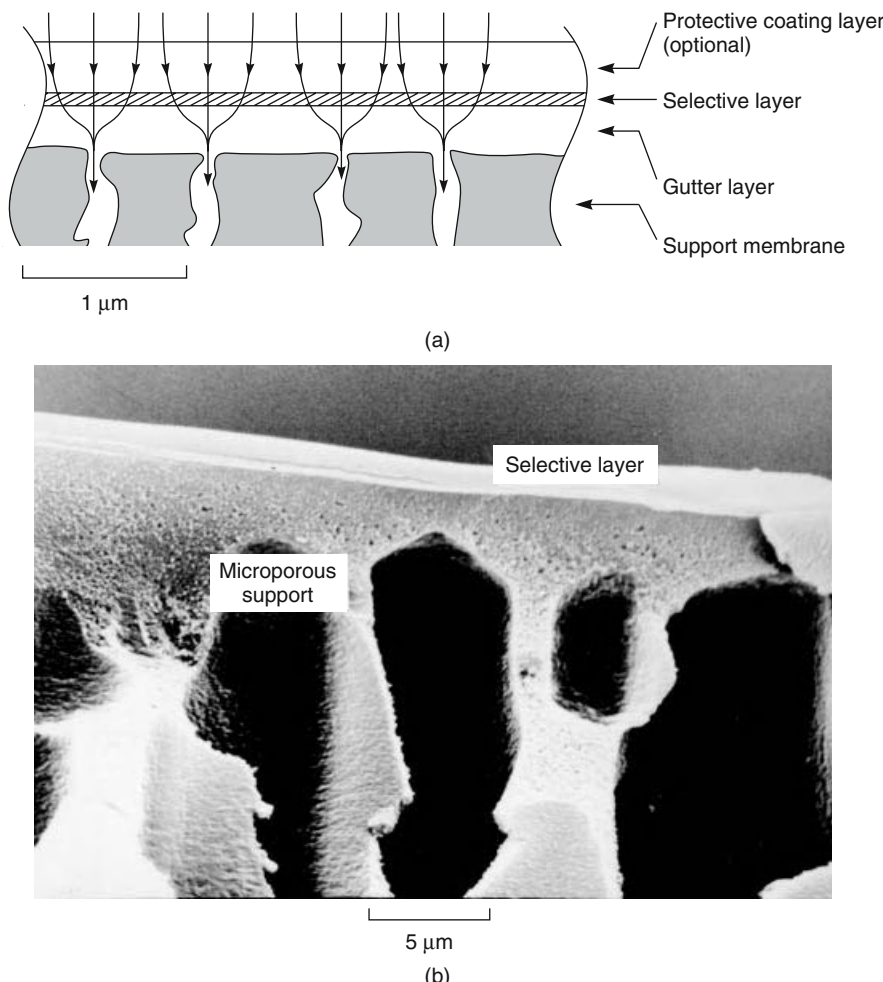


Figure 3.27 Schematic and scanning electron micrograph of a multilayer composite membrane on a microporous support. Reprinted with permission from Membrane Technology and Research, Inc. Copyright (2012) MTR.

Plasma polymerization of monomers proceeds by a complex mechanism involving ionized molecules and radicals, and is completely different from conventional polymerization reactions. In general, the polymer films are highly crosslinked and may contain radicals that slowly react on standing. The stoichiometry of the film may also be quite different from the original monomer due to fragmentation of monomer molecules during the plasma polymerization process. The susceptibility of monomers to plasma polymerization or the characteristics of the resulting polymer film are difficult to predict. For example, many vinyl and acrylic monomers polymerize very slowly, whereas unconventional monomers such as benzene and hexane polymerize readily. The vapor pressure of the monomers, the power and voltage used in the discharge reaction, and the type

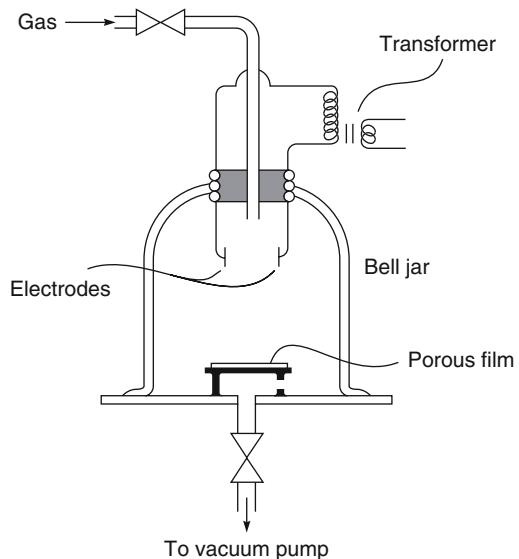


Figure 3.28 Simple bell jar plasma coating apparatus

and temperature of the substrate all affect the polymerization reaction. The inert gas used in the plasma may also enter into the reaction. Nitrogen and carbon monoxide, for example, are particularly reactive. In summary, the products of plasma polymerization are ill-defined and vary according to the experimental procedures. However, the resulting films can be very thin and have been shown to be quite selective.

3.3.4.2 Spin Coating

Spin coating is widely used in the electronics industry to coat photoresists and photolithographic films onto silicon wafers. The technique is also used in the laboratory to make composite membranes 0.5–10 µm thick. An excess of dilute polymer solution is placed on the substrate, which is then rotated at high speed. Fluid spins off the edge of the rotating substrate until the desired film thickness is achieved. The coating layer thickness can be decreased by increasing the rotation speed or decreasing the polymer concentration in the applied solution. A schematic of a typical laboratory spin coater is shown in Figure 3.29.

3.3.4.3 Dynamically Formed Membranes

In the late 1960s and early 1970s, much attention was devoted to preparing dynamically formed anisotropic membranes, principally by Johnson, Kraus, and others at Oak Ridge National Laboratory [67, 68]. The general procedure is to form a layer of inorganic or polymeric colloids on the surface of a microporous support membrane by filtering a solution containing suspended colloid through the support membrane. A thin colloidal layer is laid down on the membrane surface and acts as a semipermeable membrane. Over time the colloidal surface layer is lost, and membrane performance falls. The support membrane is then cleaned, and a new layer of colloid is deposited. In the early development

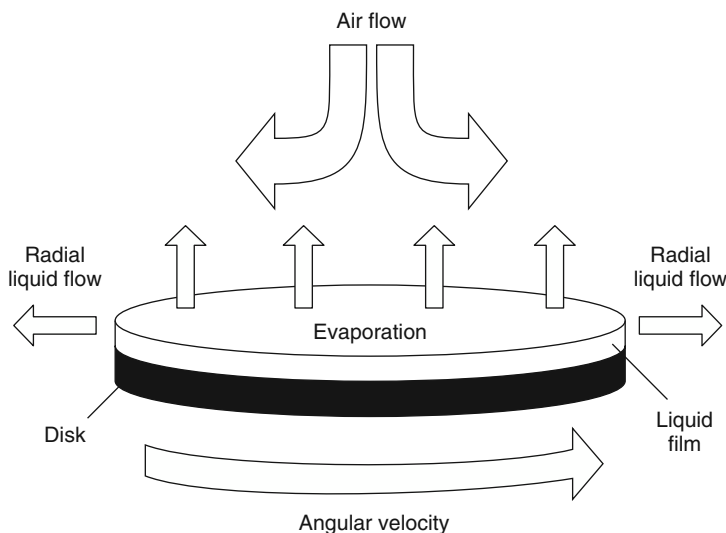


Figure 3.29 Schematic of a spin-coating process. Reprinted with permission from [66]. Copyright (2005) Royal Society of Chemistry.

of this technique a wide variety of support membranes were used. Later, microporous ceramic or porous carbon tubes became the most commonly used materials. Typical colloidal materials used to make the selective membrane layer are polyvinyl methyl ether, acrylic acid copolymers, or hydrated metal oxides such as zirconium hydroxide.

Dynamically formed membranes were pursued for many years for reverse osmosis applications, because of their high water fluxes and relatively good salt rejection with brackish water feeds. However, the membranes proved to be unstable and difficult to reproduce reliably and consistently. For these reasons, and because high-performance interfacial composite membranes were developed in the meantime, dynamically formed reverse osmosis membranes fell out of favor. A small application niche in high-temperature nanofiltration and ultrafiltration processes was found, and Rhône-Poulenc continued their production for a number of years. The principal application was poly(vinyl alcohol) recovery from hot wash water produced in textile dyeing operations.

3.3.4.4 Reactive Surface Treatment

Recently several groups have tried to improve the properties of anisotropic gas separation membranes by chemically modifying the surface selective layer. For example, Langsam at Air Products and Paul *et al.* at the University of Texas, Austin have treated films and membranes with dilute fluorine gas [69–74]. In this treatment, fluorine chemically reacts with the polymer structure. By careful control of the process conditions, the reaction can be limited to a 100–200 Å surface layer. The dramatic improvements in selectivity produced by this surface treatment are illustrated by the data in Table 3.3. Scaling up this process for safe operation on a large scale will be difficult, but several groups are studying the approach. Ozone has also been suggested as a possible reactive surface treatment agent [75].

Table 3.3 Effect of fluorination on the carbon dioxide/methane selectivity of various glassy membrane materials

Base polymer	Carbon dioxide/methane selectivity	
	Before fluorination	After fluorination
Poly(1-trimethylsilyl-1- propyne) (PTMSP) [69]	2.0	48
Poly(phenylene oxide) [74]	15	50–60
Poly(4-methyl-1-pentene) [73]	5.4	30–40

3.3.5 Repairing Membrane Defects

In preparing anisotropic membranes, the goal is to make the selective layer that performs the separation as thin as possible, but still defect free. Over the past 20 years, a great deal of work has been devoted to understanding the factors that determine the properties and thickness of the selective layer. The selective layer can be dense, as in reverse osmosis or gas separation membranes, or finely microporous with pores in the 100–500 Å diameter range, as in ultrafiltration membranes. In good quality membranes, a thickness as low as 500–1000 Å can be achieved, but with layers as thin as this, formation of minute membrane defects is a problem. The defects, caused by gas bubbles, dust particles, and support fabric imperfections, can be very difficult to eliminate. Such defects may not significantly affect the performance of anisotropic membranes used in liquid separation processes, such as ultrafiltration and reverse osmosis, but can be disastrous in gas separation applications. Browall [76] solved this problem by overcoating defective solution-cast composite membranes with a second thin coating layer of a highly permeable polymer to seal defects, as shown in Figure 3.30.

Later, Henis and Tripodi [77] showed that membrane defects in anisotropic Loeb–Sourirajan membranes could be overcome in a similar way by coating the membrane with a thin layer of a relatively permeable material such as silicone rubber. A sufficiently thin coating does not change the properties of the underlying selective layer but does plug defects, through which simple convective gas flow can occur. Henis and Tripodi's membrane is

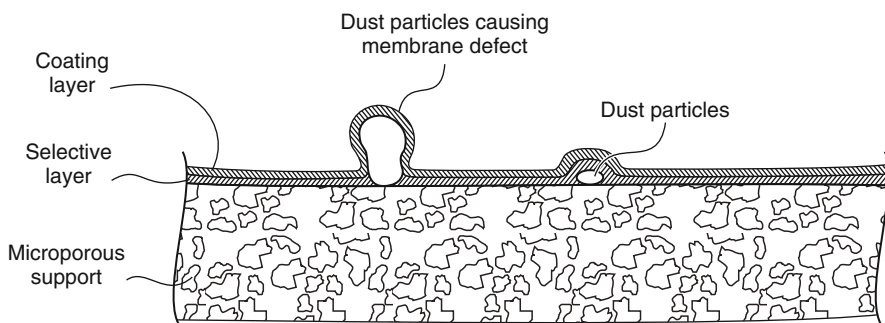


Figure 3.30 Method developed by Ward, Browell, and others at General Electric to seal membrane defects in composite membranes made by the water coating technique [76]

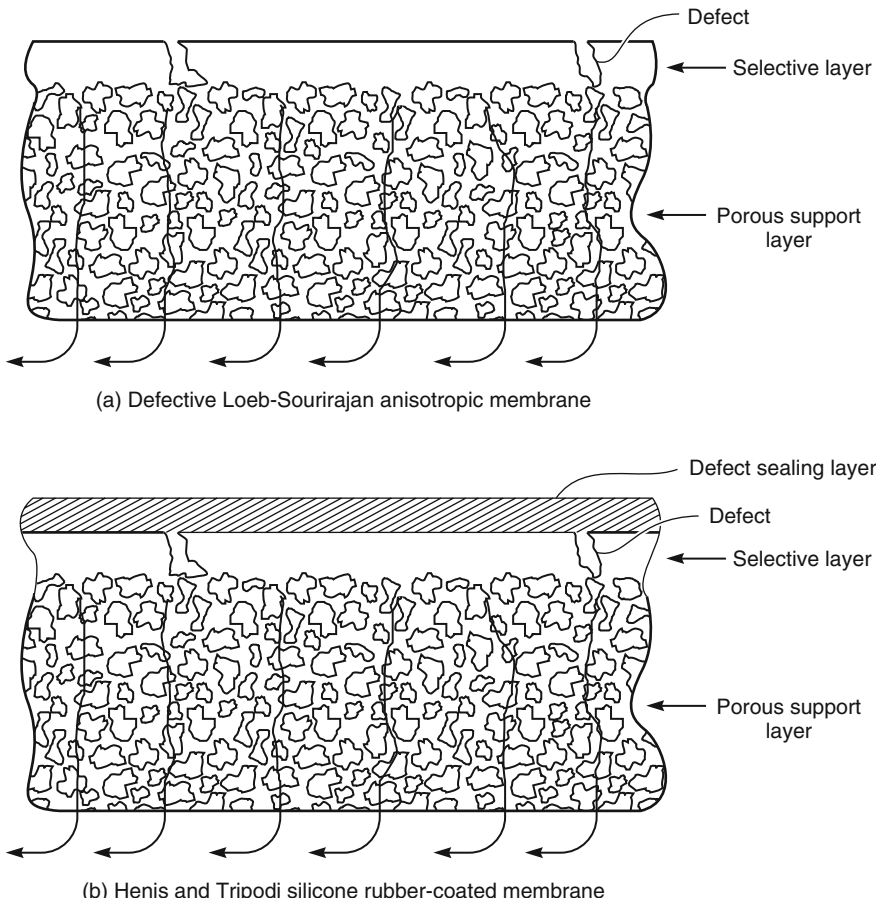


Figure 3.31 Schematic of (a) Loeb–Sourirajan and (b) Henis and Tripodi gas separation membranes [77]

illustrated in Figure 3.31. The base membrane was a polysulfone Loeb–Sourirajan membrane. The silicone rubber layer is many times more permeable than the polysulfone selective layer and does not function as a selective barrier but rather plugs defects, thereby reducing non-diffusive gas flow. The flow of gas through the portion of the silicone rubber layer over the pore is high compared to the flow through the defect-free portion of the membrane. However, because the area of membrane defects is very small, the total gas flow through these plugged defects is negligible. When this coating technique is used, the polysulfone skin layer of the Loeb–Sourirajan membrane no longer has to be completely defect free; therefore, the membrane can be made with a thinner skin than is possible with an uncoated membrane. The increase in flux obtained by decreasing the thickness of the selective skin layer more than compensates for the slight reduction in flux due to the silicone rubber sealing layer.

3.4 Metal, Ceramic, Zeolite, Carbon, and Glass Membranes

3.4.1 Metal Membranes

Metal membranes, particularly palladium-based, have been considered for hydrogen separation for a long time. In the 1950s and 1960s, Union Carbide installed and operated a palladium membrane plant to separate hydrogen from a refinery off-gas stream [78]. The plant produced 99.9% pure hydrogen in a single pass through 25 µm thick palladium membranes. However, even at a feed pressure of 450 psi, the membranes had to be operated at 370°C to obtain a useful transmembrane hydrogen flux. A further problem was the very high membrane cost: a 25 µm thick palladium membrane requires approximately 250 g palladium/m² of membrane. At current palladium costs of US\$20/g, the metal cost alone is US\$5000/m² of membrane. This is 100 times the total cost of typical polymeric membranes used for gas separations.

A breakthrough in metal permeation studies occurred in the 1960s when Hunter at Johnson Matthey discovered that palladium/silver alloy membranes showed no hydrogen embrittlement even when used to permeate hydrogen at room temperature [79, 80]. More recently, palladium–copper and palladium–gold alloys, which are more resistant to poisoning by hydrogen sulfide, have become popular. Although most work on gas permeation through metal membranes has focused on hydrogen, oxygen-permeable metal membranes are also known, but their permeabilities are low.

If noble metal membranes are ever to be used on a large scale, their cost must be reduced. One approach [81, 82] is to coat a 1000–5000 Å film of the metal on a microporous metal or polymer support. Because the film is thin, these membranes have high hydrogen fluxes. Another approach, used by Buxbaum [83, 84], is to coat a thin layer of palladium on a tantalum or vanadium support film. Tantalum and vanadium are also quite permeable to hydrogen and much less expensive than palladium. These metals cannot be used alone because they easily form an impenetrable oxide surface film. However, protected by a thin palladium layer, these membranes are quite permeable at high temperatures. Edlund [85, 86] pursued a similar approach. A detailed discussion of hydrogen permeation in metals is given in the book by Alefeld and Völkl [87].

The gas transport mechanism is the key to the high selectivity and permeance of metal membranes. Hydrogen permeation through a metal membrane is believed to follow the multistep process illustrated in Figure 3.32 [88]. Hydrogen molecules from the feed gas are sorbed on the membrane surface, where they dissociate into hydrogen atoms. Each individual hydrogen atom loses its electron to the metal lattice and diffuses through the lattice as an ion. Hydrogen atoms emerging at the permeate side of the membrane reassociate to form hydrogen molecules, then desorb, completing the permeation process. Only hydrogen is transported through the membrane by this mechanism; all other gases are excluded.

If the sorption and dissociation of hydrogen molecules is a rapid process, then the hydrogen atoms on the membrane surface are in equilibrium with the gas phase. The concentration, c , of hydrogen atoms on the metal surface is given by Sievert's law:

$$c = Kp^{1/2} \quad (3.1)$$

where K is Sievert's constant and p is the hydrogen pressure in the gas phase. At high temperatures (>300°C), the surface sorption and dissociation processes are fast, and the

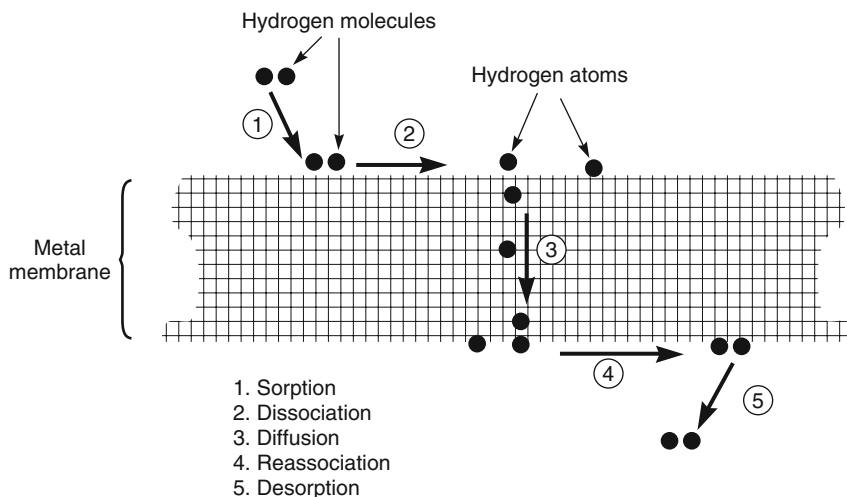


Figure 3.32 Mechanism of hydrogen permeation through metal membranes. Reprinted with permission from Pall Corporation, Filterite Division, Timonium, MD. Copyright (2012) Pall Corporation.

rate-controlling step is diffusion of atomic hydrogen through the metal lattice. This is supported by data such as that of Ma *et al.* (Figure 3.33) [81], who have shown that the hydrogen flux through the metal membrane is proportional to the difference of the square roots of the hydrogen pressures on either side of the membrane. At lower temperatures, however, the sorption and dissociation of hydrogen on the membrane surface become the rate-controlling steps, and the permeation characteristics of the membrane deviate from Sievert's law predictions.

Despite their extraordinary permeation and selectivity properties, metal membranes have found very limited industrial application. In the 1970s and early 1980s, Johnson Matthey built a number of systems to produce on-site hydrogen by separation of hydrogen/carbon dioxide mixtures made by reforming methanol [89]. This was not a commercial success, but the company and others still produce small systems using palladium–silver alloy membranes to generate ultrapure hydrogen from 99.9% hydrogen for the electronics industry and as feed gas to fuel cells.

3.4.2 Ceramic Membranes

Several companies have developed inorganic ceramic membranes for ultrafiltration and microfiltration. These microporous membranes are made from aluminum, titanium, or silicon oxides. Ceramic membranes have the advantages of being chemically inert and stable at high temperatures, conditions under which polymer membranes fail. This stability makes ceramic microfiltration/ultrafiltration membranes particularly suitable for food, biotechnology, and pharmaceutical applications in which membranes require repeated steam sterilization and cleaning with aggressive solutions. Pore diameters in ceramic membranes for microfiltration and ultrafiltration range from 0.01 to 10 μm ; these membranes are generally made by a slip coating-sintering procedure. Other

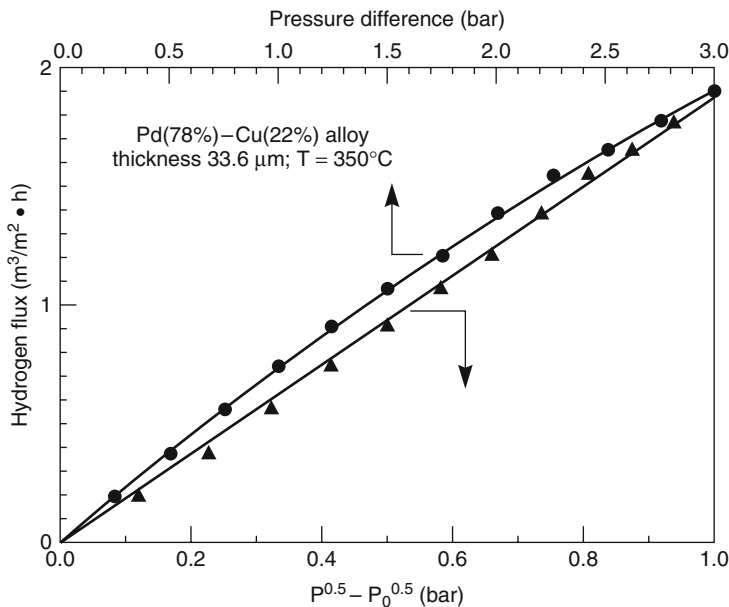


Figure 3.33 Sievert's plot for a Pd-Cu/porous stainless steel composite membrane at 350°C [81]

techniques, particularly sol–gel methods, are used to produce membranes with pores from 10 to 100 Å. Sol–gel membranes are the subject of considerable research interest, particularly for gas separation applications, but so far have found no commercial use. A number of reviews covering the general area of ceramic membrane preparation and use have appeared recently [90–92].

In the slip coating-sintering process, a porous ceramic support tube is made by pouring a dispersion of a fine-grain ceramic material and a binder into a mold and sintering at high temperature. The pores between the particles that make up this support tube are large. One surface of the tube is then coated with a suspension of finer particles in a solution of a cellulosic polymer or poly(vinyl alcohol), which acts as a binder and viscosity enhancer to hold the particles in suspension. This mixture is called a slip suspension; when dried and sintered at high temperatures, a finely microporous surface layer remains. Usually several slip-coated layers are applied in series, each layer being formed from a suspension of progressively finer particles and resulting in an anisotropic structure. Most commercial ceramic ultrafiltration membranes are made this way, generally in the form of tubes or perforated blocks. A scanning electron micrograph of the surface of this type of multilayer membrane is shown in Figure 3.34.

The slip coating-sintering procedure can be used to make membranes with pore diameters down to about 100–200 Å. These membranes are mostly used in ultrafiltration or as supports for denser membranes used in gas separation. More finely porous gas separation membranes are made by sol–gel techniques. In the sol–gel process, slip coating is taken to the colloidal level. Generally, the substrate to be coated with the sol–gel is a microporous ceramic tube formed by the slip coating-sintering technique. This support

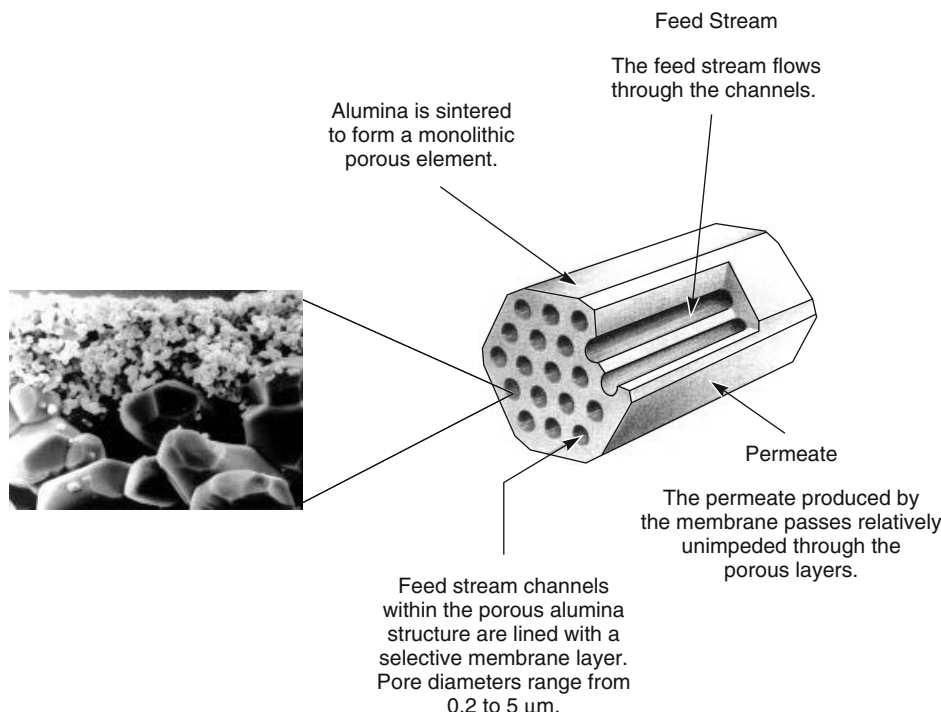
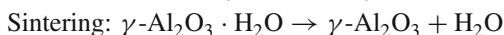
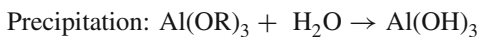


Figure 3.34 Cross-sectional scanning electron micrograph of a three-layered alumina membrane/support (pore sizes of 0.2, 0.8, and 12 µm, respectively). Reprinted with permission from [93]. Copyright (2000) Elsevier Ltd.

is then solution coated with a colloidal or polymeric gel of an inorganic hydroxide. These solutions are prepared by controlled hydrolysis of metal salts or metal alkoxides to hydroxides.

Sol–gel methods fall into two categories, depending on how the colloidal coating solution is formed. The processes are shown schematically in Figure 3.35 [92–94]. In the particulate–sol method, a metal alkoxide dissolved in alcohol is hydrolyzed by addition of excess water or acid. The precipitate that results is maintained as a hot solution for an extended period during which the precipitate forms a stable colloidal solution. This process is called peptization (from the Greek pep – to cook). The colloidal solution is then cooled and coated onto the microporous support membrane. The layer formed must be dried carefully to avoid cracking the coating. In the final step the film is sintered at 500–800°C. The overall process can be represented as:



In the polymeric sol–gel process, partial hydrolysis of a metal alkoxide dissolved in alcohol is accomplished by adding the minimum of water to the solution. The active

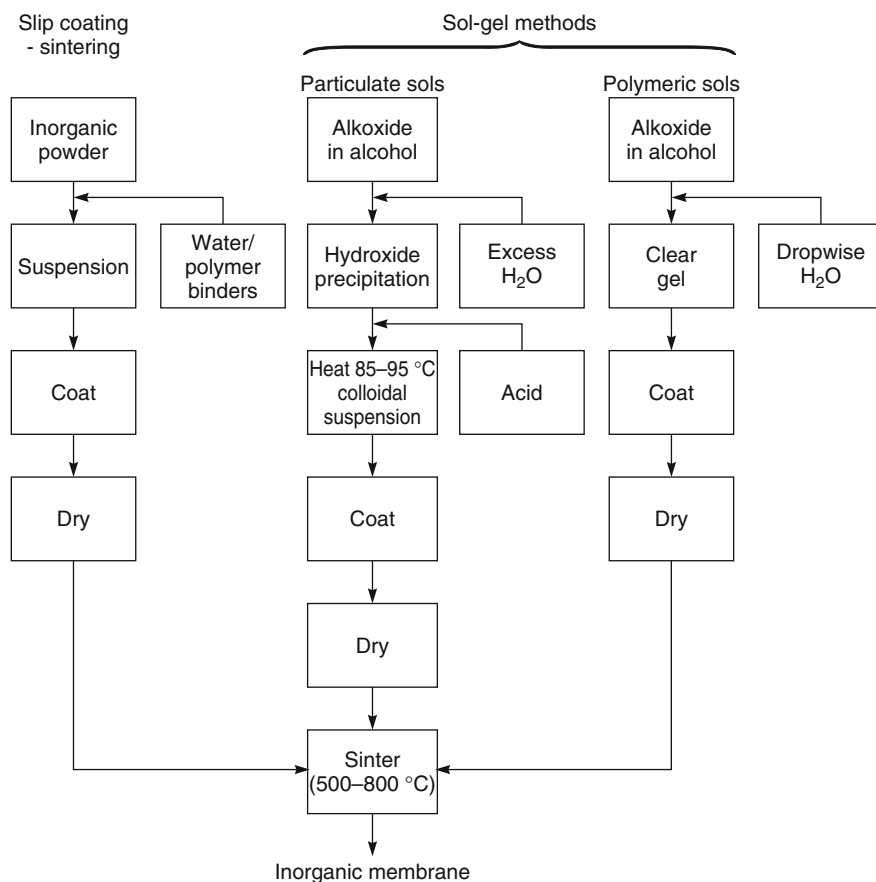
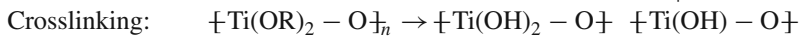


Figure 3.35 Slip coating-sintering and sol-gel processes used to make ceramic membranes. Reprinted with permission from [95]. Copyright (2006) John Wiley and Sons, Ltd.

hydroxyl groups on the alkoxides then react to form an inorganic polymer molecule that can then be coated onto the ceramic support. On drying and sintering, the metal oxide film forms. Chemically the polymeric sol–gel process can be represented as:



Depending on the starting material and the coating procedure, a wide range of membranes can be made by the sol–gel process. The problem of cracking the films on drying and sintering can be alleviated by adding small amounts of a polymeric binder to the coating

solution. The coating process may also be repeated several times to give a defect-free film. With care, membranes with pore sizes in the 10–100 Å range can be made by this method. In principle these membranes could be useful in a number of processes – membrane reactors, for example. Currently the technology is still at the laboratory stage.

3.4.3 Zeolite Membranes

In recent years, there have been a number of attempts to develop zeolite (molecular sieve) membranes. Zeolites are silicalite or aluminosilicate materials formed from a three-dimensional network of SiO_4 and AlO_4 tetrahedra. The tetrahedra are linked by shared oxygen atoms to form cages. In a zeolite structure, these individual cages are linked together in various geometric forms that create pore openings with defined regular shapes and sizes. Figure 3.36 shows how one type of building block, the sodalite β -cage, can form several structures with pores ranging from 3 to 8 Å. There are over 140 known zeolite structures [95].

Aluminosilicate structures carry a negative charge which is usually balanced by Na^+ , K^+ , or Ca^{2+} counter ions. Fine tuning of the pore openings of the zeolite structure is possible by exchanging K^+ and Ca^{2+} for Na^+ counter ions.

Zeolite membranes can be formed on microporous aluminum oxide or stainless steel supports by the *in situ* hydrothermal synthesis techniques illustrated in Figure 3.37. A ceramic substrate is immersed in precursor solution with the correct Si/Al stoichiometry, pH, and ionic strength. The solution is heated in a sealed autoclave for a predetermined time. The type of zeolite that will form is determined by many factors described elsewhere [96, 97]. Often, a structure-directing reagent is added, which leads to the formation of one particular type of zeolite. For example, the tetrapropyl ammonium ion (TPA^+) leads exclusively to MFI or silicalite zeolites. After hydrothermal synthesis,

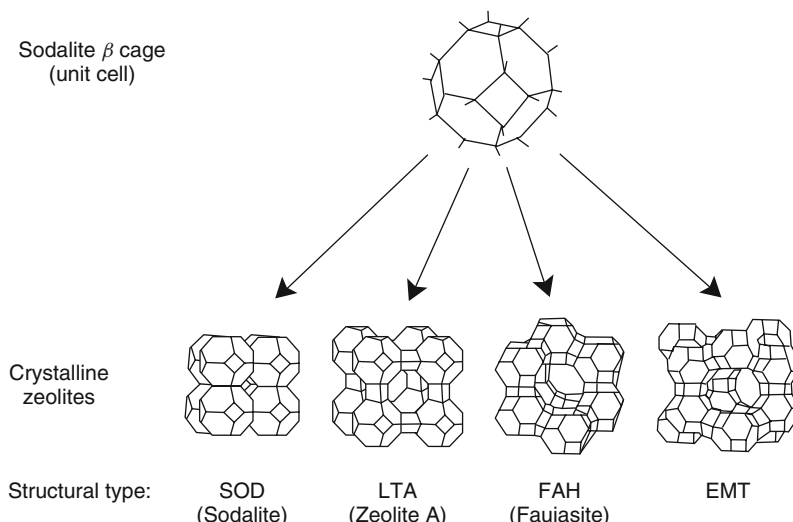


Figure 3.36 Sodalite $\text{SiO}_4/\text{AlO}_4$ β -unit cells can link together to form a variety of zeolite structures, each with its own geometry and pore size [95]

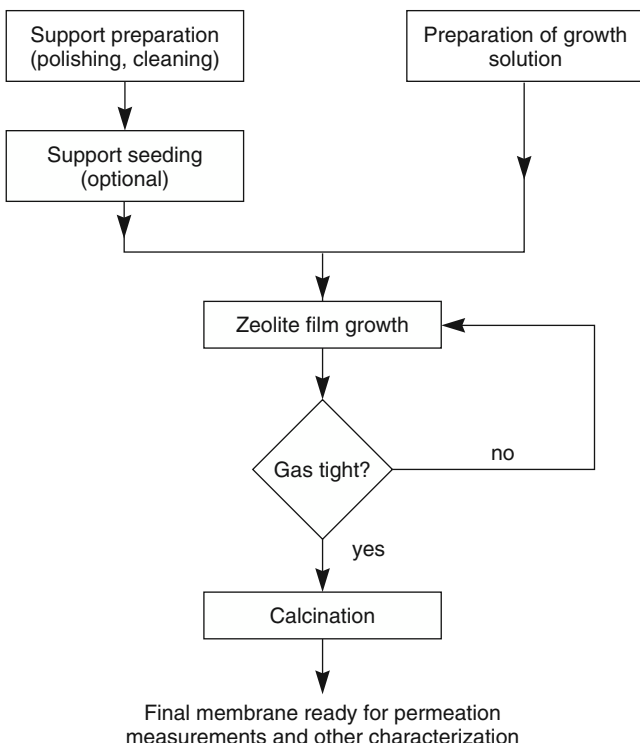
In Situ Hydrothermal Synthesis

Figure 3.37 Methods of preparing zeolite membranes [97]

the membrane is tested to see if it is gas tight. If not, the sample is reimmersed in the precursor solution and autoclaved a second time. When the sample is gas tight, it is calcined. The sample is then ready for evaluation.

More recently, a technique of seeding the support structure with small seed crystals of the desired zeolite has been developed, as shown in Figure 3.38. The seed crystals are prepared by separately synthesizing the required zeolite or grinding a sample to the required size ($\sim 0.5\text{ }\mu\text{m}$). The support must be thoroughly cleaned to promote uniform and good coverage of the seed crystal solution on the support. The sample is then heated with an appropriate $\text{AlO}_4/\text{SiO}_4$ solution in an autoclave. In this process, somewhat simpler solutions can be used and structure-directing reagents may not be needed. The crystal nucleation technique generally leads to thinner and more defect-free zeolites. Nonetheless, zeolite membranes must normally be $20\text{--}50\text{ }\mu\text{m}$ thick to be defect-free so fluxes are often quite low, although selectivities in many separations are very good. For the most part, zeolite membranes are still at the laboratory stage of development, except for the work of Sato *et al.* at the Bussan Nanotech Research Institute (XNRI) subsidiary of Mitsui, who have brought the technology to the pilot-plant stage for the separation of water/ethanol solutions by pervaporation [98, 99].

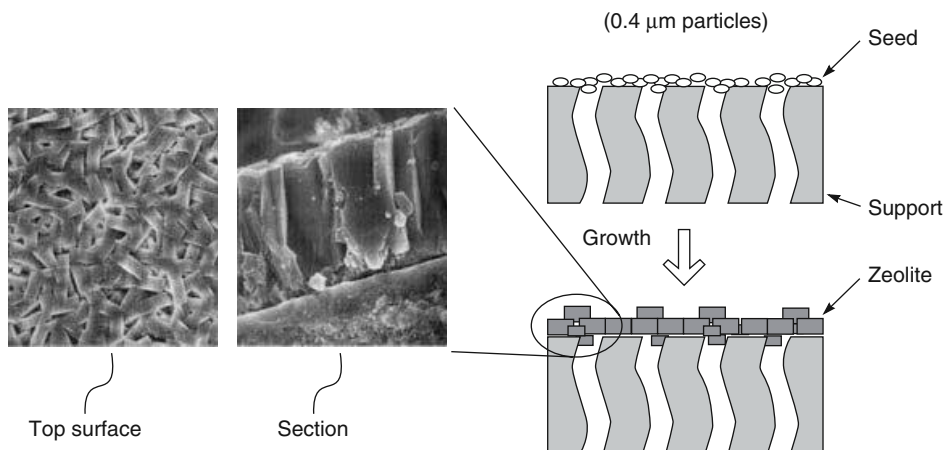


Figure 3.38 Zeolite formation by the seed nucleation and growth technique. (Adapted from Ref. [97].)

3.4.4 Mixed-Matrix Membranes

The ceramic and zeolite membranes described above have been shown to have exceptional selectivities for a number of important separations. However, the membranes are difficult to make, and are usually more than $10 \mu\text{m}$ thick so permeances are low. As a consequence, the membranes are prohibitively expensive for most separations. One solution that has been suggested is to prepare membranes consisting of zeolite particles dispersed in a polymer matrix. Makers of these membranes hope to combine the selectivity of zeolite membranes with the low cost and ease of manufacture of polymer membranes. Such membranes are called mixed-matrix membranes.

Mixed-matrix membranes have been a subject of research interest for more than 20 years. The concept is illustrated in Figure 3.39. At relatively low loadings of zeolite

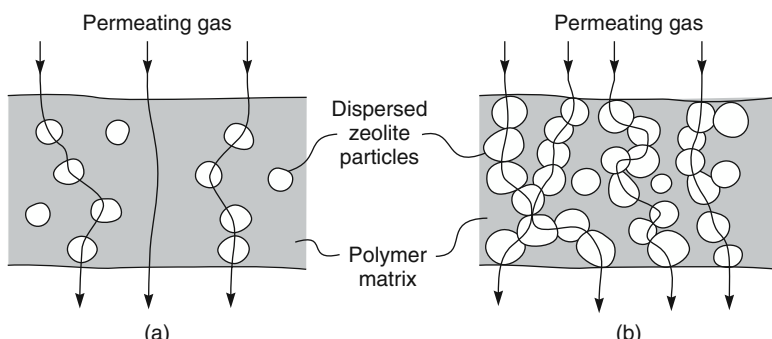


Figure 3.39 Gas permeation through mixed-matrix membranes containing different amounts of dispersed zeolite particles

particles, permeation occurs by a combination of diffusion through the polymer phase and diffusion through the permeable zeolite particles. The relative permeation rates through the two phases are determined by their permeabilities. At low loadings of zeolite, the effect of the permeable zeolite particles on permeation can be expressed mathematically by the expression shown below, first developed by Maxwell in the 1870s [100].

$$P = P_c \left[\frac{P_d + 2P_c - 2\Phi(P_c - P_d)}{P_d + 2P_c + \Phi(P_c - P_d)} \right] \quad (3.2)$$

where P is the overall permeability of the mixed-matrix material, Φ is the volume fraction of the dispersed zeolite phase, P_c is the permeability of the continuous polymer phase, and P_d is the permeability of the dispersed zeolite phase.

At low loadings of dispersed zeolite, individual particles can be considered to be well separated. At higher loadings, some small islands of interconnected particles form; at even higher loadings, these islands grow and connect to form extended pathways. At loadings above a certain critical value, continuous channels form within the membrane, and almost all the zeolite particles are connected to the channels. This value is called the percolation threshold. At this particle loading, the Maxwell equation is no longer used to calculate the membrane permeability. The percolation threshold is achieved at particle loadings of about 30 vol%.

Figure 3.40, adapted from a plot by Robeson *et al.* [101], shows a calculated plot of permeation of a model gas through zeolite-filled polymer membranes in which the zeolite phase is 1000 times more permeable than the polymer phase. At low zeolite particle loadings, the average particle is only in contact with one or two other particles, and a modest increase in average permeability occurs following the Maxwell model. At particle loadings of 25–30 vol% the situation is different – most particles touch two or more particles, and most of the permeating gas can diffuse through interconnected zeolite channels. The percolation threshold has been reached, and the Maxwell model no longer applies. Gas permeation is then best described as permeation through two interpenetrating, continuous phases. At very high zeolite loadings, the mixed-matrix membrane may be best described as a continuous zeolite phase containing dispersed particles of polymer. The Maxwell model may then again apply, with the continuous and the dispersed phases in Equation 3.2 reversed.

The figure also shows that the highly permeable zeolite only has a large effect on polymer permeability when the percolation threshold is reached. That is, useful membranes must contain more than 30 vol% zeolite. This observation is borne out by the available experimental data.

Despite a great deal of recent research on preparation of mixed-matrix membranes, performance results to date have been modest. Two general approaches have been used. The first, investigated by the groups of Koros [102–104], Smolders [105], and Peinemann [106], is to use the expected difference in the diffusion coefficients of gases in the zeolite particles. Koros, in particular, has focused on zeolites with small aperture sizes; for example, Zeolite 4A, with an effective aperture size of 3.8–4.0 Å, has been used to separate oxygen (Lennard-Jones (LJ) diameter 3.47 Å) from nitrogen (LJ diameter 3.8 Å). The theoretical oxygen/nitrogen selectivity of a Zeolite 4A membrane has been calculated to be 37, with an oxygen permeability of 0.8 Barrer – this would

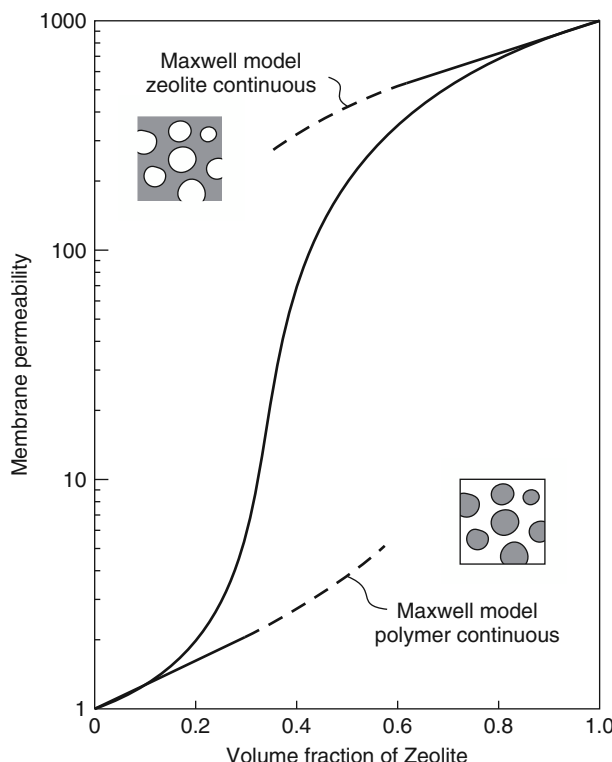


Figure 3.40 Change in membrane permeabilities for mixed-matrix membranes containing different volume fractions of zeolite. Reprinted with permission from [108]. Copyright (2010) Elsevier.

be an exceptional membrane. To maximize the effect of the zeolite in his mixed-matrix membrane, Koros used relatively low permeability polymers, such as Matrimid® and other polyimides, or poly(vinyl acetate). Some of his best results, shown in Figure 3.41, illustrate the potential and the problems of the mixed-matrix approach [107].

The best membrane material reported by Koros, 40 vol% Zeolite 4A in PVAc, had an oxygen/nitrogen selectivity of 9.7–10.4 and an oxygen permeability of about 0.3 Barrer. Such a material would be of interest to producers of nitrogen-from-air separation systems. However, because the zeolite particles were 1–2 µm in diameter, the mixed-matrix membrane films were 20–50 µm thick, resulting in low fluxes. Commercial membranes are typically 0.05–0.2 µm thick, with much higher flux values. Another problem with such large zeolite particles was obtaining good physical contact between the glassy PVAc matrix polymer and the zeolite particles, leading to gas bypass around the edges of the particles. The bypass issue becomes more of a problem as the zeolite loading increases.

The second type of zeolite mixed-matrix membrane relies on relative sorption of different permeants to obtain an improved separation. For example, Smolders *et al.* [108], at the University of Twente, and Peinemann and coworkers at GKSS, Geesthacht [109], showed that silicalite–silicone rubber mixed-matrix membranes had exceptional selectivities for

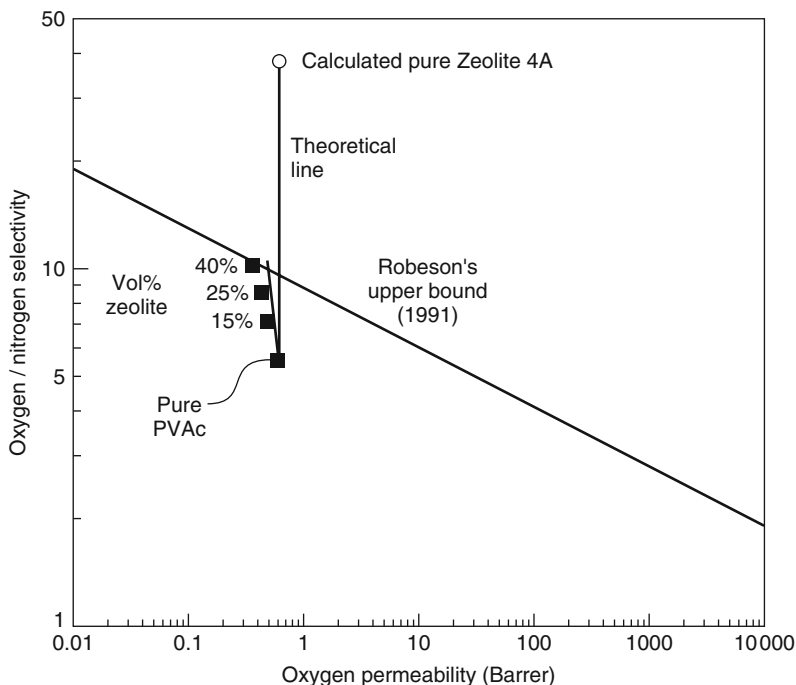


Figure 3.41 Performance of PVAc-zeolite 4A [107] mixed-matrix membranes for oxygen/nitrogen separations. The Robeson upper bound line shows the empirical trade-off between selectivity and flux observed by Robeson for polymeric membranes in 1991. The Robeson plot is discussed in more detail in Chapter 8

the permeation of ethanol (kinetic diameter 4.5 Å) over water (kinetic diameter 2.6 Å). These zeolites separate by virtue of their higher sorption of ethanol compared to water on the hydrophobic silicalite surface. Differences in diffusion coefficients favor permeation of water, but this effect is overcome by the sorption effect. The net result is an increase in the relative permeability of ethanol over water, compared to pure silicone rubber membranes. Because the aperture diameter of the silicalite particles is relatively large, permeabilities through the zeolite phase are also high, allowing rubbery, relatively high-permeability polymers to be used as the matrix phase. Although 10–20 µm thick, the resulting membranes still have useful permeances. The problem of permeate bypass around the edges of the zeolite particles is also less of a problem with these rubbery polymers.

Some data comparing the performance of a simple silicone rubber membrane and a silicone rubber–silicalite mixed-matrix membrane are shown in Figure 3.42 [110]. The improved selectivity achieved by adding zeolite particles to a silicone rubber matrix is produced by a combination of increasing the permeability to ethanol and decreasing the permeability to water. It appears that ethanol passes through the zeolite particles faster than through the silicone polymer matrix, and thus the ethanol permeabilities are enhanced. Water cannot permeate through the zeolite particles and so these particles increase the tortuous path taken by the permeating water. The result is a decrease in water permeability.

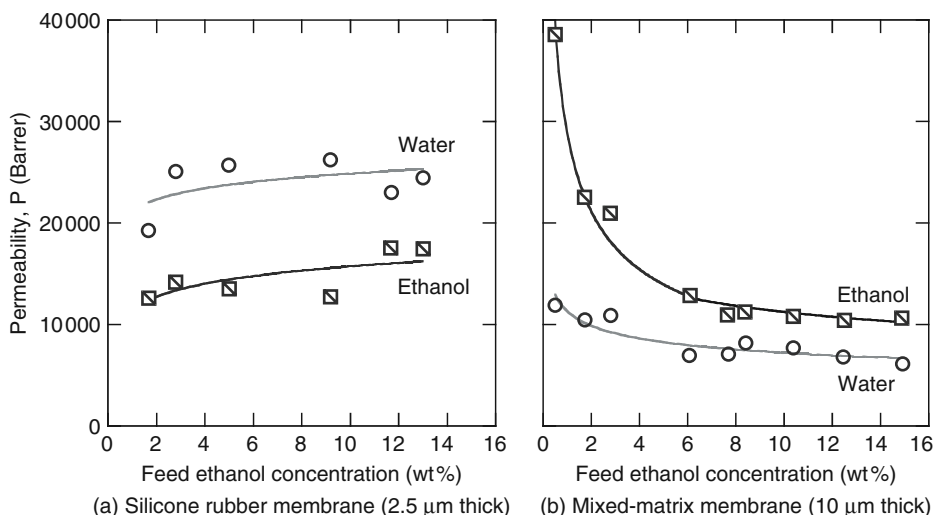


Figure 3.42 Pervaporation permeability (Equation 2.86) of ethanol and water obtained with a 2.5 μm -thick pure silicone rubber membrane and a 10 μm zeolite (60 wt%)-silicone rubber mixed-matrix membrane (flow through test cells at 75°C, permeate pressure <5 torr, stage-cut per cell less than 0.2%) [110]. (Reprinted from J. Membr. Sci., 348 (1-2), R.W. Baker, J.G. Wijmans and Y. Huang, Permeability, permeance and selectivity: a preferred way of reporting pervaporation performance data, p. 346–352, Copyright 2010, with permission from Elsevier.)

A number of problems have to be solved before mixed-matrix membranes are going to be widely used. First, to achieve connectivity of the zeolite phase, more than 30 vol% of the membrane must be zeolite. At these very high loadings, the membranes are chalky, mechanically weak and difficult to make defect-free. Second, it is critical that no gaps exist between the polymer phase and the zeolite particles [111]. If present, these gaps act as channels to allow the permeating gas mixture to bypass the zeolite particles unseparated. Finally, zeolite membranes can be plugged by minor components in the feed mixture that penetrate and permanently adsorb into the zeolite, severely reducing permeation of the target permeant. Some progress is being made on all of these problems, but these membranes are still a long way from commercial use.

3.4.5 Carbon Membranes

The first microporous carbon membranes were produced by Barrer in the 1950s and 1960s by compressing high surface area carbon powders at very high pressures [112, 113]. The resulting porous plugs had pores of 5–30 Å diameter and were used to study diffusion of gases and vapors. Later, Koresh and Soffer produced extremely finely porous hollow fiber microporous carbon membranes by pyrolyzing preformed polyacrylonitrile or polyimide membranes in an inert atmosphere at 500–800°C [114]. This technology was brought to the small module stage, but failed commercially because the membranes were very brittle and difficult to make defect-free on a large scale. However, the membranes had exceptional separation properties for some gas mixtures and so the preparation of carbon

membranes remains an active area of research for gas separation and some pervaporation applications. There are active research groups in Japan [115–117], Korea [118], and the United States [119–123].

The general procedure used to prepare carbon membranes is shown in Figure 3.43. A wide variety of precursor polymer membranes can be used. Polyacrylonitrile, poly(vinylidene chloride), and poly(furfuryl alcohol) easily carbonize and have been widely used but other research groups prefer polyimides. As the precursor membrane is heated, there is a gradual loss of weight. The amount and composition of the material lost depends on the polymer. Most polymers lose 10–20 wt% by the time the polymer has been heated to 300–500°C. At this point, the polymer becomes yellow to brown. Heating at higher temperatures produces more weight loss and most polymers lose their hetero atoms

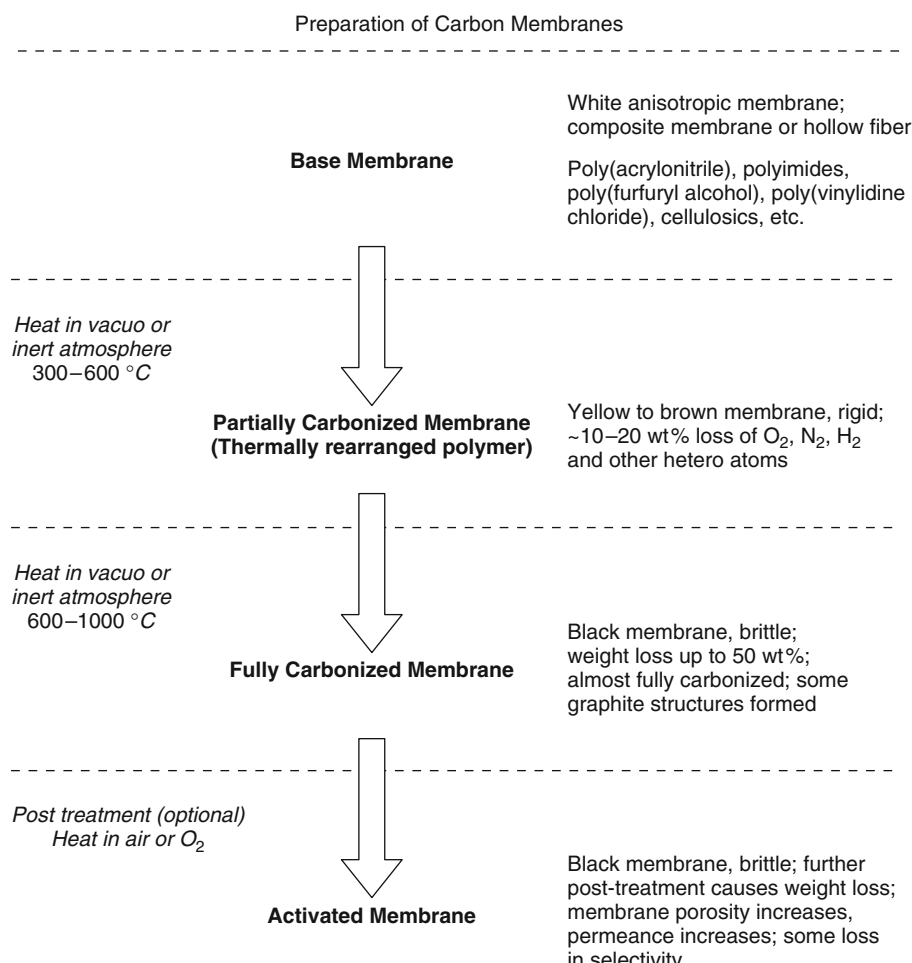


Figure 3.43 Typical changes seen in the character of carbon membranes during the preparation process

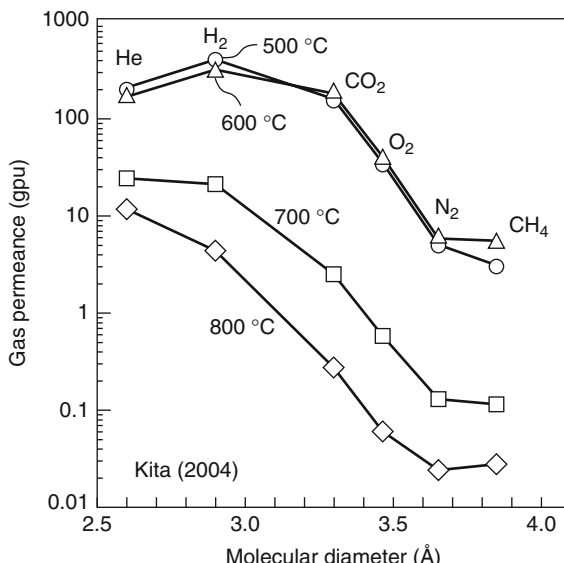


Figure 3.44 Changes in the gas permeances of carbon membranes made from phenolic resin heated to different carbonizing temperatures [117]

by the time the polymer reaches 800–1000°C. During this carbonization process, the membrane usually becomes denser and the permeance falls, but the selectivity increases. Some results of Kita *et al.* [117] that illustrate this point are shown in Figure 3.44. The base polymer membrane was a thin phenolic resin layer coated onto a microporous ceramic support. After heating to 500°C, the hydrogen permeance is ~500 gpu, but the H₂/CO₂ selectivity is only 3–4. After heating to 800°C, the hydrogen permeance is 100-fold less, but the H₂/CO₂ selectivity is now more than 20. The permeation properties of carbonized membranes are sometimes adjusted by a post-treatment step in which the membrane is heated in air or oxygen at 100–300°C. A further weight loss is produced and the membrane appears to become a little more microporous. The permeance increases, but selectivity usually decreases.

Like ceramic and zeolite membranes, carbon membranes separate by a combination of size sieving and surface diffusion; they are also susceptible to poisoning by strongly adsorbed minor components in the feed gas. Rao and Sirkar at Air Products made finely porous carbon membranes to separate light hydrocarbons from hydrogen. The light hydrocarbons (C₁ to C₄) adsorbed on the surface of the membrane pores and permeated by surface diffusion [119]. Unfortunately, small amounts of C₆₊ hydrocarbons present in the feed gas were also strongly, even permanently, adsorbed and accumulated in the membrane. The result was a steady loss of membrane permeance. Others have noticed similar problems. Koros, for example, reported that as little as a few parts per million of C₆₊ hydrocarbons decreased membrane permeability by over 60% in less than one day. Jones and Koros [121–123] saw the same effect with low concentrations of water. The best target application for carbon membranes appears to be separation of olefin/paraffin mixtures, but membrane stability problems must be solved first.

3.4.6 Microporous Glass Membranes

Microporous glass membranes in the form of tubes and fibers have been made by Corning, PPG, and Schott. Currently only the Corning membranes are still available, under the trade name Vycor®. The leaching process used to make this type of membrane has been described by Beaver [124]. The starting material is a glass containing 30–70% silica, as well as oxides of zirconium, hafnium, or titanium and extractable materials. The extractable materials comprise one or more boron-containing compounds and alkali metal oxides and/or alkaline earth metal oxides. Glass hollow fibers produced by melt extrusion are treated with dilute hydrochloric acid at 90°C for 2–4 hours to leach out the extractable materials, washed to remove residual acid, and then dried.

3.5 Liquid Membranes

Liquid membranes containing carriers to facilitate selective transport of gases or ions were the subject of a considerable research effort in the 1970s and 1980s. A number of published reviews summarize this work [125, 126]. Although these membranes are still being studied, improvements in selective conventional polymer membranes have diminished the interest in processes using liquid membranes. The preparation and use of liquid membranes and other facilitated transport membranes are described in Chapter 11.

3.6 Hollow Fiber Membranes

The membrane preparation techniques described so far were developed to produce flat-sheet membranes. However, these techniques can be adapted to produce membranes in the form of thin tubes or fibers. An important advantage of hollow fiber membranes is that compact modules with high membrane surface areas can be formed. However, this advantage is offset by the generally lower fluxes of hollow fiber membranes compared to flat-sheet membranes made from the same materials. Nonetheless, the development of hollow fiber membranes by Mahon and the group at Dow Chemical in 1966 [127] and their later commercialization by Dow, Monsanto, Du Pont, and others represents one of the major events in membrane technology. A good review of the early development of hollow fiber membranes is given by Baum *et al.* [128]. Reviews of more recent developments are given by Moch [129], McKelvey *et al.* [130], and Chung [131].

The diameter of hollow fibers varies over a wide range, from 50 to 3000 µm. Fibers can be made with a uniformly dense structure, but preferably are formed as a microporous structure having a dense selective layer on the outside or inside surface. The dense surface layer can be either integral with the fiber or a separate layer coated onto the porous support fiber. Many fibers must be packed into bundles and potted into tubes to form a membrane module; modules with a surface area of even a few square meters require kilometers of fibers. Because a module must contain no broken or defective fibers, hollow fiber production requires high reproducibility and stringent quality control.

The types of hollow fiber membranes in production are illustrated in Figure 3.45. Fibers of 50–200 µm diameter are usually called hollow fine fibers. Such fibers can withstand very

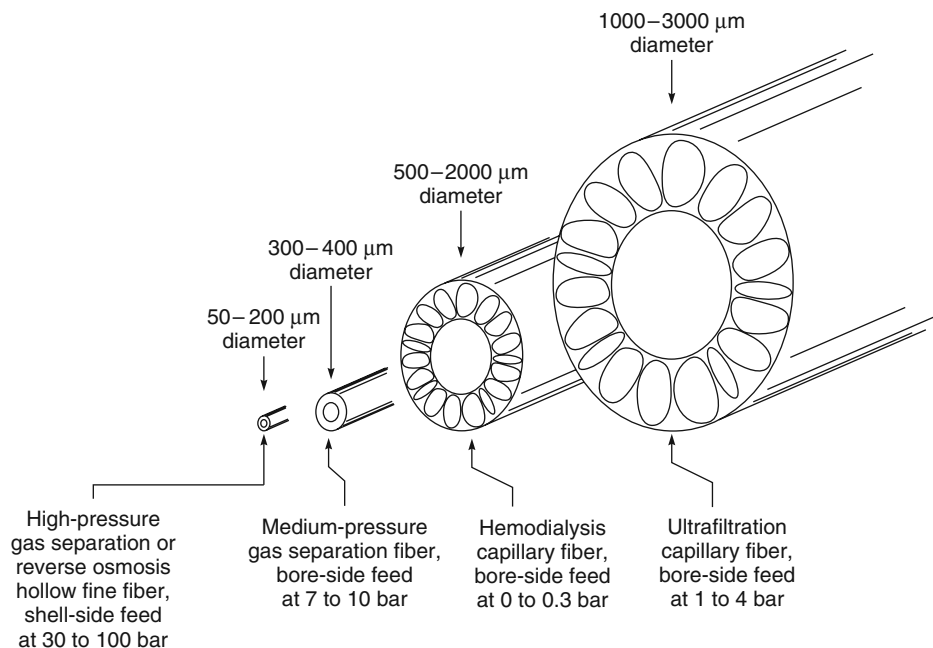


Figure 3.45 Schematic of the principal types of hollow fiber membranes

high hydrostatic pressures applied from the outside, so they are used in reverse osmosis or high-pressure gas separation applications in which the applied pressure can be 60 bar or more. The feed fluid is applied to the outside (shell side) of the fibers, and the permeate is removed down the fiber bore. When the fiber diameter is greater than 200–500 µm, the feed fluid is commonly applied to the inside bore of the fiber, and the permeate is removed from the outer shell. This technique is used for low-pressure gas separation and for applications such as hemodialysis or ultrafiltration. Fibers with a diameter of greater than 500 µm are called capillary fibers.

Two methods are used to prepare hollow fibers: solution spinning and melt spinning [128–131]. The most common process is solution spinning or wet spinning, in which a 20–30 wt% polymer solution is extruded and precipitated into a nonsolvent, generally water. Fibers made by solution spinning have the anisotropic structure of Loeb–Sourirajan membranes. This technique is used to make relatively large, porous hemodialysis and ultrafiltration fibers. In the alternative technique of melt spinning, a hot polymer melt is extruded from an appropriate die and is then cooled and solidified in air prior to immersion in a quench tank. Melt-spun fibers are usually denser and have lower fluxes than solution-spun fibers, but, because the fiber can be stretched after it leaves the die, very fine fibers can be made. Melt-spun fibers can also be produced at high speeds. The technique is usually used to make hollow fine fibers for high-pressure reverse osmosis and gas separation applications and is also used with polymers such as poly(trimethylpentene), which are not soluble in convenient solvents and are difficult to form by wet spinning. The distinction between solution spinning and melt spinning has gradually faded over the

years. To improve fluxes, solvents and other additives are generally added to melt spinning dopes so spinning temperatures have fallen considerably. Many melt spun fibers are now produced from spinning dopes containing as much as 30–60 wt% solvent, which requires the spinner to be heated to only 70–100°C to make the dope flow. These fibers are also often cooled and precipitated by spinning into a water bath, which also helps to form an anisotropic structure.

The first hollow fiber spinneret system was devised by Mahon at Dow [127]. Mahon's spinneret consisted of two concentric capillaries, the outer capillary having a diameter of approximately 400 µm, and the central capillary having an outer diameter of approximately 200 µm and an inner diameter of 100 µm. Polymer solution is forced through the outer capillary, while air or liquid is forced through the inner one. The rate at which the core fluid is injected into the fibers relative to the flow of polymer solution governs the ultimate wall thickness of the fiber. Figure 3.46 shows a cross-section of this type of spinneret, which is widely used to produce the large-diameter fibers used in ultrafiltration. Experimental details of this type of spinneret can be found elsewhere [130–132]. A complete hollow fiber spinning system is shown in Figure 3.47.

In the laboratory, a fiber spinning system will usually only have a single spinneret, but industrial systems can have 5–50 spinnerets manifolded together using the same spinning solution. These systems operate continuously for weeks or months at a time. Individual spinnerets may be taken offline if malfunctions occur, while the remaining units continue to operate.

The evaporation time between the solution exiting the spinneret and entering the coagulation bath is a critical variable, as are the compositions of the bore fluid and the coagulation bath. The position of the dense anisotropic skin can be adjusted by varying the bath and bore solutions. For example, if water is used as the bore fluid and the coagulation bath contains some solvent, precipitation will occur first and most rapidly on the inside surface of the fiber. If the solutions are reversed so that the bore solution contains some solvent

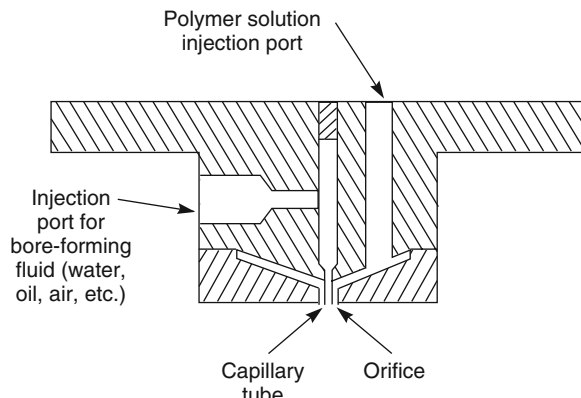


Figure 3.46 Twin-orifice spinneret design used in solution-spinning of hollow fiber membranes. Polymer solution is forced through the outer orifice, while bore-forming fluid is forced through the inner capillary

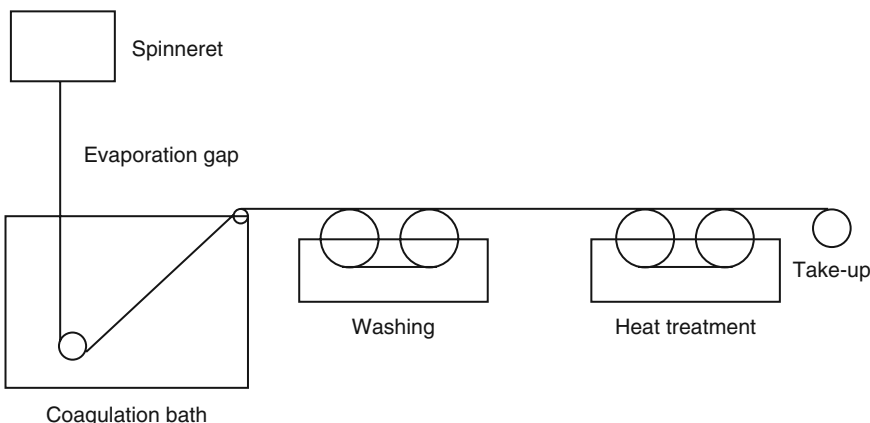


Figure 3.47 A complete hollow fiber solution-spinning system. The fiber is spun into a coagulation bath, where the polymer spinning solution precipitates forming the fiber. The fiber is then washed, dried, and taken up on a roll

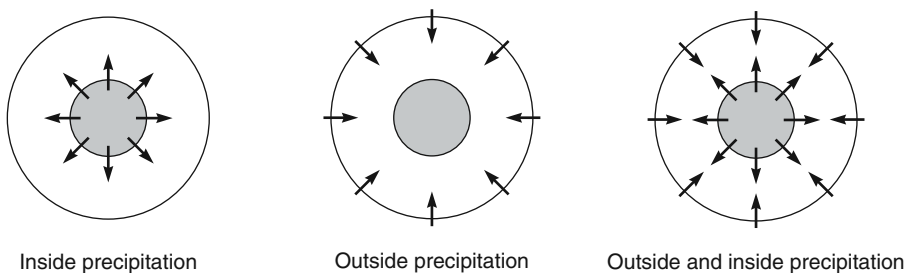


Figure 3.48 Depending on the bore fluid and the composition of the coagulation bath, the selective skin layer can be formed on the inside, the outside or both sides of the hollow fiber membrane. Reprinted with permission from [138]. Copyright (2007) Elsevier.

and the coagulation bath is water, the skin will tend to be formed on the outside surface of the fiber, as shown in Figure 3.48. In many cases precipitation will begin on both surfaces of the fiber, and a dense layer will form on both inside and outside surfaces. This ability to manipulate the position of the dense skin is important, because in use the skin should normally face the feed fluid to be separated.

Generally, the spinning dope used in solution spinning has a higher polymer concentration and is more viscous than the casting solutions used to form equivalent flat-sheet membranes. This is because hollow fiber membranes must be able to perform the separation required and to withstand the applied pressure of the process without collapsing. The mechanical demands placed on the microporous substructure of hollow fiber membranes are more demanding than for their flat-sheet equivalents. Consequently, a finer, stronger, and higher density microporous support structure is required. Because more concentrated casting solutions are used, the thickness of the skin layer of hollow fiber

membranes is also greater than their flat-sheet equivalents, and lower membrane fluxes usually result. However, the low cost of producing a large membrane area in hollow fiber form compensates for the lower flux.

Hollow fiber spinning dopes and preparation procedures vary over a wider range than their flat-sheet equivalents; some representative dopes and spinning conditions taken from the patent literature [127, 132, 133] are given in Table 3.4.

Recently, interest in forming more complex hollow fibers has developed; for example, composite hollow fibers in which the microporous shell of the fiber provides the mechanical strength, but the selective layer is a coating of a different material. Ube, Praxair, Air Products, and Medal all produce this type of fiber for gas separation applications. Various techniques are described in the patent literature [134–136]. One method of producing composite hollow fibers, described by Kusuki *et al.* at Ube [137] and Kopp *et al.* at Memtec [138], is to spin double-layered fibers with a double spinneret of the type shown in Figure 3.49. This system allows different spinning solutions to be used for the outer and inner surface of the fibers and gives more precise control of the final structure. Considerable optimization of the spinning solutions and spinning conditions is needed to produce defect-free fibers this way [139, 140]. Delamination at the interface between the different polymer layers is a problem. Scanning electron micrographs of a two-layer pervaporation hollow fiber made this way are shown in Figure 3.50 [141].

One reason for the popularity of these types of dual-layer composite hollow fiber membranes is that different polymers can be used to form the mechanically strong support and the selective layer. This allows each layer of the membrane to be separately optimized for the function it must perform. A second reason these membranes are used is

Table 3.4 Preparation parameters for various hollow fiber membranes

Casting dope	Bore fluid	Precipitation bath	Membrane type
37 wt% polysulfone (Udel P3500)	Water	Water 25–50°C	Gas separation fiber O_2/N_2 selectivity = 5.2, ~50 µm diameter, anisotropic outside-skinned fibers, finely microporous substrate [132]
36 wt% <i>N</i> -methyl pyrrolidone			
27 wt% propionic acid (spun at 15–100°C)			
25 wt% polyacrylonitrile-vinyl acetate copolymer	10 wt% dimethyl formamide in water	40 wt% dimethyl formamide in water 4°C	Ultrafiltration capillary membrane, inside skin, 98% rejection to 110 000 MW dextran [133]
68 wt% dimethyl formamide			
7 wt% formamide (spun at 65°C)			
69 wt% cellulose triacetate (spun at 200°C)	Air	No precipitation bath used; fiber forms on cooling.	Early (Dow) 80-µm-diameter fine fiber reverse osmosis membrane [127]
17.2 wt% sulfolane			
13.8 wt% polyethylene glycol (MW 400)		Solvents removed in later extraction step	

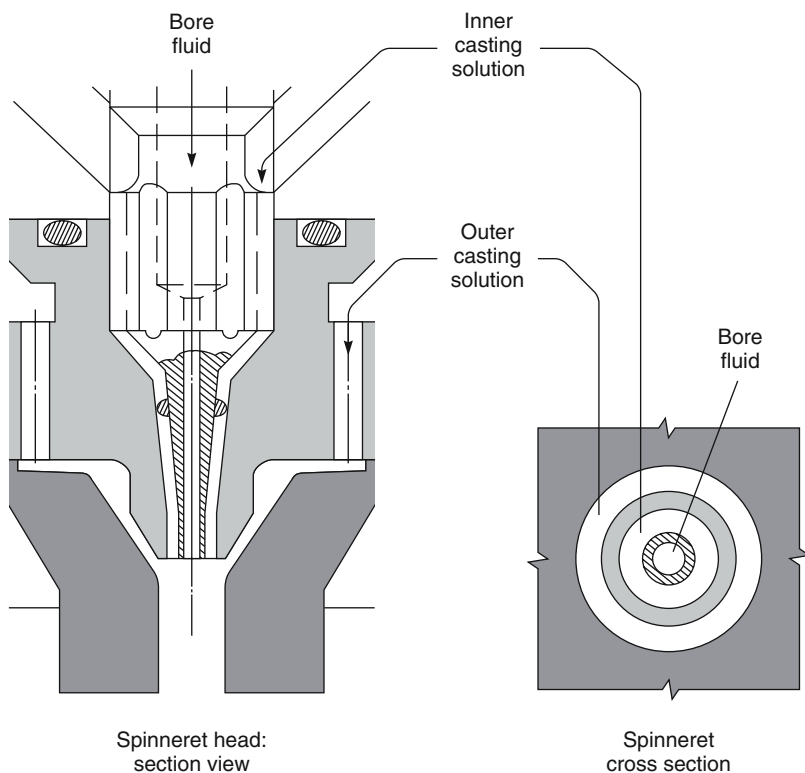


Figure 3.49 A double capillary spinneret sometimes used to produce two-layer hollow fibers. (After Kopp et al. [138].)

to reduce the amount of selective polymer required. The tailor-made polymers developed for gas separation applications can cost as much as US\$5–10/g. Single-layer hollow fiber membranes contain 10–20 g of polymer per square meter of membrane, for a material cost alone of US\$50–200/m². Using a composite structure consisting of a relatively inexpensive core polymer material coated with a thin layer of the expensive selective polymer reduces the overall membrane material cost significantly.

Another type of dual-layer capillary hollow fiber is illustrated in Figure 3.51. These fibers consist of one or two coating layers deposited on a knitted tubular braid of the type sometimes used to cover electrical wires. The braid increases the strength of the hollow fibers substantially. These fibers are difficult to break by pulling. Discovery of these very robust fibers was a key step in the development of air-sparged hollow fiber submerged membrane reactors (described in more detail in Chapter 7).

The first braid-supported membranes of this type were reported by Hayano *et al.* of Asahi [143] in 1977, but the importance of the development was not widely recognized until Zenon introduced their Zeeweed hollow fibers in the 1990s [144]. The spinneret shown in Figure 3.51 applies two coating solutions to the braid. The first (inner) solution has a lower concentration of polymer so it penetrates into the braid, thus achieving good

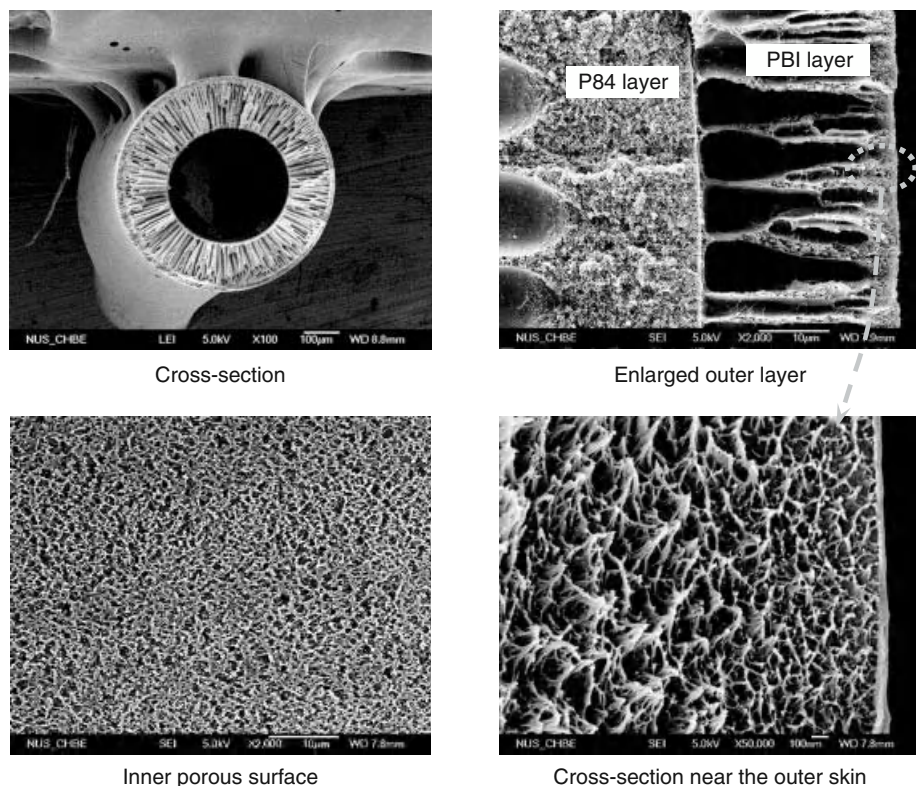


Figure 3.50 Scanning electron micrographs of dual-layer hollow fiber membranes made from an inner core of P84 polyimide and an outer shell of PBI. Reprinted with permission from [142]. Copyright (1965) American Chemical Society.

adhesion to the braid. The second (outer) solution has a higher polymer concentration and is designed to form the selective membrane layer when the coated braid is immersed in the water precipitation bath.

3.7 Membrane Modules

Industrial membrane plants often require hundreds to thousands of square meters of membrane to perform the separation required on a commercial scale. Before a membrane separation can be performed industrially, therefore, methods of economically and efficiently packaging large areas of membrane are required. These packages are called membrane modules. The development of the technology to produce low-cost membrane modules was one of the breakthroughs that led to commercial membrane processes in the 1960s and 1970s. The earliest designs were based on simple filtration technology and

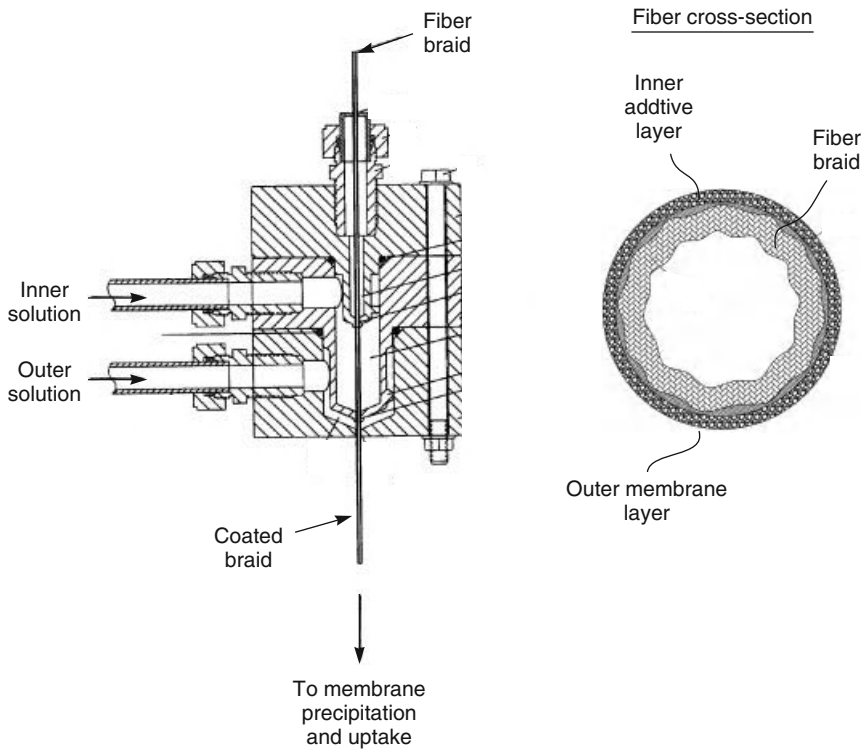


Figure 3.51 Dual-layer spinneret used to make braid-reinforced hollow fiber membranes [142]

consisted of flat sheets of membrane held in a type of filter press: these are called plate-and-frame modules. Membranes in the form of 1–3 cm diameter tubes were developed at about the same time. Both designs are still used, but because of their high cost, they have been largely displaced in most applications by two other designs – the spiral-wound module and the hollow fiber module.

Despite the importance of membrane module technology, many researchers are astonishingly uninformed about module design issues. In part this is because module technology has been developed within companies, and developments are only found in patents, which are not read by many academics. The following sections give an overview of the principal module types, followed by a section summarizing the factors governing selection of particular types for different membrane processes. Cost is always important, but equally important are reliability, membrane fouling, and concentration polarization.

3.7.1 Plate-and-Frame Modules

Plate-and-frame modules were one of the earliest types of membrane system. An early plate-and-frame design proposed by Stern *et al.* [145] for Union Carbide plants to recover helium from natural gas is shown in Figure 3.52. Membrane, feed spacers, and product

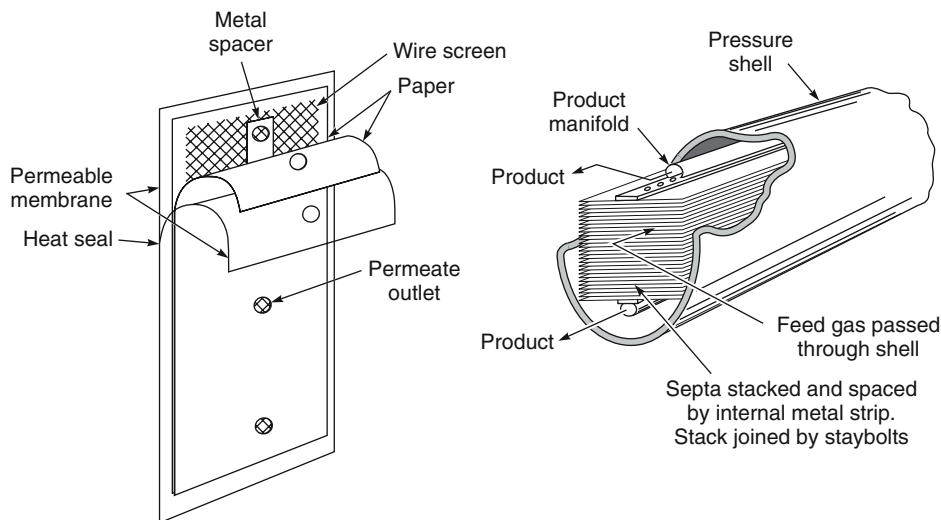


Figure 3.52 Early plate-and-frame design developed by Stern et al. [145] for the separation of helium from natural gas. Reprinted with permission from Koch Membrane Systems Inc. Copyright (2011) Koch Membrane Systems Inc.

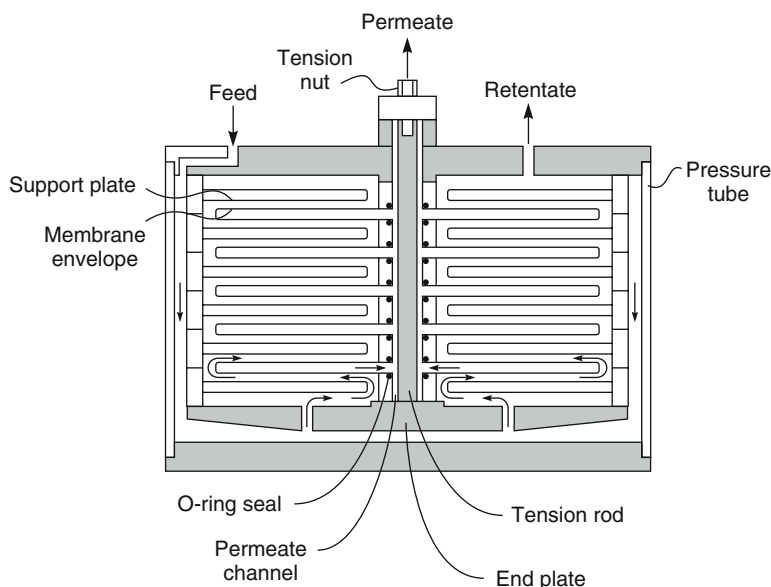


Figure 3.53 Schematic of a plate-and-frame module. Plate-and-frame modules provide good flow control on both the permeate and feed side of the membrane, but the large number of spacer plates and seals lead to high module costs. The feed solution is directed across each plate in series. Permeate enters the membrane envelope and is collected through the central permeate collection channel [146]

spacers are layered together between two end plates. The feed mixture is forced across the surface of the membrane. A portion passes through the membrane, enters the permeate channel, and makes its way to a central permeate collection manifold.

Plate-and-frame units have been developed for some small-scale applications, but these units are expensive compared to the alternatives, and leaks through the gaskets required for each plate are a problem. Plate-and-frame modules are now only used in electrodialysis and pervaporation systems and in a limited number of reverse osmosis and ultrafiltration applications with highly fouling feeds. An example of one of these reverse osmosis units is shown in Figure 3.53 [146].

3.7.2 Tubular Modules

Tubular modules are now generally limited to ultrafiltration applications, for which the benefit of resistance to membrane fouling due to good fluid hydrodynamics outweighs their high cost. Typically, the tubes consist of a porous paper or fiberglass support with the membrane formed on the inside of the tubes, as shown in Figure 3.54.

The first tubular membranes were between 2 and 3 cm in diameter, but more recently, as many as five to seven smaller tubes, each 0.5–1.0 cm in diameter, are nested inside a single, larger tube that serves as the pressure vessel. This produces a larger membrane area in the same size module housing. In a typical tubular membrane system, many tubes are manifolded in series. The permeate is removed from each tube and sent to a permeate collection header. A drawing of a 30-tube system is shown in Figure 3.55. The



Figure 3.54 Typical tubular ultrafiltration module design. The membrane is usually cast on a porous fiberglass or paper support, which is then nested inside a plastic or steel support tube. In the past, each plastic housing contained a single 2–3 cm-diameter tube. More recently, several 0.5–1.0 cm-diameter tubes, nested inside single housings, have been introduced. (Courtesy of Koch Membrane Systems.)

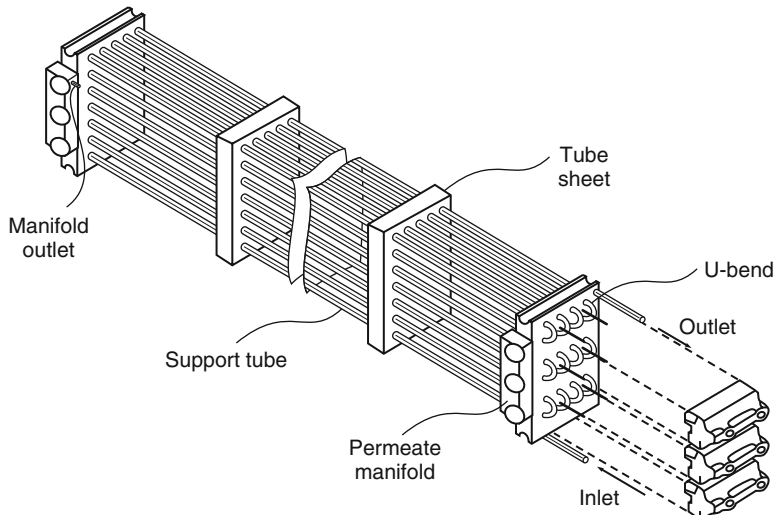


Figure 3.55 Exploded view of a tubular ultrafiltration system in which 30 tubes are connected in series. Permeate from each tube is collected in the permeate manifold

feed solution is pumped through all 30 tubes connected in series. This maintains a high fluid velocity in the tubes, which helps to control membrane fouling.

3.7.3 Spiral-Wound Modules

Spiral-wound modules were used in a number of early artificial kidney designs, but were fully developed for industrial membrane separations at Gulf General Atomic. This work, directed at reverse osmosis membrane modules, was carried out under the sponsorship of the Office of Saline Water [147–149]. The design shown in Figure 3.56 is the simplest, consisting of a membrane envelope of spacers and membrane wound around a perforated central collection tube; the module is placed inside a tubular pressure vessel. Feed passes axially down the module across the membrane envelope. A portion of the feed permeates into the membrane envelope, where it spirals toward the center and exits through the collection tube.

Small laboratory spiral-wound modules consist of a single membrane envelope wrapped around the collection tube, as shown in Figure 3.56. The membrane area of these modules is typically 0.2–1.0 m². This type of module is widely used in “under-the-sink” nanofiltration modules to remove calcium and other divalent ions from hard drinking water. Industrial-scale modules contain many membrane envelopes, each with an area of 1–2 m², wrapped around the central collection pipe. The multi-envelope design developed at Gulf General Atomic by Bray [148] and others is illustrated in Figure 3.57. Multi-envelope designs minimize the pressure drop encountered by the permeate fluid traveling toward the central pipe. If a single membrane envelope were used in a large-membrane-area module, the path taken by the permeate to reach the central collection pipe would be several meters long. Such a long permeate path would result in a large pressure drop in the permeate collection channel. By using multiple short envelopes, the pressure drop

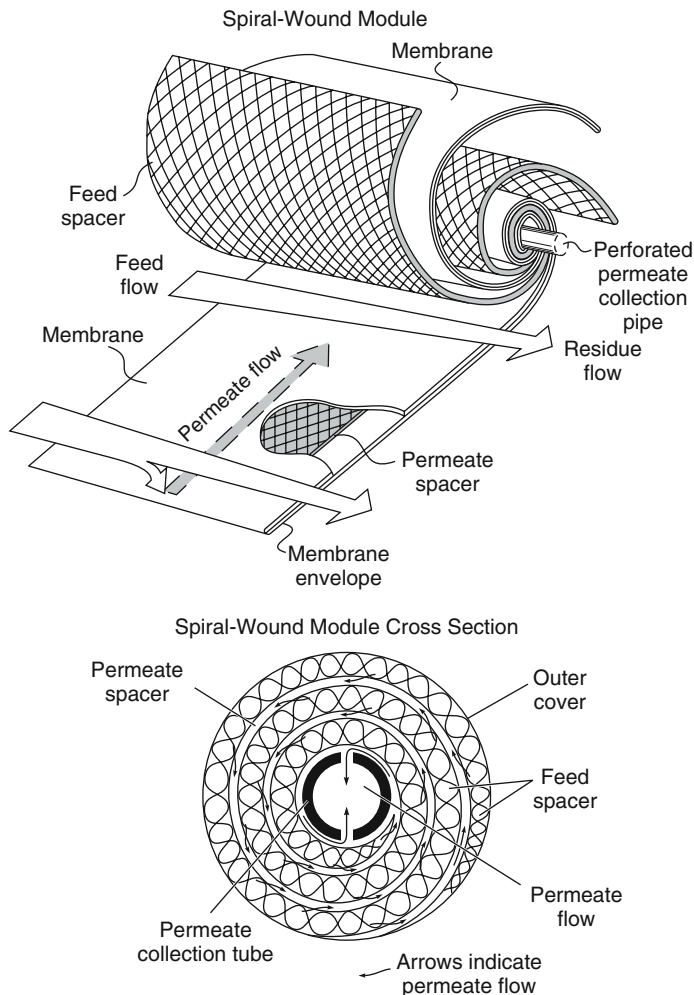


Figure 3.56 Exploded view and cross-section drawings of a spiral-wound module. Feed solution passes across the membrane surface. A portion passes through the membrane and enters the membrane envelope where it spirals inward to the central perforated collection pipe. One solution enters the module (the feed) and two solutions leave (the residue and the permeate). Spiral-wound modules are the most common module design for reverse osmosis and ultrafiltration as well as for high-pressure gas separation applications in the natural gas industry. Reprinted with permission from [147]. Copyright (1988) Taylor and Francis.

in any one envelope is kept at a manageable level. For many years, the standard industrial reverse osmosis/gas separation spiral-wound module had an 8-in. diameter and was 40 in. long. However, there is a trend toward increasing the module diameter, and large reverse osmosis plants now use 16-in. diameter modules. The approximate membrane area and number of membrane envelopes used in industrial 40-in. long spiral-wound modules are given in Table 3.5.

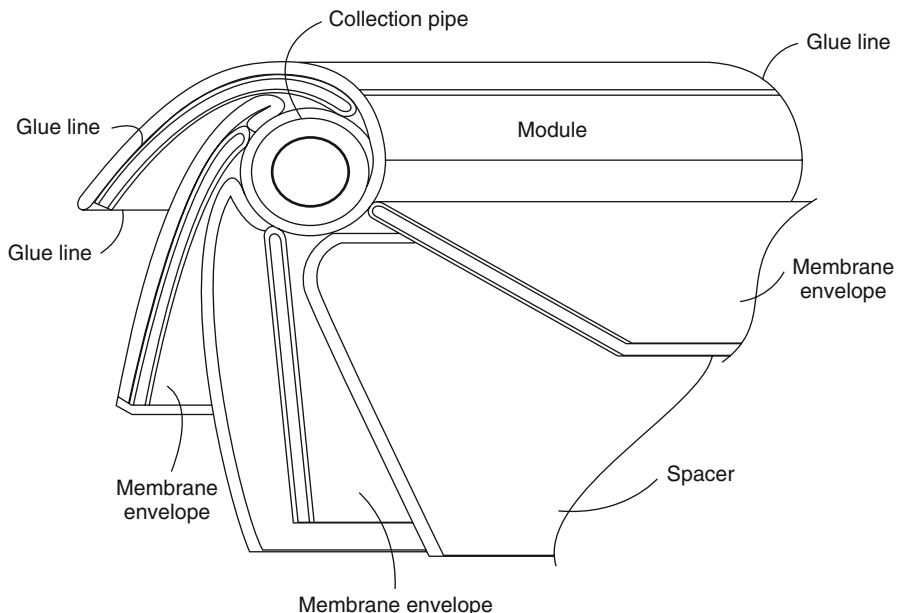


Figure 3.57 Multi-envelope spiral-wound module, used to avoid excessive pressure drops on the permeate side of the membrane. Large-diameter modules may have as many as 50 membrane envelopes, each with a membrane area of 1–2 m². Reprinted with permission from [147]. Copyright (1988) Taylor and Francis.

Table 3.5 Typical membrane area and number of membrane envelopes for 40-in.-long industrial spiral-wound modules. The thickness of the membrane spacers used for different applications causes the variation in membrane area

Module diameter (in.)	4	6	8	16
Number of membrane envelopes	4–6	6–10	15–30	50–100
Membrane area (m ²)	3–6	6–12	20–40	80–150

Four to six spiral-wound membrane modules are normally connected in series inside a single pressure vessel (tube). A typical 8-in. diameter tube containing six modules has 150–250 m² of membrane area. An exploded view of a membrane tube containing two modules is shown in Figure 3.58 [150]. The end of each module is fitted with an anti-telescoping device (ATD) which is designed to prevent the module leaves shifting under the feed-to-residue pressure difference required to force feed fluid through the module. The ATD is also fitted with a rubber seal to form a tight connection between the module and the pressure vessel. This seal prevents fluid bypassing the module in the gap between the module and the vessel wall.

In some applications of reverse osmosis and ultrafiltration spiral-wound modules in the food industry, it may be desirable to allow a small portion of the feed solution to bypass the module to prevent bacteria growing in the otherwise stagnant fluid. One way to achieve this bypass is by perforating the ATD, as illustrated in Figure 3.59 [150].

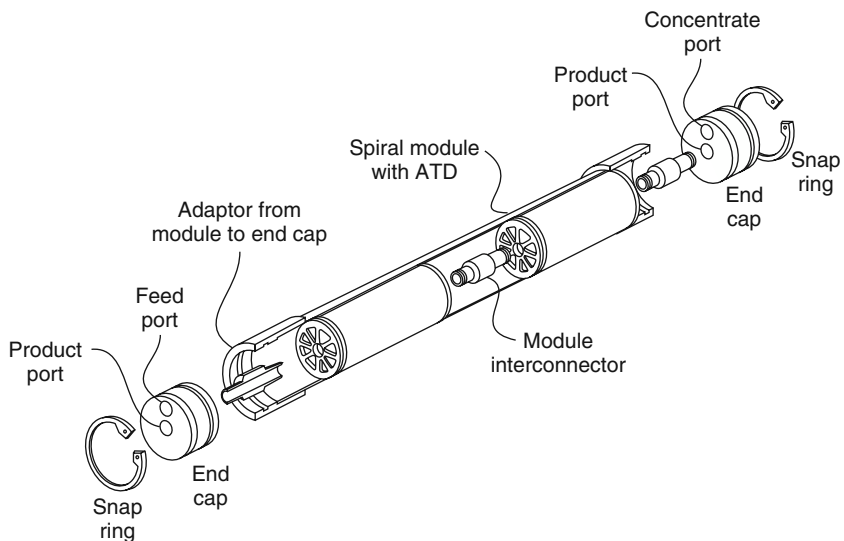


Figure 3.58 Schematic of a spiral-wound module [150] installed in a multimodule pressure vessel. Typically, four to six modules are installed in a single pressure vessel. (Reprinted from Reverse Osmosis Technology, B.S. Parekh (ed.), Marcel Dekker, New York (1988), p. 81, by courtesy of Marcel Dekker, Inc.)

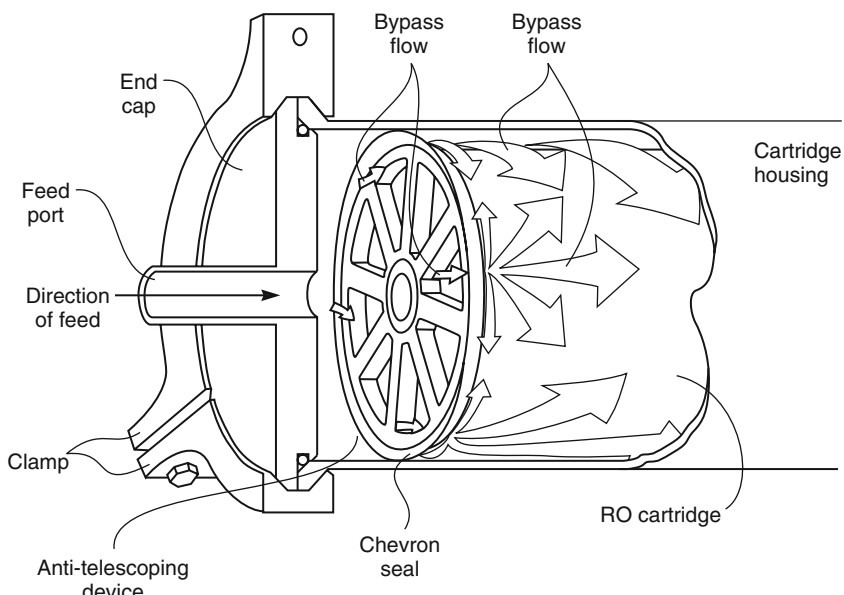


Figure 3.59 By perforating the anti-telescoping device, a small controlled bypass of fluid past the module seal is achieved to eliminate the stagnant area between the reverse osmosis module and the pressure vessel walls. This device is used in food and other sanitary applications of spiral-wound modules [150]. (Reprinted from Reverse Osmosis Technology, B.S. Parekh (ed.), Marcel Dekker, New York (1988), p. 359, by courtesy of Marcel Dekker, Inc.)

3.7.4 Hollow Fiber Modules

Hollow fiber membrane modules are formed in two basic geometries. The first is the shell-side feed design illustrated in Figure 3.60a and used, for example, by Monsanto in their hydrogen separation systems and by Du Pont (until about the year 2000) in their reverse osmosis systems. In such a module, a loop or a closed bundle of fibers is contained in a pressure vessel. The system is pressurized from the shell side; permeate passes through the fiber wall and exits through the open fiber ends. This design is easy to make and allows very large membrane areas to be contained in an economical system. Because the fiber wall must support considerable hydrostatic pressure, the fibers usually have small diameters and thick walls, typically 50 µm internal diameter and 100–200 µm outer diameter.

The second type of hollow fiber module is the bore-side feed type illustrated in Figure 3.60b. The fibers in this type of unit are open at both ends, and the feed fluid is circulated through the bore of the fibers. To minimize pressure drop inside the fibers, the diameters are larger than those of the fine fibers used in the shell-side feed system and are generally made by solution spinning. These so-called capillary fibers are used in ultrafiltration, pervaporation, and some low- to medium-pressure gas applications. Feed pressures are usually limited to below 150 psig in this type of module.

In bore-side feed modules, it is important to ensure that all of the fibers have identical fiber diameters and permeances. Even fiber variation as small as $\pm 10\%$ from the average fiber can lead to large variations in module performance [151, 152]. The flow of fluid through the fiber bore is proportional to the fiber diameter to the fourth power, whereas the membrane area only changes by the second power. The effect is particularly important in the production of nitrogen from air and in hollow fiber kidney modules, in which high levels of removal of the permeable component in a single pass are desired. If the fibers have different diameters, a few overly large or overly small fibers can significantly affect the removal achieved by the module.

Concentration polarization is well controlled in bore-side feed modules. The feed solution passes directly across the active surface of the membrane, and no stagnant dead spaces are produced. This is far from the case in shell-side feed modules in which flow channeling and stagnant areas between fibers cause significant concentration polarization problems [153]. Also, any suspended particulate matter in the feed solution is easily trapped in these stagnant areas, leading to irreversible fouling of the membrane. Baffles to direct the feed flow have been tried [154, 155], but are not widely used. A more common method of minimizing concentration polarization is to direct the feed flow normal to the direction of the hollow fibers as shown in Figure 3.61. This produces a cross-flow module with relatively good flow distribution across the fiber surface. Several membrane modules may be connected in series, so high feed solution velocities can be used. A number of variants on this basic design have been patented [156, 157] and are reviewed by Koros and Fleming [158].

A second problem in shell-side feed hollow fine fibers is permeate-side parasitic pressure drops. The bore channel in these fibers is so narrow, and presents such a resistance to fluid passage, that a significant pressure drop develops along the length of the bore-permeate channel, reducing the pressure difference across the membrane that provides the driving force for permeation. In applications involving separation of mixtures of relatively impermeable components, such as oxygen and nitrogen in air, the pressure

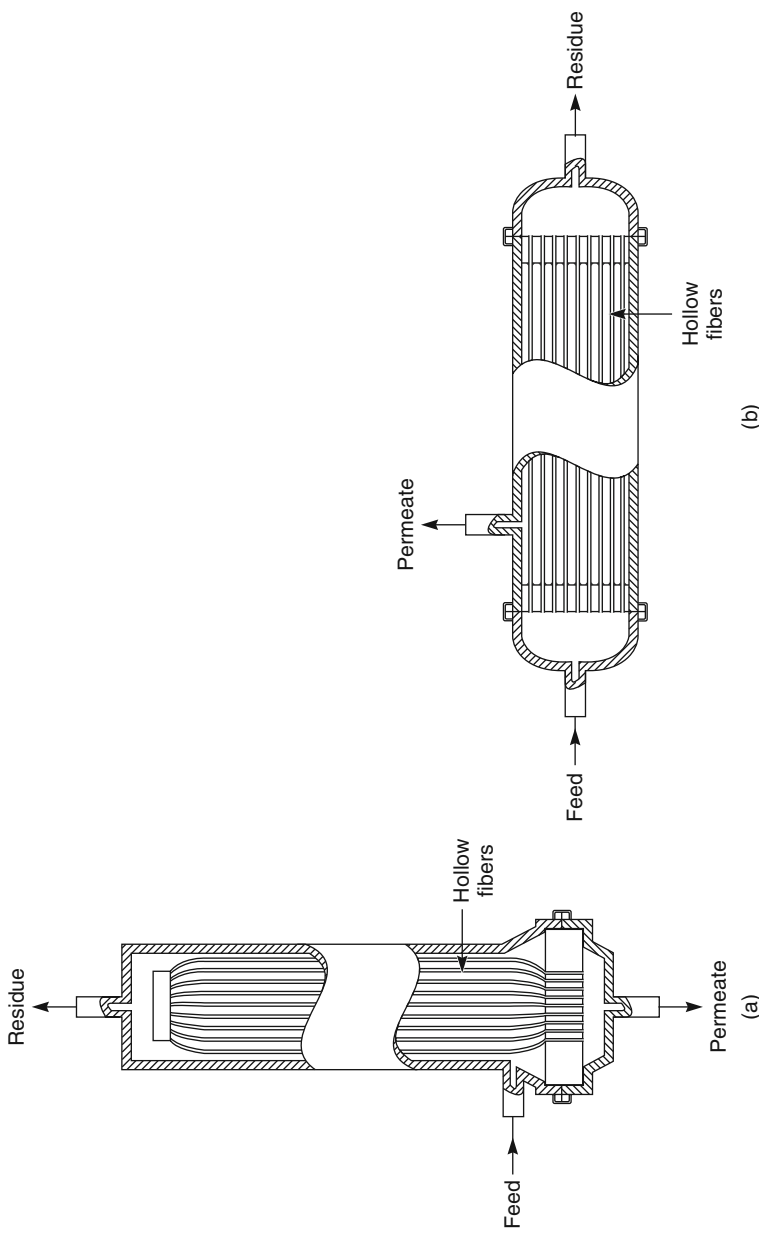


Figure 3.60 Two types of hollow fiber modules used for gas separation, reverse osmosis, and ultrafiltration applications. Shell-side feed modules are generally used for high-pressure applications up to 1000 psig. Fouling on the feed side of the membrane can be a problem with this design, and pretreatment of the feed stream to remove particulates is required. Bore-side feed modules are generally used for medium-pressure feed streams up to 150 psig, for which good flow control to minimize fouling and concentration polarization on the feed side of the membrane is desired

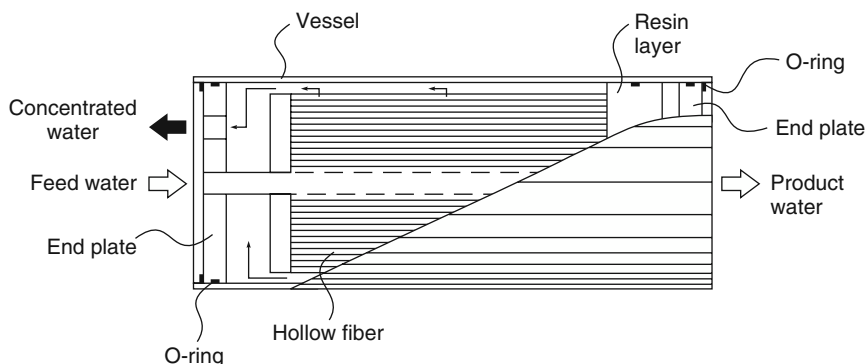


Figure 3.61 A cross-flow hollow fiber module used to obtain better flow distribution and reduce concentration polarization (the Toyobo Hollosep reverse osmosis module). Feed enters through the perforated central pipe and flows toward the module shell. Many hollow fiber gas separation modules also have this geometry.

drop that develops is small and unimportant. But in separations of more permeable gas mixtures, such as hydrogen or carbon dioxide from methane, the pressure drop can be a significant fraction of the total applied pressure. Permeate-side pressure drops also tend to develop in spiral-wound modules. However, because the permeate channels are wider in this type of module, pressure drops are usually smaller and less significant.

The greatest single advantage of hollow fiber modules is the ability to pack a very large membrane area into a single module. The magnitude of this advantage can be gauged by the membrane area per module data shown in Table 3.6. This table shows the calculated membrane area contained in an 8-in. diameter, 40-in. long module; a spiral-wound module of this size would contain about 20–40 m² of membrane area. The equivalent hollow fiber module, filled with fibers with a diameter of 100 µm, will contain approximately 300 m² of membrane area, 10 times the area in a spiral-wound module. As the diameter of the fibers in the module increases, the membrane area decreases. Capillary ultrafiltration membrane modules have almost the same area as equivalent-sized spiral-wound modules.

Table 3.6 also shows the huge numbers of hollow fibers required for high-surface-area modules. A hollow fine fiber module with an area of 300 m² will contain 1000 km of

Table 3.6 Effect of fiber diameter on membrane area and the number of fibers in a module 20 cm (8 in.) in diameter and 1 m (40 in.) long. Twenty-five percent of the module volume is filled with fiber. A spiral-wound module of this size contains approximately 20–40 m² of membrane area and has a packing density of 6–13 cm²/cm³

Module use	High-pressure reverse osmosis and gas separation	Low-pressure gas separation	Ultrafiltration		
Fiber diameter (µm)	100	250	500	1000	2000
Number of fibers/module (thousands)	1000	250	40	10	2.5
Membrane area (m ²)	315	155	65	32	16
Packing density (cm ² /cm ³)	100	50	20	10	5

fiber. Expensive, sophisticated, high-speed automated spinning and fiber handling and module fabrication equipment is required to produce these modules. A hollow fiber spinning operation may have 50–100 spinnerets. In general, the capital investment for a hollow fine fiber production plant is so large that the technology can only be considered when large numbers of modules are being produced on a round-the-clock basis. The technology is maintained as a trade secret within the handful of companies that produce this type of module. A clue to the type of machinery involved can be obtained from the patent literature. Figure 3.62, for example, shows a module winding machine from an old Du Pont patent [159]. Fibers from several bobbins are wound around a porous paper sheet, laying down the bundle that ultimately becomes the module insert.

3.7.5 Other Module Types

3.7.5.1 Vibrating and Rotating Modules

In all the module designs described thus far, the fluid to be separated (gas or liquid) is pumped across the surface of the membrane at high velocity to control concentration

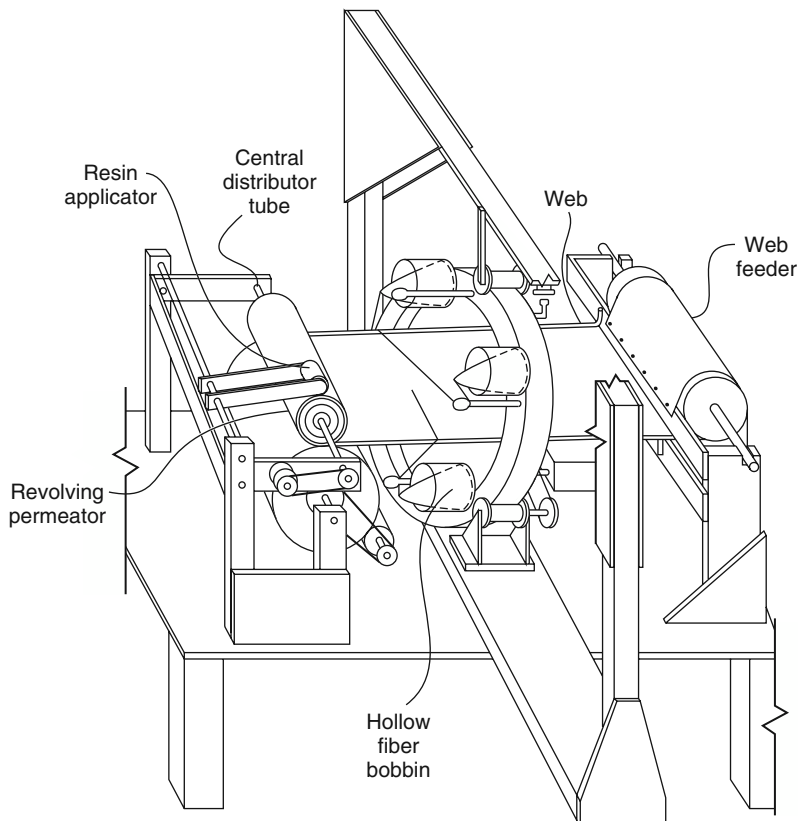


Figure 3.62 Hollow fiber module winding apparatus from a 1972 Du Pont patent [159]. Machines of this general type are still used to produce hollow fiber modules

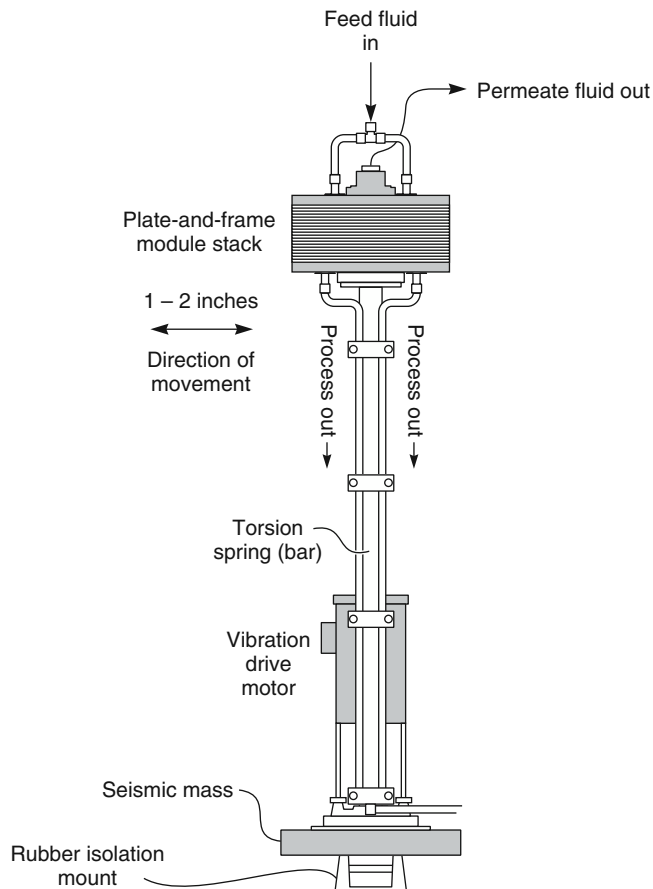


Figure 3.63 New Logic International vibrating plate-and-frame module design [160]. A motor taps a metal plate (the seismic mass) supported by a rubber mount at 60 times/s. A bar that acts as a torsion spring connects the vibrating mass to a plate-and-frame membrane module, which then vibrates by 1–2 in. at the same frequency. By shaking the membrane module, high turbulence is induced in the pressurized feed fluid flowing through the module. The turbulence occurs directly at the membrane surface, providing good control of membrane fouling

polarization. A few vibrating or rotating modules, in which the membrane moves, and moves much faster than the fluid flowing across its surface, have been developed. One such design, a vibrating module from New Logic International, is shown in Figure 3.63 [160–162]. Vibration of the membrane at high speed creates agitation of the feed solution directly at the membrane surface. These modules can ultrafilter extremely concentrated, viscous solutions that cannot be treated by conventional module designs. Currently, the modules are expensive – in the range of US\$2000–5000/m² membrane – compared to alternative designs. This limits their application to high-value separations that cannot be performed by other processes.

3.7.5.2 Submerged Membranes for Microfiltration/Membrane Bioreactors

The development of low-pressure operating membranes with short cycle back-flushing combined with air scrubbing has transformed the application of ultrafiltration/microfiltration membranes to water treatment at sewage treatment plants. The design and operation of these modules is described in Chapter 7.

3.7.5.3 Membrane Contactors and Counter-Flow Sweep Modules

Most of the membrane modules described in this chapter operate in a cross-flow operating mode. The benefits of counter-flow operation are well known in heat transfer operations and can also be beneficial in some membrane operations. The design of this type of membrane module is described in more detail in Chapter 4.

3.8 Module Selection

The choice of the most suitable membrane module type for a particular membrane separation must balance a number of factors. The principal parameters that enter into the decision are summarized in Table 3.7.

Cost – always important – is difficult to quantify because the actual selling price of the same module design varies widely, depending on the application. For example, spiral-wound modules for reverse osmosis are produced by three or four manufacturers in large volumes, resulting in severe competition and low prices. Similar modules used in ultrafiltration are produced in much lower numbers and so are much more expensive. Hollow fiber modules are significantly cheaper, per square meter of membrane, than spiral-wound or plate-and-frame modules but can only be economically produced for very high volume applications that justify the expense of developing and building the spinning and module fabrication equipment. This cost advantage is often offset by the lower fluxes of the membranes compared with their flat-sheet equivalents. Generally, high-pressure modules are more expensive than low-pressure or vacuum modules. An estimate of module manufacturing cost is given in Table 3.7; the selling price is typically two to five times higher.

Two other major factors determining module selection are concentration polarization control and resistance to fouling. Concentration polarization control is a particularly

Table 3.7 Parameters for membrane module design

Parameter	Hollow fine fibers	Capillary fibers	Spiral-wound	Plate-and-frame	Tubular
Manufacturing cost (US\$/m ²)	5–20	10–50	5–100	50–200	50–200
Concentration polarization control	Poor	Good	Moderate	Good	Very good
Permeate-side pressure drop	High	Moderate	Moderate	Low	Low
Suitability for high-pressure operation	Yes	No	Yes	Yes	Marginal
Limited to specific types of membrane material	Yes	Yes	No	No	No

important issue in liquid separations such as reverse osmosis and ultrafiltration. In gas separation applications, concentration polarization is more easily controlled but is still a problem with high-flux, highly selective membranes. Hollow fine fiber modules are notoriously prone to fouling and concentration polarization and can be used in reverse osmosis applications only when extensive, costly feed solution pretreatment removes all particulates. These fibers cannot be used in ultrafiltration applications at all.

Another factor is the ease with which various membrane materials can be fabricated into a particular module design. Almost all membranes can be formed into plate-and-frame, spiral-wound, and tubular modules, but many membrane materials cannot be fabricated into hollow fine fibers or capillary fibers. Finally, the suitability of the module design for high-pressure operation and the relative magnitude of pressure drops on the feed and permeate sides of the membrane can be important factors.

The types of modules generally used in some of the major membrane processes are listed in Table 3.8.

In reverse osmosis, the commonly used modules are spiral-wound. Plate-and-frame and tubular modules are limited to a few applications in which membrane fouling is particularly severe; for example, in food applications or processing heavily contaminated industrial wastewater. The hollow fiber reverse osmosis modules used in the past have now been almost completely displaced by spiral-wound modules, which are inherently more fouling resistant, and require less feed pretreatment.

For ultrafiltration applications, hollow fine fibers have never been seriously considered because of their susceptibility to fouling. If the feed solution is extremely fouling, tubular systems are still used. Recently, however, spiral-wound modules with improved resistance to fouling have been developed; these modules are increasingly displacing the more expensive tubular systems. This is particularly the case with clean feed solutions, for

Table 3.8 *Module designs most commonly used in the major membrane separation processes*

Application	Module type
Reverse osmosis: seawater	Spiral-wound modules dominate. Only one hollow fiber producer remains
Reverse osmosis: industrial and brackish water	Spiral-wound modules used almost exclusively; fine fibers too susceptible to scaling and fouling
Ultrafiltration	Tubular, capillary, and spiral-wound modules all used. Tubular generally limited to highly fouling feeds (automotive paint), spiral-wound to clean feeds (ultrapure water)
Gas separation	Hollow fibers for high volume applications with low flux, low selectivity membranes in which concentration polarization is easily controlled (nitrogen from air) Spiral-wound when fluxes are higher, feed gases more contaminated, and concentration polarization a problem (natural gas separations, vapor permeation)
Pervaporation	Most pervaporation systems are small so plate-and-frame systems were used in the first systems. Spiral-wound and capillary modules being introduced

example, in the ultrafiltration of boiler feed water or municipal water to make ultrapure water for the electronics industry. Capillary systems are also used in some ultrafiltration applications.

For high-pressure gas separation applications, hollow fine fibers have a major segment of the market. Hollow fiber modules are clearly the lowest cost design per unit membrane area, and their poor resistance to fouling is not a problem in many gas separation applications because gaseous feed streams can easily be filtered. Also, gas separation membrane materials are often rigid glassy polymers such as polysulfones, polycarbonates, and polyimides, which are easily formed into hollow fine fibers. Spiral-wound modules are used to process natural gas streams, which are relatively dirty, often containing oil mist and condensable components that would foul hollow fine fiber modules rapidly.

Spiral-wound modules are much more commonly used in low-pressure or vacuum gas separation applications, such as the production of oxygen-enriched air or the separation of organic vapors from air. In these applications, the feed gas is at close to ambient pressure, and a vacuum is drawn on the permeate side of the membrane. Parasitic pressure drops on the permeate side of the membrane and the difficulty in making high-performance hollow fine fiber membranes from the rubbery polymers used to make them, both work against hollow fine fiber modules for such applications.

Pervaporation operates under constraints similar to those for low-pressure gas separation. Pressure drops on the permeate side of the membrane must be small, and many pervaporation membrane materials are rubbery, so both spiral-wound modules and plate-and-frame systems are in use. Plate-and-frame systems are competitive in this application despite their high cost, primarily because they can be operated at high temperatures with relatively aggressive feed solutions, conditions under which spiral-wound modules might fail.

3.9 Conclusions and Future Directions

The technology to fabricate ultrathin high-performance membranes into high surface area membrane modules has steadily improved during the modern membrane era. As a result, the inflation-adjusted cost of membrane separation processes has decreased dramatically over the years. The first anisotropic membranes made by Loeb–Sourirajan processes had an effective thickness of 0.2–0.4 μm . Currently, several techniques are used to produce commercial membranes with a thickness of 0.1 μm or less. The permeability and selectivity of membrane materials have also increased two- to threefold during the same period. As a result, today's membranes have 5–10 times the flux and better selectivity than membranes available 30 years ago. These trends are continuing. Membranes with an effective thickness of less than 0.05 μm have been made in the laboratory using advanced composite membrane preparation techniques or surface treatment methods.

As a result of these improvements in membrane performance, the major factors determining system performance have become concentration polarization and membrane fouling. All membrane processes are affected by these problems, so membrane modules with improved fluid flow to minimize concentration polarization and modules formed from membranes that can be easily cleaned if fouled are likely to become increasingly important development areas.

References

1. Gardner, H.A. and Sward, G.G. (1950) *Physical and Chemical Examination of Paints, Varnishes, Lacquers, and Colors*, 11th edn, H.A. Gardner Laboratory, Maryland.
2. Mackenzie, K.J. (1992) Film and sheeting material, *Kirk-Othmer Encyclopedia of Chemical Technology*, 4th edn, John Wiley & Sons, Inc., Hoboken, NJ, vol. **10**, p. 761.
3. Fleischer, R.L., Alter, H.W., Furman, S.C., Price, P.B and Walker, R.M. (1972) Particle track etching. *Science*, **172**, 225.
4. Porter, M.C. (1974) A novel membrane filter for the laboratory. *Am. Lab.*, **6**, 63.
5. Gingrich, J.E. (1988) The Nuclepore story. The 1988 Sixth Annual Membrane Technology/Planning Conference, Cambridge, MA.
6. Bierenbaum, H.S., Isaacson, R.B., Druin, M.L., and Plovan, S.G. (1974) Microporous polymeric films. *Ind. Eng. Chem. Proc. Res. Dev.*, **13**, 2.
7. Gore, R.W. (1980) Porous products and process therefor. US Patent 4,187,390, Feb. 1980.
8. Kim, J.J., Jang, T.S., Kwon, Y.D., Kim, U.Y. and Kim, S.S. (1994) Structural study of microporous polypropylene hollow fiber membranes made by the melt-spinning and cold-stretching method. *J. Membr. Sci.*, **93**, 209.
9. Kim, J., Kim, S.S., Park, M., and Jang, M. (2008) Effects of precursor properties on the preparation of polyethylene hollow fiber membranes by stretching. *J. Membr. Sci.*, **318** (1–2), 201–209.
10. Okuyama, K. and Mizutani, H. (1986) Process for preparing air-permeable film. US Patent 4,585,604, April 1986.
11. Mizutani, Y., Nakamura, S., Kaneko, S., and Okamura, K. (1993) Microporous polypropylene sheets. *Ind. Eng. Chem. Res.*, **32**, 221.
12. Chau, C.C. and Im, J.-H. (1989) Process of making a porous membrane. US Patent 4,874,568, Oct. 1989.
13. Ichikawa, T., Takahara, K., Shimoda, K., Seita, Y. and Emi, M. (1987) Hollow fiber membrane and method for manufacture thereof. US Patent 4,708,800, Nov. 1987.
14. Lopatin, G., Yen, L.Y., and Rogers, R.R. (1989) Microporous membranes from polypropylene. US Patent 4,874,567, Oct. 1989.
15. Loeb, S. and Sourirajan, S. (1963) Sea water demineralization by means of an osmotic membrane, in *Saline Water Conversion II*, Advances in Chemistry Series Number, Vol. **38** (ed. R.F. Gould), American Chemical Society, Washington, DC, pp. 117–132.
16. Cadotte, J.E. (1985) Evolution of composite reverse osmosis membranes, in *Materials Science of Synthetic Membranes*, ACS Symposium Series Number, Vol. **269** (ed. D.R. Lloyd), American Chemical Society, Washington, DC, pp. 273–294.
17. Ward, W.J., Browall, W.R., and Salemme, R.M. III (1976) Ultrathin silicone rubber membranes for gas separations. *J. Membr. Sci.*, **1**, 99.

18. Francis, P.S. (1966) Fabrication and Evaluation of New Ultrathin Reverse Osmosis Membranes. Offices of Saline Water Report, National Information Technical Service, NTIS# PB-177083, February 1966.
19. Riley, R.L., Lonsdale, H.K., Lyons, C.R., and Merten, U. (1967) Preparation of ultrathin reverse osmosis membranes and the attainment of theoretical salt rejection. *J. Appl. Polym. Sci.*, **11**, 2143.
20. Strathmann, H., Kock, K., Amar, P., and Baker, R.W. (1975) The formation mechanism of anisotropic membranes. *Desalination*, **16**, 179.
21. Manjikian, S. (1967) Desalination membranes from organic casting solutions. *Ind. Eng. Chem. Prod. Res. Dev.*, **6**, 23.
22. Saltonstall, C.W. Jr. (1969) Development and testing of high-retention reverse-osmosis membranes. International Conference PURAQUA, Rome, Italy, February 1969.
23. Michaels, A.S. (1971) High flow membranes. US Patent 3,615,024 Oct. 1971.
24. Pinna, I. and Koros, W.J. (1990) Defect free ultra high flux asymmetric membranes. US Patent 4,902,422, Feb. 1990.
25. Strathmann, H., Scheible, P., and Baker, R.W. (1971) A rationale for the preparation of Loeb-Sourirajan-type cellulose acetate membranes. *J. Appl. Polym. Sci.*, **15**, 811.
26. So, M.T., Eirich, F.R., Strathmann, H., and Baker, R.W. (1973) Preparation of anisotropic Loeb-Sourirajan membranes. *Polym. Lett.*, **11**, 201.
27. Strathmann, H. and Kock, K. (1977) The formation mechanism of phase inversion membranes. *Desalination*, **21**, 241.
28. Wijmans, J.G. and Smolders, C.A. (1986) Preparation of anisotropic membranes by the phase inversion process, in *Synthetic Membranes: Science, Engineering, and Applications* (eds P.M. Bungay, H.K. Lonsdale, and M.N. de Pinho), D. Reidel Publishing Company, Dordrecht, pp. 39–56.
29. Altena, F.W. and Smolders, C.A. (1982) Calculation of liquid-liquid phase separation in a ternary system of a polymer in a mixture of a solvent and nonsolvent. *Macromolecules*, **15**, 1491.
30. Reuvers, A.J., Van den Berg, J.W.A., and Smolders, C.A. (1987) Formation of membranes by means of immersion precipitation. *J. Membr. Sci.*, **34**, 45.
31. Mulder, M. (1991) *Basic Principles of Membrane Technology*, Kluwer Academic Publishers, Dordrecht.
32. Pinna, I. and Koros, W.J. (1993) A qualitative skin layer formation mechanism for membranes made by dry/wet phase inversion. *J. Polym. Sci., Part B: Polym. Phys.*, **31**, 419.
33. Koros, W.J. and Pinna, I. (1994) Membrane formation for gas separation processes, in *Polymeric Gas Separation Membranes* (eds D.R. Paul and Y.P. Yampolskii), CRC Press, Boca Raton, FL, pp. 209–272.
34. van de Witte, P., Dijkstra, P.J., van den Berg, J.W.A., and Feijen, J. (1996) Phase separation processes in polymer solutions in relation to membrane formation. *J. Membr. Sci.*, **117** (1-2), 1–31.

35. Castro, A.J. (1981) Methods for making microporous products. US Patent 4,247,498, Jan. 1981.
36. Lloyd, D.R., Barlow, J.W., and Kinzer, K.E. (1988) Microporous membrane formation via thermally-induced phase, in *New Membrane Materials and Processes for Separation*, AIChE Symposium Series, Vol. **261** (eds K.K. Sirkar and D.R. Lloyd), AIChE, New York, p. 84.
37. Vadalia, H.J.C., Lee, H.K., Meyerson, A.S., and Levon, K. (1994) Thermally induced phase separations in ternary crystallizable polymer solutions. *J. Membr. Sci.*, **89**, 37.
38. Caneba, G.T. and Soong, D.S. (1985) Polymer membrane formation through the thermal-inversion process. *Macromolecules*, **18**, 2538.
39. Minegishi, S.-I., Henmi, M., Ishizaki, T., and Dan, K. (2007) Hollow fiber membrane and method of producing the same. US Patent 7,182,870, Feb. 2007.
40. Hiatt, W.C., Vitzthum, G.H., Wagener, K.B. *et al.* (1985) Microporous membranes via upper critical temperature phase separation, in *Materials Science of Synthetic Membranes*, ACS Symposium Series Number, Vol. **269** (ed. D.R. Lloyd), American Chemical Society, Washington, DC, p. 229.
41. Lloyd, D.R., Kim, S.S., and Kinzer, K.E. (1991) Microporous membrane formation in thermally induced phase separation. *J. Membr. Sci.*, **64**, 1.
42. Bechhold, H. (1907) Kolloidstudien mit der filtrationsmethode. *Z. Phys. Chem.*, **60**, 257.
43. Elford, W.J. (1937) Principles governing the preparation of membranes having graded porosities. The properties of 'Gradocol' membranes as ultrafilters. *Trans. Faraday Soc.*, **33**, 1094.
44. Pierce, H.F. (1927) Nitrocellulose membranes of graded permeability. *J. Biol. Chem.*, **75**, 795.
45. Ferry, J.D. (1936) Ultrafilter membranes and ultrafiltration. *Chem. Rev.*, **18**, 373.
46. Zsigmondy, R. and Bachmann, W. (1918) Über neue filter. *Z. Anorg. Chem.*, **103**, 119.
47. Zeman, L. and Fraser, T. (1994) Formation of air-cast cellulose acetate membranes. *J. Membr. Sci.*, **87**, 267.
48. Riley, R.L., Lonsdale, H.K., LaGrange, L.D., and Lyons, C.R. (1969) Development of Ultra-Thin Membranes. Office of Saline Water Research and Development Progress Report No. 386, National Information Technical Service, PB# 207036, January 1969.
49. Zeman, L.J. and Zydny, A.L. (1996) *Microfiltration and Ultrafiltration: Principles and Applications*, Marcel Dekker, New York.
50. Rozelle, L.T., Cadotte, J.E., Cobian, K.E., and Kopp, C.V. Jr. (1977) Nonpolysaccharide membranes for reverse osmosis: NS-100 membranes, in *Reverse Osmosis and Synthetic Membranes* (ed. S. Sourirajan), National Research Council Canada, Ottawa, pp. 249–262.
51. Petersen, R.J. (1993) Composite reverse osmosis and nanofiltration membranes. *J. Membr. Sci.*, **83**, 81.
52. Riley, R.L., Fox, R.L., Lyons, C.R. *et al.* (1976) Spiral-wound poly(ether/amide) thin-film composite membrane system. *Desalination*, **19**, 113.

53. Kamiyama, Y., Yoshioka, N., Matsui, K., and Nakagome, E. (1984) New thin-film composite reverse osmosis membranes and spiral wound modules. *Desalination*, **51**, 79.
54. Cadotte, J.E. (1981) Interfacially synthesized reverse osmosis membrane. US Patent 4,277,344, July 1981.
55. Larson, R.E., Cadotte, J.E., and Petersen, R.J. (1981) The FT-30 seawater reverse osmosis membrane-element test results. *Desalination*, **38**, 473.
56. Forester, R.H. and Francis, P.S. (1970) Method of producing an ultrathin polymer film laminate. US Patent 3,551,244, Dec. 1970.
57. Riley, R.L., Lonsdale, H.K., and Lyons, C.R. (1971) Composite membranes for seawater desalination by reverse osmosis. *J. Appl. Polym. Sci.*, **15**, 1267.
58. Tsai, F.-J., Kang, D., and Anand, M. (1995) Thin film composite gas separation membranes: on the dynamics of thin film formation mechanism on porous substrates. *Sep. Sci. Technol.*, **30**, 1639.
59. Pinnau, I. (1989) Ultrathin ethyl cellulose/poly(4-methyl pentene-1) permselective membranes. US Patent 4,871,378, Oct. 1989.
60. Heinzelmann, W. (1991) Fabrication methods for pervaporation membranes, *Proceedings of the Fifth International Conference on Pervaporation Processes in the Chemical Industry*, Bakish Material Corporation, Englewood, NJ, 22–30.
61. Pinnau, I., Wijmans, J.G., Blume, I., Kuroda, T. and Peinemann, K.-V. (1988) Gas separation through composite membranes. *J. Membr. Sci.*, **37**, 81.
62. Yasuda, H. (1984) Plasma polymerization for protective coatings and composite membranes. *J. Membr. Sci.*, **18**, 273.
63. Yasuda, H. (1977) Composite reverse osmosis membranes prepared by plasma polymerization, in *Reverse Osmosis and Synthetic Membranes* (ed. S. Sourirajan), National Research Council Canada, Ottawa, pp. 263–294.
64. Stancell, A.R. and Spencer, A.T. (1972) Composite permselective membrane by deposition of an ultrathin coating from a plasma. *J. Appl. Polym. Sci.*, **16**, 1505.
65. Kawakami, M., Yamashita, Y., Iwamoto, M., and Kagawa, S. (1984) Modification of gas permeabilities of polymer membranes by plasma coating. *J. Membr. Sci.*, **19**, 249.
66. Norrman, K., Ghanbari-Siahkali, A., and Larsen, N.B. (2005) Studies of spin-coated polymer films. *Annu. Rep. Prog. Chem., Sect. C: Phys. Chem.*, **101**, 174–201.
67. Johnson, J.S., Kraus, K.A., Fleming, S.M., Cochran, H.D. and Perona, J.J. (1968) Hyperfiltration studies. *Desalination*, **5**, 359.
68. Kraus, K.A., Shor, A.J., and Johnson, J.S. (1967) Hyperfiltration studies. *Desalination*, **2**, 243.
69. Langsam, M. (1987) Fluorinated polymeric membranes for gas separation processes. US Patent 4,657,564, April 1987.
70. Langsam, M. and Savoca, C.L. (1988) Polytrialkylgermylpropyne polymers and membranes. US Patent 4,759,776, July 1988.
71. Langsam, M., Anand, M., and Karwacki, E.J. (1988) Substituted propyne polymers I. Chemical surface modification of poly[1-(trimethylsilyl)propyne] for gas separation membranes. *Gas. Sep. Purif.*, **2**, 162.
72. Mohr, J.M., Paul, D.R., Pinnau, I., and Koros, W.J. (1991) Surface fluorination of polysulfone anisotropic membranes and films. *J. Membr. Sci.*, **56**, 77.

73. Mohr, J.M., Paul, D.R., Taru, Y., Misna, T. and Lagow, R.J. (1991) Surface fluorination of composite membranes. *J. Membr. Sci.*, **55**, 149.
74. Le Roux, J.D., Paul, D.R., Arendt, M.F., Yuan, Y. and Cabasso, I. (1994) Surface Fluorination of Poly(phenylene oxide) Composite Membranes. *J. Membr. Sci.*, **90**, 37.
75. Kramer, P.W., Murphy, M.K., Stookey, D.J., Henis, J.M.S. and Stedronsky, E.R. (1993) Membranes having enhanced selectivity and methods of producing such membranes. US Patent 5,215,554, June 1993.
76. Browall, W.R. (1976) Method for sealing breaches in multi-layer ultrathin membrane composites. US Patent 3,980,456, Sep. 1976.
77. Henis, J.M.S. and Tripodi, M.K. (1980) A novel approach to gas separation using composite hollow fiber membranes. *Sep. Sci. Technol.*, **15**, 1059.
78. McBride, R.B. and McKinley, D.L. (1965) A new hydrogen recovery route. *Chem. Eng. Prog.*, **61**, 81.
79. Hunter, J.B. (1956) Silver-palladium film for separation and purification of hydrogen. US Patent 2,773,561, Dec. 1956.
80. Hunter, J.B. (1960) A new hydrogen purification process. *Platinum Met. Rev.*, **4**, 130.
81. Ma, Y.H. (2008) Hydrogen separation membranes, in *Advanced Membrane Technology and Applications* (eds N.N. Li, A.G. Fane, W.S.W. Ho, and T. Matsuura), John Wiley & Sons, Inc., Hoboken, NJ, pp. 451.
82. Athayde, A.L., Baker, R.W., and Nguyen, P. (1994) Metal composite membranes for hydrogen separation. *J. Membr. Sci.*, **94**, 299.
83. Buxbaum, R.E. (1993) Composite metal membrane for hydrogen extraction. US Patent 4,215,729, June 1993.
84. Buxbaum, R.E. and Marker, T.L. (1993) Hydrogen transport through non-porous membranes of palladium-coated niobium, tantalum, and vanadium. *J. Membr. Sci.*, **85**, 29.
85. Edlund, D.J. and Friesen, D.T. (1993) Hydrogen-permeable composite metal membrane and uses thereof. US Patent 5,217,506, June 1993.
86. Edlund, D.J., Friesen, D.T., Johnson, B., and Pledger, W. (1994) Hydrogen-permeable metal membranes for high-temperature gas separations. *Gas. Sep. Purif.*, **8**, 131.
87. Alefeld, G. and Völkl, J. (eds) (1978) *Hydrogen in Metals I: Basic Properties*, Springer-Verlag, Berlin.
88. Hunter, J.B. (1963) Ultrapure hydrogen by diffusion through palladium alloys. *Disv. Pet. Chem. Prepr.*, **8**, 4.
89. Philpott, J.E. (1985) Hydrogen diffusion technology, commercial applications of palladium membrane. *Platinum Met. Rev.*, **29**, 12.
90. Li, K. (2007) *Ceramic Membranes for Separation and Reaction*, John Wiley & Sons, Ltd, Chichester.
91. Keizer, K., Uhlhorn, R.J.R., and Burggraaf, T.J. (1995) Gas separation using inorganic membranes, in *Membrane Separation Technology, Principles and Applications* (eds R.D. Noble and S.A. Stern), Elsevier, Amsterdam, pp. 553–584.

92. Burggraaf, T.J. and Keizer, K. (1991) Synthesis of inorganic membranes, in *Inorganic Membranes Synthesis, Characteristics, and Applications* (ed. R.R. Bhave), Chapman & Hall, New York, pp. 10–63.
93. Larbot, A., Fabre, J.P., Guizard, C., and Cot, L. (1988) Inorganic membranes obtained by sol-gel techniques. *J. Membr. Sci.*, **39**, 203.
94. Anderson, M.A., Gieselmann, M.J., and Xu, Q. (1988) Titania and alumina ceramic membranes. *J. Membr. Sci.*, **39**, 243.
95. Ramsay, J.D.F. and Kallus, S. (2000) Zeolite membranes, in *Membrane Science and Technology*, vol. **6** (ed. N.K. Kanellopoulos), Elsevier, pp. 373–395.
96. Barrer, R.M. (1982) *Hydrothermal Chemistry of Zeolites*, Academic Press, London.
97. Gavalas, G.R. (2006) Zeolite membranes for gas and liquid separations, in *Materials Science of Membranes for Gas and Vapor Separation* (eds Y. Yampolskii, I. Pinnau, and B.D. Freeman), John Wiley & Sons, Ltd, Chichester, 307–336.
98. Sato, K., Sugimoto, K., and Nakane, T. (2008) Synthesis of industrial scale NaY zeolite membranes and ethanol permeating performance in pervaporation and vapor permeation up to 130°C and 570 kPa. *J. Membr. Sci.*, **310** (1–2), 161–173.
99. Sato, K., Sugimoto, K., and Nakane, T. (2008) Mass-production of tubular NaY zeolite membranes for industrial purpose and their application to ethanol dehydration by vapor permeation. *J. Membr. Sci.*, **319** (1–2), 244–255.
100. Maxwell, J.C. (1873) *Treatise on Electricity and Magnetism*, vol. **I**, Oxford University Press, London.
101. Robeson, L.M., Noshay, A., Matzner, M., and Merian, C.N. (1973) Physical property characteristics of polysulfone/poly(dimethyl siloxane) block copolymers. *Angew. Makromol. Chem.*, **29**, 47.
102. Mahajan, R. and Koros, W.J. (2000) Factors controlling successful formation of mixed-matrix gas separation materials. *Ind. Eng. Chem. Res.*, **39**, 2692.
103. Mahajan, R. and Koros, W.J. (2002) Mixed-matrix materials with glassy polymers part 1. *Polym. Eng. Sci.*, **42**, 1420.
104. Mahajan, R. and Koros, W.J. (2002) Mixed-matrix materials with glassy polymers part 2. *Polym. Eng. Sci.*, **42**, 1432.
105. Duval, J.-M., Folkers, B., Mulder, M.H.V., Desgrandchamps, G. and Smolders, C.A. (1993) Adsorbent filled membranes for gas separation. *J. Membr. Sci.*, **80**, 189.
106. Jia, M., Peinemann, K.-V., and Behling, R.-D. (1991) Molecular sieving effect of the zeolite-filled silicone rubber membranes in gas permeation. *J. Membr. Sci.*, **57** (2–3), 289–292.
107. Zimmerman, C.M., Singh, A., and Koros, W.J. (1997) Tailoring mixed matrix composite membranes for gas separations. *J. Membr. Sci.*, **137** (1–2), 145–154.
108. te Hennepe, H.J.C., Bargeman, D., Mulder, M.H.V., and Smolders, C.A. (1987) Zeolite-filled silicone rubber membranes part I: membrane preparation and pervaporation results. *J. Membr. Sci.*, **35**, 39.
109. Jia, M.-D., Peinemann, K.-V., and Behling, R.-D. (1992) Preparation and characterization of thin-film zeolite-PDMS composite membranes. *J. Membr. Sci.*, **73**, 119.

110. Baker, R.W., Wijmans, J.G., and Huang, Y. (2010) Permeability, permeance and selectivity: a preferred way of reporting pervaporation performance data. *J. Membr. Sci.*, **348** (1–2), 346–352.
111. Hillock, A.M.W. (2008) Crosslinked mixed matrix membranes for the purification of natural gas: effects of sieve surface modification. *J. Membr. Sci.*, **314**, 193.
112. Ash, R., Barrer, R.M., and Pope, C.G. (1963) Flow of adsorbable gases and vapours in microporous medium. *Proc. R. Soc. Lond., Ser. A*, **271**, 19.
113. Ash, R., Baker, R.W., and Barrer, R.M. (1967) Sorption and surface flow in graphitized carbon membranes. *Proc. R. Soc. Lond., Ser. A*, **299**, 434.
114. Koresh, J.E. and Soffer, A. (1983) Molecular sieve carbon selective membrane. *Sep. Sci. Technol.*, **18**, 723.
115. Morooka, S., Kusakabe, K., and Kusuki, Y. (2000) Microporous carbon membranes, in *Membrane Science and Technology, Recent Advances in Gas Separation by Microporous Ceramic Membranes*, Vol. **6** (ed. N.K. Kanellopoulos), Elsevier Science B.V., Amsterdam, pp. 323–334.
116. Kita, H. (2006) Gas and vapor separation membranes based on carbon membranes, in *Materials Science of Membranes for Gas and Vapor Separation* (eds Y. Yam-polskii, I. Pinna, and B.D. Freeman), John Wiley & Sons, Ltd, Chichester, pp. 337–354.
117. Kita, H., Nanbu, K., Maeda, H., and Okamoto, K.-i. (2004) Gas separation and pervaporation through microporous carbon membranes derived from phenolic resin, *Advanced Materials for Membrane Separations*, ACS Symposium Series, Vol. **876**, American Chemical Society, Washington, DC, pp. 203–217.
118. Kim, Y.K., Park, H.B., and Lee, Y.M. (2004) Carbon molecular sieve membranes derived from thermally labile polymer containing blend polymers and their gas separation properties. *J. Membr. Sci.*, **243**, 9–17.
119. Rao, M.B. and Sirkar, S. (1993) Nanoporous carbon membranes for separation of gas mixtures by selective surface flow. *J. Membr. Sci.*, **85** (3), 253–264.
120. Williams, P.J. and Koros, W.J. (2008) Gas separation by carbon membranes, in *Advanced Membrane Technology and Applications* (eds N.N. Li, A.G. Fane, W.S.W. Ho, and T. Matsuura), John Wiley & Sons, Inc., Hoboken, NJ, pp. 599–631.
121. Jones, C.W. and Koros, W.J. (1995) Characterization of ultramicroporous carbon membranes with humidified feeds. *Ind. Eng. Chem. Res.*, **34**, 158–163.
122. Jones, C.W. and Koros, W.J. (1994) Carbon molecular sieve gas separation membranes – I. Preparation and characterization based on polyimide precursors. *Carbon*, **32** (8), 1419–1425.
123. Jones, C.W. and Koros, W.J. (1994) Carbon molecular sieve gas separation membranes – II. Regeneration following organic exposure. *Carbon*, **32** (8), 1427–1432.
124. Beaver, R.P. (1988) Method of production porous hollow silica-rich fibers. US Patent 4,778,499, Oct. 1988.
125. Baker, R.W. and Blume, I. (1990) Coupled transport membranes, in *Handbook of Industrial Membrane Technology* (ed. M.C. Porter), Noyes Publications, Park Ridge, NJ, pp. 511–558.

126. Cussler, E.L. (1994) Facilitated and active transport, in *Polymeric Gas Separation Membranes* (eds D.R. Paul and Y.P. Yampolskii), CRC Press, Boca Raton, FL, pp. 273–300.
127. Mahon, H.I. (1966) Permeability separatory apparatus, permeability separatory membrane element, method of making the same and process utilizing the same. US Patent 3,228,876, Jan. 1966.
128. Baum, B., Holley, W. Jr., and White, R.A. (1976) Hollow fibers in reverse osmosis, dialysis, and ultrafiltration, in *Membrane Separation Processes* (ed. P. Meares), Elsevier, Amsterdam, pp. 187–228.
129. Moch, I. Jr. (1995) Hollow fiber membranes, *Encyclopedia of Chemical Technology*, Vol. 13, 4th edn, John Wiley-Interscience Publishing, New York, p. 312.
130. McKelvey, S.A., Clausi, D.T., and Koros, W.J. (1997) A guide to establishing fiber macroscopic properties for membrane applications. *J. Membr. Sci.*, **124**, 223.
131. Chung, T.S.N. (2008) Fabrication of hollow-fiber membranes by phase inversion, in *Advanced Membrane Technology and Applications* (eds N.N. Li, A.G. Fane, W.S.W. Ho, and T. Matsura), John Wiley & Sons, Inc., Hoboken, NJ, pp. 821–839.
132. Malon, R.F. and Cruse, C.A. (1991) Anisotropic gas separation membranes having improved strength. US Patent 5,013,767, May 1991.
133. Takao, S. (1983) Process for producing acrylonitrile separation membranes in fibrous form. US Patent 4,409,162, Oct. 1983.
134. Puri, P.S. (1989) Continuous process for making coated composite hollow fiber membranes. US Patent 4,863,761, Sep. 1989.
135. Sluma, H.-D., Weizenhofer, R., Leeb, A., and Bauer, K. (1993) Method of making a multilayer capillary membrane. US Patent 5,242,636, Sep. 1993.
136. Haubs, M. and Hassinger, W. (1992) Method and apparatus for applying polymeric coating. US Patent 5,156,888, Oct. 1992.
137. Kusuki, Y., Yoshinaga, T., and Shimazaki, H. (1992) Aromatic polyimide double layered hollow filamentary membrane and process for producing the same. US Patent 5,141,642, Aug. 1992.
138. Kopp, C.V., Streeton, R.J.W., and Khoo, P.S. (1994) Extrusion head for forming polymeric hollow fiber. US Patent 5,318,417, June 1994.
139. Widjojo, N., Chung, T.S., and Krantz, W.B. (2007) A morphological and structural study of Ultem/P84 copolyimide dual-layer hollow fiber membranes with delamination-free morphology. *J. Membr. Sci.*, **294**, 132–146.
140. Pereira, C.C., Nobrega, R., Peinemann, K.-V., and Borges, C.P. (2003) Hollow fiber membranes obtained by simultaneous spinning of two polymer solutions: a morphological study. *J. Membr. Sci.*, **226**, 35–50.
141. Wang, K.Y., Chung, T.-S., and Rajagopalan, R. (2007) Dehydration of tetrafluoropropanol (TFP) by pervaporation via novel PBI/BTDA-TDI/MDI co-polyimide (P84) dual-layer hollow fiber membranes. *J. Membr. Sci.*, **287**, 60–66.
142. Ji, J. (2006) Method for producing defect free composite membranes. US Patent 7,081,273, July, 2006.
143. Hayano, F., Hashino, Y., and Ichikawa, K. (1977) Semipermeable composite membranes. US Patent 4,061,821, Dec. 1977.

144. Mailvaganam, M., Fabbricino, L., Rodrigues, C.F., and Donnelly, A.R. (1995) Hollow fiber semipermeable membrane of tubular braid. US Patent 5,472,607, Dec. 1995.
145. Stern, S.A., Sinclaire, T.F., Gareis, P.J., Vahldieck, N.P. and Mohr, P.H. (1965) Helium recovery by permeation. *Ind. Eng. Chem.*, **57**, 49.
146. Günther, R., Perschall, B., Reese, D., and Hapke, J. (1996) Engineering for high pressure reverse osmosis. *J. Membr. Sci.*, **121**, 95.
147. Westmoreland, J.C. (1968) Spirally wrapped reverse osmosis membrane cell. US Patent 3,367,504, Feb. 1968.
148. Bray, D.T. (1968) Reverse osmosis purification apparatus. US Patent 3,417,870, Dec. 1968.
149. Kremen, S.S. (1977) Technology and engineering of ROGA spiral-wound reverse osmosis membrane modules, in *Reverse Osmosis and Synthetic Membranes* (ed. S. Sourirajan), National Research Council Canada, Ottawa, pp. 371–386.
150. Parekh, B.S. (ed.) (1988) *Reverse Osmosis Technology*, Marcel Dekker, New York.
151. Crowder, R.O. and Cussler, E.L. (1997) Mass transfer in hollow-fiber modules with non-uniform fibers. *J. Membr. Sci.*, **134**, 235.
152. Lemanski, J. and Lipscomb, G.G. (2000) Effect of fiber variation on the performance of counter-current hollow-fiber gas separation modules. *J. Membr. Sci.*, **167**, 241.
153. Lemanski, J. and Lipscomb, G.G. (2002) Effect of shell-side flows on the performance of hollow-fiber gas separation modules. *J. Membr. Sci.*, **195**, 215.
154. Prasad, R., Runkle, C.J., and Shuey, H.F. (1994) Spiral-wound hollow fiber cartridge and modules having flow directing baffles. US Patent 5,352,361, Oct. 1994.
155. Schucker, R.C., Darnell, C.P., and Hafez, M.M. (1992) Hollow fiber module using fluid flow control baffles. US Patent 5,169,530, Dec. 1992.
156. Eckman, T.J. (1995) Hollow fiber cartridge. US Patent 5,470,469, Nov. 1995.
157. de Filippi, R.P. and Pierce, R.W. (1970) Membrane device and method. US Patent 3,536,611, Oct. 1970.
158. Koros, W.J. and Fleming, G.K. (1993) Membrane based gas separation. *J. Membr. Sci.*, **83**, 1.
159. McGinnis, P.R. and O'Brien, G.J. (1972) Permeation separation element. US Patent 3,690,465, Sep. 1972.
160. Culkin, B., Plotkin, A., and Monroe, M. (1998) Solve membrane fouling with high-shear filtration. *Chem. Eng. Prog.*, **94**, 29.
161. Al Akoum, O., Jaffrin, M.Y., Ding, L., Paullier, P. and Vanhoutte, C. (2002) An hydrodynamic investigation of microfiltration and ultrafiltration in a vibrating membrane module. *J. Membr. Sci.*, **197**, 37.
162. Akoum, O., Jaffrin, M.Y., Ding, L.H., and Frappart, M. (2004) Treatment of dairy process waters using a vibrating filtration system and NF and RO membranes. *J. Membr. Sci.*, **235**, 111–122.

4

Concentration Polarization

4.1 Introduction

In membrane separation processes, a gas or liquid mixture contacts the feed side of the membrane, and a permeate enriched in one of the components of the mixture is withdrawn from the downstream side of the membrane. Because feed mixture components permeate at different rates, concentration gradients can form in the fluids on both sides of the membrane. In this case, the concentrations at the membrane surfaces are not the same as the bulk fluid concentrations. This changes permeation through the membrane. The phenomenon is called concentration polarization. Figure 4.1 illustrates a dialysis experiment in which a membrane separates two solutions containing different concentrations of dissolved solute. Solute (*i*) diffuses from right to left; solvent (*j*) diffuses from left to right. Unless the solutions are well stirred, concentration gradients form in the solutions on both sides of the membrane. The layer of solution immediately adjacent to the membrane surface becomes depleted in the permeating solute on the feed side of the membrane and enriched in this component on the permeate side. Equivalent gradients form for the other component. This concentration polarization reduces the permeating component's concentration difference across the membrane, lowering its flux and the membrane selectivity. A similar phenomenon occurs in other processes that involve transport of heat or mass across an interface. Mathematical descriptions of these processes can be found in monographs on heat and mass transfer; for example, in the books of Carslew and Jaeger [1]; Bird *et al.* [2]; and Crank [3].

The importance of concentration polarization depends on the membrane separation process. Concentration polarization can significantly affect membrane performance in reverse osmosis, but it is usually well controlled in industrial systems. On the other hand, membrane performance in ultrafiltration, electrodialysis, and some pervaporation processes is seriously affected by concentration polarization.

Figure 4.1 shows concentration polarization gradients on both sides of the membrane. However, in most membrane processes there is a bulk flow of liquid or gas through

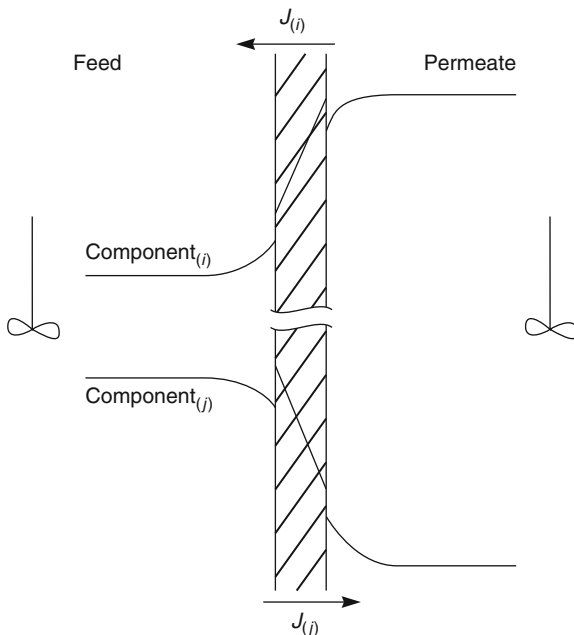


Figure 4.1 Concentration gradients formed when a dialysis membrane separates two solutions of different concentrations

the membrane, and the permeate-side composition depends only on the ratio of the components permeating the membrane. When this is the case, concentration gradients only form on the feed side of the membrane.

Two approaches have been used to describe the effect of concentration polarization. One has its origins in the dimensional analysis used to solve heat transfer problems. In this approach, the resistance to permeation across the membrane and the resistance in the fluid layers adjacent to the membrane are treated as resistances in series. Nothing is assumed about the thickness of the various layers or the transport mechanisms taking place.

Using this model and the assumption that concentration polarization occurs only on the feed side of the membrane, the flux J_i across the combined resistances of the feed-side boundary layer and the membrane can be written as

$$J_i = k_{ov}(c_{ib} - c_{ip}) \quad (4.1)$$

where k_{ov} is the overall mass transfer coefficient, c_{ib} is the concentration of component i in the bulk feed solution, and c_{ip} is the concentration of component i in the bulk permeate solution. Likewise, the flux across the boundary layer is also J_i and can be written as

$$J_i = k_{bl}(c_{ib} - c_{io}) \quad (4.2)$$

where k_{bl} is the fluid boundary layer mass transfer coefficient, and c_{i_o} is the concentration of component i in the fluid at the feed/membrane interface, and the flux across the membrane can be written as

$$J_i = k_m(c_{i_o} - c_{i_p}) \quad (4.3)$$

where k_m is the mass transfer coefficient of the membrane.

Since the overall concentration drop ($c_{i_b} - c_{i_p}$) is the sum of the concentration drops across the boundary layer and the membrane, a simple restatement of the resistances-in-series model using the terms of Equations 4.1–4.3 is

$$\frac{1}{k_{ov}} = \frac{1}{k_m} + \frac{1}{k_{bl}} \quad (4.4)$$

When the fluid layer mass transfer coefficient (k_{bl}) is large, the resistance $1/k_{bl}$ of this layer is small, and the overall resistance is determined only by the membrane. When the fluid layer mass transfer coefficient is small, the resistance term $1/k_{bl}$ is large, and becomes a significant fraction of the total resistance to permeation. The overall mass transfer coefficient (k_{ov}) then becomes smaller, and the flux decreases. The boundary layer mass transfer coefficient is thus an arithmetical fix used to correct the membrane permeation rate for the effect of concentration polarization. Nothing is revealed about the causes of concentration polarization.

The boundary layer mass transfer coefficient is known from experiments to depend on many system properties; this dependence can be expressed as an empirical relationship of the type

$$k_{bl} = \text{constant } Q^\alpha h^\beta D^\gamma T^\delta \dots \quad (4.5)$$

where, for example, Q is the fluid velocity through the membrane module, h is the feed channel height, D is the solute diffusion coefficient, T is the feed solution temperature, and so on. Empirical mass transfer correlations obtained this way can be used to estimate the performance of a new membrane unit by extrapolation from an existing body of experimental data [4–7]. However, these correlations have a limited range of applicability and must be reformulated with different coefficients for each new process and module design. The correlations cannot be used to obtain an *a priori* estimate of the magnitude of concentration polarization for a new process. This approach also does not provide insight into the dependence of concentration polarization on membrane properties. A more detailed and more sympathetic description of the mass transfer approach is given in recent monographs [8, 9].

The second approach to concentration polarization, and the one used in this chapter, is to model the phenomenon by assuming that a thin layer of unmixed fluid, thickness δ , exists between the membrane surface and the well-mixed bulk solution. The concentration gradients that control concentration polarization form in this layer. This boundary layer film model oversimplifies the fluid hydrodynamics occurring in membrane modules and still contains one adjustable parameter, the boundary layer thickness. Nonetheless, this simple model can explain most of the experimental data.

4.2 Boundary Layer Film Model

The usual starting point for the boundary layer film model is illustrated in Figure 4.2, which shows the velocity profile in a fluid flowing through the channel of an ultrafiltration/reverse osmosis membrane module. The average velocity of the fluid flowing down the channel is normally on the order of 10–20 cm/s. This velocity is far higher than the average velocity of the fluid flowing at right angles through the membrane, which is typically 10–20 $\mu\text{m}/\text{s}$. However, the velocity in the channel is not uniform. Friction at the fluid–membrane surface reduces the fluid velocity next to the membrane to essentially zero; the velocity increases as the distance from the membrane surface increases. Thus, the fluid flow velocity in the middle of the channel is high, the flow there is turbulent, and the fluid is well mixed. The velocity in the boundary layer next to the membrane is much lower, flow is laminar, and mixing occurs by diffusion. Concentration gradients due to concentration polarization are assumed to be confined to the boundary layer.

Figure 4.1 shows the concentration gradients that form on either side of a dialysis membrane. However, dialysis differs from most membrane processes in that the volume flow across the membrane is usually small. In processes such as reverse osmosis, ultrafiltration, and gas separation, the volume flow through the membrane from the feed to the permeate side is significant. As a result, the permeate concentration is determined by the ratio of the fluxes of the components that permeate the membrane. In these processes, concentration polarization gradients form only on the feed side of the membrane, as shown in Figure 4.3. This simplifies the description of the phenomenon. The membrane processes in which a fluid is used to sweep the permeate side of the membrane, to change the permeate-side concentration from the value set by the ratio of permeating components, are discussed in the section on cross-flow, co-flow, and counter-flow later in this chapter.

In any process, if one component is enriched at the membrane surface, then mass balance dictates that a second component is depleted at the surface. By convention, concentration polarization effects are described by considering the concentration gradient

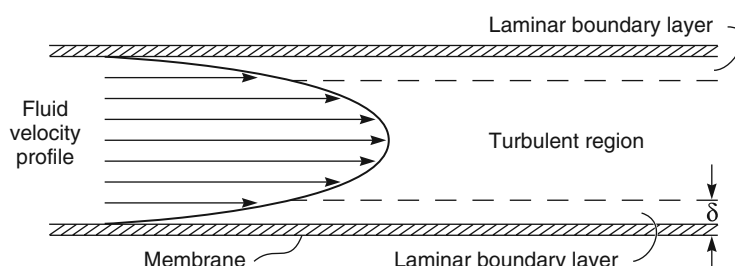


Figure 4.2 Fluid flow velocity through an ultrafiltration/reverse osmosis membrane module channel is non-uniform, being fastest in the middle and essentially zero adjacent to the membrane. In the film model of concentration polarization, concentration gradients formed due to transport through the membrane are assumed to be confined to the laminar boundary layer

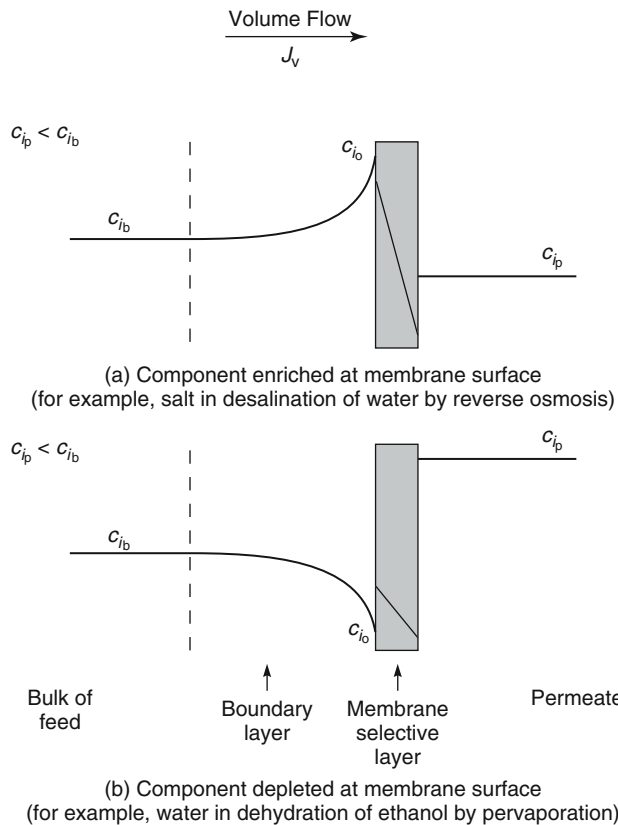


Figure 4.3 Concentration gradients formed as a result of permeation through a selective membrane. By convention, concentration polarization is usually represented by the gradient of the minor component (a) salt in the reverse osmosis example and (b) water in the pervaporation example (dehydration of an ethanol solution)

of the minor component. In Figure 4.3a, concentration polarization in reverse osmosis is represented by the concentration gradient of salt, the minor component rejected by the membrane. In Figure 4.3b, which illustrates dehydration of aqueous ethanol solutions by pervaporation, concentration polarization is represented by the concentration gradient of water, the minor component that preferentially permeates the membrane.

In the case of desalination of water by reverse osmosis illustrated in Figure 4.3a, the salt concentration c_{i_o} adjacent to the membrane surface c_{i_b} is higher than the bulk solution concentration because reverse osmosis membranes preferentially permeate water and retain salt. Water and salt are brought toward the membrane surface by the flow of solution through the membrane, designated J_v .¹ Water and a little salt permeate the membrane, but most of the salt is rejected by the membrane and retained at the membrane surface. Salt accumulates at the membrane surface until a sufficient concentration gradient has formed to allow the salt to diffuse to the bulk solution. Steady state is then reached.

¹ In this chapter, the term J_v is the volume flux ($\text{cm}^3/\text{cm}^2/\text{s}$) through the membrane measured at the feed-side conditions of the process.

In the case of dehydration of ethanol by pervaporation illustrated in Figure 4.3b, the water concentration c_{i_0} adjacent to the membrane surface is lower than the bulk solution concentration c_{i_b} because the pervaporation membrane preferentially permeates water and retains ethanol. Water and ethanol are brought toward the membrane surface by the flow of solution through the membrane. Water and a little ethanol permeate the membrane, but most of the ethanol is retained at the membrane surface. Ethanol accumulates at the membrane surface until a sufficient concentration gradient has formed to allow it to diffuse back to the bulk solution. An equal and opposite water gradient must form; thus, water becomes depleted at the membrane surface.

The formation of these concentration gradients can be expressed in mathematical form. Figure 4.4 shows the steady-state salt gradient that forms across a reverse osmosis membrane.

The salt flux through the membrane is given by the product of the permeate volume flux J_v and the permeate salt concentration c_{i_p} . For dilute liquids, the permeate volume flux is within 1–2% of the volume flux on the feed side of the membrane because the densities of the two solutions are almost equal. This means that, at steady state, the net salt flux at any point within the boundary layer must be equal to the permeate salt flux, $J_v c_{i_p}$. In the boundary layer, this net salt flux is equal to the convective salt flux toward the

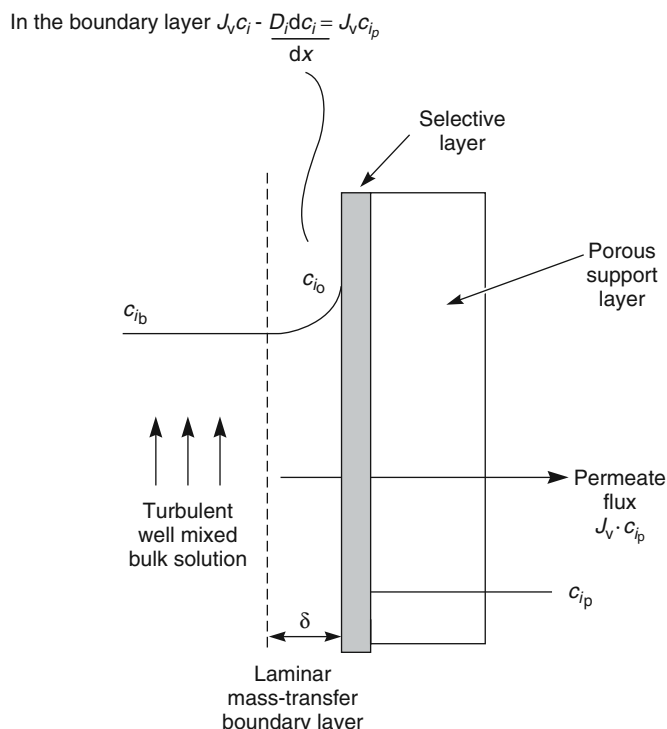


Figure 4.4 Salt concentration gradients adjacent to a reverse osmosis desalination membrane. The mass balance equation for solute flux across the boundary layer is the basis of the film model description of concentration polarization

membrane, $J_v c_i$, minus the diffusive salt flux away from the membrane expressed by Fick's law ($D_i dc_i/dx$). So, from simple mass balance, transport of salt at any point within the boundary layer can be described by the equation

$$J_v c_i - D_i dc_i/dx = J_v c_{i_p} \quad (4.6)$$

where D_i is the diffusion coefficient of the salt, x is the coordinate perpendicular to the membrane surface, and J_v is the volume flux in the boundary layer generated by permeate flow through the membrane. The mass balance equation (Equation 4.6) can be integrated over the thickness of the boundary layer to give the well-known polarization equation first derived by Brian [10] for reverse osmosis:

$$\frac{c_{i_o} - c_{i_p}}{c_{i_b} - c_{i_p}} = \exp(J_v \delta / D_i) \quad (4.7)$$

In this equation, c_{i_o} is the concentration of solute in the feed solution at the membrane surface, and δ is the thickness of the boundary layer. An alternative form of Equation 4.7 replaces the concentration terms by an enrichment factor E , defined as c_{i_p}/c_{i_b} . The enrichment obtained in the absence of a boundary layer, that is, the intrinsic enrichment of the membrane, E_o , is then defined as c_{i_p}/c_{i_o} , and Equation 4.7 can be written as

$$\frac{1/E_o - 1}{1/E - 1} = \exp(J_v \delta / D_i) \quad (4.8)$$

In the case of reverse osmosis, the actual and intrinsic enrichment factors of salt (E and E_o) are much less than 1.0, typically about 0.01, because the membrane rejects salt almost completely and permeates water. For other processes, such as dehydration of aqueous ethanol by pervaporation, the enrichment factor for water will be greater than 1.0, and perhaps as high as 10–20, because the membrane selectively permeates the water.

The increase or decrease in the concentration of the permeating component at the membrane surface c_{i_o} , compared to the bulk solution concentration c_{i_b} , determines the extent of concentration polarization. The ratio of the two concentrations, c_{i_o}/c_{i_b} , is called the concentration polarization modulus and is a useful measure of the extent of concentration polarization. When the modulus is 1.0, the concentration at the membrane surface (c_{i_o}) is equal to the bulk concentration (c_{i_b}), and no concentration polarization occurs. As the modulus deviates farther from 1.0, the effect of concentration polarization on membrane selectivity and flux becomes increasingly important. From the definitions of E and E_o , the concentration polarization modulus is equal to E/E_o , that is, the actual enrichment factor divided by the intrinsic enrichment factor, and from Equations 4.7 and 4.8, the modulus can be written as

$$\frac{c_{i_o}}{c_{i_b}} = \frac{\exp(J_v \delta / D_i)}{1 + E_o [\exp(J_v \delta / D_i) - 1]} \quad (4.9)$$

Depending on the intrinsic enrichment (E_o) of the membrane, the modulus can be larger or smaller than 1.0. For reverse osmosis, E_o is less than 1.0 and the concentration

polarization modulus is normally between 1.1 and 1.5; that is, the concentration of salt at the membrane surface is 1.1–1.5 times larger than it would be in the absence of concentration polarization. The salt leakage through the membrane and the osmotic pressure that must be overcome to produce a flow of water are increased proportionately. Fortunately, modern reverse osmosis membranes are extremely selective and permeable, and can still produce useful desalinated water under these conditions. In other membrane processes, such as pervaporation or ultrafiltration, the concentration polarization modulus may be as large as 5–10 or as small as 0.2–0.1, and may seriously affect the performance of the membrane.

Equation 4.9 shows the factors that determine the magnitude of concentration polarization, namely the boundary layer thickness δ , the intrinsic membrane enrichment E_o , the volume flux through the membrane J_v , and the diffusion coefficient of the solute in the boundary layer fluid D_i . The effect of changes in each of these parameters on the concentration gradients formed in the membrane boundary layer are illustrated graphically in Figure 4.5 for a process in which the intrinsic enrichment (E_o) is greater than 1.0, for example, dehydration of ethanol by pervaporation.

Of the four factors that affect concentration polarization, the one most easily changed is the boundary layer thickness. As δ decreases, Equation 4.9 shows that the concentration polarization modulus becomes exponentially smaller. Thus, the most straightforward way of minimizing concentration polarization is to reduce the boundary layer thickness by increasing turbulent mixing at the membrane surface. Factors affecting turbulence in membrane modules are described in detail in the review of Belfort *et al.* [11]. The most direct technique to promote mixing is to increase the fluid flow velocity past the membrane surface. Therefore, many membrane modules operate at relatively high feed fluid velocities. However, the energy consumption of the pumps required to produce high feed fluid velocities places a practical limit on the turbulence that can be obtained in a membrane module. Membrane spacers made of open mesh plastic netting are also widely used to promote turbulence by disrupting fluid flow in the module channels, as shown in Figure 4.6. The selection of appropriate feed channel spacers is an important issue for membrane module producers. Most producers select their spacers based on module performance results. In recent years, attempts have been made to put spacer selection on a more scientific basis using laboratory measurements and computer-aided design [12–14]. Pulsing the feed fluid flow through the membrane module is another technique used to control polarization [15].

The membrane's intrinsic enrichment E_o also affects concentration polarization. If the membrane is completely unselective, $E_o = 1$. The relative concentrations of the components passing through the membrane do not change, so concentration gradients are not formed in the boundary layer. As the difference in permeability between the more permeable and less permeable components increases, the intrinsic enrichment E_o achieved by the membrane increases, and the concentration gradients that form become larger. As a practical example, in pervaporation of organics from water, concentration polarization is much more important when the solute is toluene (with an intrinsic enrichment E_o of 5000 over water) than when the solute is methanol (with an intrinsic enrichment E_o less than 5).

Another important characteristic of Equation 4.9 is that it is the intrinsic enrichment E_o produced by the membrane at the operating conditions of the separation processes, not the intrinsic selectivity, that determines the concentration polarization modulus. Enrichment

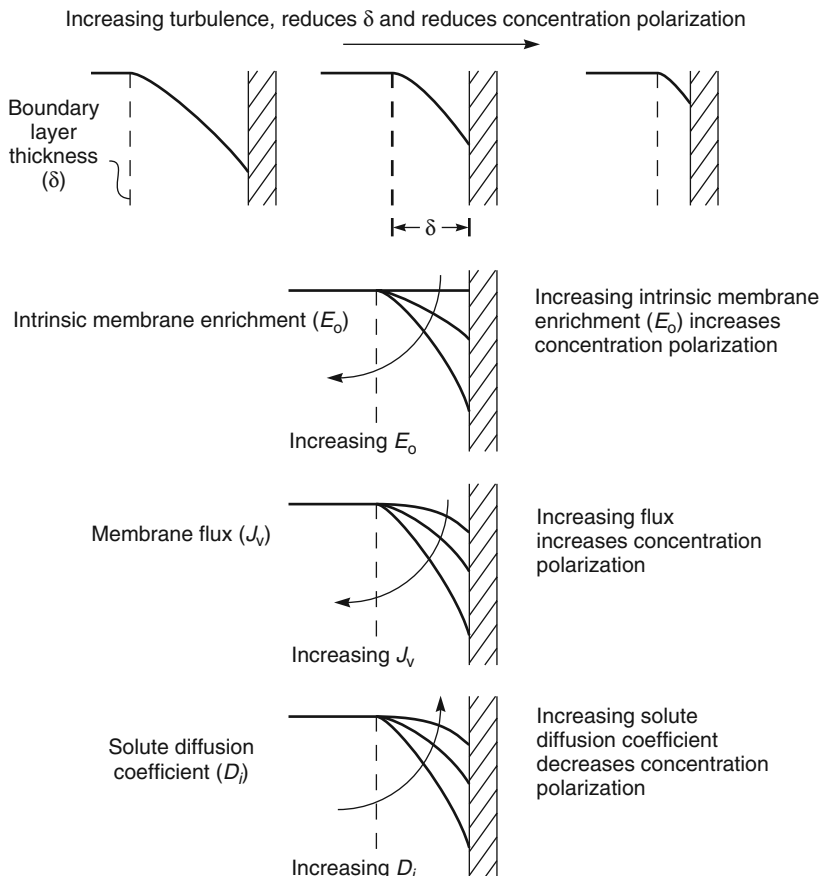


Figure 4.5 The effect of changes in boundary layer thickness δ , intrinsic membrane enrichment E_o , membrane flux J_v , and solute diffusion D_i on concentration gradients in the stagnant boundary layer ($E_o > 1$)

and intrinsic selectivity are linked but are not identical. This distinction is illustrated by the separation of hydrogen from inert gases in ammonia plant purge gas streams, which typically contain 30% hydrogen. Hydrogen is 100–200 times more permeable than the inert gases nitrogen, methane, and argon, so the intrinsic selectivity of the membrane is very high. The high selectivity means that the membrane permeate is 97% hydrogen; even so, because the feed gas contains 30% hydrogen, the enrichment E_o is only 97/30, or 3.3, so the concentration polarization modulus is negligible. On the other hand, as hydrogen is removed, its concentration in the feed gas falls. When the feed gas contains 5% hydrogen, the permeate will be 90% hydrogen and the intrinsic enrichment 90/5 or 18. Under these conditions, concentration polarization may affect the membrane performance.

Equation 4.9 shows that concentration polarization increases exponentially as the total volume flow J_v through the membrane increases. This is one of the reasons why modern spiral-wound reverse osmosis membrane modules are operated at low pressures. Modern

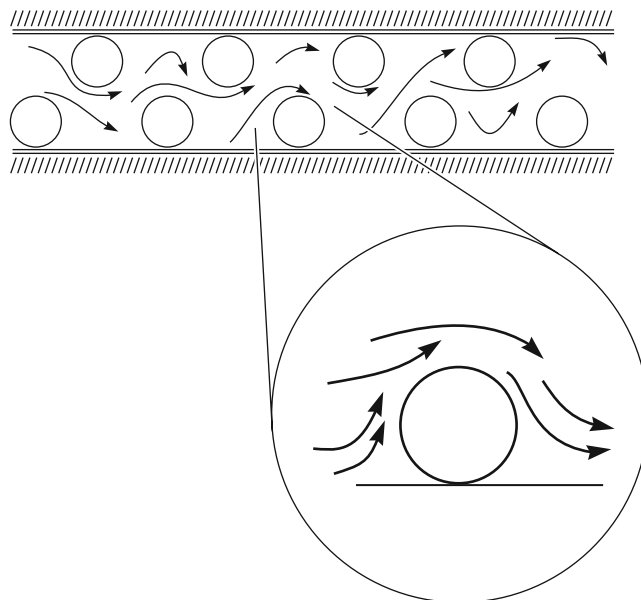


Figure 4.6 Flow dynamics around the spacer netting often used to promote turbulence in a membrane module and reduce concentration polarization

membranes have two to five times the water permeability, at equivalent salt selectivities, of the first-generation cellulose acetate reverse osmosis membranes. If membrane modules containing these new membranes were operated at the same pressures as early cellulose acetate modules, two to five times the desalinated water throughput could be achieved with the same number of modules. However, at such high fluxes, spiral-wound modules suffer from excessive concentration polarization, which leads to increased salt leakage and scale formation. This is one of the reasons modern, high permeance modules are operated at about the same volume flux as the early modules, but at lower applied pressures. This reduces energy costs and controls concentration polarization.

The final parameter in Equation 4.9 that determines the value of the concentration polarization modulus is the diffusion coefficient D_i of the solute away from the membrane surface. The size of the solute diffusion coefficient explains why concentration polarization is a greater factor in ultrafiltration than in reverse osmosis. Ultrafiltration membrane fluxes are usually higher than reverse osmosis fluxes, but the difference between the values of the diffusion coefficients of the retained solutes is more important. In reverse osmosis the solutes are dissolved salts, whereas in ultrafiltration the solutes are colloids and macromolecules. The diffusion coefficients of these high-molecular-weight components are about 100 times smaller than those of salts.

In Equation 4.9, the balance between convective transport and diffusive transport in the membrane boundary layer is characterized by the term $J_v \delta / D_i$. This dimensionless number represents the ratio of the convective transport J_v and diffusive transport D_i / δ and is commonly called the Peclet number. When the Peclet number is large ($J_v \gg D_i / \delta$), the convective flux through the membrane cannot easily be balanced by

diffusion in the boundary layer, and the concentration polarization modulus is large. When the Peclet number is small ($(J_v \ll D_i/\delta)$), convection is easily balanced by diffusion in the boundary layer, and the concentration polarization modulus is close to unity.

Wijmans *et al.* [16] calculated the concentration polarization modulus using Equation 4.9 as a function of the Peclet number $J_v\delta/D_i$, that is, the varying ratio of convection to diffusion. The resulting, very informative plot is shown in Figure 4.7. This figure is divided into two regions depending on whether the concentration polarization modulus, c_{i_o}/c_{i_b} , is smaller or larger than 1.

- The polarization modulus is smaller than 1 when the permeating minor component is enriched in the permeate. In this case, the component becomes depleted in the boundary layer, for example, in the dehydration of ethanol by pervaporation shown in Figure 4.3b.
- The polarization modulus is larger than 1 when the permeating minor component is depleted in the permeate. In this case, the component is enriched in the boundary layer, for example, in the reverse osmosis of salt solutions shown in Figure 4.3a.

As might be expected, the concentration polarization modulus deviates increasingly from unity as the Peclet number increases; that is, the convective volume flux term becomes larger relative to the diffusion term. At high values of the ratio $J_v\delta/D_i$, the exponential term in Equation 4.9 increases toward infinity, and the concentration polarization modulus c_{i_o}/c_{i_b} approaches a limiting value of $1/E_o$.

A striking feature of Figure 4.7 is its asymmetry with respect to enrichment and rejection of the minor component by the membrane. This means that, under comparable conditions, concentration polarization is much larger when the minor component of the feed is preferentially permeated by the membrane than when it is rejected. This follows

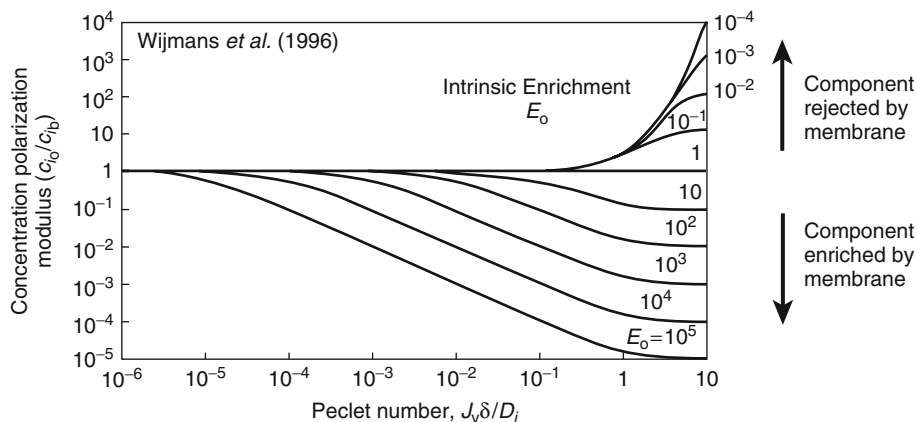


Figure 4.7 Concentration polarization modulus c_{i_o}/c_{i_b} as a function of the Peclet number $J_v\delta/D_i$ for a range of values of the intrinsic enrichment factor E_o . Lines calculated through Equation 4.9. This figure shows that components that are enriched by the membrane ($E_o > 1$) are affected more by concentration polarization than components that are rejected by the membrane ($E_o < 1$) [16]

from the form of Equation 4.9. Consider the case when the Peclet number $J_v\delta/D_i$ is 1. The concentration polarization modulus expressed by Equation 4.9 then becomes

$$\frac{c_{i_o}}{c_{i_b}} = \frac{\exp(1)}{1 + E_o[\exp(1) - 1]} = \frac{2.72}{1 + E_o(1.72)} \quad (4.10)$$

For components rejected by the membrane ($E_o \leq 1$), the enrichment E_o produced by the membrane lies between 1 and 0. The concentration polarization modulus c_{i_o}/c_{i_b} then lies between 1 (no concentration polarization) and a maximum value of 2.72. That is, the flux of the less permeable component cannot be more than 2.72 times higher than that in the absence of concentration polarization. In contrast, for a component enriched by the membrane in the permeate ($E_o \geq 1$), no such limitation on the magnitude of concentration polarization exists. For dilute solutions (c_{i_b} small) and selective membranes, the intrinsic enrichment can be 100–1000 or more. The concentration polarization modulus can then change from 1 (no concentration polarization) to close to zero (complete concentration polarization). These two cases are illustrated in Figure 4.8.

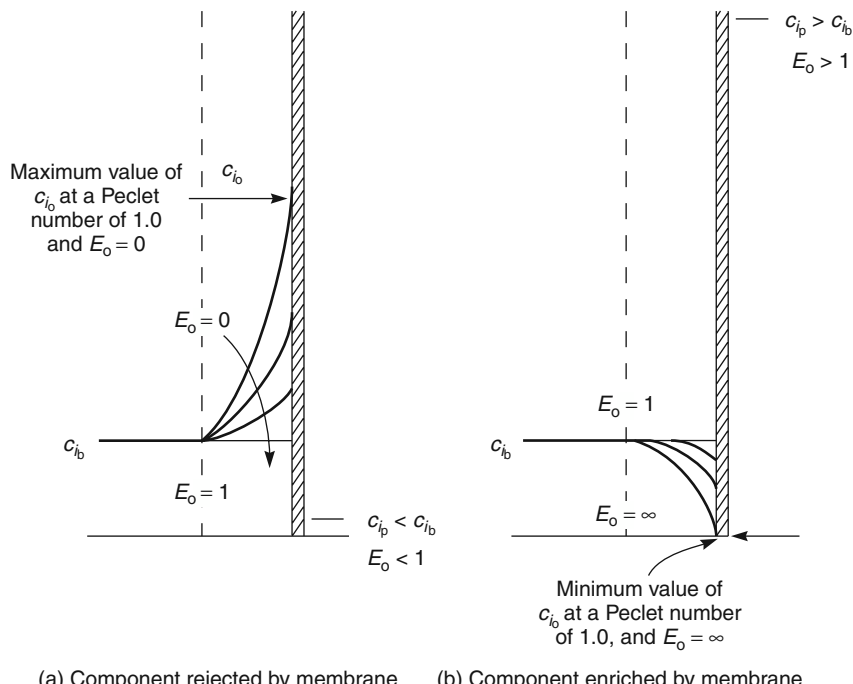


Figure 4.8 Concentration gradients that form adjacent to the membrane surface for components (a) rejected or (b) enriched by the membrane. The Peclet number, characterizing the balance between convection and diffusion in the boundary layer, is the same $J_v\delta/D_i = 1$. When the component is rejected, the concentration at the membrane surface c_{i_o} cannot be greater than 2.72 c_{i_b} , irrespective of the membrane selectivity. When the minor component permeates the membrane, the concentration at the membrane surface can decrease to close to zero, so the concentration polarization modulus can become very large

4.3 Determination of the Peclet Number

Equation 4.9 and Figure 4.7 are powerful tools to analyze the importance of concentration polarization in membrane separation processes. However, before these tools can be used, the appropriate value to be assigned to the Peclet number $J_v\delta/D_i$ must be determined. The volume flux J_v through the membrane is easily measured, so determining the Peclet number becomes a problem of measuring the coefficient D_i .

One approach to the boundary layer problem is to determine the ratio D_i/δ experimentally. This can be done using a procedure first proposed by Wilson [17]. The starting point for Wilson's approach is Equation 4.8, which can be written as

$$\ln \left(1 - \frac{1}{E} \right) = \ln \left(1 - \frac{1}{E_o} \right) - J_v \delta / D_i \quad (4.11)$$

The boundary layer thickness δ in Equation 4.11 is a function of the feed solution velocity u in the module feed flow channel; thus, the term D_i/δ can be expressed as

$$\frac{D_i}{\delta} = k_o u^n \quad (4.12)$$

where u is the superficial velocity in the feed flow channel and k_o and n are adjustable coefficients. Equation 4.11 can then be rewritten as

$$\ln \left(1 - \frac{1}{E} \right) = \ln \left(1 - \frac{1}{E_o} \right) - \frac{J_v}{k_o u^n} \quad (4.13)$$

Equation 4.13 can be used to calculate the dependence of pervaporation system performance on concentration polarization. One method is to use data obtained with a single module operated at various feed solution velocities. A linear regression analysis is used to fit data obtained at different feed velocities to obtain an estimate for k_o and E_o ; the exponent n is adjusted to minimize the residual error. Figure 4.9 shows some data obtained in pervaporation experiments with dilute aqueous toluene solutions and silicone rubber membranes [18]. Toluene is considerably more permeable than water through these membranes. In Figure 4.9, when the data were regressed, the best value for n was 0.96. The values of E_o , the intrinsic enrichment of the membrane, and k_o , obtained by regression analysis, are 3600 and 7.1×10^{-4} , respectively. The boundary layer coefficient, D_i/δ , is then given by

$$\frac{D_i}{\delta} = 7.1 \times 10^{-4} u^{0.96} \quad (4.14)$$

where u is the superficial velocity in the module.

A second method of determining the coefficient (D_i/δ) and the intrinsic enrichment of the membrane E_o is to use Equation 4.11. The term $\ln(1 - 1/E)$ is plotted against the permeate flux measured at constant feed solution flow rates, but different permeate pressures or feed solution temperatures. This type of plot is shown in Figure 4.10 for data obtained with aqueous trichloroethane solutions in pervaporation experiments with silicone rubber membranes.

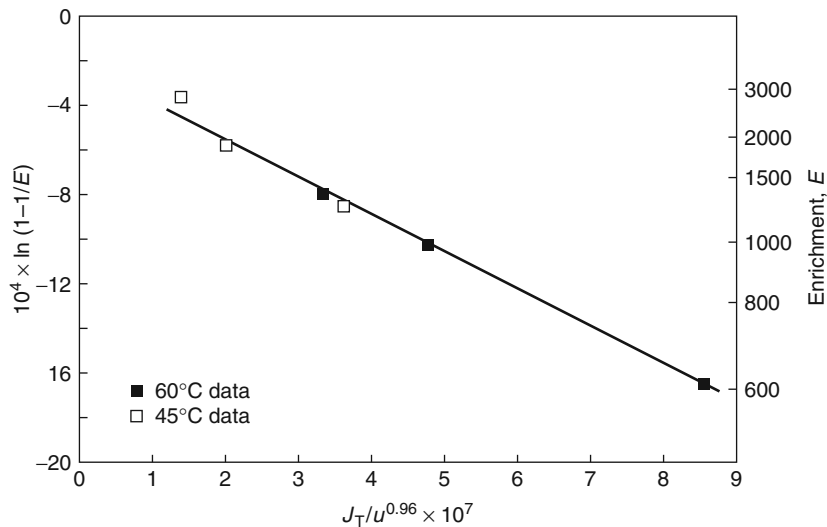


Figure 4.9 Derivation of the mass transfer coefficient by Wilson's method. Toluene/water enrichments are plotted as a function of feed solution superficial velocity in pervaporation experiments. Enrichments were measured at different feed solution superficial velocities with spiral-wound membrane modules [18]

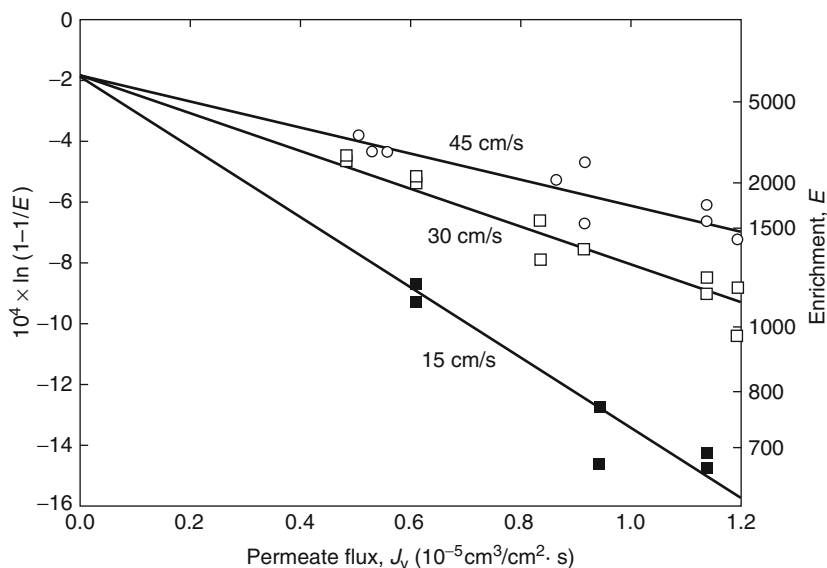


Figure 4.10 Trichloroethane enrichment ($\ln(1 - 1/E)$) as a function of permeate flux J_v in pervaporation experiments with silicone rubber membranes in spiral-wound modules using solutions of 100 ppm trichloromethane in water at different feed solution flow rates [18]. The ratio D_i/δ can be calculated from the slope of the lines using Equation 4.13

The coefficients D_i/δ obtained from the slopes of the lines at each velocity in Figure 4.10 can then be plotted as a function of the feed superficial velocity. The data show that the ratio D_i/δ varies with the superficial velocity according to the equation

$$\frac{D_i}{\delta} = 9 \times 10^{-4} u^{0.8} \quad (4.15)$$

From Equations 4.14 and 4.15, the value of the term D_i/δ at a fluid velocity of 30 cm/s is $1.6 \times 1.8 \times 10^{-2}$ cm/s. Based on a trichloroethane diffusion coefficient in the boundary aqueous layer of 2×10^{-5} cm²/s, this yields a boundary layer thickness of 10–15 µm. This boundary layer thickness is in the same range as values calculated for reverse osmosis with similar modules.

4.4 Concentration Polarization in Liquid Separation Processes

The effect of concentration polarization on specific membrane processes is discussed in the individual application chapters. However, a brief comparison of the magnitude of concentration polarization is given in Table 4.1 for processes involving liquid feed solutions. The key simplifying assumption is that the boundary layer thickness is 20 µm for all processes. This boundary layer thickness is typical of values calculated for separation of solutions with spiral-wound modules in reverse osmosis, pervaporation, and ultrafiltration. Tubular, plate-and-frame, and bore-side feed hollow fiber modules, because of

Table 4.1 Representative values of the concentration polarization modulus calculated for a variety of liquid separation processes. For these calculations, a boundary layer thickness of 20 µm, typical of that in most spiral-wound membrane modules, is assumed

Process	Typical intrinsic enrichment, E_o	Typical flux (in engineering units and as J_v (10 ⁻³ cm/s))	Diffusion coefficient (10 ⁻⁶ cm ² /s)	Peclet number, $J_v\delta/D_i$	Concentration polarization modulus (Equation 4.9)
Reverse osmosis					
Seawater desalination	0.01	50 l/m ² ·h (1.4)	10	0.28	1.3
Brackish water desalination	0.01	90 l/m ² ·h (2.3)	10	0.46	1.5
Ultrafiltration					
Protein separation	0.01	50 l/m ² ·h (1.4)	0.5	5.6	70
Pervaporation					
Ethanol dehydration	20	0.1 kg/m ² ·h (0.003)	20	0.0003	1.0
VOC from water	2000	1.0 kg/m ² ·h (0.03)	20	0.003	0.14
Coupled transport					
Copper from water	1000	60 mg/cm ² ·min (0.001)	10	0.0002	0.8

their better flow velocities, generally have lower calculated boundary layer thicknesses. Hollow fiber modules with shell-side feed generally have larger calculated boundary layer thicknesses because of their poor fluid flow patterns.

Table 4.1 shows typical enrichments and calculated Peclet numbers for membrane processes with liquid feeds. In this table, it is important to recognize the difference between enrichment and separation factor. The enrichments shown are calculated for the minor component. For example, in the dehydration of ethanol, a typical feed solution of 96% ethanol and 4% water yields a permeate containing about 80% water; the enrichment, that is, the ratio of the permeate to feed concentration, is about 20. In Figure 4.11, the calculated Peclet numbers and enrichments shown in Table 4.1 are plotted on the Wijmans graph to show the relative importance of concentration polarization for the processes listed.

In coupled transport and solvent dehydration by pervaporation, concentration polarization effects are generally modest and controllable, with a concentration polarization modulus of 1.5 or less. In reverse osmosis, the Peclet number of 0.3–0.5 was calculated on the basis of typical fluxes of current reverse osmosis membrane modules, which are 50–90 l/m²h. Concentration polarization modulus values in this range are between 1.0 and 1.5.

Figure 4.11 shows that ultrafiltration and pervaporation for the removal of organic solutes from water are both seriously affected by concentration polarization. In ultrafiltration, the low diffusion coefficient of macromolecules produces a concentration of retained solutes 70 times the bulk solution volume at the membrane surface. At these high concentrations, macromolecules precipitate, forming a gel layer at the membrane surface and reducing flux. The effect of this gel layer on ultrafiltration membrane performance is discussed in Chapter 6.

In the case of pervaporation of dissolved volatile organic compounds (VOCs) from water, the magnitude of the concentration polarization effect is a function of the

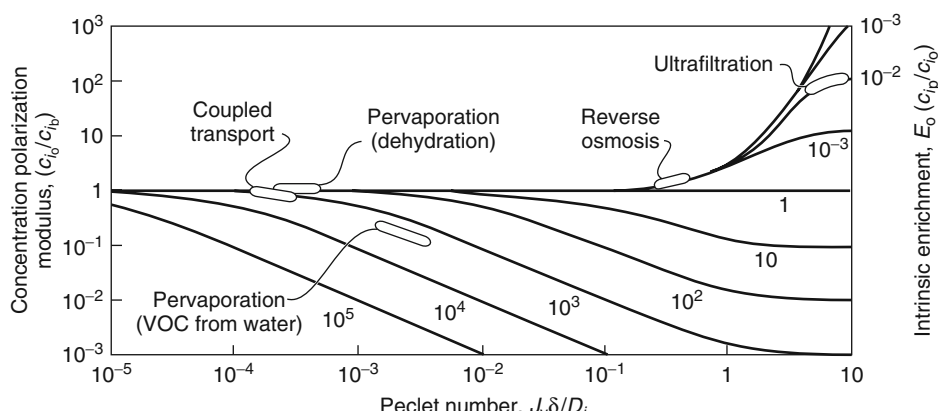


Figure 4.11 Peclet numbers and intrinsic enrichments for the membrane separation processes shown in Table 4.1 superimposed on the concentration polarization plot of Wijmans et al. [16]

enrichment factor. The selectivity of pervaporation membranes to different VOCs varies widely, so the intrinsic enrichment and the magnitude of concentration polarization effects depend strongly on the solute. Table 4.2 shows experimentally measured enrichment values for a series of dilute VOC solutions treated with silicone rubber membranes in spiral-wound modules [18]. When these values are superimposed on the Wijmans plot as shown in Figure 4.12, the concentration polarization modulus varies from 1.0, that is, no concentration polarization, for isopropanol, to 0.1 for trichloroethylene, which has an enrichment of 5700.

In liquid separation processes where concentration polarization occurs, the problem is often managed by maintaining a high feed flow rate across the surface of the membrane.

Table 4.2 Enrichment factors measured for the pervaporation of VOCs from dilute solutions with silicone rubber spiral-wound modules

Solute	Enrichment (E_o)
Trichloroethylene	5700
Toluene	3600
Ethyl acetate	270
Isopropanol	18

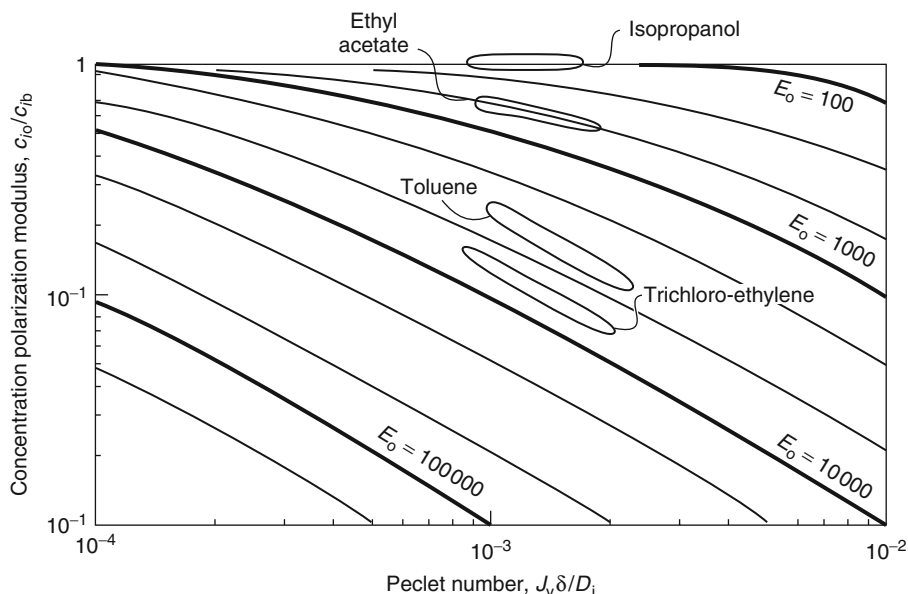


Figure 4.12 A portion of the Wijmans plot shown in Figure 4.7 expanded to illustrate concentration polarization in pervaporation of dilute aqueous organic solutions. With solutes such as toluene and trichloroethylene, high intrinsic enrichments produce severe concentration polarization. Concentration polarization is much less with solutes such as ethyl acetate (enrichment 270), and is essentially eliminated with isopropanol (enrichment 18) [18]

This reduces the boundary layer thickness and so increases the Peclet number shown in Table 4.1 and Figure 4.11. For this reason, membrane systems that contain several membrane modules often have the modules arranged in series (high feed velocity) rather than in parallel (low feed velocity). In some processes, particularly ultrafiltration, inter-stage feed pumps may also be used to maintain high feed velocities through the modules.

4.5 Concentration Polarization in Gas Separation Processes

Concentration polarization in gas separation processes has not been widely studied, but usually the effect can be assumed to be small because of the high diffusion coefficients of gases. In calculating the expression for the concentration polarization modulus of gases, the simplifying assumption that the volume fluxes on each side of the membrane are equal cannot be made. The starting point for the calculation is the mass-balance equation (Equation 4.6), which for gas permeation is written

$$J_{v_f} c_i - \frac{D_i dc_i}{dx} = J_{v_p} c_{i_p} \quad (4.16)$$

where J_{v_f} is the volume flux of gas on the feed side of the membrane and J_{v_p} is the volume flux on the permeate side. These volume fluxes ($\text{cm}^3/\text{cm}^2/\text{s}$) can be linked by correcting for the pressure on each side of the membrane using the expression

$$J_{v_f} p_o = J_{v_p} p_\ell \quad (4.17)$$

where p_o and p_ℓ are the gas pressures on the feed and permeate sides of the membrane. Hence,

$$J_{v_f} \frac{p_o}{p_\ell} = J_{v_f} \varphi = J_{v_p} \quad (4.18)$$

where φ is the pressure ratio p_o/p_ℓ across the membrane. Substituting Equation 4.18 into Equation 4.16 and rearranging gives

$$-D_i \frac{dc_i}{dx} = J_{v_f} (\varphi c_{i_p} - c_i) \quad (4.19)$$

Integrating across the boundary layer thickness, as before, gives

$$\frac{c_{i_o}/\varphi - c_{i_p}}{c_{i_b}/\varphi - c_{i_p}} = \exp \left(\frac{J_{v_f} \delta}{D} \right) \quad (4.20)$$

For gases, the enrichment terms, E and E_o , are most conveniently expressed in volume fractions, so that

$$E_o = \frac{c_{i_p}}{p_\ell} \frac{p_o}{c_{i_o}} = \frac{c_{i_p}}{c_{i_o}} \varphi \quad (4.21)$$

and

$$E = \frac{c_{i_p}}{p_\ell} \times \frac{p_o}{c_{i_b}} = \frac{c_{i_p}}{c_{i_b}} \times \varphi \quad (4.22)$$

Equation 4.20 can then be written as

$$\exp\left(\frac{J_{v_f}\delta}{D_i}\right) = \frac{1 - 1/E_o}{1 - 1/E} \quad (4.23)$$

which on rearranging gives

$$E/E_o = c_{i_o}/c_{i_b} = \frac{\exp(J_{v_f}\delta/D_i)}{1 + E_o[\exp(J_{v_f}\delta/D_i) - 1]} \quad (4.24)$$

Equation 4.24 has the same form as the expression for the concentration polarization modulus of liquids, Equation 4.9.

When Equation 4.24 is used to calculate the concentration polarization modulus, the Peclet number is very small, so no polarization is expected for most gas separation applications. Only in a few applications, such as the separation of VOCs from air, or water from ethanol, where very high permeance membranes are used, can measurable concentration polarization be observed or expected. Channeling, in which a portion of the feed gas completely bypasses contact with the membrane through some poor flow distribution in the module, can also reduce module efficiency in a way that is difficult to separate from concentration polarization. Channeling is much more noticeable in gas permeation modules than in liquid permeation modules.

4.6 Cross-Flow, Co-Flow, and Counter-Flow

In the discussion of concentration polarization to this point, the assumption is made that the concentration on the permeate side of the membrane is only determined by the ratio of the component fluxes. However, in some membrane processes, a lateral flow of permeate is used to change the concentration underneath the membrane and thus the permeance through the membrane.

An example of this type of process is illustrated in Figure 4.13, which shows the separation of nitrogen from air using a membrane that preferentially permeates oxygen. The feed air, containing approximately 20 vol% oxygen, is introduced under pressure at one end of the module. The permeate gas at this end of the module typically contains about 50 vol% oxygen (at a lower pressure). As the feed gas travels down the membrane module it becomes increasingly depleted in oxygen (enriched in nitrogen) and leaves the module as a residue gas containing 99% nitrogen. The permeate gas at this end of the module contains about 5 vol% oxygen and 95 vol% nitrogen. If this gas is directed to flow counter to the incoming feed gas, as shown in Figure 4.13, the effect is to sweep the

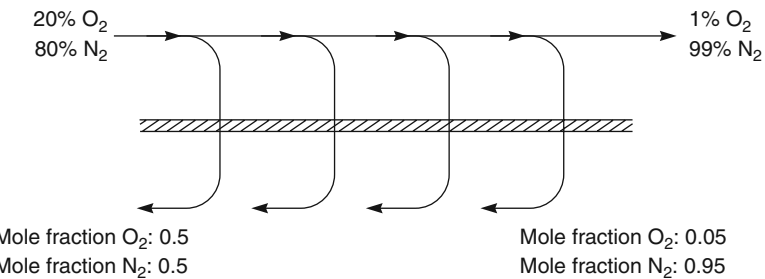


Figure 4.13 An illustration of a counter-flow module for the separation of nitrogen from air. Directing the permeate to flow counter to the feed sweeps the permeate side of the membrane with a flow of oxygen-depleted gas. This increases the oxygen flux and decreases the nitrogen flux through the membrane

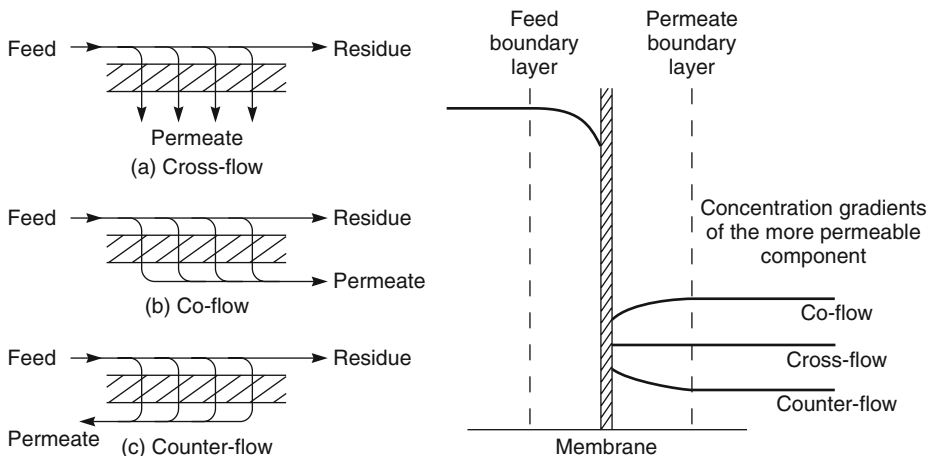


Figure 4.14 (a) Cross-, (b) co-, and (c) counter-flow schemes in a membrane module and the changes in the concentration gradients that occur across a median section of the membrane

permeate side of the membrane with a flow of oxygen-depleted, nitrogen-enriched gas. This is beneficial because the oxygen gradient through the membrane is increased, which increases oxygen flux through the membrane. Simultaneously the nitrogen gradient is reduced, which decreases nitrogen flux through the membrane. An opposite negative impact would result if the permeate gas were moved in the same direction as the feed gas (that is co-flow). This would have the effect of sweeping the permeate side of the membrane with oxygen-enriched gas.

Co-, counter-, and cross-flow schemes for membrane modules are illustrated in Figure 4.14, together with the resulting concentration gradients across a median section of the membrane for each flow scheme. It follows from Figure 4.14 that system performance can be improved by operating a module in an appropriate flow mode (generally counter-flow). However, such improvements require that the concentration at

the membrane permeate surface equals the bulk concentration of the permeate at that point; that is, significant concentration gradients do not form in the microporous support layer between the permeate membrane surface and the bulk fluid. This condition is difficult to achieve with processes such as ultrafiltration or reverse osmosis in which the permeate fluid is a liquid. In these processes, the selective side of the membrane faces the feed solution, and a microporous support layer faces the permeate. This microporous layer forms a stagnant liquid film and concentration gradients build up easily in this boundary layer, completely outweighing the benefit of counter-flow. Thus, counter-flow (sweep) module designs are usually limited to gas separation and pervaporation processes. In these processes, the permeate is a gas, and membrane permeate-side concentration gradients are more easily controlled because diffusion coefficients in gases are high.

The likelihood of concentration gradients forming in the permeate-side membrane microporous support layer can be determined by calculating the permeate-side Peclet number. For example, consider the case of dehydration of air, a process in which counter-flow sweep operation is commonly used. The average permeance of the membranes used in this application is about 10 gpu ($10 \times 10^{-6} \text{ cm}^3(\text{STP})/\text{cm}^2 \cdot \text{s} \cdot \text{cmHg}$). Under typical operating conditions of the process (10 bar feed, 1 bar permeate), the volume flux through the membrane at the permeate-side pressure is then about $6.8 \times 10^{-3} \text{ cm}^3/\text{cm}^2 \cdot \text{s}$. This is the J_v term in the Peclet number. Assuming the microporous support layer that separates the permeate membrane surface from the well-stirred counter-flowing gas is $100 \mu\text{m}$ thick (δ), and taking the diffusion coefficient of air at atmospheric pressure to be $\sim 0.2 \text{ cm}^2/\text{s}$, it follows that the permeate-side Peclet number, $J_v \delta / D$, in this application is $\sim 3.4 \times 10^{-4}$. A Peclet number this small implies that diffusion is much larger than convection in the permeate support layer. Concentration gradients in the boundary layer are then small, and counter-flow operation can be very beneficial.

In liquid permeation processes, the balance between convection and diffusion in the microporous support layer is very different. For example, consider the process of pressure retarded osmosis (PRO), described in Chapter 13, which also uses permeate-side sweep to generate the driving force for permeation. In this process, the membrane permeance is typically about $2 \text{l/m}^2 \cdot \text{h}$ bar and the pressure difference across the membrane, feed to permeate, is about 10 bar. The volume flux of permeate in the microporous support layer is then about $5.6 \times 10^{-4} \text{ cm}^3/\text{cm}^2 \cdot \text{s}$. The diffusion coefficient of salt (D_i) in the $100 \mu\text{m}$ thick boundary layer (δ) is $\sim 0.6 \times 10^{-5} \text{ cm}^2 \cdot \text{s}$. The permeate-side Peclet number in this application, $J_v \delta / D_i$, is then about 0.9. A Peclet number close to 1 implies that convection and diffusion effects are closely matched. This calculation is in accord with industrial experience, which has shown that permeate-side concentration polarization is one of the most important issues affecting the operation of PRO systems.

It follows from the discussion above that the benefit obtained from counter-flow depends on the particular separation, and it can be substantial, especially in gas separation and pervaporation processes. A comparison of cross-flow, counter-flow, and counter-flow/sweep modules used to dehydrate natural gas is shown in Figure 4.15. Water is a smaller molecule and much more condensable than methane, the main component of natural gas, so membranes with a water/methane selectivity of 400–500 are readily available. In the calculations shown in Figure 4.15, the membrane is assumed to have a pressure-normalized methane flux of $5 \times 10^{-6} \text{ cm}^3(\text{STP})/\text{cm}^2 \cdot \text{s} \cdot \text{cmHg}$ and

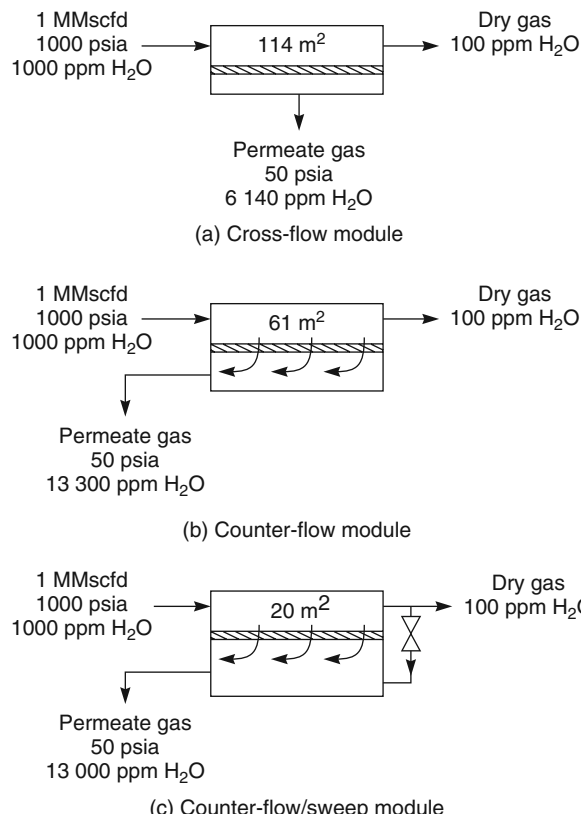


Figure 4.15 Comparison of (a) cross-flow, (b) counter-flow, and (c) counter-flow sweep module performance for the separation of water vapor from natural gas. Pressure-normalized methane flux: $5 \times 10^{-6} \text{ cm}^3(\text{STP})/\text{cm}^2 \cdot \text{s} \cdot \text{cmHg}$; membrane selectivity, water/methane: 200. The separation performance of the membrane shown was calculated using a differential element computer model

a water/methane selectivity of 200. Counter-flow/sweep modules have a substantial advantage in this separation because the separation is completely pressure-ratio-limited.²

² The importance of the pressure ratio in separating gas mixtures can be illustrated by considering the separation of a gas mixture with component concentrations (mol%) n_{i_0} and n_{i_ℓ} at a feed pressure of p_o . A flow of component across the membrane can only occur if the partial pressure of component i on the feed side of the membrane, $n_{i_0} p_o$, is greater than the partial pressure of component i on the permeate side of the membrane, $n_{i_\ell} p_\ell$. That is,

$$n_{i_0} p_o > n_{i_\ell} p_\ell$$

It follows that the maximum enrichment achieved by the membrane can be expressed as

$$\frac{n_{i_\ell}}{n_{i_0}} \leq \frac{p_o}{p_\ell}$$

This means that the enrichment can never exceed the pressure ratio of p_o/p_ℓ , no matter how selective the membrane. In the example above (and Figure 4.15), the maximum water vapor enrichment across the membrane is 20 (1000/50 psia) even though the membrane is 200 times more permeable to water than methane. The effect of pressure ratio in gas separation is described in more detail in Chapter 8.

In the cross-flow module illustrated in Figure 4.15a, the average concentration of water on the feed side of the membrane as it decreases from 1000 to 100 ppm is 310 ppm (the log mean). The pooled permeate stream has a concentration of 6140 ppm. The counter-flow module illustrated in Figure 4.15b performs substantially better, providing a pooled permeate stream with a concentration of 13 300 ppm. Not only does the counter-flow module perform twice as good a separation, it also requires only half the membrane area.

In the case of the counter-flow/sweep membrane module illustrated in Figure 4.15c, a portion of the dried residue gas stream is expanded across a valve and used as the permeate-side sweep gas. The separation obtained depends on how much gas is used as a sweep. In the calculation illustrated, 5% of the residue gas is used as a sweep; even so, the result is dramatic. The concentration of water vapor in the permeate gas is 13 000 ppm, almost the same as the perfect counter-flow module shown in Figure 4.15b, but the membrane area required to perform the separation is one-third of the counter-flow case. *Mixing separated feed gas with the permeate gas improves the separation!*

The cause of this paradoxical result is illustrated in Figure 4.16 and discussed in a number of papers by Cussler and coworkers [19]. Figure 4.16a shows the concentration of water vapor on the feed and permeate sides of the membrane module in the case of a simple counter-flow module. On the high-pressure side of the module, the water vapor concentration in the feed gas drops from 1000 to about 310 ppm halfway through the module and to 100 ppm at the residue end. The graph directly below the module drawing shows the theoretical maximum concentration of water vapor on the permeate side of the membrane. This maximum is determined by the feed-to-permeate pressure ratio of 20 as described in footnote 2 of this chapter. The actual calculated permeate-side concentration is also shown. The difference between these two lines is a measure of the driving force for water vapor transport across the membrane. At the feed end of the module, this difference is about 1000 ppm, but at the residue end the difference is only about 100 ppm.

Figure 4.16b shows an equivalent figure for a counter-flow module in which 5% of the residue gas containing 100 ppm water vapor is expanded to 50 psia and introduced as a sweep gas at the residue end of the module. The water vapor concentration in the permeate gas at the residue end of the module then falls from 1900 to 100 ppm, producing a dramatic increase in water vapor permeation through the membrane at the residue end of the module. The result is a two-thirds reduction in the size of the module.

In the discussion above, a counter-flow of permeate gas is used as a sweep gas to change the concentration underneath the membrane. In the laboratory, the sweep effect could be produced by another gas. Figure 4.17 illustrates a laboratory gas permeation experiment of this type. As the pressurized feed gas mixture is passed over the membrane surface, certain components permeate the membrane. On the permeate side of the membrane, a lateral flow of helium or other inert gas sweeps the permeate from the membrane surface. In the absence of the sweep gas, the composition of the gas mixture on the permeate side of the membrane is determined by the flow of components from the feed. If a large flow of sweep gas is used, the partial pressure of the permeating components on the permeate side of the membrane is reduced to a low value. The difference in partial pressure of the permeating gases from the feed to the permeate side of the membrane is thereby increased, and the flow across the membrane increases proportionately. Sweep

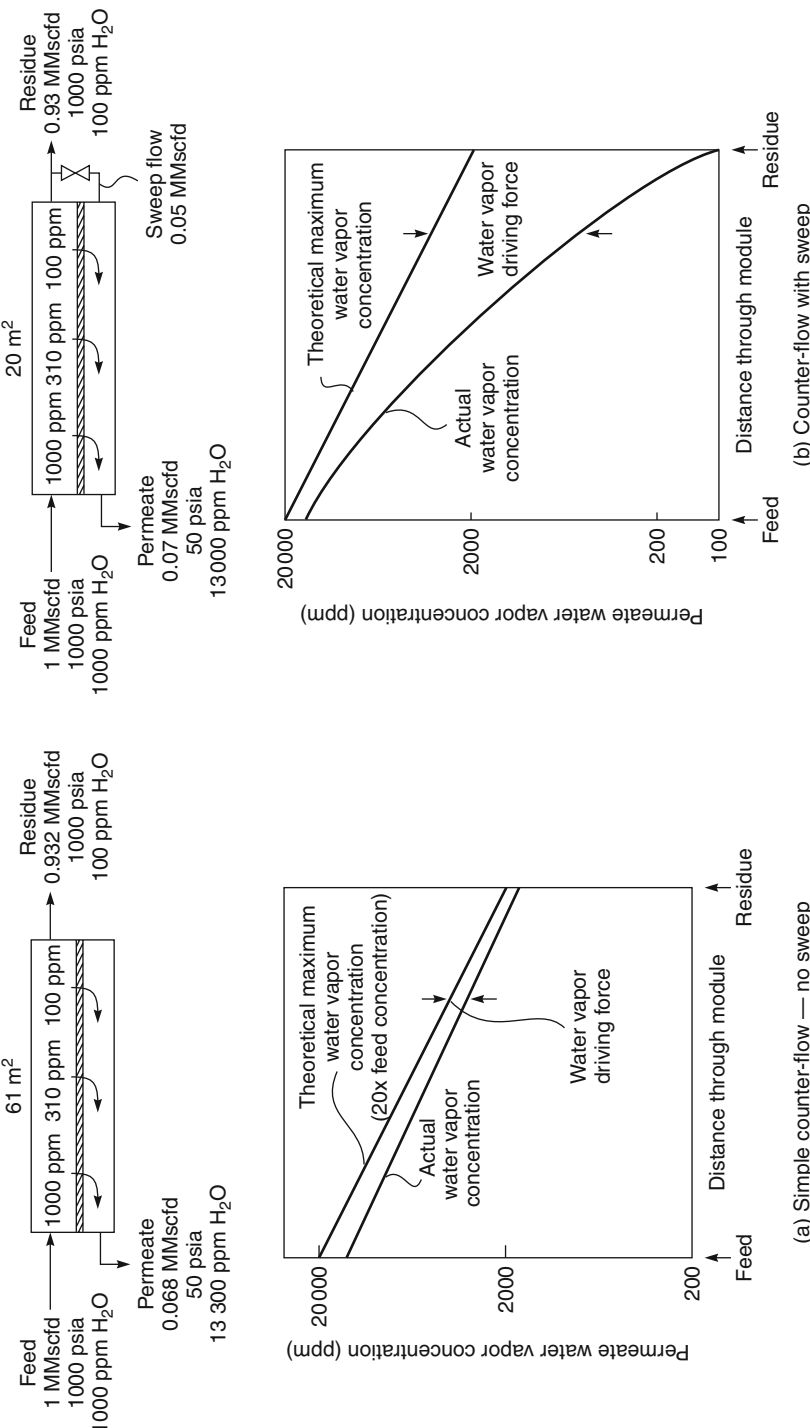


Figure 4.16 The effect of a small permeate-side, counter-flow sweep on the water vapor concentration on the permeate side of a membrane. In this example calculation, the sweep flow reduces the required membrane area for the separation by two-thirds

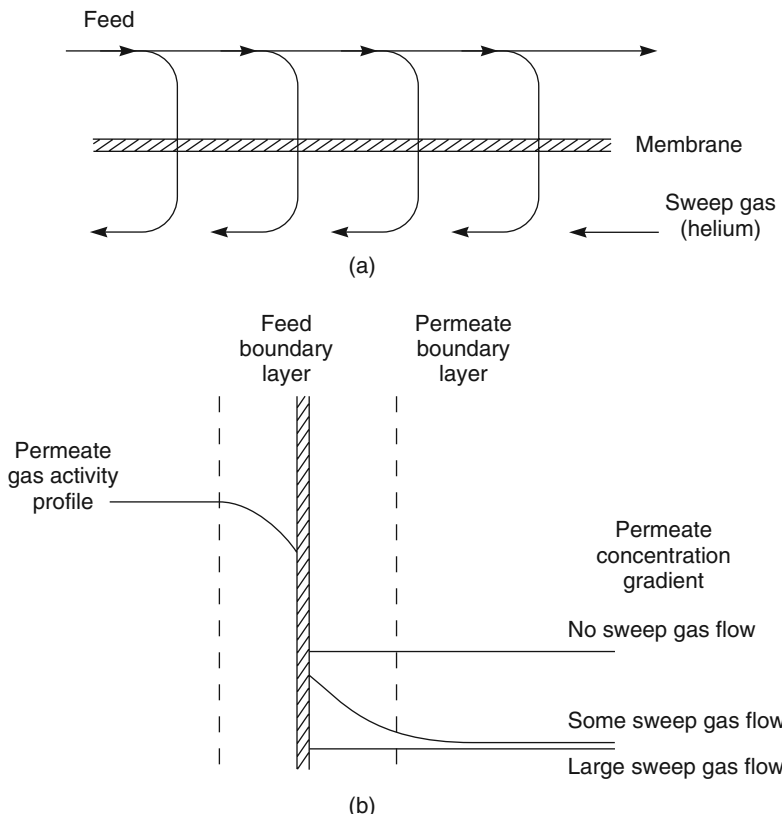


Figure 4.17 (a) Flow schematic of permeation using a permeate-side sweep gas (sometimes used in laboratory gas separation and pervaporation experiments). (b) The concentration gradients that form on the permeate side of the membrane depend on the volume of sweep gas used. In laboratory experiments, a large sweep-gas-to-permeate-gas flow ratio is used, so the concentration of permeate at the membrane surface is very low

gases are sometimes used in gas permeation and pervaporation laboratory experiments. The sweep gas is generally helium and the helium/permeate gas mixture is fed to a gas chromatograph for analysis.

Using an external permeate-side sweep gas to lower the partial pressure on the permeate side of the membrane in an industrial process has the drawback that the sweep gas and permeating component must subsequently be separated. In some cases this may not be difficult; some processes that have been suggested but rarely used are shown in Figure 4.18. In two of these examples, the sweep gas is steam and the separation of the sweep gas and the permeating component is achieved by condensation [20–22]. If the permeating gas is itself condensed easily, an inert gas such as nitrogen can be used as the sweep [23].

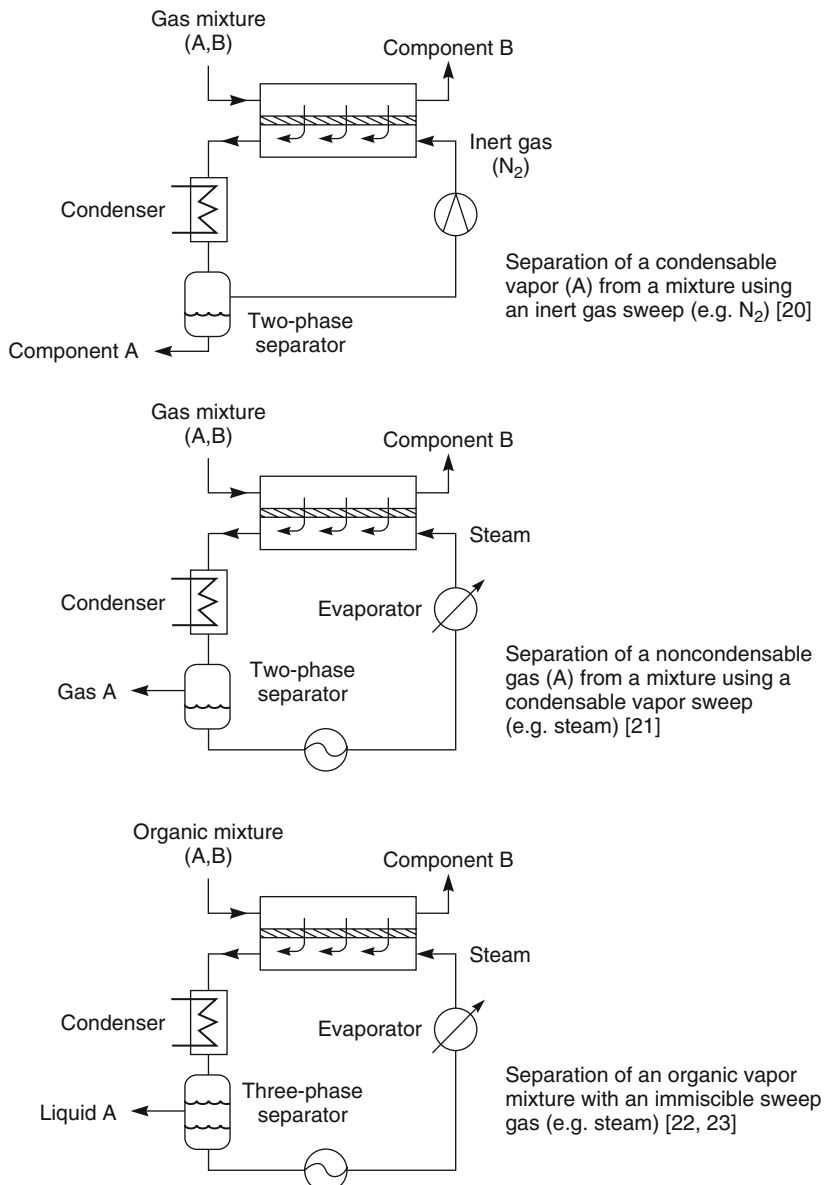


Figure 4.18 Sweep gas systems proposed for industrial processes

4.7 Conclusions and Future Directions

Few membrane processes are unaffected by concentration polarization, and the effect is likely to become more important as membrane materials and membrane fabrication techniques improve. The improvements in membrane flux and selectivity achieved will

increase concentration polarization effects. In the laboratory, concentration polarization is controlled by increasing the turbulence of the feed fluid. However, in industrial systems this approach has practical limits. In ultrafiltration and electrodialysis, for example, liquid recirculation pumps are already a major portion of the plant's capital cost and consume 20–40% of the power used for the separation. In recent years, there has been a trend toward operating microfiltration and ultrafiltration membrane modules at very low feed pressures. This lowers the flux through the membrane, but makes concentration polarization much easier to control. Air sparging and pulsed feed flow are also now widely used to promote increased turbulence in the feed solution.

References

1. Carslaw, H.S. and Jaeger, J.C. (1947) *Conduction of Heat in Solids*, Oxford University Press, London.
2. Bird, R.B., Stewart, W.E., and Lightfoot, E.N. (1960) *Transport Phenomena*, John Wiley & Sons, Inc., New York.
3. Crank, J. (1956) *The Mathematics of Diffusion*, Oxford University Press, London.
4. Porter, M.C. (1972) Concentration polarization with membrane ultrafiltration. *Ind. Eng. Chem. Prod. Res. Dev.*, **11**, 234.
5. Lepore, J.V. and Ahlert, R.C. (1988) Fouling in membrane processes, in *Reverse Osmosis Technology* (ed. B.S. Parekh), Marcel Dekker, New York, pp. 141–184.
6. Wickramasinghe, S.R., Semmens, M.J., and Cussler, E.L. (1992) Mass transfer in various hollow fiber geometries. *J. Membr. Sci.*, **69**, 235.
7. Mi, L. and Hwang, S.T. (1999) Correlation of concentration polarization and hydrodynamic parameters in hollow fiber modules. *J. Membr. Sci.*, **159**, 143.
8. Cussler, E.L. (1997) *Diffusion Mass Transfer in Fluid Systems*, 2nd edn, Cambridge University Press, New York and Cambridge.
9. Zeman, L.J. and Zydny, A.L. (1996) *Microfiltration and Ultrafiltration: Principles and Applications*, Marcel Dekker, New York.
10. Brian, P.L.T. (1966) Mass transport in reverse osmosis, in *Desalination by Reverse Osmosis* (ed. U. Merten), MIT Press, Cambridge, MA, pp. 161–292.
11. Belfort, G., Davis, R.H., and Zydny, A.L. (1994) The behavior of suspensions and macromolecular solutions in cross flow microfiltration. *J. Membr. Sci.*, **96**, 1.
12. Da Costa, A.R., Fane, A.G., and Wiley, D.E. (1994) Spacer characterization and pressure drop modeling in spacer-filled channels for ultrafiltration. *J. Membr. Sci.*, **87**, 79.
13. Schwinge, J., Neal, P.R., Wiley, D.E. et al. (2004) Spiral wound modules and spacers: review and analysis. *J. Membr. Sci.*, **242** (1–2), 129.
14. Li, F., Meindersma, W., de Haan, A.B., and Reith, T. (2005) Novel spacers for mass transfer enhancement in membrane separations. *J. Membr. Sci.*, **253** (1–2), 1.
15. Jaffrin, M.Y., Gupta, B.B., and Paullier, P. (1994) Energy savings pulsatile mode crossflow filtration. *J. Membr. Sci.*, **86**, 281.
16. Wijmans, J.G., Athayde, A.L., Daniels, R., Ly, J.H., Kamaruddin, H.D. and Pinna, I. (1996) The role of boundary layers in the removal of volatile organic compounds from water by pervaporation. *J. Membr. Sci.*, **109**, 135.

17. Wilson, E.E. (1915) A basis for rational design of heat transfer apparatus. *Trans. ASME*, **37**, 47.
18. Baker, R.W., Wijmans, J.G., Athayde, A.L. *et al.* (1997) The effect of concentration polarization on the separation of volatile organic compounds from water by pervaporation. *J. Membr. Sci.*, **137**, 159.
19. Wang, K.L., McCray, S.H., Newbold, D.N., and Cussler, E.L. (1992) Hollow fiber air drying. *J. Membr. Sci.*, **72**, 231.
20. Walker, R.J., Drummond, C.J., and Ekmann, J.M. (1985) Evaluation of Advanced Separation Techniques for Application to Flue Gas Cleanup Processes for the Simultaneous Removal of Sulfur Dioxide and Nitrogen Oxides. Department of Energy, DE85102227, May 1985.
21. Robertson, A.E. (1969) Separation of hydrocarbons. US Patent 2,475,990, July 1969.
22. Baker, R.W., Cussler, E.L., Eykamp, W., Koros, W.J., Riley, R.L. and Strathmann, H. (1991) *Membrane Separation Systems*, Noyes Data Corporation, Park Ridge, NJ, p. 155.
23. Frey, F.E. (1939) Process for concentrating hydrocarbons. US Patent 2,159,434, May 1939.

5

Reverse Osmosis

5.1 Introduction and History

Reverse osmosis is a process for desalting water using membranes that are permeable to water but essentially impermeable to salt. Pressurized water containing dissolved salts contacts the feed side of the membrane; water depleted of salt is withdrawn as a low-pressure permeate. The ability of membranes to separate small solutes from water has been known for a very long time. Pfeffer, Traube, and others studied osmotic phenomena with ceramic membranes as early as the 1850s. In 1931, the process was patented as a method of desalting water, and the term reverse osmosis was coined [1]. Modern interest dates from the work of Reid and Breton, who in 1959 showed that cellulose acetate films could perform this type of separation [2]. Their films were 5–20 µm thick so fluxes were very low, but by pressurizing the feed salt solution to 65 bar, they obtained salt removals of better than 98% in the permeate water. The breakthrough discovery that made reverse osmosis a practical process was the development of the Loeb–Sourirajan anisotropic cellulose acetate membrane [3]. This membrane had 10 times the flux of the best membrane of Reid and Breton and equivalent rejections. With these membranes, water desalination by reverse osmosis became a potentially practical process, and within a few years small demonstration plants were installed. The first membrane modules were tubular or plate-and-frame systems, but Westmoreland, Bray, and others at the San Diego Laboratories of Gulf General Atomics (the predecessor of Fluid Systems, Inc.) soon developed spiral-wound modules [4, 5]. Later, Du Pont [6], building on the earlier work of Dow, introduced polyaramide hollow fine fiber reverse osmosis modules under the name Permasep®.

Anisotropic cellulose acetate membranes were the industry standard through the 1960s to the mid-1970s, until Cadotte, then at North Star Research, developed the interfacial polymerization method of producing composite membranes [7]. Interfacial composite membranes had extremely high salt rejections, combined with good water fluxes. Fluid Systems introduced the first commercial interfacial composite membrane in 1975. The

construction of a large seawater desalination plant at Jeddah, Saudi Arabia, using these membranes was a milestone in reverse osmosis development [8]. Later, at FilmTec, Cadotte developed a fully aromatic interfacial composite membrane based on the reaction of phenylenediamine and trimesoyl chloride [9, 10]. This membrane has become the new industry standard. Over the past 30 years, the performance of membranes and membrane modules has steadily improved. The improvements and better process designs have cut the cost of seawater desalination to below \$0.50/m³ of water. The energy used by the process has also been reduced from 6.1 kWh/m³ for the Jeddah plant to ~2.0–3.0 kWh/m³ for a new plant fitted with today's membrane modules and energy recovery devices on the high-pressure brine concentrate solution.

The most recent development, beginning in the mid-1980s, was the introduction of low-pressure nanofiltration membranes by all of the major reverse osmosis companies [11, 12]. These membranes are used to separate trace amounts of salts and other dissolved solutes from already good-quality water to produce ultrapure water for the electronics industry.

Currently, approximately 10 million m³/day of water are desalinated by reverse osmosis, providing approximately 1% of the world's drinking water supply. Half of this capacity is installed in the Middle East and other desert regions to produce municipal water from wastewater, brackish groundwater, or the sea. The remainder is installed in the United States, Europe, and Japan, principally to produce ultrapure industrial water. More than 20 seawater desalination plants with capacities of more than 100 000 m³/day are now in operation. These plants each contain from 0.2 to 1.0 million m² of membrane.

The interfacial composite membrane has displaced the anisotropic cellulose acetate membrane in almost all applications. Interfacial composite membranes are supplied in spiral-wound module form; the market share of cellulose acetate membranes, principally supplied as hollow fibers, is now less than 10% of new installed capacity and shrinking [13]. Tubular and plate-and-frame systems are only competitive for small niche applications involving particularly highly fouling water, and have less than 1% of the market.

Reverse osmosis is almost completely limited to water treatment, but an important advance has been the development of similar membrane processes to separate solutes from organic solvents. This technology, perhaps better called hyperfiltration, is still largely a laboratory-scale operation, but a few industrial plants have been installed. The first large plant of this type was developed by Grace Davison (operating division of W.R. Grace & Co.), working with Mobil Oil (now ExxonMobil). The plant was installed at a Beaumont, Texas, refinery in 1998 to separate a solution of methyl ethyl ketone and lube oil in an oil dewaxing process.

Some of the milestones in the development of the reverse osmosis industry are summarized in Figure 5.1.

5.2 Theoretical Background

Salt and water permeate reverse osmosis membranes according to the solution-diffusion transport mechanism described in Chapter 2. The water flux, J_i , is linked to the pressure

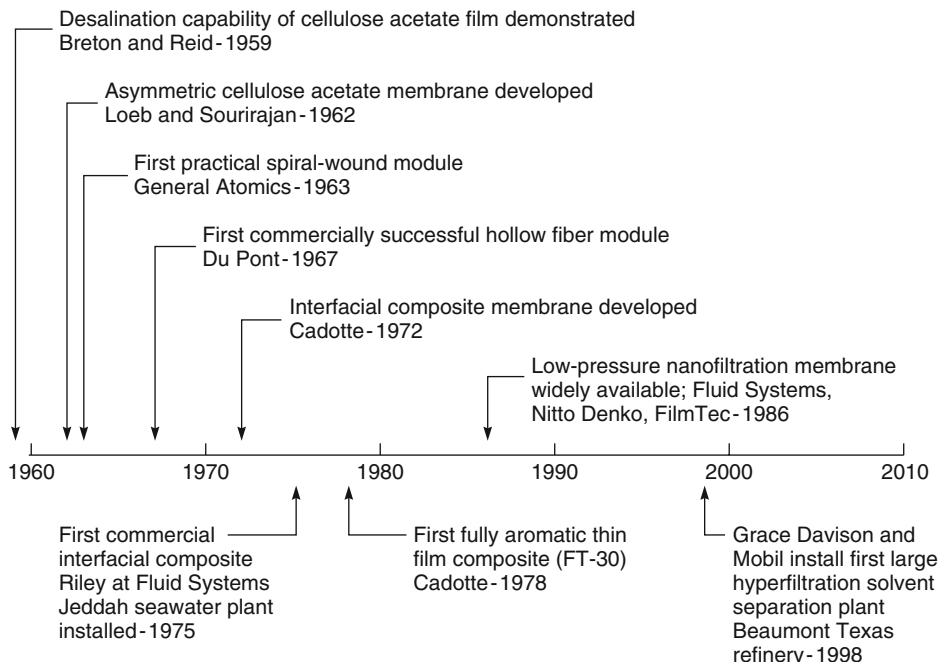


Figure 5.1 Milestones in the development of reverse osmosis

and concentration gradients across the membrane by the equation

$$J_i = A(\Delta p - \Delta\pi) \quad (5.1)$$

where Δp is the pressure difference across the membrane, $\Delta\pi$ is the osmotic pressure differential across the membrane, and A is a constant. As this equation shows, at a low applied pressure, when $\Delta p < \Delta\pi$, water flows from the dilute to the concentrated salt-solution side of the membrane by normal osmosis. When $\Delta p = \Delta\pi$, no flow occurs, and when the applied pressure is higher than the osmotic pressure, $\Delta p > \Delta\pi$, water flows from the concentrated to the dilute salt-solution side of the membrane.

The salt flux, J_j , across a reverse osmosis membrane is described by the equation

$$J_j = B(c_{j_o} - c_{j_e}) \quad (5.2)$$

where B is the salt permeability constant and c_{j_o} and c_{j_e} , respectively, are the salt concentrations on the feed and permeate sides of the membrane. The concentration of salt in the permeate solution (c_{j_e}) is usually much smaller than the concentration in the feed (c_{j_o}), so Equation 5.2 can be simplified to

$$J_j = Bc_{j_o} \quad (5.3)$$

It follows from the above equations that the water flux is proportional to the applied pressure, but the salt flux is independent of pressure. This means that the membrane becomes more selective as the pressure increases. Selectivity can be measured in a number of ways, but most commonly, it is measured as the salt rejection coefficient \mathbb{R} , defined as

$$\mathbb{R} = \left[1 - \frac{c_{j_e}}{c_{j_o}} \right] \times 100\% \quad (5.4)$$

The salt concentration on the permeate side of the membrane can be related to the membrane fluxes by the expression

$$c_{j_e} = \frac{J_j}{J_i} \cdot \rho_i \quad (5.5)$$

where ρ_i is the density of water (g/cm^3). By combining Equations 5.1 to 5.3, the membrane rejection can be expressed as

$$\mathbb{R} = \left[1 - \frac{\rho_i \cdot B}{A(\Delta p - \Delta \pi)} \right] \times 100\% \quad (5.6)$$

The effects of the most important operating parameters on membrane water flux and salt rejection are shown schematically in Figure 5.2 [14]. The effect of feed pressure on membrane performance is shown in Figure 5.2a. As predicted by Equation 5.1, at a pressure equal to the osmotic pressure of the feed (23 bar), the water flux is zero; thereafter, it increases linearly as the pressure is increased. The salt rejection also extrapolates to zero at a feed pressure of 23 bar as predicted by Equation 5.6, but increases very rapidly with increased pressure to reach salt rejections of more than 99% at an applied pressure of ~ 45 bar (twice the feed solution osmotic pressure).

The effect of increasing the concentration of salt in the feed solution on membrane performance is illustrated in Figure 5.2b. Increasing the salt concentration effectively increases the osmotic pressure term in Equation 5.1; consequently, at a constant feed pressure, the water flux falls with increasing salt concentration. At a feed pressure of ~ 45 bar the water flux approaches zero when the salt concentration is about 10 wt%, at which point the osmotic pressure equals the applied hydrostatic pressure. The salt rejection also extrapolates to zero rejection at this point but increases rapidly with decreasing salt concentration. Salt rejections of more than 99% are reached at salt concentrations below 6%, corresponding to a net applied pressure of about 27 bar.

The effect of temperature on salt rejection and water flux illustrated in Figure 5.2c is more complex. Transport of salt and water, represented by Equations 5.1 and 5.3, is an activated process, and both increase exponentially with increasing temperature. As Figure 5.2c shows, the effect of temperature on the water flux of membranes is quite dramatic: the water flux doubles as the temperature is increased by 30°C . However, the effect of temperature on the salt flux is even more marked. This means that the salt rejection coefficient, proportional to the ratio B/A in Equation 5.6, actually declines slightly as the temperature increases.

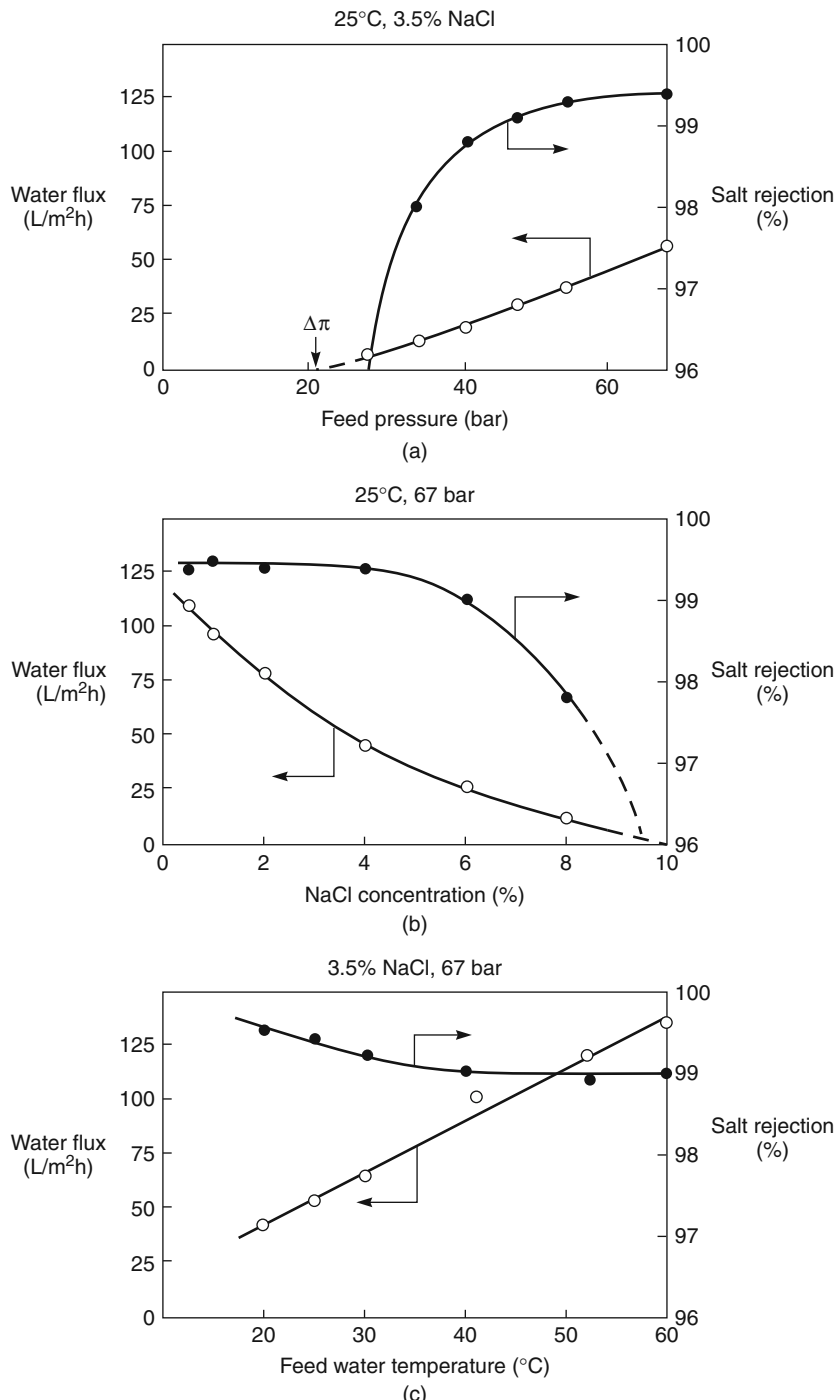


Figure 5.2 (a) Effect of pressure, (b) feed salt concentration and (c) and feed temperature on the properties of a seawater desalination membrane (SW-30) [14]

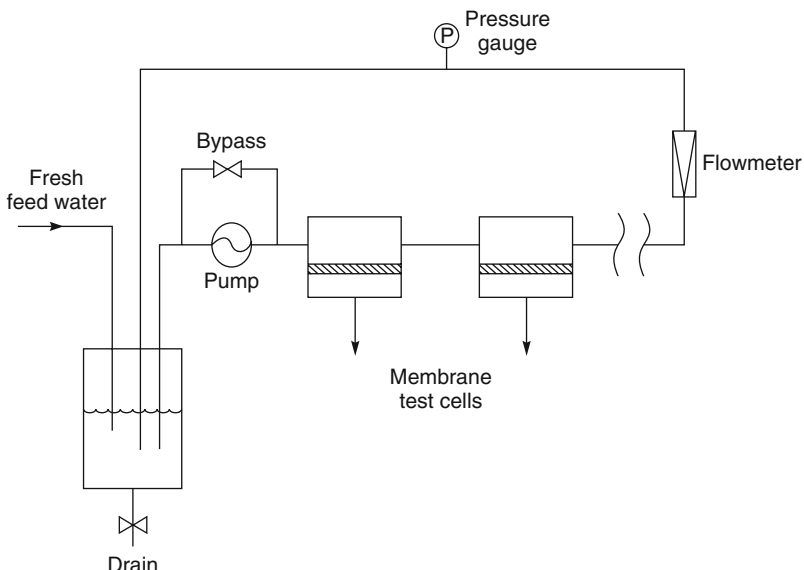


Figure 5.3 Flow schematic of a high-pressure laboratory reverse osmosis test system

Measurements of the type shown in Figure 5.2 are typically obtained with small laboratory test cells. A laboratory test system is illustrated in Figure 5.3. Such systems are often used in general membrane quality control tests with a number of cells arranged in series through which fluid is pumped. The system is usually operated with a test solution of 0.2–1.0 wt% sodium chloride at pressures ranging from 10 to 40 bar. The storage tank and flow recirculation rate are made large enough that changes in concentration of the test solution due to loss of permeate can be ignored.

Some confusion can occur over the rejection coefficients quoted by membrane module manufacturers. The intrinsic rejection of good quality seawater membranes measured in a laboratory test system might be in the range 99.7–99.8%, whereas the same membrane in module form may have a salt rejection of 99.6–99.7%. This difference is due to small membrane defects introduced during module production and to concentration polarization, which has a small but measurable effect on module rejection. Manufacturers call the module value the nominal rejection. However, manufacturers will generally only guarantee a lower figure, for example, 99.5%, for the initial module salt rejection to take into account variations between modules. To complicate matters further, module performance generally deteriorates slowly during the one- to three-year guaranteed module lifetime due to membrane compaction, membrane fouling, and membrane degradation from hydrolysis, chlorine attack, or membrane cleaning. A decrease in the membrane flux by 20% over the lifetime of typical modules is not unusual, and the rejection can fall by 0.1–0.2%. Reverse osmosis system manufacturers allow for this decline in performance when designing systems. The lifetime of a membrane module in one of today's well-maintained and operated plants is about seven years.

5.3 Membranes and Materials

A number of membrane materials and membrane preparation techniques have been used to make reverse osmosis membranes. The target of much of the early work was seawater desalination (approximately 3.5 wt% salt), which requires membranes with salt rejections of greater than 99.3% to produce an acceptable permeate containing less than 500 ppm salt. Early membranes could only meet this target performance when operated at very high pressures, up to 100 bar. As membrane performance has improved, the operating pressure has dropped to 50–60 bar. Recently, membranes to desalt water feeds with salt concentrations of 0.1–0.5 wt% have been developed. For these applications, membranes are typically operated at pressures in the 10–30 bar range with a target salt rejection of about 99%. With the growth of the electronics industry, the demand for membranes to produce ultrapure water to wash silicon wafers has increased. The feed to an ultrapure water reverse osmosis plant is often municipal drinking water, which may only contain 100–200 ppm dissolved salts, mostly divalent ions. The target membrane performance in this case may be 98–99% sodium chloride rejection, but more than 99.5% divalent ion rejection. These membranes are operated at low pressures, typically in the 8–12 bar range. Many manufacturers tailor the properties of a single membrane material to meet the requirements of different applications. Invariably, a significant trade-off between flux and rejection is involved.

A brief description of the commercially important membranes in current use follows. More detailed descriptions can be found in specialized reviews [13, 15, 16]. Petersen's review on interfacial composite membranes is particularly worth noting [17].

5.3.1 Cellulosic Membranes

Cellulose acetate was the first high-performance reverse osmosis membrane material discovered. The flux and rejection of cellulose acetate membranes have now been surpassed by interfacial composite membranes. However, cellulose acetate membranes still maintain a small fraction of the market because they are easy to make, mechanically tough, and resistant to degradation by chlorine and other oxidants, a problem with interfacial composite membranes. Cellulose acetate membranes can tolerate continuous exposure of up to 1 ppm chlorine, so chlorination can be used to sterilize the feed water, a major advantage with feed streams having significant bacterial loading.

The water and salt permeability of cellulose acetate membranes is extremely sensitive to the degree of acetylation of the polymer used to make the membrane [2, 18, 19]. The effect of degree of acetylation on salt and water permeability is illustrated in Figure 5.4 [20]. Fully substituted cellulose triacetate (44.2 wt% acetate) has an extremely high water-to-salt permeability ratio, reflecting its very high selectivity. Unfortunately, the water permeability is low, so these membranes have low water fluxes. Nonetheless, cellulose triacetate hollow fine fiber membranes are still produced for some seawater desalination plants because salt rejections of about 99.6% with a seawater feed are attainable. However, many commercial cellulose acetate membranes use a polymer containing about 40 wt% acetate with a degree of acetylation of 2.7. These membranes generally achieve 98–99% sodium chloride rejection and have good fluxes. The permeability data

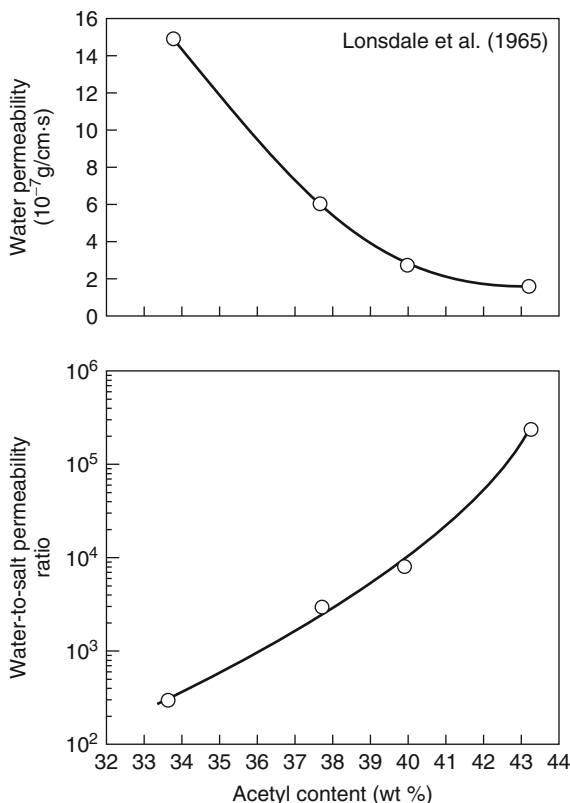


Figure 5.4 Permeabilities of cellulose acetate to water and sodium chloride as a function of acetyl content at 25°C (Data from Lonsdale et al. [20].)

shown in Figure 5.4 can be replotted to show expected salt rejections, as shown in Figure 5.5.

The data in Figure 5.5 show that thick films of cellulose acetate made from 39.8 wt% acetate polymer should reject 99.5% sodium chloride. In practice, this theoretical rejection is very difficult to obtain with practical thin membranes [21]. Figure 5.6 shows the salt rejection properties of 39.8 wt% acetate membranes made by the Loeb–Sourirajan process [22]. The freshly formed membranes have very high water fluxes of almost 300 l/m² h, but almost no rejection of sodium chloride. The membranes appear to have a finely microporous structure and are permeable to quite large solutes such as sucrose. The salt rejection of these membranes can be greatly improved by heating the membrane in a bath of hot water for a few minutes. This annealing procedure is used with all cellulose acetate membranes and modifies the salt rejection layer of the membrane by eliminating the micropores and producing a denser, more salt-rejecting skin. The water flux decreases, and the sodium chloride rejection increases. The temperature of this annealing step determines the final properties of the membrane. A typical rejection/flux curve for various annealed membranes is shown in Figure 5.6. Because their

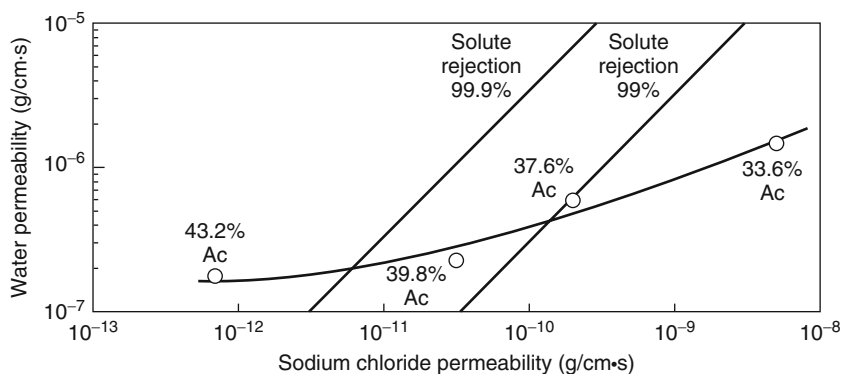


Figure 5.5 Water permeability as a function of sodium chloride permeability for membranes made from cellulose acetate of various degrees of acetylation (% Ac). The expected rejection coefficients for these membranes, calculated for dilute salt solutions using Equation 5.6, are shown

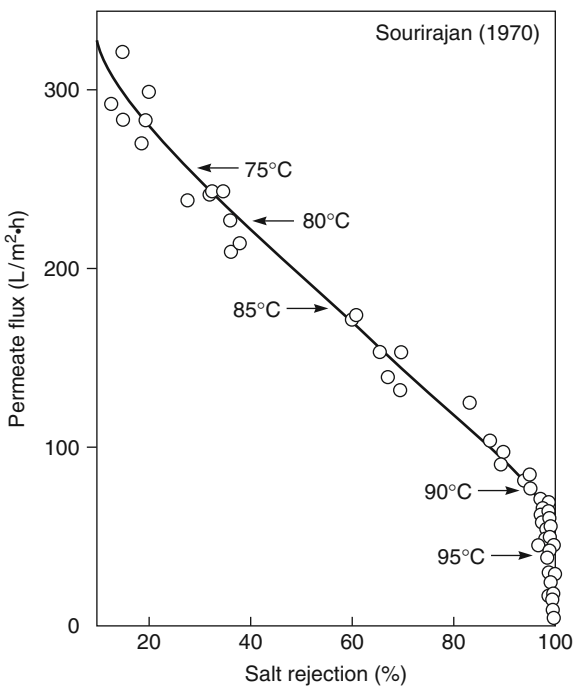


Figure 5.6 The effect of annealing temperatures on the flux and rejection of cellulose acetate membranes. The annealing temperature is shown on the figure (cellulose diacetate membranes tested at 1500 psig with 0.5 M NaCl). Reprinted with permission from [22]. Copyright (1970) Elsevier.

properties change on heating, cellulose acetate membranes are generally not used above about 35°C. The membranes also slowly hydrolyze over time, so the feed water is usually adjusted to pH 4–6, the range in which the membranes are most stable [23].

Throughout the 1960s considerable effort was expended on understanding the Loeb–Sourirajan membrane production process to improve the quality of the membranes produced. The casting solution composition is critically important. Other important process steps are the time of evaporation before precipitation, the temperature of the precipitation bath, and the temperature of the annealing step. Most of the early membranes were made of 39.8 wt% acetate polymer because this material was readily available and had the most convenient solubility properties. By the 1970s, however, a number of workers, particularly Saltonstall and others at Envirogenics (Envirogenics Technology Design International Company, Inc.), had developed better membranes by blending the 39.8 wt% acetate polymer with small amounts of triacetate polymer (44.2 wt% acetate) or other cellulose esters such as cellulose acetate butyrate [24]. These blends are generally used to form current cellulose acetate membranes. Good-quality blend membranes with seawater salt rejections of 99.0–99.5%, close to the theoretical salt rejection determined by thick film measurements, can be made, but the flux of these membranes is modest. However, most applications of cellulose acetate membranes do not require such high salt rejections, so the typical commercial cellulose acetate membranes used to process industrial water streams have good fluxes and sodium chloride rejection of about 96%.

5.3.2 Noncellulosic Polymer Membranes

During the 1960s and 1970s, the Office of Saline Water sponsored development of noncellulosic reverse osmosis membranes. Many polymers were evaluated as Loeb–Sourirajan membranes, but few matched the properties of cellulose acetate. Following the development of interfacial composite membranes by Cadotte, this line of research was largely abandoned. Nevertheless, a few commercially successful noncellulosic membrane materials were developed. In particular, polyamide membranes were developed by several groups. Aliphatic polyamides have low rejections and modest fluxes, but aromatic polyamide membranes were successfully developed by Toray [25], Chemstrand (Monsanto) [26], and Permasep® (Du Pont) [27], all in hollow fiber form. These membranes have good seawater salt rejections of up to 99.5%, but the fluxes are low, in the 2–6 l/m² h range. The Permasep® membrane, made in hollow fine fiber form to overcome the low water permeability problem, was produced under the names B-10 and B-15 for seawater desalination plants until the year 2000. The structure of the Permasep B-15 polymer is shown in Figure 5.7. The polymer contains a few

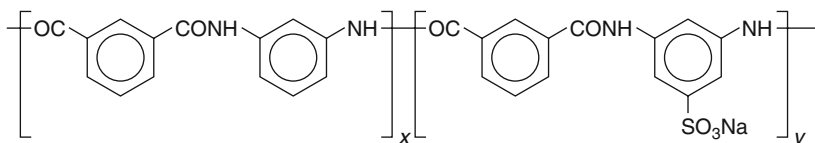


Figure 5.7 Aromatic polyamide used by Du Pont in its Permasep B-15 hollow fine fibers [27]

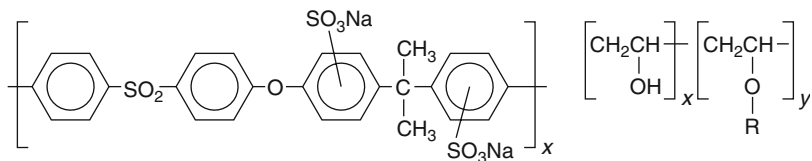


Figure 5.8 Membranes based on sulfonated polysulfone and substituted poly(vinyl alcohol) are produced by Hydranautics (Nitto Denko Corporation) for nanofiltration applications

sulfonic acid groups to make it more hydrophilic and raise its water flux. Polyamide membranes, like interfacial composite membranes, are susceptible to degradation by chlorine because of their amide bonds.

Loeb–Sourirajan membranes based on sulfonated polysulfone and substituted poly(vinyl alcohol) produced by Hydranautics (Nitto Denko Corporation) have also found a commercial market as high-flux, low-rejection membranes in water softening applications because their divalent ion rejection is high. These membranes are also chlorine-resistant and have been able to withstand up to 40 000 ppm h of chlorine exposure without degradation.¹ The structures of the polymers used by Hydranautics are shown in Figure 5.8.

5.3.3 Interfacial Composite Membranes

Since the discovery by Cadotte and his coworkers that high-flux, high-rejection reverse osmosis membranes can be made by interfacial polymerization [7, 9, 10], membranes made by this method have become the industry standard. Interfacial composite membranes have significantly higher salt rejections and fluxes than cellulose acetate membranes. The first membranes made by Cadotte had salt rejections in tests with 3.5% sodium chloride solutions (synthetic seawater) of greater than 99% and fluxes of 30 l/m² h at a pressure of 100 bar. The membranes could also be operated at temperatures above 35°C, the temperature ceiling for Loeb–Sourirajan cellulose acetate membranes. Today's interfacial composite membranes are significantly better. Typical membranes, tested with 3.5% sodium chloride solutions, have a salt rejection of 99.7% and a water flux of 50 l/m² h at 35 bar; this is less than half the salt passage of the cellulose acetate membranes and twice the water flux. The rejection of low-molecular-weight dissolved organic solutes by interfacial membranes is also far better than cellulose acetate. The only drawback of interfacial composite membranes, and a significant one, is the rapid, permanent loss in selectivity that results from exposure to even ppb levels of chlorine or hypochlorite disinfectants [28]. Although the chlorine resistance of interfacial composite membranes has been improved, these membranes still cannot be used with feed water containing more than a few ppb of chlorine.

The chemistry and properties of some of the important interfacial composite membranes developed over the past 25 years are summarized in Table 5.1 [10, 12, 29, 30].

¹ The ability of a reverse osmosis membrane to withstand chlorine attack without showing significant loss in rejection is measured in parts per million hours (ppm h). This is the product of chlorine exposure expressed in parts per million and the length of exposure expressed in hours. Thus, 1000 ppm h is 1 ppm chlorine for 1000 hours or 10 ppm chlorine for 100 hours or 1000 ppm chlorine for 1 hour, and so on.

Table 5.1 Characteristics of major interfacial polymerization reverse osmosis membranes

Membrane	Developer	Properties
NS100 Polyethylenimine crosslinked with toluene 2,4-diisocyanate	Cadotte <i>et al.</i> [29] North Star Research	The first interfacial composite membrane achieved seawater desalination characteristics of >99% rejection, 30 l/m ² h at 100 bar with seawater
PA 300/RC-100 Epamine (epichlorohydrin-ethylenediamine adduct) crosslinked with isophthaloyl chloride or toluene 2,4-diisocyanate	Riley <i>et al.</i> [30] Fluid Systems, San Diego	PA 300, based on isophthaloyl chloride (IPC), was introduced first, but RC-100, based on toluene 2,4-diisocyanate (TDI), proved more stable. This membrane was used at the first large reverse osmosis seawater desalination plant (Jeddah, Saudi Arabia)
NF40 and NTR7250 Piperazine crosslinked with trimesoyl chloride	Cadotte FilmTec [10] and Kamiyama Nitto Denko [12]	The first all-monomeric interfacial membrane. Only modest seawater desalination properties, but a good brackish water membrane. More chlorine-tolerant than earlier membranes because of the absence of secondary amine bonds
FT-30/SW-30 <i>m</i> -Phenylenediamine crosslinked with trimesoyl chloride	Cadotte FilmTec [10]	An all-aromatic, highly crosslinked structure giving exceptional salt rejection and very high fluxes. By tailoring the preparation techniques, brackish water or seawater membranes can be made. Seawater version has a salt rejection of 99.5–99.7% at 55 bar. Brackish water version has >99% salt rejection at 40 l/m ² h and 15 bar. All the major reverse osmosis companies produce variations of this membrane

The chemistry of the FT-30 membrane, which has an all-aromatic structure based on the reaction of phenylenediamine and trimesoyl chloride, is widely used. This chemistry, first developed by Cadotte [9] and shown in Figure 5.9, is now used in modified form by all the major reverse osmosis membrane producers.

For a few years after the development of the first interfacial composite membranes, it was believed that the amine portion of the reaction chemistry had to be polymeric to obtain good membranes. This is not the case, and the monomeric amines, piperazine and phenylenediamine, have been used to form membranes with very good properties. Interfacial composite membranes based on urea or amide bonds are subject to degradation by chlorine attack. Chlorine appears to first replace the hydrogen atoms of any secondary amide groups in the polymer. This mode of attack is slowed significantly if tertiary aromatic amines are used and the membranes are highly crosslinked. A slower, but

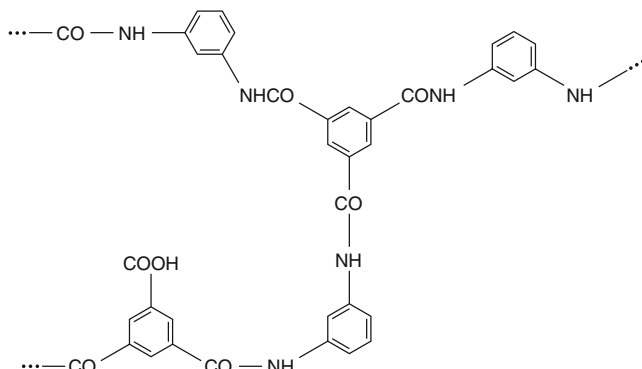


Figure 5.9 Chemical structure of the FT-30 membrane developed by Cadotte using the interfacial reaction of phenylenediamine with trimesoyl chloride

ultimately more destructive, mode of attack is direct attack of the aromatic rings in the polymer [31]. Chemistries based on all-aromatic or piperazine structures are moderately chlorine tolerant and can withstand very low level exposure to chlorine for prolonged periods or exposure to parts per million levels for a few days. Early interfacial composite membranes such as the NS100 or PA300 membrane showed significant degradation at a few hundred parts per million hours. Current membranes, such as the fully aromatic FilmTec FT-30 or the Hydranautics ESPA membrane, can withstand up to 1000 ppm h chlorine exposure. A number of chlorine tolerance studies have been made over the years; a discussion of the literature has been given by Glater *et al.* [32]. Heavy metal ions such as iron appear to strongly catalyze chlorine degradation. For example, the FT-30 fully aromatic membrane is somewhat chlorine resistant in heavy-metal-free water, but in natural waters, which normally contain heavy metal ions, chlorine resistance is low. The rate of chlorine attack is also pH sensitive.

5.3.4 Other Membrane Materials

An interesting group of composite membranes with very good properties is produced by condensation of furfuryl alcohol with sulfuric acid. The first membrane of this type was made by Cadotte at North Star Research and was known as the NS200 membrane [33]. These membranes are not made by the interfacial composite process; rather, a polysulfone microporous support membrane is contacted first with an aqueous solution of furfuryl alcohol and then with sulfuric acid. The coated support is then heated to 140°C. The furfuryl alcohol forms a polymerized, crosslinked layer on the polysulfone support; the membrane is completely black. The chemistry of condensation and reaction is complex, but a possible polymerization scheme is shown in Figure 5.10.

These membranes have exceptional properties, including seawater salt rejections of up to 99.6% and fluxes of 40 l/m² h at 30 bar. Unfortunately, they are even more sensitive to oxidants such as chlorine or dissolved oxygen than the polyamide/polyurea interfacial composites. The membranes lose their excellent properties after a few hundred hours of operation unless the feed water is completely free of dissolved chlorine and oxygen. A great deal of work was devoted to stabilizing this membrane, with little success.

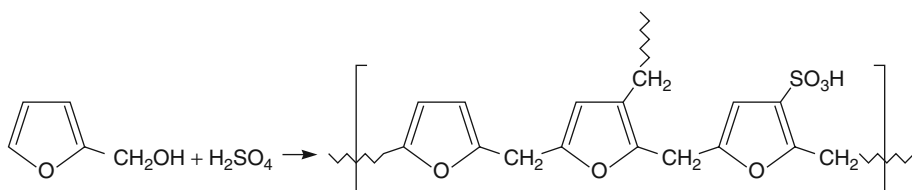


Figure 5.10 Formation of the NS200 condensation membrane

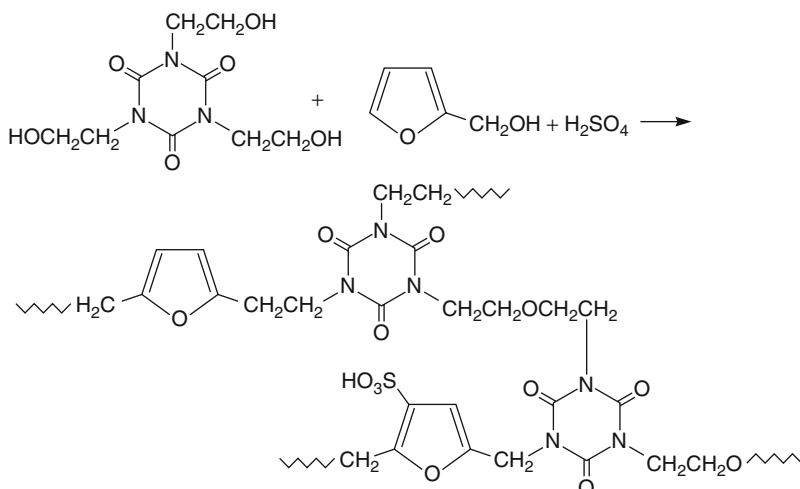


Figure 5.11 Reaction sequence for Toray's PEC-1000 membrane

Later, Kurihara and coworkers [34] at Toray produced a related membrane, using 1,3,5-tris(hydroxyethyl)isocyanuric acid as a co-monomer. A possible reaction scheme is shown in Figure 5.11. This membrane, commercialized by Toray under the name PEC-1000, has the highest rejection of any membrane developed, with seawater rejections of 99.9% and fluxes of 20 l/m² h at 65 bar. The membrane also shows the highest known rejections to low-molecular-weight organic solutes, typically more than 95% from relatively concentrated feed solutions [35]. Unfortunately, these exceptional selectivities are accompanied by the same sensitivity to dissolved oxidants as the NS200 membrane. This problem was never completely solved, so the PEC-1000 membrane, despite its unsurpassed rejection properties, is no longer commercially available.

5.4 Reverse Osmosis Membrane Categories

Reverse osmosis membranes can be grouped into three main categories:

- Seawater and brackish water desalination membranes operated with 0.5–5 wt% salt solutions at pressures of 10–60 bar.

- Low-pressure nanofiltration membranes operated with 200–5000 ppm salt solutions at pressures of 5–10 bar.
- Hyperfiltration membranes used to separate solutes from organic solvent solutions.

5.4.1 Seawater and Brackish Water Desalination Membranes

The relative performances of membranes produced for the seawater desalination market are shown in Figure 5.12, a plot of sodium chloride rejection as a function of membrane flux. The figure is divided into two sections by a dotted line at a rejection of 99.3%. This salt rejection is generally considered to be the minimum sodium chloride rejection that can produce potable water from seawater in a single-stage reverse osmosis plant. Membranes with lower sodium chloride rejections can be used to desalinate seawater, but at least a portion of the product water must be treated in a second-stage operation to achieve the target average permeate salt concentration of less than 500 ppm.

As Figure 5.12 shows, Toray's PEC-1000 crosslinked furfuryl alcohol membrane has by far the best sodium chloride rejection combined with good fluxes. This explains the sustained interest in this membrane despite its extreme sensitivity to dissolved chlorine and oxygen in the feed water. Hollow fine fiber membranes made from cellulose triacetate by Toyobo or aromatic polyamides by Permasep (Du Pont) are also comfortably in the one-stage seawater desalination performance range, but the water fluxes of these

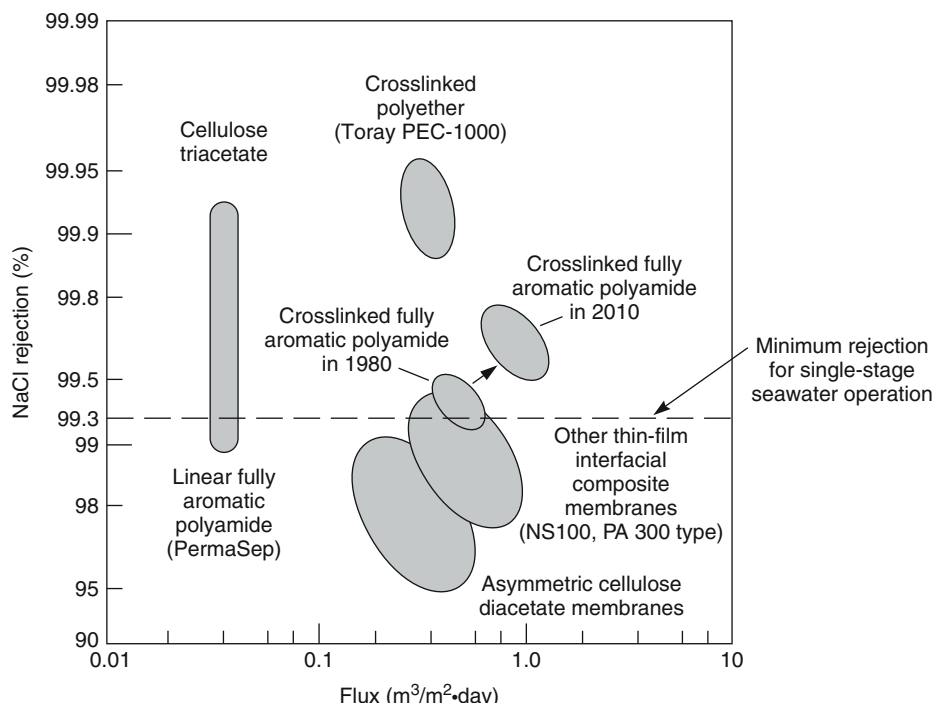


Figure 5.12 Performance characteristics of membranes operating on seawater at 60 bar and 25°C [13, 36]

membranes are low. However, because large-surface-area, hollow fine fiber, reverse osmosis modules can be produced very economically, these membranes remained competitive until 2000, when DuPont finally ceased production. Toyobo still produces cellulose triacetate hollow fibers, particularly for use in the Red Sea/Persian Gulf region where evaporation can increase the salt concentration in seawater to as much as 5%. The high salt rejection of cellulose triacetate membranes allows good water recovery to be achieved even from this high osmotic pressure feed [37]. With this exception, new seawater desalination plants are based on interfacial composite membranes of the fully aromatic type, produced by Dow, Hydranautics (Nitto Denko), and Toray. Figure 5.12 shows the properties of the first generation interfacial composite membrane (the NS100 and PA 300 type) and the first fully aromatic membrane when it first became available in about 1980. The improvement in the performance of this last membrane over the following 30 years is also shown. Membrane rejections have increased to 99.5–99.7% and fluxes have increased to more than $1.0 \text{ m}^3/\text{m}^2\text{ day}$ ($40 \text{ l/m}^2 \text{ h}$). Even the best Loeb–Sourirajan cellulose diacetate membranes are not suitable for one-stage seawater desalination because their maximum salt rejection is less than 99%.

Brackish water generally has a salt concentration in the 2000–10 000 ppm range. Groundwater aquifers with these salt levels must be treated to make the water useful. Similar membranes are used in various industrial processes such as recycling of boiler condensate water. The objective of the desalination plant is to convert 80–90% of the feed water to a desalinated permeate containing 200–500 ppm salt and a concentrated brine that is reinjected into the ground, sent to an evaporation pond, or discharged to the sea. In this application, membranes with 95–98% sodium chloride rejections are often adequate. For this reason some brackish water plants still use cellulose acetate membranes with salt rejections of 96–98%, although interfacial composite membranes are more common. The fluxes and rejections of the composite membranes at the same operating pressures are usually greater than those of cellulose acetate membranes. Therefore, composite membranes are always preferred for large operations such as municipal drinking water plants, which can be built to handle the membrane's chlorine sensitivity. Some small system operators, on the other hand, still prefer cellulose acetate membranes because of their greater stability. The membranes are then often operated at higher pressures to obtain the required flux and salt rejection.

The comparative performance of high-pressure, high-rejection reverse osmosis membranes, medium-pressure brackish water desalting membranes, and low-pressure nanofiltration membranes is shown in Table 5.2. Generally, the performance of a membrane with a particular salt can be estimated reliably once the performance of the membrane with one or two marker salts, such as sodium chloride and magnesium sulfate, is known. The rejection of dissolved neutral organic solutes is less predictable. For example, the PEC-1000 membrane had rejections of greater than 95% for almost all dissolved organics, but the rejections of even the best cellulose acetate membrane are usually no greater than 50–60%.

5.4.2 Nanofiltration Membranes

The goal of most of the early work on reverse osmosis was to produce desalination membranes with sodium chloride rejections greater than 99%. More recently, membranes with lower sodium chloride rejections but much higher water permeabilities have been

Table 5.2 Properties of current good-quality commercial membranes

Parameter	Seawater membrane (SW-30)	Brackish water membrane (CA)	Nanofiltration membrane (NTR-7250)
Pressure (bar)	60	30	10
Solution concentration (%)	1–5	0.2–0.5	0.05
Rejection (%)			
NaCl	99.7	97	60
MgCl ₂	99.9	99	89
MgSO ₄	99.9	99.9	99
Na ₂ SO ₄	99.8	99.1	99
NaNO ₃	90	90	45
Ethylene glycol	70	—	—
Glycerol	96	—	—
Ethanol	—	20	20
Sucrose	100	99.9	99.0

produced. These membranes, which fall into a transition region between pure reverse osmosis membranes and pure ultrafiltration membranes, are called loose reverse osmosis, low-pressure reverse osmosis, or more commonly, nanofiltration membranes. Typically, nanofiltration membranes have sodium chloride rejections between 20 and 80% and molecular weight cutoffs for dissolved organic solutes of 200–1000 Da. These properties are intermediate between reverse osmosis membranes with a salt rejection of more than 90% and molecular weight cutoff of less than 50 and ultrafiltration membranes with a salt rejection of less than 5%.

Although some nanofiltration membranes are based on cellulose acetate, most are based on interfacial composite membranes. The preparation procedure used to form these membranes can result in acid groups attached to the polymeric backbone. Neutral solutes such as lactose, sucrose, and raffinose are not affected by the presence of charged groups and their membrane rejection increases in proportion to solute size. Nanofiltration membranes with molecular weight cut-offs to neutral solutes between 150 and 1500 Da are produced. Typical rejection curves for low molecular weight solutes by two representative membranes are shown in Figure 5.13 [38].

The rejection of salts by nanofiltration membranes is more complicated and depends on both molecular size and Donnan exclusion effects caused by the acid groups attached to the polymer backbone. The phenomenon of Donnan exclusion is described in more detail in Chapter 10. In brief, fixed charged groups on the polymer backbone tend to exclude ions of the same charge, particularly multivalent ions, while being freely permeable to ions of the opposite charge, particularly multivalent ions.

Some results obtained by Peters *et al.* that illustrate the type of results that can be produced are shown in Figure 5.14 [39], in which the permeation properties of neutral, positively charged, and negatively charged membranes are compared.

The neutral nanofiltration membrane rejects the various salts in proportion to molecular size, so the order of rejection is simply



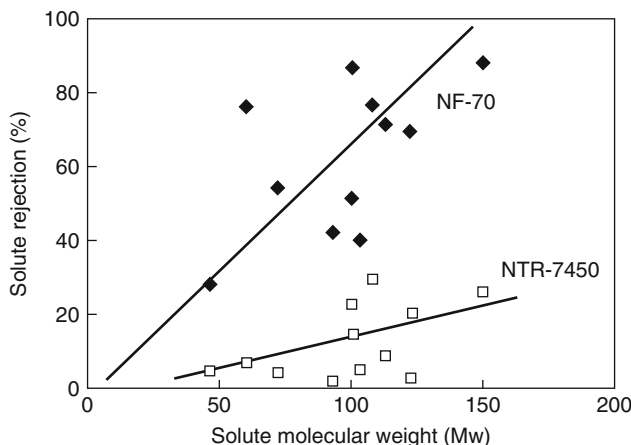


Figure 5.13 Rejection of neutral solutes by two membrane types spanning the range of commonly available nanofiltration membranes [38]

The anionic nanofiltration membrane has positive groups attached to the polymer backbone. These positive charges repel positive cations, particularly divalent cations such as Ca^{2+} , while attracting negative anions, particularly divalent anions such as SO_4^{2-} . The result is an order of salt rejection



The cationic nanofiltration membrane has negative groups attached to the polymer backbone. These negative charges repel negative anions, such as SO_4^{2-} , while attracting positive cations, particularly divalent cations such as Ca^{2+} . The result is an order of salt rejection



Many nanofiltration membranes follow these rules, but often the behavior is more complex. Nanofiltration membranes frequently combine both size and Donnan exclusion effects to minimize the rejection of all salts and solutes. These so-called low-pressure reverse osmosis membranes have very high rejections and high permeances of salt at low salt concentrations, but lose their selectivity at salt concentrations above 1000 or 2000 ppm salt in the feed water. The membranes are therefore used to remove low levels of salt from already relatively clean water. The membranes are usually operated at very low pressures of 3–10 bar.

5.4.3 Hyperfiltration Organic Solvent Separating Membranes

A promising new application of reverse osmosis under development is the processing of nonaqueous (organic solvent) solutions. Directly separating organic solvent mixtures is difficult because of the high osmotic pressures that must be overcome. This issue was discussed in Chapter 2. Osmotic pressures are less of a problem if the retained

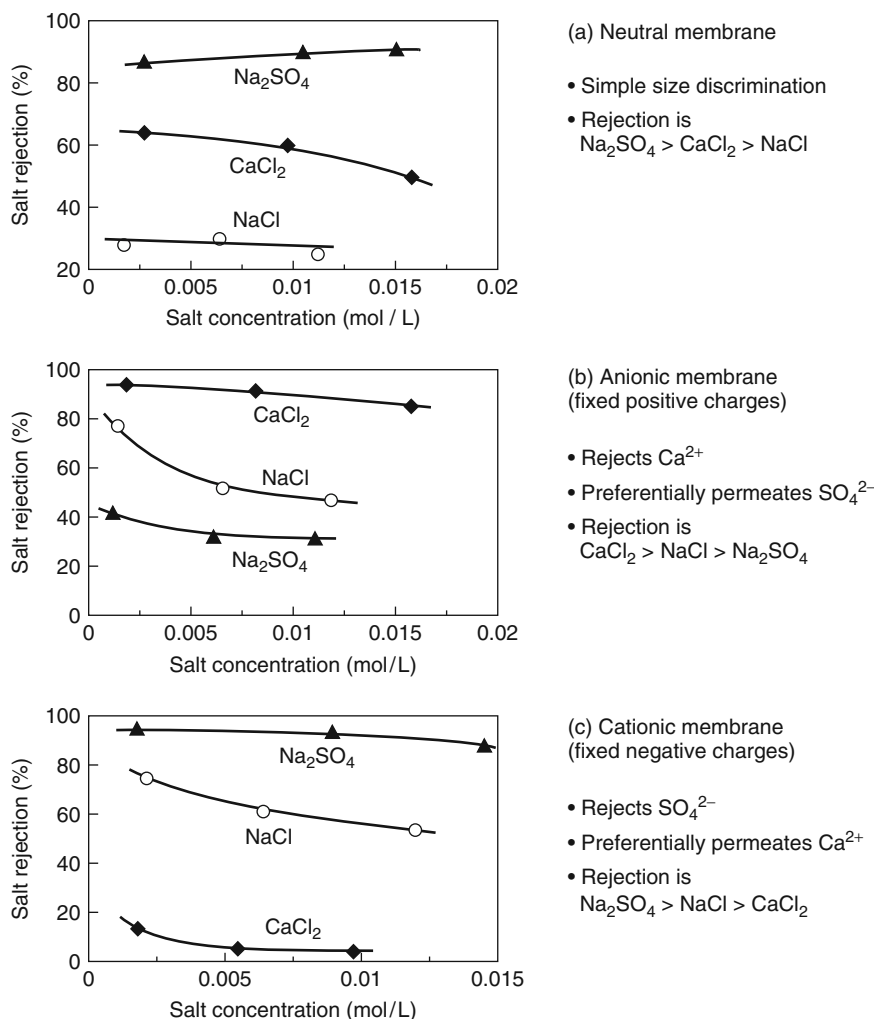


Figure 5.14 Salt rejection with (a) neutral, (b) anionic, and (c) cationic nanofiltration membranes showing the effect of Donnan exclusion and solute size on relative rejections (Data of Peters *et al.* [39].)

component has a high molecular weight and is also the minor component. This is a nanofiltration type of application and the membranes used can be considered to be finely microporous with pores in the 10–20 Å range, capable of retaining compounds with molecular weights of 200–400 Da, while being freely permeable to organic solvents with molecular weights of less than 100 Da.

Two very different types of membranes are being developed for these applications. One approach is to make a composite membrane consisting of a thin, dense, crosslinked rubbery layer (most commonly silicone rubber), supported on an inert microporous support layer. When contacted by a hexane solution, silicone rubber absorbs more than its

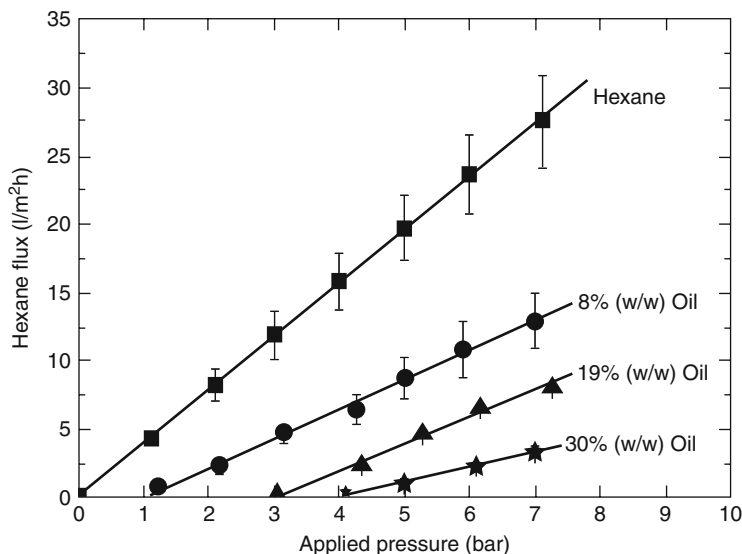


Figure 5.15 Hexane flux as a function of applied pressure for various sunflower oil/hexane feed solutions. The 1–2-µm thick silicone rubber composite membrane used had an oil rejection of 85–90%. Reprinted with permission from [40]. Copyright (2004) Elsevier.

own weight of hexane. The polymer is only prevented from dissolving by interchain crosslinks. In this swollen form, the membrane is quite permeable to hexane in the presence of a hydrostatic pressure of a few bar. However, the microvolumes between the silicone chains are small enough to almost completely reject larger solutes, such as vegetable oil ($MW = 900$) [40, 41]. Some results obtained with this type of membrane are shown in Figure 5.15. At low applied pressures, the hexane flux produced is very small, but once the osmotic pressure of the rejected sunflower oil component is exceeded, the flux increases linearly with pressure. This sort of result is similar to what would be expected with a conventional nanofiltration membrane used with aqueous solutions.

The permeance and rejection of this type of membrane changes substantially depending on the solvent used. Solvents that swell the membrane the most have the highest fluxes and lowest selectivities. Some results that illustrate this effect are shown in Figure 5.16. The rejected solute is a large polynuclear aromatic ($MW = 330$). The rejection at 8 bar varies from 20 to 50%, depending on the solvent in which the solute is dissolved [42]. This type of silicone rubber-based membrane has found a limited application in removing asphaltenes and other color bodies from various refinery naphtha streams.

The second category of nanofiltration membrane being developed uses rigid solvent-resistant materials to form finely porous membranes. In the 1980s, Nitto Denko developed polyimide-based ultrafiltration membranes that found a small use in separating polymers and pigments from toluene, ethyl acetate, hexane, and other solvents in waste paint and polymer solutions [43]. More recently, ceramic membranes have been developed for the same type of separation. The current most commonly used membranes have been

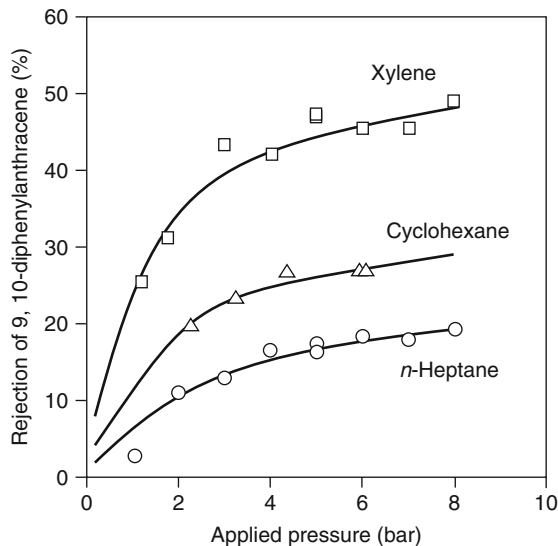


Figure 5.16 Rejection of 9,10-diphenylanthracene dissolved in different hydrocarbon solvents by a silicone rubber composite membrane. The solvent that swells the membrane the most (*n*-heptane) has the lowest rejection. Reprinted with permission from [42]. Copyright (2005) Elsevier.

developed by W.R. Grace and produced under the trade name Starmem® [44, 45]. These membranes are made by a modified Loeb–Sourirajan process from Matrimide®-type polyimides. The Matrimide polyimide structure is extremely rigid, with a T_g of 305°C; the polymer remains glassy and relatively unswollen even in aggressive solvents. This type of membrane typically has a molecular weight cutoff of 300–400. Like the silicone rubber membranes, the flux and rejection of these membranes change, depending on the solvent used [45, 46].

5.5 Membrane Selectivity

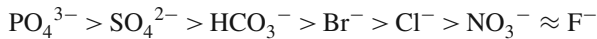
Rautenbach and Albrecht [47] have proposed some general guidelines for reverse osmosis membrane selectivity in aqueous solutions that can be summarized as follows:

1. Multivalent ions are retained better than monovalent ions. Although the absolute values of the salt rejection vary over a wide range, the ranking for the different salts is the same for all membranes. In general, the order of rejection of ions by reverse osmosis membranes is as shown below.

For cations:



For anions:



2. Dissolved gases such as ammonia, carbon dioxide, sulfur dioxide, oxygen, chlorine, and hydrogen sulfide always permeate well.
3. Rejection of weak acids and bases is highly pH dependent. When the acid or base is in the ionized form, the rejection will be high, but in the nonionized form, rejection will be low [48, 49]. Data for a few weak acids are shown in Figure 5.17. At pH values above the acid pK_a , the solute rejection rises significantly, but at pH values below the pK_a , when the acid is in the neutral form, the rejection falls.
4. Rejection of neutral organic solutes generally increases with the molecular weight (or diameter) of the solute. Components with molecular weights above 100 are well rejected by all reverse osmosis membranes. Although differences between the rejection of organic solutes by different membranes are substantial, as the data in Figure 5.18 show, the rank order is generally consistent between membranes. Caprolactam, for example, has a higher rejection than ethanol in all reverse osmosis membranes. The dependence of solute rejection on molecular weight is shown for three different membranes in Figure 5.19.
5. Negative rejection coefficients, that is, a higher concentration of solute in the permeate than in the feed, are occasionally observed, for example, for phenol and benzene with cellulose acetate membranes [50].

5.6 Membrane Modules

Currently, spiral-wound modules 8 in. in diameter, 40 in. in length and containing about 40 m^2 of membrane are the type most commonly used for reverse osmosis, but the industry has recently adopted a new 16-in. diameter, 40-in. long standard module containing about 150 m^2 of membrane. These larger modules achieve economies of scale and are

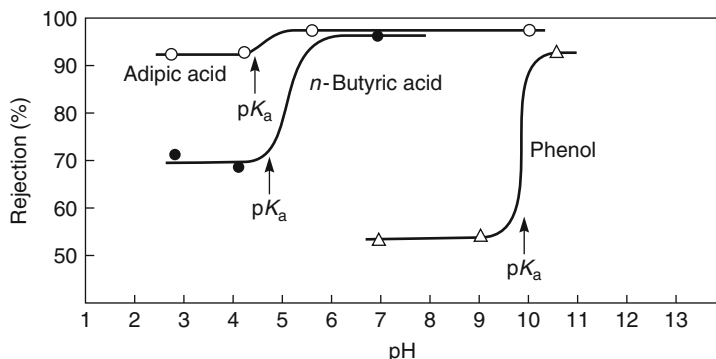


Figure 5.17 Effect of pH on rejection of organic acids. Solute rejection increases at the pK_a as the acid converts to the ionized form (Data from T. Matsuura and Sourirajan [48, 49].)

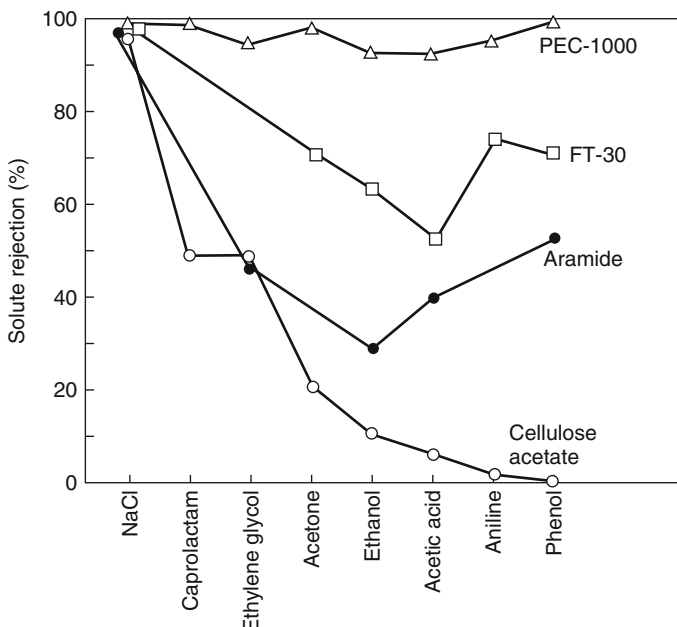
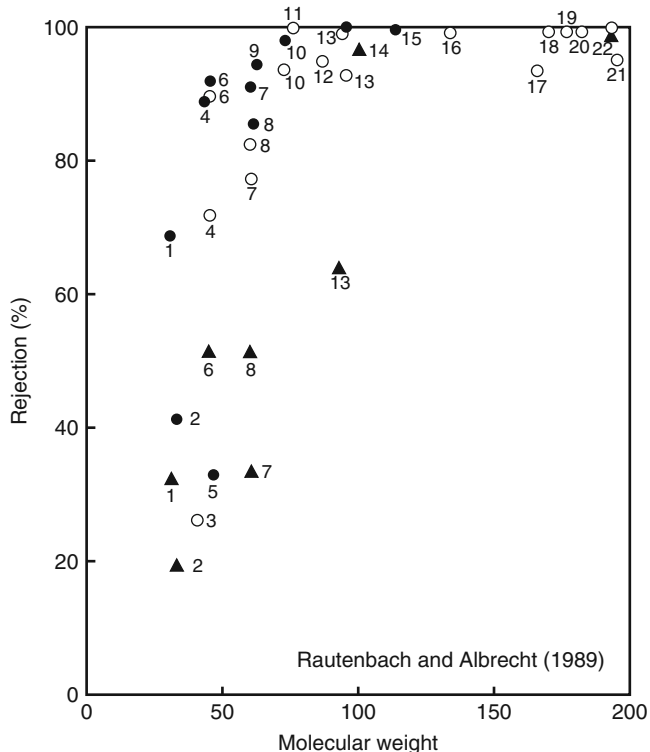


Figure 5.18 Organic rejection data for the PEC-1000 membrane compared to FT-30, anisotropic aramide, and anisotropic cellulose membranes [28]

likely to be widely used in the future. The production process used by the major manufacturers of spiral-wound modules is completely automated and so production costs are low. Costs in 2010 were estimated at $\sim \$400/40\text{ m}^2$ -8-in.-diameter module, or approximately $\$10/\text{m}^2$ of membrane. Five to seven modules are housed inside a filament-wound, fiber-glass-reinforced plastic tube. Longer modules, up to 60 in. in length, are produced by some manufacturers but have not been widely adopted. The module elements can be removed from the pressure vessels and exchanged as needed. A photograph of a typical skid-mounted system is shown in Figure 5.20. A typical spiral-wound 8-in.-diameter membrane module will produce 8000–10 000 gal/day of permeate, so the 75-module industrial water plant shown in Figure 5.20 has a capacity of about 700 000 gal/day ($2700\text{ m}^3/\text{day}$).

Hollow fine fiber modules made from cellulose triacetate or aromatic polyamides were produced in the past for seawater desalination. These modules incorporated the membrane around a central tube, and feed solution flowed outward to the shell. Because the fibers were extremely tightly packed inside the pressure vessel, flow of the feed solution was quite slow. As much as 40–50% of the feed could be removed as permeate in a single pass through the module. However, the low flow and many constrictions meant that extremely good pretreatment of the feed solution was required to prevent membrane fouling from scale or particulates. A schematic illustration of such a hollow fiber module was shown in Figure 3.61.



Rautenbach and Albrecht (1989)

Number	Name	Number	Name
1	Formaldehyde	12	Ethyl acetate
2	Methanol	13	Phenol
3	Acetonitrile	14	<i>n</i> -Methyl-2-pyrrolidone
4	Acetaldehyde	15	Caprolactam
5	Formic acid	16	D,L-aspartic acid
6	Ethanol	17	Tetrachloroethylene
7	Acetic acid	18	<i>o</i> -Phenyl phenol
8	Urea	19	Butyl benzoate
9	Ethylene glycol	20	Trichlorobenzene
10	Methyl ethyl ketone	21	Dimethyl phthalate
11	Glycine	22	Citric acid

Figure 5.19 Organic solute rejection as a function of solute molecular weight for three representative reverse osmosis membranes: the interfacial composite membranes, (○) PA300 (UOP) and (▲) NTR 7197 (Nitto); and the crosslinked furfuryl alcohol membrane (●) PEC 1000 (Toray). Reprinted with permission from [47]. Copyright (1989) John Wiley & Sons, Inc.

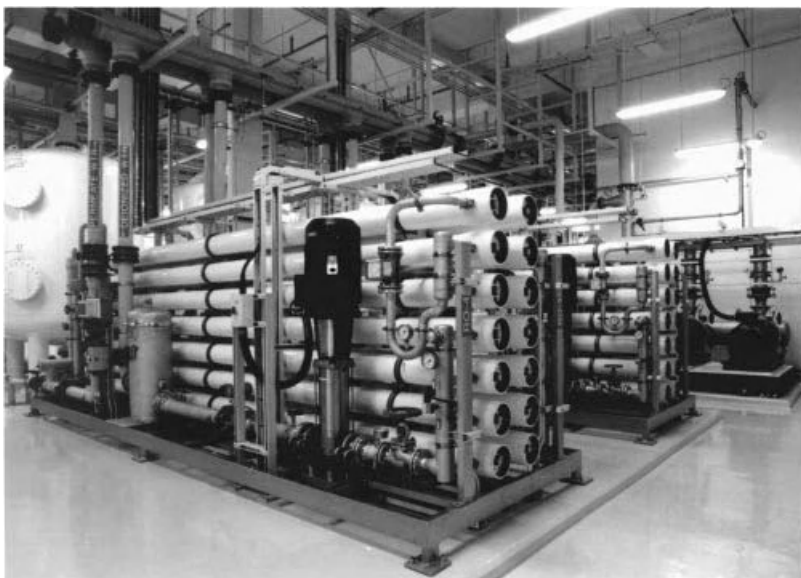


Figure 5.20 Skid-mounted reverse osmosis plant able to produce 700 000 gal/day of desalted water. Reprinted with permission from Christ Water Technology Group, now part of the Ovivo group of companies

5.7 Membrane Fouling Control

Membrane fouling is the main cause of permeant flux decline and loss of product quality in reverse osmosis systems, so fouling control dominates reverse osmosis system design and operation. The cause and prevention of fouling depend greatly on the feed water being treated, and appropriate control procedures must be devised for each plant. In general, sources of fouling can be divided into four principal categories: scale, silt, bacteria, and organic. More than one category may occur in the same plant.

Fouling control involves pretreatment of the feed water to minimize fouling as well as regular cleaning to handle any fouling that still occurs. Fouling by particulates (silt), bacteria, and organics such as oil is generally controlled by a suitable pretreatment procedure; this type of fouling affects the first modules in the plant the most. Fouling by scaling is worse with more concentrated feed solutions; therefore, the last modules in the plant are most affected because they are exposed to the most concentrated feed water.

5.7.1 Scale

Scale is caused by precipitation of dissolved metal salts in the feed water on the membrane surface. As salt-free water is removed in the permeate, the concentration of ions in the feed increases until at some point the solubility limit of some components is exceeded. Salt then precipitates on the membrane surface as scale. The proclivity of a particular type of feed water to produce scale can be determined by performing an analysis of the feed water and calculating the expected concentration factor in the brine.

The ratio of the product water flow rate to feed water flow rate is called the recovery rate, which is equivalent to the term stage-cut used in gas separation.

$$\text{recovery rate} = \frac{\text{product flow rate}}{\text{feed flow rate}} \quad (5.7)$$

Assuming all the ions remain in the brine solution, the concentration factor is given by

$$\text{concentration factor} = \frac{1}{1 - \text{recovery rate}} \quad (5.8)$$

The relationship between brine solution concentration factor and water recovery rate is shown in Figure 5.21. With plants that operate below a concentration factor of 2, that is, 50% recovery rate, scaling is not normally a problem. However, many brackish water reverse osmosis plants operate at recovery rates of 80 or 90%. This implies salt concentration factors of 5–10. Salt concentrations on the brine side of the membrane may then be above the solubility limit. In order of importance, the salts that most commonly form scale are

- calcium carbonate;
- calcium sulfate;
- silica complexes;
- barium sulfate;
- strontium sulfate;
- calcium fluoride.

Scale control is complex; the particular procedure depends on the composition of the feed water. Fortunately, calcium carbonate scale, by far the most common problem, is easily controlled by acidifying the feed or by using an ion exchange water softener to exchange calcium for sodium. Alternatively, an antiscalant chemical such as a polycarboxylate, polyacrylate, polyphosphonate, or polyphosphate can be added. Antiscalants

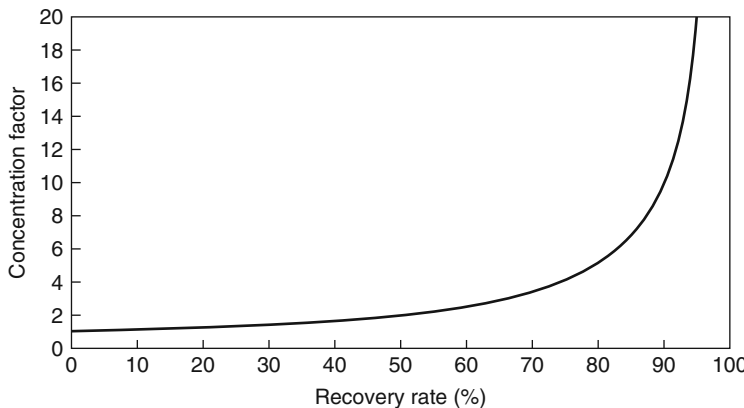


Figure 5.21 The effect of water recovery rate on the brine solution concentration factor

interfere with the precipitation of the insoluble salt and maintain the salt in solution even when the solubility limit is exceeded [51]. Polymeric antiscalants may also be used, sometimes in combination with a dispersant to break up any flocs that occur.

Silica can be a particularly troublesome scalant because no effective antiscalant or dispersant is available. The solubility of silica is a strong function of pH and temperature, but in general the brine should not exceed 120 ppm silica. Once formed, silica scale is difficult to remove.

5.7.2 Silt

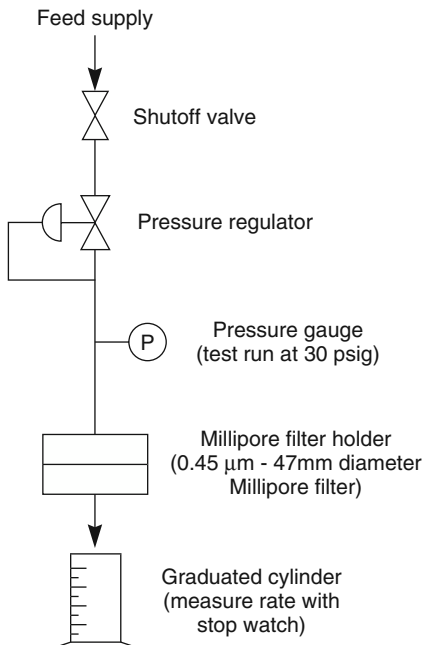
Silt is formed by suspended particulates of all types that accumulate on the membrane surface. Typical sources of silt are organic colloids, iron corrosion products, precipitated iron hydroxide, algae, and fine particulate matter. A good predictor of the likelihood of a particular feed water to produce fouling by silt is the silt density index (SDI) of the feed water. The SDI, an empirical measurement (ASTM Standard D-4189-82, 1987), is the time required to filter a fixed volume of water through a standard 0.45- μm pore size microfiltration membrane. Suspended material in the feed water that plugs the microfilter increases the sample filtration time, giving a higher SDI. The test procedure is illustrated in Figure 5.22 [52].

An SDI of less than 1 means the reverse osmosis system can run for several years without colloidal fouling. An SDI of less than 3 means the system can run several months between cleanings. An SDI of 3–5 means particulate fouling is likely to be a problem and frequent, regular cleaning will be needed. An SDI of more than 5 is unacceptable and indicates that additional pretreatment is required to bring the feed water into an acceptable range. The maximum tolerable SDI also varies with membrane module design. Spiral-wound modules generally require an SDI of less than 5, whereas hollow fine fiber modules are more susceptible to fouling and require an SDI of less than 3.

To avoid fouling by suspended solids, some form of feed water filtration is required. All reverse osmosis units are fitted with a 0.45- μm cartridge filter in front of the high-pressure pump, but a sand filter, sometimes supplemented by addition of a flocculating chemical such as alum or a cationic polymer, may be required. The target SDI after filtration is normally less than 3–5. Ground waters usually have very low SDI values, and cartridge filtration is often sufficient. However, surface or seawater may have an SDI of up to 200, requiring flocculation, coagulation, and deep-bed multimedia filtration before reverse osmosis treatment.

5.7.3 Biofouling

Biological fouling is the growth of bacteria on the membrane surface. The susceptibility of membranes to biological fouling is a strong function of the membrane composition. Cellulose acetate membranes are an ideal nutrient for bacteria and can be completely destroyed by a few weeks of uncontrolled bacterial attack. Therefore, feed water to cellulose acetate membranes must always be sterilized. Polyamide hollow fibers are also somewhat susceptible to bacterial attack, but thin-film composite membranes are generally quite resistant. Periodic treatment of such membranes with a bactericide usually controls biological fouling. Thus, control of bacteria is essential for cellulose acetate membranes.



- (1) Measure the amount of time required for 500 ml of feed water to flow through a 0.45 micrometer Millipore filter (47 mm in diameter) at a pressure of 30 psig.
- (2) Allow the feed water to continue flowing at 30 psig applied pressure and measure the time required for 500 ml to flow through the filter after 5, 10 and 15 minutes.
- (3) After completion of the test, calculate the SDI by using the equation below.

$$SDI = \frac{100 (1 - T_i / T_f)}{T_t}$$

where SDI = Silt Density Index
 T_t = Total elapsed test time (either 5, 10 or 15 minutes)
 T_i = Initial time in seconds required to collect the 500 ml sample
 T_f = Time in seconds required to collect the second 500 ml sample after test time T_t (normally after 15 minutes).

Figure 5.22 The silt density index (SDI) test. Reprinted from [52]. Copyright (1990) Noyes Publications.

and desirable for polyamides and composite membranes. Because cellulose acetate can tolerate up to 1 ppm chlorine, sufficient chlorination is used to maintain 0.2 ppm free chlorine. Chlorination can also be used to sterilize the feed water to polyamide and interfacial composite membranes, but residual chlorine must then be removed because the membranes are chlorine sensitive. Dechlorination is generally achieved by adding sodium metabisulfite. In ultrapure water systems, water sterility is often maintained by UV sterilizers. The development of low-cost ultrafiltration/microfiltration membrane processes that remove particulates and all bacteria has encouraged the use of these membranes as a pretreatment step for new reverse osmosis plants.

5.7.4 Organic Fouling

Organic fouling is the attachment of materials such as oil or grease onto the membrane surface. Such fouling may occur accidentally in municipal drinking water systems, but is more common in industrial applications in which reverse osmosis is used to treat a process or effluent stream. Removal of the organic material from the feed water by filtration or carbon adsorption is required.

An example of a complete pretreatment flow scheme for a seawater reverse osmosis plant is shown in Figure 5.23 [53]. The water is controlled for pH, scale, particulates, and biological fouling. The feed water is first treated with chlorine to sterilize the water and to bring it to a pH of 5–6. A polyelectrolyte is added to flocculate suspended matter, and two multilayer depth filters then remove suspended materials. The water is dechlorinated by dosing with sodium bisulfite followed by passage through an activated carbon bed. As a final check the pH is adjusted a second time, and the water is filtered through a 1–5- μm cartridge filter before being fed to the reverse osmosis modules. Obviously, such pretreatment is expensive and may represent as much as one-third of the operating and capital cost of the plant. Nonetheless, this type of pretreatment was used by seawater desalination plants up to 2000–2005. In recent years, the development of lower cost and

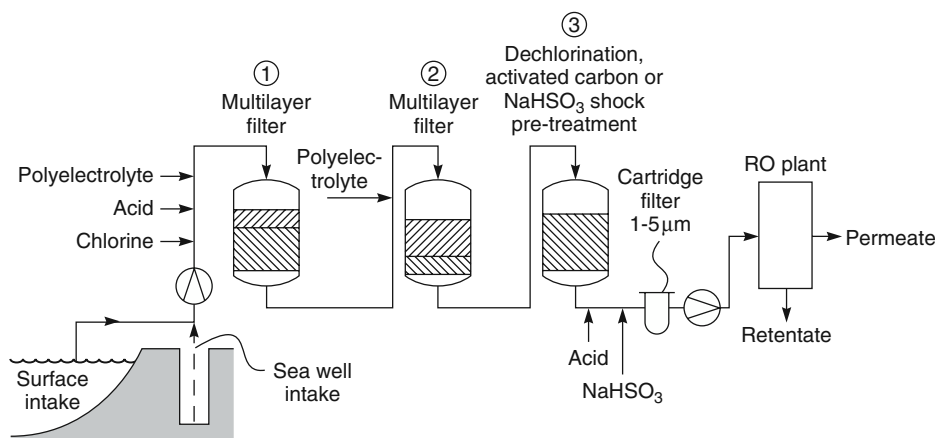


Figure 5.23 Flow scheme showing the pretreatment steps in a typical seawater reverse osmosis system [53]

more reliable ultrafiltration systems has resulted in new plants replacing much of the treatment train shown with a single ultrafiltration unit. This unit removes all suspended solids and bacteria, so chlorination of the feed water is not needed.

5.7.5 Membrane Cleaning

A good pretreatment system is essential to achieve a long reverse osmosis membrane life, but pretreatment must be backed up by an appropriate cleaning schedule. Generally this is done once or twice a year, but more often if the feed is a problem water. As with pretreatment, the specific cleaning procedure is a function of the feed water chemistry, the type of membrane, and the type of fouling. A typical cleaning regimen consists of flushing the membrane modules by recirculating the cleaning solution at high speed through the module, followed by a soaking period, followed by a second flush, and so on. The chemical cleaning agents commonly used are acids, alkalis, chelating agents, detergents, formulated products, and sterilizers.

Acid cleaning agents such as hydrochloric, phosphoric, or citric acids effectively remove common scaling compounds. With cellulose acetate membranes, the pH of the cleaning solution should not go below 2.0 or else hydrolysis of the membrane will occur. Oxalic acid is particularly effective for removing iron deposits. Acids such as citric acid are not very effective with calcium, magnesium, or barium sulfate scale; in this case a chelating agent such as ethylenediaminetetraacetic acid (EDTA) may be used.

To remove bacteria, silt, or precipitates from the membrane, alkalis combined with surfactant cleaners are often used. Biz® and other laundry detergents containing enzyme additives are useful for removing biofoulants and some organic foulants. Most large membrane module producers now distribute formulated products, which are mixtures of cleaning compounds. These products are designed for various common feed waters and often provide a better solution to membrane cleaning than devising a cleaning solution for a specific feed.

Sterilization of a membrane system is also required to control bacterial growth. For cellulose acetate membranes, chlorination of the feed water is sufficient to control bacteria. Feed water to polyamide or interfacial composite membranes need not be sterile, because these membranes are usually fairly resistant to biological attack. Periodic shock disinfection using formaldehyde, peroxide, or peracetic acid solutions as part of a regular cleaning schedule is often enough to prevent biofouling.

Repeated cleaning gradually degrades reverse osmosis membranes. Most manufacturers now supply membrane modules with a one- to two-year limited warranty depending on the application. Well-designed and maintained plants with good feed water pretreatment can usually expect membrane lifetimes of five years, and lifetimes of seven years or more are not unusual. As membranes approach the end of their useful life, the water flux will normally have dropped by at least 20%, and the salt rejection will have begun to fall. At this point, operators may try to “rejuvenate” the membrane by treatment with a dilute polymer solution. This surface treatment plugs microdefects and restores salt rejection [54]. Typical treatment polymers are poly(vinyl alcohol)/vinyl acetate copolymers or poly(vinyl methyl ether). In this procedure, the membrane modules are carefully cleaned and then flushed with dilute solutions of the rejuvenation polymer. The exact mechanism of rejuvenation is unclear.

5.8 Applications

Approximately half of the reverse osmosis systems currently installed are used for desalinating brackish water or seawater. Another 40% are producing ultrapure water for the electronics, pharmaceutical, and power generation industries. The remainder is used in small niche applications such as pollution control and food processing. A number of good reviews of reverse osmosis applications are available [36, 37, 55–57].

The relative cost of reverse osmosis compared with other desalting technologies (ion exchange, electrodialysis, and multi-effect evaporation) is shown in Figure 5.24. The operating costs of electrodialysis and ion exchange scale almost linearly in proportion to the salt concentration of the feed. Therefore, these technologies are best suited to low-salt-concentration feed streams. On the other hand, the cost of multi-effect evaporation is relatively independent of the salt concentration and is mainly proportional to the mass of water to be evaporated. Thus, desalination by evaporation is best performed with concentrated salt solution feeds. Reverse osmosis costs increase significantly with salt concentration but at a lower rate than electrodialysis costs. The result is that reverse osmosis is the lowest-cost process for streams containing between 0.2 and 5.0% salt. However, site-specific factors or plant size often make the technology the best approach for more dilute feed water streams.

The approximate operating costs for a seawater reverse osmosis plant are given in Table 5.3. Improvements in membrane technology have more than kept pace with

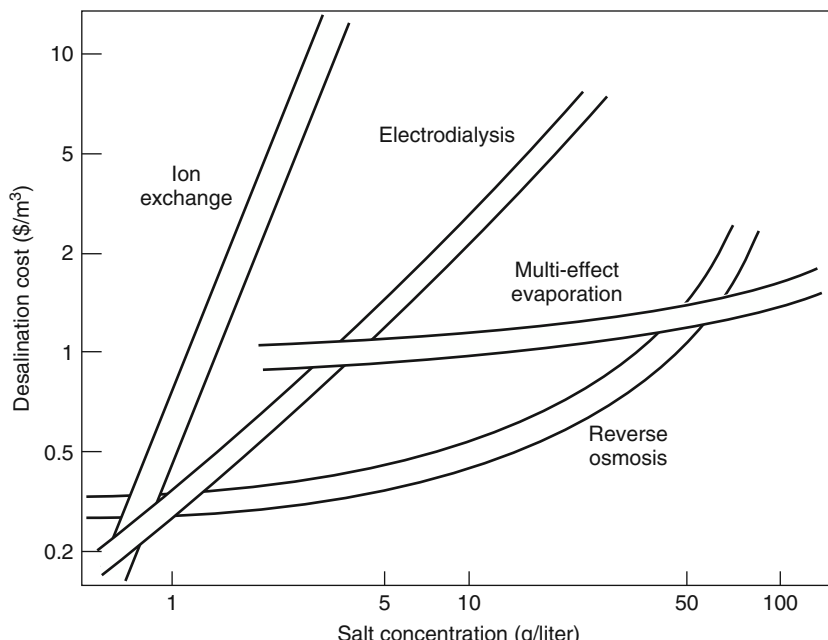


Figure 5.24 Comparative costs of the major desalination technologies as a function of salt concentration. These costs should be taken as a guide only; site-specific factors can affect costs significantly (Figure based on [58]; updated for this third edition.)

Table 5.3 Operating costs for large seawater reverse osmosis plants in 2008 [56]

Product water cost component	(US\$/m ³)
Capital cost, including land (25 years at 6.0% interest)	0.20–0.34
Electric power (0.60/kWh)	0.18–0.24
RO membrane replacement (5 years membrane life)	0.03–0.04
RO membrane replacement (7 years membrane life)	0.02–0.03
Chemicals	0.02–0.03
Maintenance and spare parts	0.02–0.04
Labor	0.02–0.04
Total product water cost	0.49–0.76

Capital costs are approximately US\$500/m³ day capacity.

inflation, so the reverse osmosis water production costs have actually fallen in the last decade. New world-scale seawater plants can now produce water at a cost of ~\$0.50/m³. Water from brackish water plants costs even less, in the region of \$0.20/m³. The initial capital cost of a seawater plant is now about \$500/m³ day (\$2/gal-day) of capacity.

5.8.1 Brackish Water Desalination

The salinity of brackish water is usually between 2000 and 10 000 mg/l. The World Health Organization (WHO) recommendation for potable water is 500 mg/l, so only 90% of the salt must be removed from these feeds in many cases. Early cellulose acetate membranes could achieve this removal easily, so treatment of brackish water was one of the first successful applications of reverse osmosis. Plants were installed as early as the 1960s.

The osmotic pressure of brackish water is approximately 0.8 bar per 1000 ppm salt, so osmotic pressure effects do not generally limit water recovery significantly. Limitations are generally due to scaling. Typical water recoveries are in the 85–90% range, which means calcium, sulfate, and silica ions present in the feed are concentrated up to 10-fold in the brine stream leaving the system. If scaling occurs, the last modules in the system are affected most and must be replaced first.

Disposal of the 10–15% of the brackish water that remains as a concentrated brine represents a significant problem. This has motivated a good deal of research into increasing the water recovery of brackish water plants to 95–98%. Cohen and coworkers [59], for example, have proposed a two-stage membrane process. In the first stage, 85–90% of the water would be permeated in the normal way. Calcium, silica, and other potential scalants in the brine would then be precipitated by addition of sodium hydroxide. The treated brine would then be reacidified, antiscalants added, and a further fraction of the water removed, thus achieving an overall water recovery of up to 98%. The final small concentrate stream can then be sent to an evaporation pond.

A simplified flow scheme for a brackish water reverse osmosis plant is shown in Figure 5.25. In this example, it is assumed that the brackish water is contaminated with suspended solids, so flocculation followed by a sand filter and a cartridge filter are used

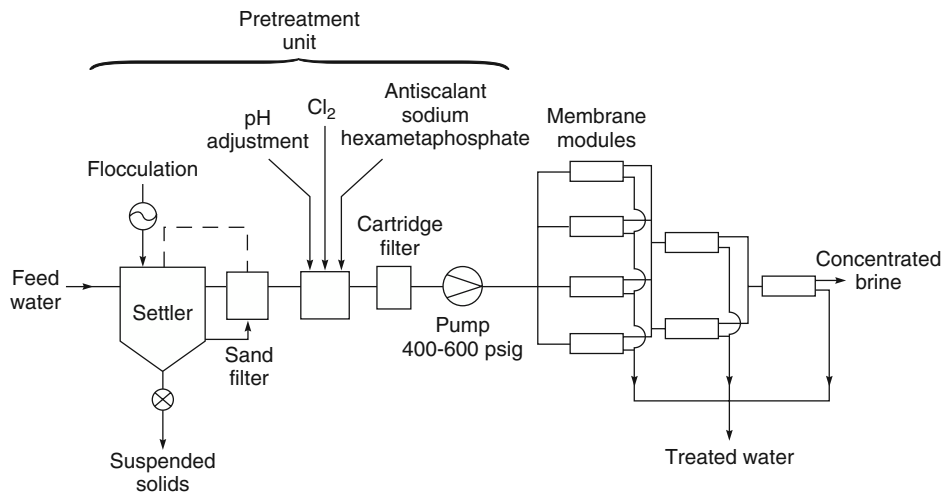


Figure 5.25 Flow schematic of a typical brackish water reverse osmosis plant. The plant contains seven pressure vessels, each containing six membrane modules. The pressure vessels are in a "Christmas tree" array to maintain a high feed velocity through the modules

to remove particulates. The pH of the feed solution might be adjusted, followed by chlorination to sterilize the water to prevent bacterial growth on the membranes and addition of an antiscalant to inhibit precipitation of multivalent salts on the membrane. Finally, if chlorine-sensitive interfacial composite membranes are used, sodium sulfite is added to remove excess chlorine before the water contacts the membrane. Generally, more pretreatment is required in plants using hollow fiber modules than in plants using spiral-wound modules. This is one reason why hollow fiber modules have been displaced by spiral-wound systems in brackish water installations.

A feature of the system design shown in Figure 5.25 is the staggered arrangement of the module pressure vessels. The volume of the feed water is reduced as water is removed in the permeate, and the number of modules arranged in parallel is reduced accordingly. In the example shown, the feed water passes initially through four modules in parallel, then through two, and finally through a single module in series. This is called a "Christmas tree" or "tapered module" design and provides a high average feed solution velocity through the modules.

The operating pressure of brackish water reverse osmosis systems has gradually fallen over the past 20 years as the permeability and rejection rates of membranes have steadily improved. The first plants operated at pressures of 50 bar, but typical brackish water plants now operate at pressures in the 10–20-bar range. Capital costs of brackish water plants have stayed remarkably constant for almost 20 years; the rule of thumb of US\$250–500/m³ day (US\$1–2/gal day) capacity is still true. Accounting for inflation, this reflects a very large reduction in real costs resulting from the better performance of today's membranes.

5.8.2 Seawater Desalination

Seawater has a salt concentration of 3.2–4.2%, depending on the region of the world. Because of this high salinity, only membranes with salt rejections of 99.3% or more can produce potable water containing less than 500 ppm dissolved salt in a single pass. Application of the first-generation cellulose acetate membranes to seawater desalination, with rejections of 97–99%, was limited. With the development of the polyamide hollow fine fibers and interfacial composites, suitable seawater membranes became available, and many plants have been installed. These membranes can produce permeate water that meets the WHO standard of <500 ppm salt in a single pass, although most municipalities require drinking water containing less than 100–200 ppm salt. This quality of water usually requires a two-pass system, typically a single stage seawater system and a single stage brackish water system connected in series. The high-pressure seawater system removes almost all of the salt. The low-pressure brackish water then removes enough residual salt to achieve the 100–200 ppm salt target. The concentrate from the brackish water system is recycled to the feed of the seawater system.

In the 1990s, membranes were not competitive for very large seawater desalination plants and multistage flash evaporation was usually used for plants larger than 100 000 m³/day capacity. These plants were often powered by waste steam from an adjacent electric power generation unit. Reductions in the cost of membrane systems and improvements in process design have significantly improved the competitive position of reverse osmosis technology. Currently, 5–10 new large seawater reverse osmosis plants are built each year. The energy consumption of these plants is now in the range of 1.5–2.0 kWh/m³ of water, far below the energy required for evaporation technology. The flexibility of membrane systems as well as their easy startup/shutdown and turndown capability are additional advantages.

Early seawater reverse osmosis plants operated at very high pressures, up to 100 bar, but as membranes improved, operating pressures dropped to 50–60 bar. The osmotic pressure of seawater is about 23 bar, and the osmotic pressure of the rejected brine can be as much as 40 bar, so osmotic pressure markedly affects the net operating pressure in a plant. This effect is illustrated in Figure 5.26. Typical seawater plants do not

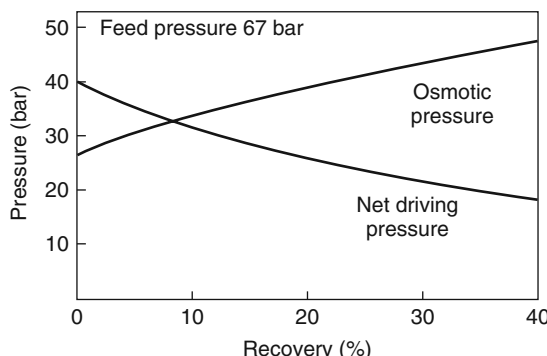


Figure 5.26 Effect of water recovery on the seawater feed osmotic pressure and net driving pressure of a plant operating at 67 bar

operate at a recovery rate of more than 35–50% because of the high brine osmotic pressure; at this modest recovery rate, more than half of the feed water leaves the plant as pressurized brine. Because of the high pressures involved in seawater desalination, recovery of compression energy from the high-pressure brine stream is almost always worthwhile. In older plants, Pelton wheel units were used that recovered 60–85% of the brine energy. More recently, more efficient turbines or isobaric energy recovery systems have been used. These systems can recover 80–95% of the energy contained in the high pressure brine.

In the last 10–15 years, the boron concentration of the water produced by reverse osmosis seawater desalination has become a concern. Typical river water has a very low boron concentration of 0.05–0.2 ppm, but seawater usually contains 4–6 ppm boron. Until 2000, reverse osmosis membrane had boron rejections of about 70–80%, so water produced from seawater could contain 1–2 ppm boron. Typical drinking water standards for boron are now 0.5–1.0 ppm, so improved treatment to reduce the boron concentration was required. All of the major membrane manufacturers have improved the boron rejection of their membranes and boron rejections of 90–93% can now be achieved. Nonetheless, some feeds may still require further treatment. The common solution is to use a nanofiltration system to filter boron from a portion of the desalinated water product.

Raw seawater requires considerable pretreatment before it can be desalinated (see Figure 5.23). For small plants, these pretreatment costs can be reduced by using shallow sea-front wells as the water source. The SDI of this water is usually quite low, and little more than a sand filter may be required for additional particulate control. However, sterilization of the water and addition of antiscalants will still be necessary. Low-pressure microfiltration/ultrafiltration units are also increasingly used as feed water pretreatment to produce clean, almost sterile, water for the desalination plant [60].

5.8.3 Ultrapure Water

Production of ultrapure water for the electronics industry is an established and growing application of reverse osmosis [61, 62]. The usual feed is municipal drinking water, which usually contains less than 200 ppm dissolved solids. However, the electronics industry requires water of extraordinarily high purity for wafer production, so extensive treatment of municipal water is required. Table 5.4 shows the target water quality required by a modern electronics plant compared to that of typical municipal drinking water.

The first ultrapure water reverse osmosis system was installed at a Texas Instruments plant in 1970 as a pretreatment unit to an ion exchange process. These systems have increased in complexity as the needs of the industry for ever better quality water have increased. The flow scheme for a typical modern ultrapure water treatment system is shown in Figure 5.27. The plant comprises a complex array of operations, each requiring careful maintenance to achieve the necessary water quality. As the key part of the process, the reverse osmosis plant typically removes more than 98% of all the salts and dissolved particulates in the feed water. Because the feed water is dilute, these systems often operate at very high recovery rates – 90% or more. Carbon adsorption then removes dissolved organics, followed by ion exchange to remove final trace amounts of ionic impurities. Bacterial growth is a major problem in ultrapure water systems; sterility is maintained by continuously recirculating the water through UV sterilizers and cartridge microfilters.

Table 5.4 Ultrapure water specifications for typical wafer manufacturing process and levels normally found in drinking water (ASTM D-5127-99)

	Ultrapure water ($\varepsilon=1.1$ type)	Typical drinking water
Resistivity at 25°C	18.2	–
TOC (ppb)	<5	5 000
Particles/liter by laser > 0.1 µm	<100	–
Bacteria/100 ml by culture	<0.1	<30
Silica, dissolved (ppb)	<0.1	3 000
Boron (ppb)	<0.02	40
Ions (ppb)		
Na ⁺	<0.02	3 000
K ⁺	<0.02	2 000
Cl ⁻	<0.05	10 000
F ⁻	<0.05	–
NO ₃ ⁻	<0.05	–
SO ₄ ²⁻	<0.02	15 000
Total ions	<0.1	<100 000

5.8.4 Wastewater Treatment

In principle, industrial wastewater pollution control should be a major application for reverse osmosis. In practice, membrane fouling, causing low plant reliability, has inhibited its widespread use in this area. The most common applications are special situations in which the chemicals separated from the water are valuable. An example is the recovery of nickel from nickel-plating rinse tanks, shown schematically in Figure 5.28. Watts nickel-plating baths contain high concentrations of nickel and other plating chemicals. After plating, a conveyor belt moves the parts through a series of connected rinse tanks. Water circulates through these tanks to rinse the parts free of nickel for the next plating operation. A typical countercurrent rinse tank produces a waste stream containing 2000–3000 ppm nickel; the water is a pollution problem and valuable material is lost. This is an ideal application for reverse osmosis because the rinse water is at nearly neutral pH, in contrast to many plating rinse waters which are very acidic [63, 64]. The reverse osmosis unit produces permeate water containing only 20–50 ppm nickel that can be reused and a small nickel concentrate stream that can be sent to the plating tank. Although the concentrate is more dilute than the plating tank drag-out, evaporation from the hot plating bath tank compensates for the extra water.

In the early days of membrane development, membranes were expected to be widely used in the tertiary treatment of water to produce drinking water from sewage. At that time, the high cost of early membrane technology kept this application from developing. At today's production cost of \$US 0.30–0.50 per m³ of water, this idea now makes much better economic sense in many water-limited regions of the world. However,

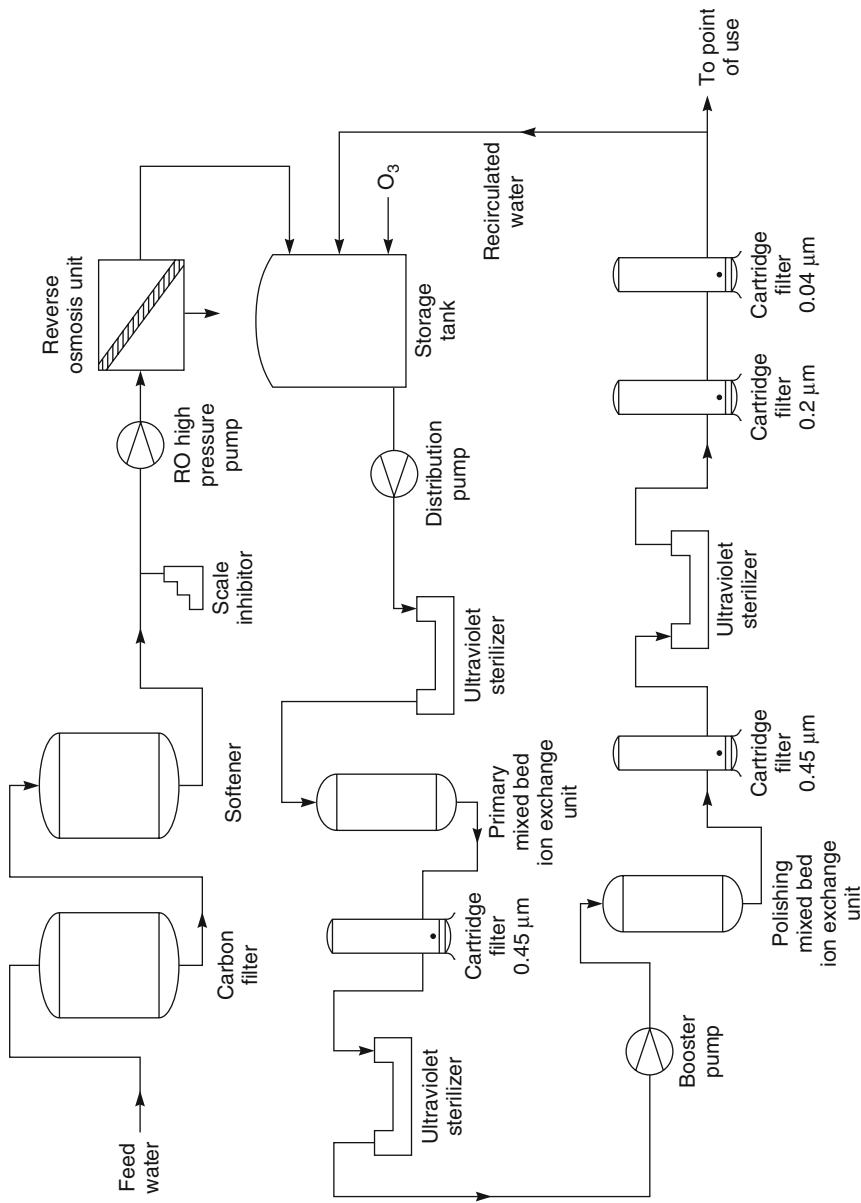


Figure 5.27 Flow schematic of an ultrapure water treatment system [61]. The RO unit operates at a high water recovery rate, so the small concentrate stream is usually discharged to the sewer

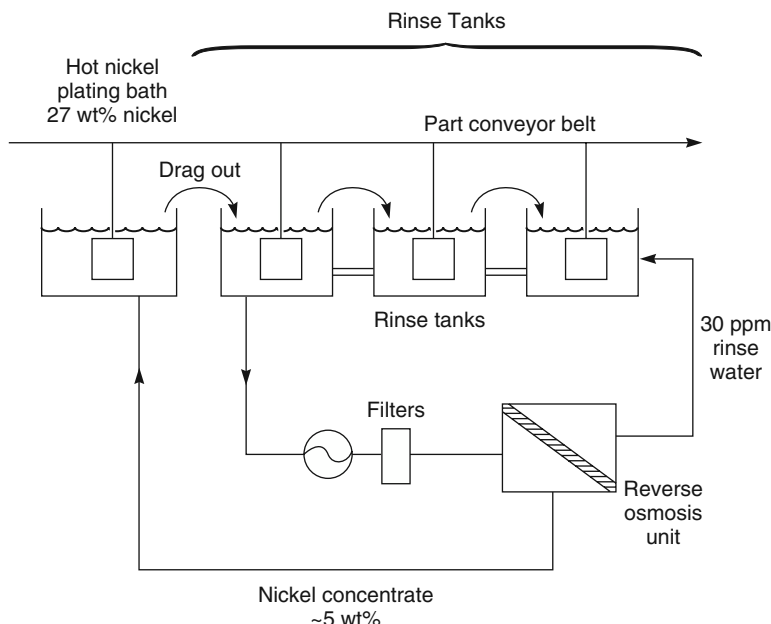


Figure 5.28 Flow scheme showing the use of a reverse osmosis system to control nickel loss from rinse water produced in a countercurrent electroplating rinse tank

psychological barriers still inhibit widespread adoption. Nonetheless, several plants have been installed in Japan, Singapore, and the Middle East, and in at least one US location. This large US plant, called Water Factory 21, is in Orange County, California, an arid region where the principal local surface water source, the Colorado River, has a total salinity of 750 ppm. Operation of this 5-million-gal/day system is described in detail by Nusbaum and Argo [65]. The system treats secondary sewage to produce good-quality water, which after purification by a reverse osmosis plant is reinjected into the aquifer below the county. The water is then mixed with natural groundwater before being removed and used as a drinking water supply elsewhere in the county. Apparently, confusing the source of the water supply in this way makes the process acceptable.

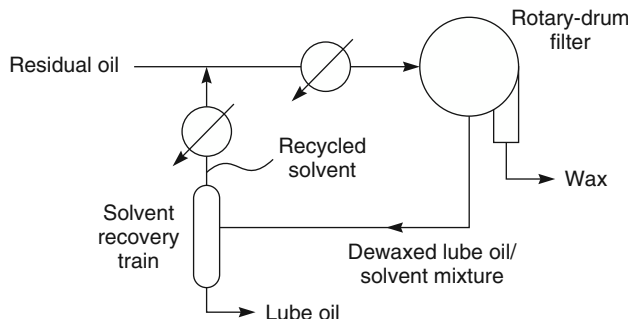
5.8.5 Nanofiltration

Nanofiltration membranes usually have high rejections to most dissolved organic solutes with molecular weights above 100–200 and good salt rejection at salt concentrations below 1000–2000 ppm salt. The membranes are also two- to fivefold more permeable than brackish and seawater reverse osmosis membranes, so they can be operated at pressures as low as 3–5 bar and still produce useful fluxes. For these reasons, their principal application has been in the removal of low levels of contaminants from already relatively clean water. For example, nanofiltration membranes are widely used as point-of-use drinking water treatment units in southern California and the southwestern United States. The water in this region contains on the order of 700 ppm dissolved salt and

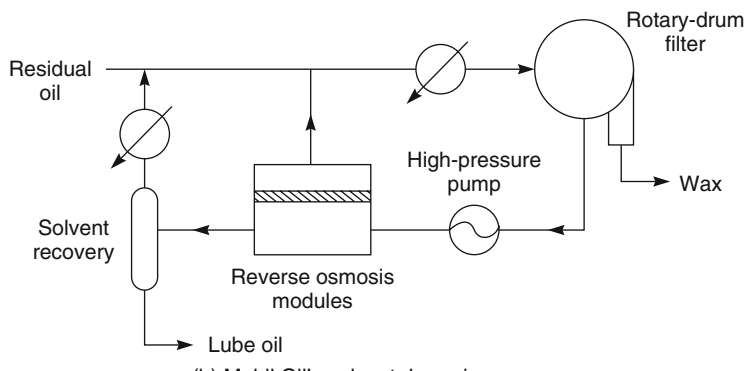
trace amounts of agricultural run-off contaminants. Many households use small 0.5-m^2 spiral-wound nanofiltration modules (under-the-sink modules) to filter this water, using the 2–3-bar pressure of tap water to provide the driving force. On a larger scale, similar membranes are used to soften municipal water by removing sulfate and divalent cations or as an initial pretreatment unit for an ultrapure water treatment plant.

5.8.6 Organic Solvent Separation

The use of membranes to separate organic solvent solutions is still at an early stage. One application that has already become commercial is the separation of small solvent molecules from larger hydrocarbons in mixtures resulting from the extraction of vacuum residual oil in refineries [66–68]. Figure 5.29a shows a simplified flow diagram of a refining lube oil separation process – these operations are very large. In a 100 000–200 000-barrel/day refinery, about 15 000–30 000 barrels/day of the oil entering the refinery remain as residual oil. A large fraction of this oil is sent to the lube oil plant, where the heavy oil is mixed with 3–10 volumes of a solvent such as methyl ethyl



(a) Conventional solvent dewaxing process



(b) Mobil Oil's solvent dewaxing process

Figure 5.29 Simplified flow schemes of (a) a conventional and (b) Mobil Oil's membrane solvent dewaxing processes. Refrigeration economizers are not shown. The first 3-million-gallon/day commercial unit was installed at Mobil's Beaumont refinery in 1998. Polyimide membranes in spiral-wound modules were used [66–68]

ketone and toluene. On cooling the mixture, the heavy wax components precipitate out and are removed by a drum filter. The light solvent is then stripped from the lube oil by vacuum distillation and recycled through the process. The vacuum distillation step is very energy intensive because of the high solvent-to-oil ratios employed.

A hyperfiltration process developed by Mobil Oil, now ExxonMobil, for this separation is illustrated in Figure 5.29b. Polyimide membranes formed into spiral-wound modules are used to separate up to 50% of the solvent from the dewaxed oil. The membranes have a flux of 20–40 l/m² h at a pressure of 30–40 bar. The solvent filtrate bypasses the distillation step and is recycled directly to the incoming oil feed. The net result is a significant reduction in the refrigeration load required to cool the oil and in the size and energy consumption of the solvent recovery vacuum distillation section.

Another refinery application developed by Shell Oil is nanofiltration of refinery naphtha fractions contaminated with color bodies and asphaltene contaminants [69]. Silicone rubber composite membranes coated onto polyacrylonitrile microporous supports are used. The process operates at about 20 bar and between 80 and 95% of the hydrocarbon is removed as a clear filtrate. The pitch black retentate is recycled to the crude distillation unit of the refinery. Shell has installed a number of these plants.

Pilot plants have also been used to separate vegetable oil/extraction solvent (hexane) mixtures in corn oil and soybean oil plants, but the process has yet to take off. Fouling of the membranes by other components in the oil has been an issue. Finally, a number of small units to separate and recover dissolved phase transfer catalysts from tetrahydrofuran and ethyl acetate solutions have been reported [70].

5.9 Conclusions and Future Directions

The reverse osmosis industry is now well established. The market is divided between four large manufacturers, who between them produce 80% of the membrane modules. These module makers supply a much larger number of system builders. The system builders buy modules almost as commodities, according to their particular needs. A handful of companies serving various niche markets produce both modules and systems. Total membrane module sales in 2010 were about US\$500 million worldwide; system sales were another US\$1–2 billion. Prospects for future growth are good. The demand for reverse osmosis systems to produce ultrapure water for the electronics and pharmaceutical industries is very strong. Municipalities in arid regions of the world also continue to buy seawater desalination units.

The industry is extremely competitive, with the manufacturers producing similar products and competing mostly on price. Many incremental improvements have been made to membrane and module performance over the past 20 years, resulting in steadily decreasing water desalination costs in inflation-adjusted dollars. Some performance values taken from a report by Dave Furukawa are shown in Table 5.5. Since 1980, just after the introduction of the first interfacial composite membranes, the cost of spiral-wound membrane modules on a per-square-meter basis has decreased seven-fold. At the same time, the water flux has doubled and the salt permeability has decreased seven-fold. Taking these improvements into account, today's membranes are almost 100 times better than those of the 1980s. This type of incremental improvement is likely to continue for some time.

Table 5.5 Advances in spiral-wound module reverse osmosis performance

Year	Cost normalized (1980 US\$)	Productivity normalized (to 1980)	Reciprocal salt passage normalized (to 1980)	Figure of merit ^a
1980	1.00	1.00	1.00	1.0
1985	0.65	1.10	1.56	2.6
1990	0.34	1.32	2.01	7.9
1995	0.19	1.66	3.52	30.8
2000	0.14	1.94	7.04	99.3

^aFigure of merit = (productivity) × (reciprocal salt passage/cost).

Source: Dave Furukawa.

The main short-term technical issue is the limited chlorine resistance of interfacial composite membranes. A number of incremental steps made over the past 10–15 years have improved resistance, but current chlorine-resistant interfacial composites do not have the rejection and flux of the best conventional membranes. All the major membrane manufacturers are working on this problem, which is slowly being solved. Three related technical issues are fouling resistance, pretreatment, and membrane cleaning. Current membrane modules are subject to fouling by particulates and scale, which is controlled by feed water pretreatment and regular membrane cleaning. The importance of these problems has declined in recent years as a result of improved membrane modules and process designs. Currently, membrane lifetimes of three to four years can be expected for well-maintained reverse osmosis systems, even with difficult feeds, and membrane lifetimes of seven years or more can be expected at seawater plants.

Development of hyperfiltration membranes to separate organic solvent mixtures is a continuing area of research. The total market for this type of application is still very small, probably only a few million dollars a year. However, this is an area where improvements in membrane performance could make a real difference to the economics of the process. Further growth is therefore likely.

References

1. Horvath, A.G. (1931) Water softening. US Patent 1,825,631, Sep. 1931.
2. Reid, C.E. and Breton, E.J. (1959) Water and ion flow across cellulosic membranes. *J. Appl. Polym. Sci.*, **1**, 133.
3. Loeb, S. and Sourirajan, S. (1963) Sea water demineralization by means of an osmotic membrane, in *Saline Water Conversion II*, Advances in Chemistry Series Number, Vol. **38** (ed. R.F. Gould), American Chemical Society, Washington, DC, pp. 117–132.
4. Westmoreland, J.C. (1968) Spirally wrapped reverse osmosis membrane cell. US Patent 3,367,504, Feb. 1968.
5. Bray, D.T. (1968) Reverse osmosis purification apparatus. US Patent 3,417,870, Dec. 1968.
6. Shields, C.P. (1979) Five years experience with reverse osmosis systems using DuPont Permasep permeators. *Desalination*, **28**, 157.

7. Cadotte, J.E. (1985) Evolution of composite reverse osmosis membranes, in *Materials Science of Synthetic Membranes*, ACS Symposium Series Number, Vol. **269** (ed. D.R. Lloyd), American Chemical Society, Washington, DC, pp. 273–294.
8. Muirhead, A., Beardsley, S., and Aboudiwan, J. (1982) Performance of the 12,000 m³/day sea water reverse osmosis desalination plant at Jeddah, Saudi Arabia (Jan. 1979–1981). *Desalination*, **42**, 115.
9. Larson, R.E., Cadotte, J.E., and Petersen, R.J. (1981) The FT-30 seawater reverse osmosis membrane-element test results. *Desalination*, **38**, 473.
10. Cadotte, J.E. (1981) Interfacially synthesized reverse osmosis membrane. US Patent 4,277,344, July 1981.
11. Eriksson, P. (1988) Water and salt transport through two types of polyamide composite membranes. *J. Membr. Sci.*, **36**, 297.
12. Kamiyama, Y., Yoshioka, N., Matsui, K., and Nakagome, E. (1984) New thin-film composite reverse osmosis membranes and spiral wound modules. *Desalination*, **51**, 79.
13. Riley, R.L. (1991) Reverse osmosis, in *Membrane Separation Systems* (eds R.W. Baker, E.L. Cussler, W. Eykamp *et al.*), Noyes Data Corporation, Park Ridge, NJ, pp. 276–328.
14. Cadotte, J.E., Petersen, R.J., Larson, R.E., and Erickson, E.E. (1980) A new thin film sea water reverse osmosis membrane. Presented at the 5th Seminar on Membrane Separation Technology, Clemson University, Clemson, SC.
15. Amjad, Z. (ed.) (1993) *Reverse Osmosis*, Van Nostrand Reinhold, New York.
16. Parekh, B.S. (ed.) (1988) *Reverse Osmosis Technology*, Marcel Dekker, New York.
17. Petersen, R.J. (1993) Composite reverse osmosis and nanofiltration membranes. *J. Membr. Sci.*, **83**, 81.
18. Rosenbaum, S., Mahon, H.I., and Cotton, O. (1967) Permeation of water and sodium chloride through cellulose acetate. *J. Appl. Polym. Sci.*, **11**, 2041.
19. Lonsdale, H.K. (1966) Properties of cellulose acetate membranes, in *Desalination by Reverse Osmosis* (ed. M. Merten), MIT Press, Cambridge, MA, pp. 93–160.
20. Lonsdale, H.K., Merten, U., and Riley, R.L. (1965) Transport properties of cellulose acetate osmotic membranes. *J. Appl. Polym. Sci.*, **9**, 1341.
21. Riley, R.L., Lonsdale, H.K., Lyons, C.R., and Merten, U. (1967) Preparation of ultrathin reverse osmosis membranes and the attainment of theoretical salt rejection. *J. Appl. Polym. Sci.*, **11**, 2143.
22. Sourirajan, S. (1970) *Reverse Osmosis*, Academic Press, New York.
23. Vos, K.D., Burris, F.O. Jr., and Riley, R.L. (1966) Kinetic study of the hydrolysis of cellulose acetate in the pH range of 2–10. *J. Appl. Polym. Sci.*, **10**, 825.
24. King, W.M., Hoernschemeyer, D.L., and Saltonstall, C.W. Jr. (1972) Cellulose acetate blend membranes, in *Reverse Osmosis Membrane Research* (eds H.K. Lonsdale and H.E. Podall), Plenum Press, New York, pp. 131–162.
25. Endoh, R., Tanaka, T., Kurihara, M., and Ikeda, K. (1977) New polymeric materials for reverse osmosis membranes. *Desalination*, **21**, 35.
26. McKinney, R. and Rhodes, J.H. (1971) Aromatic polyamide membranes for reverse osmosis separations. *Macromolecules*, **4**, 633.
27. Richter, J.W. and Hoehn, H.H. (1971) Selective aromatic nitrogen-containing polymeric membranes. US Patent 3,567,632, Mar. 1971.

28. Petersen, R.J. and Cadotte, J.E. (1990) Thin film composite reverse osmosis membranes, in *Handbook of Industrial Membrane Technology* (ed. M.C. Porter), Noyes Publications, Park Ridge, NJ, pp. 307–348.
29. Cadotte, J.E. (1977) Reverse osmosis membrane. US Patent 4,039,440, Aug. 1977.
30. Riley, R.L., Milstead, C.E., Lloyd, A.L. *et al.* (1977) Spiral-wound thin film composite membrane systems for brackish and seawater desalination by reverse osmosis. *Desalination*, **23**, 331.
31. Antony, A., Fudianto, R., Cox, S., and Leslie, G. (2010) Assessing the oxidative degradation of polyamide reverse osmosis membrane - accelerated ageing with hypochlorite exposure. *J. Membr. Sci.*, **347**, 159.
32. Glater, J., Hong, S.K., and Elimelech, M. (1994) The search for a chlorine-resistant reverse osmosis membrane. *Desalination*, **95**, 325.
33. Cadotte, J.E. (1975) Reverse osmosis membrane. US Patent 3,926,798, Dec. 1975.
34. Kurihara, M., Harumiya, N., Kannamaru, N. *et al.* (1981) Development of the PEC-1000 composite membrane for single stage sea water desalination and the concentration of dilute aqueous solutions containing valuable materials. *Desalination*, **38**, 449.
35. Nakagawa, Y., Edogawa, K., Kurihara, M., and Tonomura, T. (1985) Solute separation and transport characteristics through polyether composite (PEC)-1000 reverse-osmosis membranes, in *Reverse Osmosis and Ultrafiltration*, ACS Symposium Series, Vol. **281** (eds S. Sourirajan and T. Matsuura), American Chemical Society, Washington, DC, pp. 187–200.
36. Uemura, T. and Henmi, M. (2008) Thin-film composite membranes for reverse osmosis, in *Advanced Membrane Technology and Applications* (eds N.N. Li, A.G. Fane, W.S.W. Ho, and T. Matsuura), John Wiley & Sons, Inc., Hoboken, NJ, pp. 3–19.
37. Kumano, A. and Fujiwara, N. (2008) Cellulose triacetate membranes for reverse osmosis, in *Advanced Membrane Technology and Applications* (eds N.N. Li, A.G. Fane, W.S.W. Ho, and T. Matsuura), John Wiley & Sons, Inc., Hoboken, NJ, pp. 21–46.
38. Van der Bruggen, B., Schaep, J., Wilms, D., and Vandecasteele, C. (1999) Influence of molecular size, polarity and charge on the retention of organic molecules by nanofiltration. *J. Membr. Sci.*, **156**, 29.
39. Peters, J.M.M., Boom, J.P., Mulder, M.H.V., and Strathmann, H. (1998) Retention measurements of nanofiltration membranes with electrolyte solutions. *J. Membr. Sci.*, **145**, 199.
40. Stafie, N., Stamatialis, D.F., and Wessling, M. (2004) Insight into the transport of hexane-solute systems through tailor-made composite membranes. *J. Membr. Sci.*, **228**, 103.
41. Machado, D.R., Hasson, D., and Semiat, R. (1999) Effect of solvent properties on permeate flow through nanofiltration membranes. Part I: investigation of parameters affecting solvent flux. *J. Membr. Sci.*, **163**, 93.
42. Tarleton, E.S., Robinson, J.P., Millington, C.R., and Nijmeijer, A. (2005) Non-aqueous nanofiltration: solute rejection in low-polarity binary systems. *J. Membr. Sci.*, **252**, 123.

43. Iwama, A. and Kazuse, Y. (1982) New polyimide ultrafiltration membranes for organic use. *J. Membr. Sci.*, **11**, 279.
44. White, L.S., Wang, I.-F., and Minhas, B.S. (1993) Polyimide membranes for separation of solvents from lube oil. US Patent 5,264,166, Nov. 1993.
45. White, L.S. (2006) Development of large-scale applications in organic solvent nanofiltration and pervaporation for chemical and refining processes. *J. Membr. Sci.*, **286**, 26.
46. Silva, P., Peeva, L.G., and Livingston, A.G. (2008) Nanofiltration in organic solvents, in *Advanced Membrane Technology and Applications* (eds N.N. Li, A.G. Fane, W.S.W. Ho, and T. Matsuura), John Wiley & Sons, Inc., Hoboken, NJ, p. 451.
47. Rautenbach, R. and Albrecht, R. (1989) *Membrane Processes*, John Wiley & Sons, Ltd, Chichester.
48. Matsuura, T. and Sourirajan, S. (1972) Reverse osmosis separation of phenols in aqueous solutions using porous cellulose acetate membranes. *J. Appl. Polym. Sci.*, **15**, 2531.
49. Matsuura, T. and Sourirajan, S. (1971) Physicochemical criteria for reverse osmosis separation of alcohols, phenols, and monocarboxylic acid in aqueous solutions using porous cellulose acetate membranes. *J. Appl. Polym. Sci.*, **15**, 2905.
50. Lonsdale, H.K., Merten, U., and Tagami, M. (1967) Phenol transport in cellulose acetate membranes. *J. Appl. Polym. Sci.*, **11**, 1877.
51. Shih, W.-Y., Rahardianto, A., Lee, R.-W., and Cohen, Y. (2005) Morphometric characterization of calcium sulfate dihydrate (gypsum) scale of reverse osmosis. *J. Membr. Sci.*, **252**, 253.
52. Sudak, R.G. (1990) Reverse osmosis, in *Handbook of Industrial Membrane Technology* (ed. M.C. Porter), Noyes Publications, Park Ridge, NJ, pp. 260–306.
53. Marquardt, K. (1981) Sea water desalination by reverse osmosis, *GVC/VDI Gesellschaft Verfahrenstechnik und Chemieingenieurwesen (Seawater Desalination-Water Pretreatment and Conditioning)*, VDI Verlag, Düsseldorf.
54. Ko, A. and Guy, D.B. (1988) Brackish and seawater desalting, in *Reverse Osmosis Technology* (ed. B.S. Parekh), Marcel Dekker, New York, pp. 141–184.
55. Williams, M.E., Bhattacharyya, D., Ray, R.J., and McCray, S.B. (1992) Selected applications of reverse osmosis, in *Membrane Handbook* (eds W.S.W. Ho and K.K. Sirkar), Van Nostrand Reinhold, New York, pp. 312–354.
56. Voutchkov, N. and Semiat, R. (2008) Seawater desalination, in *Advanced Membrane Technology and Applications* (eds N.N. Li, A.G. Fane, W.S.W. Ho, and T. Matsuura), John Wiley & Sons, Inc., Hoboken, NJ, pp. 47–86.
57. Truby, R.L. (2008) Seawater desalination by ultralow-energy reverse osmosis, in *Advanced Membrane Technology and Applications* (eds N.N. Li, A.G. Fane, W.S.W. Ho, and T. Matsuura), John Wiley & Sons, Inc., Hoboken, NJ, pp. 87–100.
58. Strathmann, H. (1991) Electrodialysis in membrane separation systems, in *Membrane Separation Systems: Recent Developments and Future Directions* (eds R.W. Baker, E.L. Cussler, W. Eykamp *et al.*), Noyes Data Corporation, Park Ridge, NJ, pp. 396–420.

59. Rahardianto, A., Gao, J., Gabelich, C.J., Williams, M.D. and Cohen, Y. (2007) High recovery membrane desalting of low-salinity brackish water: integration of accelerated precipitation softening with membrane RO. *J. Membr. Sci.*, **289**, 123.
60. Côté, P., Liu, M., and Siverns, S. (2008) Water reclamation and desalination by membranes, in *Advanced Membrane Technology & Applications* (eds N.N. Li, A.G. Fane, W.S.W. Ho, and T. Matsuura), John Wiley & Sons, Inc., Hoboken, NJ, pp. 171–188.
61. Pittner, G.A. (1993) High purity water production using reverse osmosis technology, in *Reverse Osmosis* (ed. Z. Amjad), Van Nostrand Reinhold, New York.
62. Frith, C.F. Jr. (1988) Electronic-grade water production using reverse osmosis technology, in *Reverse Osmosis* (ed. B.S. Parekh), Marcel Dekker, New York, pp. 279–310.
63. Golomb, A. (1977) Application of reverse osmosis to electroplating waste treatment, in *Reverse Osmosis and Synthetic Membranes* (ed. S. Sourirajan), National Research Council Canada, Ottawa, pp. 481–494.
64. Golomb, A. (1970) Applications of reverse osmosis to electroplating waste treatment. *AES Res. Proj.*, **31**, 376.
65. Nusbaum, I. and Argo, D.G. (1984) Design and operation of a 5-mgd reverse osmosis plant for water reclamation, in *Synthetic Membrane Processes* (ed. G. Belfort), Academic Press, Orlando, FL, pp. 377–436.
66. White, L.S. and Nitsch, A.R. (2000) Solvent recovery from lube oil filtrates with polyimide membranes. *J. Membr. Sci.*, **179**, 267.
67. Gould, R.M. and Nitsch, A.R. (1996) Lubricating oil dewaxing with membrane separation of cold solvent. US Patent 5,494,566, Feb. 1996.
68. Bhore, N., Gould, R.M., Jacob, S.M. et al. (1999) New membrane process debottlenecks solvent dewaxing unit. *Oil Gas J.*, **97**, 67.
69. Cederløf, G. and Geus, E.R. (2008) Continuous process to separate colour bodies and/or asphaltene contaminants from a hydrocarbon mixture. US Patent 7,351,873, April 2008.
70. Scarpello, J.T., Nair, D., Freitas dos Santos, L.M., White, L.S. and Livingston, A.G. (2002) The separation of homogenous organometallic catalysts using solvent resistant nanofiltration. *J. Membr. Sci.*, **203**, 71.

6

Ultrafiltration

6.1 Introduction and History

Ultrafiltration uses a finely porous membrane to separate water and microsolute from macromolecules and colloids. The average pore diameter of the membrane is in the 10–1000 Å range. The first synthetic ultrafiltration membranes were prepared in the early 1900s by Bechhold from collodion (nitrocellulose) [1]. Bechhold was probably also the first to measure membrane bubble points, and he coined the term “ultrafilter.” Other important early workers in the field were Zsigmondy and Bachmann [2], Ferry [3], and Elford [4]. By the mid-1920s, collodion ultrafiltration and microfiltration membranes were commercially available for laboratory use. Although collodion membranes were widely used in laboratory studies, no industrial applications existed until the 1960s. The crucial breakthrough was the development of the anisotropic cellulose acetate membrane by Loeb and Sourirajan in 1963 [5]. Their goal was to produce high-flux reverse osmosis membranes, but others, particularly Michaels at Amicon, realized the general applicability of the technique. Michaels and his coworkers [6] produced similar anisotropic ultrafiltration membranes from cellulose acetate and other polymers including polyacrylonitrile and its copolymers, aromatic polyamides, polysulfone, and poly(vinylidene fluoride). These materials are still widely used to fabricate ultrafiltration membranes.

In 1969, Abcor (now a division of Koch Industries) installed the first commercially successful industrial ultrafiltration system. The system used tubular membrane modules [7], to recover electrocoat paint from paint shop rinse water at an automobile assembly plant. The economics were compelling, and within a few years many similar systems were installed. Shortly thereafter (1970), the first cheese whey ultrafiltration system was installed. Within a decade, 100 similar systems had been sold worldwide. These early systems used tubular or plate-and-frame modules, which were relatively expensive, but lower cost designs were gradually introduced. Hollow fiber (capillary) modules were first sold by Romicon in 1973, and spiral-wound modules, adapted to ultrafiltration applications by Abcor, became a commercial item by 1979–1980. By the 1990s, the

industry was well off the ground. All of the ultrafiltration systems installed at that time operated in a pressurized cross-flow mode. In these systems, the feed solution was circulated under pressure across the surface of the membrane. The principal problem inhibiting application of cross-flow modules for ultrafiltration was membrane fouling. The problem was controlled, but not eliminated, by use of high feed circulation rates, module and system design innovations, and regular membrane cleaning. Development of membranes with surface properties designed to minimize fouling also helped.

In the period 1988–1995, a new approach to controlling membrane fouling was developed, called constant flux operation, and it dramatically increased the market for ultrafiltration membranes. In the constant flux process, a constant flow variable pressure pump is used to withdraw solution from the permeate side of the membrane. The pump creates a negative pressure which serves to suck permeate through the membrane. Over time, as the membrane fouls, the pressure required to maintain the constant flux increases. At some point, this pressure reaches a set point and the membrane unit is taken off-line and cleaned. If the flux through the membrane is set at a low value, the time between cleanings can be kept very long, especially when constant flux operation is combined with other techniques for keeping the membrane clean, such as regular automatic back-flushing and scrubbing the membranes by air sparging. Development of this technology in the 1990s led to widespread use of ultrafiltration/microfiltration membranes to remove virus and bacteria from municipal water supplies. The US EPA and European regulators have introduced rules requiring all drinking water supplies to be treated to control *Giardia*, coliform bacteria, and viruses. Constant flux ultrafiltration/microfiltration systems have emerged as a cost-efficient method of treating this water [8].

A second application using constant flux operation is the use of ultrafiltration membranes in membrane bioreactors as a replacement for conventional sewage treatment plants. Most membrane bioreactors use submerged membrane plates or hollow fibers. The first laboratory- and pilot-scale submerged membrane systems were developed by Yamamoto *et al.* [9] in 1989. Hollow fiber membranes were submerged in a tank of raw sewage. A permeate pump was used to withdraw clean permeate at a rate below the critical flux and the fibers were maintained clean by backflushing and air sparging. It took almost 10 years before companies such as Kubota, Zenon, and Mitsui had solved all the problems involved in making industrial systems [10, 11]. However, membrane bioreactors are now widely used, and by 2006, more than 2000 municipal sewage treatment plants were using this technology.

Some of the milestones in the development of ultrafiltration membranes are charted in Figure 6.1.

6.2 Characterization of Ultrafiltration Membranes

Ultrafiltration membranes are usually anisotropic structures made by the Loeb–Sourirajan process (Chapter 3). They have a finely porous surface layer or skin supported on a much more open microporous substrate. The finely porous surface layer performs the separation; the microporous substrate provides mechanical strength. The membranes discriminate between dissolved macromolecules of different sizes and are usually characterized by their molecular weight cut-off, a loosely defined term generally taken to

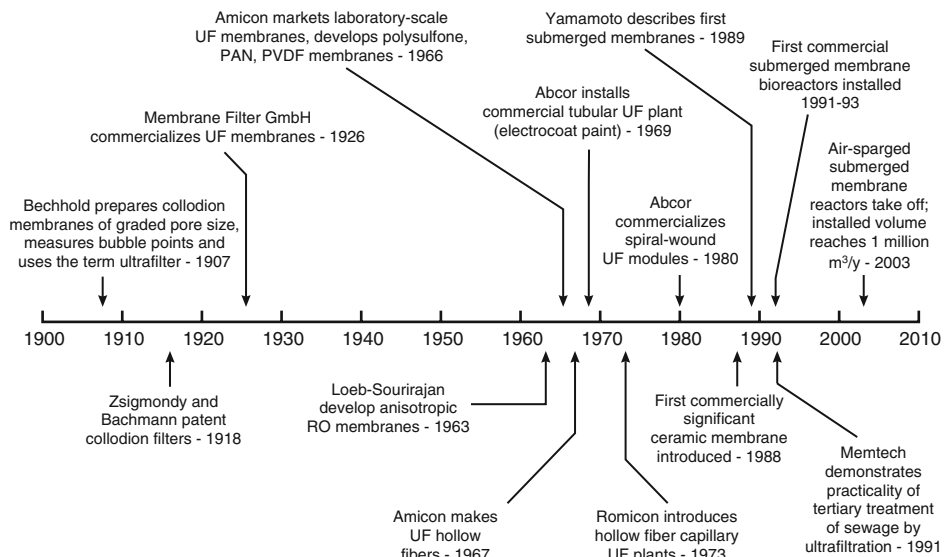


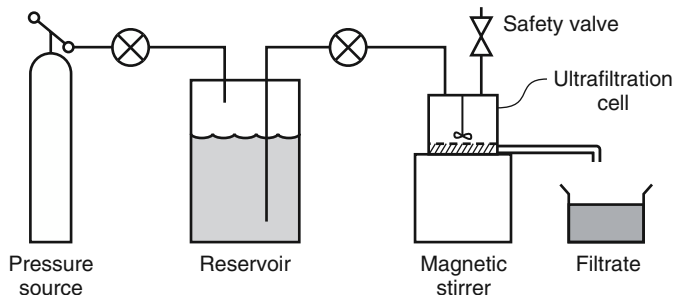
Figure 6.1 Milestones in the development of ultrafiltration

mean the molecular weight of the globular protein molecule that is 95% rejected by the membrane. Ultrafiltration and microfiltration are related processes – the distinction between the two lies in the pore size of the membrane. Microfiltration membranes have larger pores and are used to separate particles in the 0.1–10 µm range. Ultrafiltration membranes are used to separate small colloidal particles and dissolved macromolecules with diameters below 1000 Å. The pore diameter of the membrane can be inferred from the cut-off value. Ultrafiltration membranes have pore diameters in the 10–1000 Å range.

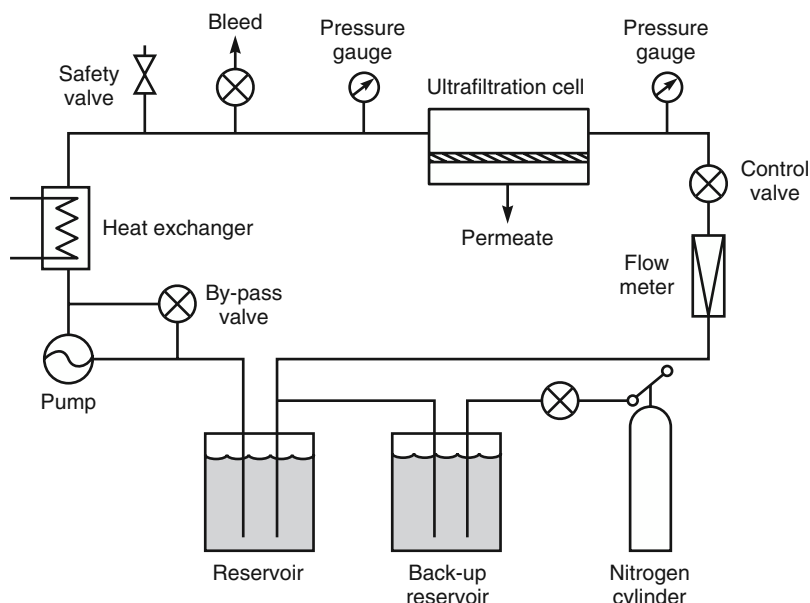
Laboratory-scale ultrafiltration experiments are performed with small, stirred batch cells, or flow-through cells in a recirculation system. Diagrams of the two types of systems are shown in Figure 6.2. A fixed pressure is applied to the feed solution and the permeate is collected at atmospheric pressure. Because ultrafiltration experiments are generally performed at pressures below 100 psi, plastic components can be used. Stirred batch cells are often used for quick experiments, but flow-through systems are preferred for systematic work. In flow-through systems, the feed solution can be more easily maintained at a constant composition, and the turbulence at the membrane surface required to control membrane fouling is high and easily reproducible. This allows reliable comparative measurements to be made.

The cut-off of ultrafiltration membranes is usually characterized by solute molecular weight, but several other factors affect permeation through these membranes. One important example is the shape of the molecule to be retained. When membrane retention measurements are performed with linear, water-soluble molecules such as polydextran, polyethylene glycol, or poly(vinyl pyrrolidone), the measured rejection is lower than the rejection measured for proteins of the same molecular weight. It is believed that linear, water-soluble polymer molecules are able to snake through the membrane pores, as illustrated in Figure 6.3. Protein molecules, however, exist in solution as tightly wound

Batch Stirred Cell



Flow Recirculation System: Flow-Through Cells

**Figure 6.2** Laboratory ultrafiltration test systems

globular coils held together by hydrogen bonds. These globular molecules cannot deform to pass through the membrane pores and are therefore rejected. Some results showing the rejection of different molecules for a polysulfone ultrafiltration membrane are listed in the table accompanying Figure 6.3 [12]. The membrane shows significant rejection to globular protein molecules as small as pepsin (MW 35 000) and cytochrome *c* (MW 13 000), but is completely permeable to a flexible linear polydextran, with an average molecular weight of more than 100 000.

The pH of the feed solution is another factor that affects permeation through ultrafiltration membranes, particularly with polyelectrolytes. For example, polyacrylic acid is usually very well rejected by ultrafiltration membranes at pH 5 and above, but is

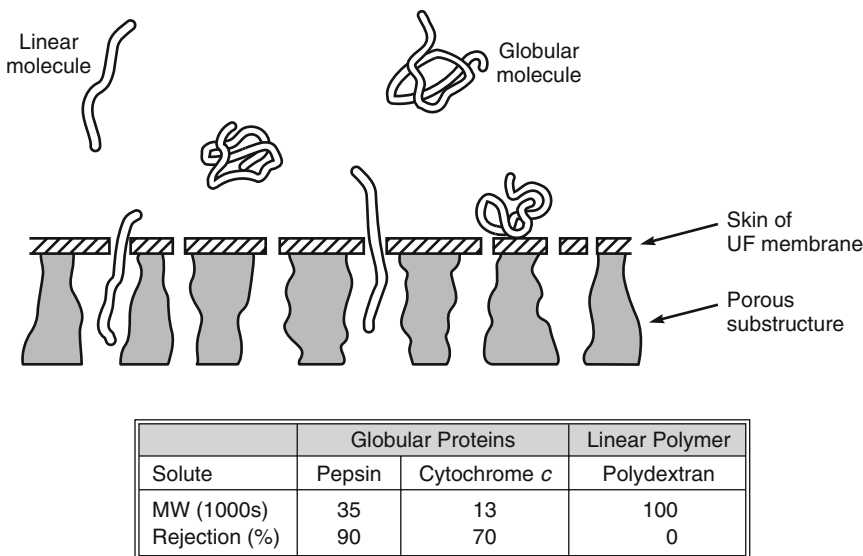


Figure 6.3 Ultrafiltration membranes are rated on the basis of nominal molecular weight cut-off, but the shape of the molecule to be retained has a major effect on retentivity. Linear molecules pass through a membrane, whereas globular molecules of the same molecular weight may be retained. The table shows typical results obtained with globular protein molecules and linear polydextran for the same polysulfone membrane [12]

completely permeable through the same membranes at pH 3 and below. This change in rejection behavior with pH is due to the change in configuration of the polyacid. At pH 5 and above, polyacrylic acid is ionized. In the ionized form, the negatively charged carboxyl groups along the polymer backbone repel each other; the polymer coil is then very extended and relatively inflexible. In this form, the molecule cannot readily permeate the small pores of an ultrafiltration membrane. At pH 3 and below, the carboxyl groups along the polyacrylic acid polymer backbone are all protonated. The resulting neutral molecule is much more flexible and can pass through the membrane pores.

6.3 Membrane Fouling

6.3.1 Constant Pressure/Constant Flux Operation

Until the mid-1990s, most laboratory ultrafiltration systems and all industrial membrane systems operated at a fixed applied pressure, typically in the range of 3–5 bar. The feed solution was circulated at a fixed pressure across the surface of the membrane and the permeate flux was measured over time. A key factor determining the performance of ultrafiltration membranes in these systems was membrane fouling, due to deposition of retained colloidal and macromolecular material on the membrane surface. A number of reviews have described the process in detail [13–16].

The pure water flux of ultrafiltration membranes is often very high – greater than $500 \text{ l/m}^2 \cdot \text{h}$ ($350 \text{ gal/ft}^2 \cdot \text{day}$). However, when membranes are used to separate macromolecular or colloidal solutions, the flux falls within seconds, typically to $50 \text{ l/m}^2 \cdot \text{h}$. This immediate drop in flux is caused by the formation of a gel layer of retained solutes on the membrane surface. This gel layer forms a secondary barrier to flow through the membrane, as illustrated in Figure 6.4 and described in detail below. The initial decline in flux is determined by the composition of the feed solution and its fluid hydrodynamics. Sometimes the resulting flux is constant for a prolonged period, and when the membrane is retested with pure water, the flux returns to the original value. More commonly, a further slow decline in flux occurs over a period of hours to weeks, depending on the feed solution. Most of this second decrease in flux is caused by slow consolidation of the secondary layer formed on the membrane surface. Formation of this consolidated gel layer, called membrane fouling, is difficult to control. Control techniques include regular membrane cleaning, backflushing, or using membranes with surface characteristics that minimize adhesion. More recently, air scrubbing is being used. Operation of the membrane at the lowest practical operating pressure also delays consolidation of the gel layer.

A typical plot illustrating the slow decrease in flux that can result from consolidation of the secondary layer is shown in Figure 6.5 [17]. The pure water flux of

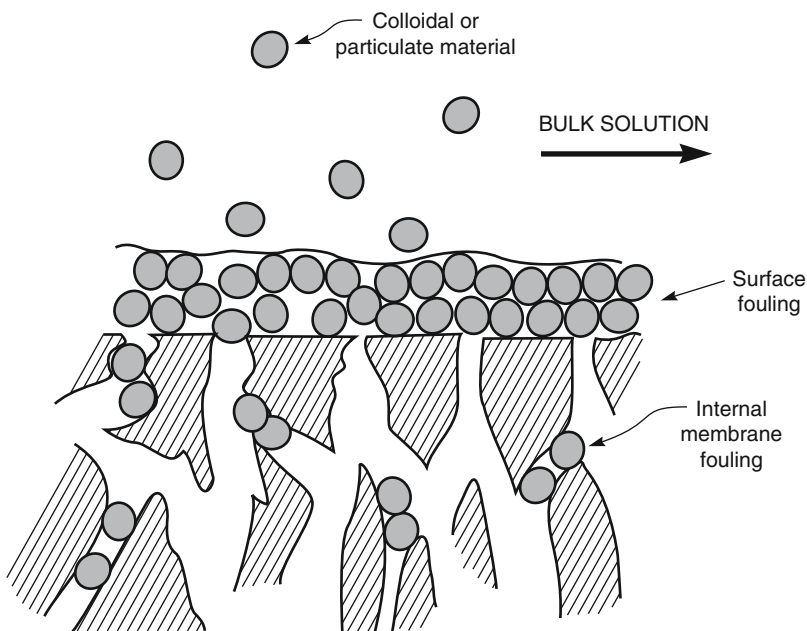


Figure 6.4 Schematic representation of fouling on an ultrafiltration membrane. Surface fouling is the deposition of solid material on the membrane that consolidates over time. This fouling layer can be controlled by high turbulence, regular cleaning, and using hydrophilic or charged membranes to minimize adhesion to the membrane surface. Surface fouling is generally reversible. Internal fouling is caused by penetration of solid material into the membrane, which results in plugging of the pores. Internal membrane fouling is generally irreversible

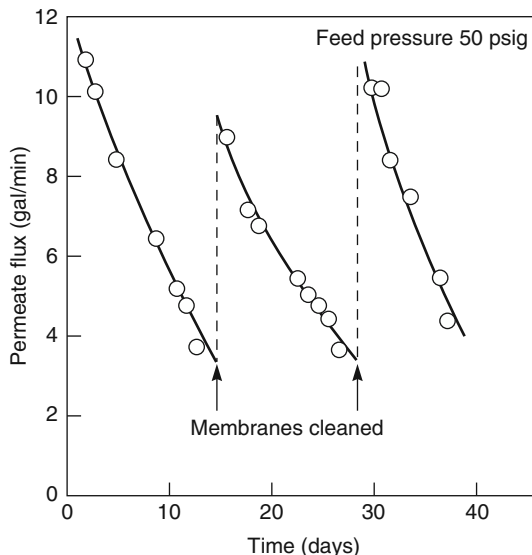


Figure 6.5 Ultrafiltration flux as a function of time for an electrocoat paint latex solution. Because of fouling, the flux declines over a period of days. Periodic cleaning is required to maintain high fluxes [17]. Reprinted from R. Walker, "Recent Developments in Ultrafiltration of Electrocoat Paint," *Electrocoat* **82**, (1982) with permission from Gardner Publications, Inc., Cincinnati, OH.

this small electrocoating plant was approximately 50 gal/min, but on contact with an electrocoat paint solution containing 10–20% latex, the flux immediately fell to about 10–12 gal/min. This first drop in flux was due to the formation of the gel layer of latex particles on the membrane surface, as shown in Figure 6.4. Thereafter, the flux steadily declined over a two-week period. This second drop in flux was caused by slow densification of the gel layer under the pressure of the system. In this particular example, the densified gel layer could be removed by periodic cleaning of the membrane. When the cleaned membrane was exposed to the latex solution again, the flux was initially restored to that of a fresh membrane.

If the regular cleaning cycle shown in Figure 6.5 is repeated many times, eventually, the membrane flux does not return to the original value when the membrane is cleaned. Part of this slow, permanent loss of flux is due to precipitates on the membrane surface that are not removed by the cleaning procedure. A further cause of the permanent flux loss is internal fouling of the membrane by material that penetrates the membrane pores and becomes lodged in the interior of the membrane, as illustrated in Figure 6.4. Ultrafiltration membranes are often used to separate colloids from water and microsolute. In this case, the tendency is to use relatively high-molecular-weight cut-off membranes, but the higher fluxes of these membranes can be transitory because they are more susceptible to internal fouling. A membrane with a lower molecular-weight cut-off, even though it may have a lower pure water flux, often provides a more sustained flux with actual feed solutions, because less internal fouling occurs. For this reason, finely porous ultrafiltration

membranes are often used to remove large colloids or bacteria with diameters of 1–2 µm from solution. Microfiltration membranes with pores in the 0.1–0.2 µm range could perform the same separation and would have higher initial water fluxes, but the resistance to internal fouling of ultrafiltration membranes is much better.

The process shown in Figure 6.5 is an example of a constant pressure cross-flow ultrafiltration. Until the mid-1990s, this was the only way industrial ultrafiltration systems were operated. Feed solution at a pressure of 3–5 bar was circulated at a fixed pressure across the surface of the membrane. As the flux declined, the feed pressure or feed recirculation rate was increased to compensate for the lower flux, or else more membrane area was turned on. When the flux declined too much, the system was taken off-line, the membranes were cleaned and the process restarted.

Beginning in about 1995, a different type of process was introduced for both ultrafiltration and microfiltration membranes. This process, called constant flux operation, is compared to the earlier constant pressure operation in Figure 6.6. In this process, the feed solution is circulated at a relatively low pressure across the feed side of the membrane and a sub-atmospheric pressure is created on the permeate side of the membrane with a constant flow/variable pressure pump. The flow through the membrane is maintained at a fixed rate by this permeate pump. As the membrane fouls, the pump has to work harder to draw liquid through the membrane and the pressure on the permeate side of the membrane falls. This increases the transmembrane pressure across the membrane. At some point, the transmembrane pressure increases to a preset cut-off value, at which point the system is taken off-line and the membrane is cleaned.

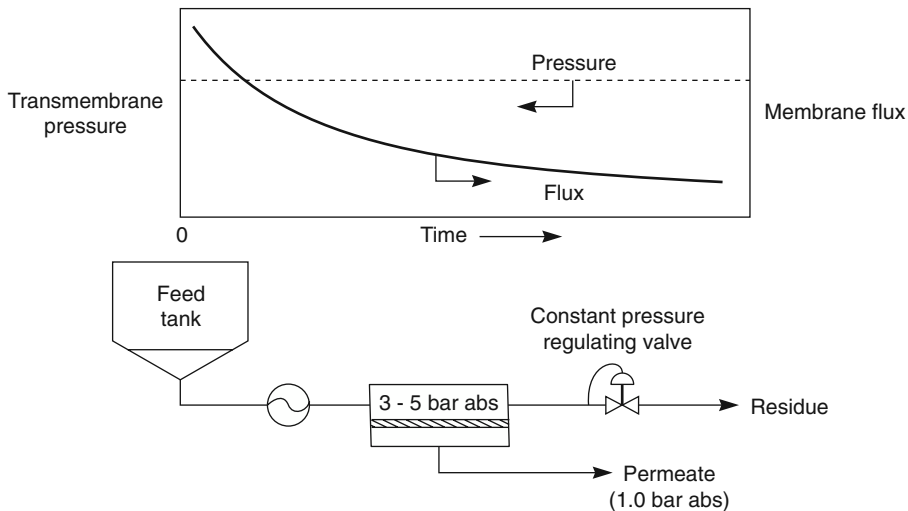
Some results illustrating constant flux/variable pressure operation are shown in Figure 6.7 [18]. In these experiments, the initial pressure difference across the membrane was very small, less than 0.02 bar. As the membrane fouled, the pressure required to maintain the flux increased. When the pressure difference across the membrane reached 0.3 bar, the membrane was considered fouled and was taken off-line for cleaning. When the flux was fixed at a high value, 50 l/m²·h, the membrane required cleaning after only five days. Reducing the flux to 25 l/m²·h increased the time between cleanings to 120 days. Reducing the flux to 14 l/m²·h increased the time between cleanings to 210 days. There is a steep trade-off in the time between cleaning cycles and membrane flux.

The transmembrane pressure-*versus*-time curves shown in Figure 6.5 have a characteristic form. The pressure initially rises at a slow and constant rate for many days until a critical value is reached. At this critical point, the rate of increase in pressure sharply increases and within a few days, the pressure reaches the set point value and the system must be taken off-line and cleaned.

This behavior is commonly observed. A number of explanations have been given [19]; the most convincing is that the membrane pores are not fouled uniformly. As some pores become blocked, the fixed permeate flux is forced through the remaining open pores. The higher flux that then occurs through these pores causes them to be fouled at a higher rate, forcing the flux to go through even fewer pores, and so on. Thus, once fouling and pore blockage begins to occur, the process rapidly accelerates, leading to complete fouling of the membrane.

Constant flux/variable (low) pressure membrane operation has become increasingly popular in recent years, especially when combined with the improved membrane cleaning methods now available.

Constant Pressure – Variable Flux Operation



Constant Flux – Variable Pressure Operation

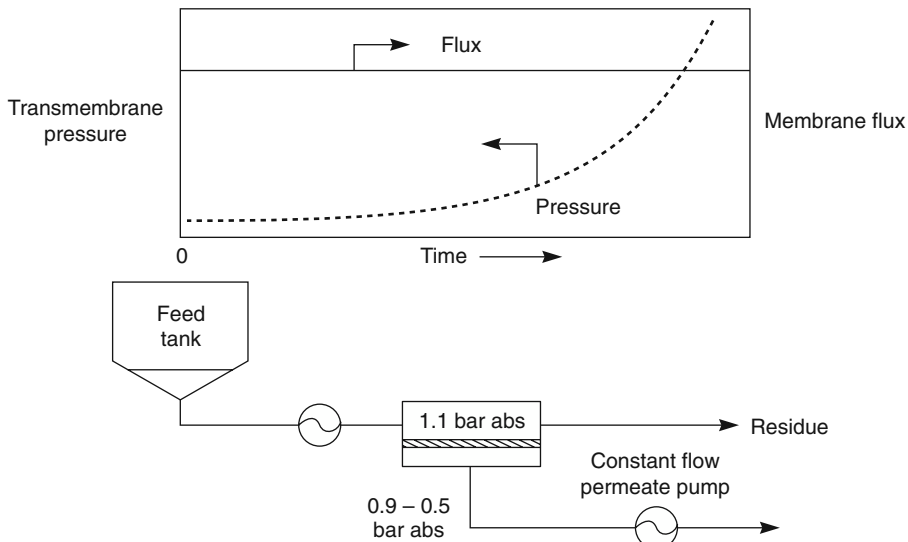


Figure 6.6 A comparison of constant pressure/variable flux and constant flux/variable pressure operations in ultrafiltration/microfiltration

6.3.2 Concentration Polarization

The primary cause of membrane fouling is concentration polarization, which results in the deposition of a layer of material on the membrane surface. The general phenomenon of concentration polarization is described in Chapter 4. In ultrafiltration, solvent and

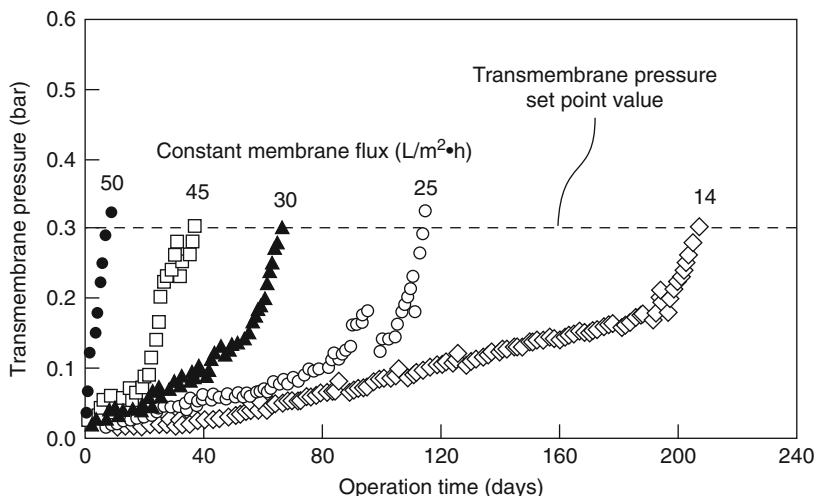


Figure 6.7 Illustration of fixed flux/variable pressure membrane operation. Feed solution is circulated across the membrane surface at ambient pressure. Permeate is removed at a fixed rate by a constant volume permeate pump. Initially, the transmembrane pressure across the membrane is very small. As the membrane fouls, the transmembrane pressure increases. When the transmembrane pressure reaches a preset value of 0.3 bar, the system is taken off-line and the membranes are cleaned. As the fixed flux decreases, the time between cleanings increases. Reprinted with permission from [18]. Copyright (2006) Elsevier.

macromolecular or colloidal solutes are carried toward the membrane surface by the solution permeating the membrane. Solvent molecules permeate the membrane, but the larger solutes accumulate at the membrane surface. Because of their size, the rate at which the rejected solute molecules can diffuse from the membrane surface back to the bulk solution is relatively low. Thus, their concentration at the membrane surface is typically 20–50 times higher than the feed solution concentration. These solutes become so concentrated at the membrane surface that a gel layer is formed and becomes a secondary barrier to flow through the membrane. The formation of this gel layer on the membrane surface is illustrated in Figure 6.8. The gel layer model was developed at the Amicon Corporation in the 1960s [12].

The formation of the gel layer is easily described mathematically. At any point within the boundary layer shown in Figure 6.8, the convective flux of solute to the membrane surface is given by the volume flux, J_v , of the solution through the membrane multiplied by the concentration of the solute, c_i . At steady state, this convective flux within the laminar boundary layer is balanced by the diffusive flux of retained solute in the opposite direction. This balance is expressed by the equation

$$J_v c_i = D_i \frac{dc_i}{dx} \quad (6.1)$$

where D_i is the diffusion coefficient of the macromolecule in the boundary layer. Once the gel layer has formed, the concentrations of solute at both surfaces of the boundary

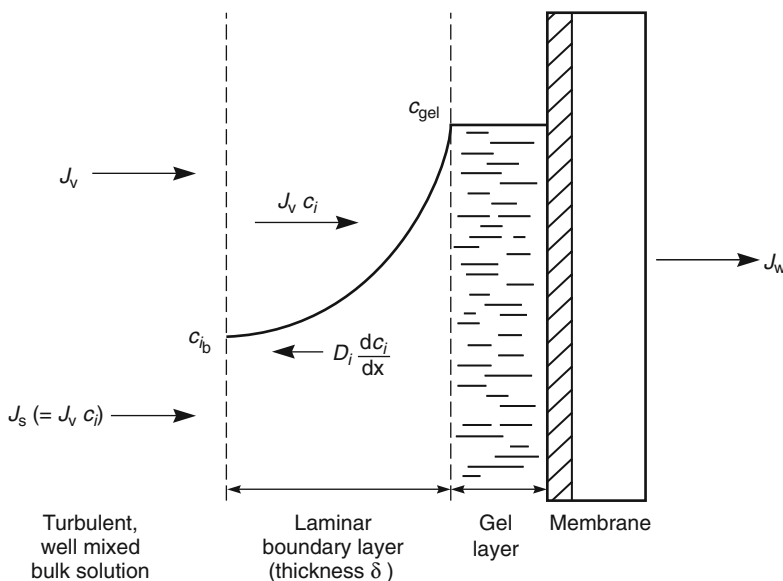


Figure 6.8 Illustration of the formation of a gel layer of colloidal material on the surface of an ultrafiltration membrane by concentration polarization

layer are fixed. At one surface, the concentration is the bulk feed solution concentration c_{ib} ; at the other surface, it is the concentration at which the solute forms an insoluble gel (c_{gel}). Integration of Equation 6.1 over the boundary layer thickness (δ) then gives

$$\frac{c_{gel}}{c_{ib}} = \exp\left(\frac{J_v \delta}{D_i}\right) \quad (6.2)$$

where c_{gel} is the concentration of retained solute at the membrane surface where the solute gels and is the concentration in the bulk solution. In any particular ultrafiltration test, the terms c_{ib} , c_{gel} , D_i , and δ in Equation 6.2 are fixed because the solution and the operating conditions of the test are fixed. From Equation 6.2, this means that the volume flux, J_v , through the membrane is also fixed and is independent of the intrinsic permeability of the membrane. In physical terms, this is because a membrane with a higher intrinsic permeability only causes a thicker gel layer to form on the surface of the membrane. This lowers the membrane flux until the rate at which solutes are brought toward the membrane surface and the rate at which they are removed are again balanced, as expressed in Equation 6.1.

The formation of a gel layer of colloidal material at the ultrafiltration membrane surface produces a limiting or plateau flux that cannot be exceeded. Once a gel layer has formed, increasing the applied pressure does not increase the flux, but merely increases the gel thickness. This is also shown in Equation 6.2, which contains no term for the applied pressure.

The effect of the gel layer on the flux through an ultrafiltration membrane at different feed pressures is illustrated in Figure 6.9. At a very low pressure p_1 , the flux J_v is low,

so the effect of concentration polarization is small, and a gel layer does not form on the membrane surface. The flux is close to the pure water flux of the membrane at the same pressure. As the applied pressure is increased to pressure p_2 , the higher flux causes increased concentration polarization, and the concentration of retained material at the membrane surface increases. If the pressure is increased further to p_3 , concentration polarization becomes enough for the retained solutes at the membrane surface to reach the gel concentration c_{gel} and form the secondary barrier layer. This is the limiting flux

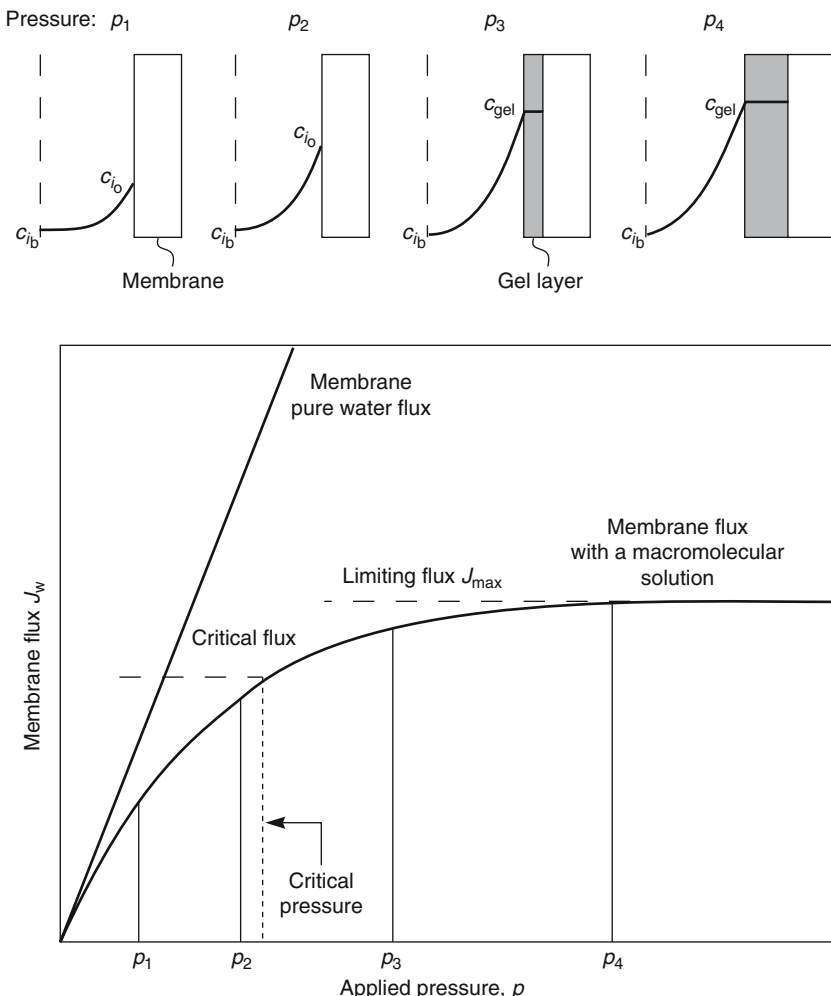


Figure 6.9 The effect of pressure on ultrafiltration membrane flux and the formation of a secondary gel layer. Ultrafiltration membranes are best operated at pressures below p_2 when the gel layer has not formed. Operation at high pressures such as those above p_3 leads to formation of thick gel layers, which consolidate over time, resulting in permanent fouling of the membrane

for the membrane. Further increases in pressure only increase the thickness of the gel layer, not the flux.

Experience has shown that the best long-term performance of an ultrafiltration membrane is obtained when the applied pressure is maintained below the pressure p_3 shown in Figure 6.9. We can call this the critical pressure. Operating at higher pressures does not increase the membrane flux but does increase the thickness and density of retained material at the membrane surface layer. Over time, material on the membrane surface can become compacted or precipitate, forming a layer of deposited material that has a lower permeability; the flux then falls from the initial value. When constant flux operation became common in the 1990s, the term critical flux was coined [20]. This flux is shown in Figure 6.9. It is the flux at which the first gel layer forms on the membrane surface. The best long-term performance of an ultrafiltration/microfiltration fixed flux system is obtained when the fixed flux is set below the critical flux.

One way of determining the critical flux is to develop a flux-applied pressure curve of the type shown in Figure 6.9 and estimate the critical flux value. A second method is illustrated in Figure 6.10, which shows data from Chen *et al.* [21]. A series of constant flux measurements were made with a membrane in a well-controlled test system. The permeate flux was increased in steps from an initial low value. The flux was held constant for 30 minutes at each step. The transmembrane pressure was measured at each step. Figure 6.10a shows the results as the permeate flux was increased stepwise to 130 l/m²·h. After each incremental change in flux, the transmembrane pressure increased, but stayed constant thereafter until the next change in flux. When the process was reversed, the transmembrane pressure decreased by almost the same amount. All of these measurements were below the critical flux for this membrane at these operating conditions.

Figure 6.10b shows a repeat of this experiment, but this time the permeate flux was increased stepwise to a higher value. Up to 130 l/m²·h, the transmembrane pressure remained constant at each step, as before, but when the permeate flux was increased to 140 l/m²·h, the transmembrane pressure no longer increased to a steady value. Instead, the pressure began to continuously increase. During the next higher flux increments (155 and 170 l/m²·h), the transmembrane pressure also continued to increase steadily, and a constant value was not reached. When the permeate flux decreased, the transmembrane pressure decreased, but did not return to the initial values measured when the permeate flux was first increased. The membrane had become permanently fouled. These measurements suggest that the critical flux at which a gel layer is formed on this membrane is about 140–150 l/m²·h.

The point at which a gel layer forms on the membrane can also be determined by constant pressure/variable flux measurements. A series of constant pressure experimental results obtained with latex solutions illustrating the effect of concentration and pressure on flux are shown in Figure 6.11 [22]. The point at which the flux reaches a plateau value depends on the concentration of the latex in the solution: the more concentrated the solution, the lower the limiting flux. The critical flux is also about 100 l/m²·h at 1% latex, but falls to about 35 l/m²·h at 20% latex. The exact relationship between the maximum flux and solute concentration can be obtained by rearranging Equation 6.2 to obtain

$$J_{\max} = -\frac{D}{\delta} (\ln c_{ib} - \ln c_{gel}) \quad (6.3)$$

where J_{\max} is the plateau or limiting flux through the membrane.

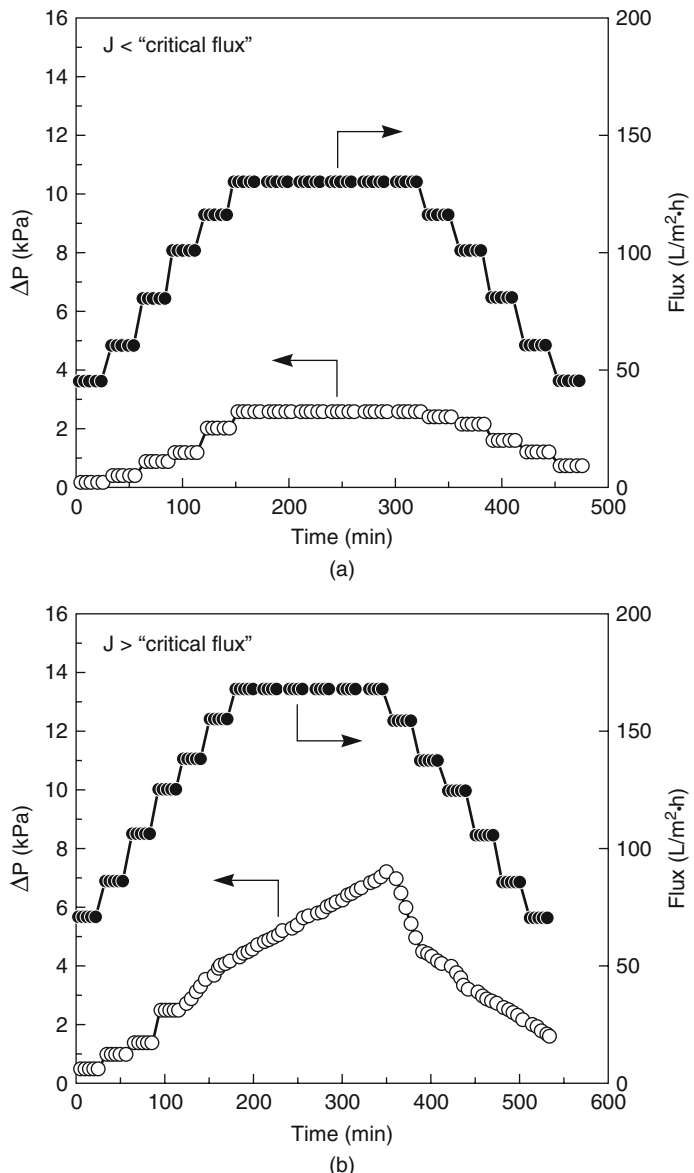


Figure 6.10 Constant flux measurements to determine limiting flux, based on data of V. Chen et al. The critical flux at which the membrane becomes fouled is between 140 and 150 $\text{L/m}^2 \cdot \text{h}$. Reprinted with permission from [21]. Copyright (1997) Elsevier.

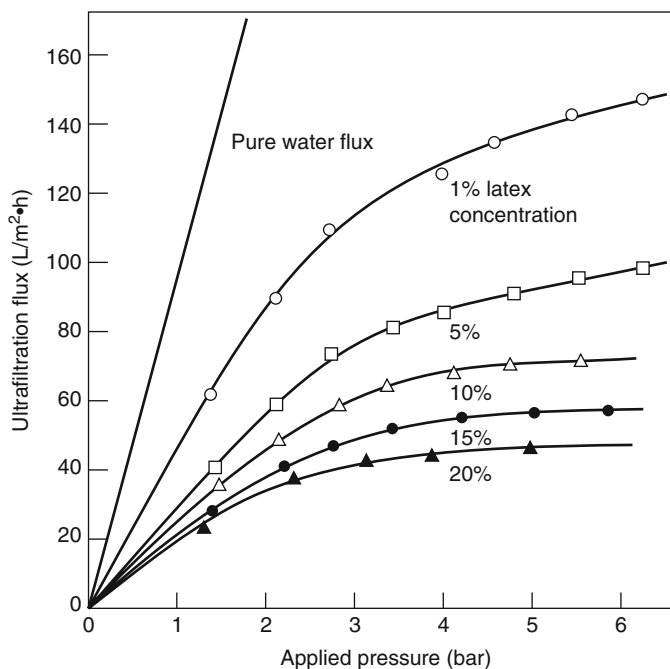


Figure 6.11 The effect of pressure on membrane flux for styrene-butadiene polymer latex solutions in a high-turbulence, thin-channel test cell [22]

Plots of the limiting flux J_{\max} as a function of solution concentration for latex solution data are shown in Figure 6.12 for a series of latex solutions at various feed solution flow rates. A series of straight line plots is obtained, and these extrapolate to the gel concentration c_{gel} at zero flux. The slopes of the plots in Figure 6.12 are proportional to the term \bar{D}/δ in Equation 6.3. The increase in flux resulting from an increase in the fluid recirculation rate is caused by the decrease in the boundary layer thickness δ .

Plots of the limiting flux as a function of solute concentration for different solutes using the same membrane under the same conditions are shown in Figure 6.13 [22]. Protein or colloidal solutions, which easily form precipitated gels, have low fluxes that extrapolate at zero flux to low gel concentrations. Particulate suspensions, pigments, latex particles, and oil-in-water emulsions, which do not easily form gels, have higher fluxes at the same concentration and operating conditions and generally extrapolate to higher gel concentrations.

The studies of concentration polarization illustrated in Figures 6.11–6.13 were performed in an exceptionally high turbulence, cross-flow laboratory test cell. Membrane fluxes were unusually high. Fluxes obtained in industrial processes, operated at less turbulent conditions, are usually lower, but the same general behavior is seen.

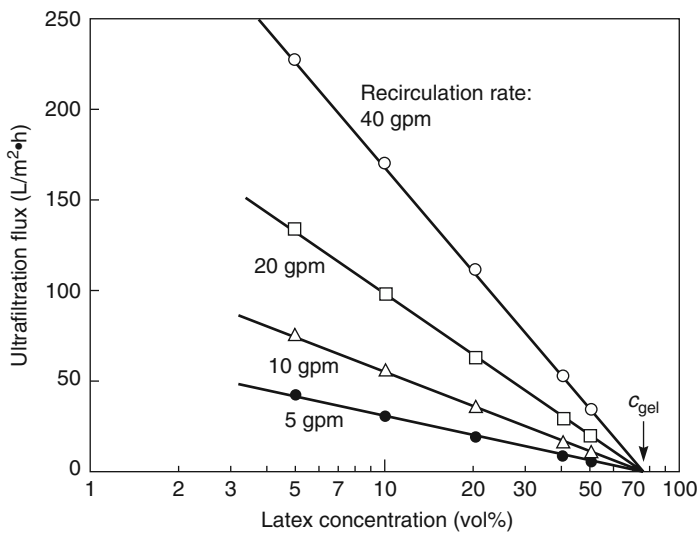


Figure 6.12 Ultrafiltration limiting flux with a latex solution at an applied pressure of 60 psi (in the limiting flux region) as a function of feed solution latex concentration. These results were obtained in an exceptionally high-turbulence, thin-channel cell. The solution recirculation rate is shown in the figure [22]

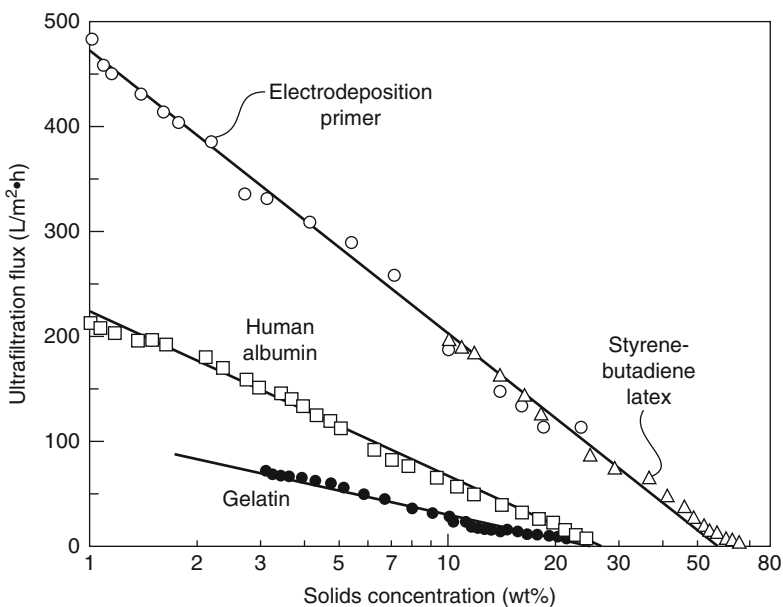


Figure 6.13 Effect of solute type and concentration on limiting flux through the same type of ultrafiltration membrane operated under the same conditions. Reprinted from [22]. Copyright (1990) Noyes Publications.

The gel layer model described by Equations 6.1–6.3 is very appealing and is widely used to rationalize the behavior of ultrafiltration membranes. Unfortunately, a number of issues cannot be easily explained by this simple model:

- The flux of many macromolecular colloidal and particulate solutions is too high (sometimes by an order of magnitude) to be rationalized by a reasonable value of the diffusion coefficient and the boundary layer thickness in Equation 6.2.
- In the plateau region of the flux/pressure curves of the type shown in Figure 6.11, different solutes should have fluxes proportional to the value of their diffusion coefficients D in Equation 6.3. Often, this is not the case, as Figure 6.13 shows. For example, latex and particulate solutes with very small diffusion coefficients typically have higher ultrafiltration limiting fluxes than protein solutions measured with the same membranes under the same conditions. This is the opposite of the expected behavior.
- Experiments with different ultrafiltration membranes and the same feed solution often yield very different ultrafiltration limiting fluxes. But according to the model shown in Figure 6.8 and represented by Equation 6.2, the ultrafiltration limiting flux is independent of the membrane type.

Contrary to the normal experience that falling bread always lands jam-side down, the trend of these observations is that experiment produces a better result than theory predicts. For this reason, the observations are lumped together and called the flux paradox [13]. The best working model seems to be that, in addition to simple diffusion, solute is also being removed from the membrane surface as undissolved gel particles by a scouring action of the feed fluid [23]. This explains why protein solutions that form tough adherent gels have lower fluxes under the same conditions than pigment and latex solutions that form looser gels. The model also explains why increasing the hydrophilicity of the membrane surface or changing the charge on the surface can produce higher limiting fluxes. Decreased adhesion between the gel and the membrane surface allows the flowing feed solution to remove gel particles more easily.

Figure 6.14 illustrates how turbulent eddies caused by the high velocity of the solution passing through the narrow channel of a spiral-wound module might remove gel particles from the membrane surface. Because of the high velocity of the feed solution and the feed spacer netting used in ultrafiltration modules, the feed liquid is normally very turbulent. Although a relatively laminar boundary layer may form next to the membrane surface, as described by the film model, periodic turbulent eddies may also occur. These eddies can dislodge gel from the membrane surface, carrying it away with the feed solution.

The most important effect of concentration polarization is to reduce the membrane flux, but it also affects the retention of macromolecules. Retention data obtained with dextran polysaccharides at various pressures are shown in Figure 6.15 [24]. Because these are stirred batch cell data, the effect of increased concentration polarization with increased applied pressure is particularly marked. A similar drop in retention with increased pressure is observed with flow-through cells, but the effect is lower than with stirred batch cells because concentration polarization is better controlled in such cells. With macromolecular solutions, the concentration of retained macromolecules at the membrane surface increases with increased pressure, so permeation of the macromolecules also increases, lowering rejection. The effect is particularly noticeable at low pressures, under which conditions increasing the applied pressure produces the largest increase in flux,

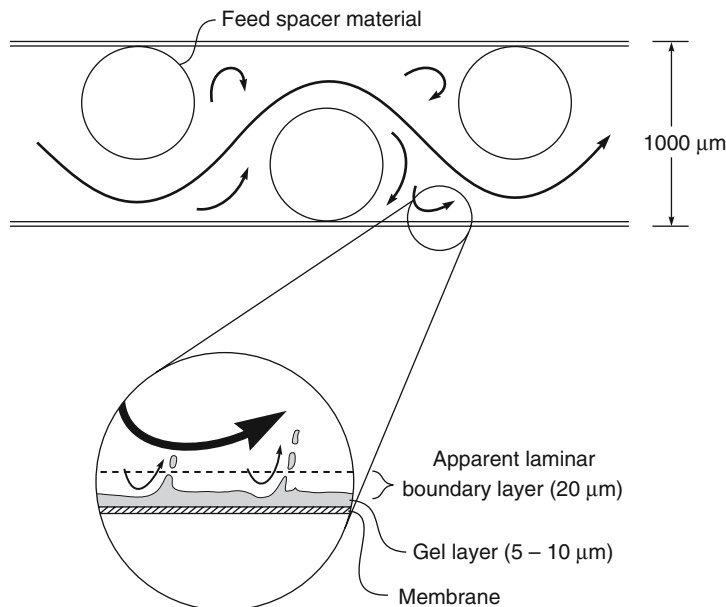


Figure 6.14 An illustration of the channel of a spiral-wound module showing how periodic turbulent eddies can dislodge deposited gel particles from the surface of ultrafiltration membranes

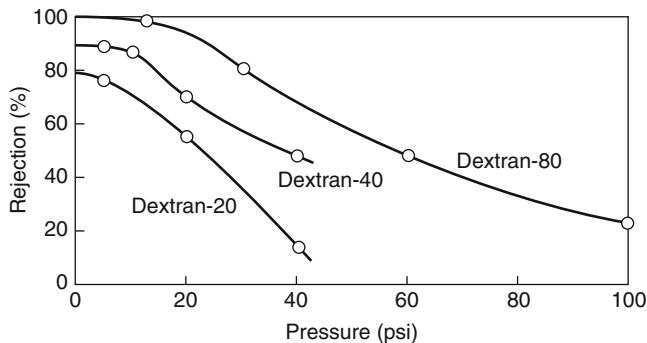


Figure 6.15 Rejection of 1% dextran solutions as a function of pressure using Dextran 20 (MW 20 000), Dextran 40 (MW 40 000), and Dextran 80 (MW 80 000). Batch cell experiments performed at a constant stirring speed [24]

and hence concentration polarization, at the membrane surface. At high pressure, the change in flux with increased pressure is smaller, so the decrease in rejection by the membrane is less apparent.

Concentration polarization can also interfere with the ability of an ultrafiltration membrane to fractionate a mixture of dissolved macromolecules. Figure 6.16 [12] shows the results of experiments for a membrane with a molecular weight cut-off of about 200 000 used to separate albumin (MW 65 000) from γ -globulin (MW 156 000). Tests with the

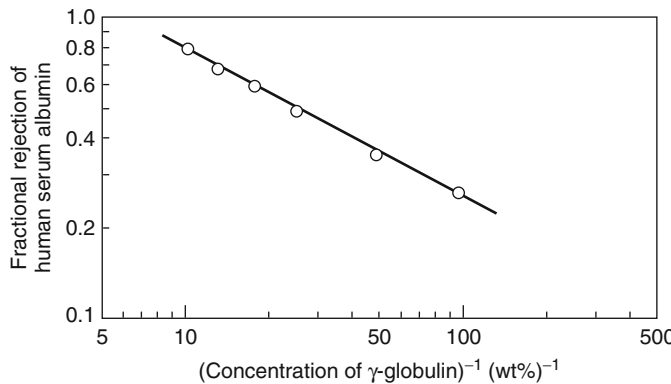


Figure 6.16 The retention of albumin (MW 65 000) in the presence of varying concentrations of γ -globulin (MW 156 000) by a membrane with a nominal molecular weight cut-off based on one-component protein solutions of MW 200 000. As the concentration of γ -globulin in the solution increases, the membrane water flux decreases, and the albumin rejection increases from 25% at 0.01 wt% γ -globulin to 80% rejection at 0.1 wt% γ -globulin [12]

pure components show that albumin passes through the membrane almost completely unhindered, but rejection of γ -globulin is significant. However, addition of even a small amount of γ -globulin to the albumin causes almost complete rejection of both components. The increased rejection is accompanied by a sharp decrease in membrane flux, suggesting that rejected globulin forms a secondary barrier layer. The secondary layer is eliminated only at very low γ -globulin concentrations, resulting in partial fractionation of the two proteins.

Because of the effect of the secondary layer on selectivity, special techniques are needed to use ultrafiltration membranes for fractionation of macromolecular mixtures. Most commercial ultrafiltration applications involve processes in which the membrane completely rejects all the dissolved macromolecular and colloidal material in the feed solution while completely passing water and dissolved microsolutes.

6.3.3 Fouling Control

Several cleaning methods are used to remove the densified gel layer of retained material from the membrane surface. The easiest is to periodically circulate an appropriate cleaning solution through the membrane modules for 1 or 2 hours. The most common ultrafiltration fouling layers – organic polymer colloids and gelatinous materials – are best treated with alkaline solutions followed by hot detergent solutions. Enzymatic detergents are particularly effective when the fouling layer is a proteinaceous gel. Calcium, magnesium, and silica scales, often a problem with reverse osmosis membranes, are generally not a problem in ultrafiltration because these ions permeate the membrane (ultrafiltration of cheese whey, in which high calcium levels can lead to calcium scaling, is an exception). Because many feed waters contain small amounts of soluble ferrous iron salts, hydrated iron oxide scaling can be a problem. In the ultrafiltration system, these salts are oxidized to ferric iron by entrained air. Ferric iron is insoluble in water, so

an insoluble iron hydroxide gel forms and accumulates on the membrane surface. Such deposits are usually removed with a citric or hydrochloric acid wash.

Regular cleaning is required to maintain the performance of all ultrafiltration membranes. The period of the cleaning cycle can vary from daily for food applications, such as ultrafiltration of whey, to once a month or even less often for ultrafiltration membranes used as polishing units in ultrapure water systems. A typical cleaning cycle is as follows:

1. Flush the system several times with hot water at the highest possible circulation rate.
2. Treat the system with an appropriate acid or alkali wash, depending on the nature of the layer.
3. Treat the system with a hot detergent solution.
4. Flush the system thoroughly with water to remove all traces of detergent; measure the pure water flux through the membrane modules under standard test conditions. Even after cleaning, some degree of permanent flux loss over time is expected. If the restoration of flux is less than expected, repeat steps 1–3.

Ultrafiltration systems should never be taken off line without thorough flushing and cleaning. Because membrane modules are normally stored wet, the final rinse solutions should contain a bacteriostat such as 0.5% formaldehyde to inhibit bacterial growth.

Backflushing is an increasingly popular way of controlling membrane fouling. The method is widely used to clean capillary and ceramic membrane modules that can withstand a flow of solution from permeate to feed without damaging the membrane. Backflushing is not usually used for spiral-wound modules because the membranes are too easily damaged. In a backflushing procedure, a slight over-pressure is applied to the permeate side of the membrane, forcing solution from the permeate side to the feed side of the membrane. The flow of solution lifts deposited materials from the surface. Backflushing must be done carefully to avoid membrane damage. Typical backflushing pressures are 0.2–0.5 bar.

One method of achieving a backflushing effect that is used with cross-flow capillary ultrafiltration modules is initiated by closing the permeate port from the membrane module, as shown in Figure 6.17 [25]. In normal operation, a pressure drop of 0.2–0.5 bar occurs between the feed and residue side of a membrane module. This pressure difference is required to drive the feed solution through the module. If the permeate port from the module is closed, the pressure on the permeate side of the membrane will increase to a pressure intermediate between those of the feed and residue streams. This produces a slight positive pressure difference at one end of the module, and a slight negative pressure difference on the other end of the module, as shown in Figure 6.17b. The pressure difference sets up a backflushing condition in which permeate-quality water that has permeated one-half of the module becomes a backflushing solution in the other half of the module. Deposited materials lifted from the membrane surface in the back-flushed area are swept away by the fast feed flow. If the direction of the feed flow is reversed, as shown in Figure 6.17c, the other half of the module is then back-flushed. This *in situ* backflushing technique is used in capillary ultrafiltration modules in which the feed-to-residue pressure drop is quite large. An advantage of the procedure is that it can be performed without stopping normal operation of the ultrafiltration system.

In the past, backflushing was used once every few days or weeks. Nowadays, the procedure is done much more frequently. In submerged membrane reactors, for example,

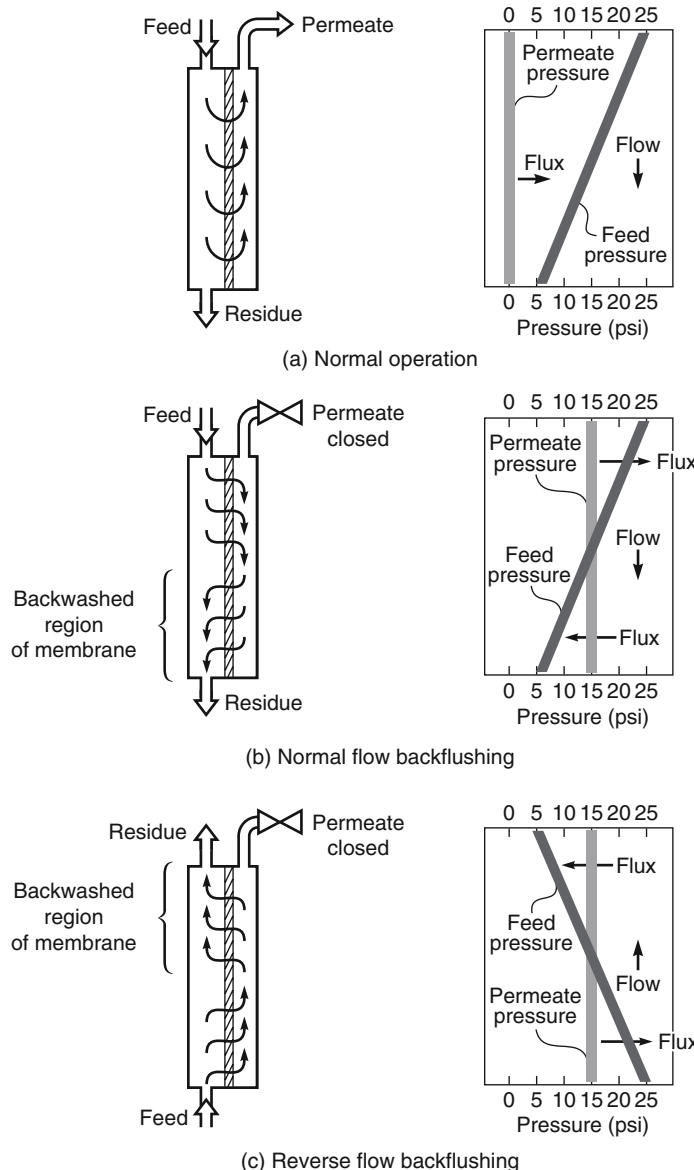


Figure 6.17 Backflushing of membrane modules by closing the permeate port. This technique is particularly applicable to capillary fiber modules

a typical backflushing cycle is 30–60 seconds every 15 minutes, and automatic equipment is used to control the backflushing process.

Because of the challenging environment in which ultrafiltration membranes are operated and the frequent routine cleaning cycles that are used, their membrane lifetimes are significantly shorter than those of reverse osmosis membranes. Ultrafiltration membrane

lifetimes are often only two to three years, and modules may be replaced annually in cheese whey or electrocoat paint applications. In contrast, reverse osmosis membranes are normally cleaned only once or twice per year, and membrane lifetimes are five to seven years.

6.4 Membranes

Most of today's ultrafiltration membranes are made by variations of the Loeb–Sourirajan process (Chapter 3). A limited number of materials are used, primarily polyacrylonitrile, poly(vinyl chloride)-polyacrylonitrile copolymers, polysulfone, poly(ether sulfone), poly(vinylidene fluoride), some aromatic polyamides, and cellulose acetate. In general, the hydrophilic membranes are more fouling-resistant than completely hydrophobic membranes. For this reason, water-soluble polymers such as poly(vinyl pyrrolidone) or poly(vinyl methyl ether) are often added to the membrane casting solutions used for hydrophobic polymers such as polysulfone or poly(vinylidene fluoride). During the membrane precipitation step, most of the water-soluble polymer is leached from the membrane, but enough remains to make the membrane surface hydrophilic.

The charge on the membrane surface is important. Many colloidal materials have a slight negative charge from carboxyl, sulfonic, or other acid groups. If the membrane surface also has a slight negative charge, adhesion of the colloidal gel layer to the membrane is reduced, which helps to maintain a high flux and inhibit membrane fouling. A slight positive charge on the membrane has the opposite effect. Charge and hydrophilic character can be the result of the chemical structure of the membrane material or can be applied to a preformed membrane surface by chemical grafting or surface treatment. The appropriate treatment depends on the application and the feed solution.

The importance of membrane surface characteristics on performance is illustrated by Figure 6.18. The feed solution in this example was an anodic electrocoat paint solution in which the paint particulates had a net negative charge. As a result, membrane flux declined rapidly with the positively charged membranes. The flux decline with essentially identical membranes that had been treated to give the surface a net negative charge was much slower [22].

6.5 Constant Pressure Modules, System Design, and Applications

Until the late 1990s, almost all industrial ultrafiltration processes used constant pressure/variable flux systems. In these systems, membrane fouling is controlled by rapid circulation of the feed solution across the membrane surface, sometimes called cross-flow operation. The modules, designs, and applications of this type of system are described in this section. In the following section, we will describe submerged membrane, constant flux/variable pressure systems that were introduced after 1995. These systems control membrane fouling by a combination of air sparging and regular backflushing of the membranes.

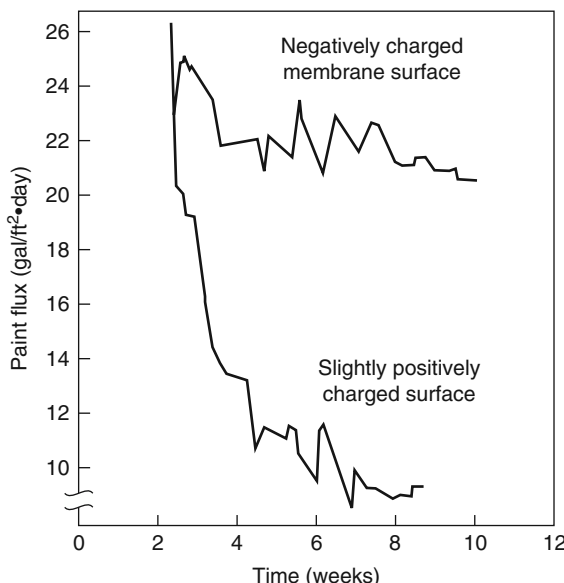


Figure 6.18 Effect of membrane surface charge on ultrafiltration flux decline. These membranes were used to ultrafilter anodic electrocoat paint, which has a net negative charge. Electrostatic repulsion made the negatively charged membrane significantly more resistant to fouling than the similar positively charged membrane [22]

6.5.1 Cross-Flow Ultrafiltration Modules

The need to control concentration polarization and membrane fouling dominates the design of ultrafiltration modules. The first commercially successful ultrafiltration systems were based on tubular and plate-and-frame modules. Over the years, many improvements have been made to these module designs, and they are still used for highly fouling solutions. However, the lower cost of spiral-wound and capillary modules has resulted in a gradual trend to replace tubular and plate-and-frame systems with these lower-cost modules. In relatively non-fouling applications, such as the use of ultrafiltration as part of a treatment train to produce ultrapure water, spiral-wound modules are universally used. Spiral-wound and capillary modules are also used in some food applications, such as ultrafiltration of cheese whey and clarification of apple juice.

Because of their large diameter, tubular ultrafiltration modules can be used to treat solutions that would rapidly foul other module types. In a number of demanding applications, such as treatment of electrocoat paint, concentration of latex solutions, or separation of oil/water emulsions, the fouling resistance and ease of cleaning of tubular modules outweighs their high cost, large footprint, and high energy consumption. In a typical tubular module system, several 5- to 8-ft-long tubes are manifolds in series. The feed solution is circulated through the module array at velocities of 2–6 m/s. This high solution velocity causes a pressure drop of 2–3 psi per tube or 10–30 psi for a module bank. Because

of the high circulation rate and the resulting pressure drop, large pumps are required, so tubular modules have the highest energy consumption of any module design. Tubular ultrafiltration plants often use 10–15 kWh of energy per cubic meter of permeate produced. At an electrical energy cost of US\$0.06/kWh, this corresponds to an energy cost of US\$0.60–0.90/m³ of permeate, a major cost factor.

The diameter of the early tubular membrane modules was 1 in. Later, more energy-efficient, higher-membrane-area modules were produced by nesting four to six smaller-diameter tubes inside a single housing (see Chapter 3). Typical tubular module costs vary widely, but are generally from US\$200 to US\$500/m². Recently, ceramic tubular modules have been introduced; these are more expensive, typically from US\$1000 to US\$2000/m². This high cost limits their use to a few applications with extreme feed operating conditions.

Plate-and-frame units compete with tubular units in some applications. These modules are not quite as fouling resistant as tubular modules, but are less expensive. Most consist of a flat membrane envelope with a rubber gasket around the outer edge. The membrane envelope, together with appropriate spacers, forms a plate that is contained in a stack of 20–30 plates. Typical feed channel heights are 0.5–1.0 mm, and the system operates in high-shear conditions. In bioseparation applications, plate-and-frame modules are supplied as sealed steam-sterilizable disposable cassettes. These units have a limited lifetime, but the high value of the separation they perform can support this cost.

Plate-and-frame systems can be operated at higher pressures than tubular or capillary modules – operating pressures up to 150 psi are not uncommon. This can be an advantage in some applications. The compact design, small hold-up volume, and absence of stagnant areas also makes sterilization easy. For these reasons, plate-and-frame units are used in pharmaceutical and food industry operations, particularly in Europe where Rhône-Poulenc (now Rhodia and Sanofi-Aventis) and De Danske Sukkerfabrikker (DDS) (now Alfa Laval) pioneered these applications in the 1970s. A photograph of an Alfa Laval plate-and-frame system is shown in Figure 6.19.

Capillary hollow fiber modules were introduced by Romicon (a joint venture of Amicon and Rohm & Haas) in the early 1970s. A typical capillary module contains 500–2000 fibers with a diameter of 0.5–1.0 mm housed in a 30-in.-long, 3-in.-diameter cartridge. Modules have a membrane area of 2–10 m². Feed solution is pumped down the bore of the fibers. Operating pressures are quite low, normally not more than 2 bar (to avoid breaking the fibers). The normal feed-to-residue pressure drop of a capillary module is 0.2–0.5 bar. Under these conditions, capillary modules achieve good throughputs with many solutions. High-temperature sanitary systems are available; this, combined with the small hold-up volume and clean flow path, has encouraged the use of these modules in biotechnology applications in which small volumes of expensive solutions are treated. A major advantage of capillary fiber systems is that the membrane can be cleaned easily by backflushing. With capillary modules it is important to avoid “blinding” the fibers with particulates caught at the fiber entrance. Prefiltration to remove all particulates larger than 1/10th of the fiber’s inside diameter is required to avoid blinding.

The use of spiral-wound modules in industrial ultrafiltration applications has increased in recent years. This design was first developed for reverse osmosis modules in which the feed channel spacer is a fine window-screen material. In ultrafiltration, a coarser feed

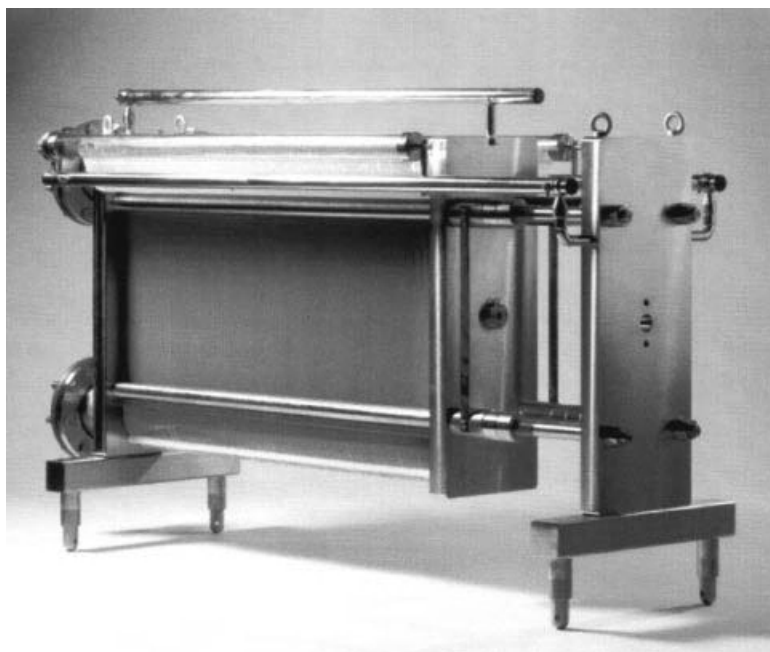


Figure 6.19 Horizontal M39 plate-and-frame ultrafiltration system. (Courtesy of Alfa Laval Nakskov A/S, Nakskov, Denmark.)

spacer material is used, often as much as 45 mil thick (1 mil = 0.001 inch). This coarse spacer prevents particulates from lodging in the spacer corners. However, prefiltration of the ultrafiltration feed down to 5–10 µm is still required for long-term operation. In the past, spiral-wound modules were limited to ultrafiltration of clean feed waters, such as preparation of ultrapure water for the electronics or pharmaceutical industries. Development of improved pretreatment and module spacer designs now allows these modules to be used for more highly fouling solutions such as cheese whey. In such food applications, the stagnant volume between the module insert and the module housing is a potentially unsterile area. To eliminate this dead space, the product seal is perforated to allow a small bypass flow to continuously flush this area.

In the last few years, a number of companies, most notably New Logic International (Emeryville, CA) and their licensees, have introduced plate-and-frame modules in which the membrane plate is vibrated or rotated. Thus, concentration polarization at the membrane surface is controlled by movement of the membrane rather than by movement of the feed solution [26]. Moving the membrane concentrates most of the turbulence right at the membrane surface, where it is most needed. These modules achieve very high turbulence at the membrane surface at a relatively low energy cost. The fluxes obtained are high and stable. Vibrating-rotating modules are considerably more expensive than cross-flow modules, so the first applications have been with high-value, highly fouling feed solutions that are difficult to treat with standard modules.

6.5.2 Constant Pressure (Cross-Flow) System Design

The common forms of constant pressure ultrafiltration systems are shown in Figure 6.20.

6.5.2.1 Batch Systems

The simplest type of ultrafiltration system is a batch unit, shown in Figure 6.20a. In such a unit, a limited volume of feed solution is circulated through the module at a high flow rate. The process continues until the required separation is achieved, after which the concentrate solution is drained from the feed tank, and the unit is ready to treat a second batch of solution. Batch processes are suited to small-scale operations common in the biotechnology and pharmaceutical industries. Such systems can be adapted to continuous use, but this requires automatic controls, which are expensive and can be unreliable.

The easiest way to calculate the performance of a batch system is to assume the membrane has a constant rejection of the solute of interest. That is,

$$\mathbb{R} = \left(1 - \frac{c_p}{c_b} \right) = 1 \quad (6.4)$$

where c_p is the solute concentration in the permeate and c_b is the solute concentration in the feed. It follows that the increase in concentration of the solute in the feed tank from the initial concentration $c_b(o)$, to the concentration at time t , $c_b(t)$ is proportional to the volume of solution remaining in the feed tank, that is,

$$\frac{c_b(t)}{c_b(o)} = \frac{V_{(o)}}{V_{(t)}} \quad (6.5)$$

where the volume of solution removed in the permeate is $V_{(o)} - V_{(t)}$. If, as is often the case, the membrane is slightly permeable to the solute ($\mathbb{R} < 1$), the concentration ratio achieved can be written as

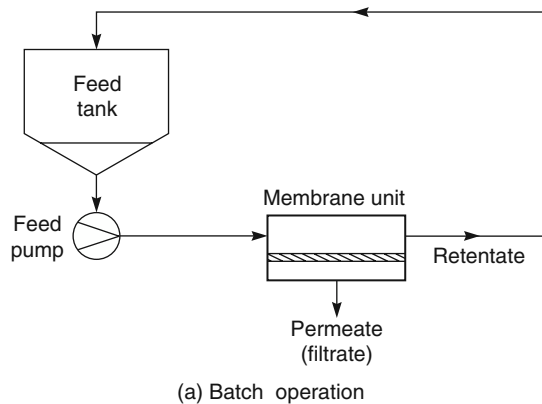
$$\ln \left[\frac{c_b(t)}{c_b(o)} \right] = \mathbb{R} \ln \left(\frac{V_{(o)}}{V_{(t)}} \right) \quad (6.6)$$

When the rejection coefficient equals one, Equation 6.6 reduces to Equation 6.5. A plot of the concentration ratio of retained solute as a function of the volume reduction for membranes with varying rejection coefficients is shown in Figure 6.21. This figure illustrates the effect of partially retentive membranes on loss of solute.

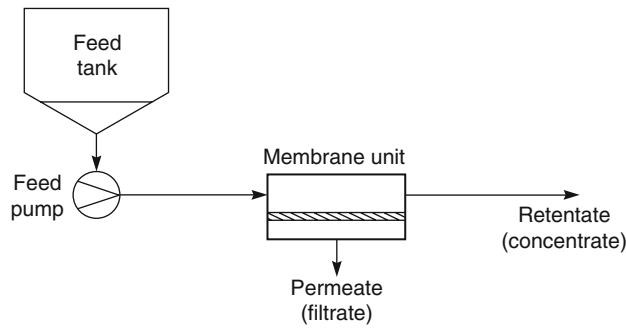
Batch systems are used in the laboratory and some biotechnology applications where small volumes of high value solutions must be processed. However, most industrial processes use some form of continuous process.

6.5.2.2 One Pass and Feed-and-Bleed (Cross-Flow) Systems

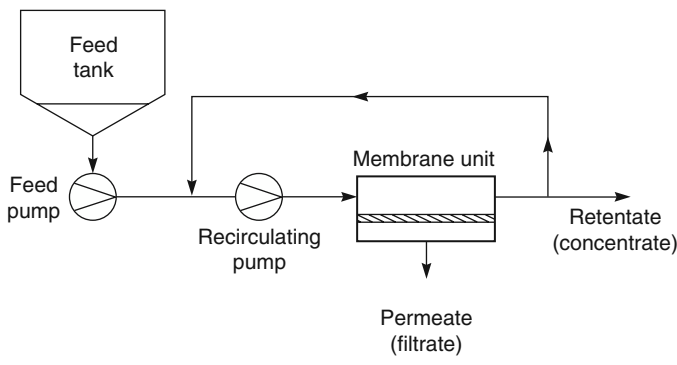
Continuous ultrafiltration processes based on Figure 6.20b, in which a series of modules are arranged in series to obtain the complete separation required in a single pass, are not common. This is because high feed solution flow rates are required to control concentration polarization; a single-pass process would not achieve the required removal under these conditions. Solution velocities in ultrafiltration modules are 5–10 times higher than in reverse osmosis. For these reasons, feed-and-bleed systems of the type



(a) Batch operation



(b) Single-pass operation



(c) Feed-and-bleed operation

Figure 6.20 Comparison of (a) batch, (b) single-pass, and (c) feed-and-bleed configurations for cross-flow filtration. After Zeman and Zydny. Reprinted with permission from [32]. Copyright (1996) Taylor & Francis.

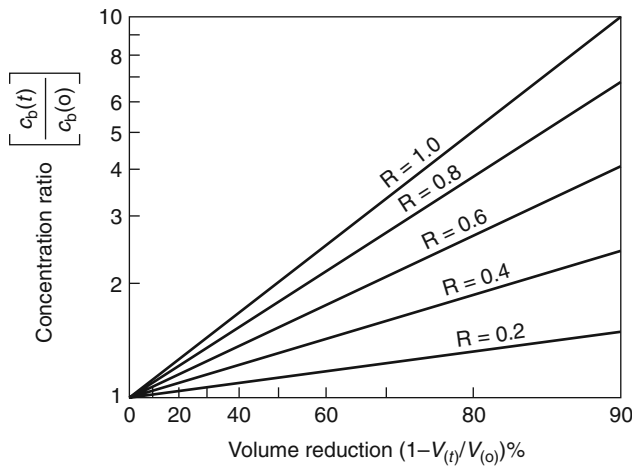


Figure 6.21 Increase in concentration of the retained feed solution as a function of volume reduction of the feed for membranes of different solute rejections. The difference between these lines and the $R = 1$ line represents loss of solute through the membrane

shown in Figure 6.20c are often used in large ultrafiltration plants. In these systems, a large volume of solution is circulated continuously through a bank of membrane modules. Concurrently, a small volume of feed solution enters the recirculation loop just before the recirculation pump, and an equivalent volume of more concentrated solution is removed (or bled) from the recirculation loop just after the membrane module. The advantage of feed-and-bleed systems is that a high feed solution velocity is easily maintained through the modules, independent of the volume of solution being treated. In most plants, the flow rate of solution in the recirculation loop is 5–10 times the feed solution flow rate. This high circulation rate means that the concentration of retained material in the circulating solution is close to the concentration of the bleed solution and is significantly higher than the feed solution concentration. Because the flux of ultrafiltration membranes decreases with increasing concentration, more membrane area is required to produce the required separation than in a batch or a once-through continuous system operated at the same feed solution velocity.

To overcome the inefficiency of one-stage feed-and-bleed designs, industrial systems are often divided into multiple stages, as shown in Figure 6.22. By using multiple stages, the difference in concentration between the solution circulating in a stage and the feed solution entering the stage is reduced. A numerical example illustrates this point. In this example, assume the membrane is completely retentive and the object of the separation is to concentrate the feed solution from 1 to 8%. If this is done in a one-stage feed-and-bleed system, the average concentration of the solution circulating through the modules is 8%, and the flux is proportionately low. In a more efficient two-stage feed-and-bleed system, the first stage concentrates the solution from 1 to 3%, and the second stage concentrates the solution from 3 to 8%. Approximately three-quarters of the permeate is removed in the first stage, and the rest in the second stage. Because the modules in the first stage operate at a concentration of 3% rather than 8%, these modules have a higher

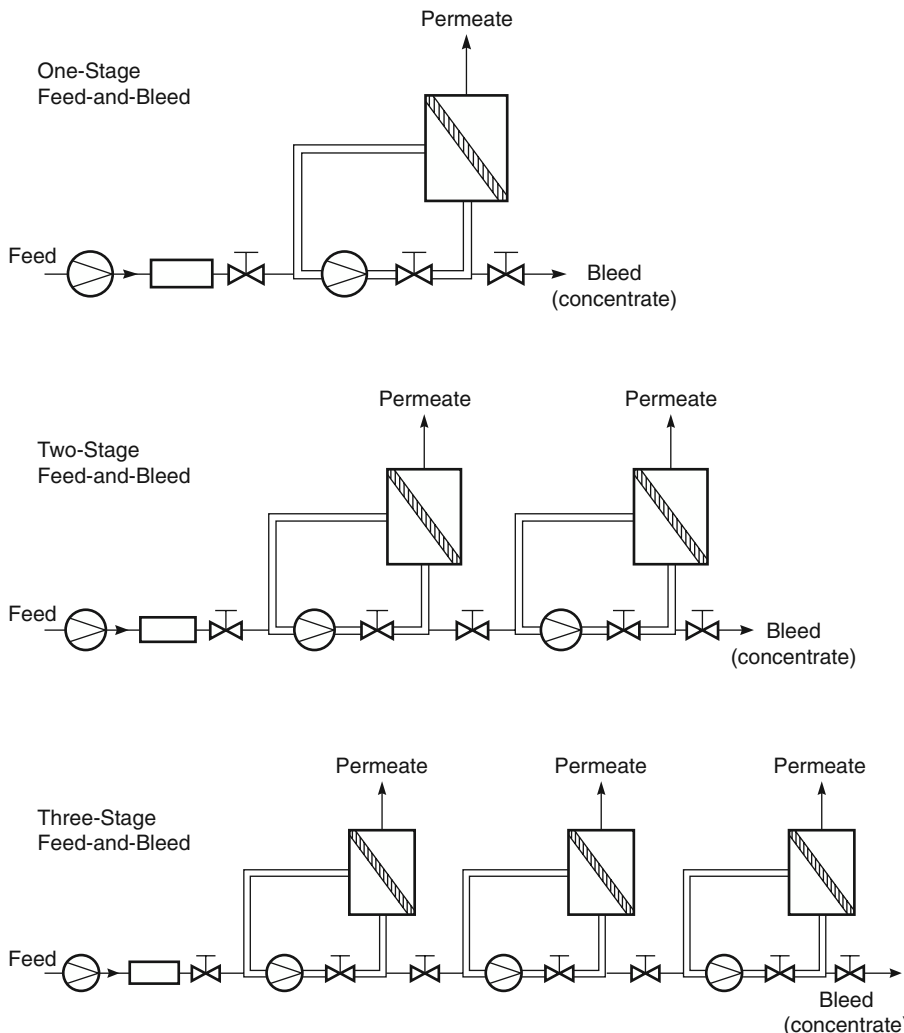


Figure 6.22 One-, two-, and three-stage feed-and-bleed systems. In general, the most efficient design is achieved when all stages have approximately the same membrane area. As the number of stages is increased, the average concentration of the solution circulating through the membrane modules decreases, and the total membrane area of the system is significantly less than for a one-stage design

membrane flux than in the one-stage unit. In fact, the membrane area of each stage is about equal, although the volume of permeate produced by each stage is very different. The two-stage feed-and-bleed design has about 60% of the area of the one-stage system. The three-stage system, which concentrates the solution in three equal-area stages – from 1 to 2% in the first stage, from 2 to 4% in the second stage, and from 4 to 8% in the third stage – is even more efficient. In this case, the total membrane area is about 40% of the area of a one-stage system performing the same separation.

Because of the significantly lower membrane areas of multistage feed-and-bleed systems, large plants may have three to five stages. The limit to the number of stages is reached when the reduction in membrane area does not offset the increase in complexity of the system. Also, because of the high fluid circulation rates involved in feed-and-bleed ultrafiltration plants, the cost of pumps can rise to 30–40% of the total cost of the system. Electricity to power the pumps is also a significant operating expense.

6.5.3 Applications of Cross-Flow Membrane Modules

In the 1960s and early 1970s, it was thought that ultrafiltration would be widely used to treat industrial and municipal wastewater. This application was slow to materialize primarily because membrane fouling made the technology too expensive and unreliable. Until the 1990s, ultrafiltration was limited to fixed pressure cross-flow systems used to treat small, concentrated waste streams from particular point sources before they were mixed with general sewer streams. Ultrafiltration was also used if the value of the components to be separated was sufficient to offset the cost of the process. Examples of this type of application exist in food processing, in which the ultrafiltered concentrate is used to produce a high-value product, or in the production of ultrapure water in the electronics industry.

The cost of industrial cross-flow ultrafiltration plants varies widely, depending on the size of the plant, the type of solution to be treated, and the separation to be performed. In general, industrial ultrafiltration plants are much smaller than reverse osmosis systems. Typical flow rates are 1000–10 000 m³/day, 1/10th that of the average reverse osmosis plant. Rogers [28] compiled the costs shown in Figure 6.23 that, adjusted for inflation, still seem reasonable. For typical plants treating 1000–10 000 m³/day of feed solution, the capital cost is in the range US\$500–1000 m³/day capacity. The typical

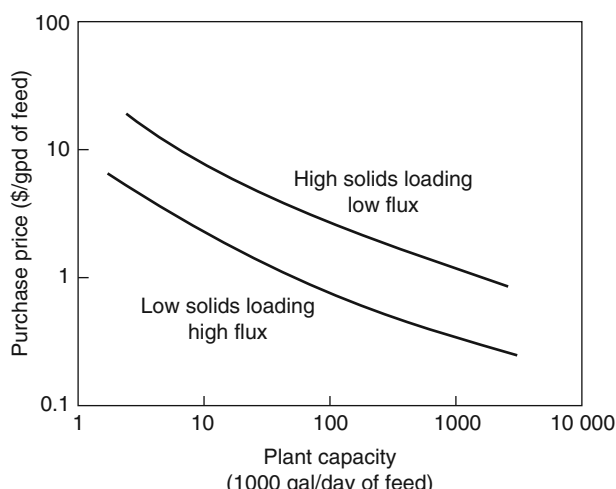


Figure 6.23 Purchase price in 2010 dollars for ultrafiltration plants as a function of plant capacity. Data of Rogers corrected for inflation. Reprinted with permission from [35]. Copyright (1984) Elsevier.

Table 6.1 Typical ultrafiltration capital and operating cost breakdown [29]

Capital Costs	Percentage
Pumps	30
Membrane modules	20
Module housings	10
Pipes, valves, frame	20
Controls/other	20
Total	100
Operating Costs	
Membrane replacement	20–40
Cleaning costs	10–30
Energy	30–40
Labor	15
Total	100

breakdown of these costs is shown in Table 6.1 [29]. Operating costs will normally be US\$750–1000/m³/day capacity, with membrane module replacement costs about 20–40%, and energy costs for the recirculation pumps 30–40%, depending on the system design.

The current food and industrial cross-flow ultrafiltration market excluding water treatment is approximately US\$400 million/year, but because the market is very fragmented, no individual segment is more than about US\$50 million/year. Also, each of the diverse applications use membranes, modules, and system designs tailored to the particular industry served. The result is little product standardization, many custom-built systems, and high costs compared to reverse osmosis. The first large successful application was the recovery of electrocoat paint in automobile plants. Later, a number of significant applications developed in the food industry [30, 31], first in the production of cheese, then in the production of apple and other juices and, more recently, in the production of beer and wine. Industrial wastewater and process water treatment is a growing application, but high costs limit growth. An overview of ultrafiltration applications is given in Cheryan and Alvarez's review article [31], Cheryan's book [32], and the book of Zeman and Zydny [27].

6.5.3.1 Paint Electrocoating

In the 1960s, automobile companies began to use electrodeposition of paint on a large scale. The paint solution is an emulsion of charged paint particles. The metal piece to be coated is made into an electrode of opposite charge to the paint particles and is immersed in a large tank of the paint. When a voltage is applied between the metal part and the paint tank, the charged paint particles migrate under the influence of the voltage and are deposited on the metal surface, forming a coating over the entire wetted surface of the metal part. After electrodeposition, the piece is removed from the tank and rinsed to remove excess paint, after which the paint is cured in an oven.

The rinse water from the washing step rapidly becomes contaminated with excess paint, while the stability of the paint emulsion is gradually degraded by ionic impurities

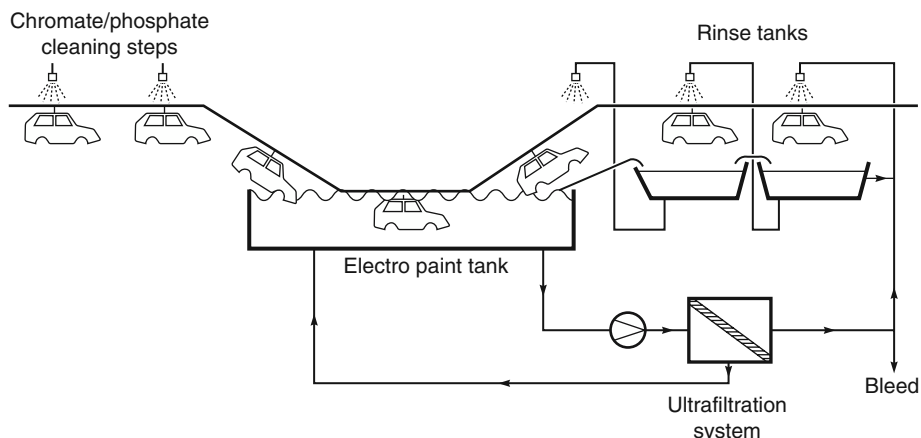


Figure 6.24 Flow schematic of an electrocoat paint ultrafiltration system. The ultrafiltration system removes ionic impurities from the paint tank carried over from the chromate/phosphate cleaning steps and provides clean rinse water for the countercurrent rinsing operation

carried over from the cleaning operation before the paint tank. Both of these problems are solved by using the ultrafiltration system shown in Figure 6.24. The ultrafiltration plant takes paint solution containing 15–20% solids and produces a clean permeate containing the ionic impurities, but no paint particles (which is sent to the countercurrent rinsing operation), and a slightly concentrated paint to be returned to the paint tank. A portion of the ultrafiltration permeate is bled from the tank and replaced with water to maintain the ionic balance of the process.

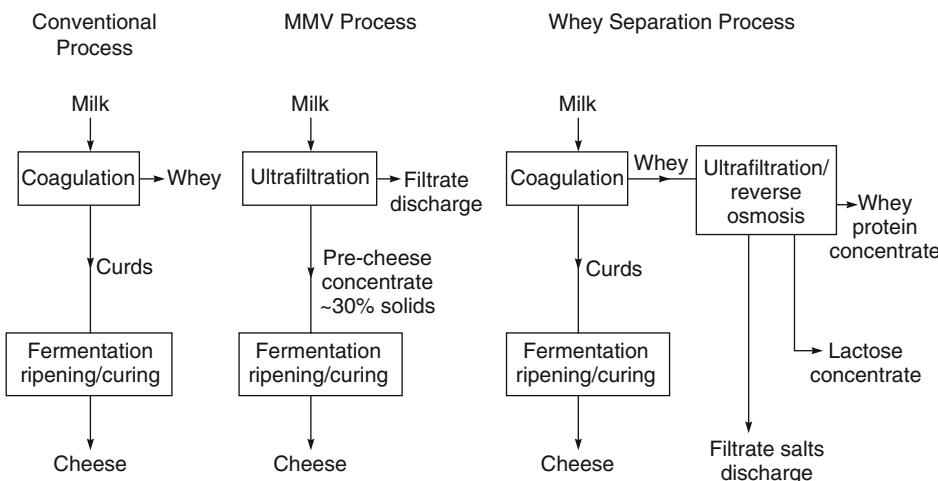
Electrocoat paint is a challenging feed solution for an ultrafiltration process. The solids content of the solution is high, typically 15–20 wt%, so a gel layer easily forms on the membrane. Gel formation results in relatively low fluxes, generally 20–30 l/m²·h. However, the value of the paint recovered from the rinse water and elimination of other rinse-water cleanup steps, made the ultrafiltration process an immediate success when introduced by Abcor. Tubular modules were used in the first plants [7] and are still installed in many electrocoat operations, although capillary and some spiral-wound modules are used in newer plants. The first electrocoat paint was cathodic because the latex emulsion particles carried a negative charge. These emulsions were best treated with membranes having a slight negative charge to minimize fouling. Anionic latex paints carrying a positive charge were introduced in the late 1970s. Ultrafiltration of these paints required development of membranes carrying a slight positive charge.

6.5.3.2 Food Industry Applications

Cheese Production. Ultrafiltration has found a major application in the production of cheese; the technology is now widely used throughout the dairy industry. During cheese production, the milk is coagulated (or curdled) by precipitation of the milk proteins. The solid that forms (curd) is sent to the cheese fermentation plant. The supernatant liquor (whey) represents a disposal problem. The compositions of milk and whey are shown in Table 6.2. Whey contains most of the dissolved salts and sugars present in the original

Table 6.2 Composition of milk and cheese whey

Component (wt%)	Milk	Whey
Total solids	12.3	7.0
Protein	3.3	0.9
Fat	3.7	0.7
Lactose/other carbohydrates	4.6	4.8
Ash	0.7	0.6

**Figure 6.25** Simplified flow schematic showing the traditional cheese production method, and two new methods using ultrafiltration to increase the production of useful products

milk and about 25% of the original protein. In the past, whey was often discharged to the sewer because its high salt and lactose content makes direct use as a food supplement difficult. Now most of the whey produced in the United States is processed to recover the protein value and reduce troublesome waste disposal problems. The traditional cheese production process and two newer processes using ultrafiltration membranes are shown in Figure 6.25.

The objective of the two membrane processes shown in Figure 6.25 is to increase the fraction of milk proteins used as cheese or some other useful product and to reduce the waste disposal problem represented by the whey. In the MMV process, named after the developers Maubois, Mocquot, and Vassal [33], whole or skimmed milk is concentrated three- to fivefold to produce a pre-cheese concentrate that can be used directly to produce soft cheeses and yogurt. Typically, the total solids level of the concentrate is about 30–35%, containing 12–17% protein. This protein concentration is sufficient for soft cheeses (Camembert, Mozzarella, and Feta) but cannot be used directly to produce hard cheeses (Cheddar and Swiss), for which protein levels of 25% are required. When ultrafiltration is used, increased milk protein utilization increases cheese production by approximately 10%, so the process has been widely adopted.

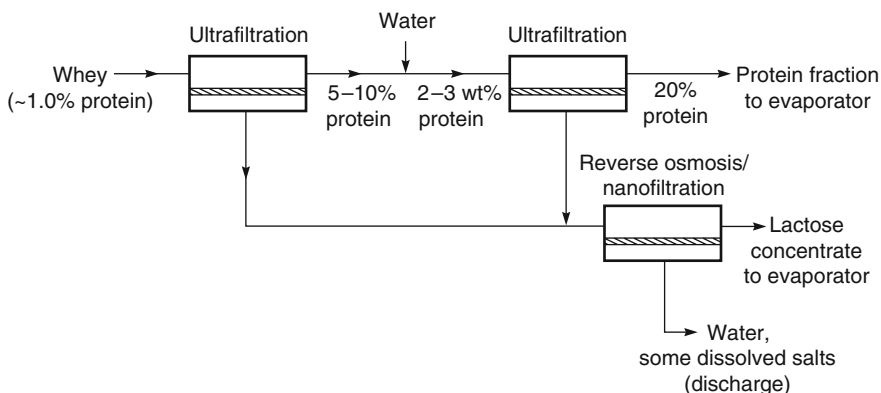


Figure 6.26 Simplified flow schematic of an ultrafiltration/reverse osmosis process to extract proteins and lactose from cheese whey. In this process, a two-step ultrafiltration unit is used to remove all the lactose and salt from the concentrated protein product to be sent to an evaporator to make dry protein

The second whey separation process uses both ultrafiltration and reverse osmosis to obtain useful protein from the whey produced in the traditional cheese manufacturing process. A flow schematic of a combined ultrafiltration/reverse osmosis process is shown in Figure 6.26. The goal is to separate the whey into three streams, the most valuable of which is the concentrated protein fraction stripped of salts and lactose. Raw whey has a high lactose concentration, so before the whey protein can be used as a concentrate, the protein concentration must be increased to at least 60–70% on a dry basis, and the lactose content reduced by 95%. The objective of the ultrafiltration membrane step is to concentrate the protein as much as possible, to minimize evaporator drying costs and to simultaneously remove the lactose. These two objectives are difficult to meet in a single ultrafiltration step because of the reduction in flux at the very high volume reduction required to achieve sufficient lactose removal. Therefore, whey plants commonly use an ultrafiltration step to achieve a 5- to 10-fold volume reduction and remove most of the lactose, after which the feed is diluted with water and reconcentrated in a second step which removes the remaining lactose. Most whey plants use spiral-wound ultrafiltration modules in multistage feed-and-bleed systems. Sanitary spiral-wound module designs are used to eliminate stagnant areas in the module housing, and the entire plant is sterilized daily with hot high- and low-pH cleaning solutions. This harsh cleaning treatment significantly reduces membrane lifetime.

Although whey protein products have several food uses, the lactose contained in the permeate is less valuable, and many plants discharge the permeate to a biological wastewater treatment plant. A few plants recover lactose as dry lactose sugar, as shown in Figure 6.26. Some plants also ferment the lactose concentrate to make ethanol. An introduction to membrane ultrafiltration in cheese production is given by Kosikowski [34].

Clarification of Fruit Juices. Apple, pear, orange, and grape juices are all clarified by ultrafiltration. Ultrafiltration of apple juice is a particularly successful application. Several hundred plants have been installed, and almost all US apple juice is clarified by this method. In the traditional process, crude filtration was performed directly after

crushing the fruit. Pectinase was added to hydrolyze pectin, which reduced the viscosity of the juice before it was passed through a series of decantation and diatomaceous filtration steps to yield clear juice with a typical yield of about 90%. By replacing these final filtration steps with ultrafiltration, a good-quality, almost-sterile product can be produced with a yield of almost 97% [34, 35].

Ultrafiltration membranes with a molecular weight cut-off of 10 000–50 000, packaged as tubular or capillary hollow fiber modules, are generally used. The initial feed solution is quite fluid, but in this application almost all of the feed solution is forced through the membrane, and overall concentration factors of 50 are normal. This means that the final residue solution is concentrated and viscous, so the solution is usually filtered at 50–55°C. Operation at this temperature also reduces bacterial growth. A flux-versus-concentration factor curve produced in this type of application is shown in Figure 6.27. As the concentration of the residue rises, the flux falls dramatically.

6.5.3.3 Industrial Oil–Water Emulsions

Oil–water emulsions are widely used in metal machining operations to provide lubrication and cooling. Although recycling of the fluids is widely practiced, spent waste streams are produced. Using ultrafiltration to recover the oil component and allow safe discharge of the water makes good economic sense. In large, automated machining operations such as automobile plants, steel rolling mills, and wire mills, a central ultrafiltration system may process up to 500 m³/day of waste emulsion. These are relatively sophisticated plants that operate continuously using several ultrafiltration feed-and-bleed stages in series. At the other end of the scale are small systems dedicated to single machines,

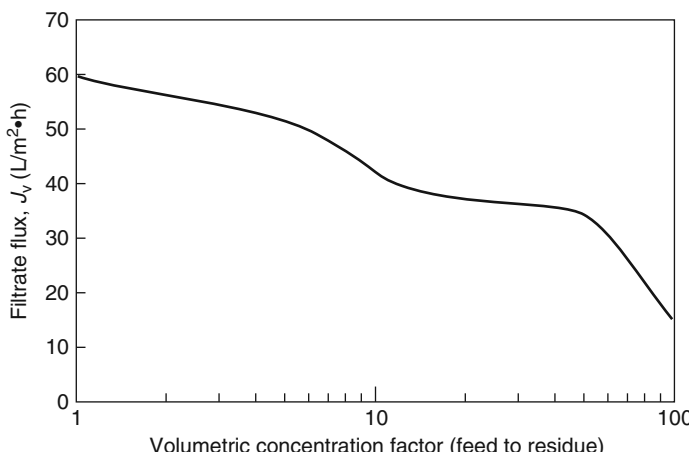


Figure 6.27 Ultrafiltration flux in apple juice clarification as a function of the volumetric feed-to-residue concentration factor. Tubular polysulfone membranes are used at 55°C [35]. R.G. Blanck and W. Eykamp, "Fruit juice ultrafiltration," in Recent Advances in Separation Techniques – III, N.N. Li (ed.), AIChE Symposium Series Number 250, 82 (1986). R.G. Blanck and W. Eykamp, "Fruit Juice Ultrafiltration," in Recent Advances in Separation Techniques-III, N.N. Li, (ed.), AIChE Symposium Series Number 250, 82 (1986). Reproduced by permission of the American Institute of Chemical Engineers. Copyright © 1986 AIChE. All rights reserved.

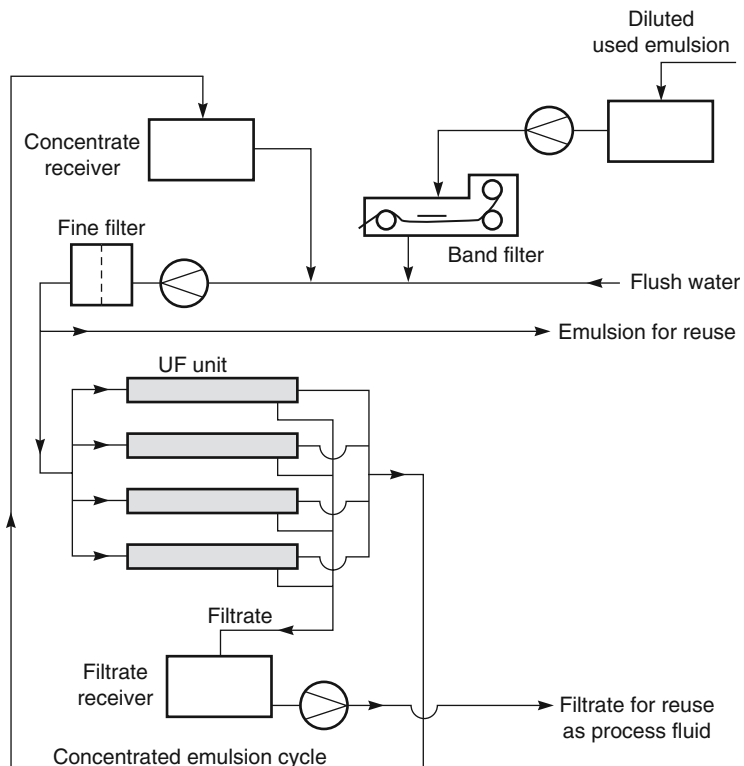


Figure 6.28 Flow diagram of a feed-and-bleed ultrafiltration unit used to concentrate a dilute oil emulsion

which process only a few gallons of emulsion per hour. The principal economic driver for users of small systems is the avoided cost of waste hauling. For larger systems, the value of the recovered oil and associated chemicals are important. In both cases, tubular or capillary hollow fiber modules are generally used because of the high fouling potential and widely variable composition of emulsified oils. A flow diagram of an ultrafiltration system used to treat large volumes of machine oil emulsions is shown in Figure 6.28. The dilute, used emulsion is filtered to remove metal cuttings and is then circulated through a feed-and-bleed ultrafiltration system, producing a concentrated emulsion for reuse and a dilute filtrate that can be discharged or reused.

6.5.3.4 Process Water and Product Recycling

Ultrafiltration has been applied to a number of process and product recycling operations. Typical applications include cleaning and recycling hot water used in food processing applications, recovery of latex particles contained in wastewater produced in production of latex paints [36, 37], and recovery of poly(vinyl alcohol) (PVA) sizing agents used as process aids in synthetic fabric weaving operations [36]. The economic driving force for the applications can come from a number of sources:

- **Water recovery.** Depending on the plant's location, reduced municipal water costs can produce savings in the US\$0.5–1.0/m³ range.
- **Heat recovery.** Many process streams are hot. Ultrafiltration usually works better with hot feeds, so hot feed solutions are not a problem. If the hot, clean permeate can be recycled without cooling, the energy savings can be considerable. If the water is 50°C above ambient temperature, the energy savings amount to about US\$1.00/m³.
- **Avoided water treatment costs.** These costs will vary over a wide range depending on the process. For a food processing plant, they are likely to be relatively modest – perhaps only US\$0.50/m³ or less – but treating latex emulsion plant effluents (called white water) can cost as much as US\$2–3/m³ or more.
- **Product recovery value.** If the product concentrated by the ultrafiltration process can be recovered and reused in the plant, this is likely to be the most important credit.

A typical example of a process water and product recycling application, shown in Figure 6.29, is the recovery of PVA sizing agent. In this application, all economic drivers listed above contribute to the total plant economics. The feed stream is produced in fabric weaving when the fiber is dipped into a solution of PVA to increase its strength. After weaving, the PVA is removed in a desizing wash bath. The solution produced in this bath is hot (55°C) and contains 0.5–1.0% PVA. The purpose of the ultrafiltration unit is to concentrate the PVA so it can be recycled to the sizing bath and to send the reclaimed, hot clean permeate back to the desizing bath. After filtration, the PVA solution is relatively particulate-free and quite viscous, so spiral-wound modules are used to reduce costs. For very small plants with flows of less than 20 l/min, batch systems are used. However, most plants are in the 50–500 l/min range and are multistage feed-and-bleed systems, as shown in Figure 6.29. The environment is challenging for the membranes, which must be cleaned weekly with detergents to remove waxy deposits and with citric acid to remove iron scale. Even so, modules must be replaced every 12–18 months, representing a major operating cost.

6.5.3.5 Biotechnology

The application of ultrafiltration to the biotechnology industry has a long history. Developers of biological drugs were early adopters of ultrafiltration in laboratory applications to separate and concentrate all types of protein, DNA, and polypeptide products. This technology has now moved to the production scale and ultrafiltration/microfiltration membranes are widely used throughout this industry. Early membrane systems used membranes and modules already in use in the food industry, but currently, modules specifically developed for biotechnology are commonly used. van Reis and Zydny [38] have written a useful review of the membrane products used in these applications.

In a typical biotechnology application, an ultrafiltration membrane is used to separate a target protein or DNA from other materials created in a recombinant cell culture process. Typical impurities are host cell proteins and debris, a variety of enzymes and virus-like particles. Batch systems are commonly used and the volume of solution to be treated in each batch is usually only 5–25 m³, which may contain 50–500 g of pure product.

An alternative technology is preparative column chromatography, but currently, a combination of ultrafiltration and chromatography is used. A first ultrafiltration separation

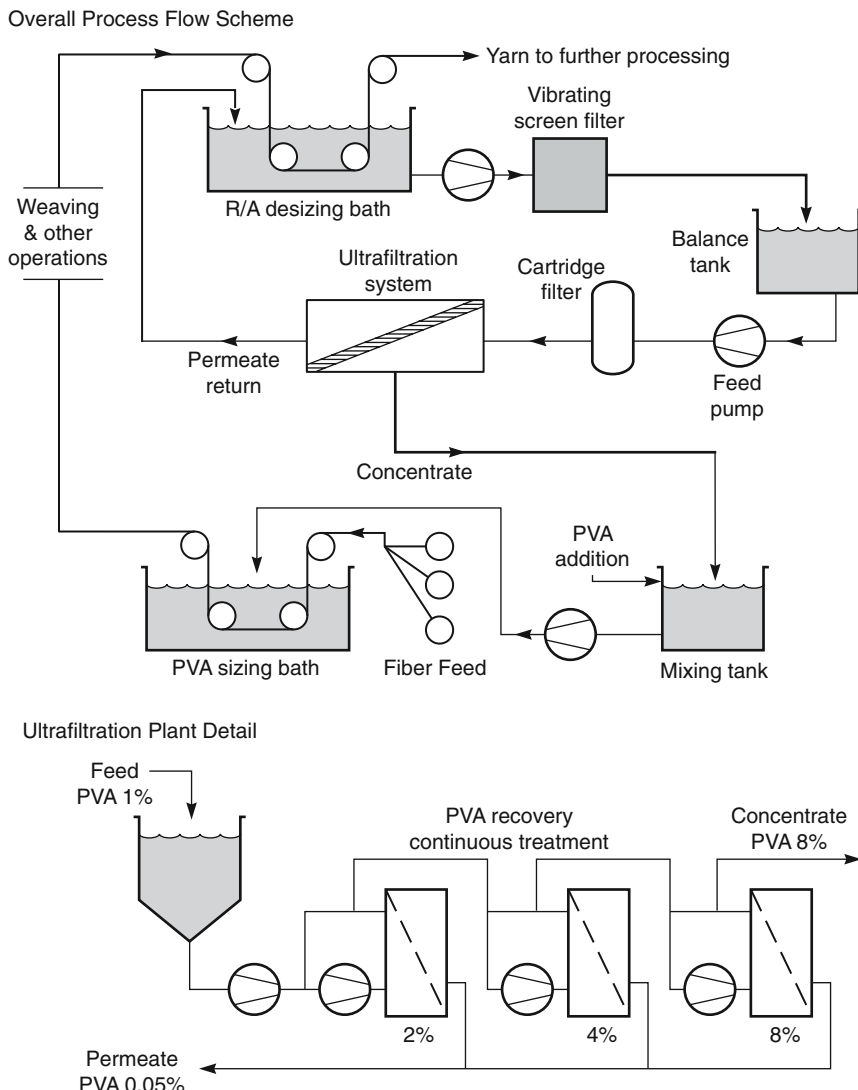


Figure 6.29 Flow schematic of a three-stage feed-and-bleed ultrafiltration system used to recover polyvinyl alcohol (PVA) sizing agents used in the production of cotton/synthetic blend fabrics [36]

is usually conducted to reduce the volume of solution and the mass of impurities. A final polishing separation using chromatography may then be used to give pure product.

In some processes where ultrafiltration is used, a particular target protein must be separated from a mixture of similar proteins. The ability of the membrane to perform the separation is often conveniently characterized by a term called the protein sieving coefficient, S , where S is simply equal to $1 - \mathbb{R}$, where \mathbb{R} is the protein rejection. In reverse osmosis, an equivalent term is called the salt passage.

The definition of the rejection coefficient in Equation 6.4 is

$$\mathbb{R} = \left(1 - \frac{c_p}{c_b} \right) \quad (6.7)$$

where c_p is the concentration of the protein in the permeate solution and c_b is the concentration in the feed. Hence, it follows that

$$S = \frac{c_p}{c_b} \quad (6.8)$$

The ability of a membrane to separate two components i and j is given by an enrichment factor

$$\gamma_{ij} = \frac{S_i}{S_j} \quad (6.9)$$

Normally, it is difficult to obtain a good separation in a single membrane step, unless components i and j are very different sizes. The trick used to overcome this problem is to choose a membrane that almost completely retains one of the components to be separated, but allows partial passage of the other components. A process called diafiltration is then used. In diafiltration, the mixed protein solution, volume V_1 , is circulated around a cross-flow ultrafiltration loop. Permeate that passes through the membrane is replaced with an equal amount of fresh solvent. The result is to wash the slightly permeable proteins through the membrane while retaining the completely rejected protein. Figure 6.30 shows the result of this process when applied to the separation of bovine serum albumin (BSA; MW = 67 000) from β -lactoglobulin (β -LG; MW = 18 000) and α -LG (MW = 14 000) [39]. The data in Figure 6.30b plot the normalized protein concentration in the feed tank as a function of the number of diafiltration volumes (V) that are collected as permeate. The concentration of the most permeable component, α -LG, decreases rapidly and less than 1% is left in the feed solution after 10 diafiltration volumes have passed through the membrane. The β -LG concentration falls less rapidly, but 75% has been removed after 10 diafiltration volumes. In contrast, the BSA concentration stays almost constant and 90% of this component remains in the retentate solution.

The dilute permeate solution is then re-concentrated by ultrafiltration with a tight membrane that retains all proteins. A second diafiltration operation is then used to separate the α - and β -LG components from the reconcentrated permeate solutions. In this case, a membrane is used that is designed to completely retain β -LG while passing a portion of the α -LG. The result of the total separation scheme is shown in Figure 6.31.

Variants of this type of process are now used by a number of biotechnology companies. Early products were highly active hormones such as insulin, human growth hormone, and erythropoietin, so small-scale equipment was used. More recently, monoclonal antibodies are being separated. These molecules act stoichiometrically by binding to a particular cell receptor. Typical drug dosing levels are much higher than with hormones, so annual production volumes can be as much as 1000 kg, and larger equipment is needed. Capillary hollow fibers and plate-and-frame module cassettes are most commonly used. Typical production equipment contains 20–200 m² of membrane, is all stainless steel, steam sterilizable, and designed to have minimum dead volume. These applications are likely to continue to grow with the increasing use of biological drug products.

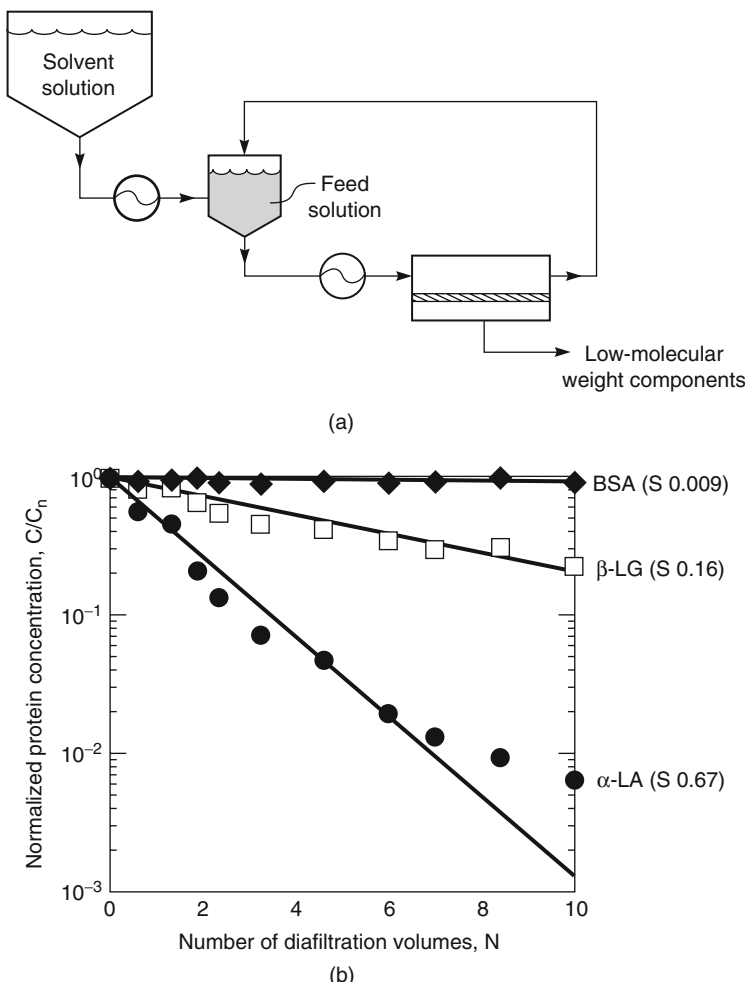


Figure 6.30 The separation of BSA from β -LG and α -LG by a batch diafiltration process. The normalized concentrations of the three proteins in the feed tank are shown as a function of the number of diafiltration volumes passing through the membrane [39]

6.6 Constant Flux Modules, System Design, and Applications

6.6.1 Constant Flux/Variable Pressure Modules

The development of constant flux/variable pressure operations beginning in about 1995 transformed the applications of ultrafiltration membranes and led to radically different module and system designs. The most important change was the development of submerged membrane modules, in which a constant flux was maintained by a variable speed pump sucking the permeate through the membrane. Membrane fouling in these modules was controlled by a combination of air sparging and regular backflushing. These developments began in the late 1980s when Kazuo Yamamoto and his coworkers began

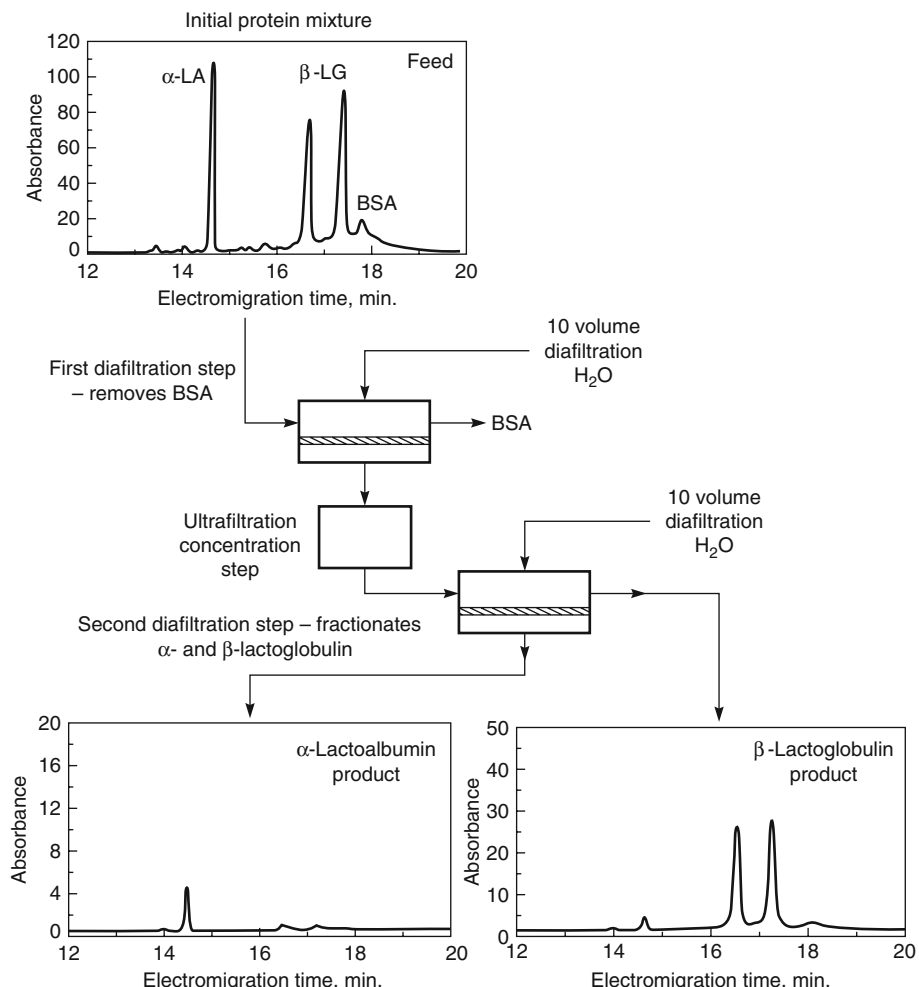


Figure 6.31 A two-stage membrane ultrafiltration/diafiltration scheme to separate α -LG, β -LG, and BSA [39]

the development of submerged hollow fiber membranes for sewage treatment [9]. Initially, these units consisted of looped hanks of hollow fibers immersed in the substrate solutions. Fouling was a serious problem, but Yamamoto showed that regular air sparging went a long way toward controlling fouling. Yamamoto's work was soon followed up by Kubota and Mitsubishi Rayon in Japan and Zenon in Canada. The total submerged membrane market now comfortably exceeds US\$2 billion and is growing rapidly [40].

6.6.2 Submerged Membrane Modules and System Design

The two most common types of submerged modules are shown in Figure 6.32 [40, 41]. Hollow fiber (capillary) modules were developed by Zenon, Memtech, and Mitsubishi, while Kubota uses an array of submerged membrane plates. All of the manufacturers use

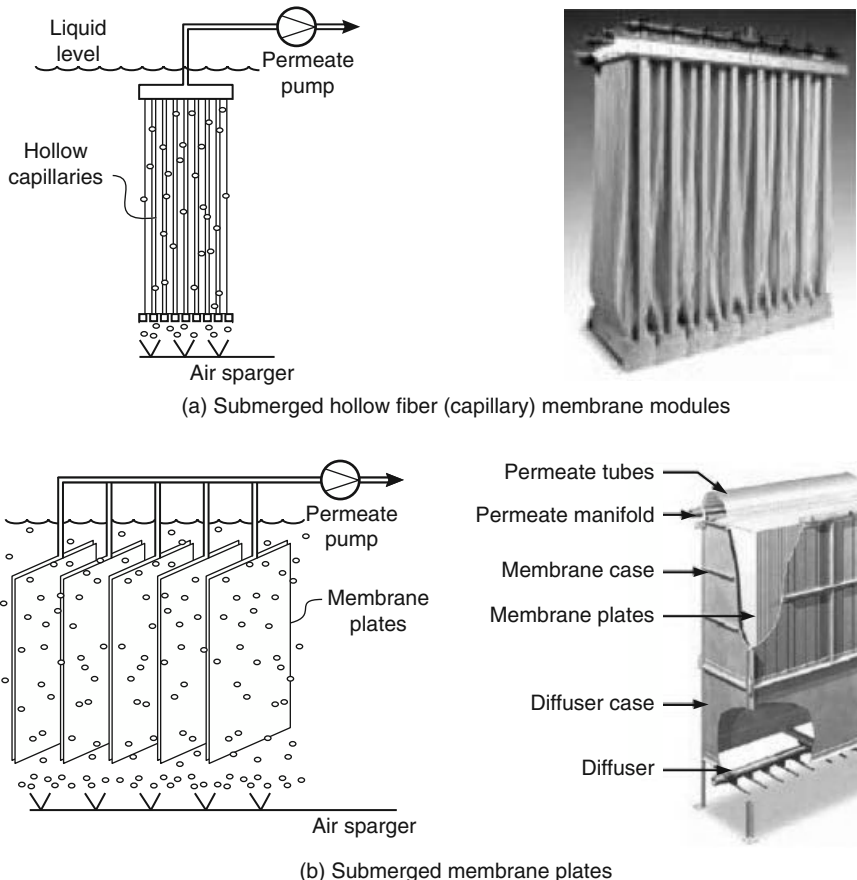


Figure 6.32 The two most common types of submerged membrane modules. Zenon, Mitsubishi, and Memcor make swayable hollow fiber (capillary) modules (a) and Kubota makes submersible plate modules (b). Air sparging is used by all manufacturers to help keep the module surfaces clean (a) Reproduced with permission from <http://workingwithwater.filtsep.com/view/24353/hollow-fibre-membrane-life-in-membrane-bioreactors/> Copyright (2012) Elsevier Ltd Last accessed 14/06/2012. (b) Reproduced with permission from <http://env.kubota.co.jp/ksmu/introduction/> Copyright (2006) Kubota Corporation Last accessed 14/06/2012.

air sparging to agitate the feed solution and scrub the membrane surface. Periodic pulses of large bubbles seem to be more effective than a continuous stream of small bubbles [42]. The capillary fiber modules are usually held loosely in between the manifolds at each end of the fiber so the fibers can sway and bubbles rise between the fiber bundles. This increases the scrubbing action and minimizes channeling. The permeate solution is usually removed from a manifold at the top of the module connected to a constant flow pump. The flow rate of this pump is usually set to maintain a flux of $10\text{--}30 \text{ l/m}^2\cdot\text{h}$, depending on the nature of the feed solution. If the solution is highly fouling, a low flow rate will be set; with low fouling feed solutions, a higher flow rate can be used. The transmembrane pressure will initially be less than 0.2 bar, but as the module is used and

slowly fouls, the pressure will rise. Most manufacturers will take the membrane off-line for chemical cleaning before the transmembrane pressure reaches about 0.5–0.8 bar.

Capillary modules are also maintained clean by automatic regular short cycle back-flushing, using 30–60 seconds every 10–20 minutes. The backflushing pressure is small, usually just enough to reverse the flow of fluid and lift off solids accumulating on the membrane surface. Typically, the back flux is one to three times the operational flux. Chemical cleaning is usually done every few days to once or twice a month, depending on the nature of the feed solution. Operation in this way can achieve membrane lifetimes of several years, even when the membranes are used in sewage treatment applications.

Kubota's plate modules are easier to keep clean by air sparging than fiber modules, but can be damaged by repeated backwashing, so backwashing is usually limited to a weekly chemical cleaning process.

The cost of submerged membranes has fallen dramatically from the time commercial systems were introduced in the early 1990s. Data reported by Judd are shown in Figure 6.33 [41]. Between 1992 and 2005, the cost of replacement modules on a per-square-meter-of-membrane basis had dropped from \$400 to less than \$50. This trend is continuing, although at a slower pace.

Concurrent with the decrease in the cost of membrane modules, the operating cost of processes using these membranes has also decreased. In part, this is because module replacement costs are lower, but also because process optimization has led to longer module replacement cycles. The operating cost of new membrane bioreactor plants using Kubota membranes is shown for the time period from 1992 to 2005 in Figure 6.34 [41, 43]. In 1992, membrane replacement was more than half of the total operating cost, while power (mostly used by the air spargers) was less than 10%. By 2005, total operating costs had come down more than 10-fold, and membrane replacement was less than 10% of the total. Power to drive air sparging is now an important contributor to operating costs, at 30–40% of the process costs. Currently, new plants consume about 1 kWh/m³ of product water, significantly more than required for a conventional bioreactor. As a consequence, development of improved ways to air sparge the membrane to reduce this power cost is a research focus for process developers.

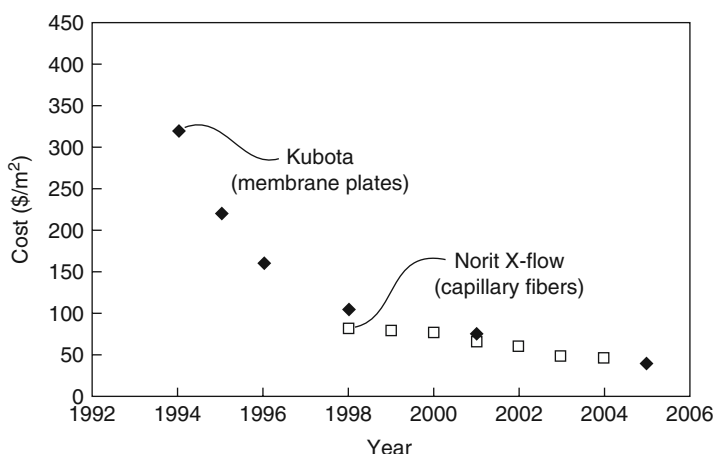


Figure 6.33 Submerged membrane replacement module costs. (Data from Judd [41].)

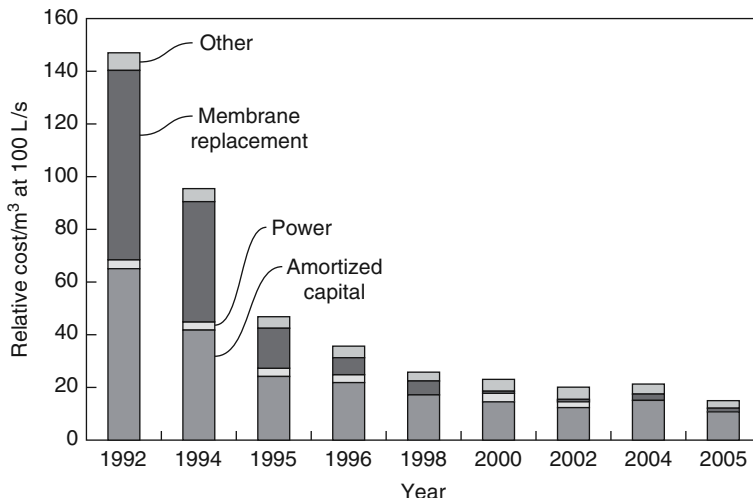


Figure 6.34 Membrane bioreactor (MBR) process operating costs (Kubota) versus time (Kennedy and Churchouse, 2005) [43]. After Judd [41]

6.6.3 Submerged Membrane Applications

The development of submerged membranes has led to a very large expansion in the size of the ultrafiltration/water treatment market. Two major applications have emerged: the first is the removal of turbidity, bacteria, viruses, and the like in municipal drinking water processing plants [44]. The feed water is relatively clean, so high fluxes and long membrane lifetimes have been achieved. The second application is in membrane bioreactors in municipal sewage treatment plants [45]. This feed water has a high level of suspended and dissolved solids and so is much more likely to foul the membrane. Nonetheless, with proper operating protocols, long membrane operating times can be achieved.

6.6.3.1 Water Treatment

Ultrafiltration/microfiltration of water to allow safe discharge or reuse has been recognized as a large potential application of membranes since the 1960s, but high capital and operating costs prohibited widespread use for a few decades. The adoption of constant flux operation reduced the capital and energy cost of the process substantially by eliminating the large recirculation pumps required for constant pressure cross-flow units. Improved fouling control using backflushing and air scrubbing has also completely changed process reliability.

The first large application of these developments was the use of ultrafiltration as a sterilizing filter to treat municipal surface water supplies [44]. A major *cryptosporidiosis* outbreak in Milwaukee, Wisconsin, in 1993 caused 100 deaths and led the EPA to mandate that better sterilization techniques be used to treat all surface water. European regulators adopted similar rules. Surface water from lakes and rivers usually has a low level of contaminants and the objective of ultrafiltration is to produce a 1000-fold

(three-decade) reduction in the level of *Giardia* and a 10 000-fold (four-decade) reduction in the level of virus contamination. This type of reduction is easily achieved by defect-free ultrafiltration membranes. It is estimated that 40 000 small water works in the United States are affected by the EPA ruling, so the potential market is very large. A related application is clarification of seawater or reclaimed water prior to treatment by a reverse osmosis plant. Again, the feed water is non-fouling, so ultrafiltration produces clear, almost sterile, water and eliminates most of the other pre-treatment steps previously used by desalination plants.

In both of these applications, because the level of fouling contaminants in the water to be treated is low, cross-flow modules of the type shown in Figure 6.35a and submerged membrane reactor modules such as those shown in Figure 6.32 can be used. The first ultrafiltration plants of this type were developed in the early 1990s [8]. The modules operated as dead-end filters for 10–20 minutes and then were backflushed with air or water for 20–30 seconds. During backflushing, the modules are swept with water to remove accumulated solids. The water is recirculated to the feed tank, after which the cycle is repeated. A photograph of one such plant is shown in Figure 6.35b. Most of these plants are fitted with capillary membrane modules; both shell and lumen side feed modules are used. Because the treated water is used as municipal drinking water, plants are carefully monitored to detect even a single broken filter that could allow unfiltered bacteria to enter the drinking water supply. A number of membrane module integrity tests have been developed [46]. These systems produce treated water that has a 10^4 - to 10^5 -fold lower level of bacteria than the feed water.

6.6.3.2 Membrane Bioreactors

Concurrently with development of water sterilization/clarification applications described above, membranes began to be used for direct filtration of water from sewage in membrane bioreactors. The first membrane bioreactors were developed by Dorr-Oliver working with Amicon in the late 1960s [47]. Cross-flow constant pressure plate-and-frame modules were used and membrane fouling was a major problem that could not be solved at that time. The development of air-sparged submerged membranes by Yamamoto *et al.* [9] and the subsequent commercial development of the processes by Kubota, Zenon, Memtech, and Mitsubishi Rayon have completely transformed the technology. The first successful plants were installed in the mid-1990s. Since then, production of dischargeable or recyclable water by direct ultrafiltration of sewage has become a well-established process. More than 2000 units have been installed at water treatment plants around the world [40, 41, 45].

A block flow diagram of a conventional biological treatment plant is shown in Figure 6.36. The plant consists of a series of unit operations. The incoming waste water is first subject to primary waste treatment where a series of screen filters and settling tanks remove large solids and grit. The clarified solution is then sent to a secondary biological treatment process. This may consist of a single aerobic biodigestion step or, as shown in Figure 6.36, a first anaerobic (anoxic) step, followed by a second aerobic step. In the anaerobic tank, a portion of the organic components present are consumed and nitrogen-containing compounds are reduced to ammonia and nitrogen. In the

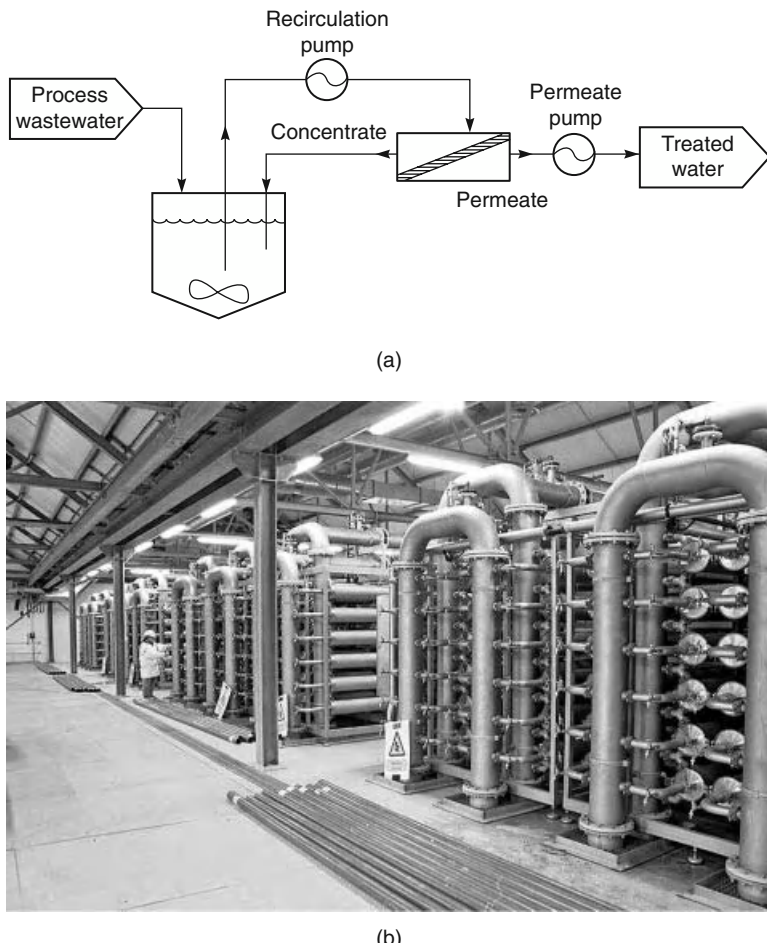


Figure 6.35 (a) Process configuration for a membrane water sterilization system. Reprinted with permission from Norit Membrane Technology BV, now part of Pentair X-flow/Pentair Process Technology and (b) photograph of a 25 million gal/day capillary hollow fiber module plant to produce potable water, installed by Norit (X-Flow) in Keldgate, UK. (Courtesy of Norit Membrane Technology BV.)

air-sparged aerobic tank that follows, the remaining organic components are removed and ammonia is converted to nitrates. Nitrogen-rich sludge that settles out in this tank is recycled to the anaerobic tank for treatment a second time. The treated water from this secondary biological step is then sent to a larger settler/filter where any suspended solids are removed. The water is then disinfected with chlorine and discharged. It can take several days for a unit of water to traverse the whole series of operations, so biological water treatment plants have a large footprint.

In a membrane bioreactor process, the submerged membranes are placed in the aerobic digestion tank [41]. The filtrate produced is clear and essentially sterile, so it can be

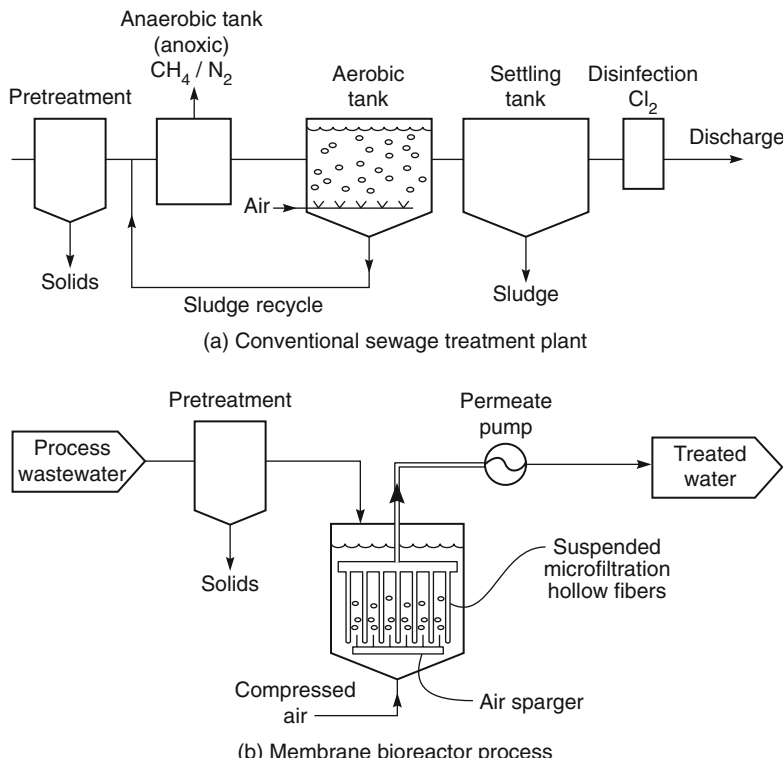


Figure 6.36 (a) Conventional sewage treatment plant and (b) membrane bioreactor process block flow diagrams. The conventional plant produces a 10- to 20-fold reduction in BOD and COD levels in the waste water; membrane bioreactor products can provide as much as 10^4 - to 10^5 -fold reductions in BOD and COD levels compared to the feed water

discharged without further treatment. The settler tanks are eliminated. Power costs for aeration of the submerged membranes are generally higher than those for conventional aerobic digesters, but these extra costs are usually more than offset by reduced footprint and far better quality of the filtrate discharged.

6.7 Conclusions and Future Directions

In the last 10 years, the use of ultrafiltration membranes has grown fivefold. The key breakthrough was the development of constant flux/variable pressure operating systems, coupled with automatic backflushing and air sparging. These innovations have gone a long way toward solving the membrane fouling problem that previously limited the applications of ultrafiltration membranes. The cost of this technology is still coming down, so submerged membrane systems are likely to gain an increasing share of the municipal water and sewage treatment market. Expansion of the technology into a host of industrial water filtration applications is also likely to take place in the next few years.

References

1. Bechhold, H. (1907) Kolloidstudien mit der filtrationsmethode. *Z. Phys. Chem.*, **60**, 257.
2. Zsigmondy, R. and Bachmann, W. (1918) Über neue filter. *Z. Anorg. Chem.*, **103**, 119.
3. Ferry, J.D. (1936) Ultrafilter membranes and ultrafiltration. *Chem. Rev.*, **18**, 373.
4. Elford, W.J. (1937) Principles governing the preparation of membranes having graded porosities. The properties of 'Gradocol' membranes as ultrafilters. *Trans. Faraday Soc.*, **33**, 1094.
5. Loeb, S. and Sourirajan, S. (1963) Sea water demineralization by means of an osmotic membrane, in *Saline Water Conversion II*, Advances in Chemistry Series, Vol. 38 (ed. R.F. Gould), American Chemical Society, Washington, DC, pp. 117–132.
6. Michaels, A.S. (1971) High flow membranes, US Patent 3,615,024, Oct. 1971.
7. Goldsmith, R.L., de Filippi, R.P., Hossain, S., and Timmins, R.S. (1971) Industrial ultrafiltration, in *Membrane Processes in Industry and Biomedicine* (ed. M. Bier), Plenum Press, New York, pp. 267–300.
8. Kolega, M., Grohmann, G.S., Chiew, R.F., and Day, A.W. (1991) Disinfection and clarification of treated sewage by advanced microfiltration. *Water Sci. Technol.*, **23**, 1609.
9. Yamamoto, K., Hiasa, M., and Mahmood, T. (1989) Direct solid-liquid separation using hollow fiber membrane in an activated sludge aeration tank. *Water Sci. Technol.*, **21**, 43.
10. Ishida, H., Yamada, Y., Izumi, K., and Moro, M. (1993) Apparatus for treating activated sludge and method of cleaning it. US Patent 5,192,456, Mar. 1993.
11. Mahendran, M., Rodrigues, C.F.F., and Pedersen, S.K. (1997) Vertical skein of hollow fiber membranes and method of maintaining clean fiber surfaces while filtering a substrate to withdraw a permeate. US Patent 5,639,373, June 1997.
12. Baker, R.W. and Strathmann, H. (1970) Ultrafiltration of macromolecular solutions with high-flux membranes. *J. Appl. Polym. Sci.*, **14**, 1197.
13. Belfort, G., Davis, R.H., and Zydny, A.L. (1994) The behavior of suspensions and macromolecular solutions in cross flow microfiltration. *J. Membr. Sci.*, **96**, 1.
14. Porter, M.C. (1972) Concentration polarization with membrane ultrafiltration. *Ind. Eng. Chem. Prod. Res. Dev.*, **11**, 234.
15. Jonsson, G. and Boesen, C.E. (1984) Polarization phenomena in membrane processes, in *Synthetic Membrane Processes* (ed. G. Belfort), Academic Press, Orlando, FL, pp. 100–130.
16. Kleinstreuer, C. and Belfort, G. (1984) Mathematical modeling of fluid flow and solute distribution in pressure-driven membrane modules, in *Synthetic Membrane Processes* (ed. G. Belfort), Academic Press, Orlando, FL, pp. 131–190.
17. Walker, R. (1982) Recent developments in ultrafiltration of electrocoat paint. *Electrocoat*, **82**, 1.
18. Wang, Z., Wu, Z., Yu, G., Liu, J. and Zhou, Z. (2006) Relationship between sludge characteristics and membrane flux determination in submerged membrane bioreactors. *J. Membr. Sci.*, **284**, 87.

19. Le-Clech, P., Chen, V., and Fane, A.G. (2006) Fouling in membrane bioreactors used in wastewater treatment. *J. Membr. Sci.*, **284**, 17.
20. Feld, R.W., Wu, D., Howell, J.A., and Gupta, B.B. (1995) Critical flux concept for microfiltration fouling. *J. Membr. Sci.*, **100**, 259.
21. Chen, V., Fane, A.G., Madaeni, S., and Wenten, I.G. (1997) Particle deposition during membrane filtration of colloids: transition between concentration polarization and cake formation. *J. Membr. Sci.*, **125**, 109.
22. Porter, M.C. (1990) Ultrafiltration, in *Handbook of Industrial Membrane Technology* (ed. M.C. Porter), Noyes Publications, Park Ridge, NJ, pp. 136–259.
23. McDonogh, R.M., Gruber, T., Stroh, N., Bauser, H., Walitza, E., Chmiel, H. and Strathmann, H. (1992) Criteria for fouling layer disengagement during filtration of feed containing a wide range of solutes. *J. Membr. Sci.*, **73**, 181.
24. Baker, R.W. (1969) Method of fractionating polymers by ultrafiltration. *J. Appl. Polym. Sci.*, **13**, 369.
25. Breslau, B.R., Testa, A.J., Milnes, B.A., and Medjanis, G. (1980) Advances in hollow fiber ultrafiltration technology, in *Ultrafiltration Membranes and Applications* (ed. A.R. Cooper), Plenum Press, New York, pp. 109–128.
26. Culkin, B., Plotkin, A., and Monroe, M. (1998) Solve membrane fouling with high-shear filtration. *Chem. Eng. Prog.*, **94**, 29.
27. Zeman, L.J. and Zydny, A.L. (1996) *Microfiltration and Ultrafiltration: Principles and Applications*, Marcel Dekker, New York.
28. Rogers, A.N. (1984) Economics of the application of membrane processes, in *Synthetic Membrane Processes* (ed. G. Belfort), Academic Press, Orlando, FL, pp. 437–476.
29. Eykamp, W. (1995) Microfiltration and ultrafiltration, in *Membrane Separation Technology: Principles and Applications* (eds R.D. Noble and S.A. Stern), Elsevier Science, Amsterdam, pp. 1–40.
30. Breslau, B.R., Larsen, P.H., Milnes, B.A., and Waugh, S.L. (1988) The application of ultrafiltration technology in the food processing industry. The 1988 6th Annual Membrane Technology/Planning Conference, Cambridge, MA, November 1988.
31. Cheryan, M. and Alvarez, F.R. (1995) Food and beverage industry applications, in *Membrane Separation Technology: Principles and Applications* (eds. R.D. Noble and S.A. Stern), Elsevier Science, Amsterdam, pp. 415–460.
32. Cheryan, M. (1998) *Ultrafiltration and Microfiltration Handbook*, Technomic Publishing Co., Lancaster, PA, p. 445.
33. Maubois, J.L., Mocquot, G., and Vassal, L. (1980) Preparation of cheese using ultrafiltration. US Patent 4,205,080.
34. Kosikowski, F.V. (1986) Membrane separations in food processing, in *Membrane Separations in Biotechnology* (ed. W.C. McGregor), Marcel Dekker, New York, pp. 201–254.
35. Blanck, R.G. and Eykamp, W. (1986) Fruit juice ultrafiltration, in *Recent Advances in Separation Techniques – III*, AIChE Symposium Series, Vol. 250 (ed. N.N. Li), AIChE, New York, p. 82.
36. Mir, L., Eykamp, W., and Goldsmith, R.L. (1977) Current and developing applications for ultrafiltration. *Ind. Water Eng.*, **14**, 1.

37. Breslau, B.R. and Buckley, R.G. (1992) The ultrafiltration of 'Whitewater', an application whose time has come! The 1992 10th Annual Membrane Technology/Separations Planning Conference, Newton, MA, October 1992.
38. van Reis, R. and Zydny, A. (2007) Bioprocess membrane technology. *J. Membr. Sci.*, **297**, 16.
39. Cheang, B. and Zydny, A.L. (2004) A two-stage ultrafiltration process for fractionation of whey protein isolate. *J. Membr. Sci.*, **231**, 159.
40. Fane, A.G. (2008) Submerged membranes, in *Advanced Membrane Technology and Applications* (eds N.N. Li, A.G. Fane, W.S.W. Ho, and T. Matsuura), John Wiley & Sons, Inc., Hoboken, NJ, pp. 239–270.
41. Judd, S. (2006) *The MBR Book: Principles and Applications of Membrane Bioreactors in Water and Wastewater Treatment*, Elsevier Ltd, Oxford.
42. Cui, Z.F., Chang, S., and Fane, A.G. (2003) The use of gas bubbling to enhance membrane processes. *J. Membr. Sci.*, **221**, 1.
43. Kennedy, S. and Churchouse, S.J. (2005) Progress in membrane bioreactors: new advances. Proceedings of the Water and Wastewater Europe Conference, Milan.
44. Côté, P., Liu, M., and Siverns, S. (2008) Water reclamation and desalination by membranes, in *Advanced Membrane Technology and Applications* (eds N.N. Li, A.G. Fane, W.S.W. Ho, and T. Matsuura), John Wiley & Sons, Inc., Hoboken, NJ, pp. 171–188.
45. Yang, W., Cicek, N., and Ilg, J. (2006) State-of-the-art of membrane bioreactors: worldwide research and commercial applications in North America. *J. Membr. Sci.*, **270**, 201.
46. Farahbakhsh, K., Adham, S.S., and Smith, D.W. (2003) Monitoring the integrity of low-pressure membranes. *J. AWWA*, **95**, 95.
47. Okey, R.W. and Stavenger, P.L. (1966) Reverse osmosis applications in industrial wastewater treatment. Membrane Processes for Industry Proceedings of the Symposium, Southern Research Institute, Birmingham, AL, May 19–20, 1966.

7

Microfiltration

7.1 Introduction and History

Microfiltration refers to filtration processes that use porous membranes to separate suspended particles with diameters between 0.1 and 10 µm. Thus, microfiltration membranes fall between ultrafiltration membranes and conventional filters. Like ultrafiltration, microfiltration has its modern origins in the development of collodion (nitrocellulose) membranes in the 1920s and 1930s. In 1926, Membranfilter GmbH was founded and began to produce collodion microfiltration membranes commercially. The market was very small, but by the 1940s, other companies including Sartorius and Schleicher and Schuell, were producing similar membrane filters.

The first large-scale application of microfiltration membranes was in laboratory tests to culture microorganisms in drinking water; this remains a significant application. The test was developed in Germany during World War II, as a rapid method to monitor the water supply for contamination. Established test methods required water samples to be cultured for at least 96 hours. Mueller and others at Hamburg University devised a method in which a liter of water was filtered through a Sartorius microfiltration membrane. Any bacteria in the water were captured by the filter, and the membrane was then placed on a pad of gelled nutrient solution for 24 hours. The nutrients diffused to the trapped bacteria on the membrane surface, allowing them to grow into colonies large enough to be easily counted under a microscope. After the war there was no US supplier of these membranes, so in 1947, the US Army sponsored a program by Goetz at CalTech to duplicate the Sartorius technology. The membranes developed there were made from a blend of cellulose acetate and nitrocellulose, and were formed by controlled precipitation with water from the vapor phase. This technology was passed to the Lowell Chemical Company, which in 1954 became the Millipore Corporation, producing the Goetz membranes on a commercial scale. Over the next 40 years, Millipore became the largest microfiltration company. Membranes made from a number of noncellulosic materials, including poly(vinylidene fluoride), polyamides, polyolefins, and poly(tetrafluoroethylene), have been developed by

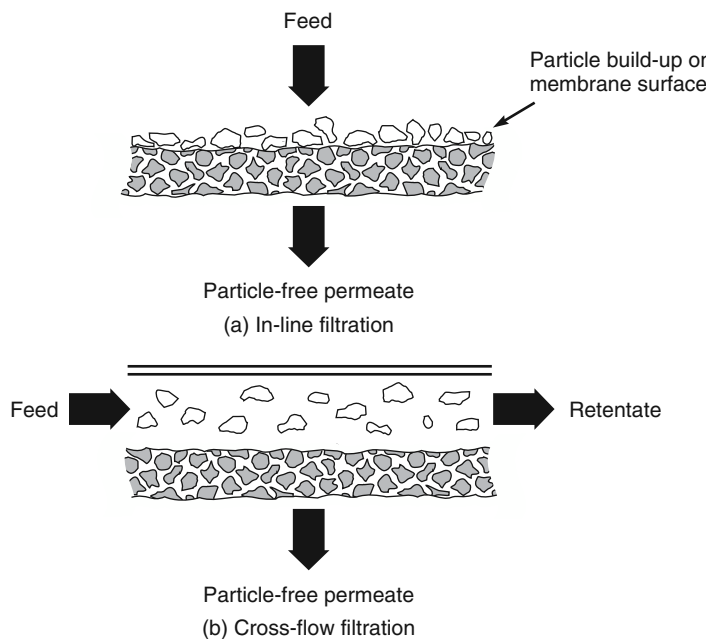


Figure 7.1 Schematic representation of (a) in-line and (b) cross-flow filtration with microfiltration membranes. The equipment used for in-line filtration is simple, but retained particles plug the membrane rapidly. The equipment required for cross-flow filtration is more complex, but the membrane lifetime is longer

Millipore and others. Nonetheless, the cellulose acetate/cellulose nitrate blend membrane remains a widely used microfilter.

Until the mid-1960s, the use of microfiltration membranes was confined to laboratory or to very small-scale industrial applications. The introduction of pleated membrane cartridges by Gelman in the 1970s was an important step forward, and made possible the use of microfiltration membranes in industrial applications. In the 1960s and 1970s, microfiltration became important in biological and pharmaceutical manufacturing, as did microfiltration of air and water in the production of microelectronics in the 1980s. The production of low-cost, single-use, disposable cartridges for pharmaceutical and electronics processes now represents a major part of the microfiltration industry. In most applications of microfiltration in these industries, trace amounts of particles are removed from solutions that are already very clean. The most widely used process design, illustrated in Figure 7.1a, is dead-end or in-line filtration, in which the entire fluid flow is forced through the membrane under pressure. As particles accumulate on the membrane surface or in its interior, the pressure required to maintain the required flow increases, until at some point the membrane must be replaced. In the 1970s, an alternative process design known as cross-flow filtration, illustrated in Figure 7.1b, began to be used.

In cross-flow systems, the feed solution is circulated across the surface of the filter, producing two streams: a clean particle-free permeate and a concentrated retentate

containing the particles. The equipment required for cross-flow filtration is more complex, but the membrane lifetime is longer than with in-line filtration. The commercial availability of ceramic tubular cross-flow filters from Membralox (now a division of US Filter), starting in the mid-1980s, increased the application of cross-flow filtration, particularly to solutions with high particle concentrations. Streams containing less than 0.1% solids are almost always treated with in-line filters; streams containing 0.5% or more solids are almost always treated with cross-flow filters. Between these two limits, both in-line and cross-flow systems can be used, depending on the particular characteristics of the application.

In the last few years, a third type of microfiltration operating system called semi-dead-end filtration has emerged. In these systems, the membrane unit is operated as a dead-end filter until the pressure required to maintain a useful flow across the filter reaches its maximum level. At this point, the filter is operated in cross-flow mode, while concurrently backflushing with air or permeate solution. After a short period of backflushing in cross-flow mode to remove material deposited on the membrane, the system is switched back to dead-end operation. This procedure is particularly applicable in microfiltration units used as final bacterial and virus filters for municipal water treatment plants. The feed water has a very low loading of material to be removed, so in-line operation can be used for a prolonged time before backflushing and cross-flow to remove the deposited solids is needed.

Beginning in 1990–1993, the first microfiltration/ultrafiltration systems began to be installed to treat municipal drinking water obtained from surface water and in membrane bioreactors in sewage treatment plants. For the most part, this equipment uses ultrafiltration membranes, so these developments are described in the chapter on ultrafiltration (Chapter 6).

Some of the important milestones in the development of microfiltration are charted in Figure 7.2.

7.2 Background

7.2.1 Types of Membrane

The two principal types of microfiltration membrane filters in use – depth filters and screen filters – are illustrated in Figure 7.3. Screen filters have small pores in their top surface that collect particles larger than the pore diameter on the surface of the membrane. Depth filters have relatively large pores on the top surface, so particles pass to the interior of the membrane. The particles are then captured at constrictions in the membrane pores or by adsorption onto the pore walls. Screen filter membranes rapidly become plugged by the accumulation of retained particles at the top surface. Depth filters have a much larger surface area available for collection of the particles, providing a larger holding capacity before fouling. The mechanism of particle capture by these membranes is described in more detail in Chapter 2.

Depth membrane filters are usually preferred for in-line filtration. As particles are trapped within the membrane, the permeability falls, and the pressure required to maintain a useful filtrate flow increases until, at some point, the membrane must be

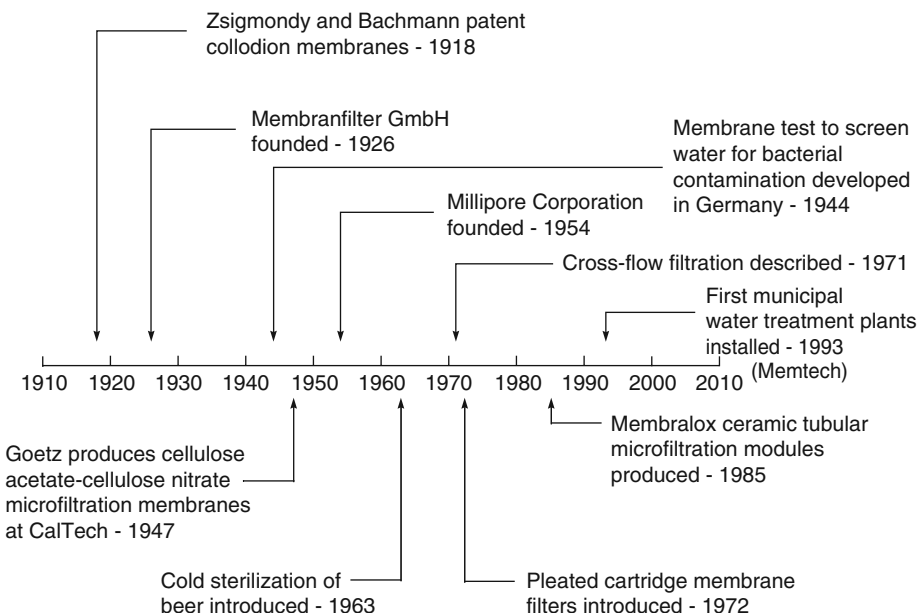


Figure 7.2 Milestones in the development of microfiltration

replaced. The useful life of the membrane is proportional to the particle loading of the feed solution. A typical application of in-line depth microfiltration membranes is final polishing of ultrapure water just prior to use. Screen membrane filters are preferred for the cross-flow microfiltration systems shown in Figure 7.1b. Because screen filters collect the retained particles on the surface of the membrane, the recirculating fluid helps to keep the filter clean.

7.2.2 Membrane Characterization

Microfiltration membranes are often used in applications for which penetration of even one particle or bacterium through the membrane can be critical. Therefore, membrane integrity, that is, the absence of membrane defects or oversized pores, is extremely important. Several tests are used to characterize membrane pore size and pore size distribution.

Characterizing the pore size of microfiltration membranes is a problem for manufacturers. Most microfiltration membranes are depth filters, so electron micrographs usually show an image similar to the right-hand side in Figure 7.3. The average pore diameter of these membranes appears to be about $5\text{ }\mu\text{m}$, yet the membranes are complete filters for particles or bacteria of about $0.5\text{-}\mu\text{m}$ diameter. All of these small particles are captured by adsorption in the interior of the membrane. Therefore, most manufacturers characterize their membranes by the size of the bacteria that are completely filtered by the membrane. The ability of a membrane to filter bacteria from solutions depends on the pore size of the membrane, the size of the bacteria being filtered, and the number

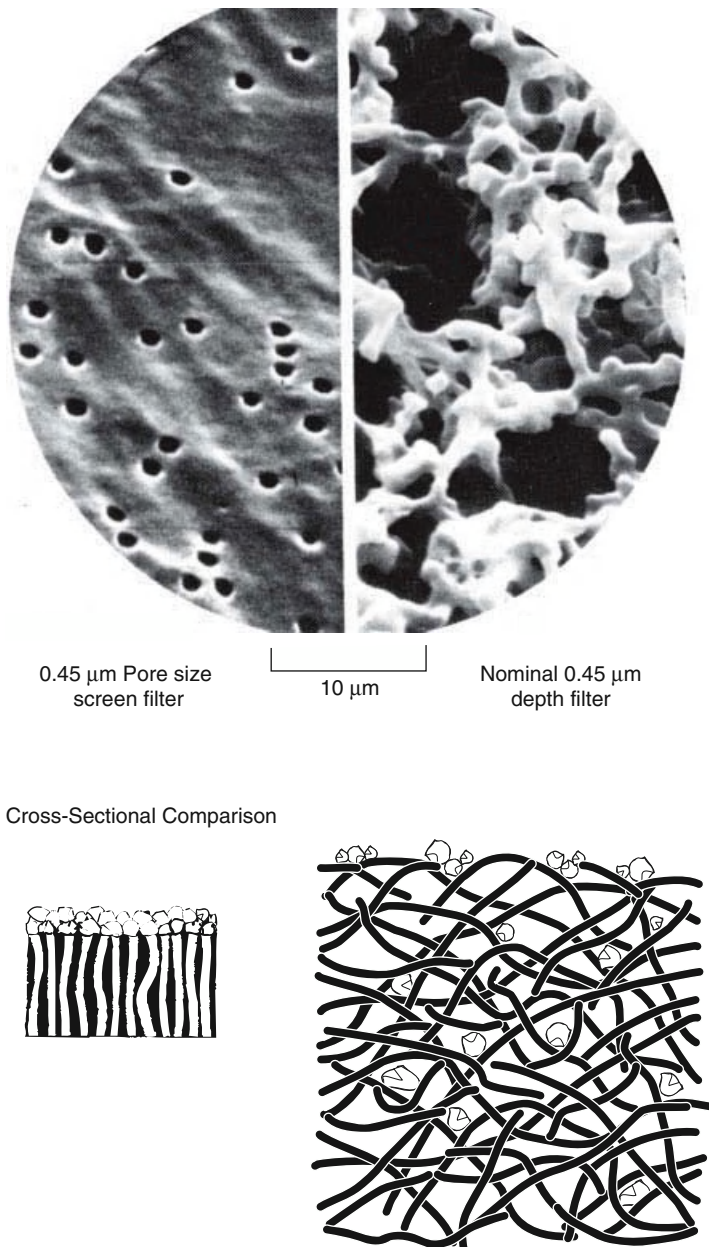


Figure 7.3 Surface scanning electron micrograph and schematic comparison of nominal 0.45- μm screen and depth filters. The screen filter pores are uniform and small and capture the retained particles on the membrane surface. The depth filter pores are almost 5–10 times larger than the screen filter equivalent. A few large 5–10 μm particles are captured on the surface of the membrane, but all particles larger than 0.45 μm are captured by adsorption in the membrane interior

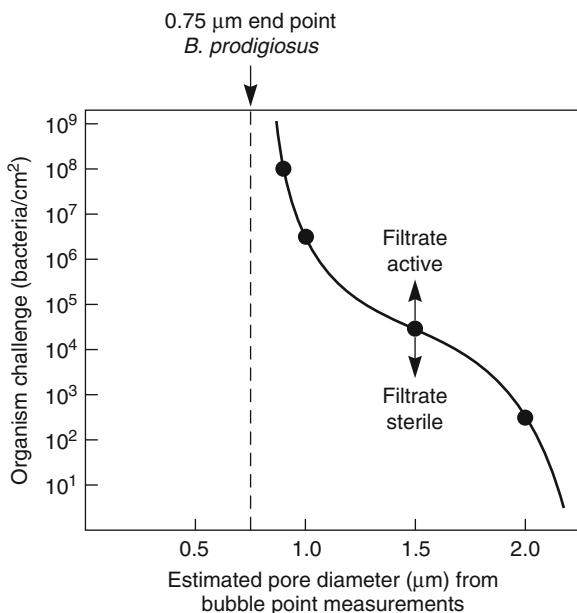


Figure 7.4 Membrane pore diameter from bubble point measurements versus *Bacillus prodigiosus* concentration. Reprinted with permission from [1]. Copyright (1933) The Royal Society.

of organisms used to challenge the membrane. Some results of Elford [1] that illustrate these effects are shown in Figure 7.4. Elford found that membranes with relatively large pores could completely filter bacteria from the challenge solution to produce a sterile filtrate, providing the challenge concentration was low. If the organism concentration was increased, breakthrough of bacteria to the filtrate occurred. However, if the membrane pore size was small enough, a point was reached at which no breakthrough of bacteria to the filtrate occurred no matter how concentrated the challenge solution. This point is taken to be the pore size of the membrane, and this pore size is much smaller than the average pore diameter seen with an electron microscope.

The industry has adopted two bacterial challenge tests to measure pore size and membrane integrity [2]. The tests are based on two bacteria: *Serratia marcescens*, originally thought to have a diameter of 0.45 µm, and *Pseudomonas diminuta*, originally thought to have a diameter of 0.22 µm. In fact, both organisms are ellipsoids with an aspect ratio of about 1.5 : 1. These tests have changed several times over the years, but by convention a membrane is designated 0.45-µm pore size if it is completely retentive when challenged with 10⁷ *S. marcescens* organisms per square centimeter and 0.22-µm pore size if it is completely retentive when challenged with 10⁷ *P. diminuta* organisms per square centimeters. Most commercial microfiltration membranes are categorized as 0.22- or 0.45-µm-diameter pore size based on these tests. Membranes with larger or smaller pore sizes are classified by the penetration tests with latex particle or bubble point measurements described below, relative to these two primary standard measurements.

Currently, most bacterial challenge tests are performed with *P. diminuta*. This organism has an average size of 0.3–0.4 µm, although the size varies significantly with the

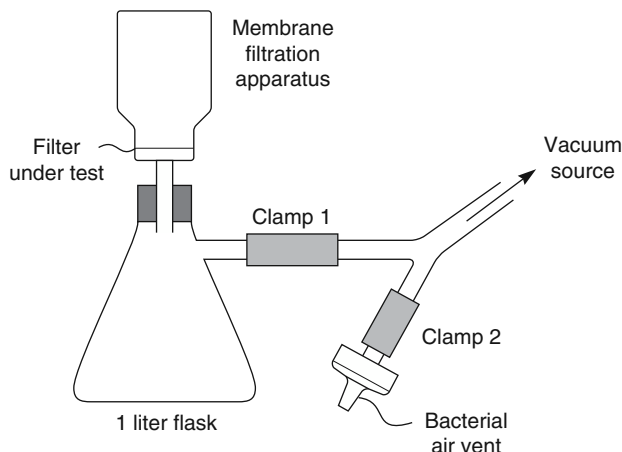


Figure 7.5 Apparatus for testing the microbial retention characteristics of membrane filters. The whole apparatus is sterilized, and initially the flask contains 140 ml of double-strength culture medium. The culture to be tested (100 ml) is passed through the filter with clamp 1 open and clamp 2 closed. The sides of the filter apparatus are washed with two 20 ml portions of sterile broth. Clamp 2 is then opened, the vacuum released, and clamp 1 closed. The filter apparatus is replaced by a sterile rubber stopper and the flask incubated. Absence of turbidity in the flask indicates that the filter has retained the test organism. Reprinted with permission from [3]. Copyright (1983) Science Tech., Courtesy of Thomas D. Brock, University of Wisconsin-Madison.

culture conditions. In a rich culture medium, the cells can form much larger clumps. Thus, to obtain consistent results, the culture characteristics must be carefully monitored and control experiments performed with already qualified 0.45- and 0.22- μm filters to confirm that no clumping has occurred. The ASTM procedure is illustrated in Figure 7.5 [2, 3]. Factors affecting this test are discussed in detail by Meltzer [4].

The performance of membranes in bacterial challenge tests is often quantified by a log reduction value (LRV), defined as

$$\text{LRV} = \log_{10} \left(\frac{c_f}{c_p} \right) \quad (7.1)$$

where c_f is the concentration of bacteria in the challenge solution and c_p is the concentration in the permeate. It follows that at 99% rejection, c_f/c_p is 100 and the LRV is 2; at 99.9% rejection, the LRV is 3; and so on. In pharmaceutical and electronic applications, an LRV of 7 or 8 is usually required. In municipal water filtration, an LRV of 4 or 5 is the target.

7.2.2.1 Latex Challenge Tests

Bacterial challenge tests require careful, sterile laboratory techniques and an incubation period of several days before the results are available. For this reason, secondary

tests based on filtration of suspensions of latex particles of precise diameters have been developed. In such a test, a monodisperse latex suspension with particle diameters from 0.1 to 10 µm is used. The test solution is filtered through the membrane, and the number of particles permeating the membrane is determined by filtering the permeate solution a second time with a tight membrane screen filter. The membrane screen filter captures the latex particles for easy counting. Although the latex challenge test has been used in fundamental studies of microfiltration membrane properties, it is not widely used by membrane producers. The bubble point test described below, backed by correlating the bubble point to the primary bacterial challenge test results, is more commonly used.

7.2.2.2 Bubble Point Test

The bubble point test is simple, quick, and reliable and is by far the most widely used method of characterizing microfiltration membranes. The membrane is first wetted with a suitable liquid, usually water for hydrophilic membranes and methanol for hydrophobic membranes. The membrane is then placed in a holder with a layer of liquid on the top surface. Air is fed to the bottom of the membrane, and the pressure is slowly increased until the first continuous string of air bubbles at the membrane surface is observed. This pressure is called the bubble point pressure and is a characteristic measure of the diameter of the largest pore in the membrane. Obtaining reliable and consistent results with the bubble point test requires care. It is essential, for example, that the membrane be completely wetted with the test liquid; this may be difficult to determine. Because this test is so widely used by microfiltration membrane manufacturers, a great deal of work has been devoted to developing a reliable test procedure to address this and other issues. The use of this test is reviewed in Meltzer's book [4].

The bubble point pressure can be correlated to the membrane pore diameter, r , by the equation

$$\Delta p = \frac{2\gamma \cos \theta}{r} \quad (7.2)$$

where Δp is the bubble point pressure, γ is the fluid surface tension, and θ is the liquid–solid contact angle. For completely wetting solutions, θ is 0°, so $\cos \theta$ equals 1. Properties of liquids commonly used in bubble point measurements are given in Table 7.1.

Table 7.1 Properties of liquids commonly used in bubble point measurements

Wetting liquid	Surface tension (dyn/cm)	Conversion factor
Water	72	42
Kerosene	30	17
Isopropanol	21.3	12
Silicone fluid ^a	18.7	11
Fluorocarbon fluid ^b	16	9

^aDow Corning 200 fluid, 2.0 centistoke.

^b3M Company, fluorochemical FC-43.

The conversion factor divided by the bubble pressure (in pounds per square inch) gives the maximum pore size (in micrometers).

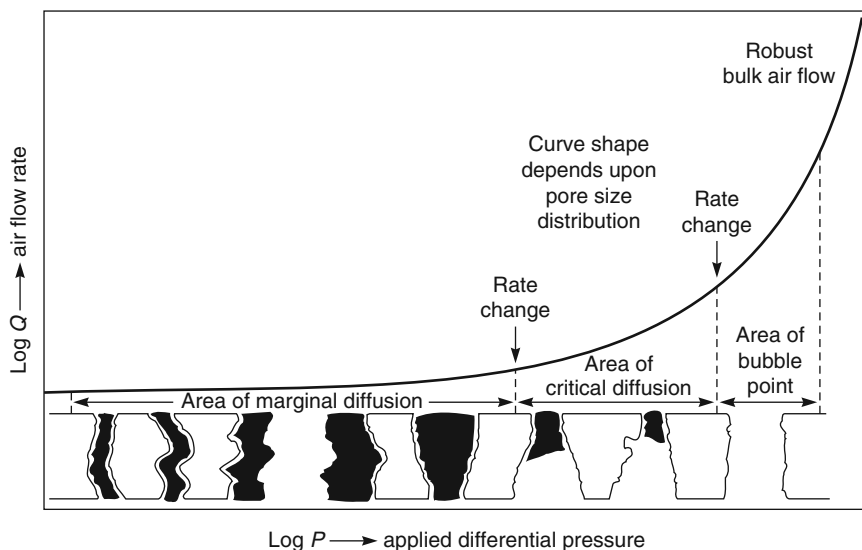


Figure 7.6 Schematic of the effect of applied gas pressure on gas flow through a wetted microporous membrane in a bubble pressure test [4]. Reprinted with permission from [4]. Copyright (1987) Taylor & Francis.

Microfiltration membranes are heterogeneous structures having a distribution of pore sizes. The effect of the applied gas pressure on the liquid in a bubble test is illustrated schematically in Figure 7.6. At pressures well below the bubble point, all pores are completely filled with liquid so gas can only pass through the membrane by diffusion through the liquid film. Just below the bubble point pressure, liquid begins to be forced out of the largest membrane pores. The diffusion rate then starts to increase until the liquid is completely forced out of the largest pore. Bubbles of gas then form on the membrane surface. As the gas pressure is increased further, liquid is forced out of more pores, and general convective flow of gas through the membrane takes place. This is sometimes called the “foam all over pressure,” and is a measure of the average pore size of the membrane.

The apparatus used to measure membrane bubble points is shown in its simplest form in Figure 7.7 [3]. Bubble point measurements are subjective, and different operators can obtain different results. Nonetheless, the test is quick and simple and is widely used as a manufacturing quality control technique. Bubble point measurements are also used to measure the integrity of filters used in critical pharmaceutical or biological operations.

Bubble point measurements are most useful to characterize sheet stock or small membrane filters. The technique is more difficult to apply to formed membrane cartridges containing several square feet of membrane because diffusive flow of gas through the liquid film masks the bubble point. To test cartridges, the cartridge is first wetted and the applied pressure is set at a few pounds per square inch below the bubble point, typically at 80% of the bubble point pressure. The diffusive flow of gas through the wetted cartridge filter is then measured [5, 6]. This provides a good integrity test of large-area

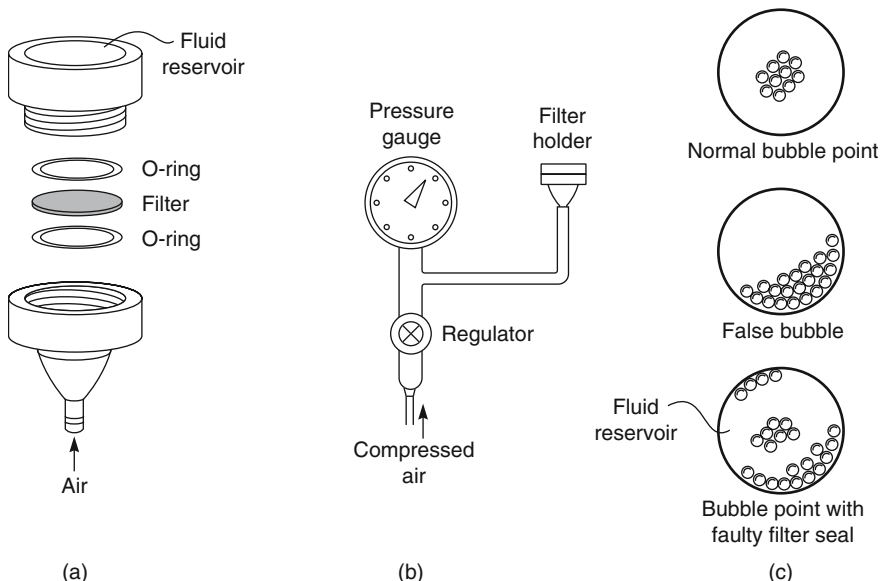


Figure 7.7 Bubble point test measurements. (a) Exploded view of filter holder; (b) test apparatus; and (c) typical bubble patterns produced. Reprinted with permission from [3]. Copyright (1983) Science Tech., Courtesy of Thomas D. Brock, University of Wisconsin-Madison.

cartridge filters, because even a small membrane defect increases gas flow significantly above the norm for defect-free cartridges.

Although bubble point measurements can be used to determine the pore diameter of membranes using Equation 7.2, the results must be treated with caution. Based on Equation 7.2, a 0.22- μm pore diameter membrane should have a bubble point of about 15 bar. In fact, based on the bacterial challenge test, a 0.22- μm pore diameter membrane has a bubble point pressure of 3–4 bar, depending on the membrane. That is, the bubble point test indicates that the membrane has a pore diameter of about 1 μm .

Figure 7.8 shows typical results comparing microbial challenge tests using 0.22- μm *P. diminuta* with membrane bubble points for a series of related membranes [7]. In these tests at a microbial reduction factor of 10^8 – 10^9 , the membrane has a bubble point pressure of only 3 bar, far below the theoretical value of 15 bar for a 0.22- μm pore diameter membrane. Such discrepancies are sometimes handled by a correction factor in Equation 7.2 to account for the shape of the membrane pores, but no reasonable shape factor can account for the fourfold discrepancy seen here. There are two possible reasons why the bubble point test overestimates the minimum pore size of the membrane. First, the test is a measure of the pore size of the membrane. However, a one-to-one relationship between the diameter of the bacteria able to penetrate the membrane and the pore diameter, assumes that the only method of bacterial capture is direct filtration of the test organism somewhere in the membrane. If no organisms penetrate the membrane even at a high concentration, the conclusion is that no pores larger than the organism's diameter exist. However, this ignores other capture mechanisms, such as adsorption and

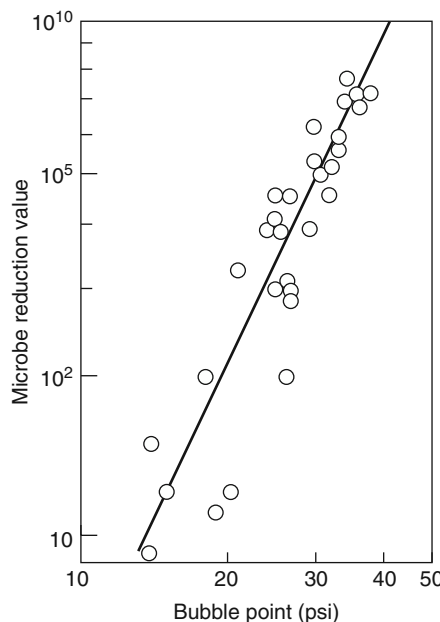


Figure 7.8 Correlation of *P. diminuta* microbial challenge and bubble point test data for a series of related membranes. Reprinted with permission from [7]. Copyright (1978) Advanstar Communications Inc.

electrostatic attraction, which remove the organism even though the pore diameter is larger than the particle. As a result, although some membrane pores may be larger than $0.22\text{ }\mu\text{m}$, leading to a low bubble point pressure, bacteria still cannot travel through these pores in a normal challenge test.

A second explanation, proposed by Williams and Meltzer [8], is illustrated in Figure 7.9. In liquid flow, all flow through the membrane is from the high-pressure (top) to the low-pressure (bottom) side of the membrane. In a bubble point test, the membrane is filled with liquid and gas is used to displace liquid from the large pores. The bubble point is reached when the first contiguous series of large pores through the membrane is formed. This path can be long and tortuous and may not follow the path taken by liquid when the membrane is used as a filter.

7.2.3 Microfiltration Membranes and Modules

The first major application of microfiltration membranes was biological testing of water. This remains an important laboratory application in microbiology and biotechnology. For this application, the early cellulose acetate/cellulose nitrate phase separation membranes made by vapor-phase precipitation with water are still widely used. In the early 1960s and 1970s, a number of other membrane materials with improved mechanical properties and chemical stability were developed. These include polyacrylonitrile-poly(vinyl chloride) copolymers, poly(vinylidene fluoride), polysulfone, cellulose triacetate, and

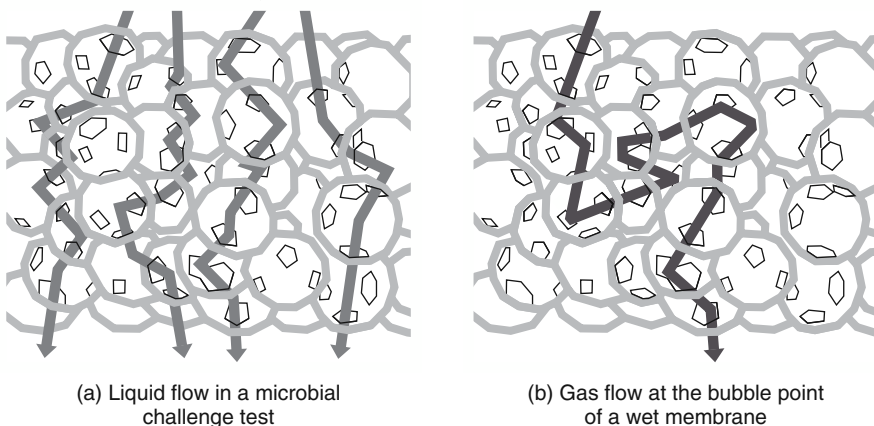


Figure 7.9 An illustration of the model of Williams and Meltzer to explain the discrepancy between membrane pore diameter measurements based on the microbial challenge test and the bubble point test. (a) Liquid flow in a microbial challenge test and (b) gas flow at the bubble point of a wet membrane. Reprinted with permission from [8]. Copyright (1983) Advanstar Communications Inc.

various nylons. Most cartridge filters use these membranes. More recently, poly (tetrafluoroethylene) membranes have come into use.

In the early 1960s and 1970s, the in-line plate-and-frame module was the only available microfiltration module. These units contained between 1 and 20 separate membrane envelopes sealed by gaskets. In most operations, all the membrane envelopes were changed after each use; the labor involved in disassembly and reassembly of the module was a significant drawback. Nonetheless, these systems are still used to process small volumes of solution. A typical plate-and-frame filtration system is shown in Figure 7.10.

More recently, a variety of cartridges that allow a much larger area of membrane to be incorporated into a disposable unit have become available. Disposable plate-and-frame cartridges have been produced, but by far the largest portion of the market is for pleated cartridges, first introduced in the early 1970s. A disposable cartridge filter of this type is shown in Figure 7.11. A typical cartridge is 25 cm long, has a diameter of 5–6 cm, and contains about 0.3 m^2 of membrane. Often the membrane consists of several layers: an outer prefilter facing the solution to be filtered, followed by a finer polishing membrane filter.

In these units, the membrane is pleated and then folded around the permeate core. The cartridge fits inside a specially designed housing into which the feed solution enters at a pressure of 1–10 bar. Pleated membrane cartridges, which are fabricated with high-speed automated equipment, are cheap, disposable, reliable, and hard to beat if the solution to be filtered has a relatively low particle level. Ideal applications are production of aseptic solutions in the pharmaceutical industry or ultrapure water for wafer manufacture in the electronics industry. The low particle load of these feed solutions allows small in-line cartridges to filter large volumes of solution before needing replacement. Manufacturers produce cartridge holders that allow a number of cartridges to be connected in series or in parallel to handle large solution flows. A multicartridge unit is shown in Figure 7.12.



Figure 7.10 Sterile filtration of a small-volume pharmaceutical solution with a 142 mm plate-and-frame filter used as a prefilter in front of a small disposable cartridge final filter

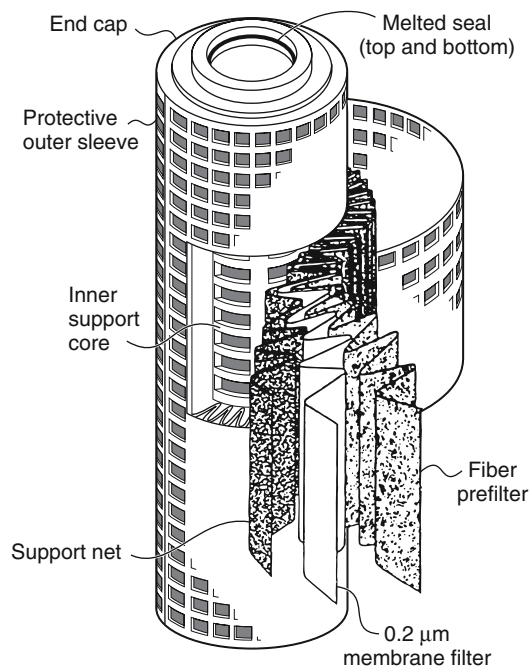


Figure 7.11 Cut-away view of a simple pleated cartridge filter. By folding the membrane, a large surface area can be contacted with the feed solution, producing a high particle loading capacity. (From Membrana product literature.)

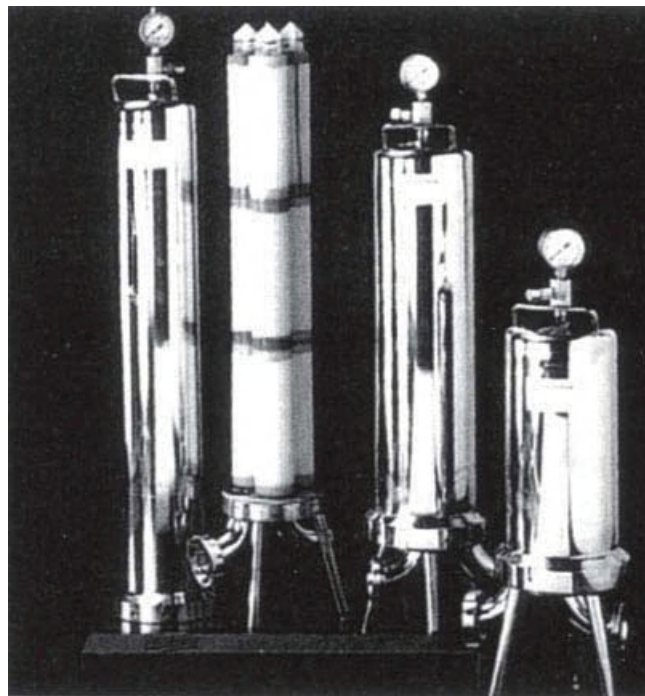


Figure 7.12 Standard-size disposable cartridges can be connected in series or parallel to handle large flows. This unit consists of nine cartridges arranged in a 3×3 array. Reprinted with permission from Sartorius product literature. Copyright (2011) Sartorius Group.

The short lifetime of in-line cartridge filters make them unsuitable for microfiltration of highly contaminated feed streams. Cross-flow filtration, which overlaps significantly with ultrafiltration technology, is used in such applications. In cross-flow filtration, long filter life is achieved by sweeping the majority of the retained particles from the membrane surface before they enter the membrane. Screen filters are preferred for this application, and an ultrafiltration membrane can be used. The design of such membranes and modules is covered under ultrafiltration (Chapter 6) and will not be repeated here.

7.2.4 Process Design

A typical in-line cartridge filtration application is illustrated in Figure 7.13. A pump forces liquid through the filter, and the pressure across the filter is measured by a pressure gauge. Initially, the pressure difference measured by the gauge is small, but as retained particles block the filter, the pressure difference increases until a predetermined limiting pressure is reached, and the filter is changed.

To extend its life, a microfiltration cartridge may contain two or more membrane filters in series or, as shown in Figure 7.13, a coarse prefilter cartridge before the final polishing filter. The prefilter captures the largest particles, allowing smaller particles to pass and be captured by the following finely porous membrane. The use of a prefilter extends the life

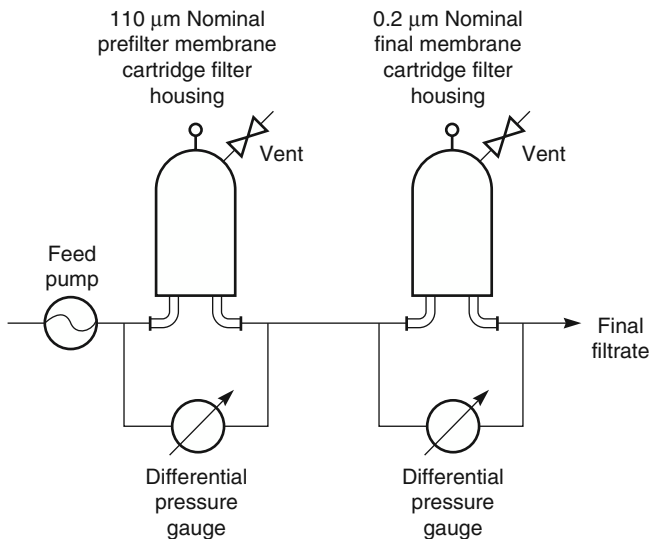


Figure 7.13 Typical in-line filtration operation using two cartridge filters in series. The prefilter removes all of the large particles and some of the smaller ones. The final polishing filter removes the remaining small particles

of the microfiltration cartridge significantly. Without a prefilter, the fine microfiltration membrane would be rapidly blinded by accumulation of large particles on the membrane surface. The correct combination of prefilter and final membrane must be determined for each application. This can be done by placing the prefilter on top of the required final filter membrane in a small test cell, or better yet, with two test cells in series. With two test cells, the pressure drop across each filter can be measured separately.

The objective of a prefilter is to extend the life of the final filter by removing the larger particles from the feed, allowing the final filter to remove the smaller particles. The results obtained with different prefilters are shown in Figure 7.14 [9]. Figure 7.14a shows the rate of pressure rise across the fine filter alone. The limited dirt-holding capacity of this filter means that it is rapidly plugged by a surface layer of large particles. Figure 7.14b shows the case when a prefilter that is too coarse is used. In this case, the pressure difference across the prefilter remains small, whereas the pressure difference across the final filter increases as rapidly as before because of plugging by particles passing the prefilter. Little improvement in performance is obtained. Figure 7.14c shows the case where the prefilter is too fine. This situation is the opposite of Figure 7.14a – the pressure difference across the prefilter increases rapidly, and the lifetime of the combination filter is limited by this filter. Figure 7.14d shows the optimum combination in which the pressure difference is uniformly distributed across the prefilter and final filter. This condition maximizes the lifetime of the filter combination.

Cartridge microfiltration is a stable area of membrane technology – few changes in cartridge design or use have occurred in the past 20 years. Most changes have focused on improving resistance to higher temperatures, solvents, and extremes of pH, to allow application of these filters in more challenging environments.

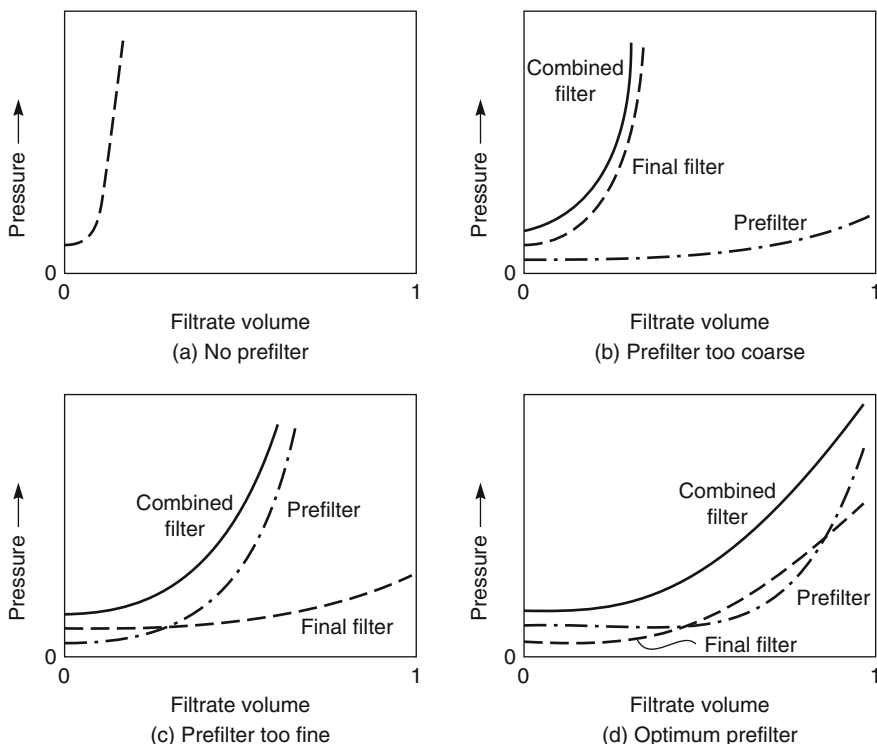


Figure 7.14 The pressure difference across the prefilter, the final filter, and the combined filters for various combinations of prefilter and final filter. The optimum prefilter distributes the particle load evenly between the two filters so both filters reach their maximum particle load at the same time. This maximizes the useful life of the combination. (a) No prefilter, (b) prefilter too coarse, (c) prefilter too fine, and (d) optimum prefilter

Recently, some membrane manufacturers have attempted to produce anisotropic microfiltration membranes in which the open microporous support is a built-in prefilter. Unlike most other applications of anisotropic membranes, these membranes are oriented with the coarse, relatively open pores facing the feed solution, and the most finely microporous layer is at the bottom of the membrane. The goal is to increase filter life by distributing the particle load more evenly across the filter than would be the case with an isotropic porous membrane.

More important recent innovations in microfiltration have mainly concerned the development of cross-flow filtration technology and membranes. The design of these processing systems closely follows that of ultrafiltration described in Chapter 6. In cross-flow filtration, the membrane must retain particles at the membrane surface; therefore, only asymmetric membranes or screen filters with their smallest pores facing the feed solutions can be used. Ceramic filters of the type made by Membralox (now part of US Filter) and others are being used increasingly in this type of application. A ceramic microfiltration cross-flow filter is shown in Figure 7.15. Capillary hollow-fiber membrane modules

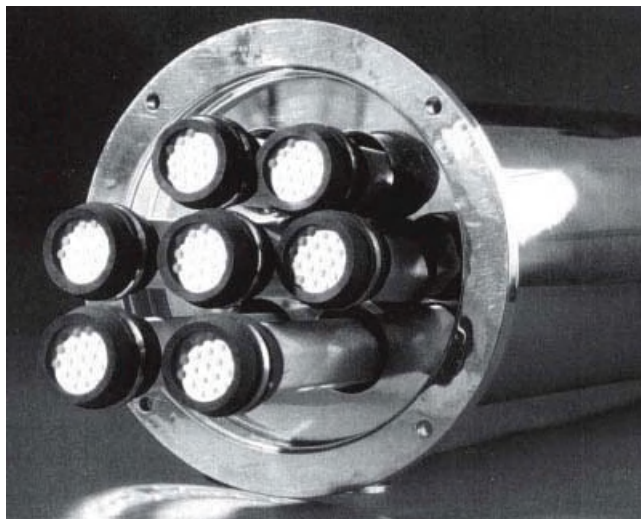


Figure 7.15 Monolithic ceramic microfilter. The feed solution passes down the bores of the channels formed in a porous ceramic block. The channel walls are coated with a finely porous ceramic layer

similar to those originally developed for ultrafiltration applications are also now being widely used for cross-flow microfiltration applications.

The key innovation that has led to increased use of cross-flow microfiltration membrane modules in the last few years has been the development of back-pulsing or backflushing to control membrane fouling [10–12]. In this procedure, the water flux through the membrane is reversed to remove any particulate and fouling material that may have formed on the membrane surface. In microfiltration, several types of backflushing can be used. A short, relatively frequent, flow reversal lasting a few seconds, and applied once every few minutes, is called back-pulsing. Longer flow reversal, lasting 1 or 2 minutes and applied once every 1 or 2 hours, is called backflushing. The balance between the duration of back pulses and their frequency depends on the particular application.

Direct observations illustrating the efficiency of back-pulsing have been made by Mores and Davis [10] using a transparent test cell and cellulose acetate microfiltration membranes fouled with yeast cells. Figure 7.16a shows a photograph of the membrane surface after 2 hours of operation with a yeast solution. The membrane surface is completely covered with yeast cells. Figures 7.16b–d shows the effect of back-pulsing for different times. Back-pulsing for 0.1 s removes about half the yeast, back-pulsing for 1 s removes about 90%, and back-pulsing for 180 s removes all but a few yeast cells.

Microfiltration cross-flow systems are often operated at a constant applied transmembrane pressure in the same way as the reverse osmosis and ultrafiltration systems described in Chapters 5 and 6. However, microfiltration membranes tend to foul and lose flux much more quickly than ultrafiltration and reverse osmosis membranes. The rapid decline in flux makes it difficult to control system operation. For this reason, microfiltration systems are now often operated as constant flux systems, and the transmembrane

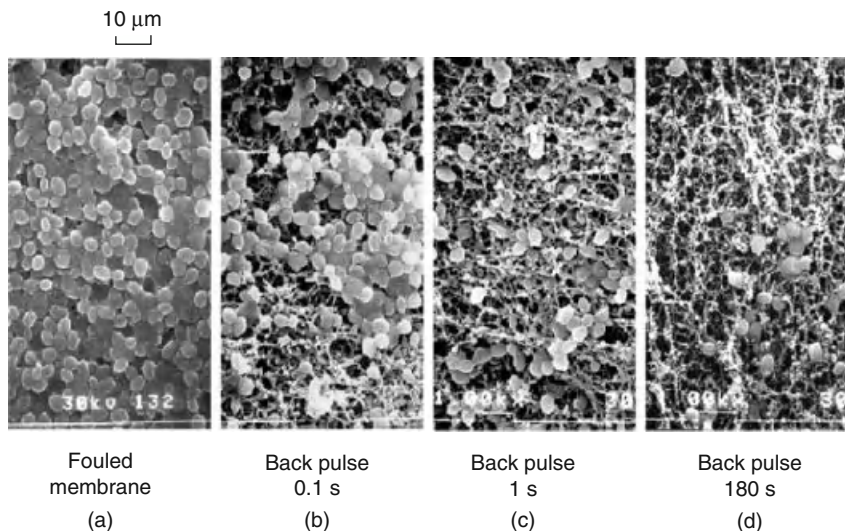


Figure 7.16 An illustration of the efficiency of back-pulsing in removing fouling materials from the surface of microfiltration membranes. Direct microscopic observations of Mores and Davis of cellulose acetate membranes fouled with a 0.1 wt% yeast suspension. The membrane was backflushed with permeate solution at 3 psi for various lengths of time. Reprinted with permission from [10]. Copyright (2001) Elsevier.

pressure across the membrane is slowly increased to maintain the flow as the membrane fouls. Most commonly, the feed pressure is fixed at atmospheric pressure, and the permeate pressure is set at a value just below the feed pressure with a constant volume pump. As the membrane is used, its permeability slowly decreases because of fouling. This decrease in permeability is compensated for by lowering the permeate pressure, thus increasing the pressure driving force. When the permeate pressure reaches some predetermined value, the module is taken off-line and cleaned or backflushed to restore its permeability.

The advantages and disadvantages of in-line microfiltration and cross-flow filtration are compared in Table 7.2. In general, in-line filtration is preferred as a polishing operation for already clean solutions, for example, to sterilize water in the pharmaceutical and electronics industries. Cross-flow filtration is more expensive than in-line filtration in this type of application, but if the water has a high particle content, cross-flow filtration is preferred.

7.3 Applications

The microfiltration market differs significantly from that of other membrane separation processes in that membrane lifetimes are often measured in hours. In a few completely passive applications, such as treating sterile air vents, membranes may last several

Table 7.2 Comparison of advantages and disadvantages of in-line and cross-flow microfiltration

In-line microfiltration	Cross-flow microfiltration
Low capital cost	High capital cost
High operating costs – membrane must be replaced after each use and disposal can be a problem	Operating costs modest – membranes have extended lifetimes if regularly cleaned
Operation is simple – no moving parts	Operation is complex – filters require regular cleaning
Best suited to dilute (low solid content) solutions. Membrane replacement costs increase with particle concentrations in the feed solution	Best suited to high solid content solutions. Costs are relatively independent of feed solution particle concentrations
Representative applications	Representative applications
Sterile filtration	Continuous culture/cell recycle
Clarification/sterilization of beer and wine	Filtration of oilfield produced water

Table 7.3 Approximate volume of fluid that can be filtered by 1 m² of a 5-μm membrane before fouling [13]

Solution	Volume filtered (m ³ /m ²)
Water from deep wells	1000
Solvents	500
Tap water	200
Wine	50
Pharmaceuticals for ampoules	50
20% glucose solution	20
Vitamin solutions	10
Parenterals	10
Peanut oil	5
Fruit juice concentrate	2
Serum (7% protein)	0.6

months; in general, the market is dominated by single-use cartridges designed to filter a relatively small mass of particles from a solution. The volume of solution that can be treated by a microfiltration membrane is directly proportional to the particle level in the feed. As a rough rule of thumb, the particle-holding capacity of a cartridge filter in a non-critical use is between 100 and 300 g/m² of membrane area. Thus, the volume of fluid that can be treated may be quite large if the microfilter is a final safety filter for an electronics plant ultrapure water system, but much smaller if treating contaminated surface water or a food-processing stream. The approximate volume of various solutions that can be filtered by a 5-μm filter before the filter is completely plugged is given in Table 7.3 [13].

Despite the limited volumes that can be treated before a filter must be replaced, microfiltration is economical because the cost of disposable cartridges is low. Currently,

a 25-cm-long pleated cartridge costs between US\$10 and US\$20 and contains 0.3–0.5 m² of active membrane area. The low cost reflects the large numbers that are produced.

The primary market for the disposable cartridge is sterile filtration for the pharmaceutical industry and final point-of-use polishing of ultrapure water for the microelectronics industry. Both industries require very high-quality, particle-free water. The cost of microfiltration compared to the value of the products is small, so these markets have driven the microfiltration industry for the past 20 years.

7.3.1 Sterile Filtration of Pharmaceuticals

Microfiltration is used widely in the pharmaceutical industry to produce injectable drug solutions. Regulating agencies require rigid adherence to standard preparation procedures to ensure a consistent, safe, sterile product. Microfiltration removes particles, and more importantly, all viable bacteria, so a 0.22-μm-rated filter is usually used. Because the cost of validating membrane suppliers is substantial, users usually develop long-term relationships with individual suppliers.

A microfilter for this industry is considered a sterile filter if it achieves a log reduction factor of better than 7. This means that if 10^7 bacteria/cm² are placed on the filter, none appears in the filtrate. A direct relationship exists between the log reduction factor and the bubble point of a membrane.

Microfiltration cartridges produced for this market are often sterilized directly after manufacture and again just prior to use. Live steam, autoclaving at 120 °C, or ethylene oxide sterilization may be used, depending on the applications. A flow schematic of an ampoule-filling station (after material by Schleicher and Schuell) is shown in Figure 7.17.

In this process, feed water is first treated by a deionization system consisting of reverse osmosis, followed by mixed bed ion exchange, and a final 5-μm microfiltration step. The requirements of water for injection are a good deal less stringent than the requirements of ultrapure water for the electronics industry, so the water treatment system is relatively straightforward. The water is first sterilized with a 0.2-μm final filter before being mixed with the drug solution, then sent to a storage tank for the ampoule-filling station. Before use, the solution is filtered at least twice more with 0.2-μm filters to ensure sterility. Because pharmaceuticals are produced by a batch process, all filters are replaced at the end of each batch.

7.3.2 Sterilization of Wine and Beer

Cold sterilization of beer using microfiltration was introduced on a commercial scale in 1963. The process was not generally accepted at that time, but has recently become more common. Sterilization of beer and wine is much less stringent than pharmaceutical sterilization. The main objective is to remove yeast cells, which are quite large, so the product is clear and bright. Bacterial removal is also desirable; a 10^6 reduction in bacteria is equivalent to the best depth filters. The industry has found that 1-μm filters can remove essentially all the yeast, as well as provide a 10^6 reduction in the common bacteria found in beer and wine. Because the cost structure of beer and wine production is very different from that of pharmaceuticals, the filtration system typically involves one or more prefilters to extend the life of the final polishing filter.

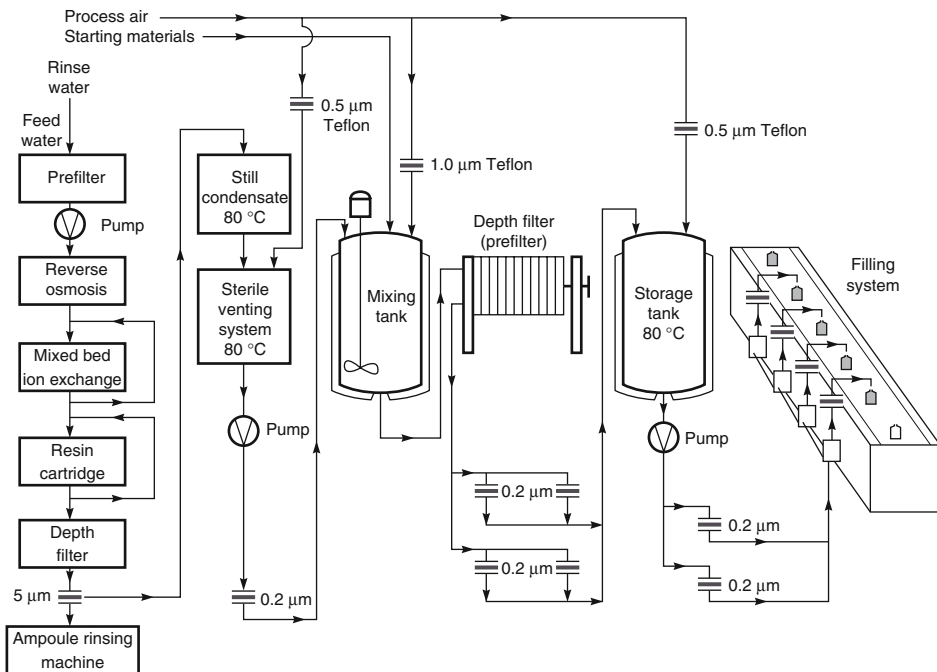


Figure 7.17 Flow diagram illustrating the use of microfiltration sterilization filters in a production line used to prepare ampoules of injectable drug solutions

7.3.3 Microfiltration in the Electronics Industry

Microfilters are used in the electronics industry, principally as final point-of-use filters for ultrapure water. The water is already very pure and almost completely particle- and salt-free, so the only potential problem is contamination in the piping from the central water treatment plant to the device fabrication area. Although fine filters with 0.1 μm pore diameter or less may be used, lifetimes are relatively long.

The electronics industry also uses a variety of reactive gases and solvents which must be particle free. Teflon® microfilters are widely used to treat these materials.

7.4 Conclusions and Future Directions

The main microfiltration market is for in-line disposable cartridge filters. These cartridges are sold into two growing industries – microelectronics and pharmaceuticals – so prospects for continued market growth of the industry are very good. In addition to these existing markets, a significant market exists for microfiltration in bacterial control of drinking water, tertiary treatment of sewage, and replacement of diatomaceous earth depth filters in the chemical processing and food industries. The market in these applications has increased rapidly in the last decade, and ultrafiltration membranes are often used. These applications are covered in more detail in Chapter 6.

References

1. Elford, W.J. (1933) The principles of ultrafiltration as applied in biological studies. *Proc. R. Soc. London, Ser. B*, **112**, 384.
2. ASTM (1983) F838-83. *Determining Bacterial Retention of Membrane Filters Utilized for Liquid Filtration*, American Society for Testing and Materials, Philadelphia.
3. Brock, T.D. (1983) *Membrane Filtration: A User's Guide and Reference*, Science Technology, Madison, WI.
4. Meltzer, T.H. (1987) *Filtration in the Pharmaceutical Industry*, Marcel Dekker, New York.
5. Hofmann, F. (1984) Integrity testing of microfiltration membranes. *J. Parenteral Sci. Technol.*, **38**, 148.
6. Farahbakhsh, K., Adham, S.S., and Smith, D.W. (2003) Monitoring the integrity of low-pressure membranes. *J. AWWA*, **95**, 95.
7. Leahy, T.J. and Sullivan, M.J. (1978) Validation of bacterial retention capabilities of membrane filters. *Pharm. Technol.*, **2**, 65.
8. Williams, R.E. and Meltzer, T.H. (1983) Membrane structure, the bubble point and particle retention. *Pharm. Technol.*, **7** (5), 36.
9. Porter, M.C. (1990) Microfiltration, in *Handbook of Industrial Membrane Technology* (ed. M.C. Porter), Noyes Publications, Park Ridge, NJ, pp. 61–135.
10. Mores, W.D. and Davis, R.H. (2001) Direct visual observation of yeast deposition and removal during microfiltration. *J. Membr. Sci.*, **189**, 217.
11. Sondhi, R. and Bhave, R. (2001) Role of backpulsing in fouling minimization in crossflow filtration with ceramic membranes. *J. Membr. Sci.*, **186**, 41.
12. Srijaroonrat, P., Julien, E., and Aurelle, Y. (1999) Unstable secondary oil/water emulsion treatment using ultrafiltration: fouling control by backflushing. *J. Membr. Sci.*, **159**, 11.
13. Hein, W. (1980) Mikrofiltration verfahren fur kritische trenn-unde reinigungsprobleme bei flussigkeiter und gasen. *Chem. Prod.*, Nov. 1980.

8

Gas Separation

8.1 Introduction and History

Gas separation only became a major industrial application of membrane technology in the past 30 years, but the study of gas permeation through membranes has a long history. Systematic studies began with Thomas Graham who, over a period of 20 years, measured the permeation rates of all the gases then known, through every diaphragm available to him [1]. This was no small task because his experiments had to start with synthesis of the gas. Graham gave the first description of the solution-diffusion model, and his work on porous membranes led to Graham's law of diffusion. Through the remainder of the nineteenth and the early twentieth centuries, the ability of gases to permeate membranes selectively had no industrial or commercial use. The concept of the perfectly selective membrane was, however, used as a theoretical tool to develop physical and chemical theories, such as Maxwell's kinetic theory of gases.

From 1943 to 1945, Graham's law of diffusion was exploited for the first time, to separate $U^{235}F_6$ from $U^{238}F_6$ as part of the Manhattan project. Finely microporous metal membranes were used. The separation plant, constructed in Knoxville, Tennessee, represented the first large-scale use of gas separation membranes and remained the world's largest membrane separation plant for the next 40 years. However, this application was unique and so secret that it had essentially no impact on the long-term development of gas separation.

In the 1940s to 1950s, Barrer [2], van Amerongen [3], Stern [4], Meares [5], and others laid the foundation of the modern theories of gas permeation. The solution-diffusion model of gas permeation developed then is still the accepted model for gas transport through membranes. However, despite the availability of interesting polymer materials, membrane fabrication technology was not sufficiently advanced, at that time, to make useful membrane systems from these polymers.

The development of high-flux anisotropic membranes and large-surface-area membrane modules for reverse osmosis applications in the late 1960s and early 1970s provided

the basis for modern membrane gas separation technology. The first company to establish a commercial presence was Monsanto, which launched its hydrogen-separating Prism® membrane in 1980 [6]. Monsanto had the advantage of being a large chemical company with ample opportunities to test pilot- and demonstration-scale systems in its own plants before launching the product. The economics were compelling, especially for the separation of hydrogen from ammonia-plant purge-gas streams. Within a few years, Prism systems were installed in many such plants [7].

Monsanto's success encouraged other companies to advance their own membrane technologies. By the mid-1980s, Cynara, Separax, and Grace Membrane Systems were producing membrane plants to remove carbon dioxide from methane in natural gas. This application has grown significantly over the years. At about the same time, Dow launched Generon®, the first commercial membrane system for nitrogen separation from air. Initially, membrane-produced nitrogen was cost-competitive in only a few niche areas, but the development by Dow, Ube, and Du Pont/Air Liquide of materials with improved selectivities has since made membrane separation much more competitive. This application of membranes has expanded very rapidly and has now captured more than half of the nitrogen production market. More than 30 000 small- to medium-sized nitrogen production systems have been installed worldwide. Gas separation membranes are also being used for a wide variety of other, smaller applications ranging from dehydration of air and natural gas to organic vapor removal from air and nitrogen streams. Application of the technology is expanding rapidly, and further growth is likely to continue for the foreseeable future. Figure 8.1 provides a summary of the development of gas separation technology.

8.2 Theoretical Background

Porous or dense membranes can be used as selective gas separation barriers; Figure 8.2 illustrates the mechanism of gas permeation. Three types of porous membranes, differing in pore size, are shown. If the pores are relatively large – from 0.1 to 10 µm – gases permeate the membrane by convective flow, and no separation occurs. If the pores are smaller than 0.1 µm, then the pore diameter is smaller than the mean free path of the gas molecules. Diffusion through such pores is governed by Knudsen diffusion, and the transport rate of a gas is inversely proportional to the square root of its molecular weight. This relationship is called Graham's law of diffusion. Finally, if the membrane pores are extremely small, of the order 5–20 Å, then gases are separated by molecular sieving. Transport through this type of membrane is complex and includes both diffusion in the gas phase and diffusion of adsorbed species on the surface of the pores (surface diffusion). These very-small-pore membranes have not been used on a large scale, but carbon, ceramic, and ultramicroporous glass membranes with extraordinarily high selectivities for similar molecules have been prepared in the laboratory.

Although microporous membranes are topics of research interest, almost all current commercial gas separations are based on the dense polymer membrane also shown in Figure 8.2. Separation through dense polymer films occurs by a solution-diffusion mechanism.

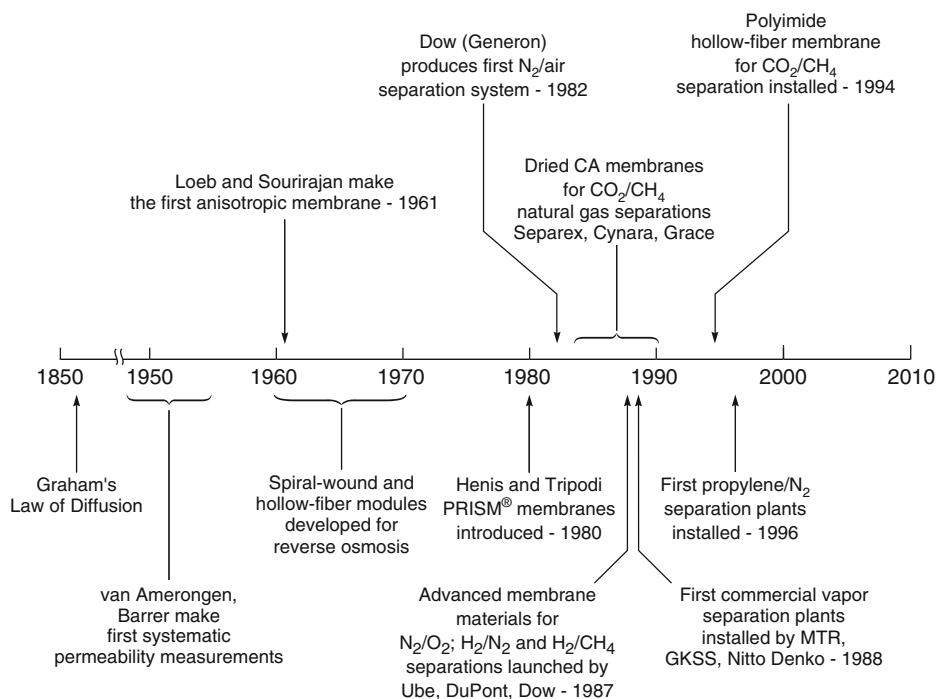


Figure 8.1 Milestones in the development of gas separation

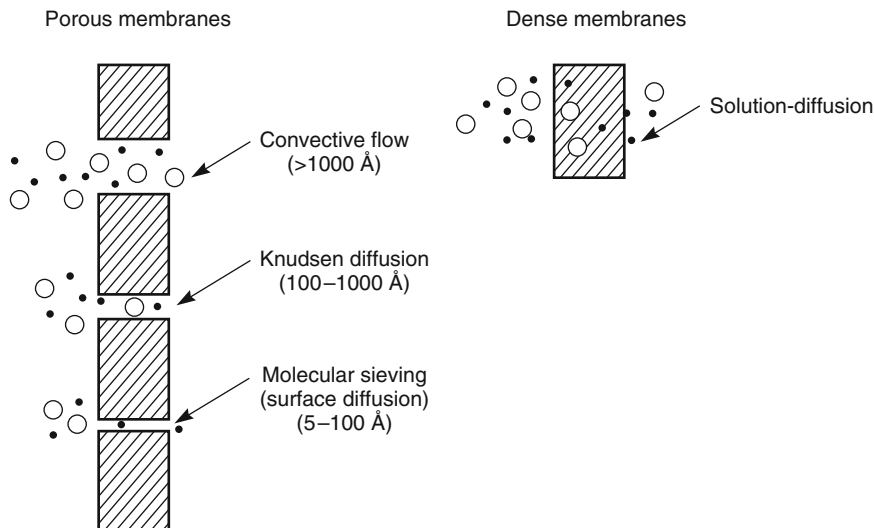


Figure 8.2 Mechanisms for permeation of gases through porous and dense gas separation membranes

In Chapter 2 (Equation 2.59), it was shown that gas transport through dense polymer membranes is governed by the expression

$$J_i = \frac{D_i K_i^G (p_{i_o} - p_{i_\ell})}{\ell} \quad (8.1)$$

where J_i is the flux of component i ($\text{g}/\text{cm}^2 \cdot \text{s}$), p_{i_o} and p_{i_ℓ} are the partial pressures of the component i on either side of the membrane, ℓ is the membrane thickness, D_i is the permeate diffusion coefficient, and K_i^G is the Henry's law sorption coefficient ($\text{g}/\text{cm}^3 \cdot \text{pressure}$). In gas permeation it is much easier to measure the volume flux through the membrane than the mass flux, and so Equation 8.1 is usually recast as

$$j_i = \frac{D_i K_i (p_{i_o} - p_{i_\ell})}{\ell} \quad (8.2)$$

where j_i is the volume (molar) flux expressed as $(\text{cm}^3(\text{STP}) \text{ of component } i)/\text{cm}^2 \cdot \text{s}$ and K_i is a sorption coefficient with units $(\text{cm}^3(\text{STP}) \text{ of component } i)/\text{cm}^3$ of polymer·pressure). The product $D_i K_i$ can be written as \mathcal{P}_i , which is called the membrane permeability, and is a measure of the membrane's ability to permeate gas, normalized for pressure driving force, and membrane thickness.¹ A measure of the ability of a membrane to separate two gases, i and j , is the ratio of their permeabilities, α_{ij} , called the membrane selectivity

$$\alpha_{ij} = \frac{\mathcal{P}_i}{\mathcal{P}_j} \quad (8.3)$$

8.2.1 Polymer Membranes

The relationship between polymer structure and membrane permeation was discussed in Chapter 2 and is revisited only briefly here. Permeability can be expressed as the product $D_i K_i$ of two terms. The diffusion coefficient, D_i , reflects the mobility of the individual molecules in the membrane material; the gas sorption coefficient, K_i , reflects the number of molecules dissolved in the membrane material. Thus, Equation 8.3 can also be written as

$$\alpha_{ij} = \left[\frac{D_i}{D_j} \right] \left[\frac{K_i}{K_j} \right] \quad (8.4)$$

The ratio D_i/D_j is the ratio of the diffusion coefficients of the two gases and can be viewed as the mobility selectivity, reflecting the different sizes of the two molecules. The ratio K_i/K_j is the ratio of the sorption coefficients of the two gases and can be

¹ The permeability of gases through membranes is most commonly measured in Barrer, defined as $10^{-10} \text{ cm}^3(\text{STP}) \cdot \text{cm}/\text{cm}^2 \cdot \text{s} \cdot \text{cmHg}$ and named after R.M. Barrer, a pioneer in gas permeability measurements. The term $j_i/(p_{i_o} - p_{i_\ell})$, best called the permeance or pressure-normalized flux, is often measured in terms of gas permeation units (gpu), where 1 gpu is defined as $10^{-6} \text{ cm}^3(\text{STP}) \cdot \text{cm}/\text{cm}^2 \cdot \text{s} \cdot \text{cmHg}$. One gpu is therefore one Barrer/ μ . Occasional academic purists insist on writing permeability in terms of $\text{mol} \cdot \text{m}/\text{m}^2 \cdot \text{s} \cdot \text{Pa}$ (1 Barrer = $0.33 \times 10^{-15} \text{ mol} \cdot \text{m}/\text{m}^2 \cdot \text{s} \cdot \text{Pa}$), but fortunately this has not caught on.

viewed as the sorption or solubility selectivity, reflecting the relative solubilities of the two gases.

In all polymers, the *diffusion coefficient* decreases with increasing permeant molecular size, because large molecules interact with more segments of the polymer chain than do small molecules. Hence, the mobility selectivity always favors the passage of small molecules over large ones. However, the magnitude of the mobility selectivity term depends greatly on whether the membrane material is above or below its glass transition temperature (T_g). If the material is below the glass transition temperature, the polymer chains are essentially fixed and segmental motion is limited. The material is then called a glassy polymer and is tough and rigid. Above the glass transition temperature, segments of the polymer chains have sufficient thermal energy to allow limited rotation around the chain backbone. This motion changes the mechanical properties of the polymer dramatically, and it becomes a rubber. The transition is quite sharp and occurs over a temperature change of just a few degrees. As characterized by their diffusion coefficients, the relative mobilities of gases differ significantly in rubbers and glasses, as illustrated in Figure 8.3 [8]. Diffusion coefficients in glassy materials are small and decrease much more rapidly with increasing permeate size than diffusion coefficients in rubbers. This means the mobility selectivity term for rubbery membranes is smaller than the mobility selectivity of glassy membranes. For example, the mobility selectivity for nitrogen over pentane in natural rubber is approximately 10. The mobility selectivity for nitrogen over pentane in poly(vinyl chloride), a rigid, glassy polymer, is more than 100 000.

The *sorption coefficient* of gases and vapors increases with increasing condensability of the permeant. This dependence on condensability means that the sorption coefficient also increases with molecular diameter, because large molecules are normally more condensable than smaller ones. The gas sorption coefficient can, therefore, be plotted against boiling point or molar volume. As shown in Figure 8.4 [9], sorption selectivity favors larger, more condensable molecules, such as hydrocarbon vapors, over permanent gases, such as oxygen and nitrogen. However, the difference between the sorption coefficients of permeants in rubbery and glassy polymers is far less marked than the difference in the diffusion coefficients.

It follows from the discussion above that the balance between the mobility selectivity term and the sorption selectivity term in Equation 8.4 [10] is different for glassy and rubbery polymers. This difference is illustrated by the data in Figure 8.5. In glassy polymers, the mobility term is usually dominant, permeability falls with increasing permeate size, and small molecules permeate preferentially. Therefore, when used to separate organic vapors from nitrogen, glassy membranes preferentially permeate nitrogen. In rubbery polymers, the sorption selectivity term is usually dominant, permeability increases with increasing permeate size, and larger molecules permeate preferentially. Therefore, when used to separate organic vapor from nitrogen, rubbery membranes preferentially permeate the organic vapor. The separation properties of polymer membranes for a number of the most important gas separation applications have been summarized by Robeson [11]. A review of structure/property relations has been given by Stern [12]. Properties of some representative and widely used membrane materials are summarized in Table 8.1.

An important tool to rationalize the properties of different membrane materials is the plot of membrane selectivity versus membrane permeability popularized by Robeson [11, 13]. A Robeson plot for the separation of oxygen and nitrogen is shown in Figure 8.6.

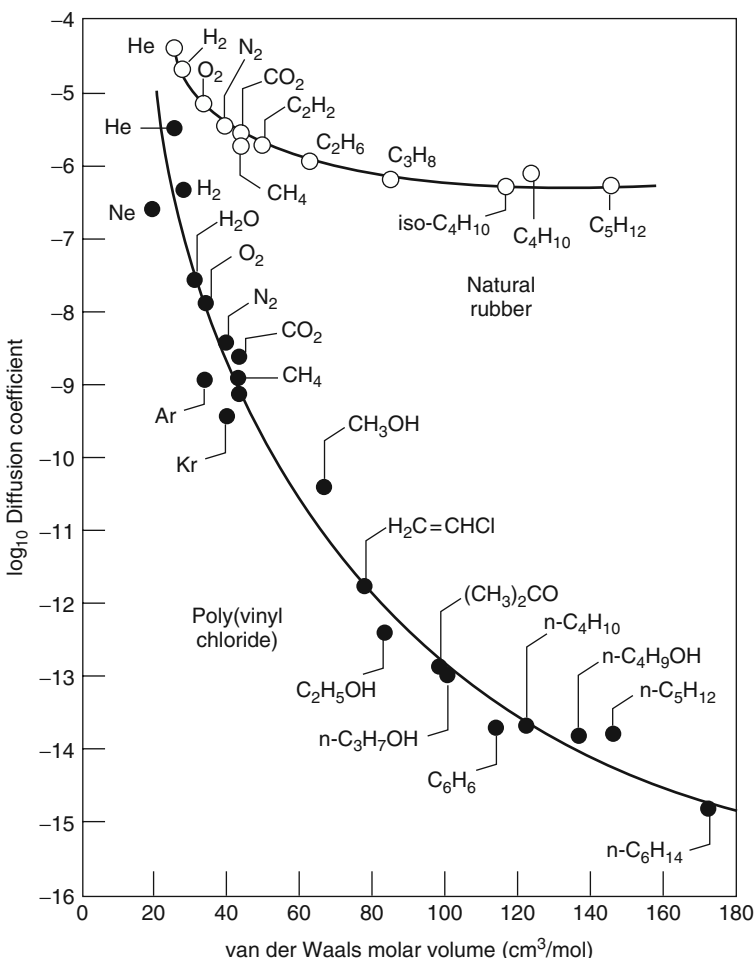


Figure 8.3 Diffusion coefficient as a function of molar volume for a variety of permeants in natural rubber and in poly(vinyl chloride), a glassy polymer. This type of plot was first drawn by Gruen [8], and has been used by many others since

Each point on the figure represents a different membrane material. A wide range of selectivity/permeability combinations are provided by different polymers, but for gas separation applications, only the most permeable polymers at a particular selectivity are of interest. The line linking these polymers is called the upper bound, beyond which no better material is currently known. There is a strong inverse relationship between permeability and selectivity. The most permeable membranes with a selectivity of 6–7 have 1% of the permeability of membranes with a selectivity of 2–3. The relative positions of the upper bound in 1991 and in 1980 show the progress that was made in producing polymers specifically tailored for this separation. Development of better materials is a continuing research topic at the major gas separation companies and in

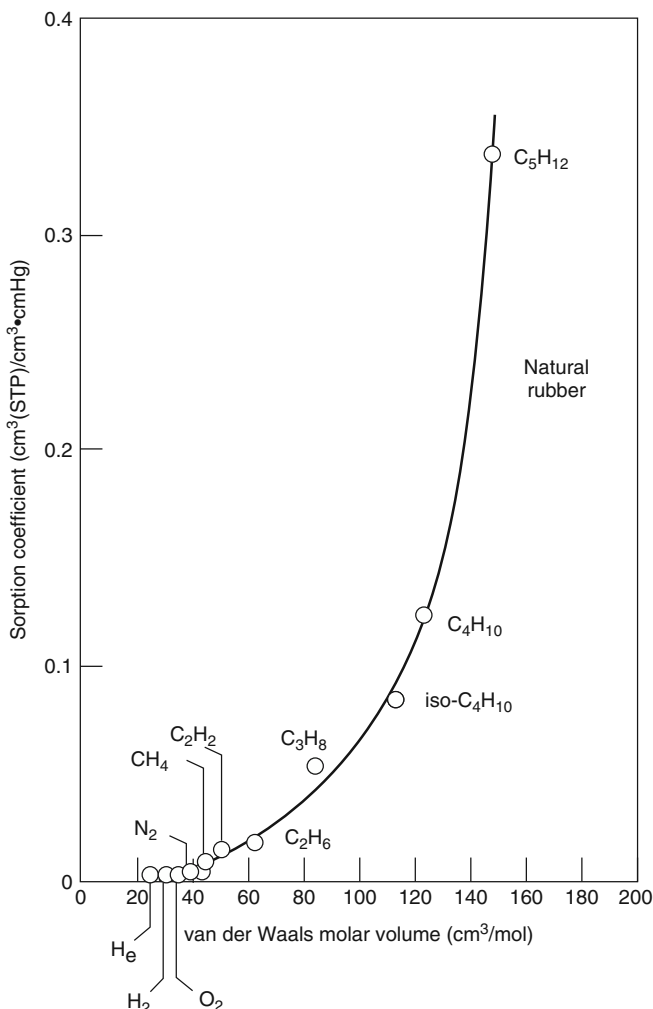


Figure 8.4 Gas sorption coefficient as a function of molar volume for natural rubber membranes. Larger permeants are more condensable and have higher sorption coefficients [9]

some universities, so further but slow movement of the upper bound may be seen in the future.

Robeson plots similar to that shown in Figure 8.6 have been created for a number of other gas pairs. The position of the upper bound lines for a number of gas pairs of commercial interest are shown in Figure 8.7. This type of plot is useful in estimating the permeability and selectivity that can be expected for the best membrane materials.

Figure 8.7 also shows that with some gas pairs it is possible to switch the selectivity of the separation by choice of the membrane material. For example, the separation of nitrogen/methane gas mixtures is of interest in the processing of natural gas [14].

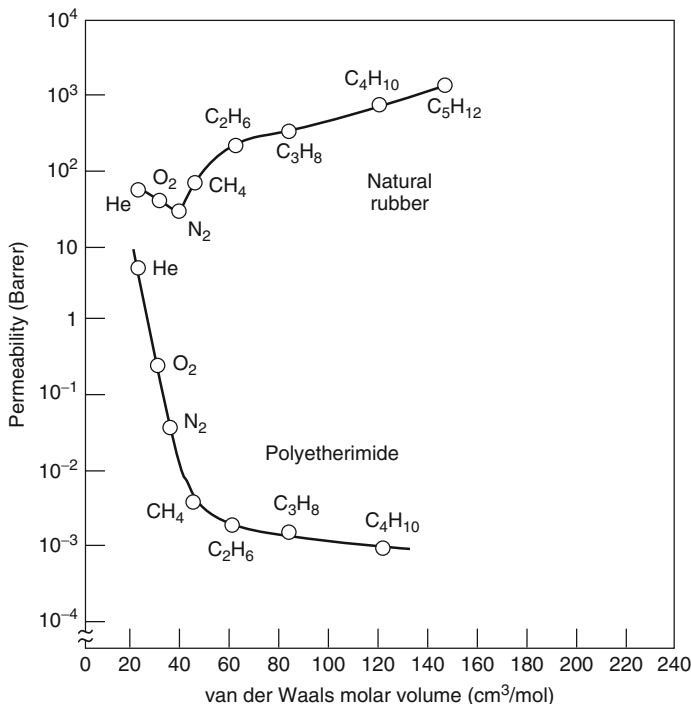


Figure 8.5 Permeability as a function of molar volume for a rubbery and a glassy polymer, illustrating the different balance between sorption and diffusion in these polymer types. The natural rubber membrane is highly permeable; permeability increases rapidly with increasing permeant size because sorption dominates. The glassy polyetherimide membrane is much less permeable; the permeability decreases with increasing permeant size because diffusion dominates [10]. Reprinted from R.D. Behling, K. Ohlrogge, K.-V. Peinemann and E. Kyburz, *The Separation of Hydrocarbons from Waste Vapor Streams*, in *Membrane Separations in Chemical Engineering*, A.E. Fouda, J.D. Hazlett, T. Matsuura and J. Johnson (eds), AIChE Symposium Series Number 272, Vol. 85, p. 68 (1989). Reproduced by permission of the American Institute of Chemical Engineers. Copyright © 1989 AIChE. All rights reserved.

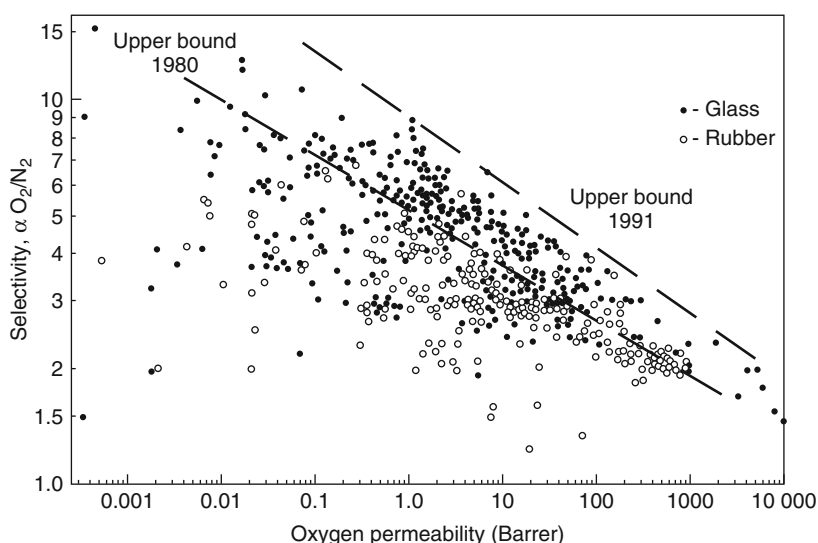
The mobility selectivity term D_{N_2}/D_{CH_4} favors permeation of the small molecule nitrogen (kinetic diameter 3.64 Å) over the larger methane (kinetic diameter 3.80 Å). On the other hand, the sorption selectivity K_{N_2}/K_{CH_4} favors sorption of the more condensable gas methane (boiling point 111 K) over the less condensable gas nitrogen (boiling point 77 K). It follows that the effects of the mobility and sorption selectivity terms in Equation 8.4 are opposed. Glassy polymers generally have low permeability and will preferentially permeate nitrogen ($\alpha_{N_2/CH_4} > 1$) because the diffusion mobility selectivity term is dominant. Rubbery polymers have higher permeabilities and preferentially permeate methane ($\alpha_{N_2/CH_4} < 1$) because the sorption selectivity term is dominant.

The upper bound lines shown in Figure 8.7 can be expressed mathematically as

$$\ln \alpha_{A/B} = \ln \beta_{A/B} - \lambda_{A/B} \ln P_A \quad (8.5)$$

Table 8.1 Pure-gas permeabilities (Barrer ($10^{-10} \text{ cm}^3(\text{STP}) \cdot \text{cm}/\text{cm}^2 \cdot \text{s} \cdot \text{cmHg}$)) of widely used polymers

Gas	Rubbers		Glasses		
	Silicone rubber at 25°C $T_g = -129^\circ\text{C}$	Natural rubber at 30°C $T_g = -73^\circ\text{C}$	Cellulose acetate at 25°C $T_g = 124^\circ\text{C}$	Polysulfone at 35°C $T_g = 186^\circ\text{C}$	Polyimide (Ube Industries) at 60°C $T_g > 250^\circ\text{C}$
H_2	550	41	24	14	50
He	300	31	33	13	40
O_2	500	23	1.6	1.4	3
N_2	250	9.4	0.33	0.25	0.6
CO_2	2700	153	10	5.6	13
CH_4	800	30	0.36	0.25	0.4
C_2H_6	2100	—	0.20	—	0.08
C_3H_8	3400	168	0.13	—	0.015
C_4H_{10}	7500	—	0.10	—	—

**Figure 8.6** Oxygen/nitrogen selectivity as a function of oxygen permeability. This plot by Robeson shows the wide range of selectivity and permeability combinations achieved by current materials. Reprinted with permission from [11]. Copyright (1991) Elsevier.

or

$$\alpha_{A/B} = \beta_{A/B} / P_A^{\lambda_{A/B}} \quad (8.6)$$

where A and B represent the two gases, $\lambda_{A/B}$ is the slope of the line in Figure 8.7, and $\ln \beta_{A/B}$ is the intercept at $\ln P_A = 0$. Freeman [15] has shown that these parameters have physical significance and can be calculated with reasonable accuracy from first

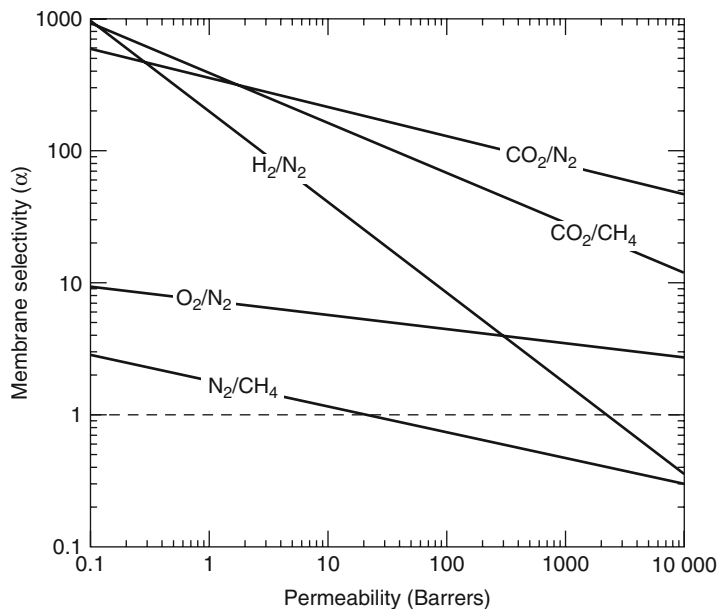


Figure 8.7 Upper bound Robeson selectivity/permeability lines for a number of commercially important gas separations. This figure allows the trade-off between selectivity and permeability to be estimated for the best available membrane materials

principle considerations. The slope $\lambda_{A/B}$ depends only on the size of the gas pair, and $\beta_{A/B}$ depends on the gas condensabilities.

Despite all of the above considerations, applying the permeability and selectivity data shown in Robeson plots to actual gas separation problems must be approached with caution. Permeabilities used to prepare Robeson plots are measured with pure gases; the selectivity obtained from the ratio of pure gas permeabilities gives the ideal membrane selectivity. However, practical gas separation processes are performed with gas mixtures. If the gases in a mixture do not interact with the membrane material, the pure gas selectivity and the mixed gas selectivity will be equal. This is usually the case for mixtures of oxygen and nitrogen, for example. In many other cases, such as the separation of carbon dioxide/methane mixtures, one of the components (carbon dioxide) is sufficiently sorbed by the membrane to affect the permeability of the other component (methane). The selectivity measured with a gas mixture may then be one-half or less of the selectivity calculated from pure gas measurements. Pure gas selectivities are much more commonly reported in the literature than gas mixture data because they are easier to measure. However, neglecting the difference between these two values has led many membrane users to seriously overestimate the ability of a membrane to separate a target gas mixture. Figure 8.8 [16] shows selected data for the separation of methane and carbon dioxide using cellulose acetate membranes. The calculated pure gas selectivity is very good, but in gas mixtures, enough carbon dioxide dissolves in the membrane to increase the methane permeability far above the pure gas methane permeability value. As a result,

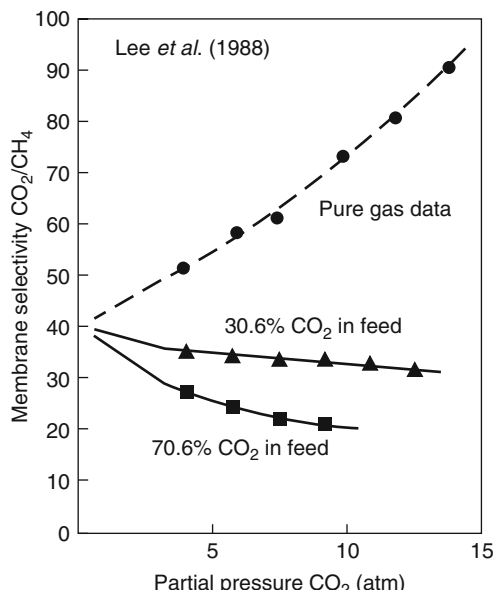


Figure 8.8 The difference between selectivities calculated from pure gas measurements and selectivities measured with gas mixtures can be large. S.Y. Lee, B.S. Minhas and M.D. Donohue, Effect of Gas Composition and Pressure on Permeation through Cellulose Acetate Membranes, in *New Membrane Materials and Processes for Separation*, K.K. Sirkar and D.R. Lloyd (eds), AIChE Symposium Series Number 261, Vol. 84, p. 93 (1988). Reproduced with permission of the American Institute of Chemical Engineers. Copyright © 1988 AIChE. All rights reserved.

the selectivities measured with gas mixtures are much lower than those calculated from pure gas data.

Most gas separation processes using polymer membranes require that the selective membrane layer be extremely thin to achieve economical fluxes. Typical membrane thicknesses are less than 0.5 μm and often less than 0.1 μm . Early gas separation membranes [17] were made by modifying cellulose acetate membranes produced for reverse osmosis by the Loeb–Sourirajan phase separation process. These membranes are produced by precipitation in water, and the water must be removed before the membranes can be used to separate gases. However, the capillary forces generated as the liquid evaporates cause collapse of the finely microporous substrate of the cellulose acetate membrane, destroying its usefulness. This problem has been overcome by a solvent-exchange process in which the water is first exchanged for an alcohol, then for hexane. The surface tension forces generated as liquid hexane evaporates are much reduced, when a dry membrane is produced. Membranes produced by this method are still used by Separex and Cynara to separate carbon dioxide from methane in natural gas.

Experience has shown that gas separation membranes are far more sensitive to minor defects in the selective membrane layer than membranes used in reverse osmosis or ultrafiltration. Even a few tiny defects can easily allow an unseparated gas flow equal

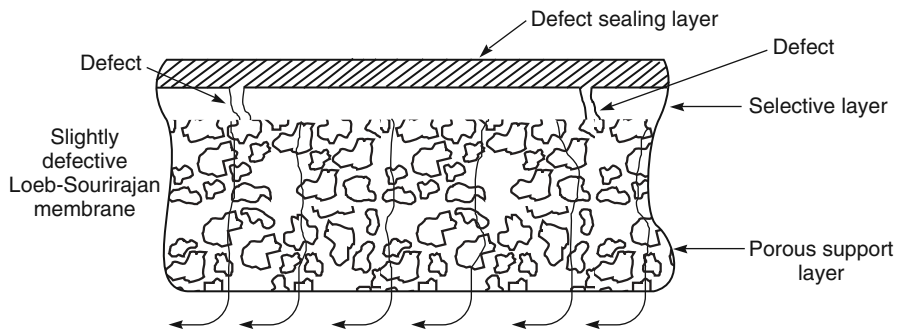


Figure 8.9 The technique devised by Henis and Tripodi [18] to seal defects in their selective polysulfone Loeb–Sourirajan membrane

to 1–2% of the total flux through the membrane. The sensitivity of gas separation membranes to defects posed a serious problem to early developers. Generation of a few defects is very difficult to avoid during membrane preparation and module formation.

In 1978, Henis and Tripodi [6, 18] at Monsanto devised an ingenious solution to the membrane defect problem; their approach is illustrated in Figure 8.9. The Monsanto group made Loeb–Sourirajan-type hollow fiber membranes (principally from polysulfone), then coated the membranes with a thin layer of silicone rubber. Silicone rubber is extremely permeable compared to polysulfone, but has a much lower selectivity; thus, the silicone rubber coating did not significantly change the selectivity or flux through the defect-free portions of the polysulfone membrane. However, the coating plugged membrane defects in the polysulfone membrane and eliminated convective flow through these defects. The silicone rubber layer also protected the membrane during handling. The development of silicone rubber-sealed anisotropic membranes was a critical step in the production of the first successful gas separation membrane for hydrogen/nitrogen separations by Monsanto.

Another type of gas separation membrane is the multilayer composite structure shown in Figure 8.10. The preparation of these membranes is described in Chapter 3. The base material that provides the mechanical strength is a finely microporous support membrane. This support is then coated with a series of thin polymer coatings. A gutter

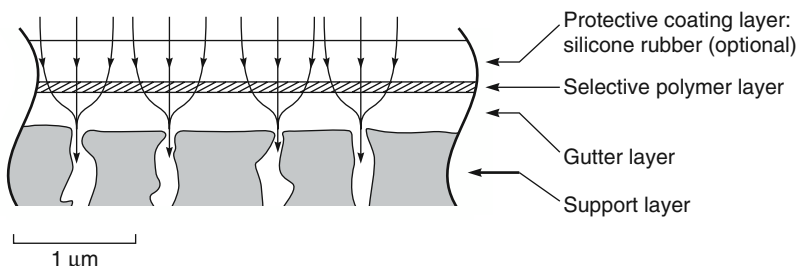


Figure 8.10 Multilayer composite membrane formed by coating thin layers of polymer on a microporous support membrane that provides mechanical strength

layer is often applied first to provide a defect-free, smooth surface onto which the ultrathin selective layer is applied. A final protective layer of silicone rubber or other highly permeable polymer is then applied to seal any defects. It is difficult to make composite membranes with glassy selective layers as thin and high-flux as good-quality Loeb–Sourirajan membranes. However, composite membranes can be made from a much wider range of materials than the Loeb–Sourirajan process allows. It is also possible to make composite membranes that use rubbery soft polymers as the selective layer, while the microporous support that provides mechanical strength is made from a tough, glassy polymer. Rubbery composite membranes of this type can withstand pressure differentials of 100 bar or more.

8.2.2 Metal Membranes

Although almost all industrial gas separation processes use polymeric membranes, interest in metal membranes continues, mostly for the high-temperature membrane reactor applications discussed in Chapter 13 and for the preparation of pure hydrogen for fuel cells. Hydrogen-permeable palladium and palladium alloy membranes are extraordinarily selective, being permeable to hydrogen, but essentially impermeable to all other gases. Membrane permeation rates are extremely high, usually 10–100 times higher than permeation rates measured with polymeric membranes. Hydrogen also permeates a number of other metals including tantalum, niobium, vanadium, nickel, iron, copper, cobalt, and platinum [19]. However, in most cases, metal membranes must be operated at high temperatures ($>300^{\circ}\text{C}$) to obtain useful permeation rates and to prevent embrittlement and cracking of the metal by sorbed hydrogen. Poisoning of the membrane surface by oxidation or sulfur deposition from trace amounts of hydrogen sulfide also occurs. The preparation and properties of these membranes are described in more detail in Chapter 3.

Despite their extraordinary permeation and selectivity properties, metal membranes have found very limited industrial application [20]. In the 1970s and early 1980s, Johnson Matthey built a number of systems to produce on-site hydrogen by separation of hydrogen/carbon dioxide mixtures made by reforming methanol. This was not a commercial success, but the company and others still produce small systems using palladium–silver alloy membranes to generate ultrapure hydrogen from 99.9% hydrogen for the electronics industry and as feed gas to fuel cells.

8.2.3 Ceramic and Zeolite Membranes

During the last few years, ceramic- and zeolite-based membranes have begun to be used for a few commercial separations. These membranes are all multilayer composite structures formed by coating a thin selective ceramic or zeolite layer onto a microporous ceramic support. Ceramic membranes are prepared by the sol-gel technique described in Chapter 3; zeolite membranes are prepared by direct crystallization, in which the thin zeolite layer is crystallized at high pressure and temperature directly onto the microporous support [21, 22] (also described in Chapter 3).

Both Mitsui [23] and ECN [24] have commercialized these membranes for dehydration of alcohols by pervaporation or vapor/vapor permeation. The membranes are made in tubular form. Extraordinarily high selectivities have been reported for these membranes, and their ceramic nature allows operation at high temperatures, so fluxes are high. These

advantages are, however, offset by the costs of the membrane modules, currently in excess of US\$3000/m² of membrane.

8.2.4 Thermally Rearranged/Microporous Carbon Membranes

When heated in a vacuum or inert atmosphere, many polymers will thermally rearrange, crosslink and, at temperatures above 300–400°C, begin to carbonize. Of particular interest are polymers that undergo these changes before they soften or melt. It is then possible to form an anisotropic or composite membrane and to partially or completely carbonize the membrane by heating it to a high temperature. The membrane left has the original asymmetric structure, but the selective layer is changed to a highly crosslinked or carbonized finely microporous film.

Koresh and Soffer were the first to prepare this type of membrane, and in 1983, reported a carbonized membrane with an oxygen/nitrogen selectivity of 7–8 [25]. Later, membranes with selectivities of 10–20 and good permeances were made. Since then, the process has been the subject of considerable development by Soffer, Lee [26, 27], Koros and Williams [28], Ube Industries in Japan [29, 30], and many others. Carbonized membranes can have exceptional separation properties. Membranes with oxygen/nitrogen selectivities of more than 10 and carbon dioxide/methane selectivities of 50–100 with good permeances have been reported many times. Membranes with propylene/propane selectivities of more than 20 have also been made [29]. These membranes, if successfully scaled up, would find use in many petrochemical applications.

Unfortunately, carbon membranes are brittle, and difficult to produce as high-surface-area membrane modules. More importantly, the finely microporous structure of the polymers can also be plugged by trace amounts of heavy hydrocarbons or even water present in the feed gas. Until these problems are solved, these membranes are likely to remain in the laboratory despite their outstanding permeation properties.

8.2.5 Mixed-Matrix Membranes

The ceramic microporous carbon and zeolite membranes described above are far too expensive for most separation applications. For this reason, despite their exceptional selectivities, these membranes are not yet used on an industrial scale. One solution to this problem is to prepare membranes from materials consisting of the inorganic particles dispersed in a polymer matrix. These mixed-matrix membranes are expected to combine the selectivity of the inorganic membranes with the low cost and ease of manufacture of polymer membranes. The development of these membranes has been described in Chapter 3. Despite a very significant effort over more than 20 years, these membranes have not left the laboratory. Low permeances are one problem, because it is difficult to make thin mixed-matrix membranes. Another problem is fouling of the membranes by minor, easily absorbed components in the feed mixture to be separated.

8.3 Membrane Modules

Gas separation membranes are formed into spiral-wound or hollow fiber modules. Particulate matter, oil mist, and other potentially fouling materials can be completely and

Table 8.2 Module designs used for various gas separation applications

Application	Typical membrane material	Selectivity (α)	Pressure-normalized flux of most permeable component ($10^{-6} \text{ cm}^3 (\text{STP})/\text{cm}^2 \cdot \text{s} \cdot \text{cmHg}$)	Commonly used module designs
O ₂ /N ₂	Polyimide	6–7	10–30	Hollow fiber–bore-side feed
H ₂ /N ₂	Polysulfone	100	100–200	Hollow fiber–shell-side feed
CO ₂ /CH ₄	Cellulose acetate	15	100–200	Spiral or hollow fiber–shell-side feed
VOC/N ₂	Silicone rubber	10–30	1000–2000	Spiral
H ₂ O/Air	Polyimide	>200	2000–5000	Capillary–bore-side feed

economically removed from gas streams by good-quality coalescing filters, so membrane fouling is generally more easily controlled in gas separation than with liquid separations. Therefore, the choice of module design is usually decided by cost and membrane flux. The high pressures used in gas separation applications require that the hollow fiber membranes used are very fine, with lumen diameters of 50–200 μm . The pressure drop required to circulate gas on the lumen side of the membrane of these small-diameter fibers can become large enough to seriously affect membrane performance. In the production of nitrogen from air, membrane permeances are relatively low, from 1 to 2 gpm, and parasitic pressure drops are not a problem. However, in the separation of hydrogen from nitrogen or methane and carbon dioxide from natural gas, membrane permeances are higher, and hollow fine fiber modules can develop excessive permeate-side pressure drops. The solution is to use capillary fibers or spiral-wound modules for this type of application. Nonetheless, these disadvantages of hollow fiber membranes may be partially offset by their lower cost per square meter of membrane. These factors are summarized for some important gas separation applications in Table 8.2.

8.4 Process Design

The three factors that determine the performance of a membrane gas separation system are illustrated in Figure 8.11. The role of membrane selectivity is obvious; not so obvious are the importance of the ratio of feed pressure (p_o) to permeate pressure (p_ℓ) across the membrane, usually called the pressure ratio, φ , and defined as

$$\varphi = \frac{p_o}{p_\ell} \quad (8.7)$$

and of the membrane stage-cut, θ , which is the fraction of the feed gas that permeates the membrane, defined as

$$\theta = \frac{\text{permeate flow}}{\text{feed flow}} \quad (8.8)$$

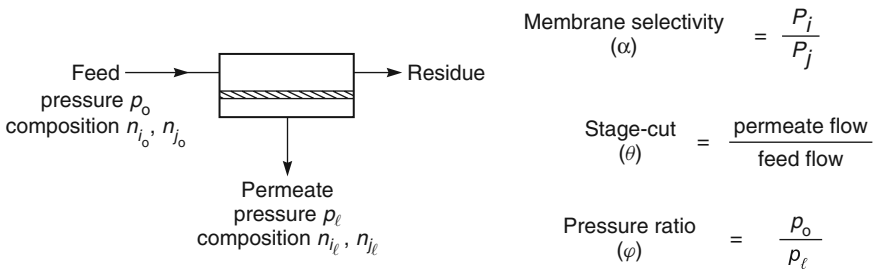


Figure 8.11 Parameters affecting the performance of membrane gas separation systems

8.4.1 Pressure Ratio

The importance of pressure ratio in the separation of gas mixtures can be illustrated by considering the separation of a gas mixture with component concentrations of n_{i_o} and n_{j_o} at a feed pressure p_o . A flow of component i across the membrane can only occur if the partial pressure of i on the feed side of the membrane ($n_{i_o} p_o$) is greater than the partial pressure of i on the permeate side of the membrane ($n_{i_e} p_e$), that is,

$$n_{i_o} p_o > n_{i_e} p_e \quad (8.9)$$

It follows that the maximum separation achieved by the membrane can be expressed as

$$\frac{p_o}{p_e} \geq \frac{n_{i_e}}{n_{i_o}} \quad (8.10)$$

That is, the separation achieved can never exceed the pressure ratio φ , no matter how selective the membrane:

$$\frac{n_{i_e}}{n_{i_o}} \leq \varphi \quad (8.11)$$

The relationship between pressure ratio and membrane selectivity can be derived from the Fick's law expression for the fluxes of components i and j

$$j_i = \frac{\mathcal{P}_i(p_{i_o} - p_{i_e})}{\ell} \quad (8.12)$$

and

$$j_j = \frac{\mathcal{P}_j(p_{j_o} - p_{j_e})}{\ell} \quad (8.13)$$

The total gas pressures on the feed and permeate side are the sum of the partial pressures. For the feed side

$$p_o = p_{i_o} + p_{j_o} \quad (8.14)$$

and for the permeate side

$$p_\ell = p_{i_\ell} + p_{j_\ell} \quad (8.15)$$

The volume fractions of components i and j on the feed side and permeate side are also related to partial pressures. For the feed side

$$n_{i_o} = \frac{p_{i_o}}{p_o} \quad n_{j_o} = \frac{p_{j_o}}{p_o} \quad (8.16)$$

and for the permeate side

$$n_{i_\ell} = \frac{p_{i_\ell}}{p_\ell} \quad n_{j_\ell} = \frac{p_{j_\ell}}{p_\ell} \quad (8.17)$$

while from mass balance considerations

$$\frac{j_i}{j_j} = \frac{n_{i_\ell}}{n_{j_\ell}} = \frac{n_{i_\ell}}{1 - n_{i_\ell}} = \frac{1 - n_{j_\ell}}{n_{j_\ell}} \quad (8.18)$$

Dividing Equation 8.12 by Equation 8.13 and using the definition of α , Equation 8.3, and Equations 8.16–8.18 lead to

$$n_{i_\ell} = \frac{1}{2} \times \frac{n_{i_o} + \frac{1}{\varphi} + \frac{1}{\alpha - 1} - \sqrt{\left(n_{i_o} + \frac{1}{\varphi} + \frac{1}{\alpha - 1}\right)^2 - \frac{4 \times \alpha \times n_{i_o}}{(\alpha - 1) \times \varphi}}}{\frac{1}{\varphi}} \quad (8.19)$$

This somewhat complex expression breaks down into two limiting cases, depending on the relative magnitudes of the pressure ratio and the membrane selectivity. First, if the membrane selectivity (α) is very much larger than the pressure ratio (φ), that is,

$$\alpha \gg \varphi \quad (8.20)$$

then Equation 8.19 becomes

$$n_{i_\ell} = n_{i_o} \varphi \quad (8.21)$$

This is called the pressure-ratio-limited region, in which the performance is determined only by the pressure ratio across the membrane and is independent of the membrane selectivity.

If the membrane selectivity (α) is very much smaller than the pressure ratio (φ), that is,

$$\alpha \ll \varphi \quad (8.22)$$

then Equation 8.19 becomes (after some manipulation and the application of the rule of l'Hôpital)

$$n_{i_e} = \frac{\alpha \cdot n_{i_o}}{n_{i_o} \cdot (\alpha - 1) + 1} \quad (8.23)$$

This is called the membrane-selectivity-limited region, in which the membrane performance is determined only by the membrane selectivity and is independent of the pressure ratio. There is, of course, an intermediate region between these two limiting cases, in which both the pressure ratio and the membrane selectivity affect the membrane system performance. These three regions are illustrated in Figure 8.12, in which the calculated permeate concentration (n_{i_e}) is plotted versus pressure ratio (φ) for a membrane with a selectivity of 30 [31]. At a pressure ratio of 1, the feed pressure is equal to the permeate pressure, and no separation is achieved by the membrane. As the difference between the feed and permeate pressure increases, the concentration of the more permeable component in the permeate gas begins to increase, first according to Equation 8.21 and then, when the pressure ratio and membrane selectivity are comparable, according to Equation 8.19. At very high pressure ratios, that is, when the pressure ratio is four to five times higher than the membrane selectivity, the membrane enters the membrane-selectivity-controlled region. In this region the permeate concentration reaches the limiting value given by Equation 8.23.

The relationship between pressure ratio and selectivity is important because of the practical limit to the pressure ratio achievable in gas separation systems. Compressing the feed stream to very high pressure or drawing a very hard vacuum on the permeate side

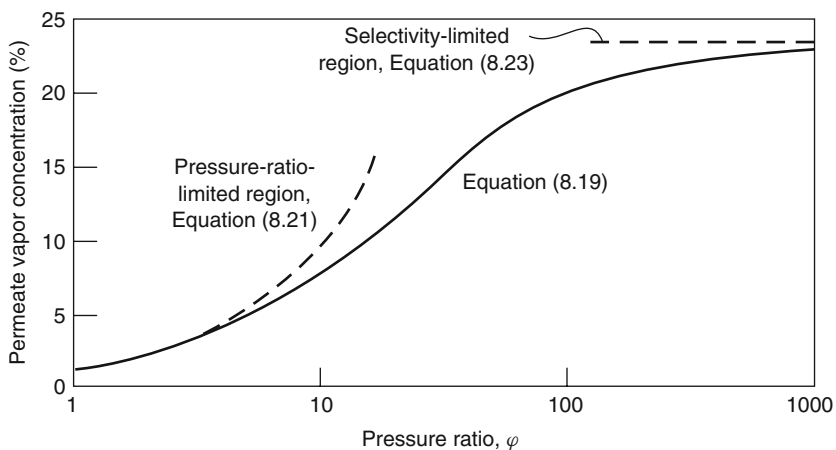


Figure 8.12 Calculated permeate vapor concentration for a vapor-permeable membrane with a vapor/nitrogen selectivity of 30 as a function of pressure ratio. The feed vapor concentration is 1%. Below pressure ratios of about 10, separation is limited by the pressure ratio across the membrane. At pressure ratios above about 100, separation is limited by the membrane selectivity [31]

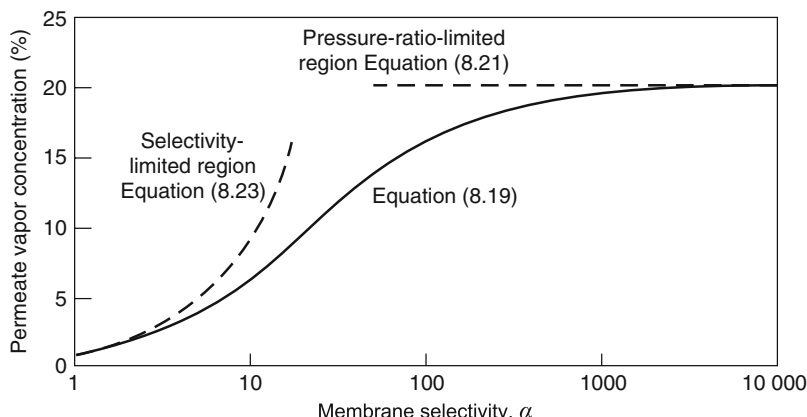


Figure 8.13 Calculated permeate vapor concentration as a function of selectivity. The feed vapor concentration is 1%; the pressure ratio is fixed at 20. Below a vapor/nitrogen selectivity of about 10, separation is limited by the low membrane selectivity; at selectivities above about 100, separation is limited by the low pressure ratio across the membrane [31]

of the membrane to achieve large pressure ratios both require large amounts of energy and expensive pumps. As a result, typical practical pressure ratios are in the range 5–20.

Because the attainable pressure ratio in most gas separation applications is limited, the benefit of very highly selective membranes is often less than might be expected. For example, as shown in Figure 8.13, if the pressure ratio is 20, then increasing the membrane selectivity from 10 to 20 will significantly improve system performance. However, a much smaller incremental improvement results from increasing the selectivity from 20 to 40. Increases in selectivity above 100 will produce negligible improvements.

8.4.2 Stage-Cut

Another factor that affects membrane system design is the degree of separation required. The usual target of a gas separation system is to produce a residue stream essentially stripped of the permeable component and a small, highly concentrated permeate stream. These two requirements cannot be met simultaneously; a trade-off must be made between removal from the feed gas and enrichment in the permeate. The system attribute that characterizes this trade-off is called the stage-cut. Analytical expressions linking the membrane and the operating conditions expressed in Equation 8.19 with the performance of a module have been developed for simple binary mixtures [32]. These expressions are clumsy for routine use, so industrial membrane producers have all developed differential element computer programs to calculate the performance of these modules. The techniques used to create these programs have been described in the literature [33, 34], but the programs themselves are not generally available.

The effect of stage-cut on module performance calculated with a differential element computer program is shown in Figure 8.14.

In the example calculation shown, the feed gas contains 50% of a permeable gas (i) and 50% of a relatively impermeable gas (j). Under the assumed operating conditions

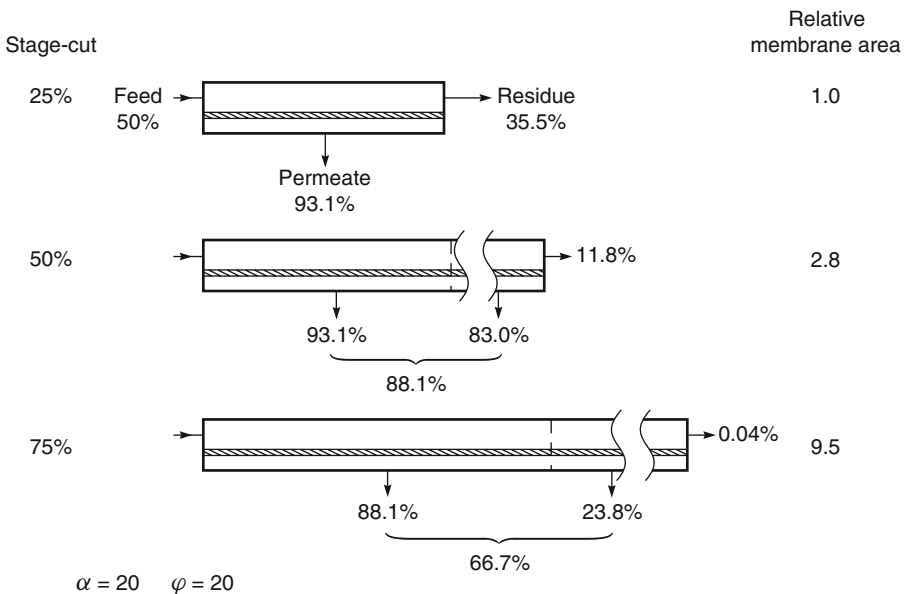


Figure 8.14 The effect of stage-cut on the separation of a 50/50 feed gas mixture (pressure ratio, 20; membrane selectivity, 20). At low stage-cuts a concentrated permeate product, but only modest removal from the residue, can be obtained. At high stage-cuts almost complete removal is obtained, but the permeate product is only slightly more enriched than the original feed

of this system (pressure ratio 20, membrane selectivity 20), it is possible at zero stage-cut to produce a permeate stream containing 94.8% of component i . But the permeate stream is tiny and the residue stream is still very close to the feed gas concentration of 50%. As the fraction of the feed gas permeating the membrane is increased by increasing the membrane area, the concentration of the permeable component in the residue and permeate streams falls. At a stage-cut of 25%, the permeate gas concentration has fallen from 94.8% (its maximum value) to 93.1%. The residue stream concentration of permeable gas is then 35.5%. Increasing the fraction of the feed gas that permeates the membrane to 50% by adding more membrane area produces a residue stream containing 11.8% of the permeable gas. However, the gas permeating the added membrane area only contains 83.0% of the permeable component, so the average concentration of permeable component in the permeate stream is reduced from 93.1 to 88.1%. If the fraction of the feed gas that permeates the membrane is increased to 75% by adding even more membrane area, the concentration of the permeable component in the residue stream is reduced to only 0.04%. However, the gas permeating the added membrane area only contains 23.8% of the permeable component, *less than the original feed gas*. The average concentration of the permeable component in the feed gas is, therefore, reduced to 66.7%. This means that half of the less permeable component has been lost to the permeate stream.

The calculations shown in Figure 8.14 illustrate the trade-off between recovery and purity. A single-stage membrane process can be designed for either maximum recovery or maximum purity, but not both. The calculations also show that membranes can produce very pure residue gas streams enriched in the less permeable component, although at low recoveries. However, the enrichment of the more permeable component in the permeate can never be more than the membrane selectivity, so a membrane with low selectivity produces an only slightly enriched permeate. This is why membranes with an oxygen/nitrogen selectivity of 4–6 can produce very pure nitrogen (>99.5%) from air on the residue side of the membrane, but the same membranes cannot produce better than 50–60% oxygen on the permeate side. If the more permeable component must be pure, very selective membranes are required or multistage or recycle membrane systems must be used.

Finally, the calculations in Figure 8.14 show that increasing the stage-cut to produce a pure residue stream requires a disproportionate increase in membrane area. As the feed gas is stripped of the more permeable component, the average permeation rate through the membrane falls toward the permeation rate of the slow gas. In the example shown, this means that permeating the first 25% of the feed gas requires a relative membrane area of 1, permeating the next 25% requires a membrane area increment of 1.8, and permeating the next 25% requires an increment of 6.7.

8.4.3 Multistep and Multistage System Designs

Because the membrane selectivity and pressure ratio achievable in a commercial membrane system are limited, a one-stage membrane system may not provide the separation desired. The problem is illustrated in Figure 8.15. By way of example, the process designs are calculated for the removal of a volatile organic compound (VOC), which is the permeable component, from a nitrogen feed gas, which contains 1 vol% of this component. Rubbery membranes such as silicone rubber permeate the VOC preferentially because of its greater condensability and hence solubility in the membrane. In this calculation, the pressure ratio is fixed at 20 by compressing the feed gas, and the permeate is maintained at atmospheric pressure. The membrane VOC/nitrogen selectivity is assumed to be 20.

Figure 8.15 shows that when 90% of the VOC in the feed stream is removed, the permeate stream will contain approximately 4% of the permeable component. In many

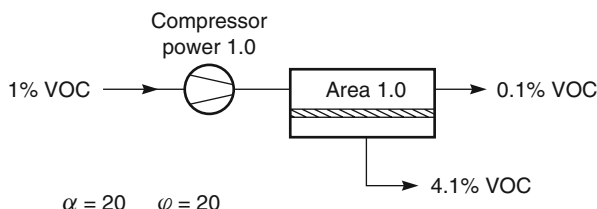


Figure 8.15 A one-stage vapor separation operation. The performance of this system was calculated for a cross-flow module using a vapor/nitrogen selectivity of 20 and a pressure ratio of 20

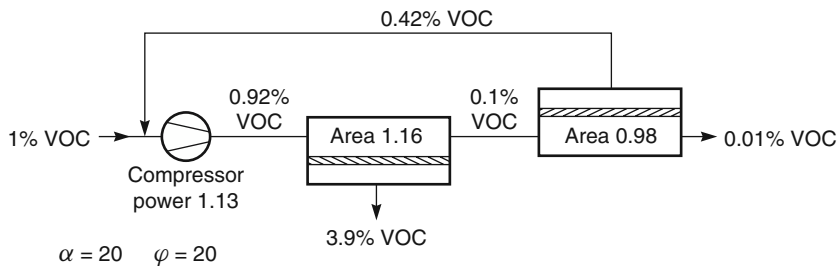


Figure 8.16 A two-step system to achieve 99% vapor removal from the feed stream. Selectivity, 20; pressure ratio, 20

cases, 90% removal of VOC from the feed stream is insufficient to allow the residue gas to be discharged, and enrichment of the component in the permeate is also insufficient.

If the main problem is insufficient VOC removal from the feed stream, a two-step system as shown in Figure 8.16 can be used. In a two-step system, the residue stream from the first membrane unit is passed to a second unit, where the VOC concentration is reduced by a further factor of 10, from 0.1 to 0.01%. Because the concentration of VOC in the feed to the second membrane unit is low, the permeate stream is relatively dilute and is recirculated to the feed stream.

A multistep design of this type can achieve almost complete removal of the permeable component from the feed stream to the membrane unit. However, greater removal of the permeable component is achieved at the expense of increases in membrane area and power consumption by the compressor. As a rule of thumb, the membrane area required to remove the last 9% of a component from the feed equals the membrane area required to remove the first 90%.

Sometimes, 90% removal of the permeable component from the feed stream is acceptable for the discharge stream from the membrane unit, but a higher concentration is needed to make the permeate gas usable. In this situation, a two-stage system of the type shown in Figure 8.17 is used. In a two-stage design, the permeate from the first

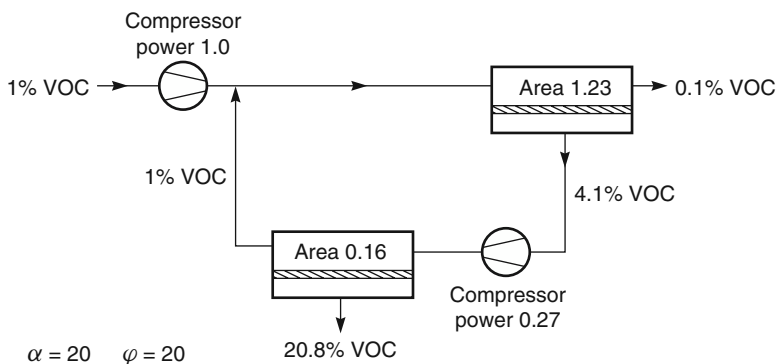


Figure 8.17 A two-stage system to produce a highly concentrated permeate stream. Selectivity, 20; pressure ratio, 20

membrane unit is recompressed and sent to a second membrane unit, where a further separation is performed. The final permeate is then twice enriched. In the most efficient two-stage designs, the residue stream from the second stage is reduced to about the same concentration as the original feed gas, with which it is mixed. In the example shown in Figure 8.17, the permeate stream, concentrated a further fivefold, leaves the system at a concentration of 21%. Because the volume of gas treated by the second-stage membrane unit is much smaller than in the first stage, the membrane area of the second stage is relatively small. Thus, incorporation of a second stage only increases the overall membrane area and power requirements by approximately 30–40%.

More complex multistage/multistep combination processes can be designed, but are seldom used in commercial systems – their complexity makes them uncompetitive with alternative separation technologies. More commonly, some form of recycle design is used.

8.4.4 Recycle Designs

A simple recycle design, sometimes called a two-and-one-half-stage system, proposed by Wijmans and Baker [35] is shown in Figure 8.18. In this design, the permeate from the first membrane stage is recompressed and sent to a two-step second stage, where a portion of the gas permeates and is removed as enriched product. The remaining gas passes to another membrane stage, which brings the gas concentration close to the original feed value. The permeate from this stage is mixed with the first-stage permeate, forming a recycle loop. By controlling the relative size of the two second stages, any desired concentration of the more permeable component can be achieved in the product. In the example shown, the permeable component is concentrated to 50% in the permeate. The increased performance is achieved at the expense of a slightly larger second-stage compressor and more membrane area. Normally, however, this design is preferable to a more complex three-stage system.

Figure 8.19 shows another type of recycle design in which a recycle loop increases the concentration of the permeable component to the point at which it can be removed

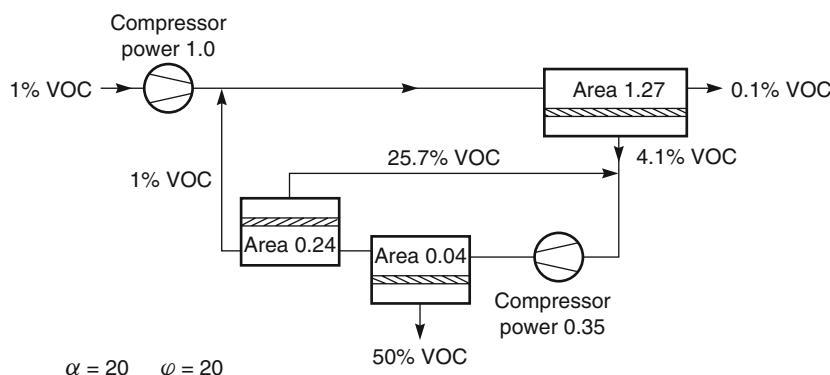


Figure 8.18 Two-and-one-half-stage system: by forming a recycle loop around the second stage, a small, very concentrated product stream is created. Selectivity, 20; pressure ratio, 20 [35]

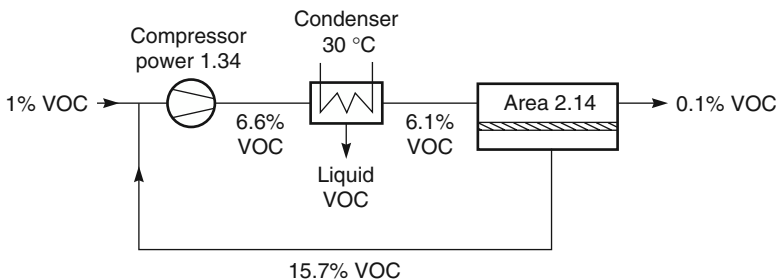


Figure 8.19 Recycle system design using one membrane stage, preceded by a compressor and condenser: feed stream, 1% vapor in nitrogen; selectivity, 20; pressure ratio, 20. The VOC is assumed to be pentane

by a second process, most commonly condensation [36]. The feed stream entering the recycle loop contains 1% of the permeable component as in Figures 8.15–8.18. After compression to 20 atm, the feed gas passes through a condenser at 30°C, but the VOC content is still below the condensation concentration at this temperature. The membrane unit separates the gas into a VOC-depleted residue stream and a vapor-enriched permeate stream, which is recirculated to the front of the compressor. Because the bulk of the vapor is recirculated, the concentration of vapor in the loop increases rapidly until the pressurized gas entering the condenser exceeds the vapor dew point of 6.1%. At this point, the system is at steady state; the mass of VOC entering the recirculation loop is equal to the mass discharged in the residue stream plus the mass removed as liquid condensate.

Recycle designs of this type are limited to applications in which the components of the gas mixture, if sufficiently concentrated, can be separated from the gas by some other technique. With organic vapors, condensation is often possible; adsorption, chemical scrubbing, or absorption can also be used. The process shown in Figure 8.19 is used to separate VOCs from nitrogen and air, or to separate propane, butane, pentane, and higher hydrocarbons from natural gas (methane).

All the example process designs illustrated in Figures 8.15–8.19 used cross-flow membrane modules. This is because the improvement in separation performance achieved by a counter-flow module does not normally compensate for the extra cost of fabrication and use of this type of module. However, some special cases do exist where this type of module can offer real benefits. The dehydration of air and natural gas with counter-flow sweep modules was discussed in Chapter 4. Counter-flow modules were also used in the continuous membrane column popularized by Hwang and Thorman [37].

Hwang's device is shown in Figure 8.20, applied to the separation of oxygen and nitrogen in air. Pressurized air is introduced at the middle of the high-pressure side of the unit. As the air travels down the bottom membrane section, the more permeable component (oxygen) permeates the membrane. The feed gas is thus continually depleted of oxygen. At the bottom of the unit, the nitrogen-enriched residue gas is removed. The permeate gas, enriched in oxygen, travels up the column on the permeate side of the membrane, countercurrent to the feed gas. A portion of this gas is removed at the top of the column while the remainder is compressed and recycled on the high-pressure side of

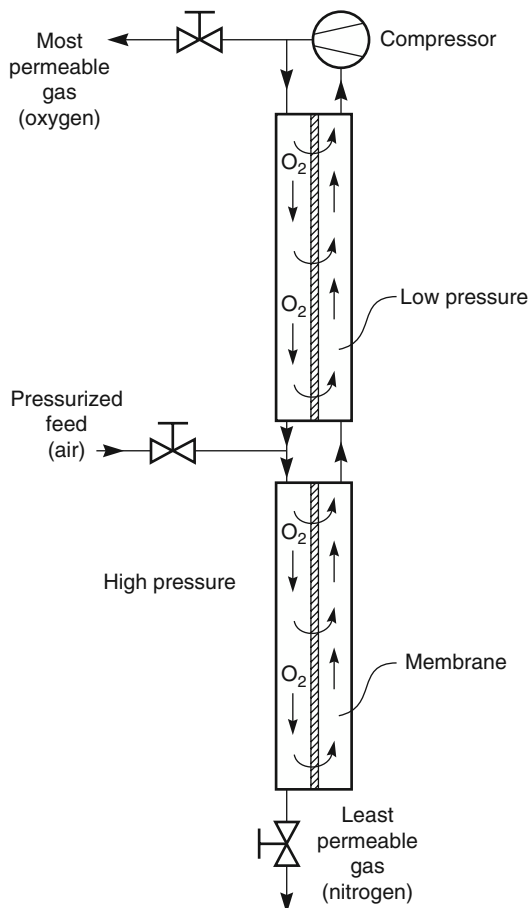


Figure 8.20 Schematic illustration of a continuous membrane column popularized by Sun-Tak Hwang and used here to separate oxygen and nitrogen in air. Reprinted with permission from [54]. Copyright (1980) John Wiley and Sons.

the top membrane section. Oxygen in this recycle gas permeates through the membrane, so the more permeable oxygen accumulates at the top of the column. The process has features in common with the reflux operation of a distillation column and, when developed by Hwang, was described in similar language. The Hwang group demonstrated that a number of spectacular separations could be achieved with the device. Unfortunately, the energy cost of the recycle operation meant the system could not compete economically with more conventional multistep/multistage membrane designs.

8.5 Applications

The membrane gas separation industry is still growing and changing. Two of the largest industrial gas companies now have membrane affiliates: Air Products (Permea) and

Air Liquide (Medal). The affiliates focus mainly on producing membrane systems to separate nitrogen from air, but also produce some hydrogen separation systems. Ube (Japan) and Aquillo (The Netherlands) are also active in these markets. Another group of companies – UOP (GMS/Separex), Cameron (Cynara), and MTR – produce membrane systems for natural gas separations. A third group of smaller independents are focusing on new applications, including vapor separation, air dehydration, and oxygen enrichment. The final size and form of this industry is still changing. The following section covers the major current applications. Overview articles on the main gas separation applications can be found in Paul and Yampol'skii [38], in Koros and Fleming [39], and elsewhere [40].

8.5.1 Hydrogen Separations

The first large-scale commercial application of membrane gas separation was the separation of hydrogen from nitrogen in ammonia purge gas streams. The process, launched in 1980 by Monsanto, was followed by a number of similar applications, such as hydrogen/methane separation in refinery off-gases and hydrogen/carbon monoxide adjustment in oxo chemical synthesis plants [7]. Hydrogen is a small, noncondensable gas, which is highly permeable compared to all other gases. This is particularly true with the glassy polymers primarily used to make hydrogen-selective membranes; fluxes and selectivities of hydrogen through some of these materials are shown in Table 8.3. With fluxes and selectivities as high as these, it is easy to understand why hydrogen separation was the first gas separation process developed. Early hydrogen membrane gas separation plants used polysulfone or cellulose acetate membranes, but now a variety of specifically synthesized materials, such as polyimides (Ube), polyaramide (Medal), or brominated polysulfone (Permea), are used.

A typical membrane system flow scheme for recovery of hydrogen from an ammonia plant purge gas stream is shown in Figure 8.21. A photograph of such a system is shown in Figure 8.22. During the production of ammonia from nitrogen and hydrogen, argon enters the high-pressure ammonia reactor as an impurity with the nitrogen stream, and methane enters the reactor as an impurity with the hydrogen. Ammonia produced in the reactor is removed by condensation, so the argon and methane impurities accumulate until they represent as much as 15% of the gas in the reactor. To control the concentration of these components, the reactor must be continuously purged. The hydrogen lost with this purge gas can represent 2–4% of the total hydrogen consumed. Ammonia plants are very large, so recovery of purged hydrogen for recycle to the reactor is economically worthwhile.

Table 8.3 Hydrogen separation membranes

Membrane (developer)	Selectivity			Hydrogen pressure-normalized flux ($10^{-6} \text{ cm}^3 (\text{STP})/\text{cm}^2 \cdot \text{s} \cdot \text{cmHg}$)
	H ₂ /CO	H ₂ /CH ₄	H ₂ /N ₂	
Polyaramide (Medal)	100	>200	>200	100
Polysulfone (Permea)	40	80	80	100
Cellulose acetate (Separex)	30–40	60–80	60–80	200
Polyimide (Ube)	50	100–200	100–200	80–200

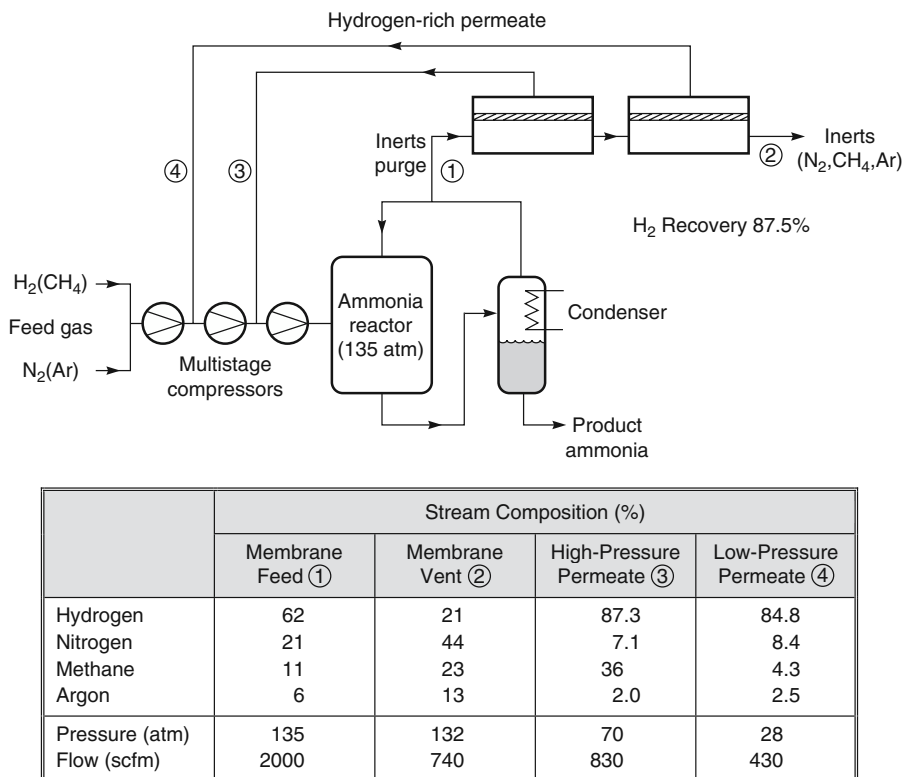


Figure 8.21 Simplified flow schematic of the PRISM® membrane system to recover hydrogen from an ammonia reactor purge stream. A two-step membrane system is used to reduce permeate compression costs

In the process shown in Figure 8.21, a two-step membrane design is used to reduce the cost of recompressing the hydrogen permeate stream to the very high pressures of ammonia reactors. In the first step, the feed gas is maintained at the reactor pressure of 135 atm, and the permeate is maintained at 70 atm, giving a pressure ratio of 1.9. The hydrogen concentration in the feed to this first step is about 62%, high enough that even at this low pressure ratio, the permeate contains about 90% hydrogen. However, by the time the feed gas hydrogen concentration has fallen to 30%, the hydrogen concentration in the permeate is no longer high enough for recycle to the reactor. This remaining hydrogen is recovered in a second membrane step operated at a lower permeate pressure of 28 atm; the resulting pressure ratio is 4.7. The increased pressure ratio increases the hydrogen concentration in the permeate significantly. By dividing the process into two steps operating at different pressure ratios, maximum hydrogen recovery is achieved at minimum permeate hydrogen recompression costs.

A second major application of hydrogen-selective membranes is recovery of hydrogen from waste gases produced in refinery operations [7, 41, 42]. A typical separation – treatment of the high-pressure purge gas from a hydrotreater – is shown in



Figure 8.22 Photograph of an Air Products and Chemicals, Inc. PRISM® membrane system installed at an ammonia plant. The modules are mounted vertically

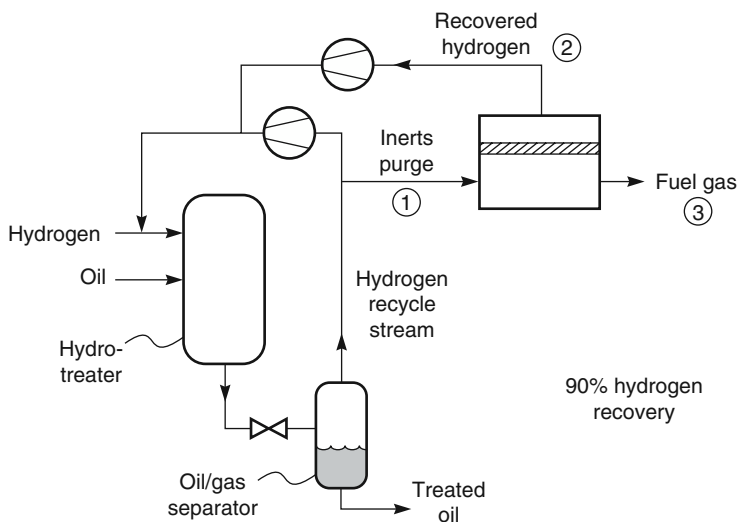
Figure 8.23. The hydrogen separation process is designed to recycle the hydrogen to the hydrotreater. As in the case of the ammonia plant, there is a trade-off between the concentration of hydrogen in the permeate and the permeate pressure and subsequent cost of recompression. In the example shown, a permeate of 96.5% hydrogen is considered adequate at a pressure ratio of 3.9.

Another example of the use of highly hydrogen-selective membranes in the petrochemical industry is the separation of hydrogen from carbon monoxide/hydrogen mixtures to obtain the correct ratio of components for subsequent synthesis operations.

8.5.2 Oxygen/Nitrogen Separation

The largest gas separation process in current use is the production of nitrogen from air. The first membranes used for this process were based on poly(4-methyl-1-pentene) (TPX) and ethyl cellulose. These polymer materials have oxygen/nitrogen selectivities of 4; the economics of the process using these membranes were marginal. The second-generation materials now used have selectivities of 6–7, providing very favorable economics, especially for small plants producing 5–500 scfm of nitrogen. In this range, membranes are the low-cost process, and most new small nitrogen plants use membrane systems.

Table 8.4 lists the permeabilities and selectivities of some of the materials that are used or have been used for this separation. There is a sharp trade-off between permeability



	Stream Composition		
	Untreated Purge ①	Recovered Hydrogen ②	Treated Purge ③
Hydrogen	82	96.5	34.8
Methane	12	2.6	43.3
Ethane	4.6	0.7	17.1
Propane	1.2	0.2	4.8
Pressure (psig)	1800	450	1450
Flow (MMscfd)	18.9	14.5	4.4

Figure 8.23 Hydrogen recovery from a hydrotreater used to lower the molecular weight of a refinery oil stream. Permea polysulfone membranes (PRISM®) are used [41]

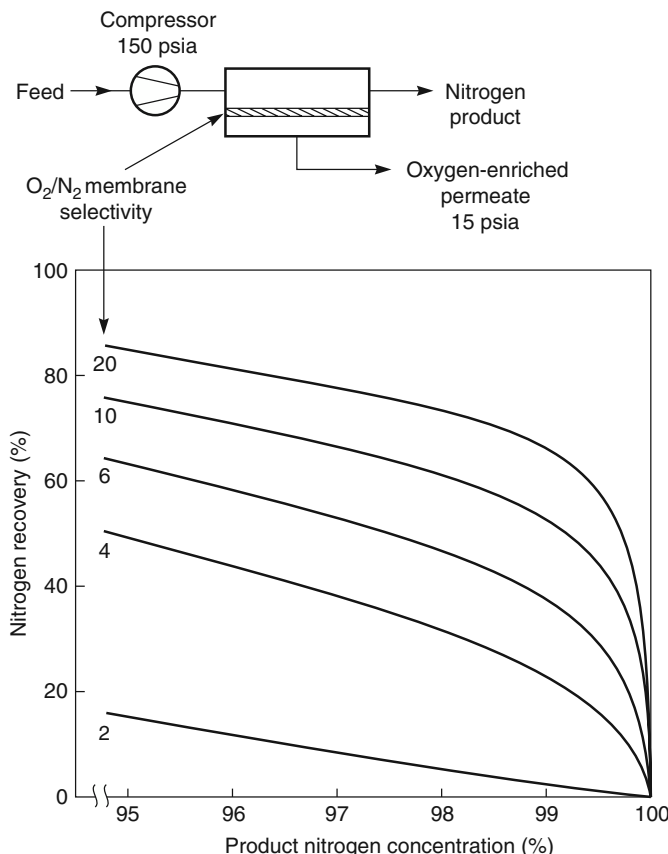
and selectivity. This trade-off was illustrated in the Robeson trade-off plot shown in Figure 8.6 [11].

High oxygen/nitrogen selectivity is required for an economical nitrogen production process. The effect of improved membrane selectivities on the efficiency of nitrogen production from air is illustrated in Figure 8.24. This figure shows the trade-off between the fraction of nitrogen in the feed gas recovered as nitrogen product gas as a function of the nitrogen concentration in the product gas. All oxygen-selective membranes, even membranes with an oxygen/nitrogen selectivity as low as 2, can produce better than 99% nitrogen, albeit at very low recoveries. The figure also shows the significant improvement in nitrogen recovery that results from an increase in oxygen/nitrogen selectivity from 2 to 20.

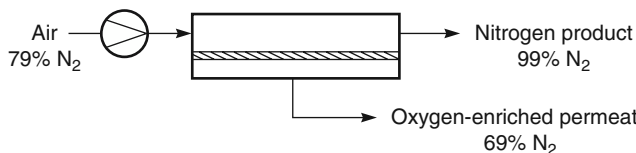
The first nitrogen production systems used membranes made from TPX with a selectivity of about 4. These membranes were incorporated into one-stage designs to produce 95% nitrogen used to render flammable-liquid storage tanks inert. As membranes

Table 8.4 Permeabilities and selectivities of polymers of interest in air separation

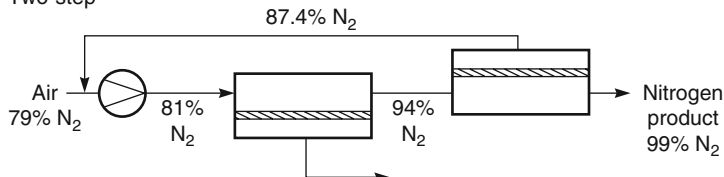
Polymer	Oxygen permeability (Barrer)	Nitrogen permeability (Barrer)	Oxygen/nitrogen selectivity
Poly(1-trimethylsilyl-1-propyne) (PTMSP)	7600	5400	1.4
Teflon AF 2400	1300	760	1.7
Silicone rubber	600	280	2.2
Poly(4-methyl-1-pentene) (TPX)	30	7.1	4.2
Poly(phenylene oxide) (PPO)	16.8	3.8	4.4
Ethyl cellulose	11.2	3.3	3.4
6FDA-DAF (polyimide)	7.9	1.3	6.2
Polyaramide	3.1	0.46	6.8
Tetrabromobisphenol A polycarbonate	1.4	0.18	7.5
Polysulfone	1.1	0.18	6.2

**Figure 8.24** Nitrogen recovery as a function of product nitrogen concentration for membranes with selectivities between 2 and 20

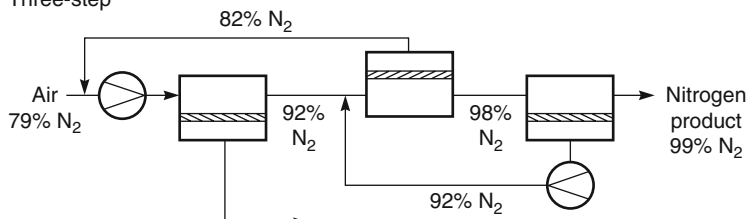
Single-step



Two-step



Three-step



Design	Relative Membrane Area	Relative Compressor HP
One-Step	1.0	1.0
Two-Step	0.94	0.94
Three-Step	0.92	0.92

Figure 8.25 Single-, two-, and three-step designs for nitrogen production from air

improved, more complex process designs, of the type shown in Figure 8.25, were used to produce purer gas containing >99% nitrogen. The first improvement was the two-step process. As oxygen is removed from the air passing through the membrane modules, the oxygen concentration in the permeating gas falls. At some point, the oxygen concentration in the permeate gas is less than the concentration in normal ambient feed air. Mixing this oxygen-depleted gas permeate with the incoming air then becomes worthwhile. The improvement is most marked when the system is used to produce high-quality nitrogen containing less than 1% oxygen. In the example shown in Figure 8.25, the second-step permeate gas contains 12.5% oxygen, and recycling this gas to the incoming feed air reduces the membrane area and compressor load by about 6%. This relatively small saving is worthwhile because it is achieved at essentially no cost by making a simple piping change to the system. In the two-step design, the 12.5% oxygen permeate recycle stream

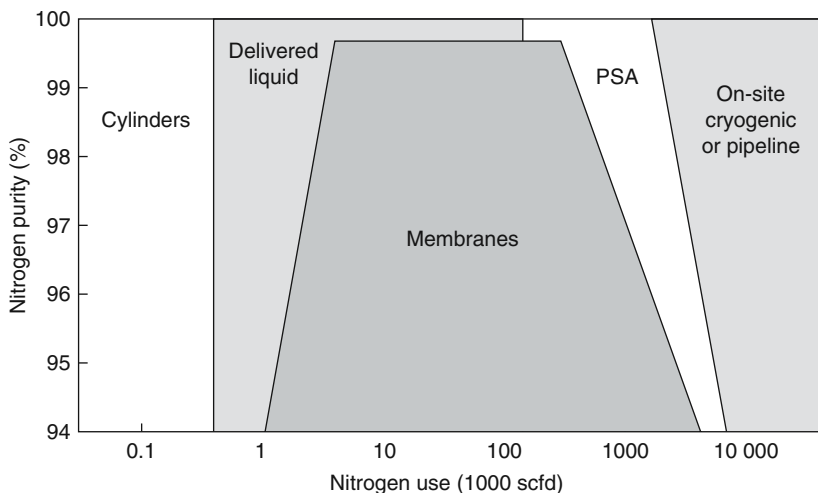


Figure 8.26 Approximate competitive range of current membrane nitrogen production systems. Many site-specific factors can affect the actual system selection

is mixed with ambient air containing 21% oxygen. A more efficient design would be to combine the recycle and feed gas where the feed gas has approximately the same concentration. This is the objective of the three-step process shown in Figure 8.25. This design saves a further 2% in membrane area and some compressor power, but now two compressors are needed. Three-step processes are, therefore, generally not used. A discussion of factors affecting the design of nitrogen plants is given by Prasad *et al.* [43, 44].

Membrane nitrogen production systems are now very competitive with alternative technologies. The competitive range of the various methods of obtaining nitrogen is shown in Figure 8.26. Very small nitrogen users generally purchase gas cylinders or delivered liquid nitrogen, but once consumption exceeds 5000 scfd of nitrogen, membranes become the low-cost process. This is particularly true if the required nitrogen purity is between 95 and 99% nitrogen. Membrane systems can still be used if high quality nitrogen (up to 99.9%) is required, but the cost of the system increases significantly. Very large nitrogen users – above 10 MMscfd of gas – generally use pipeline gas or on-site cryogenic systems. Pressure swing adsorption (PSA) systems are also used in the 1–10 MMscfd range.

A membrane process to separate nitrogen from air inevitably produces oxygen-enriched air as a by-product. Sometimes this by-product gas, containing about 35% oxygen, can be used beneficially, but usually it is vented. A market for oxygen or oxygen-enriched air exists, but because oxygen is produced as the permeate gas stream, it is much more difficult to produce high-purity oxygen than high-purity nitrogen with membrane systems. Figure 8.27 shows the maximum permeate oxygen concentration that can be produced by a one-step membrane process using membranes of various selectivities. Even at zero stage-cut and an infinite pressure ratio, the best currently available membrane, with an oxygen/nitrogen selectivity of 8, can only produce 68% oxygen. At useful stage-cuts and achievable pressure ratios, this concentration falls.

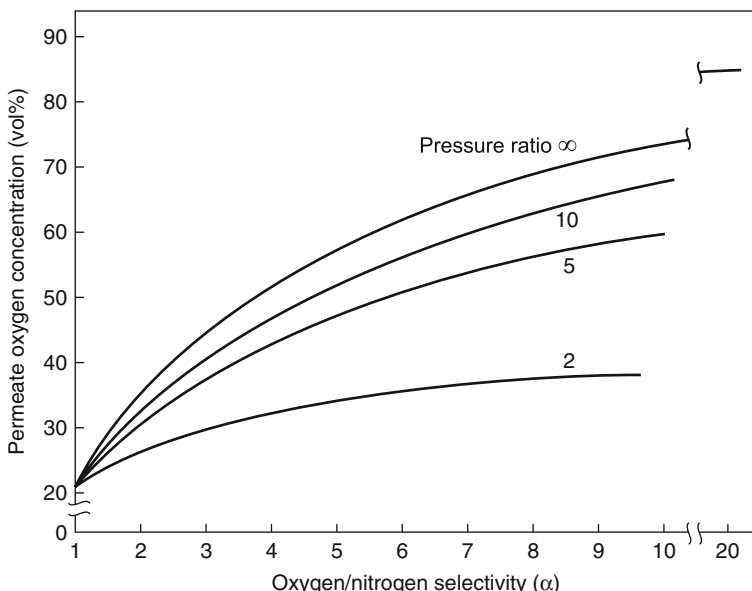


Figure 8.27 The maximum possible oxygen concentration in the permeate from a one-step membrane process with membranes of various selectivities (assumes zero stage-cut). Even the best current membrane materials, with a selectivity of 8, only produce 68% oxygen in the permeate at an infinite pressure ratio

These constraints limit membrane systems to the production of oxygen-enriched air in the 30–50% oxygen range.

Oxygen-enriched air is used in the chemical industry, in refineries, and in various fermentation and biological digestion processes, but it must be produced very cheaply for these applications. The competitive technology is pure oxygen produced cryogenically, then diluted with atmospheric air. The quantity of pure oxygen that must be blended with air to produce the desired oxygen enrichment determines the cost. This means that in membrane systems producing oxygen-enriched air, only the fraction of the oxygen above 21% can be counted as a credit. This fraction is called the equivalent pure oxygen (EPO₂) basis.

A comparison of the cost of oxygen-enriched air produced by membranes and by cryogenic separation shows that current membranes are generally uncompetitive. The only exception is for very small users in isolated locations, where the logistics of transporting liquid oxygen to the site increase the oxygen cost to US\$80–100/ton.

In the early 2000s in Japan and China, a market developed for small oxygen enrichment systems as a component in high-end room air conditioners, and in small personal oxygen-enriching devices for students working in smoke-filled rooms. These devices produced 25–28% oxygen and were filled with silicone rubber- or polyacetylene-based membranes.

Development of better membranes for producing oxygen-enriched air has been, and continues to be, an area of research because of the potential application of the gas in combustion processes. When methane, oil, and other fuels are burned with air, a large

amount of nitrogen passes as an inert diluent through the burners and is discarded as hot exhaust gas. If oxygen-enriched air were used, the energy lost with the hot exhaust gas would decrease considerably and fuel consumption would decrease. In the last few years, a market has developed in China for this type of system in regional cement plants. The high cost of natural gas in China makes the process economic. Carbon dioxide separation from the exhaust gas would also be easier – an advantage if CO₂ separation and sequestration ever becomes a real market. Use of oxygen-enriched air also improves the efficiency of diesel engines. The useful energy that can be extracted from the same amount of fuel increases significantly even if air is enriched only to 25–35% oxygen.

To make these oxygen-enrichment applications widely used, the fuel savings achieved must offset the cost of the oxygen-enriched air used. Calculations show that the process would be cost-effective for some applications at an EPO₂ cost as high as US\$60/ton and, for many applications, at an EPO₂ cost of US\$30–40/ton. Bhide and Stern [45] have published an interesting analysis of this problem, the results of which are shown in Figure 8.28. The figure shows the cost of oxygen-enriched air produced by a membrane process for membranes of various permeabilities and selectivities. The assumptions were optimistic – low-cost membrane modules (US\$54/m²) and membranes with extremely

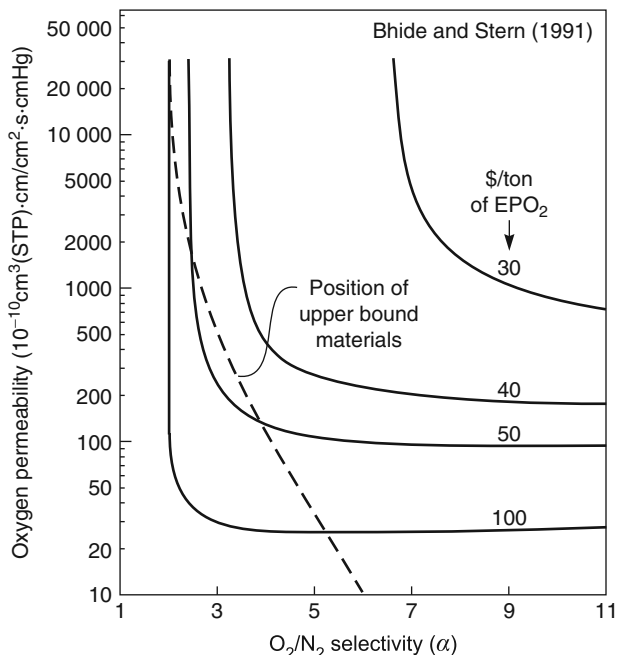


Figure 8.28 Cost of oxygen-enriched air produced by membrane separation on an EPO₂ basis as a function of the oxygen permeability and oxygen/nitrogen selectivity of the membrane. The performance of today's best membranes is represented by the upper bound performance line from Robeson's plot (Figure 8.6) [45]. Reprinted from *J. Membr. Sci.* 62, B.O. Bhide and S.A. Stern, A New Evaluation of Membrane Processes for the Oxygen-Enrichment of Air, p. 87. Copyright 1991, with permission from Elsevier.

thin selective separating layers (1000 Å). Also shown in Figure 8.28 is the portion of the upper-bound curve obtained from the permeability/selectivity trade-off plot shown in Figure 8.6. As the figure shows, a number of materials at the upper-bound limit, with oxygen/nitrogen selectivities of 3–4 and permeabilities of 50–500, are within striking distance of the US\$30–40/ton target. Production of these very high-performance membrane modules is at the outer limit of current technology, but improvements in the technology could open up new, very large applications of membranes in the future.

8.5.3 Natural Gas Separations

US production of natural gas is about 20 trillion scf/year; total worldwide production is about 100 trillion scf/year. All of this gas requires some treatment, and approximately 20% of the gas requires extensive treatment before it can be delivered to the pipeline. As a result, several billion dollars' worth of natural gas separation equipment is installed annually worldwide. The current membrane market share is about 5%, essentially all for carbon dioxide removal. However, this fraction is expected to increase as better carbon dioxide-selective membranes are developed and the application of membranes to other separations in the natural gas processing industry becomes more widespread [46–48].

Raw natural gas varies substantially in composition from source to source. Methane is always the major component, typically 75–90% of the total. Natural gas also contains significant amounts of ethane, some propane and butane, and 1–3% of other higher hydrocarbons. In addition, the gas contains undesirable impurities: water, carbon dioxide, nitrogen, and hydrogen sulfide. Although raw natural gas has a wide range of compositions, the composition of gas delivered to the pipeline is tightly controlled. Typical US natural gas specifications are shown in Table 8.5. The opportunity for membranes lies in the processing of gas to meet these specifications.

Natural gas is usually produced and transported to the gas processing plant at high pressure, in the range 500–1500 psi. To minimize recompression costs, the membrane process must remove impurities from the gas into the permeate stream, leaving the methane, ethane, and other hydrocarbons in the high-pressure residue gas. This requirement determines the type of membranes that can be used. Figure 8.29 is a graphical representation of the factors of molecular size and condensability that affect selection of membranes for natural gas separations.

As Figure 8.29 shows, water is small and condensable; therefore, it is easily separated from methane by both rubbery and glassy polymer membranes. Both rubbery and glassy

Table 8.5 Composition of natural gas required for delivery to the US national pipeline grid

Component	Specification
CO ₂	<2%
H ₂ O	<120 ppm
H ₂ S	<4 ppm
C ₃₊ content	950–1050 Btu/scf Dew point, -20°C
Total inerts (N ₂ , CO ₂ , He, etc.)	<4%

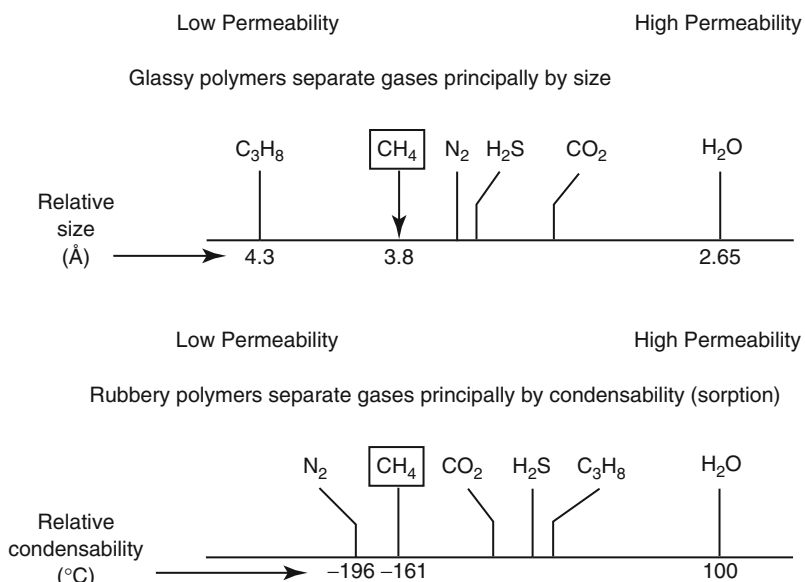


Figure 8.29 The relative size and condensability (boiling point) of the principal components of natural gas. Glassy membranes generally separate by differences in size; rubbery membranes separate by differences in condensability

membranes can also separate carbon dioxide and hydrogen sulfide from natural gas. However, in practice, carbon dioxide is best separated by glassy membranes (utilizing size selectivity) [49], whereas hydrogen sulfide, which is larger and more condensable than carbon dioxide, is best separated by rubbery membranes (utilizing sorption selectivity) [50, 51]. Nitrogen can be separated from methane by glassy membranes utilizing the difference in size, or rubbery membranes using the difference in sorption. In both cases, the differences are small, so the membrane selectivities are low. Finally, propane and other hydrocarbons, because of their condensability, are best separated from methane with rubbery sorption-selective membranes. Table 8.6 shows typical membrane materials

Table 8.6 Membrane materials and selectivities for separation of impurities from natural gas under normal operating conditions

Component to be permeated	Category of preferred polymer material	Typical polymer used	Typical selectivity over methane
CO_2	Glass	Cellulose acetate, polyimide	10–20
H_2S	Rubber	Ether-amide block copolymer	20–30
N_2	Glass	Polyimide, perfluoro polymers	2–3
N_2	Rubber	Silicone rubber	0.35
H_2O	Rubber or glass	Many	>200
Butane	Rubber	Silicone rubber	7–10

and the selectivities that can be obtained with good-quality membranes under normal natural gas processing conditions.

8.5.4 Carbon Dioxide Separation

Removal of carbon dioxide is the only membrane-based natural gas separation process currently practiced on a large scale – several hundred plants have been installed, some very large. Most were installed by Grace, Separax (UOP), and Cynara, and all use cellulose acetate membranes in hollow fiber or spiral-wound module form. More recently, hollow fiber polyamide and polyimide membranes have been introduced by Ube and Air Liquide, but their use has been slow to take off.

The designs of two typical carbon dioxide removal plants are illustrated in Figure 8.30. One-stage plants, which are simple, contain no rotating equipment, and require minimal maintenance, are preferred for small gas flows. In such plants methane loss to the permeate is often 10–15%. If there is no fuel use for this gas, it must be flared, which represents a significant revenue loss. Nonetheless, for gas wells producing 1–2 MMscfd, one-stage membrane units with their low capital and operating costs may still be the optimum treatment method.

For all but very small plants, the methane loss from a one-stage system becomes prohibitive. Often the permeate gas is recompressed and passed through a second membrane stage. This second stage reduces the methane loss to a small percentage. However,

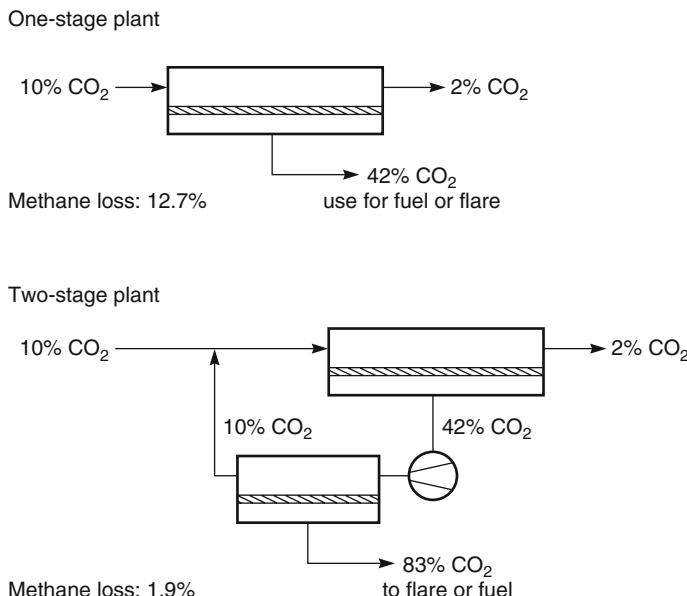


Figure 8.30 Flow scheme of one-stage and two-stage membrane separation plants to remove carbon dioxide from natural gas. Because the one-stage design has no moving parts, it is very competitive with other technologies, especially if there is a use for the low-pressure permeate gas. Two-stage processes are more expensive because a large compressor is required to compress the permeate gas. However, the loss of methane with the fuel gas is much reduced

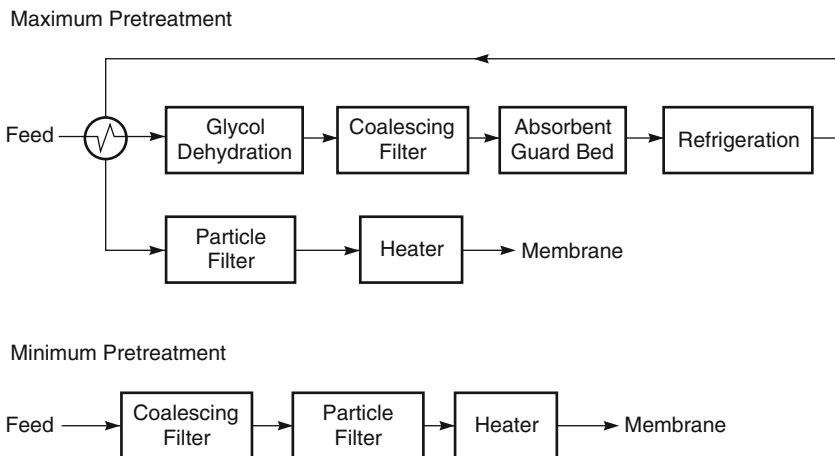


Figure 8.31 Natural gas pretreatment trains used in front of carbon dioxide membrane separation systems

because the cost of recompression is considerable, the membrane system may no longer compete with amine absorption, the alternative technology. In general, membrane systems have proven to be most competitive for gas streams containing high concentrations of carbon dioxide.

Natural gas contains a range of contaminants that can seriously affect the system performance. All carbon dioxide membrane separation units require some sort of pretreatment. Two possible pretreatment trains are illustrated in Figure 8.31. The amount of pretreatment is dependent on the membranes used and the nature of the gas to be treated. Cellulose acetate membranes, for example, are particularly sensitive to water, and therefore, glycol dehydration followed by silica bed drying would be used for most streams.

In Figure 8.31, the design labeled “maximum pretreatment” would be used for a gas that contains high levels of carbon dioxide and a high concentration of heavy hydrocarbons (for example, gas produced as a by-product of carbon dioxide flood-enhanced oil recovery projects). The pretreatment train labeled “minimum pretreatment” would be used for relatively hydrocarbon-lean gas that contains much smaller amounts of carbon dioxide [52].

The importance of adequate pretreatment was not appreciated by the builders of some of the first-generation membrane plants. Several early systems were damaged by plant upsets, which caused high levels of contaminants or liquids to reach the membranes. Better plant designs are now used to control membrane damage, and today’s membranes are also more robust.

Spillman [46], and more recently White [48], have reviewed the competitive position of membrane systems for this application. Currently the market for membrane carbon dioxide gas separation systems can be summarized as follows:

1. **Very small systems (less than 3 MMscfd).** At this flow rate, membrane units are very attractive. Often the permeate is flared or used as fuel, so the system is a simple bank of membrane modules.

2. **Small systems (3–30 MMscfd).** Two-stage membrane systems are used to reduce methane loss. In this gas flow range, amine and membrane systems compete; the choice between the two technologies depends on site-specific factors.
3. **Medium to large systems (greater than 30 MMscfd).** In general, membrane systems are too expensive to compete head-to-head with amine plants if the gas contains less than 10% CO₂. However, a number of large membrane systems have been installed on offshore platforms, where the small footprint and low weight of membrane systems are important. Membrane systems are also used in carbon dioxide enhanced oil recovery operations, or on other gas streams containing high concentrations of carbon dioxide, that favor membrane technology. As membranes improve, their market share is increasing.

In principle, the combination of membranes for bulk removal of the carbon dioxide with amine units as polishing systems offers a low-cost alternative to all-amine plants for many streams. However, this approach has not been generally used, because the savings in capital cost are largely offset by the increased complexity of the plant, which now contains two separation processes. The one exception has been in carbon dioxide flood-enhanced oil recovery projects [53, 54], in which carbon dioxide is injected into an oil formation to lower the viscosity of the oil. Water, oil, and gas are removed from the formation; the carbon dioxide is separated from the gas produced and reinjected. In these projects, the composition and volume of the gas changes significantly over the lifetime of the project. The modular nature of membrane units allows easy retrofitting to an existing amine plant, allowing the performance of the plant to be adjusted to meet the changing separation needs. Also, the capital cost of the separation system can be spread more evenly over the project lifetime. An example of a membrane/amine plant design is shown in Figure 8.32. In this design, the membrane unit removes two-thirds of the carbon dioxide, and the amine plant removes the remainder. The combined plant is usually significantly less expensive than an all-amine or all-membrane plant.

8.5.4.1 Dehydration

All natural gas must be dried before entering the national distribution pipeline, to control corrosion of the pipeline and to prevent formation of solid hydrocarbon/water hydrates

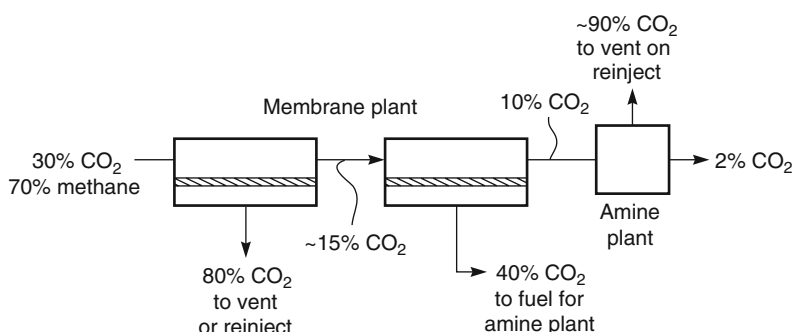


Figure 8.32 A typical membrane/amine plant for the treatment of associated natural gas produced in carbon dioxide/enhanced oil projects. The membrane permeate gas is often used as a fuel for the amine absorption plant

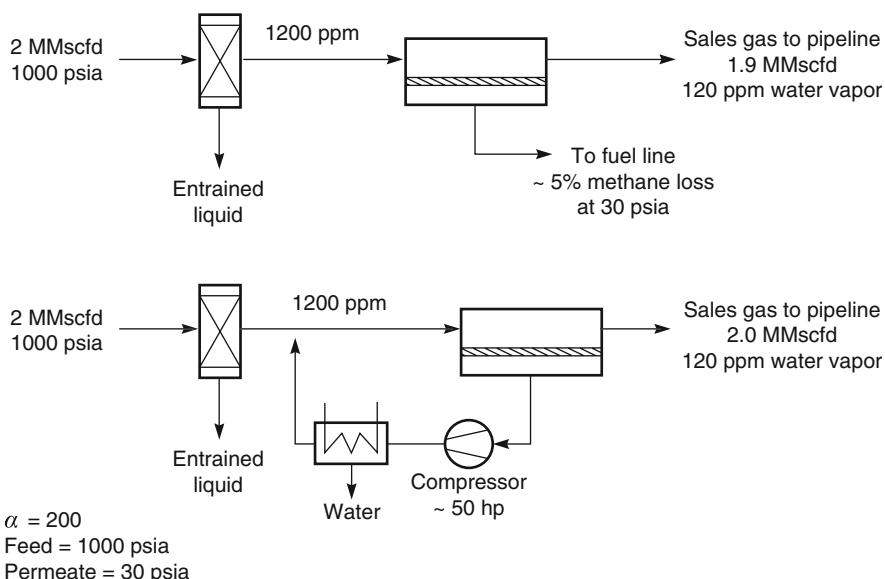


Figure 8.33 Two possible process designs for natural gas dehydration. Dehydration of natural gas is easily performed by membranes, but high cost often limits its scope to niche applications

that can choke valves. Currently, glycol dehydrators are widely used; approximately 50 000 units are in service in the United States. However, glycol dehydrators are not well suited for use on small gas streams or on offshore platforms, increasingly common sources of natural gas. In addition, these units coextract benzene, a known carcinogen and trace contaminant in natural gas, and release the benzene to the atmosphere. The Environmental Protection Agency (EPA) now requires large glycol units be fitted with benzene emission control systems.

Membrane processes offer an alternative approach to natural gas dehydration. Membranes with intrinsic selectivities for water from methane of more than 500 are easily obtained, but because of concentration polarization effects and membrane bypass, actual selectivities are typically about 200. Two possible process designs are shown in Figure 8.33. In the first design, a small one-stage system removes 90% of the water in the feed gas, producing a low-pressure permeate gas representing ~5% of the initial gas flow. The selectivity of the membrane (200) is much greater than the pressure ratio across the membrane (33), so this process is pressure ratio limited. If the permeate gas can be used as low-pressure fuel at the site, this design is economical and competitive with glycol dehydration, but normally the loss of methane to the permeate is too large to make this process economical. In the second design, the wet, low-pressure permeate gas is recompressed and cooled, so the water vapor condenses and is removed as liquid water. The natural gas that permeates the membrane is then recovered. However, if the permeate gas must be recompressed, as in the second design, the capital cost

of the system approximately doubles. Membranes are then only competitive in special situations where glycol dehydration is not possible.

8.5.4.2 Dew Point Adjustment, C_{3+} Recovery

Natural gas usually contains varying amounts of ethane, propane, butane, and higher hydrocarbons. The gas is often close to its saturation point with respect to some of these hydrocarbons, which means liquids will condense from the gas at cold spots in the pipeline transmission system. To avoid the problems caused by condensation of liquids, the dew point of US natural gas is lowered to about -20°C before delivery to the pipeline by removing portions of the propane and butane and higher hydrocarbons. For safety reasons, the Btu rating of the pipeline gas is also usually controlled within a narrow range, typically 950–1050 Btu per cubic foot. Because the Btu values of ethane, propane, and pentane are higher than that of methane, natural gas that contains significant amounts of these hydrocarbons may have an excessive Btu value, requiring their removal. Of equal importance, these higher hydrocarbons are generally more valuable as recovered liquids than as their fuel value in the natural gas stream. For all of these reasons, almost all natural gas is treated to control the C_{3+} hydrocarbon content.

The current technology used to separate the higher hydrocarbons from natural gas streams is condensation, shown schematically in Figure 8.34. The natural gas stream is cooled by refrigeration or expansion to between -20 and -40°C . The condensed liquids, which include the higher hydrocarbons and water, are separated from the gas streams and subjected to fractional distillation to recover the individual components. Because refrigeration is capital-intensive and uses large amounts of energy, there is interest in alternative techniques, such as membrane gas separation.

A flow diagram of a membrane system for C_{3+} liquids recovery is also shown in Figure 8.34. The natural gas is fed to modules containing a higher-hydrocarbon-selective membrane, which removes the higher hydrocarbons as the permeate stream. This stream is recompressed and cooled by a cold-water exchanger to condense higher hydrocarbons. The non-condensed bleed stream from the condenser will normally still contain more heavy hydrocarbons than the raw gas, so prior to returning the gas to the feed stream, the condenser bleed stream is passed through a second set of membrane modules. The permeate streams from the two sets of modules are combined, creating a recirculation loop around the condenser, which continuously concentrates the higher hydrocarbons [35].

Today's membranes, mostly silicone rubber-based, are insufficiently selective to be widely used to recover C_{3+} liquids from pipeline gas. However, these membranes have found an application in treating raw unprocessed gas often used as fuel at remote compressor stations. The unprocessed gas is rich in heavy hydrocarbons, resulting in engine knocking and frequent shutdowns. By removing the heavy hydrocarbons, the gas octane number is substantially improved at little cost [47].

8.5.4.3 Nitrogen Removal from Natural Gas

The US pipeline specification for natural gas requires the total inert content – predominantly nitrogen – to be less than 4%. Of known US natural gas reserves, 14% contain more than 4% nitrogen and, therefore, do not meet this specification. Many of these high-nitrogen gas streams can be diluted with low-nitrogen gas to meet the

Current Technology

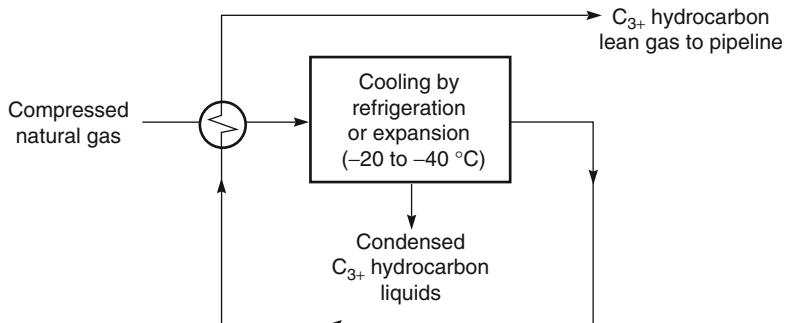
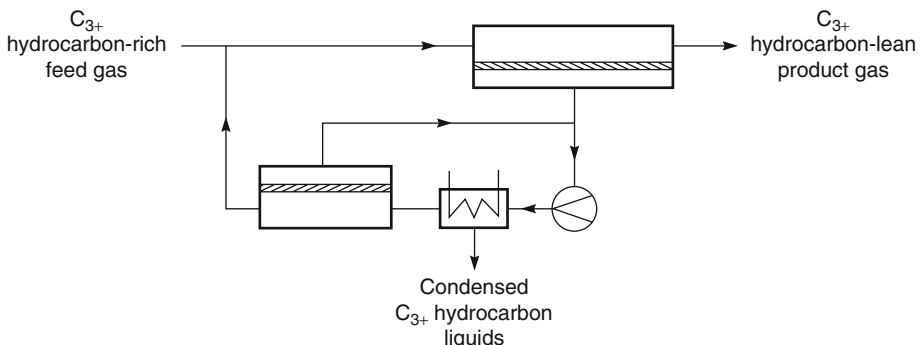
Membrane System Using C_{3+} Hydrocarbon-Selective Membranes

Figure 8.34 Recovery of C_{3+} hydrocarbons from natural gas

specification, but if dilution is not practical, a nitrogen removal unit must be installed. Cryogenic distillation is currently used to treat this gas. As of 1999, 26 cryogenic nitrogen removal plants were in operation in the United States. Cryogenic plants are most suited to large gas fields that can deliver 50–500 million scfd of gas for 10–20 years. These large gas flow rates allow the high capital cost of the cryogenic plant to be defrayed over a number of years. Many small gas wells are shut in for lack of suitable small-scale nitrogen separation technology. One technology that has been tried with some success is PSA using molecular sieves that preferentially adsorb nitrogen. Another technology is membrane separation [14]. Membranes that selectively permeate methane over nitrogen are available, but the selectivities for both types of membrane are low. For this reason, multistep or multistage systems are needed to process the gas. To date, most of the plants installed have used silicone rubber membranes that have a methane/nitrogen selectivity of 3.

A typical unit is illustrated in Figure 8.35 [14]. The operator was producing 12 MMscfd of gas that contained up to 16% nitrogen, which had a heating value of about 900 Btu/scf. The pipeline company was ready to accept the gas for dilution, provided the nitrogen

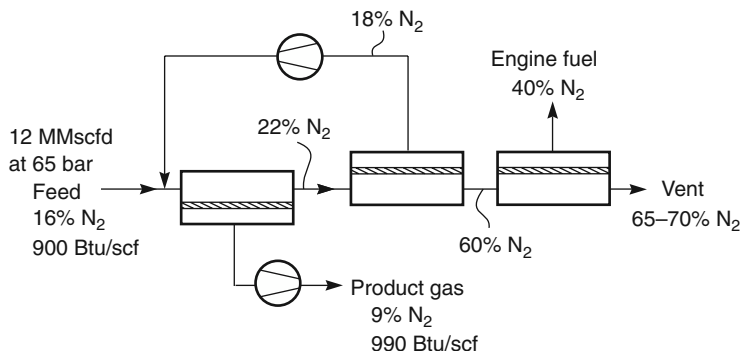


Figure 8.35 Flow diagram and a photograph of one of the two membrane skids at a 12 MMscfd membrane nitrogen removal plant installed on a high-nitrogen gas well in the Sacramento River Delta region of California

content was less than 10% and more importantly, that the gas heating value was more than 970 Btu/scf. To reach this target, the feed gas, at a pressure of 65 bar, was passed through three sets of modules in series. The permeate from the front set of modules was preferentially enriched in methane, ethane, and the C₃₊ hydrocarbons, and the nitrogen content was reduced to 9% nitrogen. These changes raised the heating value of the gas to 990 Btu/scf. This gas was compressed and sent to the pipeline. The residue gas from the first set of modules contained 22% nitrogen and was sent to a second membrane step, where it was concentrated to 60% nitrogen. The permeate from the second step contained 18% nitrogen and was recycled to mix with the feed gas. The second-step residue gas was sent to a third and final small membrane system to be fractionated. The permeate gas – containing 40% nitrogen – was used as fuel for the compressor engines.

The final residue contained 65–70% nitrogen and was essentially stripped of all C₃₊ hydrocarbons; it was vented.

Overall, this unit recovered 95% of the hydrocarbon values for delivery to the pipeline, 2% of the hydrocarbons were used as compressor fuel, and the final 3% were vented with the final residue nitrogen.

8.5.5 Vapor/Gas Separations

In the separation of vapor/gas mixtures, rubbery polymers, such as silicone rubber, can be used to permeate the more condensable vapor, or glassy polymers can be used to permeate the smaller gas. Although glassy, gas-permeable membranes have been proposed for a few applications, most installed plants use vapor-permeable membranes, often in conjunction with a second process such as condensation [31, 36] or absorption [55]. The first plants, installed in the early 1990s, were used to recover vapors from gasoline terminal vent gases or chlorofluorocarbon (CFC) vapors from the vents of industrial refrigeration plants. More recently, membranes have begun to be used to recover hydrocarbons and processing solvents from petrochemical plant purge gas. Some of these streams are quite large and discharge vapors with a recovery value of US\$2–5 million/year.

One of the most successful petrochemical applications is treatment of resin degassing vent gas in polyolefin plants [56, 57]. Olefin monomer, catalyst, solvents, and other co-reactants are fed at high pressure into the polymerization reactor. The polymer product (resin) is removed from the reactor and separated from excess monomer in a flash separation step. The recovered monomer is recycled to the reactor. Residual monomer is removed from the resin by stripping with nitrogen. The composition of this degassing vent stream varies greatly, but it usually contains 20–50% of mixed hydrocarbon monomers in nitrogen. The monomer content represents about 1% of the hydrocarbon feedstock entering the plant. This amount might seem small, but because polyolefin plants are large operations, the recovery value of the stream can be significant.

Several membrane designs can be used, but the most common is the hybrid process combining condensation and membrane separation, as shown in Figure 8.36 [58]. In this design, the compressed feed gas is sent to a condenser. On cooling of the feed gas,

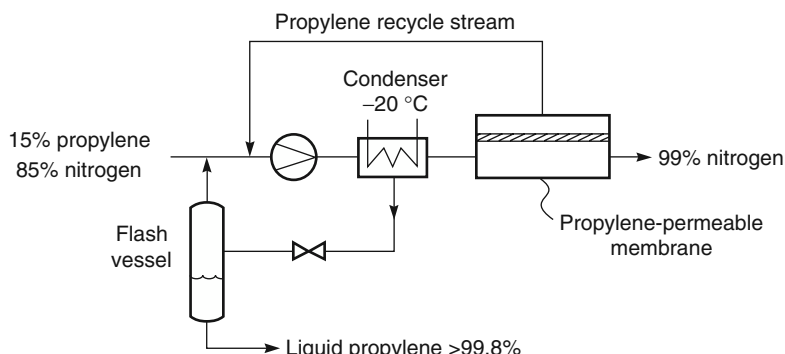


Figure 8.36 A hybrid compression–condenser–membrane process to recover propylene from a propylene/nitrogen mixture. Silicone rubber propylene-selective membranes are used



Figure 8.37 Photograph of a membrane unit used to recover nitrogen and propylene from a polypropylene plant vent gas

a portion of the propylene content is removed as a condensed liquid. The remaining, uncondensed propylene is removed by the membrane separation system to produce a 99% nitrogen stream. The permeate gas is recycled to the incoming feed gas from the purge bin.

Because the gas sent to the membrane stage is cooled, the solubility of propylene in the membrane is enhanced, and the selectivity of the membrane unit is increased. The propylene condensate contains some dissolved nitrogen so the liquid is flashed at low pressure to remove this gas, producing a better than 99.5% pure hydrocarbon product. A photograph of a propylene/nitrogen vent gas treatment system is shown in Figure 8.37.

8.5.6 Dehydration of Air

Another application of vapor/gas separation membranes is dehydration of compressed air. The competitive processes are condensation or solid desiccants, both of which are established, low-cost technologies. Membranes with water/air selectivities of more than 200 are used. The problem inhibiting their application is the loss of compressed feed air through the membrane. Compressed air is typically supplied at about 7 atm (105 psi), and the membrane permeate is at 1 atm, so the pressure ratio across the membrane is about 7. Because air dehydration membranes have a selectivity of more than 200, these membranes are completely pressure-ratio-limited. Based on Equation 8.10, this means that the permeate gas cannot be more than seven times more concentrated than the feed. The result is that a significant fraction of the feed gas must permeate the membrane to

carry away the permeate water vapor. Typically, 15–20% of the pressurized feed gas permeates the membrane, which affects the productivity of the compressor significantly. Counter-flow sweep designs of the type discussed in Chapter 4 are widely used to reduce permeant loss. Membrane air dehydration systems have found a significant market, especially for small gas streams where the reliability and simplicity of the membrane design compared to adsorbents or cooling is particularly attractive.

8.5.7 Carbon Dioxide/Hydrogen and Carbon Dioxide/Nitrogen Separations

The emergence of global warming as a significant environmental problem is likely to change the way the world produces and uses energy in the next decades [59]. The costs involved in solving the problem are huge, and so significant amounts of money are being spent looking for lower-cost solutions. A number of these solutions could involve membranes.

One of the most direct ways of addressing the problem is to separate and sequester the carbon dioxide (CO_2) produced in the production of electricity. Power production at electrical power plants is responsible for 35–40% of global CO_2 emissions. In addition, power stations are an attractive target for carbon capture, because they are large point sources of CO_2 emissions; there are about 5000 large power plants around the world. The amount of CO_2 emitted depends on the plant size and fuel feed, but an average (500 MW_e) coal-fired power plant will emit about 10 000 tons of CO_2 per day. Separating the CO_2 from these emissions and then compressing the gas to high pressure (80–100 bar) and injecting it deep underground would go a long way to mitigating the global warming problem.

Two membrane methods under development to separate CO_2 produced during power production are shown in Figure 8.38. A world-scale coal power plant (illustrated in Figure 8.38a) has a relatively straightforward flow scheme. Coal is burned with air in a boiler to make high-pressure steam, which is then sent to a steam turbine to make power. The flue gas from the boiler (at low pressure; a few inches of water above atmospheric pressure), is sent through an electrostatic precipitator to remove particulates, scrubbed to remove sulfur dioxide (SO_2) in a flue gas desulfurization unit, and then emitted directly to the atmosphere. Removal of CO_2 from the flue gas, although being considered, is not currently practiced. Amine absorption is the most commonly considered technology to separate the CO_2 , but would double the cost of the electricity produced. Membranes could be used, and a number of materials have the required CO_2/N_2 selectivities. However, for this application, extremely high permeance membranes will be needed. With the highest permeance membranes now known, plant membrane areas will be in the 1–2 million m^2 range per power plant – as large as the largest reverse osmosis plants. Possible membrane process designs are described by Merkel *et al.* [60] and Favre [61].

The Integrated Gasification Combined Cycle (IGCC) process flow scheme shown in Figure 8.38b is significantly more complex. Typically, an air separation plant is first used to produce oxygen, which together with water is then used to gasify coal at high pressure and temperature. The syngas produced (CO and H_2) is contaminated with carbon dioxide, nitrogen, methane, argon, hydrogen sulfide, particulates, and tars. The gas is quenched and scrubbed to eliminate tar and particulates. If CO_2 capture is to be used at an IGCC

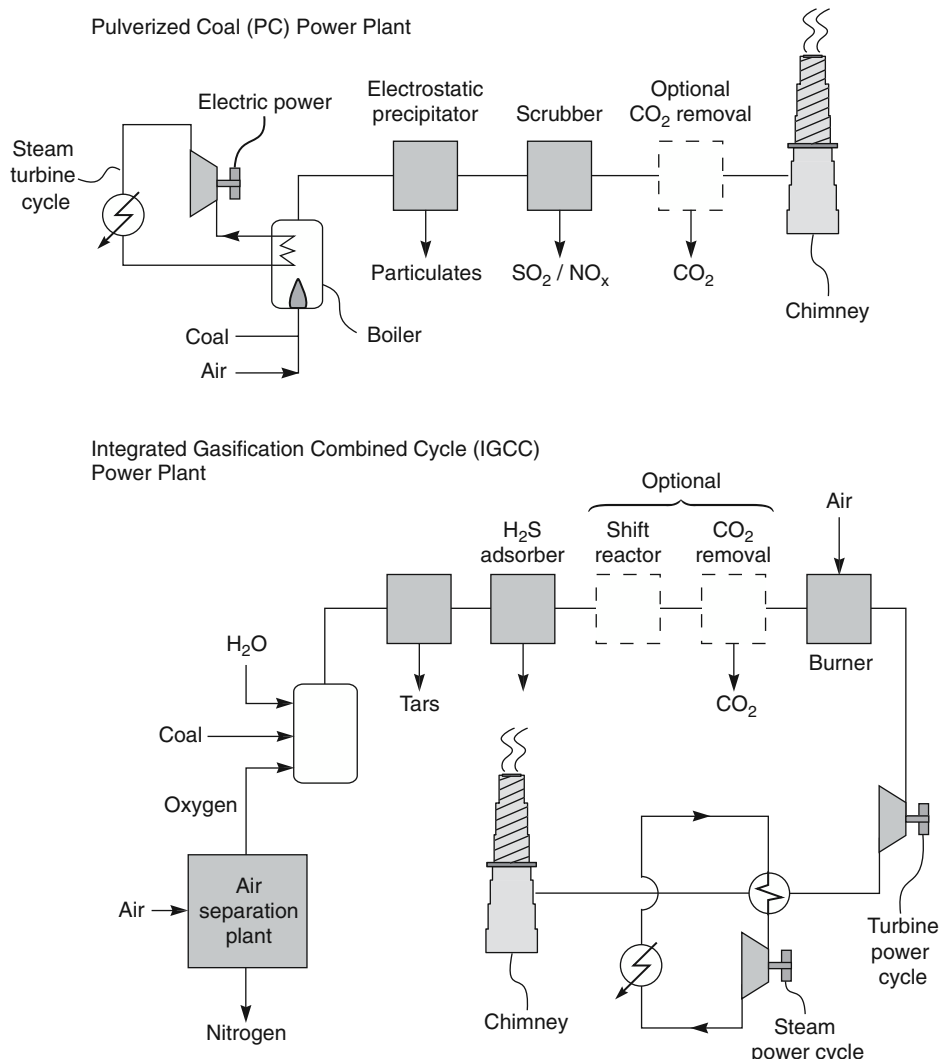


Figure 8.38 Comparison of pulverized coal (PC) and Integrated Gasification Combined Cycle (IGCC) electric power plants

plant, the syngas will be reacted with steam in a shift reactor to produce more hydrogen by the reaction:



Sulfur compounds, and optionally CO_2 , are then removed by a low-temperature absorption process. The high-pressure hydrogen is then burned with air and the hot

high-pressure gas product is used to drive a gas turbine and make electricity. The hot turbine exhaust is used to produce steam that makes additional electricity in a steam turbine. The cooled gas is vented to the atmosphere. An IGCC plant has an overall heat to electric power efficiency of about 45%, significantly better than the 35% efficiency of a conventional subcritical pulverized coal power plant. However, today this advantage is more than offset by the higher capital cost of an IGCC plant. The result is that without CO₂ capture, the electric power produced at an IGCC plant is expected to be 25% more expensive than electricity produced in subcritical pulverized coal power plants.

The real benefit of IGCC technology kicks in if a cost is placed on CO₂ emissions. This is because CO₂ removal from high-pressure, high-concentration gasification streams will be significantly less costly than CO₂ removal from conventional pulverized coal power plants. The reason for the lower cost of CO₂ removal from an IGCC plant is apparent from Figure 8.38. In a conventional coal power plant, CO₂ has to be separated from a dilute (13% CO₂) and atmospheric pressure (<1.05 bar) gas stream. The gas to be separated in an IGCC plant contains about 40–50% CO₂ and is at a much higher pressure and concentration. The gas leaving the shift reactor is usually at a pressure of ~50 bar and contains about 56% hydrogen, 40% CO₂, and 4% carbon monoxide, nitrogen, methane, argon, hydrogen sulfide. Separation of CO₂ from this gas stream is far easier and lower cost than separation from flue gas. Currently, absorption of the CO₂ in chilled methanol or ethylene glycol would be used for CO₂ capture (the Rectisol® or Selexol™ processes), but hydrogen- or CO₂-permeable membranes are being developed for this application and are likely to be significantly lower cost and be less energy intensive [62].

8.5.8 Vapor/Vapor Separations

A final group of separations likely to develop into a major application area for membranes is vapor/vapor separations, such as ethylene (bp –93.9°C) from ethane (bp –88.9°C), propylene (bp –47.2°C) from propane (bp –42.8°C), and *n*-butane (bp –0.6°C) from isobutane (bp –10°C). These close-boiling mixtures are separated on a very large scale in the synthesis of ethylene and propylene, the two largest-volume organic chemical feedstocks, and in the synthesis of isobutane in refineries to produce high-octane gasoline. Because the mixtures are close-boiling, large towers and high reflux ratios are required to achieve good separations.

If membranes are to be used for these separations, highly selective materials must be developed. Several groups have measured the selectivities of polymeric membranes for ethylene/ethane and propylene/propane mixtures. Burns and Koros have reviewed these results [63]. Much of the literature data should be treated with caution. Some authors report selectivities based on the ratio of the permeabilities of the pure gases; others use a hard vacuum or a sweep gas on the permeate side of the membrane. Both procedures produce unrealistically high selectivities. In an industrial plant, the feed gas will be at 8–10 bar and a temperature sufficient to maintain the gas in the vapor phase; the permeate gas will be at a pressure of 1–2 bar. Under these operating conditions, plasticization and loss of selectivity occur with even the most rigid polymer membranes, so selectivities are usually much lower than the ratio of pure gas permeabilities suggests. Because of these problems, this application might be one for which the benefits of ceramic or carbon

membranes can justify their high cost. Caro *et al.* have reviewed the ceramic membrane literature [21].

8.6 Conclusions and Future Directions

The application of membranes to gas separation problems has grown rapidly since the installation of the first industrial plants in the early 1980s. The current status of membrane gas separation processes is summarized in Table 8.7, in which the processes are divided into three groups. The first group consists of the *established processes*: nitrogen production from air, hydrogen recovery, natural gas processing, treatment of petrochemical purge gas, and air drying. These processes represent more than 90% of the current gas separation membrane market. All have been used on a large commercial scale for 10 years, and dramatic improvements in membrane selectivity, flux, and process designs have been made during that time. For example, today's hollow fine fiber nitrogen production module generates more than 10 times the amount of nitrogen, with better quality and lower energy consumption, than the modules produced in the early 1980s. For most of these applications, the technology has reached a point at which, barring a completely unexpected breakthrough, further changes in productivity are likely to be the result of a number of small incremental changes. The one exception is the removal of carbon dioxide from natural gas. Membranes still have a small market share. Development of more selective membranes (not an impossible dream) could improve the competitiveness of the membrane process for this application substantially.

Developing processes are the second group of applications. These include recovery of light hydrocarbons from refinery and petrochemical plant purge gases, and separation of C₃₊ hydrocarbons, hydrogen sulfide, nitrogen, and water from natural gas. All of these processes are performed on a commercial scale. Significant expansion in these applications, driven by the development of better membranes and process designs, is occurring.

The “*to be developed*” *membrane processes* represent the future expansion of gas separation technology. The production of oxygen-enriched air is a large potential application for membranes. The market size depends completely on the properties of the membranes that can be produced. Improvements in flux by a factor of 2 at current oxygen/nitrogen selectivities would probably produce a limited membrane market; improvements by a factor of 5–10 would make the use of oxygen-enriched air in natural gas combustion processes attractive. In the latter case, the market could be very large indeed. The separation of carbon dioxide from nitrogen at electric power plants or from hydrogen in coal gasification plants are two environmental applications linked to global warming. A large research effort is underway to develop membrane and other separation technologies for these applications. If governments decide that carbon dioxide separation and sequestration will be carried out, this application could be huge. The final application listed in Table 8.7 is the separation of organic vapor mixtures (for example, propylene/propane mixtures) using membranes in competition, or perhaps in combination, with distillation. Ten years ago, plants for these separations seemed to be just around the corner. Today, they do not look so near. Membranes that retain their properties at high temperature and

Table 8.7 Status of membrane gas separation processes

Process	Application	Comments
Established Processes		
Oxygen/nitrogen	Nitrogen from air	
Hydrogen/methane; hydrogen/nitrogen; hydrogen/carbon monoxide	Hydrogen recovery; ammonia plants and refineries	
Water/air	Drying compressed air	
Light hydrocarbons from nitrogen or hydrogen	Reactor purge gas, petrochemical process streams, refinery waste gas	Application is expanding
Carbon dioxide/methane	Carbon dioxide from natural gas	Many plants installed, but better membranes could change economics significantly and increase market share
Developing Processes		
VOC/air	Air pollution control applications	Several applications being developed; for example, gasoline stations and terminals, but high costs inhibit growth
C ₃₊ hydrocarbons/methane	NGL recovery from natural gas	Processes used for fuel gas conditioning, but NGL recovery requires better economics
Hydrogen sulfide, water/methane	Natural gas treatment	Niche applications, difficult for membranes to compete with existing technology for large flows
To-Be-Developed Processes		
Oxygen/nitrogen	Oxygen-enriched air	Requires better membranes to become commercial. Size of ultimate market will depend on properties of membranes developed. Could be large
Carbon dioxide/nitrogen	Carbon dioxide capture and sequestration	Potential application is enormous and technically feasible, but requires government regulation of CO ₂ emissions
Carbon dioxide/hydrogen	Hydrogen production in refineries and IGCC plants	Could be big, but also depends on adoption of government regulations for CO ₂ recovery
Organic vapor mixtures	Separation of organic mixtures in refineries and petrochemical plants	Requires better membranes and modules. Potential size of application is large

in the presence of high concentrations of organic vapors are required. This may be a separation for which ceramic membranes finally find an application. Overall, the outlook for growth in the use of membrane gas separation technology is bright.

References

1. Graham, T. (1866) On the adsorption and dialytic separation of gases by colloid septa. *Philos. Mag.*, **32**, 401.
2. Barrer, R.M. (1951) *Diffusion In and Through Solids*, Cambridge University Press, London.
3. van Amerongen, G.J. (1950) Influence of structure of elastomers on their permeability to gases. *J. Appl. Polym. Sci.*, **5**, 307.
4. Stern, S.A. (1966) Industrial applications of membrane processes: the separation of gas mixtures, *Membrane Processes for Industry, Proceedings of the Symposium*, Southern Research Institute, Birmingham, AL, pp. 196–217.
5. Meares, P. (1954) Diffusion of gases through polyvinyl acetate. *J. Am. Chem. Soc.*, **76**, 3415.
6. Henis, J.M.S. and Tripodi, M.K. (1980) A novel approach to gas separation using composite hollow fiber membranes. *Sep. Sci. Technol.*, **15**, 1059.
7. MacLean, D.L., Bollinger, W.A., King, D.E., and Narayan, R.S. (1986) Gas separation design with membranes, in *Recent Developments in Separation Science* (eds N.N. Li and J.M. Calo), CRC Press, Boca Raton, FL, p. 9.
8. Gruen, F. (1947) Diffusionmessungen an kautschuk (Diffusion in rubber). *Experimenta*, **3**, 490.
9. van Amerongen, G.J. (1946) The permeability of different rubbers to gases and its relation to diffusivity and solubility. *J. Appl. Phys.*, **17**, 972.
10. Behling, R.D., Ohlrogge, K., Peinemann, K.V., and Kyburz, E. (1989) The separation of hydrocarbons from waste vapor streams, in *Membrane Separations in Chemical Engineering*, AIChE Symposium Series Number 272, Vol. **85** (eds A.E. Fouada, J.D. Hazlett, T. Matsuura, and J. Johnson), AIChE, New York, p. 68.
11. Robeson, L.M. (1991) Correlation of separation factor versus permeability for polymeric membranes. *J. Membr. Sci.*, **62**, 165.
12. Stern, S.A. (1994) Polymers for gas separation: the next decade. *J. Membr. Sci.*, **94**, 1.
13. Robeson, L.M. (2008) The upper bound revisited. *J. Membr. Sci.*, **320**, 390.
14. Lokhandwala, K.A., Pinnau, I., He, Z., Amo, K.D., DaCosta, A.R., Wijmans, J.G. and Baker, R.W. (2010) Membrane separation of nitrogen from natural gas: a case study from membrane synthesis to commercial deployment. *J. Membr. Sci.*, **346**, 270.
15. Freeman, B.D. (1999) Basis of permeability/selectivity tradeoff relations in polymeric gas separation membranes. *Macromolecules*, **32** (2), 375.
16. Lee, S.Y., Minhas, B.S., and Donohue, M.D. (1988) Effect of gas composition and pressure on permeation through cellulose acetate membranes, in *New Membrane Materials and Processes for Separation*, AIChE Symposium Series Number 261, Vol. **84** (eds K.K. Sirkar and D.R. Lloyd), AIChE, New York, p. 93.

17. Merten, U. and Gantzel, P.K. (1968) Method and apparatus for gas separation by diffusion. US Patent 3,415,038, Dec. 1968.
18. Henis, J.M.S. and Tripodi, M.K. (1980) Multicomponent membranes for gas separations. US Patent 4,230,436, Oct. 1980.
19. Alefeld, G. and Völkl, J. (eds) (1978) *Hydrogen in Metals I: Basic Properties*, Springer-Verlag, Berlin.
20. Philpott, J.E. (1985) Hydrogen diffusion technology, commercial applications of palladium membrane. *Platinum Met. Rev.*, **29**, 12.
21. Caro, J., Noack, M., Kolsch, P., and Schäfer, R. (2000) Zeolite membranes: state of their development and perspective. *Microporous Mesoporous Mater.*, **38**, 3.
22. Brinker, J., Tsai, C.Y., and Lu, Y. (2003) Inorganic dual-layer microporous supported membranes. US Patent 6,536,604, Mar. 2003.
23. Kondo, M., Komori, M., Kita, H., and Okamoto, K. (1997) Tubular-type pervaporation module with zeolite NaA membrane. *J. Membr. Sci.*, **133**, 133.
24. Castricum, H.L., Kreiter, R., van Veen, H.M., Blank, D.H.A., Vente, J.F. and ten Elshof, J.E. (2008) High-performance hybrid pervaporation membranes with superior hydrothermal and acid stability. *J. Membr. Sci.*, **324**, 111.
25. Koresh, J.E. and Soffer, A. (1983) Molecular sieve carbon selective membrane. *Sep. Sci. Technol.*, **18**, 723.
26. Kim, Y.K., Park, H.B., and Lee, Y.M. (2005) Gas separation properties of carbon molecular sieve membranes derived from polyimide/polyvinylpyrrolidone blends: effect of the molecular weight of polyvinylpyrrolidone. *J. Membr. Sci.*, **251**, 159.
27. Park, H.B., Kim, Y.K., Lee, J.M., Lee, S.Y. and Lee, Y.M. (2004) Relationship between chemical structure of aromatic polyimides and gas permeation properties of their carbon molecular sieve membranes. *J. Membr. Sci.*, **229**, 117.
28. Williams, P.J. and Koros, W.J. (2008) Gas separation by carbon membranes, in *Advanced Membrane Technology and Applications* (eds N.N. Li, A.G. Fane, W.S.W. Ho, and T. Matsuura), John Wiley & Sons, Inc., Hoboken, NJ, pp. 599–631.
29. Yoshino, M., Nakamura, S., Kita, H., Okamoto, K.-i., Tanihara, N. and Kusuki, Y. (2003) Olefin/paraffin separation performance of carbonized membranes derived from an asymmetric hollow fiber membrane of 6FDA/BPDA-DDBT. *J. Membr. Sci.*, **215**, 169.
30. Tanihara, N., Shimazaki, H., Hirayama, Y., Nakanishi, S., Yoshinaga, T. and Kusuki, Y. (1999) Gas permeation properties of asymmetric carbon hollow fiber membranes prepared from asymmetric polyimide hollow fiber. *J. Membr. Sci.*, **160**, 179.
31. Baker, R.W. and Wijmans, J.G. (1994) Membrane separation of organic vapors from gas streams, in *Polymeric Gas Separation Membranes* (eds D.R. Paul and Y.P. Yampolskii), CRC Press, Boca Raton, FL, pp. 353 –398.
32. Weller, S. and Steiner, W.A. (1950) Fractional permeation through membranes. *Chem. Eng. Prog.*, **46**, 585.
33. Coker, D.T., Freeman, B.D., and Fleming, G.K. (1998) Modeling multicomponent gas separation using hollow fiber membrane contactors. *AICHE J.*, **44** (6), 1289.
34. Stern, S.A. and Wang, S.C. (1978) Countercurrent and cocurrent gas separation in a permeation stage: comparison of computation methods. *J. Membr. Sci.*, **4**, 141.

35. Baker, R.W. and Wijmans, J.G. (1993) Two-stage membrane process and apparatus. US Patents 5,256,295 and 5,256,296, Oct. 1993.
36. Wijmans, J.G. (1992) Process for removing condensable components from gas streams. US Patents 5,199,962, April 1993 and 5,089,033, Feb. 1992.
37. Hwang, S.T. and Thorman, J.M. (1980) The continuous membrane column. *AIChE J.*, **26** (4), 558.
38. Paul, D.R. and Yampolskii, Y.P. (eds) (1994) *Polymeric Gas Separation Membranes*, CRC Press, Boca Raton, FL.
39. Koros, W.J. and Fleming, G.K. (1993) Membrane based gas separation. *J. Membr. Sci.*, **83**, 1.
40. Baker, R.W. (2002) Future directions of membrane gas separation technology. *Ind. Eng. Chem. Res.*, **41**, 1393.
41. Bollinger, W.A., MacLean, D.L., and Narayan, R.S. (1982) Separation systems for oil refining and production. *Chem. Eng. Prog.*, **78**, 27.
42. Henis, J.M.S. (1994) Commercial and practical aspects of gas separation membranes, in *Polymeric Gas Separation Membranes* (eds D.R. Paul and Y.P. Yampolskii), CRC Press, Boca Raton, FL, pp. 441–530.
43. Prasad, R., Shaner, R.L., and Doshi, K.J. (1994) Comparison of membranes with other gas separation technologies, in *Polymeric Gas Separation Membranes* (eds D.R. Paul and Y.P. Yampolskii), CRC Press, Boca Raton, FL, pp. 531–614.
44. Prasad, R., Notaro, F., and Thompson, D.R. (1994) Evolution of membranes in commercial air separation. *J. Membr. Sci.*, **94**, 225.
45. Bhide, B.O. and Stern, S.A. (1991) A new evaluation of membrane processes for the oxygen-enrichment of air. *J. Membr. Sci.*, **62**, 87.
46. Spillman, R.W. (1989) Economics of gas separation by membranes. *Chem. Eng. Prog.*, **85**, 41.
47. Baker, R.W. and Lokhandwala, K.A. (2008) Natural gas processing with membranes: an overview. *Ind. Eng. Chem. Res.*, **47**, 2109.
48. White, L.S. (2010) Evolution of natural gas treatment with membrane systems, in *Membrane Gas Separation* (eds Y. Yampolskii and B.D. Freeman), John Wiley & Sons, Ltd, Chichester, pp. 313 –332.
49. Schell, W.J., Wensley, C.G., Chen, M.S.K., Venugopal, K.G., Miller, B.D. and Stuart, J.A. (1989) Recent advances in cellulosic membranes for gas separation and pervaporation. *Gas. Sep. Purif.*, **3**, 162.
50. Chatterjee, G., Houde, A.A., and Stern, S.A. (1997) Poly(urethane) and poly(ether urethane urea) membranes with high H_2S/CH_4 selectivity. *J. Membr. Sci.*, **135**, 99.
51. Lokhandwala, K.A., Baker, R.W., and Amo, K.D. (1995) Sour gas treatment process. US Patent 5,407,467, April 1995.
52. Dortmundt, D. and Doshi, K. (2002) Recent developments in CO_2 removal membrane technology, *Proceedings of the Laurance Reid Gas Conditioning Conference*, University of Oklahoma, Norman, OK, p. 22.
53. Parro, D. (1985) Membrane carbon dioxide separation. *Energy Prog.*, **5**, 51.
54. Hamaker, R.J. (1991) Evolution of a gas separation membrane, 1983–1990, in *Effective Industrial Membrane Processes* (ed. M.K. Turner), Elsevier, New York, pp. 337–344.

55. Ohlrogge, K., Wind, J., and Behling, R.D. (1995) Off gas purification by means of membrane vapor separation systems. *Sep. Sci. Technol.*, **30**, 1625.
56. Baker, R.W. and Jacobs, M.L. (1996) Improve monomer recovery from polyolefin resin degassing. *Hydrocarbon Process.*, **75**, 49.
57. Baker, R.W., Lokhandwala, K.A., Jacobs, M.L., and Gottschlich, D.E. (2000) Recover feedstock and product from reactor vent streams. *Chem. Eng. Prog.*, **96**, 51.
58. Baker, R.W., Wijmans, J.G., and Kaschemekat, J. (1998) The design of membrane vapor-gas separation systems. *J. Membr. Sci.*, **151**, 55.
59. Pacala, S. and Socolow, R. (2004) Stabilization wedges: solving the climate problem for the next 50 years with current technologies. *Science*, **305**, 968.
60. Merkel, T.C., Lin, H., Wei, X., and Baker, R.W. (2010) Power plant post-combustion carbon dioxide capture: an opportunity for membranes. *J. Membr. Sci.*, **359**, 126.
61. Favre, E. (2007) Carbon dioxide recovery from post-combustion processes: can gas permeation membranes compete with absorption? *J. Membr. Sci.*, **294**, 50.
62. Merkel, T.C., Zhou, M., and Baker, R.W. (2012) Carbon dioxide capture with membranes at an IGCC power plant. *J. Membr. Sci.*, **389**, 441.
63. Burns, R.L. and Koros, W.J. (2003) Defining the challenges for C₃H₆/C₃H₈ separation using polymeric membranes. *J. Membr. Sci.*, **211**, 299.

9

Pervaporation

9.1 Introduction and History

A pervaporation process to separate liquid mixtures is illustrated in Figure 9.1. A heated feed liquid mixture contacts one side of a membrane; permeate vapor is removed from the other side. Transport through the membrane is induced by the vapor pressure difference between the heated feed solution and the permeate vapor. This vapor pressure difference can be maintained in several ways. In the laboratory, a vacuum pump is used to draw a vacuum on the permeate side of the system. Industrially, the permeate vacuum is most economically generated by cooling the permeate vapor, causing it to condense; condensation spontaneously creates a partial vacuum.

The origins of pervaporation can be traced to the nineteenth century, but the word itself was coined by Kober in 1917 [1]. The process was first studied in a systematic fashion by Binning and coworkers at American Oil in the 1950s [2–5]. Binning was interested in applying the process to the separation of organic mixtures. Although this work was pursued at the laboratory and bench scales for a number of years and several patents were obtained, the process was not commercialized. Membrane technology at that time could not produce the high-performance membranes and modules required for a commercially competitive process. Research on the process was picked up in the 1970s by Eli Perry and others at Monsanto. More than a dozen patents assigned to Monsanto were issued from 1973 to 1980, and covered a wide variety of pervaporation applications [6], but none of this work led to a commercial process. Academic research on pervaporation was also carried out by Aptel, Neel, and others at the University of Toulouse [7, 8]. Only by the 1980s had advances in membrane technology made it possible to prepare economically viable pervaporation systems.

The most important current application of pervaporation is the removal of water from organic solvent solutions, most importantly, ethanol solutions. GFT Membrane Systems, now owned by Sulzer Chemtech, is the leader in this field. GFT installed the first pilot plant in 1982 [9]. The ethanol feed to the membrane typically contains about 10% water. Pervaporation removes the water as permeate, producing a residue of pure ethanol

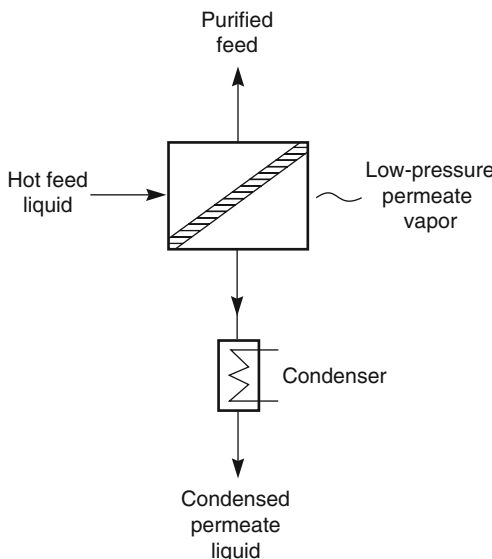


Figure 9.1 In a pervaporation process, a hot liquid mixture contacts a selective membrane. The components of the liquid mixture pass through the membrane and are removed from the permeate side as a vapor mixture. The vapor, enriched in the more permeable component, is cooled and condensed, spontaneously generating a vacuum that drives the process

containing less than 1% water. All the problems of azeotropic distillation are avoided. More than 200 small plants have been installed by Sulzer (GFT) and its licensees for this type of application [10, 11]. Most of these plants were used to remove water from ethanol and isopropyl alcohol streams produced in the pharmaceutical and fine chemicals industries. In the last 10 years, a much larger potential application has emerged, and that is dehydration of fuel bioethanol. Approximately 23 billion gal/year of fuel bioethanol are produced worldwide (2010); 13 billion gal/year in the United States, mostly from corn; 8 billion gal/year in Brazil from sugar; and approximately 2 billion gal/year elsewhere from a mixture of crops. Essentially all of the existing ethanol plants use a combination of distillation and molecular sieve drying to separate the ethanol/water feed mixture. Membrane technology was not sufficiently developed to be used when these plants were built. Fortunately, membrane producers will have another chance to bite the apple when the next generation of cellulose-to-ethanol plants come online. More than 500 of these plants will be needed in the United States if the Department of Energy's biofuels program is to meet its 2022 targets. Additional plants will be built in Brazil and elsewhere.

Although the bulk of current industrial research is focused on dehydration applications, pervaporation processes are being evaluated for separation of small amounts of volatile organic components (VOCs) from water, for environmental pollution control, and some food applications [12–14]. Pilot plants to separate organic/organic mixtures have also been built by Separex [15, 16], Exxon/ExxonMobil [17–19], and W.R. Grace [20]. A timeline illustrating some of the key milestones in development of pervaporation is shown in Figure 9.2.

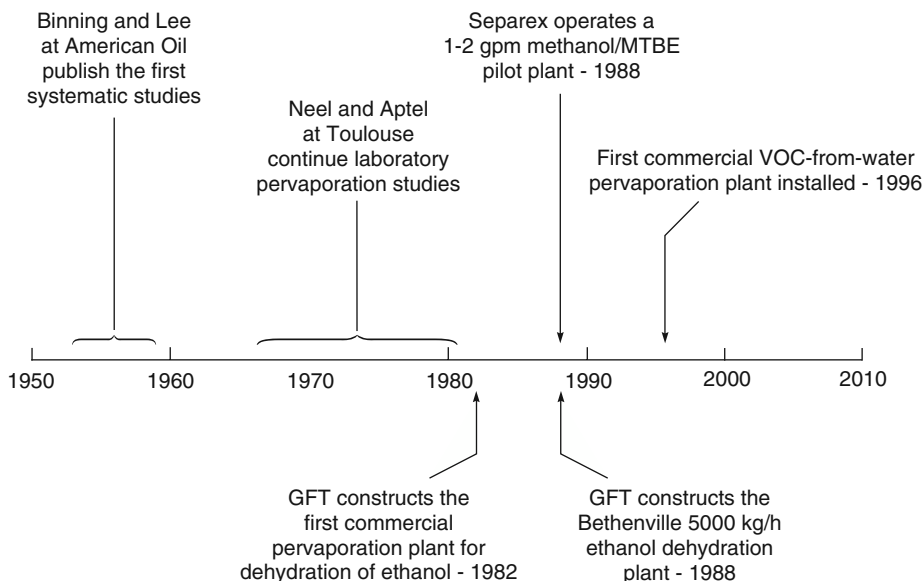


Figure 9.2 Milestones in the development of pervaporation

Although this chapter is titled “Pervaporation”, the section covering commercial application of pervaporation also includes examples of vapor permeation processes. Pervaporation and vapor permeation can both be used to perform the same separations, often times with the same membrane supplied by the same manufacturer. Since industrial producers do not make a major distinction between the two processes, especially when applied to the group of applications discussed here, we have also chosen to treat them together.

9.2 Theoretical Background

The link between pervaporation and vapor permeation is illustrated in Figure 9.3. The right-hand side of the figure shows a pervaporation process. A portion of the heated feed liquid is circulated from the large feed tank past the pervaporation membrane. The membrane removes a small amount of the feed as a low pressure permeate vapor. After cooling and condensing, this permeate vapor forms the condensed permeate.

The left-hand side of Figure 9.3 shows a vapor permeation process. A portion of feed vapor that is in equilibrium with the feed liquid is circulated past the vapor permeation membrane. The membrane removes a small amount of the feed as a low pressure permeate vapor. After cooling and condensing, this permeate vapor also forms a condensed permeate.

The membranes in these two examples are in contact with two very different fluids, but because the vapor feed fluid is in equilibrium with the liquid feed fluid, the driving force for permeation through both membranes is the same [21]. For the vapor permeation case, the flux of component i (J_i) through the membrane is described by Equation 2.65,

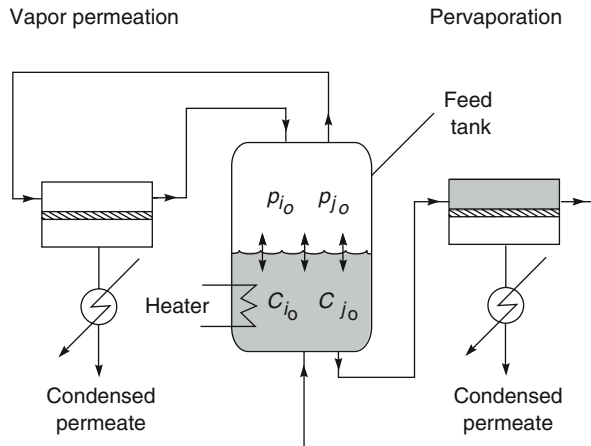


Figure 9.3 A schematic illustration of the equivalence of vapor permeation and pervaporation. The vapor feed to the vapor permeation membrane and the liquid feed to the pervaporation membrane are in equilibrium with each other. This means the driving force across both membranes is equivalent and identical membranes will produce identical permeation fluxes and separations [21]

derived in Chapter 2, as

$$J_i = \frac{D_i K_i^G (p_{i_o} - p_{i_\ell})}{\ell} = \frac{P_i^G}{\ell} (p_{i_o} - p_{i_\ell}) \quad (9.1)$$

where p_{i_o} and p_{j_o} are the partial vapor pressures of components i and j in equilibrium with the feed liquid of composition c_i and c_j , and p_{i_ℓ} and p_{j_ℓ} are the partial pressures of the permeating vapors on the permeate side of the membrane.

For the pervaporation case, the flux of component i through the membrane is described by Equation 2.80, derived in Chapter 2, as

$$J_i = \frac{D_i (K_i^L c_{i_o} - K_i^G p_{i_\ell})}{\ell} \quad (9.2)$$

where K_i^G is the gas phase sorption coefficient of component i in the membrane and K_i^L is the liquid phase sorption coefficient of component i in the membrane. In Chapter 2, it was then shown that Equation 9.2 can be rearranged (Equations 2.80–2.86) to yield

$$J_i = \frac{D_i K_i^G (p_{i_o} - p_{i_\ell})}{\ell} = \frac{P_i^G}{\ell} (p_{i_o} - p_{i_\ell}) \quad (9.3)$$

Equations 9.1 and 9.3 can also be written in molar form as described in Chapter 2, Equation 2.70. Thus

$$j_i = \frac{\mathcal{P}_i^G}{\ell} (p_{i_o} - p_{i_\ell}) \quad (9.4)$$

where j_i is the molar flux of i , ℓ is the membrane thickness, and \mathcal{P}_i^G is the gas separation permeability coefficient. A similar equation can be written for component j .

$$j_j = \frac{\mathcal{P}_j^G}{\ell} (p_{j_o} - p_{j_e}) \quad (9.5)$$

The pervaporation Equation 9.3 has the same form as the gas permeation Equation 9.1. These equations are easily applied to gas permeation since the partial pressures on the feed and permeate sides of the membrane are readily calculated from the measured total pressures and the feed and permeate concentrations. In pervaporation separations, calculating the vapor pressure driving force is not as easy; p_{i_o} and p_{i_e} are the vapor pressures of component i on the feed and permeate sides of the membrane, and the permeability term (\mathcal{P}_i^G) is the same as the gas permeability of the same membrane. Determining the permeate-side vapor pressure in pervaporation is straightforward; the total permeate pressure and the permeate gas composition are all that is required. The problem is to calculate the feed-side vapor pressure; conversion of the measured liquid phase composition and temperature into component vapor pressures is required. Today, the availability of computer process simulation programs (ChemCad, HYSYS, ProSim) makes calculation of the partial vapor pressure a trivial exercise, provided the correct equation of state is selected. Most computer process simulators do a good job of selecting the appropriate equation of state and the activity coefficients required for simple two-component mixtures. The vapor pressures calculated this way are normally within a small percentage of the experimental values. However, obtaining reliable vapor pressures for multi-component mixtures is more difficult and may not be possible if one of the components is an electrolyte. Fortunately, the vast bulk of laboratory pervaporation data involve only two-component mixtures.

Researchers who do not have access to a process simulator can find experimental vapor pressure data and the predictions of several equations of state for many common binary mixtures in compilations such as the DECHEMA Vapor–Liquid Equilibrium Data Collection. The appropriate equations and suggested numerical coefficients can then be used to calculate the vapor pressures from known liquid compositions at known temperatures.

Having obtained membrane permeabilities or permeances as described above, the membrane selectivity, defined as the ratio of the molar permeabilities or permeances, can then be determined:

$$\alpha_{ij} = \frac{\mathcal{P}_i^G}{\mathcal{P}_j^G} = \frac{\mathcal{P}_i^G / \ell}{\mathcal{P}_j^G / \ell} \quad (9.6)$$

In these definitions (Equations 9.4–9.6), the permeability and selectivity are given in molar terms to allow direct comparison of pervaporation data with the larger body of gas permeation data.

Describing pervaporation data in terms of membrane permeabilities, permeances, and selectivities as described above is the preferred method of reporting the data, since it links pervaporation to the related processes of gas and vapor separation. Unfortunately, in much of the published literature, the separation performed by the pervaporation process shown on the right-hand side of Figure 9.1 is characterized in terms of the component

fluxes J_i and J_j , and a separation factor β_{pervap} defined as

$$\beta_{\text{pervap}} = \frac{c_{i_\ell}/c_{j_\ell}}{c_{i_o}/c_{j_o}} \quad (9.7)$$

or

$$\beta_{\text{pervap}} = \frac{p_{i_\ell}/p_{j_\ell}}{c_{i_o}/c_{j_o}} \quad (9.8)$$

since the ratio of the permeate-side component partial vapor pressures is also the ratio of the component concentrations.

The factors that determine the pervaporation separation factor, β_{pervap} , can be illustrated by considering the thermodynamically equivalent vapor permeation process shown on the left-hand side of Figure 9.3. The process can be divided into two steps [21]. The first step is evaporation, governed by the vapor–liquid equilibrium of the liquid mixture. Evaporation produces a separation because of the different volatilities of the components of the feed liquid. The separation can be defined as β_{evap} , the ratio of the component concentrations in the feed vapor to their concentrations in the feed liquid:

$$\beta_{\text{evap}} = \frac{p_{i_o}/p_{j_o}}{c_{i_o}/c_{i_\ell}} \quad (9.9)$$

The second step is permeation of components i and j through the membrane; this step is equivalent to conventional gas permeation. The driving force for permeation is the difference in the vapor pressures of the components in the feed and permeate vapors. The separation achieved in this step, β_{mem} , can be defined as the ratio of the components in the permeate vapor to the ratio of the components in the feed vapor

$$\beta_{\text{mem}} = \frac{p_{i_\ell}/p_{j_\ell}}{p_{i_o}/p_{j_o}} \quad (9.10)$$

It follows from Equations 9.8–9.10 that the separation achieved in pervaporation is equal to the product of the separation achieved by evaporation of the liquid and the separation achieved by selective vapor permeation through the membrane.¹

$$\beta_{\text{pervap}} = \beta_{\text{evap}} \cdot \beta_{\text{mem}} \quad (9.11)$$

Equation 9.11 is useful in showing the two processes that contribute to the total pervaporation permeation process. The first step is evaporation of the feed liquid to form a

¹ Figure 9.3 illustrates the concept of permeation from a saturated vapor phase in equilibrium with the feed liquid as a tool to obtain Equation 9.11. A number of workers have experimentally compared vapor permeation and pervaporation separations and have sometimes shown that permeation from the liquid is faster and less selective than permeation from the equilibrium vapor. This is an experimental artifact. In vapor permeation experiments, the vapor in contact with the membrane is not completely saturated. This means that the activities of the feed components in vapor permeation experiments are less than their activity in pervaporation experiments. Because sorption by the membrane in this range is extremely sensitive to activity, the vapor permeation fluxes are lower than pervaporation fluxes. Kataoka *et al.* [22] have illustrated this point in a series of careful experiments.

saturated vapor in contact with the membrane; the second step is diffusion of this vapor through the membrane to the low-pressure permeate side.

Equation 9.11 illustrates the problem with reporting data in terms of fluxes and separation factors. These values are not only a function of the intrinsic properties of the membranes used, but also depend on the vapor–liquid equilibrium of the feed solution and the operating conditions of the experiments (feed concentration, permeate pressure, feed temperature): change the operating conditions and all the numbers change [23]. Using flux and separation factors makes comparison of pervaporation data sets obtained under different operating conditions difficult. Combining all of the contributing terms into a single parameter also masks each term's individual effect.

The benefit of reporting pervaporation data in terms of molar permeances (vapor-pressure normalized fluxes) and membrane selectivities is apparent from the experimental data shown in Figures 9.4 and 9.5 [23]. Figure 9.4 shows plots of membrane flux and separation factor as a function of feed water concentration for a series of pervaporation experiments performed with ethanol/water mixtures and a hydrophilic cellulose ester membrane. At a low water concentration in the feed, the membrane is very selective for water from ethanol and the separation factor is high, but the flux of water and ethanol through the membrane is low. As the water concentration in the feed is increased, both the ethanol and water fluxes increase and the membrane separation factor falls. At a water concentration of about 70 wt%, the ethanol flux reaches a maximum value. At higher water concentrations, the ethanol flux declines, going to zero ethanol flux at zero ethanol concentration in the feed. The water flux continues to increase sharply, reaching about $34 \text{ kg/m}^2 \text{ h}$ at 100 wt% water. Something is going on, probably related to plasticization of the membrane by water, but it is hard to sort this out from the membrane flux and separation factor data as presented in Figure 9.4.

The same data are re-plotted as permeances and selectivities *versus* feed concentration in Figure 9.5. The situation is now clearer. At low water concentrations in the feed, the membrane is extremely selective; for example, at a water concentration of less than 5 wt%, the membrane has a water permeance of about 5000 gpu ($1 \text{ gpu} \equiv 1 \times 10^{-6} \text{ cm}^3(\text{STP})/\text{cm}^2 \cdot \text{s} \cdot \text{cmHg}$) and the ethanol permeance is below 10 gpu. As the water concentration increases, the ethanol and water permeances both increase. This increase is probably due to swelling of the membrane by water, leading to plasticization. Plasticization increases the water permeance from 5000 gpu at less than 5 wt% water to 32 000 gpu at 100 wt% water, but has a much larger relative effect on ethanol permeance. The corresponding ethanol permeance increases from less than 10 gpu at less than 5 wt% water to more than 6000 gpu at 100 wt% water, an almost 600-fold increase. As a consequence, the water/ethanol selectivity falls to a selectivity of only 5 at very high water concentrations.

The data in Figure 9.5 also highlight the very high permeances of these water permeable pervaporation membranes. In the concentration range for which these membranes are usually used, 0–20 wt% water, the membrane has a water permeance of 5000–10 000 gpu. This permeance is almost 1000 times higher than the oxygen permeance of membranes used to separate oxygen from air, and about 50 times the CO_2 permeance of membranes used to separate CO_2 from natural gas.

Membrane selectivities and permeances are intrinsic properties of the membrane, while the membrane separation factor, β_{mem} , is affected by the properties of the membrane, the

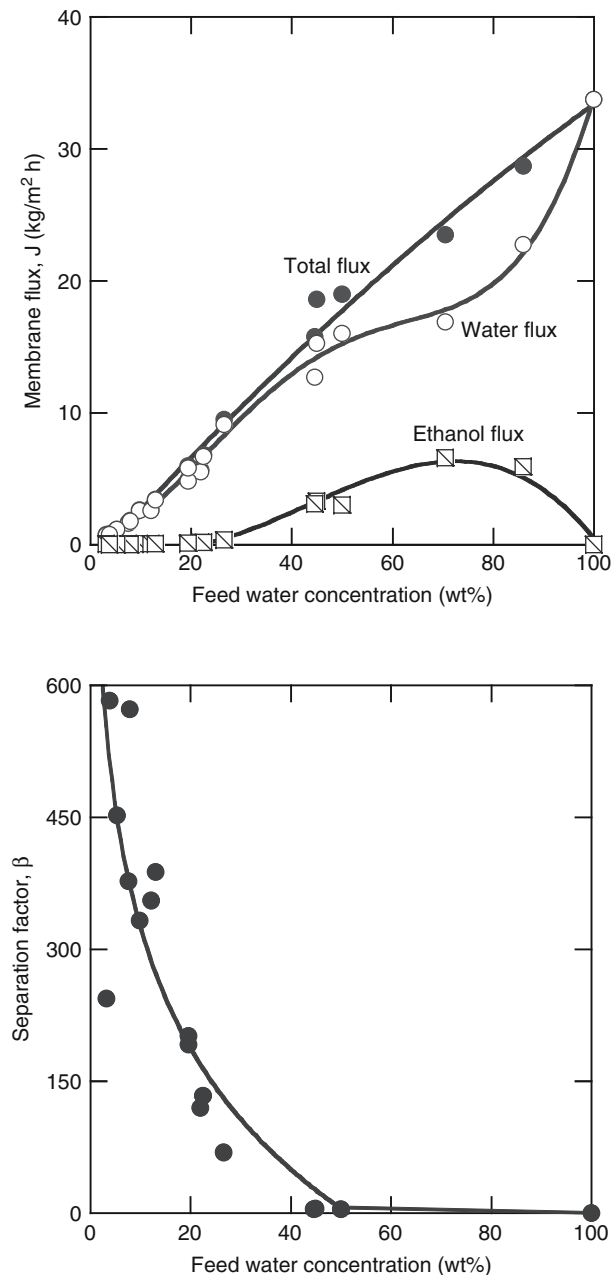


Figure 9.4 Dehydration of ethanol/water solutions with a commercial cellulose ester membrane (75°C , permeate pressure <5 torr), reported as membrane flux and water/ethanol separation factor data [23]. Reprinted from *J. Membr. Sci.*, **348**, (1–2), R.W. Baker, J.G. Wijmans and Y. Huang, Permeability, Permeance and Selectivity: A Preferred Way of Reporting Pervaporation Performance Data, p. 346–352. Copyright 2010, with permission from Elsevier.

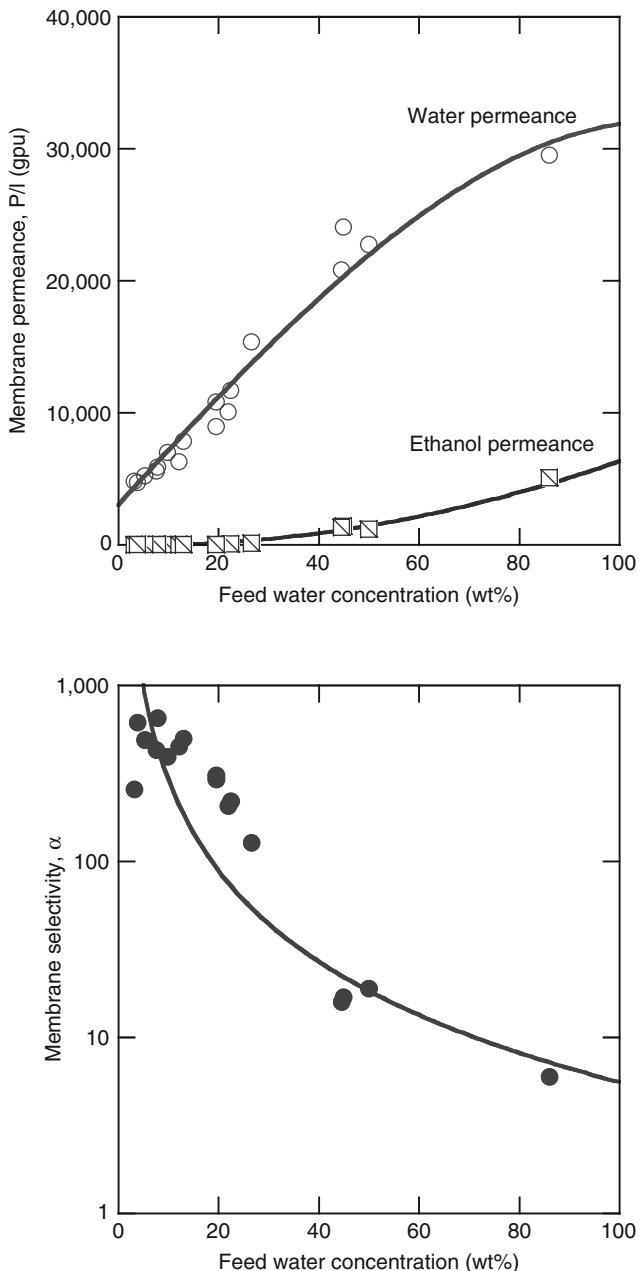


Figure 9.5 Data from Figure 9.4, re-plotted as membrane permeance and selectivity data [23]. Reprinted from *J. Membr. Sci.* 348 (1-2), R.W. Baker, J.G. Wijmans and Y. Huang, Permeability, Permeance and Selectivity: A Preferred Way of Reporting Pervaporation Performance Data, p. 346–352, Copyright 2010, with permission from Elsevier.

vapor–liquid equilibrium diagram of the feed solution, and the process operating conditions. However, the different terms can be linked. Thus, combining Equations 9.4–9.6, we can write

$$\frac{j_i}{j_j} = \frac{\mathcal{P}_i^G}{\mathcal{P}_j^G} \frac{(p_{i_o} - p_{i_\ell})}{(p_{j_o} - p_{j_\ell})} \quad (9.12)$$

The ratio of the molar fluxes is also the same as the ratio of the permeate partial pressures

$$\frac{j_i}{j_j} = \frac{p_{i_\ell}}{p_{j_\ell}} \quad (9.13)$$

And so combining Equations 9.6, 9.12, and 9.13 yields

$$\beta_{\text{pervap}} = \frac{\beta_{\text{evap}} \alpha_{\text{mem}} (p_{i_o} - p_{i_\ell})}{(p_{j_o} - p_{j_\ell}) (p_{i_o}/p_{j_o})} \quad (9.14)$$

Equation 9.14 identifies the three factors that determine the performance of a pervaporation system. The first factor, β_{evap} , is the vapor–liquid equilibrium, determined mainly by the feed liquid composition and temperature; the second is the membrane selectivity, α_{mem} , an intrinsic permeability property of the membrane material; and the third includes the feed and permeate vapor pressures, reflecting the effect of operating parameters on membrane performance.

At very low permeate pressures, that is, when a hard vacuum is applied to the permeate side of the membrane, Equation 9.14 reduces to

$$\beta_{\text{pervap}} = \beta_{\text{evap}} \alpha_{\text{mem}} \text{ as } p_{i_\ell} \rightarrow 0, p_{j_\ell} \rightarrow 0 \quad (9.15)$$

As in gas separation, the separation achieved by pervaporation is determined both by the membrane selectivity and by the membrane pressure ratio. The interaction of these two factors is expressed in Equation 9.14. The related expression for gas separation is Equation 8.19 in Chapter 8. As in gas separation, there are two limiting cases in which one of the two factors dominates the separation achieved. The first limiting case is when the membrane selectivity is very large compared to the vapor pressure ratio between the feed liquid and the permeate vapor:

$$\alpha_{\text{mem}} \gg \frac{p_o}{p_\ell} \quad (9.16)$$

This means that for a membrane with infinite selectivity for component i , the permeate vapor pressure of component i will equal the feed partial vapor pressure of i . That is,

$$p_{i_\ell} = p_{i_o} \quad (9.17)$$

Equation 9.17 combined with Equation 9.10 gives

$$\beta_{\text{mem}} = \frac{p_{j_o}}{p_{j_\ell}} \quad (9.18)$$

which, combined with Equation 9.11, leads to the limiting case

$$\beta_{\text{pervap}} = \beta_{\text{evap}} \cdot \frac{p_{j_o}}{p_{j_\ell}} \text{ when } \alpha_{\text{mem}} \gg \frac{p_o}{p_\ell} \quad (9.19)$$

Similarly, in the case of a very large membrane selectivity in favor of component j ,

$$\beta_{\text{pervap}} = \beta_{\text{evap}} \cdot \frac{p_{i_o}}{p_{i_\ell}} \quad (9.20)$$

For the special case in which component i is the minor component in the feed liquid, p_{j_o} approaches p_o , p_{j_ℓ} approaches p_ℓ , and Equation 9.19 reverts to

$$\beta_{\text{pervap}} = \beta_{\text{evap}} \frac{p_o}{p_\ell} \quad (9.21)$$

where p_o/p_ℓ is the feed-to-permeate ratio of the total vapor pressures.

The second limiting case occurs when the vapor pressure ratio is very large compared to the membrane selectivity. This means that the permeate partial pressure is smaller than the feed partial vapor pressures, and p_{i_ℓ} and $p_{j_\ell} \rightarrow 0$. Equation 9.14 then becomes

$$\beta_{\text{pervap}} = \beta_{\text{evap}} \alpha_{\text{mem}} \text{ when } \alpha_{\text{mem}} \ll \frac{p_o}{p_\ell} \quad (9.22)$$

The relationship between the three separation factors, β_{pervap} , β_{evap} , and β_{mem} , is illustrated for an ethanol-selective membrane in Figure 9.6. This type of plot was introduced by Shelden and Thompson [24] to illustrate the effect of permeate pressure on pervaporation separation, and is a convenient method to represent the pervaporation process graphically. When the permeate pressure, $p_\ell = p_{i_\ell} + p_{j_\ell}$, approaches the feed vapor pressure, $p_o = p_{i_o} + p_{j_o}$, the vapor pressure ratio across the membrane shown on the right-hand axis of the figure approaches unity. No separation is produced by the membrane, and the composition of the permeate vapor approaches the composition obtained by simple evaporation of the feed liquid. This composition is shown by the line labeled β_{evap} in the figure. As the permeate pressure decreases to below the feed vapor pressure, the vapor pressure ratio across the membrane increases. The overall separation obtained, β_{pervap} , is then the product of the separation due to evaporation of the feed liquid, β_{evap} , and the separation due to permeation through the membrane, β_{mem} . The line labeled "permeate composition" in Figure 9.6 is calculated from Equation 9.14. As the permeate pressure decreases, the feed-to-permeate pressure ratio across the membrane increases and a better separation is obtained.

9.3 Membrane Materials and Modules

9.3.1 Membrane Materials

The selectivity (α_{mem}) of pervaporation membranes critically affects the overall separation obtained and depends on the membrane material. Therefore, membrane materials are tailored for particular separation problems. As with other solution-diffusion membranes, the permeability of a component is the product of the membrane sorption coefficient and

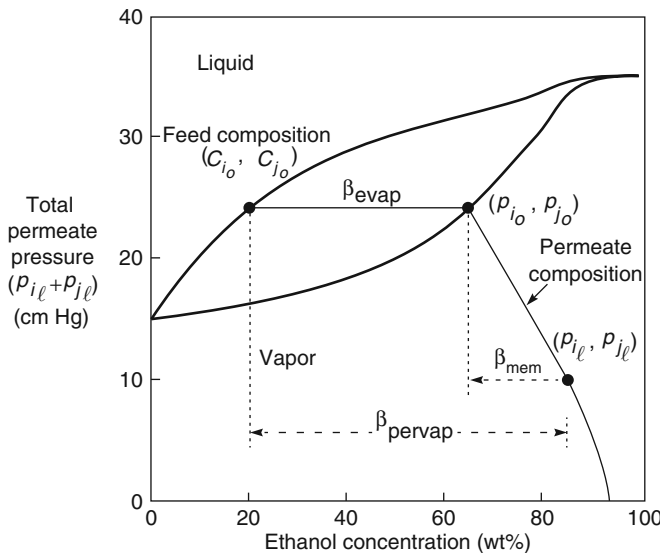


Figure 9.6 The permeate composition of an ethanol-selective pervaporation membrane used to separate ethanol from an ethanol/water feed solution containing 20 wt% ethanol at 60°C. The total separation, β_{pervap} , is made up of two contributions: β_{evap} , due to the evaporative VLE contribution, and β_{mem} , due to selective permeation of ethanol through the membrane. The line labeled permeate composition is calculated from Equation 9.14 and shows that the membrane performance improves as the permeate pressure decreases.

the diffusion coefficient (mobility). The membrane selectivity term α_{mem} in Equation 9.6 can be written as

$$\alpha_{\text{mem}} = \frac{\mathcal{P}_i^G}{\mathcal{P}_j^G} = \left(\frac{D_i}{D_j} \right) \left(\frac{K_i^G}{K_j^G} \right) \quad (9.23)$$

(see Equation 8.4). This expression shows that membrane selectivity is the product of the mobility selectivity (D_i/D_j) of the membrane material, generally governed by the relative mobility of the permeants, and the solubility selectivity (K_i^G/K_j^G), generally governed by the chemistry of the membrane material. In gas permeation, the total sorption of gases by the membrane material is usually low, often less than 1 wt%, so the membrane selectivity measured with gas mixtures is often close to the selectivity calculated from the ratio of the pure gas permeabilities. In pervaporation, the membrane is in contact with the feed liquid, and typical sorptions are 2–20 wt%. Sorption of one of the components of the feed can then change the sorption and diffusion of the second component. As a rule of thumb, the total sorption of the feed liquid by the membrane material should be in the range 3–10 wt%. Below 3 wt% sorption, the membrane selectivity may be good, but the flux through the material will be low. Above 10 wt% sorption, fluxes will be high, but the membrane selectivity will generally be low because the mobility selectivity will decrease as the material becomes more swollen and plasticized. The sorption selectivity will also tend toward unity.

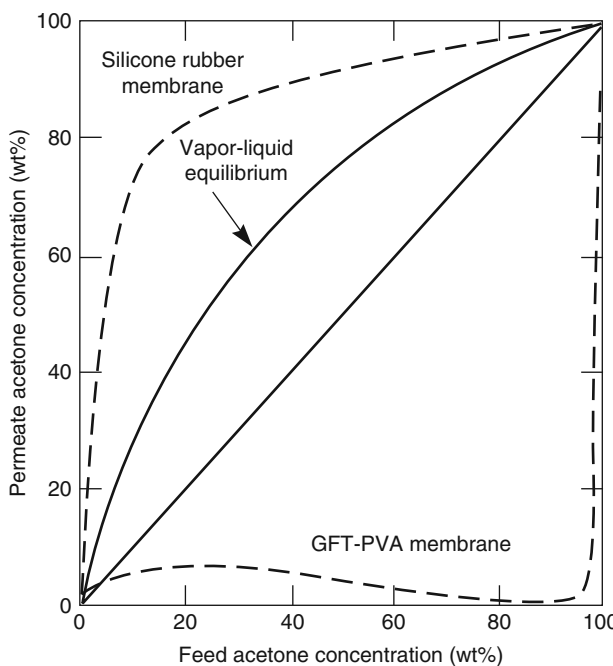


Figure 9.7 Pervaporation separation of acetone/water mixtures achieved with a water-selective membrane [poly(vinyl alcohol) (PVA)], and an acetone-selective membrane (silicone rubber).[25]. Reprinted from Hollein et al., p. 1051 by courtesy of Marcel Dekker, Inc

By manipulating the chemistry of membrane materials, either sorption- or diffusion-selectivity-controlled membranes can be made. The range of results that can be obtained with different membranes with the same liquid mixture is illustrated in Figure 9.7 for the separation of acetone from water [25]. The figure shows the concentration of acetone in the permeate as a function of the concentration in the feed. The two membranes shown have dramatically different properties. The silicone rubber membrane, made from a hydrophobic rubbery material, preferentially sorbs acetone, the more hydrophobic organic compound. For rubbery materials, the diffusion selectivity term – which would favor permeation of the smaller component (water), is small. Therefore, the silicone rubber membrane is sorption-selectivity-controlled and preferentially permeates acetone. In contrast, the poly(vinyl alcohol) membrane is made from a hydrophilic, rigid, crosslinked material. Because poly(vinyl alcohol) is hydrophilic, the sorption selectivity favors permeation of water, the more hydrophilic polar component. Also, because poly(vinyl alcohol) is glassy and crosslinked, the diffusion selectivity favoring the smaller water molecules over the larger acetone molecules is substantial. As a result, poly(vinyl alcohol) membranes permeate water several hundred times faster than acetone.

In any membrane process, it is desirable for the minor components to permeate the membrane, so the acetone-selective silicone rubber membrane is best used to treat dilute acetone feed streams, concentrating most of the acetone in a small volume of permeate. The water-selective poly(vinyl alcohol) membrane is best used to treat concentrated

Table 9.1 Widely used pervaporation membrane materials

Dehydration of organics	Microporous polyacrylonitrile support membrane coated with a 5–20 µm layer of crosslinked poly(vinyl alcohol) is the most commonly used commercial material [10, 26]. Chitosan [27] and polyelectrolyte membranes such as Nafion [28, 29] have equivalent properties
VOC/water separation	
Toluene/water	
Trichloroethylene/water	
Methylene chloride/water	Membranes comprising silicone rubber coated onto polyimides, polyacrylonitrile, or other microporous supports are widely used [12, 13]. Other rubbers such as ethylene-propylene terpolymers have been reported to have good properties also [30]. Polyamide-polyether block copolymers have also been used for pervaporation of some polar VOCs [31, 32]
Organic/organic separation	The membrane used depends on the nature of the organics. Poly(vinyl alcohol) and cellulose acetate [15] have been used to separate alcohols from ethers. Polyurethane-polyimide block copolymers have been used for aromatic/aliphatic separations [17–19]

acetone feed streams, concentrating most of the water in a small volume of permeate. Both membranes are more selective than distillation, which relies on the vapor–liquid equilibrium to achieve separation.

Table 9.1 summarizes the principal commercial pervaporation applications and the membrane materials most commonly used.

9.3.2 Dehydration Membranes

Water forms azeotropes with a number of commonly used solvents, so a membrane process that could separate these mixtures, alone or in combination with distillation, would be widely used. The vapor–liquid equilibrium diagrams for some of the potential candidate applications are shown in Figure 9.8.

A huge body of pervaporation data dealing with solvent/water mixtures has been published and is reviewed elsewhere [26]. Most of this data has little value to industrial developers of the technology. The materials studied are usually tested as thick films (50–100 µm thick) at low temperatures of 30–60°C. These conditions are far from those found in industrial applications. Industrial membranes are normally made as composite membranes with a selective layer 1–5 µm thick. In solvent dehydration applications, these membranes are used with solvent/water feed solutions heated to 100–120°C to maximize the vapor pressure driving force across the membrane. Many of the materials described in the literature will fail at these temperatures.

Crosslinked poly(vinyl alcohol) was one of the first membrane materials used commercially by GFT and it remains a widely used material [10]. Chitosan [27] and Nafion® [28, 29] provide equivalent performance in pervaporative dehydration of organics. Various cellulose esters and ethers have also been used. Data shown in Figures 9.4 and 9.7 are typical of these polymeric membranes.

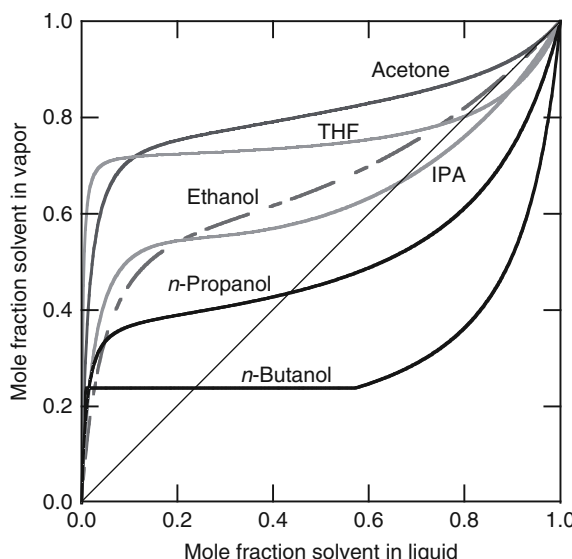


Figure 9.8 Vapor–liquid equilibrium diagrams for various solvent/water mixtures that are potential candidate applications for water-selective pervaporation membrane processes [11]. Reprinted with permission from [45]. Copyright (2010) American Chemical Society.

More recently, there has been increasing interest in ceramic membrane materials. Mitsui and the Bussan Research Institute brought tubular NaY and NaA zeolite membranes to the commercial stage [33, 34] and a demonstration plant was built. Membrane water/ethanol selectivities are very high and at temperatures of 100–150°C, high fluxes have also been obtained. The membranes can be used for pervaporation or vapor permeation. However, high costs have limited commercial use to date.

Energy Research Centre of the Netherlands (ECN) has also developed silica membranes which are at the early commercial stage.

9.3.3 Organic/Water Separation Membranes

Silicone rubber composite membranes are the state-of-the-art materials used to separate VOCs from water. Silicone rubber is easy to fabricate, is mechanically and chemically strong, and has good separation factors for many common organic compounds, as shown in Table 9.2. These representative data were obtained with industrial-scale modules under normal operating conditions. The performance of silicone membranes in laboratory test cells operated under ideal conditions is usually better.

A number of academic studies have produced rubbery hydrophobic membrane materials with higher selectivities than silicone rubber. For example, Nijhuis *et al.* [30] measured the separation factors of various rubbery membranes with dilute toluene and trichloroethylene (TCE) solutions. The separation factor of silicone rubber was in the 4000–5000 range, but other materials had separation factors as high as 40 000. However, in practice, an increase in membrane separation factor beyond about 1000 provides very little additional benefit. Once a separation factor of this magnitude is obtained, other factors, such as

Table 9.2 Typical silicone rubber membrane module pervaporation separation factors (VOC removal from water)

Separation factor for VOC over water	Volatile organic compound (VOC)
200–1000	Benzene, toluene, ethylbenzene, xylenes, TCE, chloroform, vinyl chloride, ethylene dichloride, methylene chloride, perchlorofluorocarbons, hexane
20–200	Ethyl acetate, propanols, butanols, MEK, aniline, amyl alcohol
5–20	Methanol, ethanol, phenol, acetaldehyde
1–5	Acetic acid, ethylene glycol, DMF, DMAc

ease of manufacture, mechanical strength, chemical stability, and control of concentration polarization become more important. This is why silicone rubber remains prevalent for VOC/water separations, even though polymers with higher selectivities are known.

Membranes with improved separation factors would be useful for hydrophilic VOCs such as ethanol and methanol, for which the separation factor of silicone rubber is 5–10. As yet, no good replacement for silicone rubber has been developed. The most promising results to date have been obtained with silicone rubber membranes containing dispersed zeolite particles [30]. Apparently, ethanol preferentially permeates the pores of the zeolite particles; membranes have been produced in the laboratory with ethanol/water separation factors of 40 or more. The evaporative separation factor (β_{evap}) is 12–15, so from Equation 9.11, separation factors of 40 imply a membrane selectivity of about 3. Membranes with these properties could be applied in fermentation processes and solvent recovery [35]. Unfortunately, the membranes are not stable when used with industrial solutions. Small amounts of esters or long-chain alcohols present in the solution penetrate the zeolite pores and are adsorbed and block the ethanol transport.

Polyamide-polyether block copolymers (Pebax[®], Elf Atochem, Inc., Philadelphia, PA) have been used successfully with polar organics such as phenol and aniline [31, 32, 36]. The separation factors obtained with these organics are greater than 100, far higher than the separation factors obtained with silicone rubber. The improved selectivity reflects the greater sorption selectivity obtained with the polar organic in the relatively polar polyamide-polyether membrane. On the other hand, toluene separation factors obtained with polyamide-polyether membranes are below those measured with silicone rubber.

9.3.4 Organic/Organic Separation Membranes

For the separation of organic/organic mixtures, current membranes are only moderately selective, generally because the differences in sorption between different organic molecules is small, and also because many membrane materials swell excessively in organic solvent mixtures, especially at high temperatures. The goal is to find a membrane material that will absorb between 3 and 10 wt% of the organic mixture at the high temperatures of the application. One approach is to use rigid backbone polymers to control swelling (for example, the Matrimid[®] polyimides developed by Grace [37]). However, the permeability of these materials is often low. Another approach, used by ExxonMobil [18, 19], is to use block copolymers consisting of rigid polyimide segments that provide

a strong network and softer segments formed from more flexible polymers through which permeant transport occurs. The permeation properties of the polymer can be controlled by tailoring the size and chemistry of the two blocks. Another approach is to use amorphous but polar rubbery or glassy polymers. Because of their polar nature, sorption of hydrophobic organics is limited. Notwithstanding this work, development of more selective membranes is still required before the application of pervaporation to important organic/organic separations, such as separation of aromatics from aliphatics and olefins from paraffins, become practical.

9.3.5 Membrane Modules

One of the major problems affecting pervaporation modules and process designs is the need to supply heat to the feed solution to maintain its feed temperature during the separation. The feed solution cools because of the latent heat of liquid evaporation required to create the permeate vapor removed from the feed liquid. This pervaporative cooling produces a feed solution temperature drop of about 5°C for every 1% of the feed that permeates the membrane. In industrial pervaporation processes, an average of 3–5% of the feed permeates the membrane per module. The corresponding temperature drop is then about $15\text{--}25^{\circ}\text{C}$. Conventionally, this temperature drop is restored by a series of individual heater/heating cycles between each module. The use of heat exchangers to maintain a constant feed solution temperature is illustrated in Figure 9.9. Four heating/pervaporation steps are shown, but in an industrial plant, more feed reheating/pervaporation steps may be required. The cost of piping, valves, and flanges for these operations is a significant fraction of the final plant cost.

Batch pervaporation systems are a lower cost solution to the reheating problem, particularly for small feed streams. A flow diagram of this type of system, together with some performance data, is shown in Figure 9.10. In this unit, the incoming feed solution is collected in a surge tank. A portion of this solution is then transferred to the

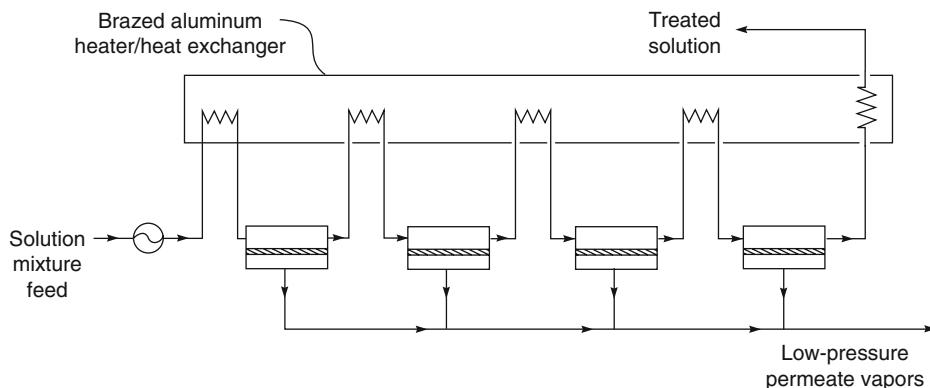


Figure 9.9 Conventional layout of heater/heat exchangers used to maintain the feed solution temperature of pervaporation modules

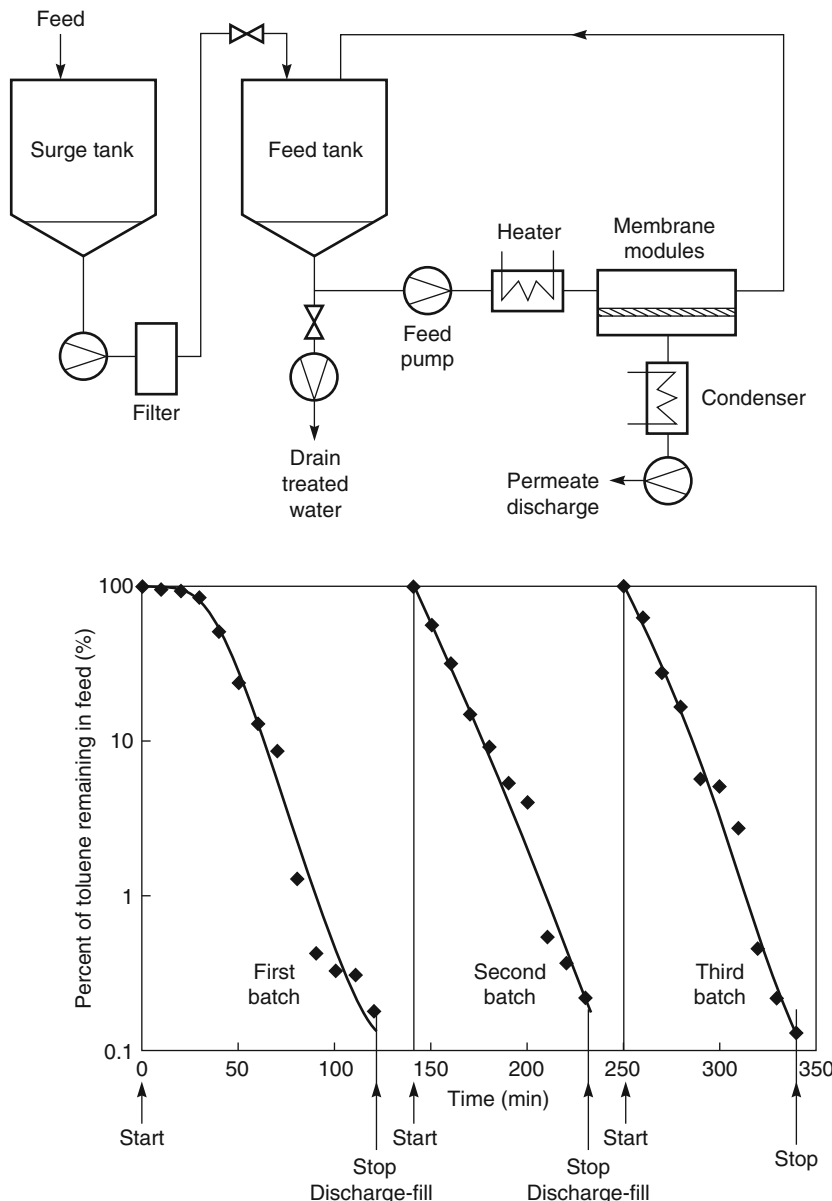


Figure 9.10 Flow diagram and typical performance for a 50-gal cyclic batch pervaporation system. The treatment time for the first 50-gal batch was set at 120 minutes because the unit was cold; thereafter, the cycle time was set at 90 minutes. The system achieved 99.8% removal of toluene from the feed water that initially contained about 500 ppm toluene [13]

feed tank and circulated at high velocity through the feed pervaporation modules. The stage-cut per pass through the modules can be set at a low value of $\sim 1\%$ or less. Cooling of the feed solution is then small and the solution can be easily maintained at the set temperature by the in-line heater shown. When the feed solution has reached the desired concentration – in the example shown, 99.8% removal of toluene from the feed solution – the treated solution is removed from the feed tank. The tank is then loaded with a new batch of feed solution and the cycle is repeated. Automatic controls can be used to operate the unit in a semi-continuous fashion.

The first successful pervaporation modules produced were made by GFT (Sulzer) and used a plate-and-frame design. A photograph of one of these units is shown in Figure 9.11. All of the membrane plates were arranged in parallel, so multiple modules with interstage heating were required for a complete plant. Two to four modules were normally stacked inside the vacuum chamber of the system shown.

In later years, Sulzer (working with W.R. Grace) developed tubular modules housed in a shell-and-tube (heat exchanger) design (see Figure 9.12) [39]. The tubular modules were mounted inside perforated steel tubes. Permeate passing through the perforated tubes collected in the low-pressure central shell of the unit. The U-tube manifolds at each end of the tubes were contained inside steam-heated end chambers separated from the central vacuum chamber by a tube sheet. As the feed circulated through these manifolds, it was reheated to the set temperature.

Tubular and plate-and-frame modules have been used in many small plants using tens to a few hundred square meters of membrane. More recently, the focus of industrial pervaporation research has moved to dehydration of bioethanol. These plants will require several thousand square meters of membrane, so more economical module designs are required. Ube in Japan has developed hollow fiber polyimide membranes for this application. Other companies are adapting spiral-wound module technology to pervaporation.

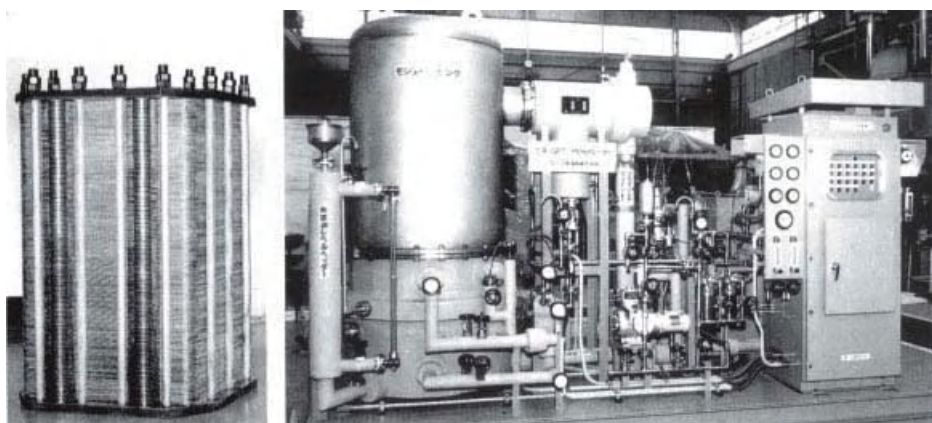


Figure 9.11 Photograph of a 50-m^2 GFT plate-and-frame module and an ethanol dehydration system fitted with this type of module. The module is contained in the large vacuum chamber on the left-hand-side of the pervaporation system [38]

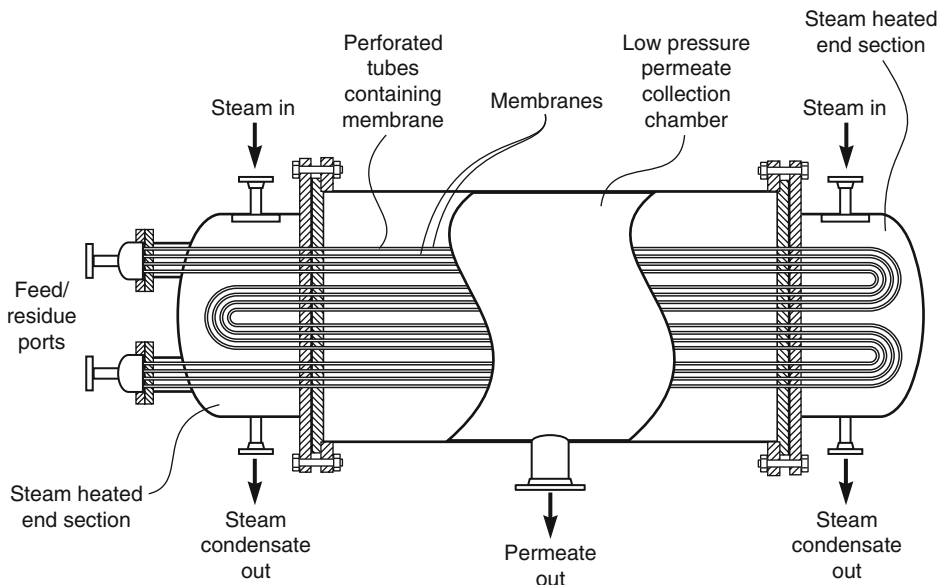


Figure 9.12 Sulzer-Grace shell-and-tube pervaporation module design, from U.S. Patent 7,655,141 [39]. The feed liquid pumped through the tubular membranes is reheated every time it passes into the steam-heated end sections of the module

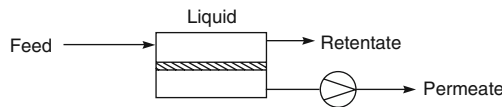
9.4 System Design

Transport through pervaporation membranes is produced by maintaining a vapor pressure gradient across the membrane. As in gas separation, the flux through the membrane is proportional to the vapor pressure difference (Equation 9.5), but the separation obtained is determined by the membrane selectivity and the pressure ratio (Equation 9.14). Figure 9.13 illustrates a number of ways to achieve the required vapor pressure gradient.

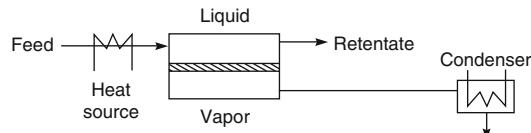
In the laboratory, the low vapor pressure required on the permeate side of the membrane is often produced with a vacuum pump, as shown in Figure 9.13a. In a commercial-scale system, however, the vacuum pump requirement would be impossibly large. In the early days of pervaporation research, the calculated vacuum pump size was sometimes used as proof that pervaporation would never be commercially viable. An attractive alternative to a vacuum pump, illustrated in Figure 9.13b, is to cool the permeate vapor to condense the liquid; condensation of the liquid spontaneously generates the permeate-side vacuum. The feed solution may also be heated to increase the vapor pressure driving force. In this process, the driving force is the difference in vapor pressure between the hot feed solution and the cold permeate liquid at the temperature of the condenser. This type of design is preferred for commercial operations, because the cost of providing the required cooling and heating is much less than the cost of a vacuum pump, and the process is operationally more reliable.

A third possibility, illustrated in Figure 9.13c, is to sweep the permeate side of the membrane with a countercurrent flow of carrier gas. In the example shown, the carrier gas is cooled to condense and recover the permeate vapor, and the gas is recirculated. If

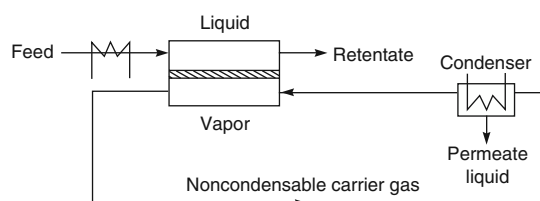
(a) Vacuum driven pervaporation



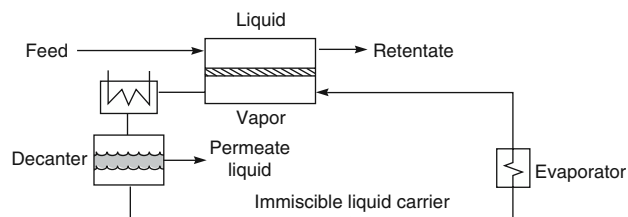
(b) Temperature gradient driven pervaporation



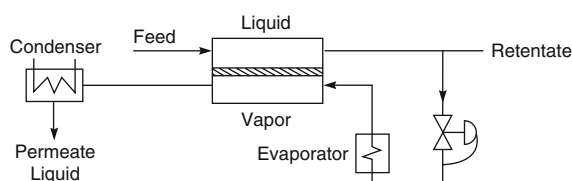
(c) Carrier gas pervaporation



(d) Pervaporation with a condensable and immiscible carrier



(e) Pervaporation with a condensable miscible carrier



(f) Pervaporation with a two-phase permeate and partial recycle

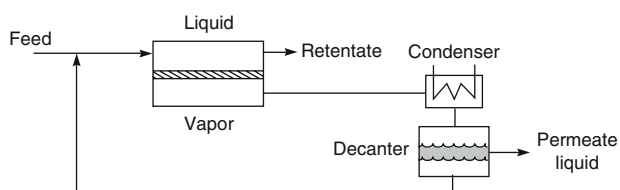


Figure 9.13 Schematics of potential pervaporation process configurations that have been suggested but not necessarily practiced

the permeate has no value and can be discarded without condensation (for example, in the pervaporative dehydration of an organic solvent with an extremely water-selective membrane), this is the preferred mode of operation. In this case, the permeate would contain only water plus a trace of organic solvent and could be discharged or incinerated at low cost. No permeate refrigeration is required.

An alternative carrier gas system uses a condensable gas, such as steam, as the carrier sweep fluid. One variant of this system is illustrated in Figure 9.13d. Low-grade steam is often available at low cost, and, if the permeate is immiscible with the condensed carrier – water – it can be recovered by decantation. The condensed water will contain some dissolved organic and can be recycled to the evaporator and then to the permeate side of the module. This operating mode is limited to water-immiscible permeates and to feed streams for which contamination of the feed liquid by water vapor permeating from the sweep gas is not a problem. This idea has been discovered, rediscovered, and patented a number of times, but never used commercially [40, 41]. If the permeate is soluble in the condensable sweep generated, then the sweep gas is best obtained by evaporating a portion of the residue liquid as shown in Figure 9.13e. The final pervaporation process, illustrated in Figure 9.13f, is a system of particular interest for removing low concentrations of dissolved VOCs from water. The arrangement shown is used when the solubility of the permeating solvent in water is limited. In this case, the condensed permeate liquid separates into two phases: an organic phase, which can be treated for reuse, and an aqueous phase saturated with organic, which can be recycled to the feed stream for reprocessing.

In the process designs shown in Figure 9.13, the permeate vapor is condensed to yield a single liquid permeate condensate. A simple improvement to the pervaporation process is to use fractional condensation of the permeate vapor to achieve an improved separation [42, 43]. Two process designs are shown in Figure 9.14. In Figure 9.14a, the permeate vapor is condensed in two condensers in series. In the example shown, the recovery of ethanol from water, the first (higher temperature) condenser produces a first condensate containing about 5% ethanol that is recycled to the incoming feed. The second (lower temperature) condenser condenses the remaining vapor to produce an ethanol product stream containing about 50% ethanol.

The condensation system shown in Figure 9.14b uses a vertical heat exchanger (sometimes called a dephlegmator) to achieve an even better separation. Warm, low-pressure permeate vapor from the pervaporation unit enters the heat exchanger at the bottom. As the vapor rises up the column, some condenses on the cold tube wall. The resultant liquid flows downward within the feed passage countercurrent to the rising feed vapor. Mass transfer between the liquid and vapor enriches the liquid in the less volatile components as the more volatile components are re-vaporized. As a result, several theoretical stages of separation are achieved. The separation achieved with this approach can be impressive. In the example shown, the 20 wt% ethanol vapor is separated into a 5 wt% bottoms, which is recycled to the pervaporation unit, and a 90–95 wt% overhead ethanol product stream [43].

9.5 Applications

The three current applications of pervaporation are dehydration of solvents, water purification, and organic/organic separations as an alternative to distillation. Currently, dehydration

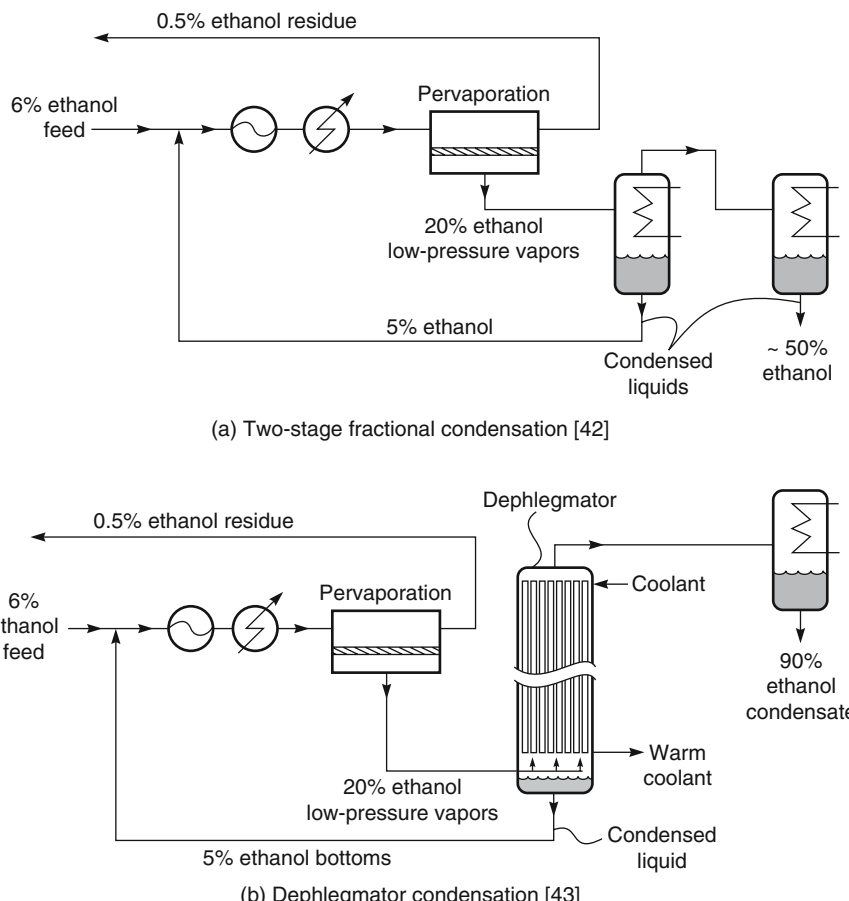


Figure 9.14 The use of permeate vapor fractional condensation systems to improve the separation achieved in pervaporation of dilute ethanol solutions: (a) two-stage fractional condensation [42] and (b) dephlegmator condensation [43]

of solvents, in particular ethanol and isopropanol, is the process most commonly installed on an industrial scale. The market for these systems is about US\$30 million/year, mostly for small systems sold to the pharmaceutical and fine chemicals industries. However, a major potential application is the use of pervaporation/vapor permeation technology to dehydrate bioethanol. If this application takes off, the market size would grow 10-fold or more. Each of these applications is described separately below.

9.5.1 Solvent Dehydration

Several hundred plants have been installed for the dehydration of ethanol by pervaporation. This is a particularly favorable application for pervaporation because ethanol forms an azeotrope with water at ~ 95 wt% ethanol and a 99.5% pure product is needed. The presence of the ethanol/water azeotrope means that distillation alone cannot produce

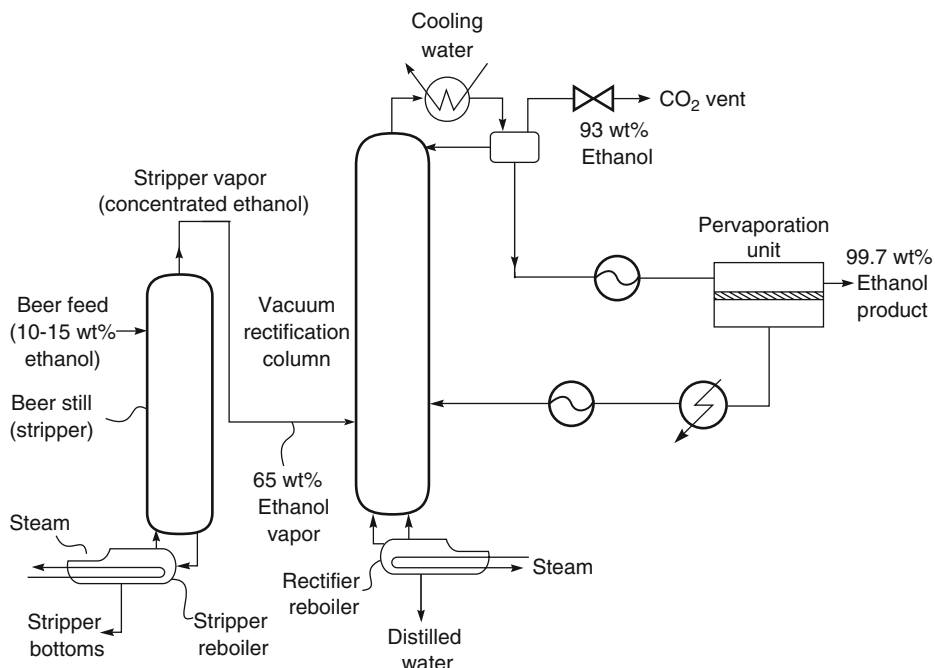


Figure 9.15 Integrated distillation/pervaporation plant for ethanol recovery from fermenters

dry ethanol, and some second process, such as a molecular sieve drying process or a liquid–liquid extraction process, must be used. Most ethanol/water separator units currently use molecular sieve driers. The flow scheme of a bioethanol distillation-membrane system in which the membrane unit is used to replace the molecular sieve dryer is shown in Figure 9.15. A stripper column followed by a rectification column produces azeotropic ethanol. This ethanol is fed to the pervaporation system. To maximize the vapor pressure difference and the pressure ratio across the membrane, the pervaporation module usually operates in the temperature range 105–130°C, with a corresponding feed stream vapor pressure of 2–4 bar. Despite these harsh conditions, the membrane lifetime is good and a number of small plants have been installed.

A comparison of the separation performance obtained by various pervaporation membranes and the vapor–liquid equilibrium line that controls separation obtained by distillation is shown in Figure 9.16 [42]. The membranes all achieve a good separation, but the GFT poly(vinyl alcohol) membrane performance is the best. Most pervaporation dehydration systems installed to date have been equipped with this type of hydrophilic, glassy, crosslinked membrane, although Mitsui is producing zeolite tubular modules [33, 34, 44].

Figure 9.15 shows a single-stage pervaporation unit. In practice, three to five pervaporation units are usually used in series, with additional heat supplied to the ethanol feed between each stage. This compensates for pervaporative cooling of the feed and maintains the feed temperature. The heat required is obtained by thermally integrating

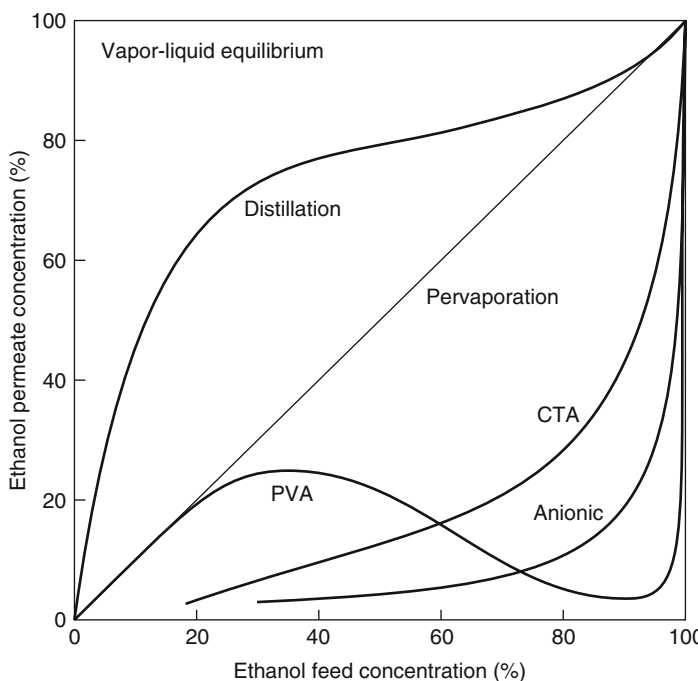


Figure 9.16 Comparison of separation of ethanol/water mixtures by distillation and by three pervaporation membranes: cellulose triacetate (CTA), an anionic polyelectrolyte membrane, and GFT's poly(vinyl alcohol) (PVA) membrane [42]

the pervaporation system with the condenser of the final distillation column. Therefore, most of the energy used in the process is low-grade heat.

No attempt to reduce the energy consumption of the dehydration process has been made for the pervaporation processes shown in Figure 9.15. For this reason, use of this type of unit has been limited to small processes where energy costs are a minor consideration. Recently, there has been considerable interest in applying the technology to bioethanol production. These process streams are much larger and the energy consumption of the plant is important.

Most of the new designs being worked on employ vapor permeation of ethanol/water mixtures. One suggested design is shown in Figure 9.17 [11]. An initial separation of the ethanol/water mixture is performed with a vacuum stripper column, as in a conventional bioethanol plant. This stripper produces an ethanol-free ($\leq 0.1\%$) bottoms and an overhead vapor at a pressure of 0.5 bar, containing ~ 65 wt% ethanol. This vapor is then compressed to 3 bar. Compression increases the temperature of the vapor, and a heat exchanger (not shown) integrated with the reboiler is used to cool this vapor to about 120°C (about 5°C above the dew point). The compressed gas is then sent to the membrane separation unit. A single membrane unit could be used to separate the overhead vapor, but as explained below, it is often more efficient to separate the membrane unit into two parts. The first membrane unit lowers the water content of the overhead vapor from 35 to ~ 10 wt% water. The permeate vapor from this unit has a high water concentration (93 wt% water) and contains the bulk

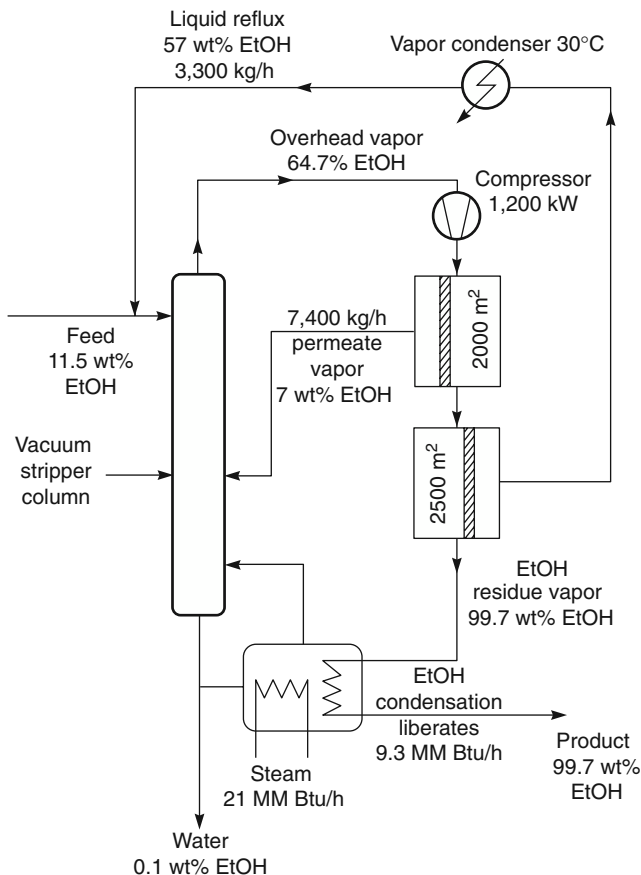


Figure 9.17 Design of a distillation-membrane hybrid process for the separation of a 100 000 kg/h ethanol/water mixture (equivalent to 30 million gal/year of ethanol production). The membrane used has a water permeance of 2000 gpu and an ethanol permeance of 50 gpu. The assumed efficiency of the compressor is 75%. A simple stripper column is used in this design (no rectification section) [11]

of the water content of the overhead vapor. This stream is recycled without condensation to the vacuum stripper, thus saving all of the latent heat of the stream. The remaining water is removed by a second membrane unit. This unit lowers the water concentration from ~10 to 0.3 wt% water. Because the vapor being treated by this unit has a lower average water concentration, the permeate contains less water and more ethanol. The permeate is condensed and remixed with the feed fermentation broth. The dry ethanol residue vapor stream produced by the second membrane unit is condensed in the stripper column reboiler to recover its latent heat content. In this design, the bulk of the heat used to create the stripper overhead is recovered and recycled to the column. This significantly lowers the steam usage of the column reboiler. Even when the energy consumption of the required compressor is taken into account, the energy needed to produce dry ethanol is cut in half.

Two membrane separation units are used for the process shown in Figure 9.17 because of the problem of pressure ratio. The first unit lowers the water concentration from 35 wt% (58 mol%) water to 10 wt% (22 mol%) water, so the average feed water concentration in this unit is about 40 mol%. The feed pressure is 3 bar and the permeate pressure is 0.5 bar, so the pressure ratio is 6. At this high water feed concentration, the first membrane unit is not affected by the pressure ratio limitation (Equation 9.19). The second membrane unit shown in Figure 9.17 also operates at close to 3 bar in the feed. This unit is used to reduce the water concentration in the ethanol product from 10 wt% (22.1 mol%) in the feed to 0.3 wt% (0.76 mol%) in the dry ethanol product. The performance of the unit is very much affected by the pressure ratio. If the unit were operated at a pressure ratio of 6, this unit would be completely controlled by the pressure ratio. The permeate vapor at any point in the membrane unit would never be more than six-fold more concentrated than the feed vapor at the same point. The problem of this enrichment limitation is particularly acute at the residue end of the unit, where the water concentration falls to the 1–2 mol% range. This means that the permeate vapor water concentration cannot be more than 6–12 mol% water (88–94 mol% of the permeate has to be ethanol) no matter how selective the membrane is. This result implies a large and wasteful recycle of ethanol back to the beer still.

The solution to this problem is to increase the pressure ratio across the second membrane unit by reducing the pressure on the permeate side of the membrane to 0.1 bar. This can easily be done by cooling the permeate vapor to 30°C, which completely condenses the vapor and spontaneously creates the vacuum required. At a pressure ratio of 30 (feed pressure 3 bar/permeate pressure 0.1 bar), the feed end of the second membrane unit is not affected by the pressure ratio limitation of Equation 9.19, and the effect at the residue end of the second membrane unit is much reduced, although not completely eliminated. Increasing the pressure ratio across the second membrane step from 6 to 30 increases the concentration of water in the permeate stream from 19 to 43 wt%. It also reduces the membrane area required to perform the same separation from 14 000 to 2500 m². These benefits are achieved at the expense of cooling and condensing the permeate vapor, which means the latent heat of vaporization of this stream is lost. Fortunately, this stream is much smaller than the permeate vapor stream from the first membrane unit, so the impact on the total process energy consumption of losing this fraction of the permeate latent heat is not large.

Most of the early solvent dehydration systems were installed for ethanol dehydration. More recently, pervaporation has been applied to dehydration of other solvents, particularly isopropanol used as a cleaning solvent in the electronics industry. Ube in Japan has installed a number of these systems [45]. A simplified process flow scheme is shown in Figure 9.18. Cold semiconductor wafers or electronics parts are lowered into a warm IPA vapor atmosphere in the drying unit. The IPA vapor condenses on the wafer surfaces, and any surface water or oil contaminants dissolve in the IPA and are removed with the condensate liquid. This liquid is pumped to a vaporizer chamber. The liquid is vaporized, leaving the solid contaminants in the chamber and producing a vapor consisting of IPA and some water. This vapor flows across the surface of a water-permeable membrane that selectively removes the vapor. A nitrogen sweep gas is usually used to increase the process driving force. The dry vapor then passes to an evaporation chamber. Some additional heat may be supplied here to vaporize any condensate and circulate the vapor to the vaporizer unit.

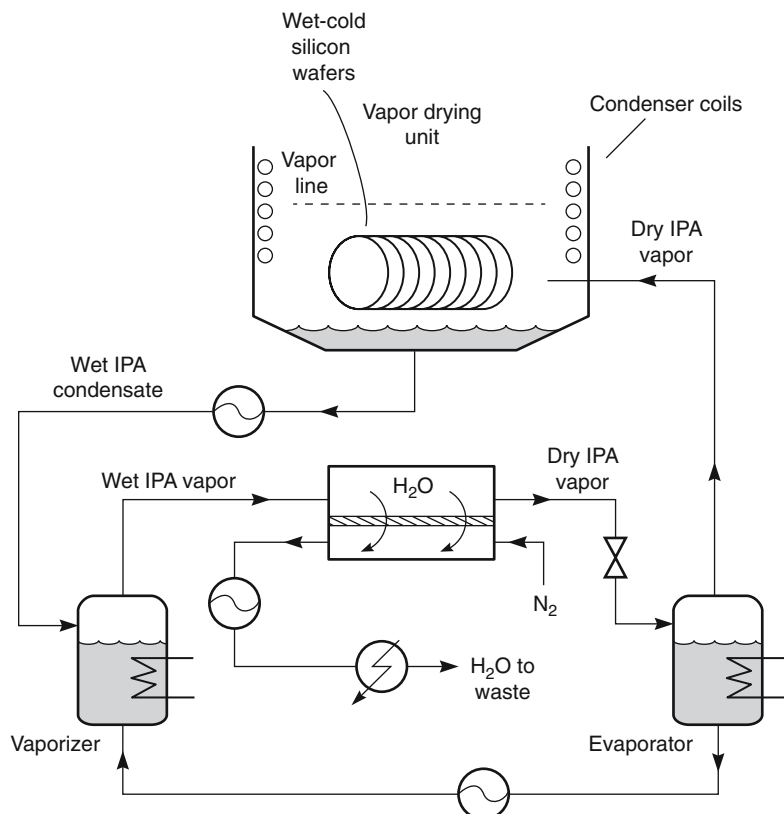
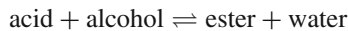


Figure 9.18 Flow diagram of a membrane vapor permeation drying unit

A final interesting application of dehydration membranes is to shift the equilibrium of chemical reactions. For example, esterification reactions of the type



are usually performed in batch reactors, and the degree of conversion is limited by buildup of water in the reactor. By continuously removing the water, the equilibrium reaction can be forced to the right. In principle, almost complete conversion can be achieved. This process was first suggested by Jennings and Binning in the 1960s [46]. A number of groups have since studied this type of process, and a few commercial plants have been installed [47, 48].

9.5.2 Separation of Dissolved Organics from Water

A number of pervaporation applications exist for removal or recovery of VOCs from water. If the aqueous stream is very dilute, pollution control is the principal economic driving force. However, if the stream contains more than 1–2% VOC, recovery for eventual reuse can enhance the process economics.

Several types of membrane have been used to separate VOCs from water and are discussed in the literature [12, 13, 30–32, 35]. Usually the membranes are made from rubbery polymers such as silicone rubber, polybutadiene, and polyamide-polyether copolymers. Rubbery pervaporation membranes are remarkably effective at separating hydrophobic organic solutes from dilute aqueous solutions. The concentration of VOCs such as toluene or TCE in the condensed permeate is typically more than 1000 times that in the feed solution. For example, a feed solution containing 100 ppm of such VOCs yields a permeate vapor containing 10–20% VOC. This concentration is well above the saturation limit, so condensation produces a two-phase permeate. This permeate comprises an essentially pure condensed organic phase and an aqueous phase containing a small amount of VOC that can be recycled to the aqueous feed. The flow scheme for this process is shown in Figure 9.13f. The separations achieved with moderately hydrophobic VOCs, such as ethyl acetate, methylene chloride, and butanol, are still impressive, typically providing at least 100-fold enrichment in the permeate. However, the separation factors obtained with hydrophilic solvents, such as methanol, acetic acid, and ethylene glycol, are usually modest, at 5 or below.

Some data showing measured pervaporation separation factors for dilute aqueous VOC solutions are shown in Figure 9.19, in which the total separation factor, β_{pervap} , is plotted against the theoretical evaporative separation factor, β_{evap} , obtained from the equation of state. Two sets of data, both obtained with silicone rubber membranes, are shown. One set was obtained with thick membranes in laboratory test cells under very well stirred conditions [32] that largely eliminate concentration polarization. The other set was obtained with high-flux membranes in spiral-wound modules [13, 49]. The difference

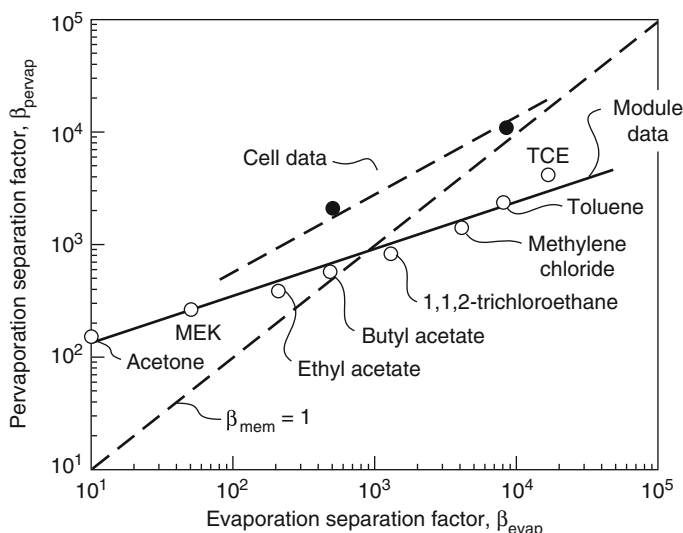


Figure 9.19 Pervaporation separation factor, β_{pervap} , as a function of the VOC evaporation separation factor, β_{evap} . Data were obtained with laboratory-scale spiral-wound modules containing a composite silicone rubber membrane and with thick membranes in laboratory cells

between the curves is due to the concentration polarization effects discussed in Chapter 4. With VOCs such as acetone, methyl ethyl ketone (MEK), and ethyl acetate, the difference between separation factors measured in the laboratory test cells and in spiral-wound modules is relatively small. The difference becomes very large for more hydrophobic VOCs with high separation factors. Concentration polarization effects can reduce the separation factor for VOCs such as toluene or TCE 5- to 10-fold.

The data in Figure 9.19 also allow determination of the relative contributions of the evaporative separation term β_{evap} and the membrane selectivity term α_{mem} to the total separation achieved by pervaporation β_{pervap} (Equation 9.15). Earlier it was shown that membranes used to dehydrate ethanol achieved almost all of the total pervaporation separation as a result of a high membrane selectivity term, in the 100–500 range. In dehydration applications where the solvent/water feed mixture composition is close to the azeotropic composition, the evaporative separation term is close to 1. In the case of the separation of VOCs from water, the relative contribution of evaporation and membrane permeation to the separation is quite different. For example, MEK has a pervaporation separation factor of approximately 280. In this case, the evaporation contribution β_{evap} is 40; therefore, from Equation 9.15, the membrane contribution α_{mem} is ~7. For more hydrophobic VOCs, the total separation factor increases, because the evaporative separation term is larger. For example, the separation factor β_{pervap} for toluene measured in cell experiments is an impressive 10 000, but most of the separation is due to the evaporation step factor, β_{evap} , which is 8000. The membrane contribution α_{mem} is only 1.2, and the approximate selectivity of the membrane falls to 0.3 when concentration polarization effects are taken into account.

Concentration polarization plays a dominant role in the selection of membrane materials, operating conditions, and system design in the pervaporation of VOCs from water. Selection of the appropriate membrane thickness and permeate pressure is discussed in detail elsewhere [49]. In general, concentration polarization effects are not a major problem for VOCs with separation factors less than 100–200. With solutions containing such VOCs, very high feed solution flow rates through the membrane modules are needed to control concentration polarization, so a continuous once-through process design cannot be used, because it is not possible to balance the fluid velocity required to control concentration polarization with the residence time required to achieve the target VOC removal in a single pass. In this case, a batch system with recycle may be needed.

Applications for VOC-from-water pervaporation systems include treatment of contaminated wastewaters and process streams in the chemical industry, removal of small amounts of VOCs from contaminated groundwater, and the recovery of volatile flavor and aroma elements from streams produced in the processing of fruits and vegetables. Commercial development of pervaporation for VOC removal/recovery has been slower than many predicted; only a few plants have been installed. An early target application was removal of VOCs from waste water, but pervaporation could not compete with steam and air stripping, or carbon adsorption technologies. The first significant applications are likely to be in the food industry, processing aqueous condensate streams generated in the production of concentrated orange juice, tomato paste, apple juice, and the like. These condensates contain a complex mixture of alcohols, esters, and ketones that are the flavor elements of the juice. Steam distillation can be used to recover these elements, but the high temperatures involved damage the product. Pervaporation recovers essentially all of

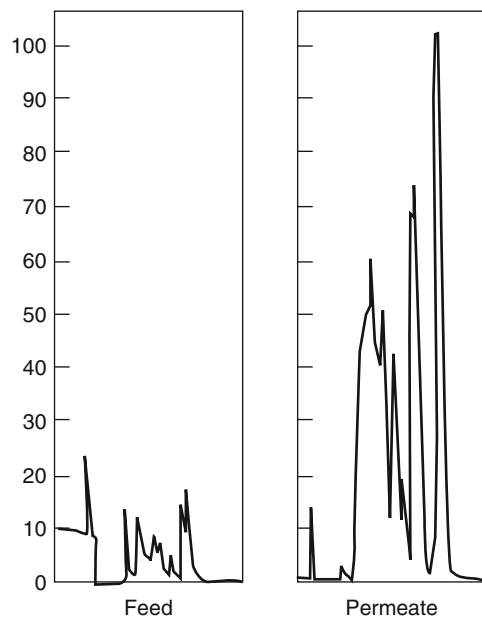


Figure 9.20 GC traces showing recovery of flavor and aroma components from orange juice evaporator condensate

these components, producing a concentrated, high-value oil, without exposing the flavor elements to high temperatures [50, 51]. Figure 9.20 shows gas chromatography (GC) traces of the feed and permeate streams produced by pervaporation of an orange juice evaporator condensate stream.

9.5.3 Separation of Organic Mixtures

The third application area for pervaporation is the separation of organic/organic mixtures. The competitive technology is generally distillation, a well-established and familiar technology. However, a number of azeotropic and close-boiling organic mixtures cannot be efficiently separated by distillation; pervaporation can be used to separate these mixtures, often in a combination membrane/distillation process. White [20] and Lipnizki *et al.* [52] have reviewed the most important applications.

The degree of separation of a binary mixture is a function of the relative volatility of the components, the membrane selectivity, and the operating conditions. For azeotropic or close-boiling mixtures, the relative volatility is close to 1, so separation by simple distillation is not viable. However, if the membrane permeation selectivity is much greater than 1, a significant separation is possible using pervaporation. An example of such a separation is given in Figure 9.21, which shows a plot of the pervaporation separation of benzene/cyclohexane mixtures using a 20- μm -thick crosslinked cellulose acetate-poly(styrene phosphate) blend membrane [53]. The vapor–liquid equilibrium for the mixture is also shown; the benzene/cyclohexane mixture forms an azeotrope at approximately 50% benzene. A typical distillation stage could not separate a feed stream

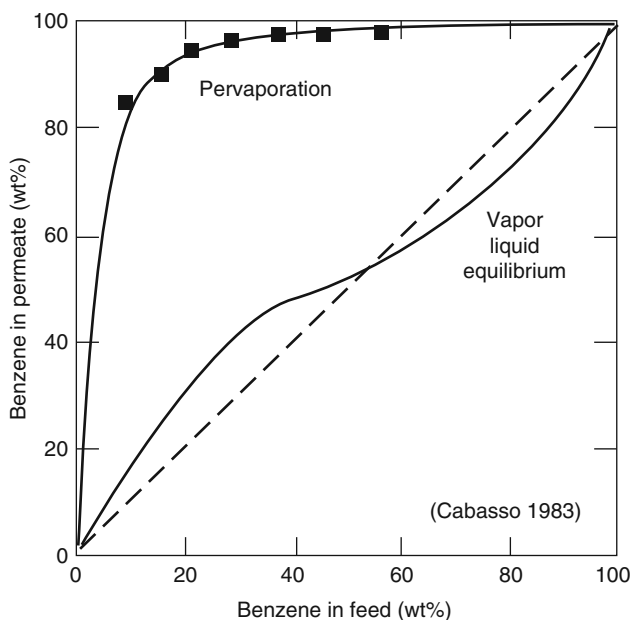


Figure 9.21 Fraction of benzene in permeate as a function of feed mixture composition for pervaporation at the reflux temperature of a binary benzene/cyclohexane mixture. A 20- μm -thick crosslinked blend membrane of cellulose acetate and poly(styrene phosphate) was used [53]. Reprinted with permission from [55]. Copyright (1983) American Chemical Society.

of this composition. However, pervaporation treatment of this mixture produces a vapor permeate containing more than 95% benzene. This example illustrates the advantages of pervaporation over simple distillation for separating azeotropes and close-boiling mixtures.

It would be unusual for a pervaporation process to perform an entire organic/organic separation. Rather, pervaporation will be most efficient when combined with distillation in a hybrid process [45, 54]. The two main applications of pervaporation/distillation hybrid processes most likely to develop commercially are in breaking azeotropes and in removing a single-component, high-purity side stream from a multicomponent distillation separation. Figure 9.22 shows some potential pervaporation–distillation combinations. In Figure 9.22a, pervaporation is combined with distillation to break an azeotrope that is concentrated in one component (>90%). This approach is used in the production of high-purity ethanol. The ethanol/water azeotrope from the top of the distillation column is fed to a pervaporation unit where the water is removed as the permeate and returned to the column as a reflux.

Figure 9.22b illustrates the use of pervaporation with two distillation columns to break a binary azeotrope such as benzene/cyclohexane. The feed is supplied at the azeotropic composition and is split into two streams by the pervaporation unit. The residue stream, rich in cyclohexane, is fed to a distillation column that produces a pure bottom product and an azeotropic top stream, which is recycled to the pervaporation unit. Similarly,

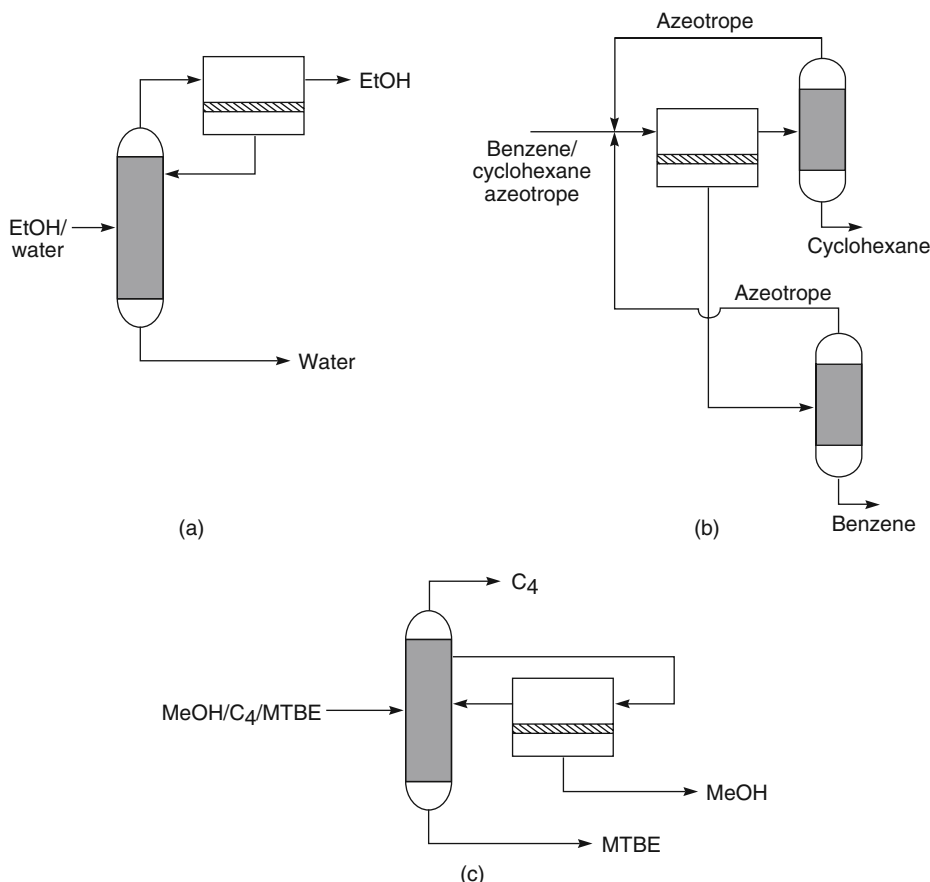


Figure 9.22 (a–c) Potential configurations for pervaporation/distillation hybrid processes

the other distillation column treats the benzene-rich stream to produce a pure benzene product and an azeotropic mixture that is returned to the pervaporation unit.

Pervaporation can also be used to unload a distillation column, thereby reducing energy consumption and operating cost while increasing throughput. The example shown in Figure 9.22c is for the recovery of pure methanol by pervaporation of a side stream from a column separating a methanol/isobutene/methyl tertiary butyl ether (MTBE) feed mixture [15, 16].

The principal problem hindering the development of commercial pervaporation systems for organic/organic separations is the lack of membranes and modules able to withstand long-term exposure to organic compounds at the elevated temperatures required for pervaporation. Membrane and module stability problems are not insurmountable, however, as shown by the successful demonstration of a pervaporation process for the separation of methanol from an isobutene/MTBE mixture [16].

Another application that has developed to the pilot scale is the separation of aromatic/aliphatic mixtures in refining crude oils into transportation fuels [17–19, 55]. For

hydrocarbons with approximately the same boiling point range, the permeability is generally in the order aromatics > unsaturated hydrocarbons > saturated hydrocarbons. For aliphatic hydrocarbons in approximately the same boiling point range, the order of permeabilities is straight chain > cyclic chain > branched chain. The goal in these processes is to perform a bulk separation of the hydrocarbon mixture by pervaporation; therefore, the membrane must be highly permeable and selective. The general approach [18, 19, 56] is to prepare segmented block copolymers consisting of hard segments not swollen by the hydrocarbon oil, to control the swelling of the soft segments through which the oil would permeate. Crosslinking is also used to control swelling of the membrane materials, polyester-polyimide, and polyurea-polyurethane polymers.

Recently Sulzer, working with Grace Davison [37, 57] and using polyimide, polysiloxane, or polyurea urethane membranes; and ExxonMobil [58], using Nafion® or cellulose triacetate membranes, have described processes to separate sulfur compounds from various refinery streams.

9.6 Conclusions and Future Directions

The use of pervaporation/vapor permeation membranes as a low-energy alternative to distillation has been proposed for more than 30 years, yet the current market for this technology is not more than US\$30 million/year, almost all for the separation of water from ethanol or isopropanol in the pharmaceutical and fine chemicals industry. In the early 1990s, major oil companies such as Exxon, Texaco, and Mobil all had research programs focused on developing membrane technology for refinery separations. Most of these programs have since been abandoned or scaled back. The problem was not the lack of suitably selective membrane materials, but the difficulty of making reliable and economical membranes and membrane modules. Membrane and module components able to operate at temperatures above 100°C in hydrocarbon liquids were required. Also, early developers of the technology often linked the membrane systems and distillation as a simple series of unit operations. This overlooked the very substantial reductions in the energy of separation achieved when heat integrated process designs are used. Significant progress has been made in solving all of these problems in the last 10 years, especially the last 3–4 years.

Dehydration of bioethanol is the largest potential commercial target for pervaporation/vapor permeation technology. The next generation of bioethanol plants are expected to begin coming online in 2012–2015. If this occurs, and the plants integrate pervaporation/vapor permeation technology into their process trains, a very large market for membrane systems could develop. We will see.

References

1. Kober, P.A. (1917) Pervaporation, perstillation, and percrystallization. *J. Am. Chem. Soc.*, **39**, 944.
2. Binning, R.C. and Stuckey, J.M. (1960) Method of separating hydrocarbons using ethyl cellulose selective membrane. US Patent 2,958,657, Nov. 1960.

3. Binning, R.C., Lee, R.J., Jennings, J.F., and Martin, E.C. (1961) Separation of liquid mixtures by permeation. *Ind. Eng. Chem.*, **53**, 45.
4. Binning, R.C. and Johnston, W.F. Jr. (1961) Aromatic separation process. US Patent 2,970,106, Jan. 1961.
5. Binning, R.C., Jennings, J.F., and Martin, E.C. (1962) Process for removing water from organic chemicals. US Patent 3,035,060, May 1962.
6. Strazik, W.F. and Perry, E. Process for removing water from organic chemicals. US Patent 3,776,970, Dec, 1973. Also US Patents 4,067,805 and 4,218,312 and many others.
7. Aptel, P., Challard, N., Cuny, J., and Neel, J. (1976) Application of the pervaporation process to separate azeotropic mixtures. *J. Membr. Sci.*, **1**, 271.
8. Neel, J., Nguyen, Q.T., Clement, R., and Le Blanc, L. (1983) Fractionation of a binary liquid mixture by continuous pervaporation. *J. Membr. Sci.*, **15**, 43.
9. Ballweg, A.H., Brüschke, H.E.A., Schneider, W.H., Tüscl, G.F., and Böddeker, K.W. (1982) Pervaporation membranes. Proceedings of the 5th International Alcohol Fuel Technology Symposium, Auckland, New Zealand, May 1982, pp. 97–106.
10. Brüschke, H.E.A. (1988) State of art of pervaporation, in *Proceedings of the 3rd International Conference on Pervaporation Processes in the Chemical Industry* (ed. R. Bakish), Bakish Materials Corporation, Englewood, NJ, pp. 2–11.
11. Huang, Y., Baker, R.W., and Vane, L.M. (2010) Low-energy distillation-membrane separation process. *Ind. Eng. Chem. Res.*, **49**, 3760–3768.
12. Blume, I., Wijmans, J.G., and Baker, R.W. (1990) The separation of dissolved organics from water by pervaporation. *J. Membr. Sci.*, **49**, 253.
13. Athayde, A.L., Baker, R.W., Daniels, R., Le, M.H. and Ly, J.H. (1997) Pervaporation for wastewater treatment. *Chemtech*, **27**, 34.
14. Cox, G. and Baker, R.W. (1998) Pervaporation for the treatment of small volume VOC-contaminated waste water streams. *Ind. Wastewater*, **6**, 35.
15. Chen, M.S.K., Eng, R.M., Glazer, J.L., and Wensley, C.G. (1988) Pervaporation process for separating alcohols from ethers, US Patent 4,774,365, Sep. 1988.
16. Chen, M.S.K., Markiewicz, G.S., and Venugopal, K.G. (1989) Development of membrane pervaporation TRIMTM process for methanol recovery from CH₃OH/MTBE/C₄ mixtures, in *Membrane Separations in Chemical Engineering*, AIChE Symposium Series, Vol. 272 (eds A.E. Fouad, J.D. Hazlett, T. Matsuura, and J. Johnson), AIChE, New York, p. 85.
17. Schucker, R.C. (1995) Separation of organic liquids by perstraction, in *Proceedings of the 7th International Conference on Pervaporation Processes in the Chemical Industry* (ed. R. Bakish), Bakish Materials Corporation, Englewood, NJ, pp. 321–332.
18. Schucker, R.C. (1991) Highly aromatic polyurea/urethane membranes and their use for the separation of aromatics from non-aromatics, US Patent 5,063,186, Nov. 1991, US Patent 5,055,632, Oct. 1991 and many others.
19. Schucker, R.C. (1991) Isocyanurate crosslinked polyurethane membranes and their use for the separation of aromatics from non-aromatics. US Patent 4,983,338, Jan. 1991 and many others.

20. White, L.S. (2006) Development of large-scale applications in organic solvent nanofiltration and pervaporation for chemical and refining processes. *J. Membr. Sci.*, **286**, 26.
21. Wijmans, J.G. and Baker, R.W. (1993) A simple predictive treatment of the permeation process in pervaporation. *J. Membr. Sci.*, **79**, 101.
22. Kataoka, T., Tsuro, T., Nakao, S.I., and Kimura, S. (1991) Permeation equations developed for prediction of membrane performance in pervaporation, vapor permeation and reverse osmosis based on the solution-diffusion model. *J. Chem. Eng. Jpn.*, **24**, 326–333.
23. Baker, R.W., Wijmans, J.G., and Huang, Y. (2010) Permeability, permeance and selectivity: a preferred way of reporting pervaporation performance data. *J. Membr. Sci.*, **348** (1–2), 346–352.
24. Shelden, R.A. and Thompson, E.V. (1978) Dependence of diffusive permeation rates on upstream and downstream pressures. *J. Membr. Sci.*, **4**, 115.
25. Hollein, M.E., Hammond, M., and Slater, C.S. (1993) Concentration of dilute acetone-water solutions using pervaporation. *Sep. Sci. Technol.*, **28**, 1043.
26. Chapman, P.D., Oliveira, T., Livingston, A.G., and Li, K. (2008) Membranes for the dehydration of solvents by pervaporation. *J. Membr. Sci.*, **318**, 5.
27. Watanabe, K. and Kyo, S. (1992) Pervaporation performance of hollow-fiber chitosan-polyacrylonitrile composite membrane in dehydration of ethanol. *J. Chem. Eng. Jpn.*, **25**, 17.
28. Wenzlaff, A., Böddeker, K.W., and Hattenbach, K. (1985) Pervaporation of water-ethanol through ion exchange membranes. *J. Membr. Sci.*, **22**, 333.
29. Cabasso, I. and Liu, Z.Z. (1985) The permselectivity of ion-exchange membranes for non-electrolyte liquid mixtures. *J. Membr. Sci.*, **24**, 101.
30. Nijhuis, H.H., Mulder, M.V.H., and Smolders, C.A. (1988) Selection of elastomeric membranes for the removal of volatile organic components from water, in *Proceedings of the 3rd International Conference on Pervaporation Processes in the Chemical Industry* (ed. R. Bakish), Bakish Materials Corporation, Englewood, NJ, pp. 239–251.
31. Böddeker, K.W. and Bengtson, G. (1990) Pervaporation of low volatility aromatics from water. *J. Membr. Sci.*, **53**, 143.
32. Böddeker, K.W. and Bengtson, G. (1991) Selective pervaporation of organics from water, in *Pervaporation Membrane Separation Processes* (ed. R.Y.M. Huang), Elsevier, Amsterdam, pp. 437–460.
33. Kondo, M., Komori, M., Kita, H., and Okamoto, K. (1997) Tubular-type pervaporation module with zeolite NaA membrane. *J. Membr. Sci.*, **133**, 133.
34. Sato, K., Sugimoto, K., and Nakane, T. (2008) Synthesis of industrial scale NaY zeolite membranes and ethanol permeating performance in pervaporation and vapor permeation up to 130°C and 570 kPa. *J. Membr. Sci.*, **310** (1–2), 161–173.
35. Vane, L.M. (2005) A review of pervaporation for product recovery from biomass fermentation processes. *J. Chem. Technol. Biotechnol.*, **80**, 603.
36. Meckl, K. and Lichtenhaller, R.N. (1992) Hybrid-processes including pervaporation for the removal of organic compounds from process and waste water, in *Proceedings of the 6th International Conference on Pervaporation Processes in the Chemical*

- Industry (ed. R. Bakish), Bakish Materials Corporation, Englewood, NJ, p. 32, pp. 476–483.
- 37. White, L.S., Wormsbecher, R.F., and Lesmann, M. (2005) Membrane separation for sulfur reduction. US Patent 6,896,796, May 2005.
 - 38. Abouchar, R. and Brüschke, H. (1992) Long-term experience with industrial pervaporation plants, in *Proceedings of the 6th International Conference on Pervaporation Processes in the Chemical Industry* (ed. R. Bakish), Bakish Materials Corporation, Englewood, NJ, pp. 494–502.
 - 39. Brüschke, H.E.A., Wynn, N., and Marggraff, F.K. (2010) Membrane pipe module. US Patent 7,655,141, Feb. 2010.
 - 40. Robertson, A.E. (1949) Separation of hydrocarbons. US Patent 2,475,990, Jul. 1949.
 - 41. Friesen, D.T., Newbold, D.D., and McCray, S.B. (1995) Pervaporation by counter-current condensable sweep. US Patent 5,464,540, Nov. 1995.
 - 42. Kaschemekat, J., Barbknecht, B., and Böddeker, K.W. (1986) Konzentrierung von ethanol durch pervaporation. *Chem. Ing. Tech.*, **58**, 740.
 - 43. Vane, L.M., Alvarez, F.R., Mairal, A.P., and Baker, R.W. (2004) Separation of vapor-phase alcohol/water mixtures via fractional condensation using a pilot-scale dephlegmator: enhancement of the pervaporation process separation factor. *Ind. Eng. Chem. Res.*, **43**, 173.
 - 44. Shah, D., Kissick, K., Ghorpade, A., Hannah, R. and Bhattacharyya, D. (2000) Pervaporation of alcohol-water and dimethylformamide-water mixtures using hydrophilic zeolite NaA membranes: mechanisms and results. *J. Membr. Sci.*, **179**, 185.
 - 45. Kase, Y. (2008) Gas separation by polyimide membranes, in *Advanced Membrane Technology and Applications* (eds N.N. Li, A.G. Fane, W.S.W. Ho, and T. Matsuura), John Wiley & Sons, Inc., Hoboken, NJ, pp. 581–598.
 - 46. Jennings, J.F. and Binning, R.C. (1960) Organic chemical reactions involving liberation of water. US Patent 2,956,070, Oct. 1960.
 - 47. Dams, A. and King, J. (1991) Pervaporation aided esterification-alternative in plant extension for an existing chemical process, in *Proceedings of the 5th International Conference on Pervaporation Processes in the Chemical Industry* (ed. R. Bakish), Bakish Materials Corporation, Englewood, NJ, pp. 338–348.
 - 48. Zhu, Y., Minet, R.G., and Tsotsis, T.T. (1996) A continuous pervaporation membrane reactor for the study of esterification reactions using a composite polymeric/ceramic membrane. *Chem. Eng. Sci.*, **51**, 4103.
 - 49. Baker, R.W., Wijmans, J.G., Athayde, A.L., Daniels, R., Ly, J.H., and Le, M. (1998) Separation of volatile organic compounds from water by pervaporation. *J. Membr. Sci.*, **137**, 159.
 - 50. Rajagopalan, N. and Cheryan, M. (1995) Pervaporation of grape juice aroma. *J. Membr. Sci.*, **104**, 243.
 - 51. Karlsson, H.O.E. and Trägårdth, G. (1996) Applications of pervaporation in food processing. *Trends Food Sci. Technol.*, **7**, 78.
 - 52. Lipnizki, F., Feld, R.F., and Ten, P.K. (1999) Pervaporation-based hybrid processes: a review of process design applications and economics. *J. Membr. Sci.*, **153**, 183.

53. Cabasso, I. (1983) Organic liquid mixtures separation by permselective polymer membranes. 1. Selection and characteristics of dense isotropic membranes employed in the pervaporation process. *Ind. Eng. Chem. Prod. Res. Dev.*, **22**, 313.
54. Stephan, W., Noble, R.D., and Koval, C.A. (1995) Design methodology for a membrane/distillation hybrid process. *J. Membr. Sci.*, **99**, 259.
55. Matsui, S. and Paul, D.R. (2003) Pervaporation separation of aromatic/aliphatic hydrocarbons by a series of ionically crosslinked poly(n-alkyl acrylate) membranes. *J. Membr. Sci.*, **213**, 67–83.
56. Tanihara, N., Umeo, N., Kawabata, T., Tanaka, K., Kita, H., and Okamoto, K. (1995) Pervaporation of organic liquids through poly(etherimide) segmented copolymer membranes. *J. Membr. Sci.*, **104**, 181.
57. Balko, J., Bourdillon, G., and Wynn, N. (2003) Membrane separation for producing gasoline. *Petrol. Q.*, **8**, 17.
58. Minhas, B., Chuba, R.R., and Saxton, R.J. (2002) Membrane process for separating sulfur compounds from FCC light naphtha. US Patent Application US 2002/0111524, Aug. 2002.

10

Ion Exchange Membrane Processes – Electrodialysis

10.1 Introduction/History

Ion exchange membranes are used in a number of separation processes, the most important of which are electrodialysis and membrane chlor-alkali cells. In ion exchange membranes, charged groups are attached to the polymer backbone of the membrane material. These fixed charge groups partially or completely exclude ions of the same charge from the membrane. This means that an anionic membrane with fixed positive groups excludes positive ions but is freely permeable to negatively charged anions. Similarly, a cationic membrane with fixed negative groups excludes negative ions but is freely permeable to positively charged cations, as illustrated in Figure 10.1.

Electrodialysis was the first industrial process to use ion exchange membranes on a large scale. In an electrodialysis system, anionic and cationic membranes are formed into a multicell arrangement built on the plate-and-frame principle, to form up to 100 cell pairs in a stack. The cation and anion exchange membranes are arranged in an alternating pattern between the anode and cathode. Each set of anion and cation membranes forms a cell pair. Salt solution is pumped through the cells while an electrical potential is maintained across the electrodes. The positively charged cations in the solution migrate toward the cathode and the negatively charged anions migrate toward the anode. Cations easily pass through the negatively charged cation exchange membrane but are retained by the positively charged anion exchange membrane. Similarly, anions pass through the anion exchange membrane but are retained by the cation exchange membrane. The overall result of the process is that one cell of the pair becomes depleted of ions while the adjacent cell becomes enriched in ions. The process, which is widely used to remove dissolved ions from water, is illustrated in Figure 10.2.

Experiments with ion exchange membranes were described as early as 1890 by Ostwald [1]. Work by Donnan [2] a few years later led to development of the concept of membrane potential and the phenomenon of Donnan exclusion. These early

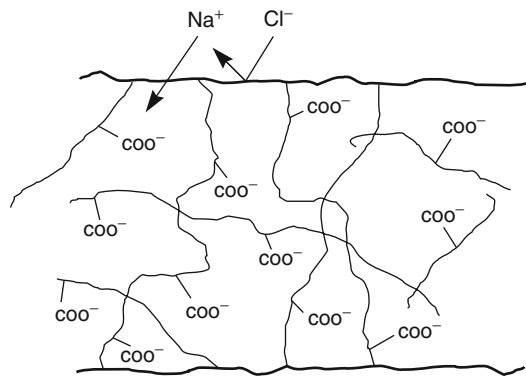


Figure 10.1 This cationic membrane with fixed carboxylic acid groups is permeable to cations such as sodium but is impermeable to anions such as chloride

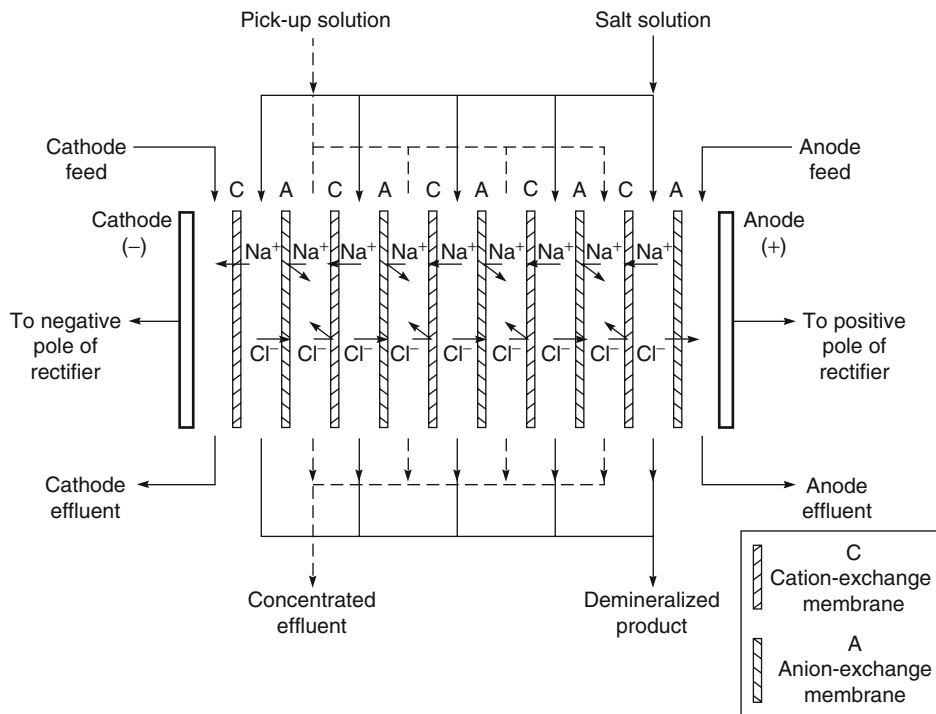


Figure 10.2 Schematic diagram of a plate-and-frame electrodialysis stack. Alternating cation- and anion-permeable membranes are arranged in a stack of up to 100 cell pairs

charged membranes were made from natural materials or chemically treated collodion membranes – their mechanical and chemical properties were very poor. Nonetheless, as early as 1939, Manegold and Kalauch [3] suggested the application of selective anionic and cationic exchange membranes to separate ions from water, and within another year Meyer and Straus [4] described the concept of a multicell arrangement between a single pair of electrodes. The advances in polymer chemistry during and immediately after World War II led to the production of much better ion exchange membranes by Kressman [5], Murphy *et al.* [6], and Juda and McRae [7] at Ionics. With the development of these membranes, electrodialysis became a practical process. Ionics was the principal early developer and installed the first successful plant in 1952; by 1956, eight plants had been installed.

In the United States, electrodialysis was developed primarily for desalination of water, with Ionics, now a division of General Electric, being the industry leader. In Japan, Asahi Glass, Asahi Chemical (a different company), and Tokuyama Soda developed the process to concentrate seawater [8]. This application of electrodialysis is confined to Japan, which has no domestic salt sources. Electrodialysis membranes concentrate the salt in seawater to about 18–20% solids, after which the brine is further concentrated by evaporation, and the salt recovered by crystallization.

All of the electrodialysis plants installed in the 1950s through the 1960s were operated unidirectionally, that is, the polarity of the two electrodes, and hence the position of the dilute and concentrated cells in the stack, were fixed. In this mode of operation, formation of scale on the membrane surface by precipitation of colloids and insoluble salts was often a severe problem. To prevent scale, pH adjustment and addition of antiscalant chemicals to the feed water was required, together with regular membrane cleaning using detergents and descaling chemicals. Nevertheless, scaling and membrane fouling remained major problems, affecting plant on-stream time and widespread acceptance of the process. In the early 1970s, a breakthrough in system design, known as electrodialysis polarity reversal, was made by Ionics [9]. In these systems, the polarity of the DC power applied to the membrane electrodes is reversed two to four times per hour. When the electrode polarity is reversed, the desalted water and brine chambers are also reversed by automatic valves that control the flows in the stack. By switching cells and reversing current direction, freshly precipitated scale is flushed from the membrane before it can solidify. The direction of movement of colloidal particulates drawn to the membrane by the flow of current is also reversed, so colloids do not form a film on the membrane. Electrodialysis plants using the reverse polarity technique have been operating since 1970 and have proven more reliable than their fixed polarity predecessors.

Electrodialysis is now a mature technology, with Ionics remaining the worldwide industry leader except in Japan. Desalting of brackish water and the production of boiler feed water and industrial process water were the main applications until the 1990s, but electrodialysis has since lost market share due to stiff competition from improved reverse osmosis membranes. Beginning in the 1990s, electrodeionization, a combination process using electrodialysis and ion exchange, began to be used to achieve very good salt removal in ultrapure water plants. This is now a major use of electrodialysis. Other applications are control of ionic impurities from industrial effluent streams, water softening, and desalting certain foods, particularly milk whey [10, 11].

Over the last 30 years, a number of other uses of ion exchange membranes have been found. One important application is the development by Asahi, Dow, and DuPont of perfluoro-based ion exchange membranes with exceptional chemical stability for membrane chlor-alkali cells [12]. More than 1 million square meters of chlor-alkali membrane cells have been installed. These membranes were introduced in 1979. Since then, membrane processes have almost completely displaced the mercury amalgam process and most asbestos diaphragm process plants.

Ion exchange membranes are also finding an increasing market in electrolysis processes of all types. One application that has received a great deal of attention is the use of bipolar membranes to produce acids and alkalis by electrolysis of salts. Bipolar membranes are laminates of anionic and cationic membranes. The first practical bipolar membranes were developed by Liu and others at Allied Chemicals in about 1977 [13]; they were later employed in Allied's Aquatech acid/base production process [14]. A final, growing use of ion exchange membranes is in fuel cells where the membranes regulate ion transport in the cells [15–17]. The first successful fuel cells using polymer electrolyte membranes (PEMs) were developed for the US space program in the early 1960s. Since then, a huge effort has been spent developing fuel cells for more mundane applications, but the technology has never quite taken off and the future always seems just around the corner. A time line illustrating the major milestones in the development of ion exchange membranes is shown in Figure 10.3.

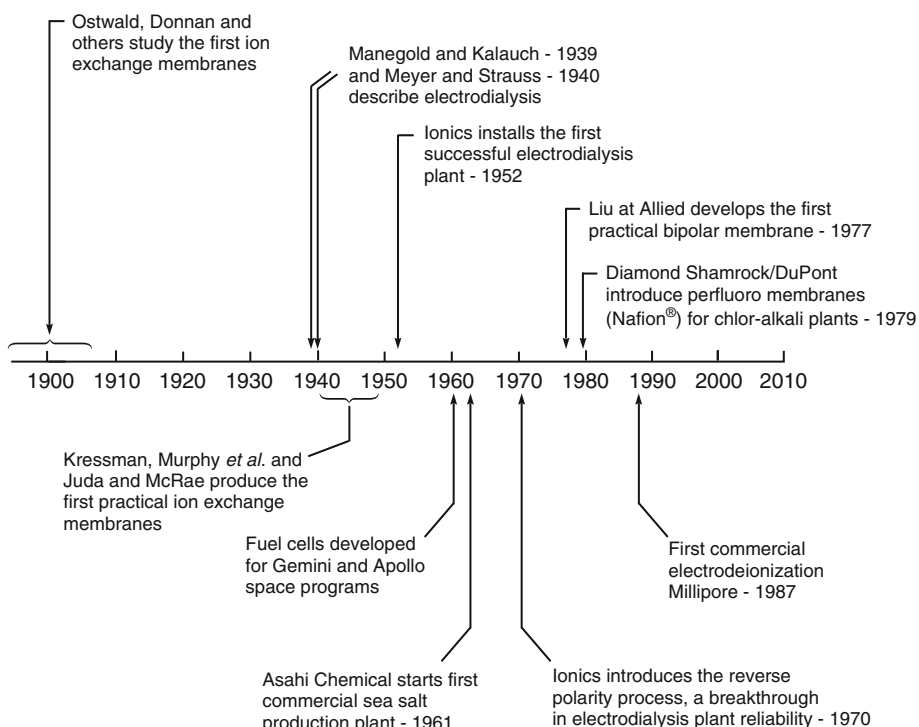


Figure 10.3 Milestones in the development of ion exchange membrane processes

10.2 Theoretical Background

10.2.1 Transport through Ion Exchange Membranes

In electrodialysis and the other separation processes using ion exchange membranes, transport of components generally occurs under the driving forces of both concentration and electric potential (voltage) gradients. However, because the two types of ion present, anions and cations, move in opposite directions under an electric potential gradient, ion exchange membrane processes are often more easily evaluated in terms of the amount of charge transported than the amount of material transported. Consider, for example, a simple univalent–univalent electrolyte such as sodium chloride, which can be considered to be completely ionized in dilute solutions. The concentration of sodium cations is then c^+ , and the concentration of chloride anions is c^- . The velocity of the cations in an externally applied field of strength, E , is u (cm/s), and the velocity of the anions measured in the same direction is $-v$ (cm/s). Each cation carries the protonic charge $+e$, and each anion the electronic charge of $-e$, so the total amount of charge transported per second across a plane of 1 cm^2 area is

$$\frac{I}{F} = c^+(u)(+e) + c^-(-v)(-e) = ce(u + v) \quad (10.1)$$

where I is the current and F is the Faraday constant to convert transport of electric charge to a current flow in amps. This equation links the electric current with the transport of ions. It has been found that the fractions of the current carried by the anions and cations do not necessarily have to be equal. The fraction of the total current carried by any particular ion is known as the transport number of that ion. Thus, the transport number for the cations is t^+ , and the transport number for the anions is t^- . It follows that

$$t^+ + t^- = 1 \quad (10.2)$$

Combining Equations 10.1 and 10.2, the transport number of the cations in the univalent–univalent electrolyte described above is given as

$$t^+ = \frac{c^+ue}{ce(u + v)} = \frac{u}{u + v} \quad (10.3)$$

and similarly for the anion

$$t^- = \frac{v}{u + v} \quad (10.4)$$

Transport numbers for different ions, even in aqueous solutions, can vary over a wide range, reflecting the different sizes of the ions. Ions with the same charge as the fixed charge groups in an ion exchange membrane are excluded from the membrane and, therefore, carry a very small fraction of the current through the membrane. In these membranes, the transport number of the excluded ions is very small, normally between 0 and 0.05. Counter ions with a charge opposite to the fixed charged groups permeate the membrane freely and carry almost all of the current through the membrane. The transport numbers of these ions are between 0.95 and 1.0. This difference in transport

number, a measure of relative permeability, allows separations to be achieved with ion exchange membranes.

Equation 10.1 shows that, as in other transport processes, the flux of the permeating component is the product of a mobility term (u or v) and a concentration term (c^+ or c^-). In ion exchange transport processes, most of the separation is achieved by manipulating the concentration terms. When the membrane carries fixed charges, the counter ions of the same charge will tend to be excluded from the membrane. As a result, the concentration of ions of the same charge is reduced, while the concentration of ions of opposite charge is elevated. This makes the membrane selective for ions of the opposite charge.

The ability of ion exchange membranes to discriminate between oppositely charged ions was put on a mathematical basis by Donnan in 1911 [2]. Figure 10.4 shows the distribution of ions between a salt solution and an ion exchange membrane containing fixed negative charges, R^- .

The equilibrium between the ions in the membrane (m) and the surrounding solution (s) can be expressed as

$$c_{(m)}^+ \cdot c_{(m)}^- = k c_{(s)}^+ \cdot c_{(s)}^- \quad (10.5)$$

where k is an equilibrium constant. Charge balance considerations lead to the expression

$$c_{(m)}^+ = c_{(m)}^- + c_{R(m)}^- \quad (10.6)$$

where $c_{R(m)}^-$ is the concentration of fixed negative charges in the membrane. For a fully dissolved salt, such as sodium chloride, the total molar concentration of the salt $c_{(s)}$ is equal to the concentration of each of the ions, so

$$c_{(s)} = c_{(s)}^+ = c_{(s)}^- \quad (10.7)$$

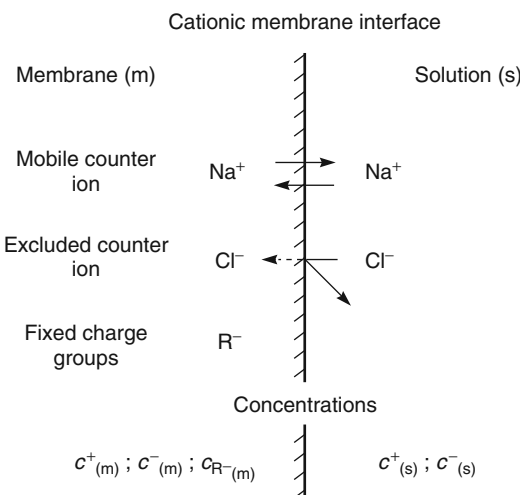


Figure 10.4 An illustration of the distribution of ions between a cationic membrane with fixed negative ions and the surrounding salt solution

Combining these three equations and rearranging gives the expression

$$\frac{c_{(m)}^+}{c_{(m)}^-} = \frac{\left[c_{(m)}^- + c_{R_{(m)}^-} \right]^2}{k [c_{(s)}]} \quad (10.8)$$

Because the membrane is cationic (fixed negative charges), the concentration of negative counter ions in the membrane will be small compared to the concentration of fixed charges, that is,

$$c_{R_{(m)}^-} \gg c_{(m)}^- \quad (10.9)$$

so it can be assumed that

$$c_{(m)}^- + c_{R_{(m)}^-} \approx c_{R_{(m)}^-} \quad (10.10)$$

Equation 10.8 can then be written

$$\frac{c_{(m)}^+}{c_{(m)}^-} = \frac{1}{k} \left(\frac{c_{R_{(m)}^-}}{c_{(s)}} \right)^2 \quad (10.11)$$

This expression shows that the ratio of sodium to chloride ions in the membrane ($c_{(m)}^+/c_{(m)}^-$) is proportional to the square of the ratio of the fixed charge groups in the membrane to the salt concentration in the surrounding solution ($c_{R_{(m)}^-}/c_{(s)}$). In commonly used ion exchange membranes, the fixed ion concentration in the membrane is very high, typically at least 3–4 meq/g. Figure 10.5 shows a plot of the sodium-to-chloride concentration ratio in a cationic membrane, calculated using Equation 10.11. The ion exchange membrane is assumed to have a fixed negative charge concentration of 3 meq/g. The plot shows that, at salt solution concentrations of less than 0.2 meq/g (~1 wt% sodium chloride), chloride ions are almost completely excluded from the ion exchange membrane. This means that in this concentration range, the transport number for sodium is close to one, and for chloride it is close to zero. Only at high salt concentrations – above about 0.6 meq/g (3 wt% sodium chloride) – does the ratio of sodium to chloride ions in the membrane fall below 30, and the membrane becomes measurably permeable to chloride ions.

10.3 Chemistry of Ion Exchange Membranes

A wide variety of ion exchange membrane chemistries has been developed. Most of this early membrane development work was aimed at electrodialysis applications, and each electrodialysis system manufacturer developed its own membrane tailored for the specific applications and equipment used. Many of these developments have been kept as trade secrets or are only described in the patent literature. Korngold [18] gives a description of early ion exchange membrane development. More recently, most ion exchange membrane development has focused on membranes for fuel cells. Reviews of these developments can be found in a book edited by Peinemann and Nunes [15].

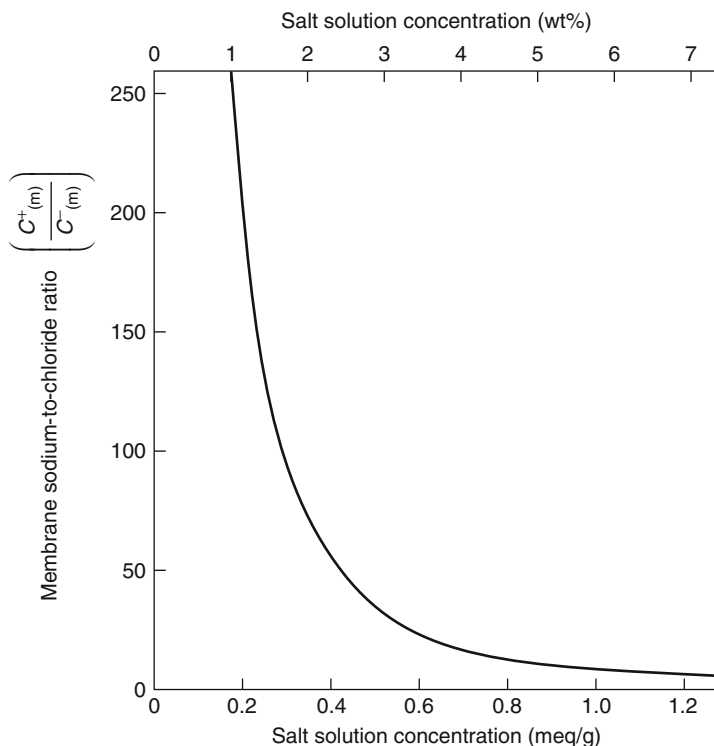


Figure 10.5 The sodium-to-chloride ion concentration ratio inside a negatively charged ion exchange membrane containing a concentration of fixed negative groups of 3 meq/g as a function of salt concentration. At salt concentrations in the surrounding solution of less than about 1 wt% sodium chloride (0.2 meq/g), chloride ions are almost completely excluded from the membrane

Ion exchange membranes contain a high concentration of fixed ionic groups, typically 3–4 meq/g or more. When placed in water, these ionic groups tend to absorb water; charge repulsion of the ionic groups can then cause the membrane to swell excessively. This is why most ion exchange membranes are highly crosslinked to limit swelling. However, high crosslinking densities make polymers brittle, so the membranes are usually stored and handled wet to allow absorbed water to plasticize the membrane. Most ion exchange membranes are produced as homogenous films 50–200 µm thick. The membrane is often reinforced by casting onto a net or fabric to maintain the shape and to minimize swelling.

Ion exchange membranes fall into two broad categories: homogeneous and heterogeneous. In homogeneous membranes, the charged groups are uniformly distributed through the membrane matrix. These membranes swell relatively uniformly when exposed to water, the extent of swelling being controlled by their crosslinking density. In heterogeneous membranes, the ion exchange groups are contained in small domains distributed throughout an inert support matrix, which provides mechanical strength. Heterogeneous membranes can be made, for example, by dispersing finely ground ion exchange particles

in a polymer support matrix. In recent years, finely dispersed heterogeneous membranes have been made by casting membrane films from ABA block copolymers. The A and B blocks phase separate as the casting solvent evaporates, forming two domain structures. The membrane film is then chemically treated to introduce fixed charges into one of the phase separated domains. This domain forms the ion conducting path through the membrane. Because of the difference in the degree of swelling between the ion exchange portion and the inert portion of heterogeneous membranes, mechanical failure, leading to leaks at the boundary between the two domains, can be a problem.

10.3.1 Homogeneous Membranes

A number of early homogeneous membranes were made by simple condensation reactions of suitable monomers, such as phenol–formaldehyde condensation reactions of the type shown in Figure 10.6.

The mechanical stability and ion exchange capacity of these condensation resins were modest. It was found that a better approach is to prepare a suitable crosslinked base membrane, which can then be converted to a charged form in a subsequent reaction. Ionics used this method to make many of their membranes. In a typical preparation procedure, a 60:40 mixture of styrene and divinylbenzene is cast onto a fabric web, sandwiched between two plates and heated in an oven to form the membrane matrix. The membrane is then sulfonated with 98% sulfuric acid or a concentrated sulfur trioxide solution. The degree of swelling in the final membrane is controlled by varying the divinylbenzene concentration in the initial mix to control crosslinking density. The degree of sulfonation can also be varied. The chemistry of the process is shown in Figure 10.7.

Anion exchange membranes can be made from the same crosslinked polystyrene membrane base by post-treatment with monochloromethyl ether and aluminum chloride to introduce chloromethyl groups into the benzene ring, followed by formation of quaternary amines with trimethylamine (Figure 10.8).

A particularly important category of ion exchange polymers is the perfluorocarbon type made by DuPont under the trade name Nafion® [19, 20]. The base polymer is made by polymerization of a sulfinol fluoride vinyl ether with tetrafluoroethylene. The copolymer formed is extruded as films about 120 µm thick, after which the sulfinol fluoride groups are hydrolyzed to form sulfonic acid groups (Figure 10.9).

Asahi Chemical [8] and Tokuyama Soda [21] have developed similar chemistries in which the $-CF_2SO_2F$ groups are replaced by carboxylic acid groups. Membranes made from these polymers have better selectivity than the perfluorosulfonic membranes.

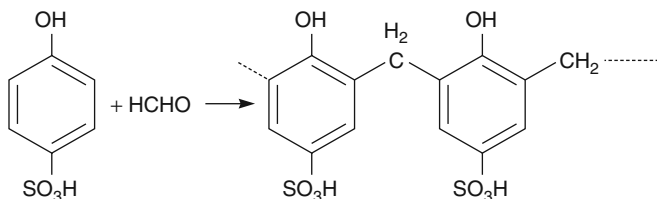


Figure 10.6 Phenol-formaldehyde condensation reaction used to make early cationic membranes

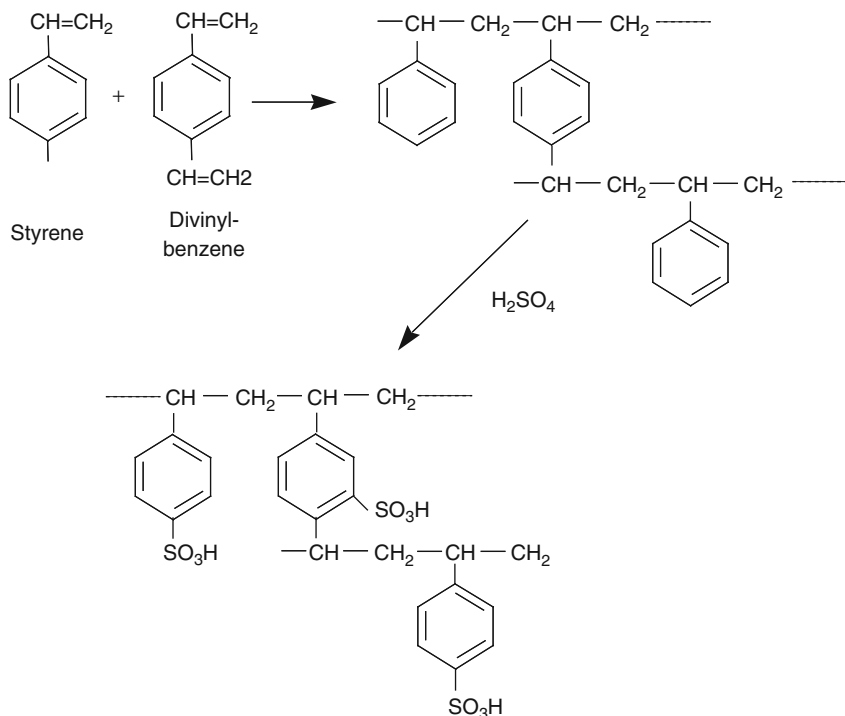


Figure 10.7 Preparation of a crosslinked matrix polymer followed by sulfonation to produce a cationic ion exchange membrane

In all these perfluoro polymers, the backbone is extremely hydrophobic whereas the charged acid groups are strongly polar. Because the polymers are not crosslinked, some phase separation into different domains takes place. The hydrophobic perfluoro polymer domains provide a nonswelling matrix, ensuring the integrity of the membrane. The ionic hydrophilic domains absorb water and form as small clusters distributed throughout the perfluoro polymer matrix. This configuration, illustrated in Figure 10.10, minimizes both the hydrophobic interaction of ions and water with the backbone and the electrostatic repulsion of close sulfonate groups. These perfluorocarbon membranes are completely inert to concentrated sodium hydroxide solutions and have been widely used in membrane electrochemical cells in the chlor-alkali industry and as PEMs in fuel cells. One drawback of the membranes is their very high cost of several hundred dollars per square meter of membrane.

10.3.2 Heterogeneous Membranes

Heterogeneous membranes have been produced by a number of Japanese manufacturers. The simplest form has very finely powdered cation or anion exchange particles uniformly dispersed in polypropylene. A film of the material is then extruded to form the membrane. The mechanical properties of these membranes are often poor because of swelling of the relatively large – 10–20 μm diameter – ion exchange particles. A much

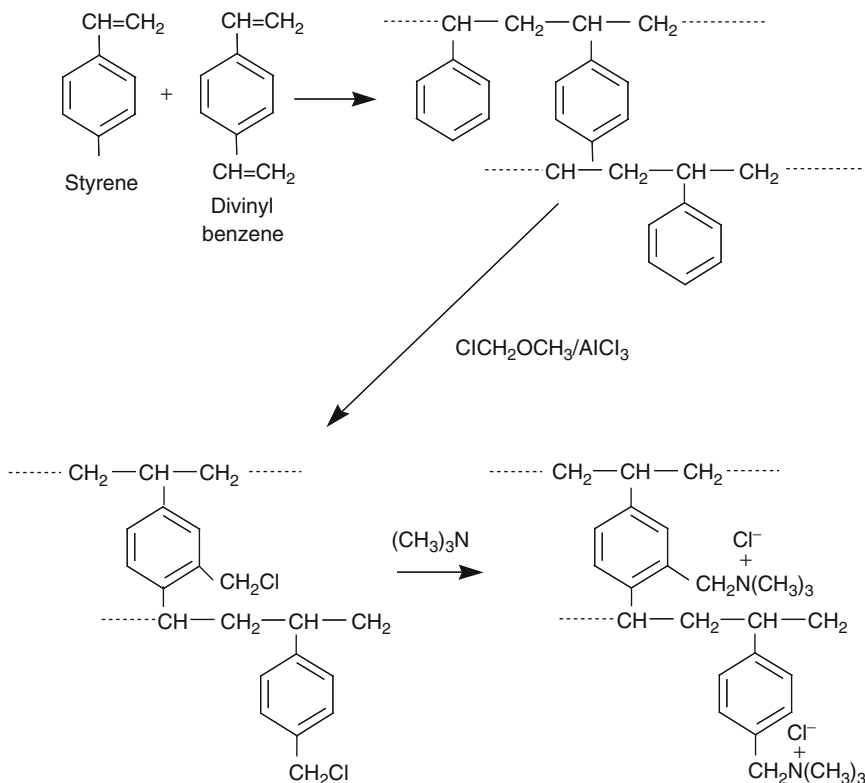


Figure 10.8 Preparation of a crosslinked matrix polymer followed by introduction of chlormethyl groups and formation of quaternary amines to produce an anionic ion exchange membrane

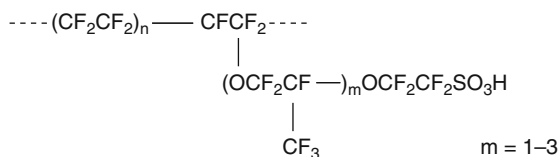


Figure 10.9 DuPont's Nafion® perfluorocarbon cationic exchange membrane

finer heterogeneous dispersion of ion exchange particles, and consequently a more stable membrane, can be made with a poly(vinyl chloride) (PVC) plastisol. A plastisol of approximately equal parts PVC, styrene monomer, and crosslinking agent in a diethyl phthalate plasticizing solvent is prepared. The mixture is then cast and polymerized as a film. The PVC and polystyrene polymers form an interconnected domain structure. The styrene groups are then sulfonated by treatment with concentrated sulfuric acid or sulfur trioxide to form a very finely dispersed but heterogeneous structure of sulfonated polystyrene in a PVC matrix, which provides toughness and strength.

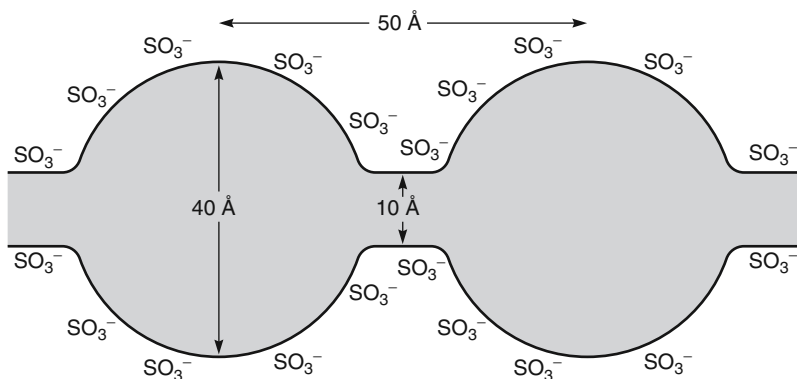


Figure 10.10 Schematic of the cluster model used to describe the distribution of sulfonate groups in perfluorocarbon-type cation exchange membranes such as Nafion® [20]

10.4 Electrodialysis

10.4.1 Concentration Polarization and Limiting Current Density

Transport of ions in an electrodialysis cell, in which the salt solutions in the chambers formed between the ion exchange membranes are very well stirred, is shown in Figure 10.11. In this example, chloride ions migrating to the left easily permeate the anionic membranes containing fixed positive groups and are stopped by the cationic membranes containing fixed negative groups. Similarly, sodium ions migrating to the right permeate the cationic membranes, but are stopped by the anionic membranes. The overall result is an increased salt concentration in alternating compartments while the other compartments are simultaneously depleted of salt. The drawing shown implies that the voltage potential drop caused by the electrical resistance of the apparatus takes place entirely across the ion exchange membrane. This is the case for a well-stirred cell, in which the solutions in the compartments are completely turbulent. In a well-stirred cell, the flux of ions across the membranes and hence the productivity of the electrodialysis system can be increased without limit by increasing the current across the stack. In practice, however, the resistance of the membrane is often small in proportion to the resistance of the water-filled compartments, particularly in the dilute compartment where the concentration of ions carrying the current is low. In this compartment, the formation of ion-depleted regions next to the membrane places an additional limit on the current and hence the flux of ions through the membranes. Ion transport through this ion-depleted aqueous boundary layer generally controls electrodialysis system performance.

Concentration polarization occurs in electrodialysis because ions permeate the membrane at different rates. This means that the concentration of some of the ions in the solution immediately adjacent to the membrane surface become significantly depleted compared to the bulk solution concentration. As the voltage across the stack is increased to increase the flux of ions through the membrane, the solution next to the membrane surface becomes increasingly depleted of the permeating ions. Depletion of the ions at the

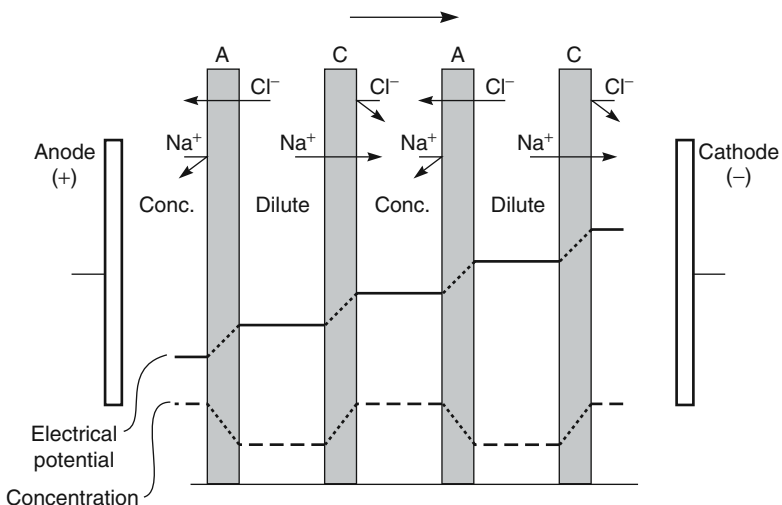


Figure 10.11 Schematic of the concentration and electrical potential gradients in a well-stirred electrodialysis membrane stack

membrane surface means that an increasing fraction of the voltage drop is dissipated in transporting ions across the boundary layer rather than through the membrane; therefore, the energy consumption per unit of ion transported increases significantly. A point can be reached at which the ion concentration at the membrane surface is zero. This represents the maximum transport rate of ions through the boundary layer. The current through the membrane at this point is called the limiting current density, that is, current per unit area of membrane (mA/cm^2). Once the limiting current density is reached, any further increase in voltage difference across the membrane will not increase ion transport or current through the membrane. Normally the extra power is dissipated by side reactions, such as dissociation of the water in the cell into ions, and by other effects. Concentration polarization can be partially controlled by circulating the salt solutions at high flow rates through the cell chambers. But even when very turbulent flow is maintained in the cells, significant concentration polarization occurs.

The formation of concentration gradients caused by the flow of ions through a single cationic membrane in the electrodialysis cell stack is shown in Figure 10.12. As in the treatment of concentration polarization in other membrane processes, the resistance of the aqueous solution is modeled as a thin boundary layer of unstirred solution separating the membrane surface from the well-stirred bulk solution. In electrodialysis, the thickness (δ) of this unstirred layer is generally $20\text{--}50\,\mu\text{m}$. Concentration gradients form in this layer because only one of the ionic species is transported through the membrane. This species is depleted in the boundary layer on the feed side and enriched in the boundary layer on the permeate side.

Figure 10.12 shows the concentration gradient of univalent sodium ions next to a cationic membrane. Exactly equivalent gradients of anions, such as chloride ions, form adjacent to the anionic membranes in the stack. The ion gradient formed on the left,

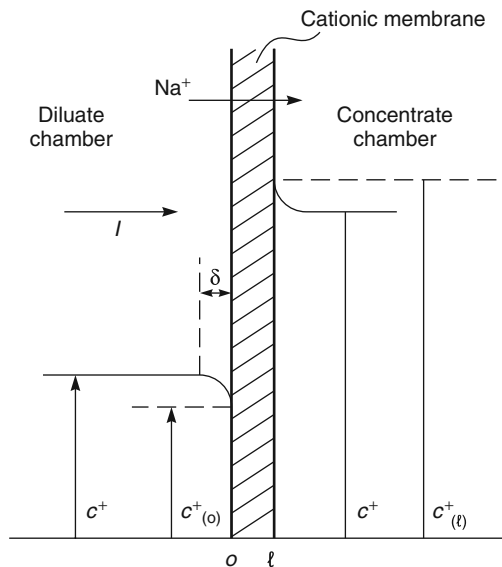


Figure 10.12 Schematic of the concentration gradients adjacent to a single cationic membrane in an electrodialysis stack. The effects of boundary layers that form on each side of the membrane on sodium ion concentrations are shown

dilute side of the membrane can be described by Fick's law. Thus the rate of diffusion of cations to the surface is given by:

$$J^+ = D^+ \frac{(c^+ - c_{(o)}^+)}{\delta} \quad (10.12)$$

where D^+ is the diffusion coefficient of the cation in water, c^+ is the bulk concentration of the cation in the solution, and $c_{(o)}^+$ is the concentration of the cation in the solution adjacent to the membrane surface (o).

The rate at which the cations approach the membrane by electrolyte transport is t^+I/F . It follows that the total flux of sodium ions to the membrane surface (J^+) is the sum of these two terms

$$J^+ = \frac{D^+ (c^+ - c_{(o)}^+)}{\delta} + \frac{t^+I}{F} \quad (10.13)$$

Transport through the membrane is also the sum of two terms, one due to the voltage difference, the other due to the diffusion caused by the difference in ion concentrations on each side of the membrane. Thus, the ion flux through the membrane can be written

$$J^+ = \frac{t_{(m)}^+ I}{F} + \frac{P^+ (c_{(o)}^+ - c_{(\ell)}^+)}{\ell} \quad (10.14)$$

where P^+ is the permeability of the sodium ions in a membrane of thickness ℓ . The quantity $P^+ (c_{(o)}^+ - c_{(\ell)}^+) / \ell$ is much smaller than transport due to the voltage gradient, so Equations 10.13 and 10.14 can be combined and simplified to

$$D^+ \frac{(c^+ - c_{(o)}^+)}{\delta} + \frac{t^+ I}{F} = \frac{t_{(m)}^+ I}{F} \quad (10.15)$$

For a selective cationic ion exchange membrane for which $t_{(m)}^+ \approx 1$, Equation 10.15 can be further simplified to

$$I = \frac{F}{1 - t^+} \cdot \frac{D^+}{\delta} (c^+ - c_{(o)}^+) \quad (10.16)$$

This important equation has a limiting value when the concentration of the ion at the membrane surface is zero ($c_{(o)}^+ \approx 0$). At this point, the current reaches its maximum value; the limiting current is given by the equation

$$I_{\text{lim}} = \frac{D^+ F c^+}{\delta (1 - t^+)} \quad (10.17)$$

This limiting current, I_{lim} , is the maximum current that can be employed in an electrodialysis process. If the potential required to produce this current is exceeded, the extra current will be carried by other processes, first by transport of anions through the cationic membrane and, at higher potentials, by hydrogen and hydroxyl ions formed by dissociation of water. Both of these undesirable processes consume power without producing any separation. This decreases the current efficiency of the process, that is, the separation achieved per unit of energy consumed. A more detailed discussion of the effect of the limiting current density on electrodialysis performance is given by Krol *et al.* [22].

The limiting current can be determined experimentally by plotting the electrical resistance across the membrane stack against the reciprocal electric current. This is called a Cowan-Brown plot after its original developers [23]; Figure 10.13 shows an example for a laboratory cell [24]. At a reciprocal current of 0.1 A^{-1} , the resistance has a minimum value. When the limiting current is exceeded, the excess current is not used to transport ions. Instead, the current causes water to dissociate into protons and hydroxyl ions. The pH of the solutions in the cell chambers then begins to change, reflecting this water splitting. This change in pH, also shown in Figure 10.13, can be used to determine the value of the limiting current density.

In industrial-scale electrodialysis systems, determining the limiting current is not so easy. In large membrane stacks, the boundary layer thickness will vary from place to place across the membrane surface. The limiting current where the boundary layer is relatively thick because of poor fluid flow distribution, will be lower than where the boundary layer is thinner. Thus, the measured limiting current may be only an approximate value. In practice, systems are operated at currents well below the limiting value.

The limiting current density for an electrodialysis system operated at a constant solution flow rate is a function of the feed solution salt concentration, as shown in

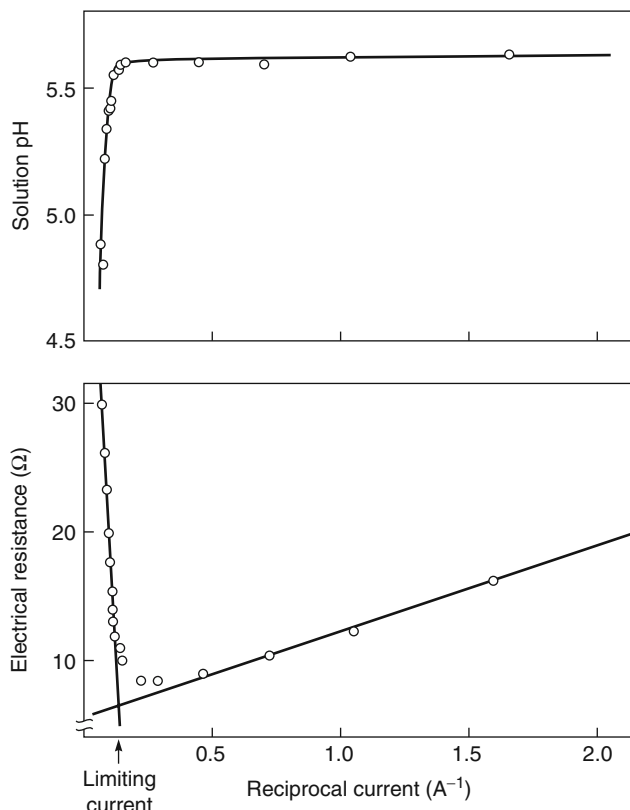


Figure 10.13 Cowan-Brown plots showing how the limiting current density can be determined by measuring the stack resistance or the pH of the dilute solution as a function of current [24]. (Redrawn from R. Rautenbach and R. Albrecht, Membrane Processes, Copyright © 1989. This material is used by permission of John Wiley & Sons, Ltd.)

Equation 10.17. As the salt concentration in the solution increases, more ions are available to transport current in the boundary layer, so the limiting current density also increases. For this reason, large electrodialysis systems with several electrodialysis stacks in series will operate with different current densities in each stack, reflecting the change in the feed water concentration as salt is removed.

Once the limiting current is reached, further changes in applied electrical potential do not increase the current through the membrane, and energy is dissipated without achieving an increase in separation. However, at very high applied potential, an increase in current does occur. This phenomenon is called the overlimiting current. An example is shown in Figure 10.14. The origins of this phenomenon have been debated for a number of years. Recent thinking is that surface heterogeneity leads to charge separation and electroconvection in the ion-depleted boundary layer of the membrane [25]. At high applied voltages, tiny convection cells are created by charge separation that convectively brings ions to the membrane surface.

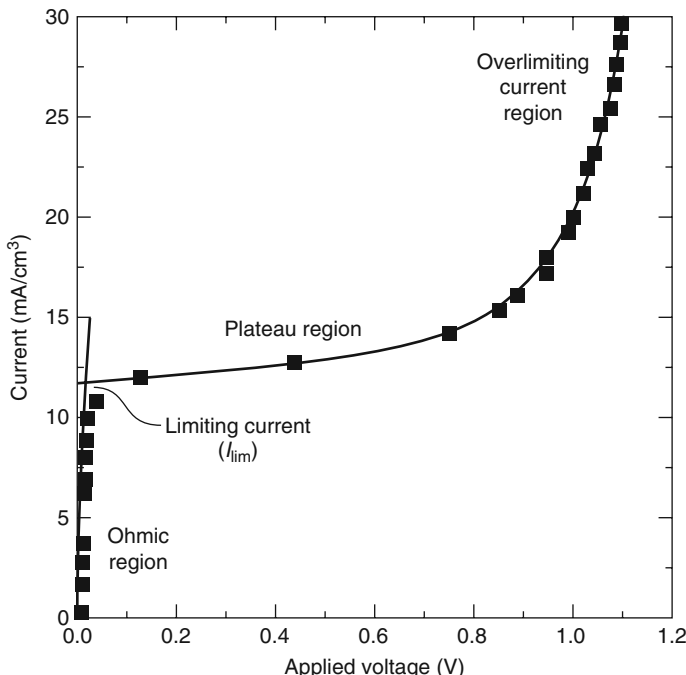


Figure 10.14 Full current-voltage (I - V) curve for an ion exchange membrane, illustrating the ohmic region controlled by the diffusion in the membrane boundary layer; the plateau region above the limiting current, where the diffusion gradient has reached its maximum value; and the overlimiting current region, where electroconvection supplements diffusion in transporting ions through the membrane boundary layer [25]

10.4.2 Current Efficiency and Power Consumption

A key factor determining the overall efficiency of an electrodialysis process is the energy consumed to perform the separation. Power consumption E in watts, is linked to the current I through the stack and the resistance R of the stack by the expression

$$E = I^2 R \quad (10.18)$$

The theoretical electric current I_{theor} required to perform the separation is directly proportional to the number of charges transported across the ion exchange membrane and is given by the expression

$$I_{\text{theor}} = z \Delta C F Q \quad (10.19)$$

where Q is the feed flow rate, C is the difference in molar concentration between the feed and the dilute solutions, z is the valence of the salt, and F is the Faraday constant. Thus the theoretical power consumption E_{theor} to achieve a given separation is given by substituting Equation 10.19 into 10.18 to give:

$$E_{\text{theor}} = IRz\Delta C Q F \quad (10.20)$$

or

$$E_{\text{theor}} = Vz \Delta C QF \quad (10.21)$$

where V is the theoretical voltage drop across the stack. In the absence of concentration polarization and any resistance losses in the membrane or solution compartments, the energy required to achieve a separation and a flow of ions out of the concentrated feed solution into the dilute solution for any cell pair is as shown in Figure 10.15.

The actual voltage drop and hence the energy consumed are higher than the theoretical value for two reasons [10, 26]. First, as shown in Figure 10.12, the concentrations of ions in the solutions adjacent to the membrane surfaces are significantly lower than the bulk solution values. That is, the actual voltage drop used in Equation 10.21 is several times larger than the voltage drop in the absence of polarization. The result is to increase the actual energy consumption 5–10 times above the theoretical minimum value. In commercial electrodialysis plants, concentration polarization is controlled by circulating the solutions through the stack at a high rate. Various feed spacer designs are used to maximize turbulence in the cells. Because electric power is used to power the feed and product solution circulation pumps, a trade-off exists between the power saved because of the increased efficiency of the electrodialysis stack and the power consumed by the pumps. In modern electrodialysis systems, the circulation pumps consume approximately one-quarter to one-half of the total power. Even under these conditions, concentration

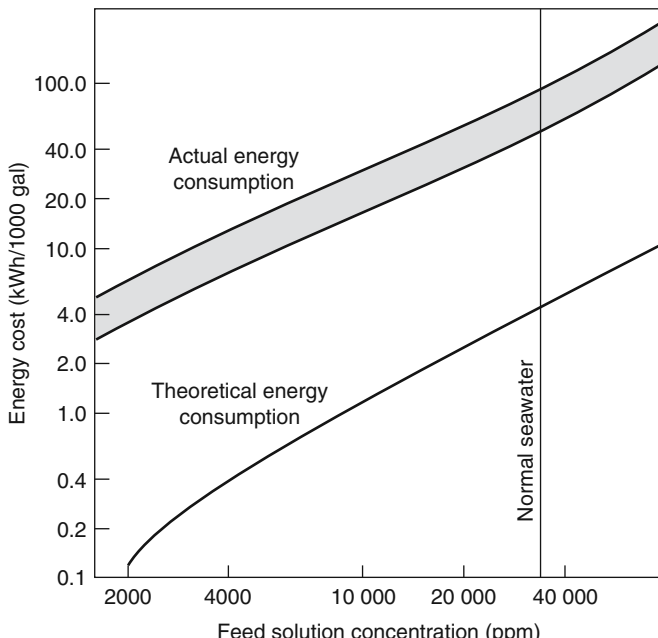


Figure 10.15 Comparison of the theoretical energy consumption and the actual energy consumption of electrodialysis desalination systems. Most of the difference results from concentration polarization effects [26]

polarization is not fully controlled and actual energy consumption is substantially higher than the theoretical value as shown in Figure 10.15.

Most inefficiencies in electrodialysis systems are related to the difficulty in controlling concentration polarization. The second cause is current utilization losses, arising from the following factors [10]:

1. Ion exchange membranes are not completely semipermeable; some leakage of co-ions of the same charge as the membrane can occur. This effect is generally negligible at low feed solution concentrations, but can be serious with concentrated solutions, such as the seawater treated for salt production in Japan.
2. Ions permeating the membrane carry solvating water molecules in their hydration shell. Also, osmotic transport of water from the dilute to the concentrated chambers can occur.
3. A portion of the electric current can be carried by the stack manifold, bypassing the membrane cell. Modern electrodialysis stack designs generally make losses due to this effect negligible.

10.4.3 System Design

An electrodialysis plant consists of several elements:

- a feed pretreatment system;
- the membrane stack;
- the power supply and process control unit;
- the solution pumping system.

Many small plants use a single electrodialysis stack, as shown in Figure 10.16. Manifolding may be used to allow the feed and brine solutions to pass through several cell pairs in series, but the entire procedure is performed in a single stack.

In large systems, using several separate electrodialysis stacks in series to perform the separation is more efficient [10, 27]. Multiple stacks are used because the current density of the first stack is higher than the current density of the last stack, which is operating on a more dilute feed solution. As in the single-stack system, the feed solution may pass through several cell pairs in each stack in series. Because concentration polarization becomes more important as the solution becomes more dilute, the solution velocity in the stacks is increased to control polarization as the solution becomes more dilute. The velocity is controlled by the number of cell pairs through which the solution passes in each stack. The number of cell pairs used in series decreases from the first to the last stack; this is known as the taper of the system. The flow scheme of a three-stage design is shown in Figure 10.17.

10.4.3.1 Feed Pretreatment

The type and complexity of the feed pretreatment system depends on the content of the water to be treated. As in reverse osmosis, most feed water is sterilized by chlorination to prevent bacterial growth on the membrane. Scaling on the membrane surface by precipitation of sparingly soluble salts such as calcium sulfate is usually controlled by adding precipitation inhibitors such as sodium hexametaphosphate. The pH may also be adjusted

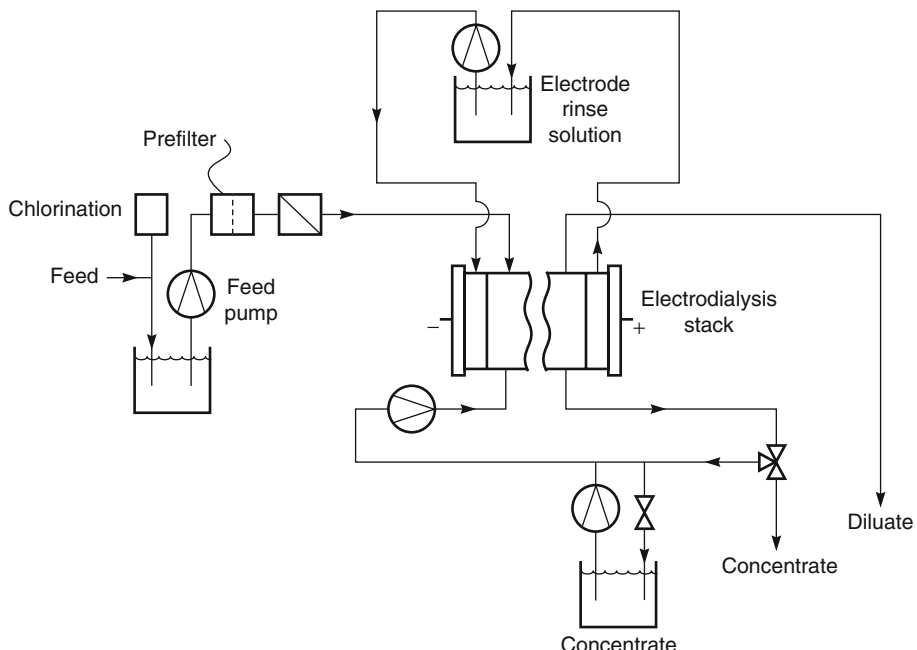


Figure 10.16 Flow diagram of a typical small electrodialysis plant [10]

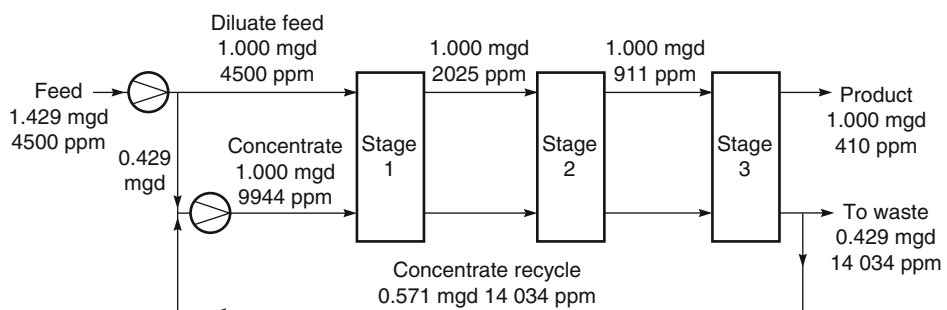


Figure 10.17 Flow scheme of a three-stage electrodialysis plant. Reprinted with permission from [27]. Copyright (1977) Elsevier.

to maintain salts in their soluble range. Large, charged organic molecules or colloids such as humic acid are particularly troublesome impurities, because they are drawn by their charge to the membrane surface but are too large to permeate. They then accumulate at the dilute solution side of the membrane and precipitate, causing an increase in membrane resistance. Filtration of the feed water may control these components, and operation in the polarity reversal mode is often effective.

10.4.3.2 Membrane Stack

After the pretreatment step, the feed water is pumped through the electrodialysis stack. This stack normally contains 100–200 membrane cell pairs, each with a membrane area between 1 and 2 m². Plastic mesh spacers form the channels through which the feed and concentrate solutions flow. Most manufacturers use one of the spacer designs shown in Figure 10.18. In the tortuous path cell design of Figure 10.18a, a solid spacer grid forms a long open channel through which the feed solution flows at relatively high velocity. The channel is not held open by netting, so the membranes must be thick and sturdy to prevent collapse of the channels. In the sheet flow design of Figure 10.18b, the gap between the membrane leaves is maintained by a polyolefin mesh spacer. The spacer is made as thin as possible without producing an excessive pressure drop.

Two membranes and two gasket spacers form a single cell pair. Holes in the gasket spacers are aligned with holes in the membrane sheet to form the manifold channels through which the dilute and concentrated solutions are introduced into each cell. The end plate of the stack is a rigid plastic frame containing the electrode compartment. The entire arrangement is compressed together with bolts between the two end flow plates. The perimeter gaskets of the gasket spacers are tightly pressed into the membranes to form the cells. A large electrodialysis stack has several hundred meters of fluid seals around each cell. Early units often developed small leaks over time, causing unsightly salt deposits on the outside of the stacks. These problems have now been largely solved. In principle, an

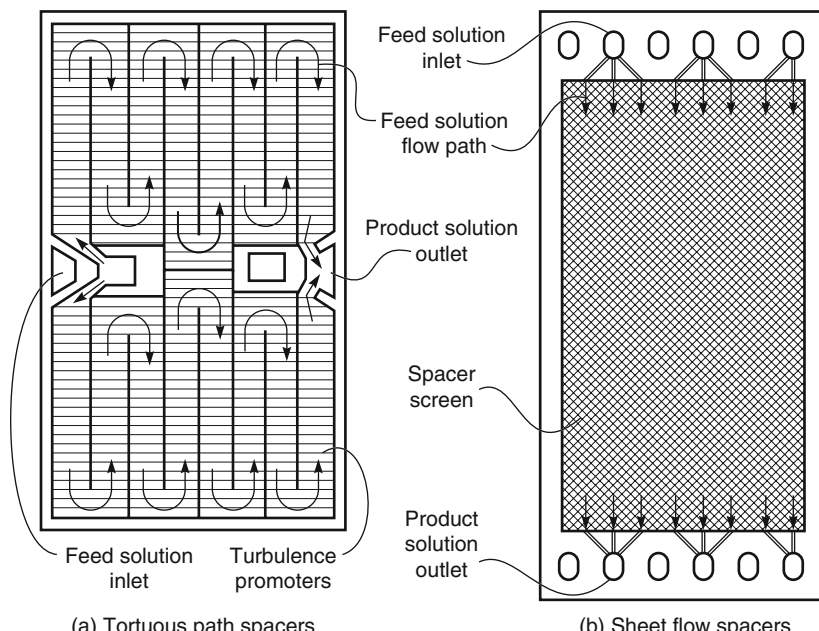


Figure 10.18 The two main types of feed solution flow distribution spacers used in electrodialysis [10]. (a) Tortuous path spacers and (b) sheet flow spacers

electrodialysis stack can be disassembled and the membranes cleaned or replaced on-site. In practice, this operation is performed infrequently and almost never in the field.

10.4.3.3 Power Supply and Process Control Unit

Electrodialysis systems use large amounts of direct current power; the rectifier required to convert AC to DC and to control the operation of the system represents a significant portion of a plant's capital cost. A typical voltage drop across a single cell pair is in the range 1–2 V, and the normal current flow is 40 mA/cm². For a 200-cell-pair stack containing 1 m² of membrane per cell, the total voltage is about 200–400 V, and the current about 400 A per stack. This is a considerable amount of electric power, and care must be used to ensure safe operation.

10.4.3.4 Solution Pumping System

A surprisingly large fraction of the total power used in electrodialysis systems is consumed by the water pumps required to circulate feed and concentrate solutions through the stacks. This fraction increases as the average salt concentration of the feed decreases and can become dominant in electrodialysis of low-concentration solutions (less than 500 ppm salt). The pressure drop per stack varies from 15 to 30 psi for sheet flow cells to as much as 70–90 psi for tortuous path cells. Depending on the separation required, the fluid will be pumped through two to four cells in series, requiring interstage pumps for each stack.

10.5 Electrodialysis Applications

10.5.1 Brackish Water Desalination

Brackish water desalination is the largest application of electrodialysis. The competitive technologies are ion exchange for very dilute saline solutions, below 500 ppm, and reverse osmosis for concentrations above 2000 ppm. In the 500–2000 ppm range, electrodialysis is often the low-cost process. One advantage of electrodialysis applied to brackish water desalination is that a large fraction, typically 80–95% of the brackish feed, is recovered as product water. These high recoveries mean that the concentrated brine stream produced is 5–20 times more concentrated than the feed. The degree of water recovery is limited by precipitation of insoluble salts in the brine.

Since the first plants were produced in the early 1950s, several thousand brackish water electrodialysis plants have been installed around the world. Modern plants are generally fully automated and require only periodic operator attention. This has encouraged production of many small trailer-mounted plants. However, a number of large plants with production rates of 10 million gal/day or more have also been installed.

The power consumption of an electrodialysis plant is directly proportional to the salt concentration of the feed water, varying from 1 kWh/m³ for 1000 ppm feed water to 2.5–4.0 kWh/m³ for 5000 ppm feed water.

10.5.2 Salt Recovery from Seawater

A second major application of electrodialysis is the production of table salt by concentration of seawater [8]. This process is only practiced in Japan, which has no other

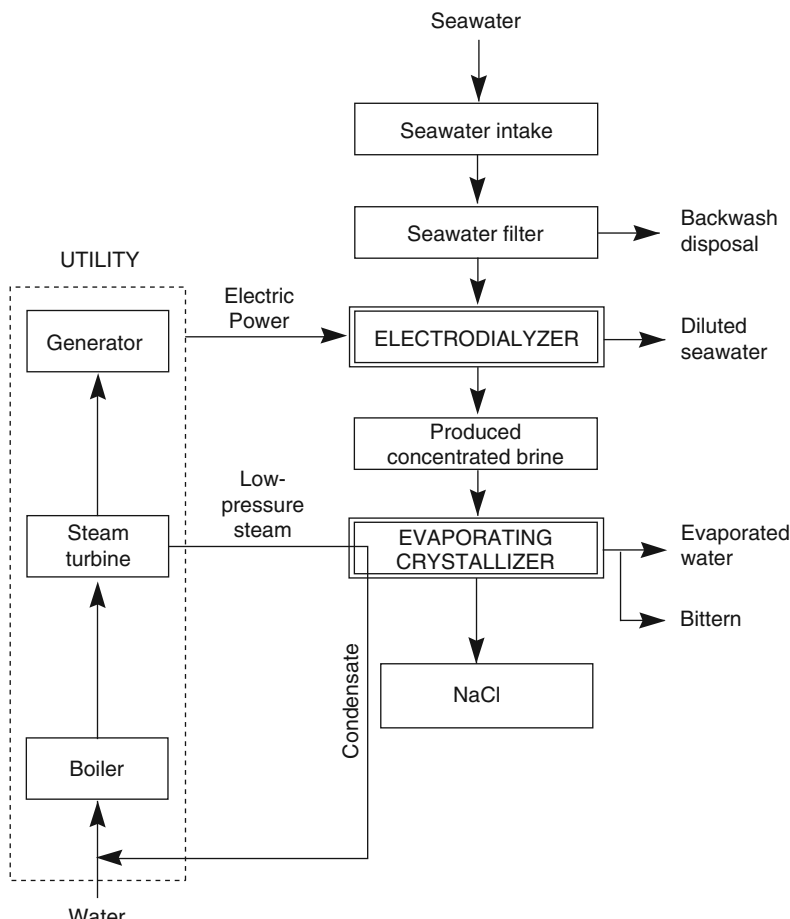


Figure 10.19 Flow scheme of the electrodialysis unit used in a seawater salt concentration plant [8]

domestic salt supply. The process is subsidized by the government, and total production is approximately 1.2 million tons/year of salt. In total, these plants use more than 500 000 m² of membrane.

A flow scheme of one such seawater salt production plant is shown in Figure 10.19. A co-generation unit produces the power required for the electrodialysis operation, which concentrates the salt in sea water to about 18–20 wt%. The waste stream from the power plant is then used to further concentrate the salt by evaporation.

Seawater contains relatively high concentrations of sulfate (SO₄²⁻), calcium (Ca²⁺), magnesium (Mg²⁺), and other multivalent ions that can precipitate in the concentrated salt compartments of the plant and cause severe scaling. This problem has been solved by applying a thin polyelectrolyte layer of opposite charge to the ion exchange membrane on the surface facing the seawater solution. A cross-section of a coated anionic membrane is shown in Figure 10.20. Because the Donnan exclusion effect is much stronger for

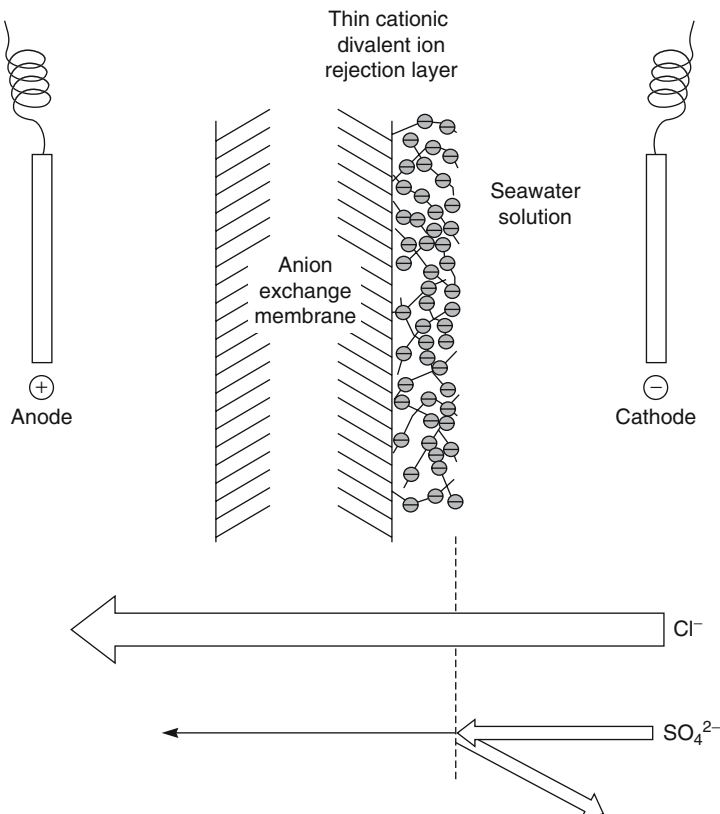


Figure 10.20 Polyelectrolyte-coated ion exchange membranes used to separate multivalent and monovalent ions in seawater salt concentration plants [8]

multivalent ions than for univalent ions, the polyelectrolyte layer rejects multivalent ions but allows the univalent ions to pass relatively unhindered.

10.5.3 Other Electrodialysis Separation Applications

The two water desalination applications described above represent the majority of the market for electrodialysis separation systems. A small application exists in softening water and, recently, markets have developed in the food industry to desalt whey and to remove tannic acid from wine and citric acid from fruit juice. A number of other applications exist in wastewater treatment, particularly regeneration of waste acids used in metal pickling operations and removal of heavy metals from electroplating rinse waters [10, 11]. These applications rely on the ability of electrodialysis membranes to separate electrolytes from nonelectrolytes and to separate multivalent from univalent ions.

The arrangement of membranes in these systems depends on the application. Figure 10.21a shows a stack comprised of cation exchange membranes to soften water, whereas Figure 10.21b shows an all-anion exchange membrane stack to deacidify

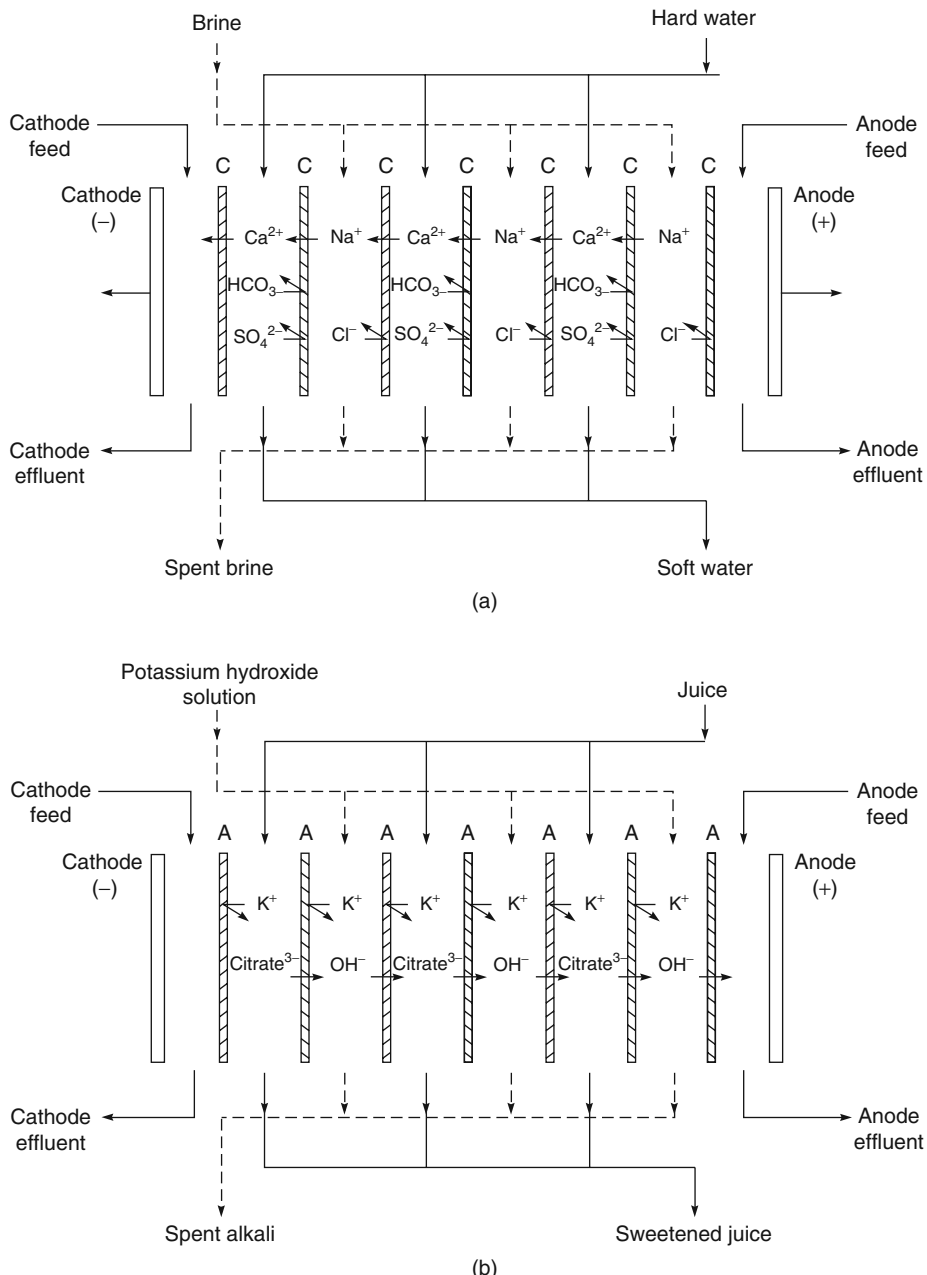


Figure 10.21 Flow schematic of electrodialysis systems used to exchange target ions in the feed solution. (a) An all-cation exchange membrane stack to exchange sodium ions for calcium ions in water softening. (b) An all-anion exchange membrane stack to exchange hydroxyl ions for citrate ions in deacidification of fruit juice

juice [28]. In the water-softening application, the objective is to exchange divalent cations such as calcium and magnesium for sodium ions. In the juice deacidification process, the all-anion stack is used to exchange citrate ions for hydroxyl ions. These are both ion exchange processes, and the salt concentration of the feed solution remains unchanged.

10.5.4 Continuous Electrodeionization and Ultrapure Water

Electrodeionization systems were first suggested to remove small amounts of radioactive elements from contaminated waters [29], but the principal application recently is the preparation of ultrapure water for the electronics and pharmaceutical industries [30, 31]. Use of this process has grown rapidly in the last 10 years and is now often used as a polishing step after the water has been pretreated with a reverse osmosis unit.

In the production of ultrapure water for the electronics industry, salt concentrations must be reduced to the ppb range. This is a problem with conventional electrodialysis units because the low conductivity of very dilute feed water streams generally limits the process to producing water in the 10 ppm range. This limitation can be overcome by filling the dilute chambers of the electrodialysis stack with fine mixed-bed ion exchange beads as shown in Figure 10.22. The ions in the chamber partition into the ion exchange resin beads as shown in Figure 10.22. The ions in the chamber partition into the ion exchange resin beads, and are concentrated many times. As a result, ions and current flow through

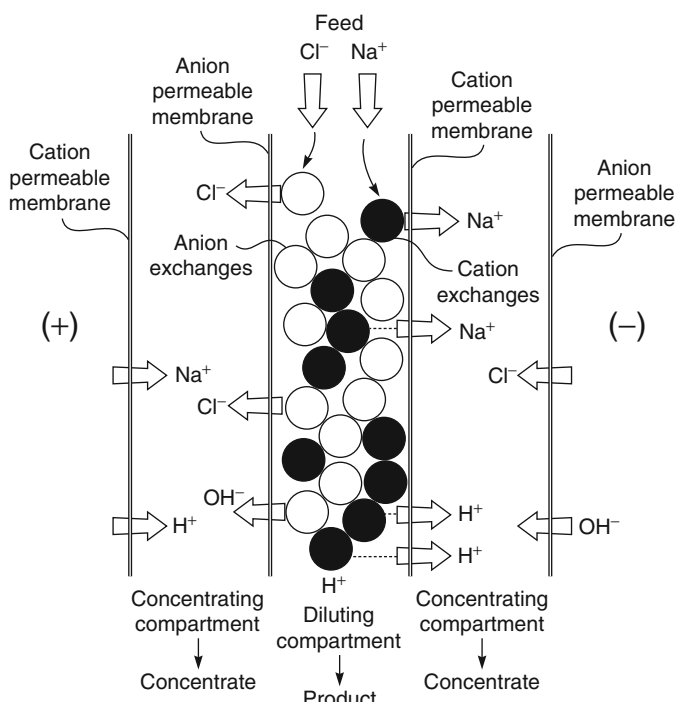


Figure 10.22 Schematic of the electrodeionization process using a mixed-bed ion exchange resin to increase the conduction of the dilute compartments of the electrodialysis stack. This type of process is often used in the production of ultrapure water for the electronics industry

the beads in the resin bed, and the resistance of the cell is much lower than for a normal cell operating on the same very dilute feed. An additional benefit is that, toward the bottom of the bed where the ion concentration is in the ppb range, a certain amount of water splitting occurs. This produces hydrogen and hydroxyl ions that also migrate to the membrane surface through the ion exchange beads. The presence of these ions maintains a high pH in the anion exchange beads and a low pH in the cation exchange beads. These extreme pHs enhance the ionization and removal of weakly ionized species such as carbon dioxide and silica that would otherwise be difficult to remove. Such electrodeionization systems can reduce most ionizable solutes to below ppb levels.

10.5.5 Bipolar Membranes

Bipolar membranes consist of an anionic and a cationic membrane laminated together [13]. When placed between two electrodes, as shown in Figure 10.23, the interface between the anionic and cationic membranes becomes depleted of ions. The only way a current can then be carried is by the water splitting reaction, which liberates hydrogen ions that migrate to the cathode and hydroxyl ions that migrate to the anode. The mechanism of water splitting in these membranes has been discussed in detail by Strathmann *et al.* [10, 32]. The phenomenon can be utilized in an electrodialysis stack composed of a number of sets of three-chamber cells between two electrodes, as shown in Figure 10.24. Salt solution flows into the middle chamber; cations migrate to the chamber on the left and anions to the chamber on the right. Electrical neutrality is maintained in these chambers by hydroxyl and hydrogen ions provided by water splitting in the bipolar membranes that bound each set of three chambers [33].

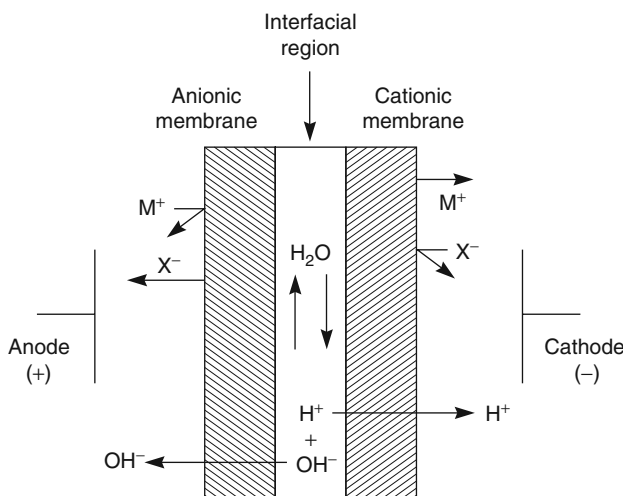


Figure 10.23 Schematic of a single bipolar membrane showing generation of hydroxyl and hydrogen ions by water splitting in the interior of the membrane. Electrolysis takes place in the thin interfacial region between the anodic and cathodic membranes. This drawing is not made to scale. The interfacial space between the 100 and 300 μm -thick anionic and cationic membranes is extremely thin, typically less than a few μm thick

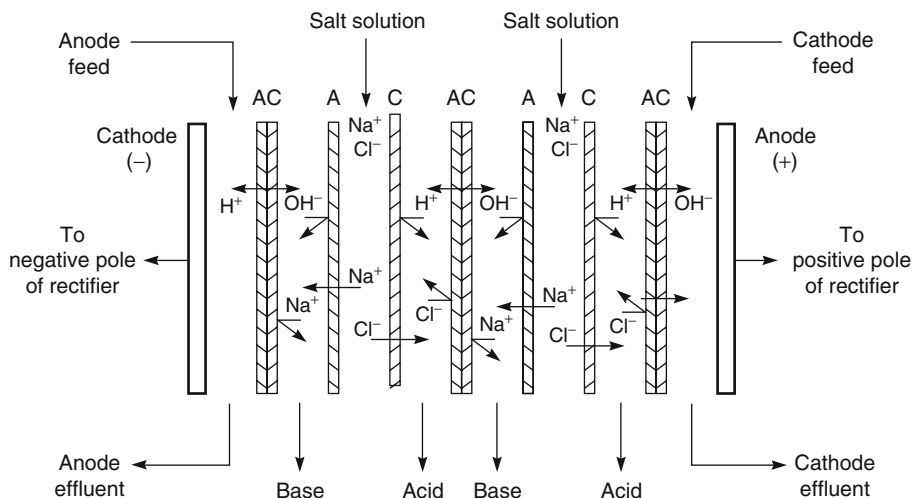


Figure 10.24 Schematic of a bipolar membrane process to split sodium chloride into sodium hydroxide and hydrochloric acid

Several other arrangements of bipolar membranes can achieve the same overall result, namely, dividing a neutral salt into the conjugate acid and base. The process is limited to the generation of relatively dilute acid and base solutions. Also, the product acid and base are contaminated with 2–4% salt. Nevertheless, the process is significantly more energy efficient than the conventional electrolysis process because no gases are created at the cell electrodes. Total current efficiency is about 80%, and the system can often be integrated into the process generating the feed salt solution. A process utilizing bipolar membranes was first reported by Liu and colleagues in 1977 [13]. Aquatech, originally a division of Allied Chemicals and now part of Graver Water, has pursued commercialization of the process for almost 30 years, but only a handful of plants have been installed. Membrane instability was an early problem, but this has been solved and prospects for the process appear to be improving. A review of bipolar membrane technology has been produced by Kemperman [34].

10.6 Fuel Cells

The operating principle of the fuel cell was described by Sir William Grove (and independently by the Swiss scientist Christian Shoenbein) in 1839. Grove's device consisted of an electrochemical cell with two electrodes. Hydrogen was bubbled over the surface of one electrode, oxygen over the other. As long as the gas supply was maintained, a current flowed through a wire connecting the two electrodes. Grove's device was a scientific curiosity until the 1940s, when Francis Bacon at Cambridge University and King's College London started to develop practical fuel cells. By the late 1950s, he had made a 6 kW fuel cell. The technology took off with the US space program in the 1960s. Spacecraft needed far more electric power than could be stored in batteries. Fuel cells

were an efficient, lightweight method of converting chemical energy into electric power. The Gemini, Apollo, and all subsequent space programs were equipped with fuel cells.

The space program remained the principal application of fuel cells until the 1990s when there was a surge of interest in developing fuel cells as the power source for all sorts of electric motor-driven cars, trucks, buses, and boats. Fuel cells also found a place in non-interruptible power systems and as portable power sources to replace batteries for laptops, computers, and military electronic devices. The industry has gone through several boom and bust cycles – one in 2000–2001 and another in 2008–2009 – but the technology's takeoff continues to be “just a few years in the future.”

Many different types of fuel cells exist, differing mostly in the nature of the barrier media separating the two electrodes. Membrane developers are mostly interested in PEM (or proton exchange membrane) fuel cells of the type shown in Figure 10.25. In this device, the membrane has three functions:

- it separates the anode and cathode to prevent an electrical short circuit;
- it separates the hydrogen and oxygen fuels to prevent a chemical short circuit;
- it selectively transports protons (H^+) from the anode to the cathode.

A hydrogen/oxygen fuel cell produces electricity by the reaction



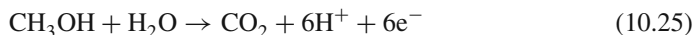
The anode electrode of the cell consists of a porous carbon fabric which allows hydrogen gas to contact one side of a cation (negatively charged) ion exchange membrane. The dissociation of hydrogen to protons is normally slow, but can be catalyzed by a finely dispersed layer of platinum at the membrane surface. In the presence of this catalyst, the hydrogen ionizes by the reaction



Electrical energy is generated as the electrons travel to the cathode through the conductor joining the two electrodes. The protons diffuse through the negatively charged ion exchange membrane. At the cathode, the protons combine with oxygen by the reaction



Two types of fuel cells use PEMs. The first is the proton exchange (or polymer electrolyte) membrane fuel cell (PEMFC) illustrated in Figure 10.25. The second is the direct methanol fuel cell (DMFC). The DMFC uses methanol instead of hydrogen at the anode of the cell. In the presence of platinum or platinum–ruthenium catalysts, methanol releases protons by the reaction



Methanol is easier to transport and use than hydrogen and has a much higher volumetric energy density, which are significant advantages. The principal problem is that cation exchange membranes, as well as being permeable to protons, are also significantly permeable to methanol. Methanol permeation (crossover) from the anode to the cathode compartment leads to several unwanted effects, including a loss in cell voltage and the

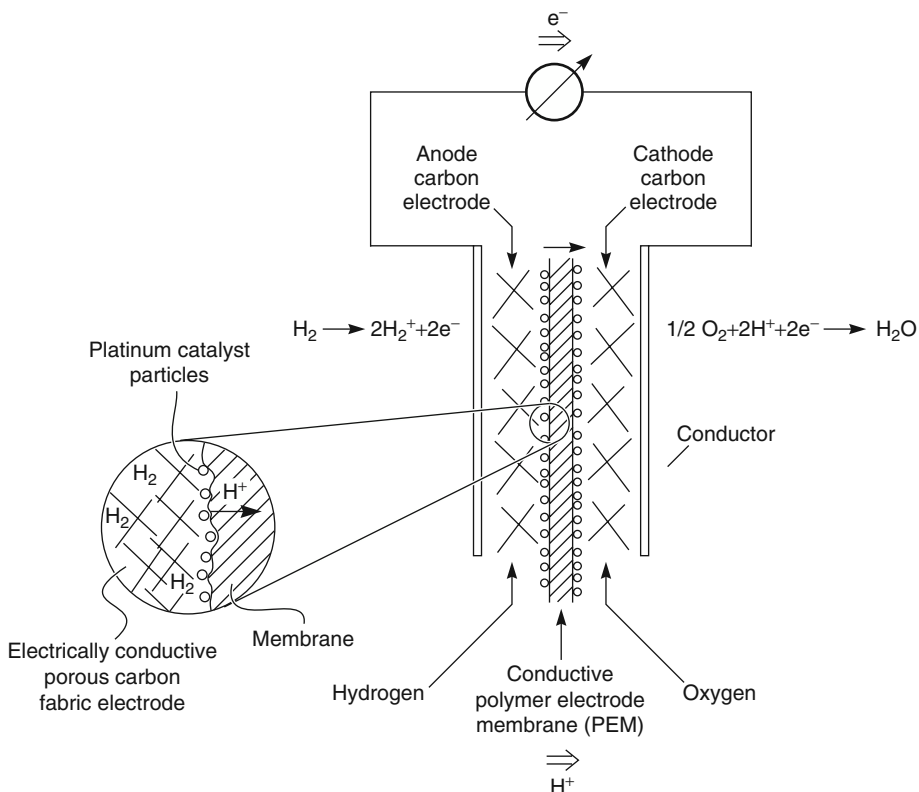
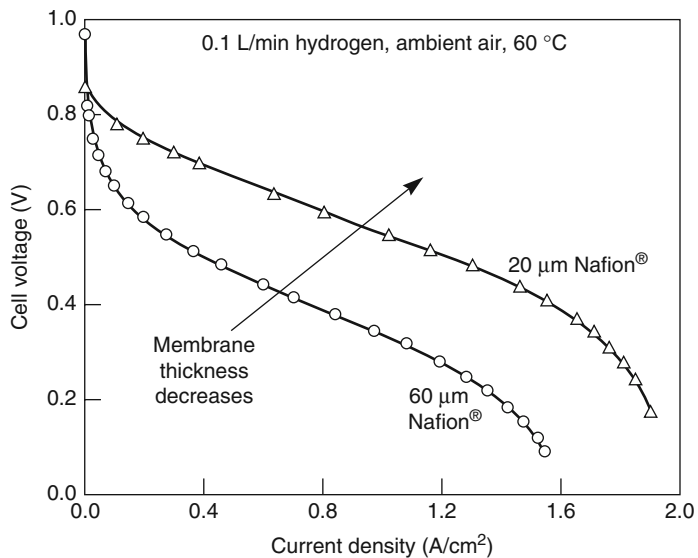


Figure 10.25 A schematic of a hydrogen-powered polymer electrolyte membrane fuel cell (PEMFC). Hydrogen at the anode electrode is converted to protons and electrons. The electrons are carried to the cathode electrode by a conductor producing useful power. The protons diffuse through the proton-permeable (cationic) membrane to the cathode electrode, where they react with oxygen to produce water

consumption of methanol and oxygen without electricity generation, lowering the fuel efficiency of the cell. By far the most important PEM material is DuPont's Nafion® perfluorosulfonic acid, for which the chemical structure was shown in Figure 10.9. The performance of Nafion® membranes in a hydrogen-powered PEMFC cell and a methanol-powered DMFC cell are shown in Figure 10.26. The power generated by the fuel cell is the product of the cell voltage and current density. The data show the hydrogen-powered PEM fuel cell gets better as the membrane becomes thinner. The only limitation is the mechanical weakness of very thin membranes. W.R. Gore has tried to circumvent this problem by impregnating Nafion® into very thin microporous PTFE membranes. The PTFE provides the mechanical strength, the Nafion® conducts the protons.

In contrast, the data for the methanol DMFC fuel cell shows the cell power achieved with this cell is significantly less than with a hydrogen-powered cell and also increases as the membrane becomes thicker. This is because of methanol crossover to the cathode.

Hydrogen (PEMFC) Fuel Cell



Methanol (DMFC) Fuel Cell

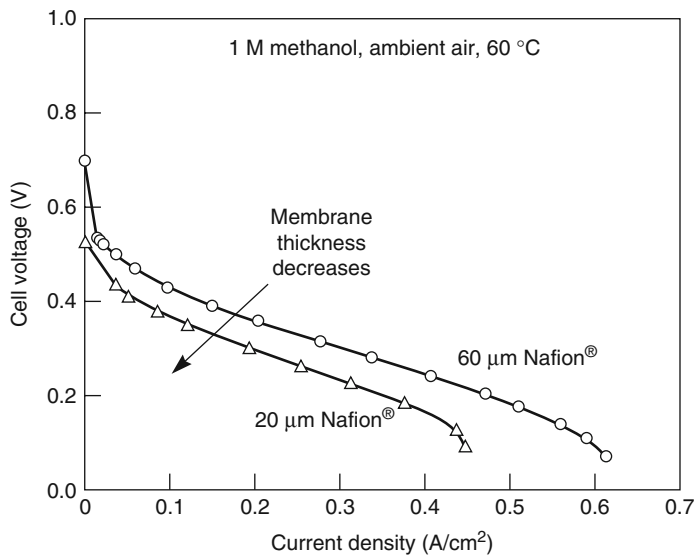


Figure 10.26 Effect of membrane thickness on full cell performance with two commercial Nafion® membranes [16]

Making the membrane thicker decreases the proton transport rate, but this is more than offset by the decrease in methanol crossover.

In the past decade, a huge amount of effort has been spent developing better PEM membranes [15, 16, 35]. However, even today, Nafion® still seems to be the material to beat, despite its very high cost.

10.7 Membranes in Chlor-Alkali Processes

Caustic soda (sodium hydroxide) and chlorine are produced by the electrolysis of aqueous sodium chloride. The process has been carried out on an industrial scale since 1892. For many years, mercury cells were used, but environmental problems caused by leakage of mercury into the environment has meant these plants have almost all been closed and replaced with membrane processes, first using asbestos diaphragms and more recently using polymeric cationic ion exchange membranes.

A schematic diagram of the membrane chlor-alkali process is shown in Figure 10.27. Sodium chloride (brine) is sent to the anode compartment of the electrolysis cell. The salt is pretreated to bring calcium, aluminum, magnesium, and other impurities down to the ppb level. Make up water is sent to the cathode compartment of the cell. The cell compartments are separated by a cationic perfluorosulfonic acid (Nafion®) or perfluorocarboxylic acid (Flemion®) membrane. When a voltage gradient is generated between the two cell electrodes, sodium ions pass through the membrane, which acts as an almost perfect barrier to chloride and hydroxyl ions. Chloride ions discharged at the anode

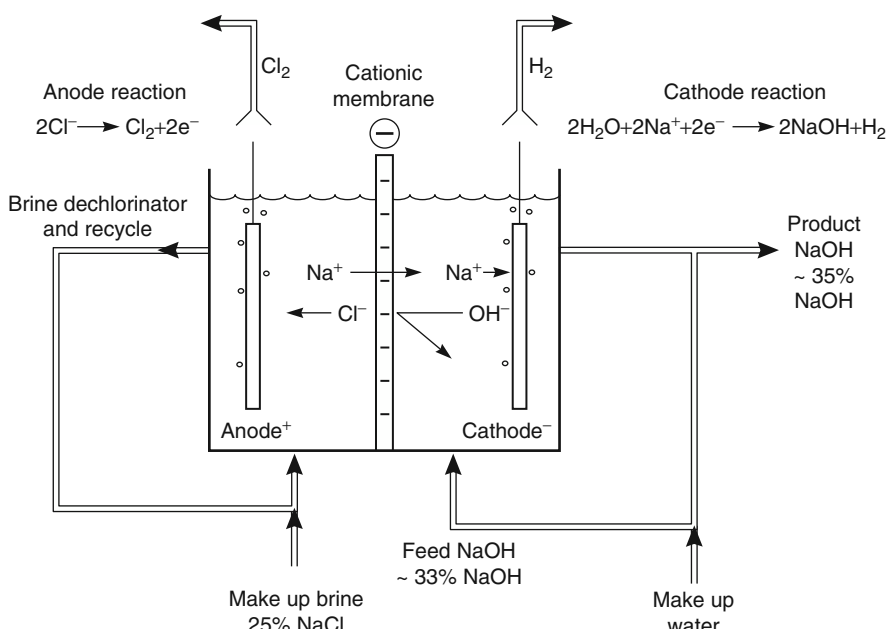


Figure 10.27 Schematic of a membrane chlor-alkali electrolysis cell

create chlorine gas, while hydroxide ions discharged at the cathode produce hydrogen and dissolved sodium hydroxide. The sodium hydroxide concentration builds up until the concentration reaches about 35%. The sodium hydroxide is then removed as a product stream. The current efficiency of the process is very high, reaching up to 97%, and in recent years better membranes have allowed the concentration of the sodium hydroxide product produced in the cathode compartment to rise to as high as 50 wt%.

The main products of the chlor-alkali industry are chlorine – used directly in the pulp and paper industry and in the production of intermediates such as ethylene dichloride and vinyl chloride – and sodium hydroxide – used in a wide variety of neutralization reactions and in the production of hypochlorite for bleach. Hydrogen is also generated as a by-product, and is usually burned for fuel. In recent years, some plants have improved the economics of the process by using a porous cathode permeated by CO₂-free air. Oxygen in the air is reduced by hydrogen at the cathode and the potential of the oxygen reduction process reduces the decomposition voltage needed for chlor-alkali electrolysis by as much as 30%. Since the consumption of electricity is a large contributor to the cost of the process, this saving is significant.

A number of other processes using ion exchange membranes (Donnan dialysis, diffusion dialysis, piezodialysis, and reverse electrodialysis) are covered in Chapter 13.

10.8 Conclusions and Future Directions

Electrodialysis and chlor-alkali cells are by far the largest uses of ion exchange membranes. These two processes are both well established, and major technical innovations that will change the competitive position of ion exchange membranes do not appear likely. Some new applications of electrodialysis exist in the treatment of industrial process streams, food processing, and wastewater treatment systems, but the total market is small. Long-term major applications for ion exchange membranes may develop in non-separation areas such as fuel cells, electrochemical reactions, and production of acids and alkalis with bipolar membranes. These processes have been worked on for decades and have found some niche applications, but have yet to fulfill the hopes of their developers.

References

1. Ostwald, W. (1890) Elektrische eigenschaften halbdurchlässiger scheidewande. *Z. Phys. Chem.*, **6**, 71.
2. Donnan, F.G. (1911) Theory of membrane equilibria and membrane potentials in the presence of non-dialyzing electrolytes. *Z. Elektrochem.*, **17**, 572.
3. Manegold, E. and Kalauch, C. (1939) Über kapillarsysteme, XXII die wirksamkeit verschiedener reinigungsmethoden (Filtration, Dialyse, Electrolyse und Ihre Kombinationen). *Kolloid Z.*, **86**, 93.
4. Meyer, K.H. and Straus, W. (1940) La permeabilité des membranes, VI, Sur la passage du courant électrique a travers des membranes selectives. *Helv. Chim. Acta*, **23**, 795.
5. Kressman, T.R.E. (1950) Ion exchange resin membranes and resin-impregnated filter paper. *Nature*, **165**, 568.

6. Murphy, E.A., Paton, F.J., and Ansell, J. (1943) Apparatus for the electrical treatment of colloidal dispersions. US Patent 2,331,494 Oct. 1943.
7. Juda, W. and McRae, W.A. (1950) Coherent ion-exchange gels and membranes. *J. Am. Chem. Soc.*, **72**, 1044.
8. Seko, M., Miyauchi, H., and Omura, J. (1983) Ion exchange membrane application for electrodialysis, electroreduction, and electrohydrodimerisation, in *Ion Exchange Membranes* (ed. D.S. Flett), Ellis Horwood Ltd, Chichester, pp. 121–136.
9. Siwak, L.R. (1992) Here's how electrodialysis reverses and why EDR works. *Desalin. Water Reuse*, **2**, 16.
10. Strathmann, H. (1991) Electrodialysis, in *Membrane Separation Systems: Recent Developments and Future Directions* (eds R.W. Baker, E.L. Cussler, W. Eykamp, W.J. Koros, R.L. Riley and H. Strathmann), Noyes Data Corporation, Park Ridge, NJ, pp. 396–448.
11. Strathmann, H. (1985) Electrodialysis and its application in the chemical process industry. *Sep. Purif. Methods*, **14**, 41.
12. Grotheer, M.P. (1992) Electrochemical processing (Inorganic), in *Kirk Othmer Encyclopedia of Chemical Technology*, 4th edn, vol. **9**, Wiley Interscience and John Wiley & Sons, Inc., New York, p. 124.
13. Nagasubramanian, K., Chlanda, F.P., and Liu, K.J. (1977) Use of bipolar membranes for generation of acid and base – an engineering and economic analysis. *J. Membr. Sci.*, **2**, 109.
14. Nagasubramanian, K., Chlanda, F.P., and Liu, K.J. (1980) Bipolar membrane technology: an engineering and economic analysis, *Recent Advances in Separation Tech - II*, AIChE Symposium Series number 1192, Vol. **76**, AIChE, New York, p. 97.
15. Peinemann, K.V. and Nunes, S.P. (eds) (2008) *Membranes for Energy Conversion*, vol. **2**, Wiley-VCH Verlag GmbH & Co. KGaA, Weinheim.
16. Pintauro, P.N. and Wycisk, R. (2008) Fuel cell membranes, in *Advanced Membrane Technology and Applications* (eds N.N. Li, A.G. Fane, W.S.W. Ho, and T. Matsuura), John Wiley & Sons, Inc., Hoboken, NJ, pp. 755–786.
17. Yeo, R.S. (1982) Applications of perfluorosulfonated polymer membranes in fuel cells, electrolyzers, and load leveling devices, in *Perfluorinated Ionomer Membranes*, ACS Symposium Series, Vol. **180** (eds A. Eisenberg and H.L. Yeager), American Chemical Society, Washington, DC, pp. 453–473.
18. Korngold, E. (1984) Electrodialysis-membranes and mass transport, in *Synthetic Membrane Processes: Fundamentals and Water Applications* (ed. G. Belfort), Academic Press, Orlando, FL, pp. 191–220.
19. Eisenberg, A. and Yeager, H.L. (1982) *Perfluorinated Ionomer Membranes*, ACS Symposium Series, Vol. **180**, American Chemical Society, Washington, DC.
20. Gierke, T.D. (1977) Ionic clustering in Nafion perfluorosulfonic acid membranes and its relationship to hydroxyl rejection and chlor-alkali current efficiency. Paper presented at the Electrochemical Society Fall Meeting, Atlanta, GA.
21. Sata, T., Motani, K., and Ohaski, Y. (1983) Perfluorinated ion exchange membrane, neosepta-f and its properties, in *Ion Exchange Membranes* (ed. D.S. Flett), Ellis Horwood Ltd, Chichester, pp. 137–150.

22. Krol, J.J., Wessling, M., and Strathmann, H. (1999) Concentration polarization with monopolar ion exchange membranes: current-voltage curves and water dissociation. *J. Membr. Sci.*, **162**, 145.
23. Cowan, D. and Brown, J. (1959) Effect of turbulence on limiting current in electrodialysis cells. *Ind. Eng. Chem.*, **51**, 1445.
24. Rautenbach, R. and Albrecht, R. (1989) *Membrane Processes*, John Wiley & Sons, Ltd, Chichester.
25. Balster, J., Yildirim, M.H., Stamatialis, D.F., Ibanez, R., Lammertink, R.G.H., Jordan, V. and Wessling, M. (2007) Morphology and microtopology of cation-exchange polymers and the origin of the overlimiting current. *J. Phys. Chem. B*, **111**, 2152.
26. Shaffer, L.H. and Mintz, M.S. (1966) Electrodialysis, in *Principles of Desalination* (eds K.S. Spiegler and A.D.K. Laird), Academic Press, New York, pp. 200–289.
27. Rogers, A.N. (1984) Economics of the application of membrane processes, in *Synthetic Membrane Processes* (ed. G. Belfort), Academic Press, Orlando, FL, pp. 437–476.
28. Zang, J.A. (1966) Sweetening citrus juice in membrane process for industry. *Proc. South Res. Inst. Conf.*, **35**.
29. Walters, W.R., Weiser, D.W., and Marek, L.J. (1955) Concentration of radioactive aqueous wastes. Electromigration through ion-exchange membranes. *Ind. Eng. Chem.*, **47**, 61.
30. Ganzi, G.C., Jha, A.D., DiMascio, F., and Wood, J.H. (1997) Electrodeionization: theory and practice of continuous electrodeionization. *Ultrapure Water*, **14**, 64.
31. Dey, A. (2008) Ultrapure water by membranes, in *Advanced Membrane Technology and Applications* (eds N.N. Li, A.G. Fane, W.S.W. Ho, and T. Matsuura), John Wiley & Sons, Inc., Hoboken, NJ, pp. 371–406.
32. Strathmann, H., Krol, J.J., Rapp, H.J., and Eigenberger, G. (1997) Limiting current density and water dissociation in bipolar membranes. *J. Membr. Sci.*, **125**, 123.
33. Carmen, C. (1994) Bipolar membrane pilot performance in sodium chloride salt splitting. *Desalin. Water Reuse*, **4**, 46.
34. Kemperman, A.J.B. (ed.) (2000) *Handbook on Bipolar Membrane Technology*, Twente University Press, Enschede.
35. Kreuer, K.D. (2001) On the development of proton conducting polymer membranes for hydrogen and methanol fuel cells. *J. Membr. Sci.*, **185**, 29.

11

Carrier Facilitated Transport

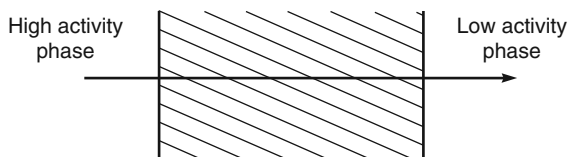
11.1 Introduction/History

Carrier facilitated transport membranes incorporate a reactive carrier in the membrane. The carrier reacts with and helps to transport one of the components of the feed across the membrane. Much of the early work on carrier facilitated transport employed liquid membranes containing a dissolved carrier agent held by capillary action in the pores of a microporous film, so the process is sometimes also called liquid membrane transport.

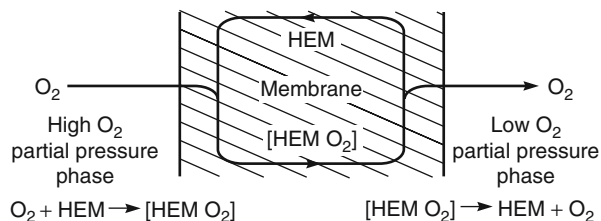
The types of transport that can occur in a liquid membrane are illustrated in Figure 11.1. *Passive diffusion* down a concentration gradient is the most familiar – this process is usually relatively slow and nonselective. In *facilitated transport*, the liquid membrane phase contains a carrier agent that chemically combines with the permeant to be transported. In the example shown, the carrier is hemoglobin, which transports oxygen. On the upstream, high-pressure side of the membrane, hemoglobin reacts with oxygen to form oxyhemoglobin, which then diffuses to the downstream, low-pressure membrane interface. There, the reaction is reversed: oxygen is liberated to the permeate gas and hemoglobin is re-formed. The hemoglobin then diffuses back to the feed side of the membrane to pick up more oxygen. In this way, hemoglobin acts as a shuttle to selectively transport oxygen through the membrane. Other gases that do not react with hemoglobin, such as nitrogen, are left behind.

Coupled transport resembles facilitated transport in that a carrier agent is incorporated into the membrane. However, in coupled transport, the carrier agent couples the flow of two species. Because of this coupling, one of the species can be moved against its concentration gradient, provided the concentration gradient of the second coupled species is sufficiently large. In the example shown in Figure 11.1, the carrier is an oxime that forms an organic-soluble complex with copper ions. The reaction is reversed by hydrogen ions. On the feed side of the membrane two oxime carrier molecules pick up a copper ion, liberating two hydrogen ions to the feed solution. The copper–oxime complex then diffuses to the downstream membrane interface, where the reaction is reversed because of the higher concentration of hydrogen ions in the permeate solution. The copper ion is

Passive diffusion



Facilitated transport



Coupled transport

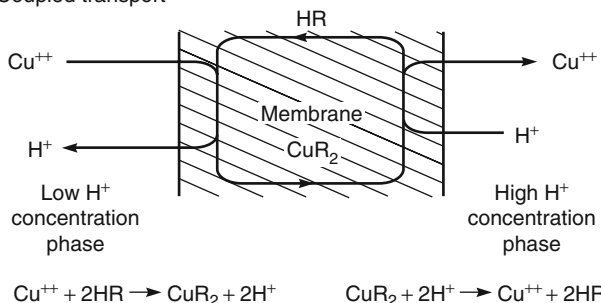


Figure 11.1 Schematic examples of passive diffusion, facilitated transport, and coupled transport in a liquid membrane. The facilitated transport example shows permeation of oxygen across a membrane using hemoglobin as the carrier agent. The coupled transport example shows permeation of copper and hydrogen ions across a membrane using a reactive mobile oxime as the carrier agent

liberated to the permeate solution, and two hydrogen ions are picked up. The re-formed oxime molecules diffuse back to the feed side of the membrane.

Because carrier facilitated transport has so often involved liquid membranes, the process is sometimes called liquid membrane transport, as noted previously, but this is a misnomer, because solid membranes containing carriers dispersed or dissolved in a polymer matrix are increasingly used. In these membranes, the reactive carrier is relatively immobile and it is the permeating components that move from immobile carrier site to carrier site.

Coupled transport was the first carrier facilitated process studied, originating in early biological experiments involving natural ion carriers contained in cell walls. As early

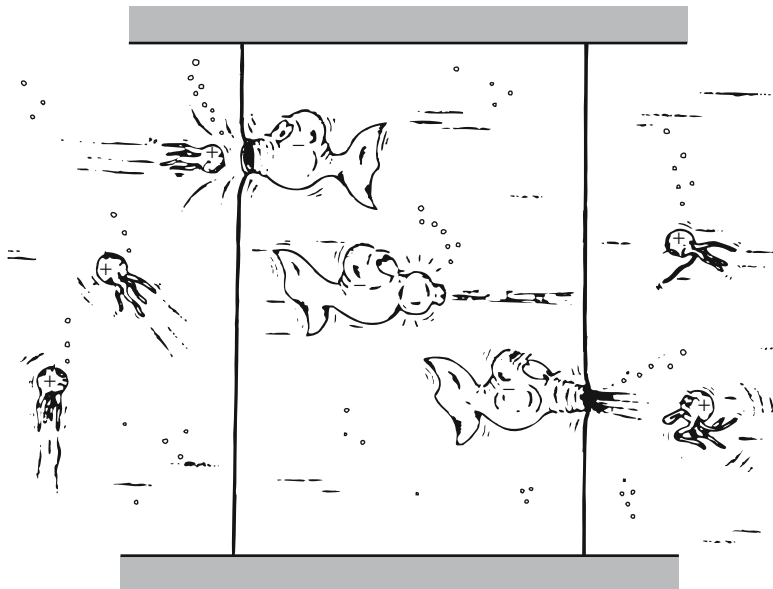


Figure 11.2 Gliozzi's biological model of coupled transport [2]

as 1890, Pfeffer postulated that the transport in these membranes involved carriers. Perhaps the first coupled transport experiment was performed by Osterhout, who studied the transport of ammonia across algaе cell walls in the 1930s [1]. A biological explanation of the coupled transport mechanism in liquid membranes is shown in Figure 11.2 [2].

By the 1950s, the carrier concept was well established, and workers began to develop synthetic analogs of the natural systems. For example, in the mid-1960s, Shean and Sollner [3] studied a number of coupled transport systems using inverted U-tube membranes. At the same time, Bloch and Vofsi published the first of several papers in which coupled transport was applied to hydrometallurgical separations, namely the separation of uranium using phosphate ester carriers [4–6]. Because phosphate esters also plasticize poly(vinyl chloride) (PVC), Bloch and Vofsi prepared immobilized liquid films by dissolving the esters in a PVC matrix. The solid PVC/ester film, containing 60 wt% ester, was cast onto a paper support. Bloch and others actively pursued this work until the early 1970s. At that time, interest in this approach lagged, apparently because the fluxes obtained could not make the process competitive with conventional separation techniques.

In immobilized liquid membranes, it is possible that the carrier complex formed at the membrane surfaces could diffuse from one side of the membrane to the other, where the carrier reaction is reversed. In solid carrier, plasticized films of the type Block and Vofsi made, this type of mechanism implies unrealistically high diffusion coefficients for the large carrier–ion complexes in a solid polymer film. In this type of matrix, a better mechanism is that the small ions being transported – metal ions in one direction, hydrogen ions in the other – rapidly exchange between relatively immobile carrier molecules. That is, the mobile ions hop from one carrier molecule to another. The ions are small, so their diffusion in this way is rapid, compared to diffusion of a large carrier–ion complex.

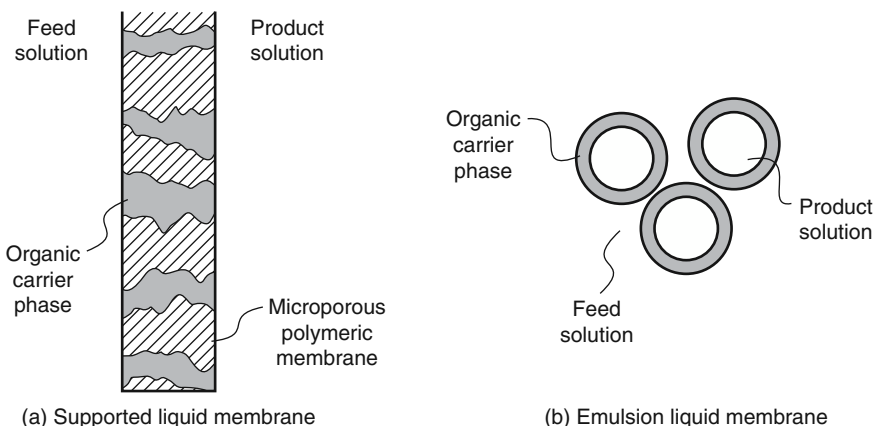


Figure 11.3 Methods of forming liquid membranes. (a) *Supported liquid membrane* and (b) *emulsion liquid membrane*

Following the work of Bloch and Vofsi, other methods of producing immobilized liquid films were introduced. In one approach, the liquid carrier phase was held by capillarity within the pores of a microporous substrate, as shown in Figure 11.3a. This approach was first used by Miyauchi [7], Largman and Sifniades [8], and others [9]. The principal objective of this early work was to recover copper, uranium, and other metals from hydrometallurgical solutions. Despite considerable effort on the laboratory scale, the first pilot plant was not installed until 1983 [10]. The main problem was instability of the liquid carrier phase held in the microporous membrane support.

Another type of liquid carrier membrane is the emulsion or “bubble” membrane. This technique employs a surfactant-stabilized emulsion, as shown in Figure 11.3b. The organic phase containing the carrier forms the wall of an emulsion droplet separating the aqueous feed from the aqueous product solution. Metal ions are removed from the outside aqueous feed and are concentrated in the interior of the droplets. When sufficient metal has been extracted, the emulsion droplets are separated from the feed, and the emulsion is broken to liberate a concentrated product solution and an organic carrier phase. The organic carrier phase is decanted from the product solution and recycled to make more emulsion droplets. One technical problem is the stability of the liquid membrane. Ideally, the emulsion membrane should be completely stable during the extraction step to prevent the two aqueous phases mixing, but should be completely broken and easily separated in the stripping step. Achieving this level of control over emulsion stability has proven to be difficult. The technique of emulsion membranes was invented and popularized by Li and his coworkers at Exxon, starting in the late 1960s and continuing for more than 20 years [11–14]. The first use of these membranes was as a passive device to extract phenol from water. In 1971–1973, Cussler used this technique with carriers to selectively transport metal ions [15, 16]. Work by the Exxon group led to the installation of a pilot plant in 1979 [17]. The process is still not commercial, although a number of pilot plants have been installed, principally using hydrometallurgical feed streams [18].

The use of membrane contactors to solve the stability problem of liquid membranes has been proposed [19–21]. The concept is illustrated in Figure 11.4. Two membrane

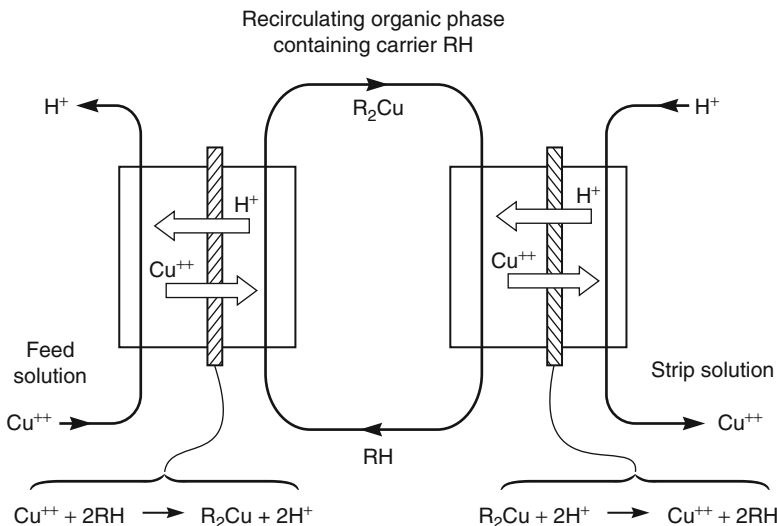


Figure 11.4 Use of two contactors in a liquid membrane process

contactors are used: one to separate the organic carrier phase from the feed, the other to separate the organic carrier phase from the permeate. In the first contactor, metal ions in the feed solution diffuse across the microporous membrane and react with the carrier, liberating hydrogen counter ions. The organic carrier solution is then pumped from the first to the second membrane contactor, where the reaction is reversed. The metal ions are liberated to the permeate solution, and hydrogen ions are picked up. The re-formed carrier solution is then pumped back to the first membrane contactor. Sirkar and his students [20] have used this system to separate metal ions. A similar process was developed to the large demonstration plant scale by Davis *et al.* at British Petroleum for the separation of ethylene/ethane mixtures, using a silver nitrate solution as the carrier for ethylene [21].

In 1993, Wiencek *et al.* [22, 23] developed a combination of emulsion membranes and membrane contactors that went a long way to solving the stability and flux problems of carrier membranes. The process is illustrated in Figure 11.5. An aqueous feed solution (containing a low concentration of heavy metal ions) passes on one side of a membrane contactor. The contactor is fitted with a hydrophobic finely microporous membrane. The pores of the membrane are filled with a water-immiscible solvent containing a dissolved carrier agent for the heavy metal. The organic liquid phase also contains dispersed droplets of aqueous strip solution that can extract and concentrate the metal ions that are extracted by the carrier agent.

As the aqueous feed passes across the membrane, metal ions in the solution react with the carrier agent and displace hydrogen ions into the feed. The metal ion–carrier complex then diffuses through the organic liquid-filled membrane to the emulsified permeate solution. The complex then reacts with the dispersed acid droplets. The metal ion is extracted into these droplets and the carrier agent is re-formed. The dispersed aqueous droplets in the permeate organic solution are much larger than the membrane pores, so mixing of the acid strip solution with the aqueous feed is completely prevented.

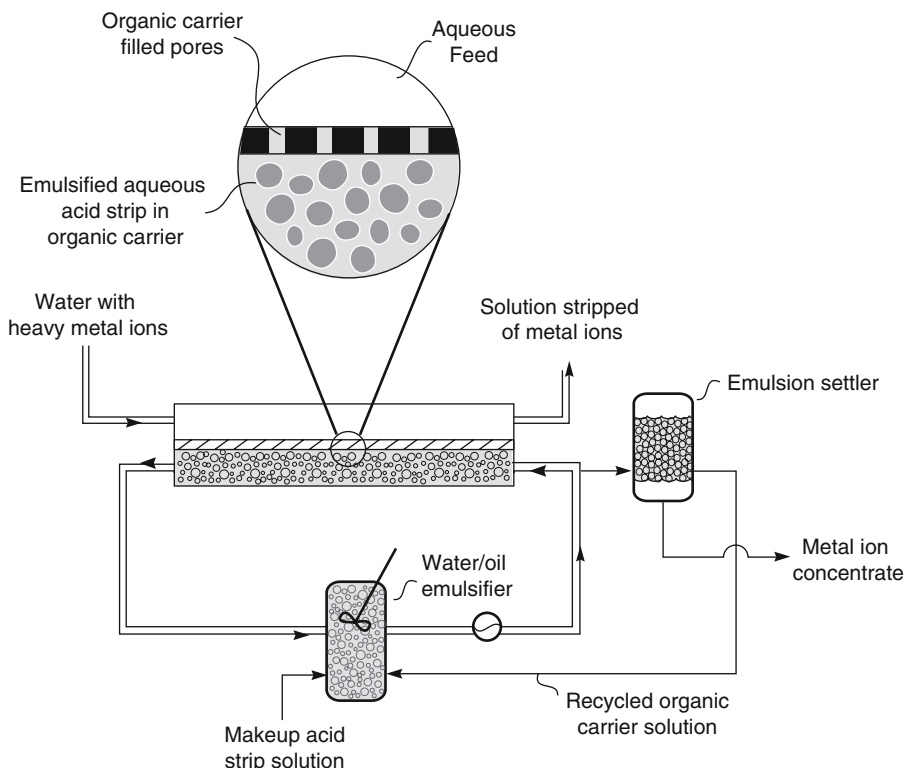


Figure 11.5 A hybrid emulsion–membrane contactor system developed for coupled transport applications by Wiencek and his students [22, 23]. The stability problems of liquid membranes and emulsion membranes are circumvented

The dispersed droplets of strip solution are circulated countercurrently to the aqueous feed. In a continuous process, a portion of the strip solution is removed from the loop and allowed to phase separate. The organic phase is returned to the emulsifier unit; the aqueous phase is the concentrated metal ion product solution.

This device has the stability of the two-contactor systems shown in Figure 11.4, but uses only half the membrane area, and produces significantly higher membrane fluxes. Fouad and Bart [24] and Ho and coworkers [25–27] have applied this idea to a number of potential coupled transport applications.

Carrier facilitated transport membranes often achieve spectacular separations between closely related species because of the selectivity of the carriers. However, no coupled transport process has advanced to the commercial stage, despite a steady stream of papers in the academic literature. The instability of the membranes is a major technical hurdle, but another issue has been low membrane fluxes, leading to marginal improvements in economics offered by coupled transport processes over conventional technologies such as solvent extraction or ion exchange. Major breakthroughs in performance are required to make coupled transport technology commercially competitive. The hybrid emulsion–contactor system proposed by Wiencek *et al.* [22, 23] may be a way forward.

Facilitated transport membranes are plagued by membrane stability and carrier stability problems. However, the economic rationale for developing facilitated transport membranes is at least clear. Practical facilitated transport membranes, capable of separating gas mixtures for which polymeric membranes have limited selectivity, would be commercially adopted. Target applications meeting this criterion are the separation of oxygen and nitrogen, and the separation of olefin/paraffin mixtures. The selectivities of current polymeric membranes are modest for both of these separations. Scholander [28] reported the first work on facilitated transport in 1960 – he studied the transport of oxygen through aqueous hemoglobin solutions. In the late 1960s through the early 1980s, a great deal of work was performed by Ward and others at General Electric [29–32] and Hughes *et al.* [33] at Standard Oil. Ward's work focused on carbon dioxide and hydrogen sulfide separation, and some remarkable selectivities were obtained. However, the problems of membrane stability and scale-up were never solved. This group eventually switched to the development of passive polymeric gas separation membranes. At Standard Oil, Steigelmann and Hughes concentrated most of their efforts on propylene/propane and ethylene/ethane separation, using concentrated silver salt solutions as carriers. Propylene/propane selectivities of several hundred were obtained, and the process was developed to the pilot plant stage. The principal problem was the chemical instability of the silver–olefin complex, which led to a decline in membrane flux and stability over 10–20 days. Although the membrane could be regenerated periodically, this was impractical in an industrial process.

Following the development of good quality polymeric gas separation membranes in the early 1980s, industrial interest in facilitated transport waned. However, in the last few years, a number of workers have shown that facilitated transport membranes can be made by dispersing or complexing the carrier into a solid polymeric film. Such membranes are more stable than immobilized liquid film membranes, and formation of these membranes into thin, high-flux membranes by conventional techniques should be possible. Nishide, Tsuchida, and others in Japan, working with immobilized oxygen carriers [34–36], Peinemann in Germany [37], and Ho [38] and Pinna *et al.* [39] in the US, working with silver salts for olefin separation, have reported promising results. Apparently, the carrier mechanism in these membranes involves the permeant gas molecule diffusing from active site to active site across the solid membrane.

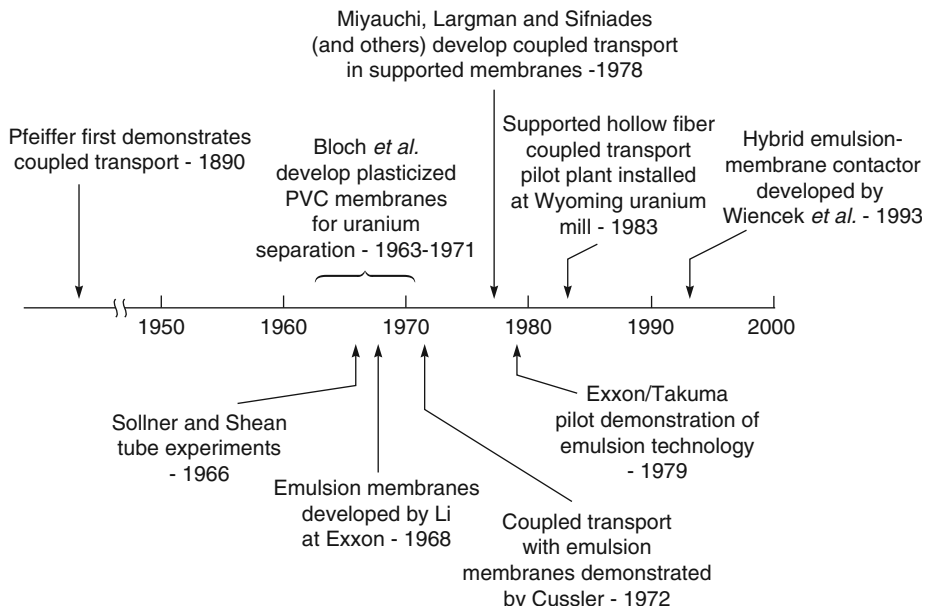
A milestone chart showing the historical development of carrier facilitated transport membranes is given in Figure 11.6. Reviews of carrier facilitated transport have been given by Ho *et al.* [18], Noble and Way [40], Krull *et al.* [41], and Figoli *et al.* [42]. Because of the differences between coupled and facilitated transport applications, these processes are described separately in the sections that follow.

11.2 Coupled Transport

11.2.1 Background

Carrier facilitated transport involves a combination of chemical reaction and diffusion. One way to model the process is to calculate the equilibrium between the various species in the membrane phase and to link them by the appropriate rate expressions to the species

Coupled Transport



Facilitated Transport

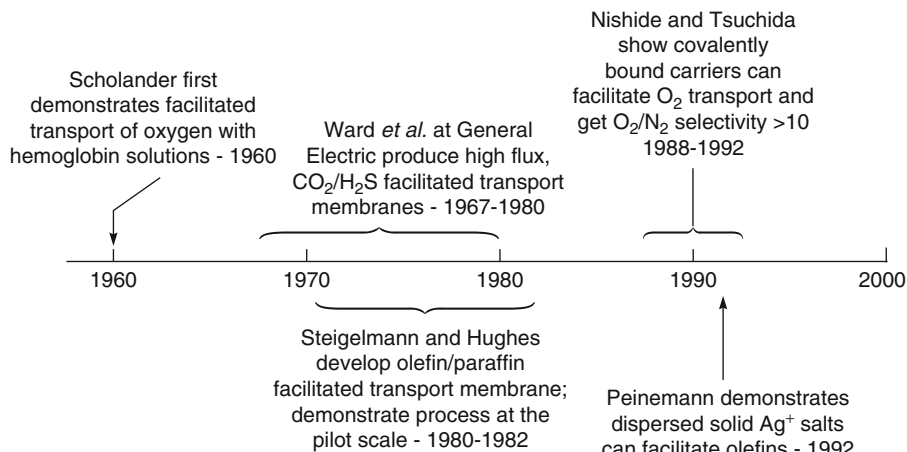
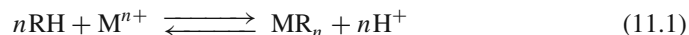


Figure 11.6 Milestones in the development of carrier facilitated transport

in adjacent feed and permeate solutions. An expression for the concentration gradient of each species across the membrane is then calculated and can be solved to give the membrane flux in terms of the diffusion coefficients, the distribution coefficients, and the rate constants for all the species involved in the process [43, 44]. Unfortunately, the resulting expressions are too complex to be widely used.

An alternative approach is to make the simplification that the rate of chemical reaction is fast compared to the rate of diffusion; that is, membrane diffusion is rate controlling. This approximation is a good one for most coupled transport processes and can be easily verified by showing that flux is inversely proportional to membrane thickness. If interfacial reaction rates were rate controlling, the flux would be constant and independent of membrane thickness. Making the assumption that chemical equilibrium is reached at the membrane interfaces allows the coupled transport process to be modeled easily [9]. The process is shown schematically in Figure 11.7, in which the reaction of the carrier (RH) with the metal (M^{n+}) and hydrogen ion (H^+) is given as



This reaction is characterized by an equilibrium constant

$$K = \frac{[MR_n][H^+]^n}{[RH]^n[M]} \quad (11.2)$$

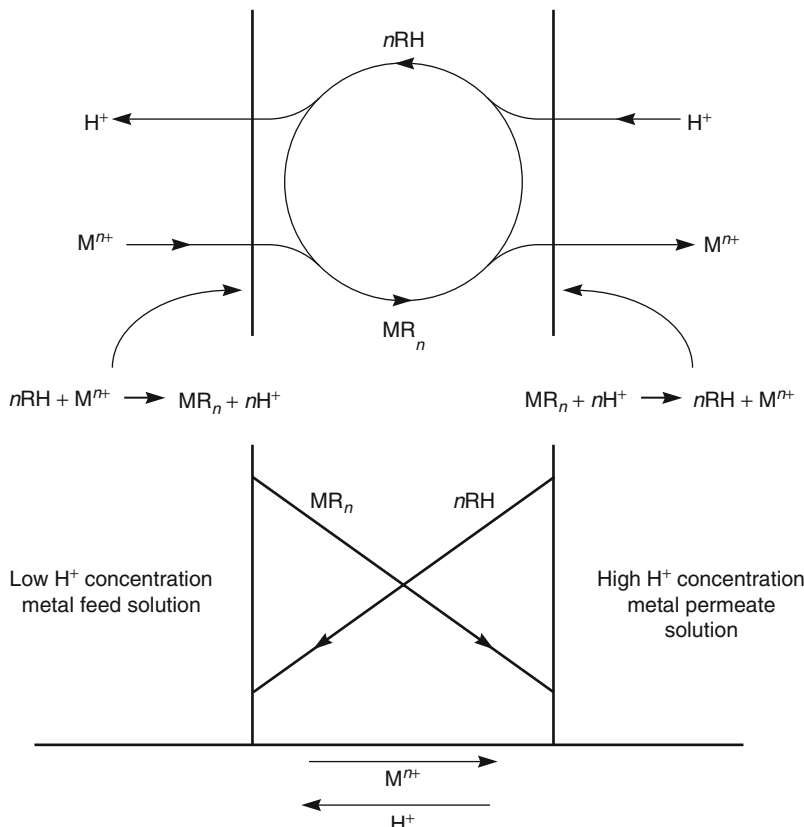


Figure 11.7 An illustration of the carrier agent concentration gradients that form in coupled transport membranes

where the terms in square brackets represent the molar concentrations of the particular chemical species. The equilibrium equation can be written for the organic phase or the aqueous phase. As in earlier chapters, the subscripts o and ℓ represent the position of the feed and permeate interfaces of the membrane. Thus the term $[\text{MR}_n]_o$ represents the molar concentration of component MR_n in the aqueous solution at the feed/membrane interface. The subscript m is used to represent the membrane phase. Thus, the term $[\text{MR}_n]_{o(m)}$ is the molar concentration of component MR_n in the membrane at the feed interface (point o).

Only $[\text{MR}_n]$ and $[\text{RH}]$ are measurable in the organic phase, where $[\text{H}]$ and $[\text{M}]$ are negligibly small. Similarly, only $[\text{H}]$ and $[\text{M}]$ are measurable in the aqueous phase, where $[\text{MR}_n]$ and $[\text{RH}]$ are negligibly small. Equation 11.2 can, therefore, be written for the feed solution interface as

$$K' = \frac{[\text{MR}_n]_{o(m)} [\text{H}]_o^n}{[\text{RH}]_{o(m)}^n [\text{M}]_o} = \frac{k_m}{k_a} \cdot K \quad (11.3)$$

where k_m and k_a are the partition coefficients of M and H between the aqueous and organic phases. This form of Equation 11.2 is preferred because all the quantities are accessible experimentally. For example, $[\text{MR}_n]_{o(m)}/[\text{M}]_o$ is easily recognizable as the distribution coefficient of metal between the organic and aqueous phases.

The same equilibrium applies at the permeate–solution interface, and Equation 11.3 can be recast to

$$K' = \frac{[\text{MR}_n]_{\ell(m)} [\text{H}]_{\ell}^n}{[\text{RH}]_{\ell(m)}^n [\text{M}]_{\ell}} \quad (11.4)$$

Consider now the situation when a counter ion concentration gradient that exactly balances the metal ion concentration gradient is established, so no flux of either ion across the membrane occurs. Under this condition, $[\text{MR}_n]_{o(m)} = [\text{MR}_n]_{\ell(m)}$ and $[\text{RH}]_{o(m)}^n = [\text{RH}]_{\ell(m)}^n$, producing the expression

$$\frac{[\text{M}]_o}{[\text{M}]_{\ell}} = \left(\frac{[\text{H}]_o}{[\text{H}]_{\ell}} \right)^n \quad (11.5)$$

Thus, the maximum concentration factor of metal ion that can be established across the membrane varies with the counter ion (hydrogen ion) concentration ratio (in the same direction) raised to the n th power, where n is the valence of the metal ion (M^{n+}).

This development, of course, says nothing about the metal ion flux across the membrane under non-equilibrium conditions; this is described by Fick's law. At steady state, the flux j_{MR_n} , in $\text{mol}/\text{cm}^2 \cdot \text{s}$, of metal complex MR_n across the liquid membrane is given by

$$j_{\text{MR}_n} = \frac{D_{\text{MR}_n} ([\text{MR}_n]_{o(m)} - [\text{MR}_n]_{\ell(m)})}{\ell} \quad (11.6)$$

where D_{MR_n} is the mean diffusion coefficient of the complex in the membrane of thickness ℓ . To put Equation 11.6 into a more useful form, the terms in $[\text{MR}_n]$ are

eliminated by introduction of Equation 11.3. This results in a complex expression involving the desired quantities $[M]$ and $[H]$, but also involving $[RH]$. However, mass balance provides the following relationship

$$n[MR_n]_{(m)} + [RH]_m = [R]_{(m)\text{tot}} \quad (11.7)$$

where $[R]_{(m)\text{tot}}$ is the total concentration of R in the membrane.

Substitution of Equations 11.3 and 11.4 into Equation 11.6 gives an expression for the metal ion flux in terms of only constants and the concentrations of metal and counter ion in the aqueous solutions on the two sides of the membrane [9]. The solution is simple only for $n = 1$, in which case

$$j_{MR_n} = \frac{D_{MR_n}}{\ell} [R]_{(m)\text{tot}} \left[\left(\frac{1}{[H]_o/[M]_o K' + 1} \right) - \left(\frac{1}{[H]_\ell/[M]_\ell K' + 1} \right) \right] \quad (11.8)$$

This equation shows the coupling effect between the metal ion $[M]$ and the hydrogen ion $[H]$ because both appear in the concentration term of the Fick's law expression linked by the equilibrium reaction constant K' . Thus, there will be a positive "uphill" flux of metal ion from the downstream to the upstream solution (that is, in the direction $\ell \rightarrow o$) as long as

$$\frac{[M]_o}{[H]_o} > \frac{[M]_\ell}{[H]_\ell} \quad (11.9)$$

When the inequality is opposite, the metal ion flux is in the conventional or "downhill" direction. The maximum concentration factor, that is, the point at which metal ion flux ceases, can be determined in terms of the hydrogen ion concentration in the two aqueous phases

$$\frac{[M]_o}{[M]_\ell} = \frac{[H]_o}{[H]_\ell} \quad (11.10)$$

This expression is identical to Equation 11.5 for the case of a monovalent metal ion.

11.2.2 Characteristics of Coupled Transport Membranes

11.2.2.1 Concentration Effects

Equations 11.1–11.10 provide a basis for rationalizing the principal features of coupled transport membranes. It follows from Equation 11.8 that coupled transport membranes can move metal ions from a dilute to a concentrated solution against the metal ion concentration gradient, provided the gradient in the second coupled ion concentration is sufficient. A typical experimental result demonstrating this unique feature of coupled transport is shown in Figure 11.8. The process is counter-transport of copper driven by hydrogen ions, as described in Equation 11.1. In this particular experiment, a pH difference of 1.5 units is maintained across the membrane. The initial product solution copper concentration is higher than the feed solution concentration. Nonetheless, copper diffuses against its concentration gradient from the feed to the product side of the membrane. The ratio of the counter hydrogen ions between the solutions on either side of the membrane

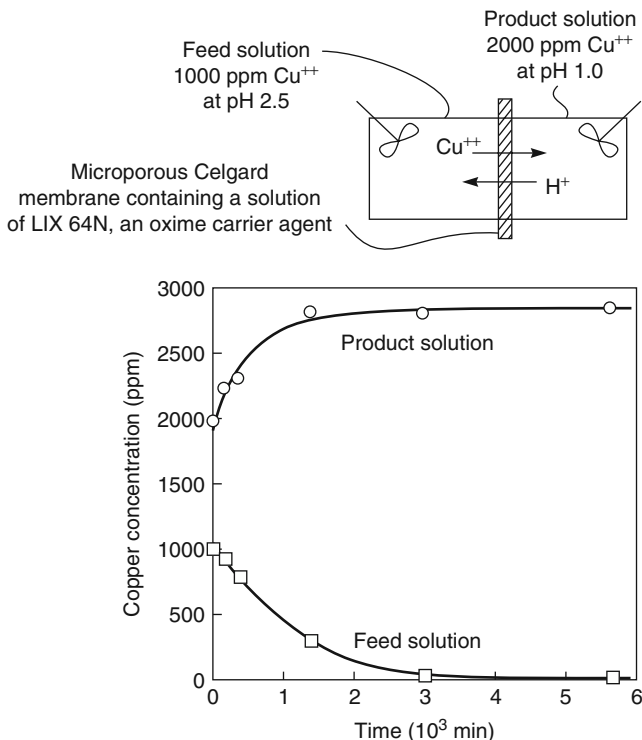


Figure 11.8 Demonstration of coupled transport. In a two-compartment cell, copper flows from the dilute (feed) solution into the concentrated (product) solution, driven by a gradient in hydrogen ion concentration [9]. Membrane, microporous Celgard 2400/LIX 64N; feed, pH 2.5; product, pH 1.0

is about 32 to 1 which, according to the appropriate form of Equation 11.5, should give a copper concentration ratio of

$$\frac{[\text{Cu}^{2+}]_e}{[\text{Cu}^{2+}]_o} = \left(\frac{[\text{H}^+]_e}{[\text{H}^+]_o} \right)^2 = (32)^2 \approx 1000 \quad (11.11)$$

In the experiment shown in Figure 11.8, this means that the feed solution copper concentration should drop to just a few parts per million, and this is the case.

A more convenient method of measuring the maximum copper concentration factor is to maintain the product solution at some high copper concentration and to allow the feed solution copper concentration to reach an easily measurable steady-state value. Figure 11.9 shows the feed copper concentration in such an experiment, in which the steady-state feed solution concentration was about 40 ppm. The feed solution was allowed to approach steady state from both directions, that is, with initial copper concentrations higher and lower than the predicted value for the given pH gradient. As Figure 11.9 shows, regardless of the starting point, the copper concentration factors measured by this method are in reasonable agreement with the predictions of Equation 11.11.

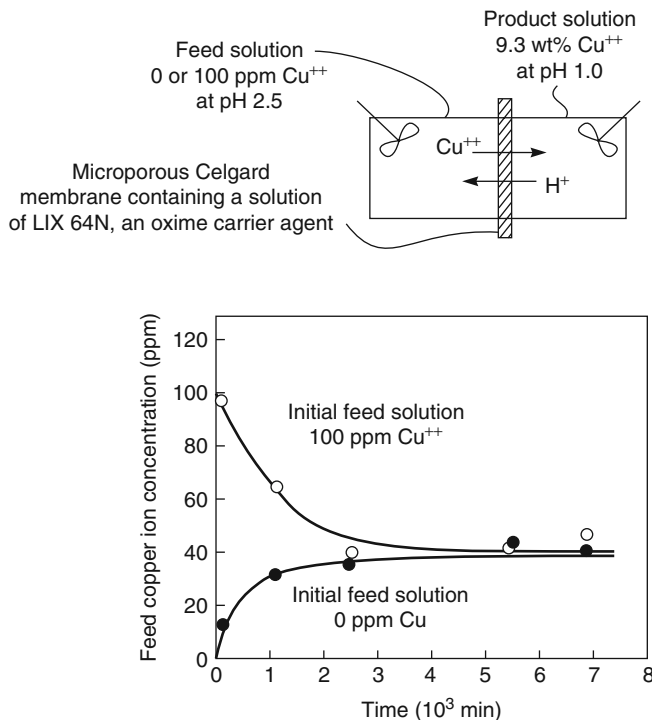


Figure 11.9 Experiments to demonstrate the maximum achievable concentration factor. Membrane, microporous Celgard 2400/LIX 64N; feed, pH 2.5, copper ion concentration, 0 or 100 ppm; product, pH 1.0, 9.3 wt% copper [9]. The concentration in the feed solution moves to a plateau value of 40 ppm, at which the copper concentration gradient across the membrane is balanced by the hydrogen ion gradient in the other direction

11.2.2.2 Feed and Product Metal Ion Concentration Effects

A second characteristic of coupled transport membranes is that the membrane flux usually increases with increasing metal concentration in the feed solution, but is usually independent of the metal concentration in the product solution. This behavior follows from the flux Equations 11.6 and 11.8. In typical coupled transport experiments, the concentration of the driving ion (H⁺) in the product solution is very high. For example, in coupled transport of copper, the driving ions are hydrogen ions, and 100 g/l sulfuric acid is often used as the product solution. As a result, on the product side of the membrane the carrier is in the protonated form, the term $[MR_n]_{\ell(m)}$ is very small compared to $[MR_n]_{o(m)}$, and Equation 11.8 reduces to

$$j_{MR_n} = \frac{D_{MR_n} [R]_{(m)\text{tot}}}{\ell} \cdot \frac{1}{[H]_o / [M]_o K' + 1} \quad (11.12)$$

The permeate solution metal ion concentration, $[M]_\ell$, does not appear in the flux equation, which means that the membrane metal ion flux is independent of the concentration of

metal on the permeate side. However, the flux does depend on the concentration of metal ions, $[M]_o$, on the feed solution side. At low values of $[M]_o$, the flux will increase linearly with $[M]_o$, but at higher concentrations the flux reaches a plateau value as the term $[H]_o/[M]_o K'$ becomes small compared to 1. At this point, all of the available carrier molecules are complexed and no further increase in transport rate across the membrane is possible. The form of this dependence is illustrated for the feed and product solution metal ion concentrations in Figure 11.10.

11.2.2.3 pH and Metal Ion Effects

It follows from flux Equation 11.12 that the concentration of the counter hydrogen ion and the equilibrium coefficient K' for a particular metal ion will affect the metal ion flux. The effect of these factors can best be understood by looking at curves of metal ion extraction versus pH. Examples are shown in Figure 11.11 for copper and other metals using the carrier LIX 64N [45]. The counter ion is hydrogen and the metal ions are extracted by reactions of the type shown in Equation 11.1.

The pH at which metal ions are extracted depends on the distribution coefficient for the particular metal and complexing agent. As a result, the pH at which the metal ions are extracted varies, as shown by the results in Figure 11.11. This behavior allows one metal to be separated from another. For example, consider the separation of copper and iron with LIX 64N. As Figure 11.11 shows, LIX 64N extracts copper at pH 1.5–2.0, but iron is not extracted until above pH 2.5. The separations obtained when 0.2% solutions of copper and iron are tested with a LIX 64N membrane at various pHs are shown in Figure 11.12. The copper flux is approximately 100 times higher than the iron flux at a feed pH of 2.5.

11.2.2.4 Carrier Agent

In the examples given in Figures 11.10–11.12 to illustrate coupled transport, the two oxime carriers used for copper were LIX 64N and Kelex 100, which have the structures

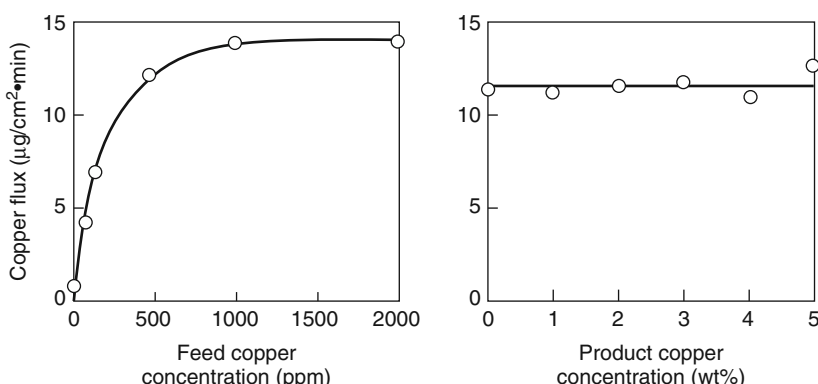


Figure 11.10 Effect of metal concentration in the feed and product solution on flux. Membrane, microporous Celgard 2400/30% Kelex 100 in Kermac 470B; feed, pH 2.5; product, 100 g/l H_2SO_4 [9]

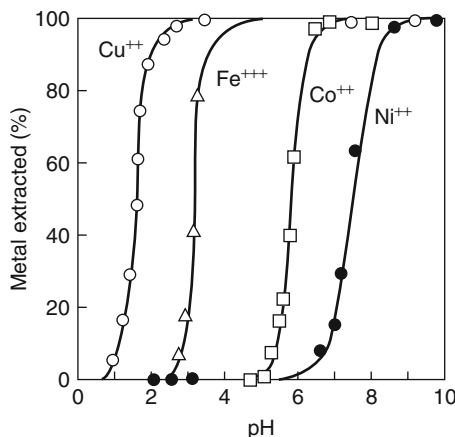


Figure 11.11 Metal extraction curves for four metal ions, using LIX 64N as a carrier agent. The aqueous phase initially contained 1000 ppm metal as the sulfate salt [45]

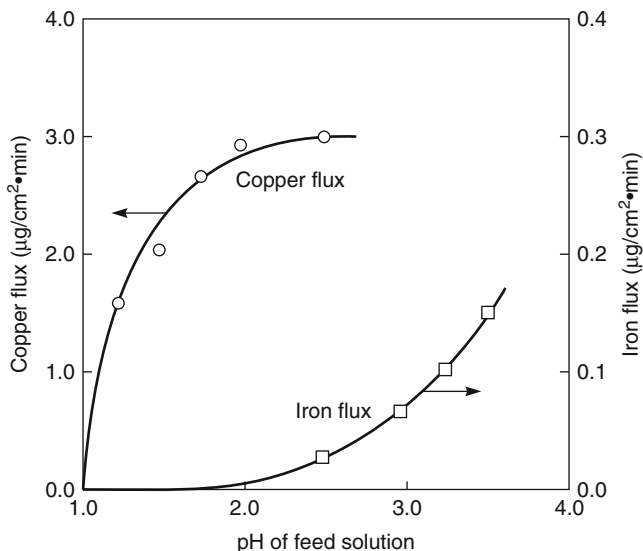


Figure 11.12 Copper and iron fluxes as a function of feed pH [9]. Membrane, Celgard 2400/LIX 64N; feed, 0.2% metal; product, pH 1.0

shown in Figure 11.13. A large number of complexing agents of all kinds with chemistries designed for specific metal ions have been reported in the literature. The tertiary amine Alamine 336 is widely used to transport anions such as $\text{UO}_2(\text{SO}_4)^{4-}$ and $\text{Cr}_2\text{O}_7^{2-}$ [46, 47]. The macrocyclic crown ether family has also been used to transport alkali and rare earth metals (see Figure 11.13) [48, 49].

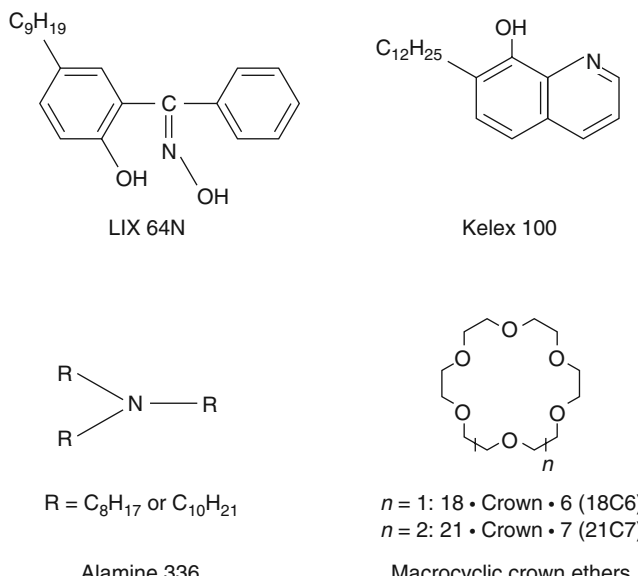


Figure 11.13 Structures of selected metal carrier agents widely used in coupled transport membranes

11.2.3 Coupled Transport Membranes

11.2.3.1 Supported Liquid Membranes

In supported liquid membranes, a microporous support impregnated with the liquid complexing agent separates the feed and product solutions. In coupled transport, the fluid on both sides of the membrane must be circulated to avoid concentration polarization, which is much more significant on the feed side than on the permeate side. In the laboratory, concentration polarization is easily avoided by using flat sheet membranes in a simple permeation cell with stirred solutions on both sides of the membrane. On a larger scale, hollow-fiber systems with the feed solution circulated down the bore of the fibers have been the most common form of membrane.

Large-scale processes require many modules to remove most of the metal from a continuous feed stream. In general, a multistage system operating in a feed-and-bleed mode is the most efficient design; a schematic representation of a three-stage system is shown in Figure 11.14 [50]. A fixed feed volume circulates through each module at a high rate to control concentration polarization. Feed solution is continuously introduced into the circulating volume of the first stage and is bled off at the same rate. The bleed from the first stage constitutes the feed for the second, and the bleed from the second stage constitutes the feed for the third. In operation, the concentration of metal in the feed solution decreases as it flows from stage 1 to stage 3, with the final raffinate concentration depending on the feed-and-bleed flow rate. The product solution flows in series through the stages. The advantage of this multistage design over a single-stage system is that only the final stage operates on feed solution depleted of metal.

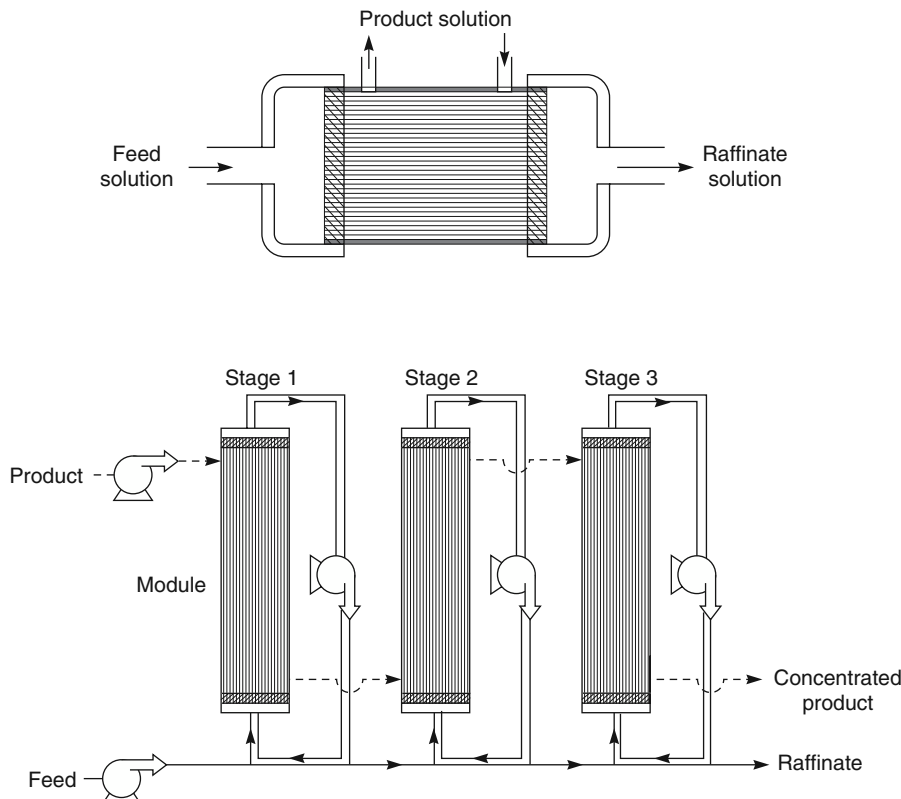


Figure 11.14 Schematic of a three-stage feed-and-bleed hollow-fiber coupled transport concentrator [50]

Liquid membranes supported by hollow fibers are relatively easy to make and operate, and the membrane fluxes are often sufficient to make the process economically feasible for some separations. For example, a flux of $10\text{--}40 \mu\text{g}/\text{cm}^2\cdot\text{min}$ corresponds to $50\text{--}200 \text{ kg}/\text{m}^2\cdot\text{year}$. However, membrane stability is a major problem. The variation in coupled transport flux during long-term tests is illustrated in Figure 11.15 [50]. The detailed mechanism for this flux instability is not completely established, but appears to be related to loss of the organic complexing agent phase from the support membrane [50–54]. Although the membrane flux of this immobilized liquid film membrane could be restored to the original value by reloading the membrane with fresh complexing agent, this is not practical in a commercial system. The stability of membranes in which the carrier is immobilized in a polymeric or gel matrix is better than when the carrier is in a liquid held by capillary action in a microporous membrane. Nonetheless, even these polymer/gel membranes are not sufficiently stable for industrial use.

11.2.3.2 Emulsion Liquid Membranes

A form of liquid membrane that received a great deal of attention in the 1970s and 1980s was the bubble or emulsion membrane, first developed by Li at Exxon [11–13].

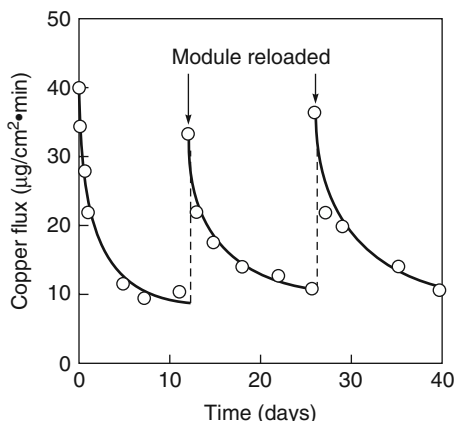


Figure 11.15 The effect of replenishing a hollow fiber coupled transport module with fresh complexing agent. Membrane, polysulfone hollow-fiber/Kelex 100 carrier; feed, 0.2% copper, pH 2.5; product, 2% copper, 100 g/l H_2SO_4 [50]

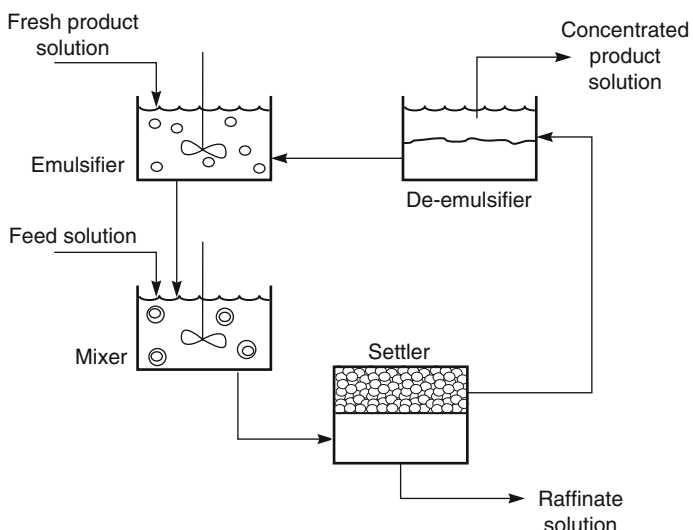


Figure 11.16 Flow diagram of a liquid emulsion membrane separation process

Figure 11.16 is a schematic illustration of an emulsion liquid membrane process, which comprises four main operations. First, fresh product solution is emulsified in the liquid organic membrane phase. This water/oil emulsion then enters a second large mixer vessel, where it is again emulsified into the feed solution to form a water/oil/water emulsion. Metal ions in the feed solution permeate by coupled transport through the walls of the emulsion to the product solution. The mixture then passes to a settler tank where the oil droplets separate from the metal-depleted raffinate solution. A single mixer/settler step

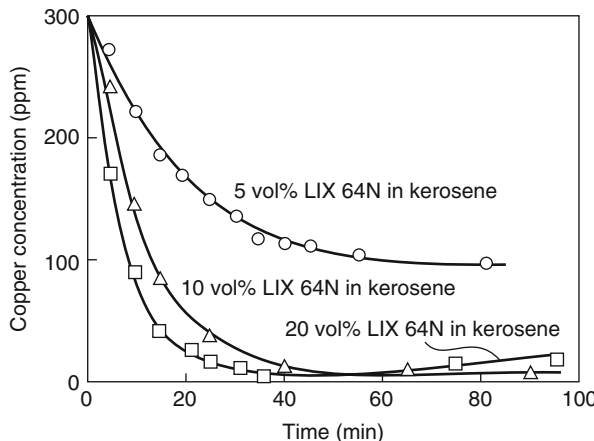


Figure 11.17 Copper extraction by a liquid emulsion membrane process. Feed, 200 ml, pH 2.0, 300 ppm Cu²⁺; membrane, 15 ml LIX 64N in kerosene, 3% Span 80; stripping solution, 15 ml H₂SO₄. Reprinted with permission from [55]. Copyright (1980) Elsevier.

is shown in Figure 11.16, but in practice a series of mixer/settlers may be used to extract the metal completely. The emulsion concentrate then passes to a de-emulsifier where the emulsion is broken and the organic and concentrated product solutions are separated. The regenerated organic solution is recycled to the first emulsifier.

The optimum operating conditions for this type of process vary a great deal. The first water/oil emulsion is typically an approximately 50/50 mixture, which is then mixed with the aqueous feed solution phase at a ratio of 1 part emulsion phase to 5–20 parts feed solution phase. Typical extraction curves for copper using LIX 64N as the carrier agent are shown in Figure 11.17. The extraction rate generally follows a first-order expression [55]. The slope of the curve in Figure 11.17 is proportional to the loading of complexing agent in the organic phase and the rate of agitation in the mixer vessel.

Figure 11.17 also illustrates one of the problems of emulsion membrane systems, namely, degradation of the emulsion, which can result from either prolonged contact with the feed solution and high-speed mixing of the product and feed solutions. Prolonged stirring of the emulsion with the feed solution causes the copper concentration to rise as some of the emulsion droplets break. Careful tailoring of the stirring rate and surfactant composition is required to minimize premature emulsion breakdown [24].

Although emulsion degradation must be avoided in the mixer and settler tanks, complete and rapid breakdown is required in the de-emulsifier in which the product solution is separated from the organic complexing agent. Currently, electrostatic coalescers seem to be the best method of breaking these emulsions. Even then, some of the organic phase is lost with the feed raffinate.

One solution to the membrane stability problem is to use the hybrid emulsion–membrane contactor described earlier and illustrated in Figure 11.5. A larger inventory of the carrier agent is required, but any reagent lost to the feed solutions can be easily replaced, so the membrane stability problem is largely circumvented [22, 23, 25].

11.2.4 Applications

The best application of coupled transport is removal and recovery of metals from large, dilute feed solutions such as contaminated ground water or dilute hydrometallurgical process streams. Treatment of such streams by chemical precipitation, conventional solvent extraction with liquid ion exchange reagents, or extraction with ion exchange resins is often uneconomical. The ability of coupled transport to treat large-volume, dilute streams with relatively small amounts of the expensive carrier agent is an advantage.

The application that has received the most attention is the recovery of copper from dilute hydrometallurgical process streams. Such streams are produced by extraction of low-grade copper ores with dilute sulfuric acid. Typically, the leach stream contains 500–5000 ppm copper and various amounts of other metal ions, principally iron. Currently, copper is removed from these streams by precipitation with iron or by solvent extraction. A scheme for recovering the copper by coupled transport is shown in Figure 11.18. The dilute copper solution from the dump leach stream forms the feed solution; concentrated sulfuric acid from the electrowinning operation forms the product solution. Copper from the feed solution permeates the membrane, producing an acidic raffinate solution containing 50–100 ppm copper, which is returned to the dump. The product solution, which contains 2–5% copper, is sent to the electrowinning tankhouse. Many papers have described this application of coupled transport with supported [9, 50] and emulsion [13, 55] membranes. Membrane stability is still a major problem and,

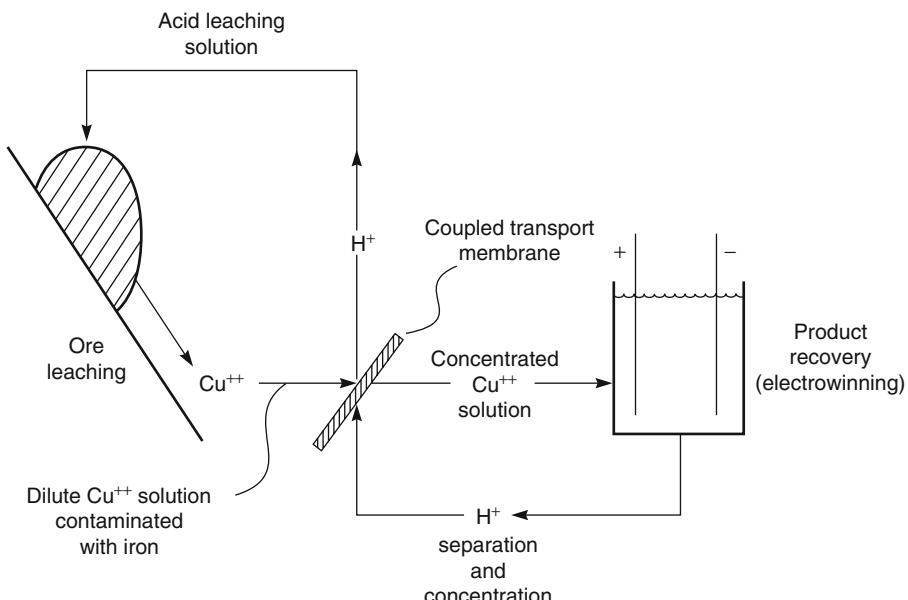


Figure 11.18 Schematic of copper recovery by coupled transport from dump leach streams. The concentrated copper solution produced by coupled transport separation of the dump leach liquid is sent to an electrolysis cell where copper sulfate is electrolyzed to copper metal and sulfuric acid

although the economics appeared promising, the advantages have not proven sufficient to encourage industrial adoption of the process.

11.3 Facilitated Transport

11.3.1 Background

The transport equations used for facilitated transport parallel those derived for coupled transport [33]. The major difference is that only one species is transported across the membrane by the carrier. The carrier–species equilibrium in the membrane is



where R is the carrier, A is the permeant transported by the carrier and RA is the permeant–carrier complex. Examples of reactions used in facilitated transport processes are shown in Table 11.1.

Table 11.1 Facilitated transport carrier reactions

CO ₂	CO ₂ + H ₂ O + Na ₂ CO ₃ ⇌ 2NaHCO ₃
O ₂	O ₂ + CoSchiffs base ⇌ CoSchiffs base (O ₂)
SO ₂	SO ₂ + H ₂ O + Na ₂ SO ₃ ⇌ 2NaHSO ₃
H ₂ S	H ₂ S + Na ₂ CO ₃ ⇌ NaHS + NaHCO ₃
CO	CO + CuCl ₂ ⇌ CuCl ₂ (CO)
C ₂ H ₄	C ₂ H ₄ + AgNO ₃ ⇌ AgNO ₃ (C ₂ H ₄)

As with coupled transport, two assumptions are made to simplify the treatment: first, that the rate of chemical reaction is fast compared to the rate of diffusion across the membrane, and second, that the amount of material transported by carrier facilitated transport is much larger than that transported by normal passive diffusion, which is ignored. The facilitated transport process can then be represented schematically as shown in Figure 11.19.

The carrier–permeate reaction within the membrane is described by the equilibrium constant

$$K = \frac{[RA]_{(m)}}{[R]_{(m)} [A]_{(m)}} \quad (11.14)$$

The concentration of permeant, [A]_(m), within the membrane phase can be linked to the concentration (pressure) of permeant A in the adjacent gas phase, [A], by the Henry's law expression

$$[A]_{(m)} = k [A] \quad (11.15)$$

Hence Equation 11.14 can be written

$$\frac{[RA]_{(m)}}{[R]_{(m)} [A]} = K \cdot k = K' \quad (11.16)$$

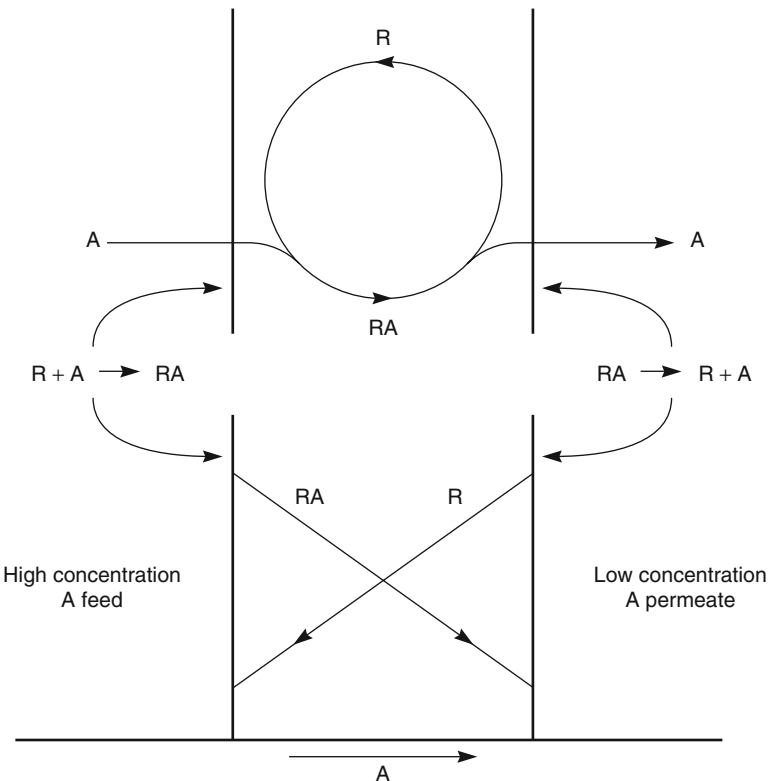


Figure 11.19 Illustration of the facilitated transport process

The components $[R]_{(m)}$ and $[RA]_{(m)}$ can be linked by a simple mass balance expression to the total concentration of carrier $[R]_{(m)\text{tot}}$ within the membrane phase, so Equation 11.16 can be rearranged to

$$[RA]_{(m)} = \frac{[R]_{(m)\text{tot}}}{1 + 1/[A]K'} \quad (11.17)$$

Equation 11.17 shows the fraction of the carrier that reacts to form a carrier complex. At very large values of the term $[A]K'$, all the carrier is complexed, and $[RA]_{(m)} \rightarrow [R]_{(m)\text{tot}}$. At low values, $[A]K' \rightarrow 0$ and none of the carrier is complexed ($[RA]_{(m)} \rightarrow 0$). Equation 11.17 allows the concentration of the carrier-permeant complex at each side of membrane to be calculated in terms of the equilibrium constant between the carrier and the permeant, and the concentration (pressure) of the permeant in the adjacent feed and permeant fluids. Transport through the membrane can then be calculated using Fick's law. The flux, j_{RA} , of RA through the membrane is given by

$$j_{RA} = \frac{D_{RA}([RA]_{o(m)} - [RA]_{\ell(m)})}{\ell} \quad (11.18)$$

Substituting Equation 11.17 into Equation 11.18 yields

$$j_{RA} = \frac{D_{RA}[RA]_{(m)tot}}{\ell} \left[\frac{1}{1 + 1/[A]_o K'} - \frac{1}{1 + 1/[A]_\ell K'} \right] \quad (11.19)$$

To illustrate the dependence of the membrane flux, j_{RA} , on the equilibrium constant K' and the pressure gradient across the membrane, the permeant pressure [A] can be set to zero, that is, $[A]_\ell \approx 0$, and Equation 11.19 becomes

$$j_{RA} = \frac{D_{RA}[R]_{(m)tot}}{\ell} \left(\frac{1}{1 + 1/[A]_o K'} \right) \quad (11.20)$$

This expression is plotted in Figure 11.20 as flux as a function of feed pressure for different values of the equilibrium constant, K' . In this example, at an equilibrium constant K' of 0.01 atm^{-1} , very little of carrier R reacts with permeant A even at a feed pressure of 10 atm, so the flux is low. As the equilibrium constant increases, the fraction of carrier reacting with permeant at the feed side of the membrane increases, so the flux increases. This result would suggest that, to achieve the maximum flux, a carrier with the highest possible equilibrium constant should be used. For example, the calculations illustrated in Figure 11.20 indicate a carrier with an equilibrium constant of 10 atm^{-1} or more will provide maximum flux.

The calculations illustrated in Figure 11.20 assume that a hard vacuum is maintained on the permeate side of the membrane. The operating and capital costs of vacuum and compression equipment prohibit these conditions in practical systems. More realistically,

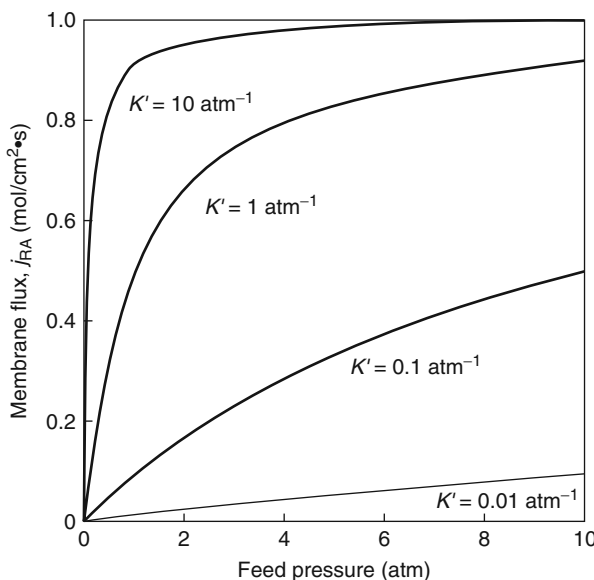


Figure 11.20 Flux through a facilitated transport membrane calculated using Equation 11.20 and setting $[A]_\ell \approx 0$ and $D_{RA}[R]_{(m)tot}/\ell \approx 1$

a carrier facilitated process would be operated either with a compressed gas feed and atmospheric pressure on the permeate side of the membrane, or with an ambient pressure feed gas and a vacuum of about 0.1 atm on the permeate side. By substitution of specific values for the feed and permeate pressures into Equation 11.19, the optimum values of the equilibrium constant can be calculated. A plot illustrating this calculation for compression and vacuum operation is shown in Figure 11.21.

Under the assumptions of this calculation, the optimum equilibrium constant is 0.3 atm^{-1} for compression operation (feed pressure, 10 atm; permeate pressure, 1 atm), and 3 atm^{-1} for vacuum operation (feed pressure, 1 atm; permeate pressure, 0.1 atm). The results show that rather precise control of the equilibrium constant is required to achieve a useful facilitated transport process. In this example calculation, although carriers with equilibrium constants lower than 0.3 atm^{-1} or greater than 3 atm^{-1} can transport the permeant across the membrane, obtaining the maximum flux for the process would require operation at feed and permeate pressures likely to make the process uneconomical. This issue is usually ignored in much of the academic literature. Very commonly, the permeate pressure is maintained as a hard vacuum and the feed pressure is set at 2–3 bar, usually far from the practical application conditions. For this reason, much of the published membrane performance data has to be treated with caution.

11.3.2 Process Designs

Until quite recently, most of the facilitated transport results reported in the literature were obtained with supported liquid membranes held in microporous films by capillarity.

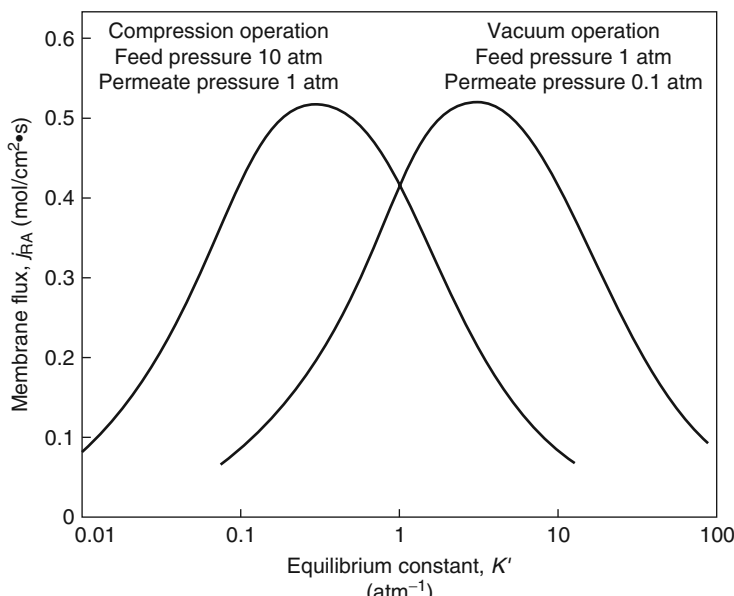


Figure 11.21 Illustration of the effect of feed and permeate pressure on the optimum carrier equilibrium constant, $D_{RA}[R]_{(m)\text{tot}}/\ell \approx 1$. Vacuum operation: feed pressure 1 atm, permeate pressure 0.1 atm; compression operation: feed pressure 10 atm, permeate pressure 1 atm

The instability of these membranes has inhibited commercial application of the process. Three factors contribute to this instability and the consequent loss of membrane performance over time:

1. Evaporation of the solvent used to prepare the liquid membrane, leading to membrane failure.
2. Expulsion of liquid held by capillarity within the microporous membrane pores. The membrane must always be operated well below the average bubble point of the membrane, because liquid expulsion from even a few larger-than-average pores can cause unacceptable leakage of gas.
3. Chemical degradation of the carrier agent by the permeant gas or by minor components such as water, carbon dioxide, or hydrogen sulfide in the feed gas.

Significant progress has been made in alleviating the first two physical causes of membrane instability. The magnitude of the long-term chemical stability problem depends on the separation being conducted. It is a major issue for carriers used to transport oxygen and olefins, but for carriers used to transport carbon dioxide, chemical stability is less of a problem. For this reason, if facilitated transport membranes ever reach the industrial scale, separation of carbon dioxide from other gases may be the first application.

Several techniques can minimize the pressure difference across supported liquid membranes, in order to improve mechanical membrane stability. In the laboratory, flow of an inert sweep gas such as helium on the permeate side can be used to maintain low partial pressure of the permeating component, while the hydrostatic pressure is about equal to that of the feed. A variation on this approach, proposed by Ward [29, 30], is to use a condensable sweep gas such as steam. The permeate/steam mixture is cooled and condensed, separating the permeate gas from the condensed water, which is then sent to a boiler to regenerate the steam [31, 32]. A simplified flow scheme of this process is shown in Figure 11.22a. An alternative approach is to sweep the permeate side of the membrane with an absorbent liquid in which the permeate gas dissolves. Hughes *et al.* [33], for example, used liquid hexane to sweep the permeate side of their propylene/propane separating membrane, as illustrated in Figure 11.22b. The hexane/propylene permeate mixture leaving the membrane separator is sent to a small distillation column to recover the hexane liquid and a concentrated propylene gas stream. The stripped hexane is then recycled to the permeate side of the membrane.

Both techniques shown in Figure 11.22 increase the complexity of the separation process significantly, and neither has advanced to a commercial process. The focus of much of the recent work on facilitated transport has been to produce membranes that are inherently stable and can be used in conventional gas separation systems. Krull *et al.* have reviewed this work [41].

One approach used with ionic carriers is to impregnate ion exchange membranes with the carrier feed solution. Ion exchange sites in the membrane are ion-paired to the facilitated transport carrier [56, 57]. The membrane is swollen with a solvent – usually water but sometimes glycerol – so that the carrier ions have some mobility. These membranes are, in effect, swollen polymeric gels, so the problem of carrier fluid displacement from the membrane pores if the bubble pressure is exceeded does not occur. Evaporation of the solvent remains a problem, and addition of solvent vapor to the feed gas is generally required.

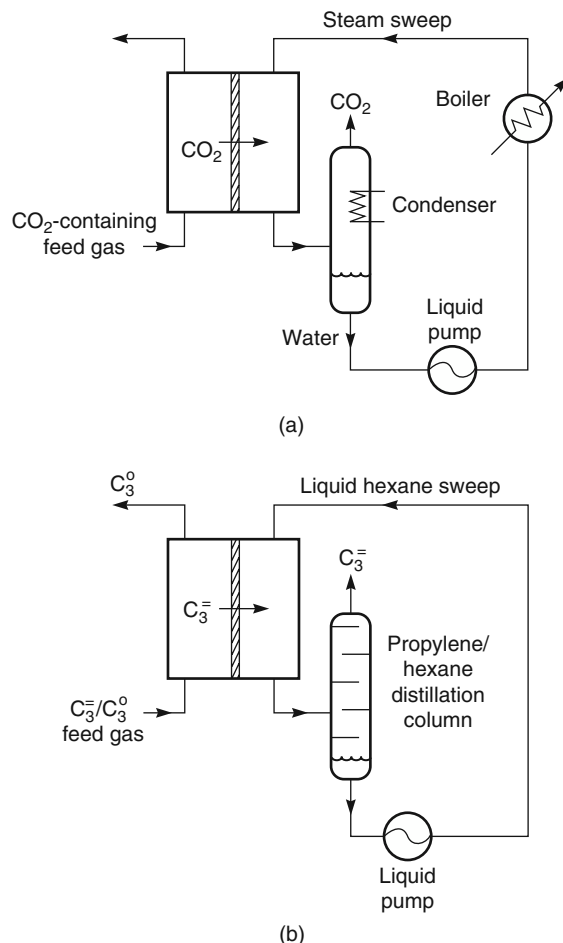


Figure 11.22 Flow schematics of (a) a steam sweep configuration used in the facilitated transport of carbon dioxide [31, 32] and (b) a liquid hexane sweep used in the transport of propylene [33]

Another method of solving the solvent evaporation problem (devised by Pez, Laciak, and others [58–61] at Air Products) uses carriers in the form of organic salts that become liquids (molten salts) at ambient temperatures. Examples of such salts are:

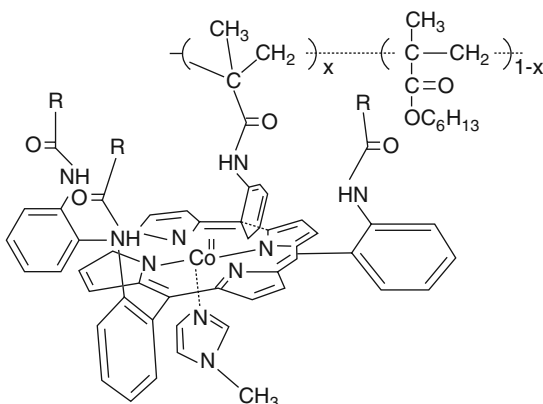
- triethyl ammonium chlorocuprate ($C_2H_5)_3NHCuCl_2$, a carrier for carbon monoxide;
- tetrahexyl ammonium benzoate ($C_6H_{13})_4N^+C_6H_5CO_2^-$, a carrier for carbon dioxide;
- tetrahexyl ammonium fluoride tetrahydrate ($C_6H_{13})_4NF \cdot 4H_2O$, a carrier for carbon dioxide.

Under the membrane test conditions, these carrier salts are liquids with essentially no vapor pressure, so the solvent evaporation problem is eliminated.

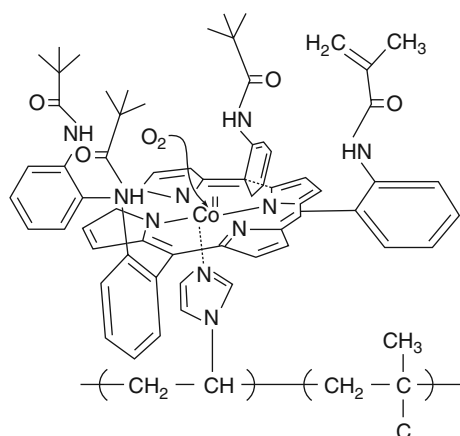
Yet another approach to stabilizing facilitated transport membranes is to form multilayer structures in which the supported liquid-selective membrane is encapsulated

between thin layers of very permeable but nonselective dense polymer layers. The coating layers must be very permeable to avoid reducing the gas flux through the membrane; materials such as silicone rubber or poly(trimethylsiloxane) are usually used [32].

Despite many years of effort, none of these methods of stabilizing liquid membranes has had real success. For this reason, a number of workers are trying to develop solid or polymer-bound carrier facilitated membranes. Several approaches are being tried. One of the most promising is covalent linking of the carrier complex to the matrix polymer. This approach was first tried by Nishide and coworkers at Wasada University [36]. A porphyrin oxygen carrier group was chemically bound to the polymer backbone, as shown in Figure 11.23. The resulting material was then used to form a dense polymer



(a) An oxygen carrier chemically bonded to the polymer backbone



(b) An oxygen carrier chemically bonded to the polymer backbone through a donor base

Figure 11.23 Methods of forming bound oxygen carriers used by Nishide et al. [36]. (a) An oxygen carrier chemically bonded to the polymer backbone and (b) an oxygen carrier chemically bonded to the polymer backbone through a donor base

film containing no solvent. Unfortunately, the fluxes and oxygen/nitrogen selectivities of the membranes produced were only moderate.

More recently, this same approach has been tried with amine-containing groups, which are potential carriers for carbon dioxide [25, 62, 63]. This work has been more successful. Membranes with very high carbon dioxide/nitrogen and carbon dioxide/hydrogen selectivities have been made with good carbon dioxide permeabilities. However, the results reported are often obtained under operating conditions far from that expected in real applications (for example, a hard vacuum on the permeate and a low feed pressure). Some tailoring of the equilibrium binding constant between carbon dioxide and the carrier is required, as described in the text relating to Figures 11.20 and 11.21.

Another approach to producing stable membranes is to make membranes in which the polymer matrix acts as a partial solvent for the carrier. For example, poly(ethylene oxide) or ethylene oxide copolymers can dissolve covalent salts such as silver tetrafluoroborate (AgBF_4), a facilitated transport carrier for olefins [37–39, 64–66]. Significant facilitation of some gases has been achieved with these membranes, but stability remains a problem.

Solid matrix membranes often show clear evidence of a percolation threshold. At low carrier loadings, little or no facilitation is observed, but as the carrier loading is increased, a certain critical loading is reached at which facilitation occurs [65, 67]. Some results illustrating this effect are shown in Figure 11.24. At loadings below 70 wt% AgBF_4 , essentially no facilitation is seen; at loadings greater than this threshold value, facilitation occurs. It is believed that the percolation threshold level is the point at which carrier sites are close enough that the permeating complex molecule can hop from carrier site to carrier site through the membrane.

The third approach to obtaining stable membranes uses membrane contactors in series, as illustrated in Figure 11.4. Good separations have been obtained with ethylene/ethane mixtures and silver nitrate carrier solutions [19, 68, 69]. However, this work has yet to move out of the laboratory.

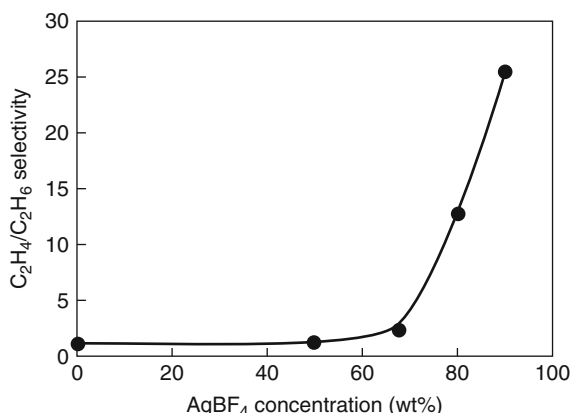


Figure 11.24 Mixed gas ethylene/ethane selectivity of a solid polymer electrolyte membrane as a function of AgBF_4 concentration in a polyamide-polyether matrix. Reprinted with permission from [32]. Copyright (1977) American Chemical Society.

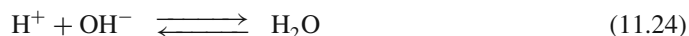
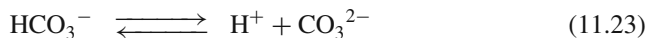
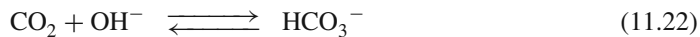
11.3.3 Applications

Over the last 40 years, a variety of facilitated transport carriers have been studied for a number of important separation problems, reviewed briefly below.

11.3.3.1 Carbon Dioxide/Hydrogen Sulfide Separation

From the late 1960s to the early 1980s, Ward and others at General Electric studied facilitated transport membranes, particularly for separation of the acid gases carbon dioxide and hydrogen sulfide from methane and hydrogen [29–32]. This work was finally abandoned after the development of selective polymeric membranes for this separation in the 1980s. In the last few years, interest in the process has been picked up again, mostly aimed at CO_2/CH_4 and CO_2/N_2 separations [25, 62, 63].

Although many carriers are available for carbon dioxide and hydrogen sulfide transport, one of the most studied chemistries uses aqueous carbonate/bicarbonate solutions. Four principal reactions occur in the film



Equations 11.21 and 11.22 are measurably slow reactions; Reactions 11.23 and 11.24 are essentially instantaneous. All four reactions determine the equilibrium concentrations, but the process can be illustrated in simple form by Figure 11.25 [31].

At the feed side of the membrane, carbon dioxide dissolves in the aqueous carbonate/bicarbonate solution and reacts with water and carbonate ions according to

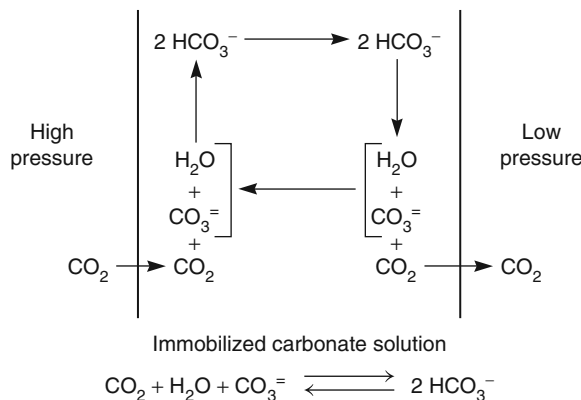
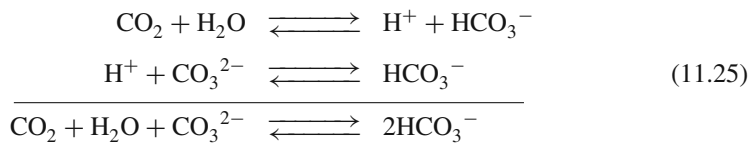


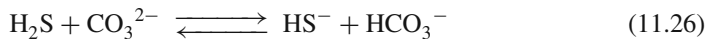
Figure 11.25 Facilitated transport of carbon dioxide through an immobilized carbonate/bicarbonate solution. Reprinted with permission from [31]. Copyright (1979) Taylor and Francis.

Equations 11.21 and 11.23.



At the permeate side of the membrane the reaction is reversed, and bicarbonate ions form carbon dioxide, water, and carbonate ions.

Coupled transport of hydrogen sulfide through the same carbonate/bicarbonate membrane is shown in Figure 11.26 [32]. The overall reaction is simple



but, again, a number of reactions occur simultaneously to establish the equilibrium concentrations.

Because some of the reactions involved in establishing equilibrium at the membrane surface are slow compared to diffusion, the calculated concentration gradients formed in the liquid membrane do not have a simple form. The equations for partial reaction rate control have been derived by Ward and Robb [29].

The transport rates of carbon dioxide and hydrogen sulfide through these carbonate membranes can be significantly increased by adding catalysts to increase the rates of the slow reactions of Equations 11.21 and 11.22. A variety of materials can be used, but the anions of the weak acids such as arsenite, selenite, and hypochlorite have been found to be the most effective. Small concentrations of these components increase permeation rates three- to five-fold.

Membranes selective to carbon dioxide and hydrogen sulfide have been considered for removal of these gases from natural gas and various synthetic gas streams. Again,

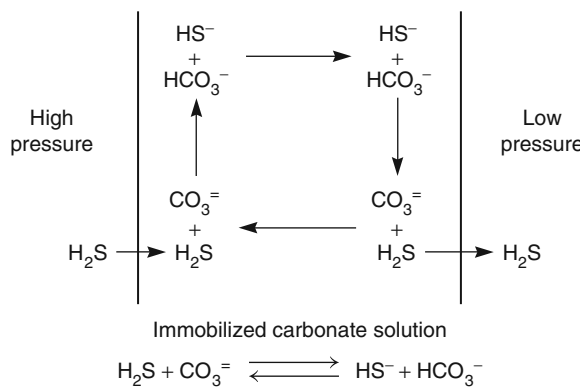


Figure 11.26 Facilitated transport of hydrogen sulfide through an immobilized carbonate/bicarbonate solution. Reprinted with permission from [32]. Copyright (1977) American Chemical Society.

the main problem has been instability of available supported liquid membranes under the typical pressure gradients of 10 to 30 bar. Because the membranes are generally more permeable to hydrogen sulfide than to carbon dioxide, their use to selectively remove hydrogen sulfide from streams contaminated with both gases has also been studied.

In the last few years, the need to develop high selectivity, high permeance membranes to separate carbon dioxide from nitrogen for sequestration has led to the development of polymeric carrier membranes [25, 62, 63]. This application is still under development, but may become the first place where facilitated transport membranes are used on an industrial scale.

11.3.3.2 Olefin Separation

Concurrently with the early work on carbon dioxide and hydrogen sulfide facilitated transport at General Electric, Steigelmann and Hughes [33] and others at Standard Oil were developing facilitated transport membranes for olefin separations. The principal target was the separation of ethylene/ethane and propylene/propane mixtures. Both separations are performed on a massive scale by distillation, but the differences in the relative volatilities of the olefins and paraffins are so small that large columns with up to 200 trays are required. In the facilitated transport process, concentrated aqueous silver salt solutions, held in microporous cellulose acetate flat sheets or hollow fibers, were used as the carrier.

Silver ions react readily with olefins, forming a silver–olefin complex according to the reaction:



Hughes and Steigelmann used silver nitrate solutions mainly because of the low cost and relatively good stability compared to other silver salts. Silver tetrafluoroborate (AgBF_4) has been used by others. The absorption isotherm of ethylene obtained with a 4 M silver nitrate solution equilibrated with ethylene is shown in Figure 11.27 [32]. The propylene isotherm is reported to be very similar. Based on these data, silver salt membranes are best used with pressurized ethylene feed streams; pressures of 3–6 atm are generally used. The Standard Oil work was continued for a number of years and was taken to the pilot plant stage using hollow fiber modules containing almost 40 m^2 membrane area. Some typical data are shown in Figure 11.28 [33]. In these experiments, the feed pressure was maintained at 5–13 atm, with liquid hexane circulated on the permeate side of the fibers to remove the permeating olefin. In laboratory tests, propylene/propane selectivities of more than 100 were obtained routinely; in the large pilot system, the initial selectivity was not quite as high, but was still very good. Unfortunately, the selectivity and flux deteriorated over a period of a few weeks, partly due to loss of water from the fibers, which could not be prevented even when the feed gas was humidified. Periodic regeneration by pumping fresh silver nitrate solution through the fibers partially restored their properties. However, this technique is not practical in an industrial plant. These instability problems caused Standard Oil to halt the program, which remains the largest facilitated transport trial to date.

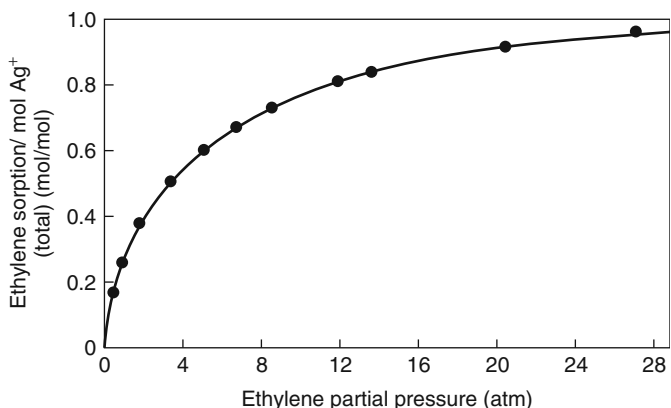


Figure 11.27 Solubility of ethylene in a 4 M silver nitrate solution. Reprinted with permission from [32]. Copyright (1977) American Chemical Society.

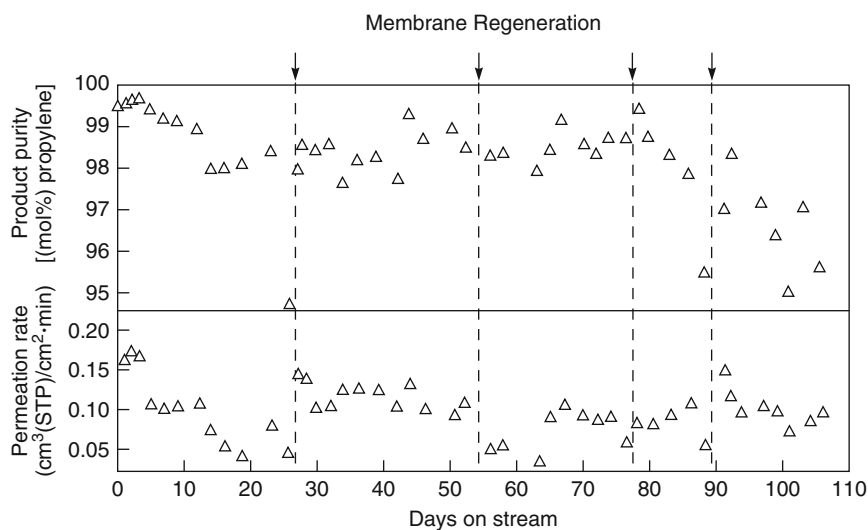


Figure 11.28 Performance of a 37 m² hollow fiber silver-nitrate-impregnated facilitated transport membrane for the separation of propylene/propane mixtures. The feed pressure was 5–13 atm; the permeate was a hexane liquid sweep stream. The vertical dotted lines show when the membrane was regenerated with fresh silver nitrate solution. Reprinted with permission from [33]. Copyright (1986) Taylor & Francis.

The best hope for olefin/paraffin facilitated membrane separations seems to be the solid polymer electrolyte membranes or the membrane contactor approach discussed earlier, the results of which were shown in Figure 11.24. If stable membranes with these properties can be produced on an industrial scale, significant applications could develop in treating gases from steam crackers that manufacture ethylene and from polyolefin plants.

11.3.3.3 Oxygen/Nitrogen Separations

The first demonstration of facilitated transport of oxygen was performed by Scholander [28] using thin films of cellulose acetate impregnated with aqueous hemoglobin solutions. Later Bassett and Schultz [70] demonstrated the process with cobalt dihistidine, a synthetic carrier. The enhancements obtained in these experiments were low, but Johnson and others [71] demonstrated very large enhancements using a series of cobalt-based metal chelate carriers. The chemical structures of two typical cobalt Schiffs-base carriers of the type used in this study and in most later work are shown in Figure 11.29. All of these compounds have a central cobalt(II) ion with four coordinating atoms in a planar array. The oxygen molecule coordinates with the cobalt ion from one side of the plane while another coordinating atom, usually a nitrogen group, acts as an electron-donating axial base. In compound I, referred to as Co(3-MeOsaltmen), the coordinating base is usually an imidazole or pyridine group, which must be present for oxygen complexation to occur. In compound II, referred to as Co(SalPr), the coordinating base group is provided by a donor nitrogen atom that is part of the structure.

With Schiff's-base carriers, a high degree of facilitation can be achieved. Some data from Johnson's work, plotted on the Robeson plot [72] for conventional polymeric oxygen/nitrogen separating membranes described in Chapter 8, are shown in Figure 11.30. This figure shows the promise of facilitated transport membranes and why, even after many failures, interest in this topic has not waned. If stable, thin membranes with these permeabilities and selectivities could be made, major reductions in the cost of membrane-produced oxygen and nitrogen – the second and third largest volume industrial chemicals – would result.

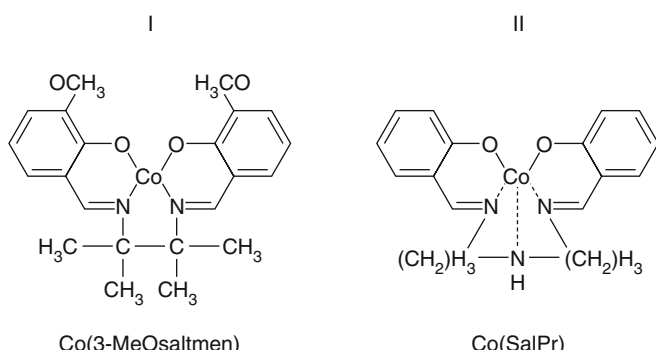


Figure 11.29 Examples of cobalt Schiffs-base agents used as facilitated transport oxygen carriers [71].

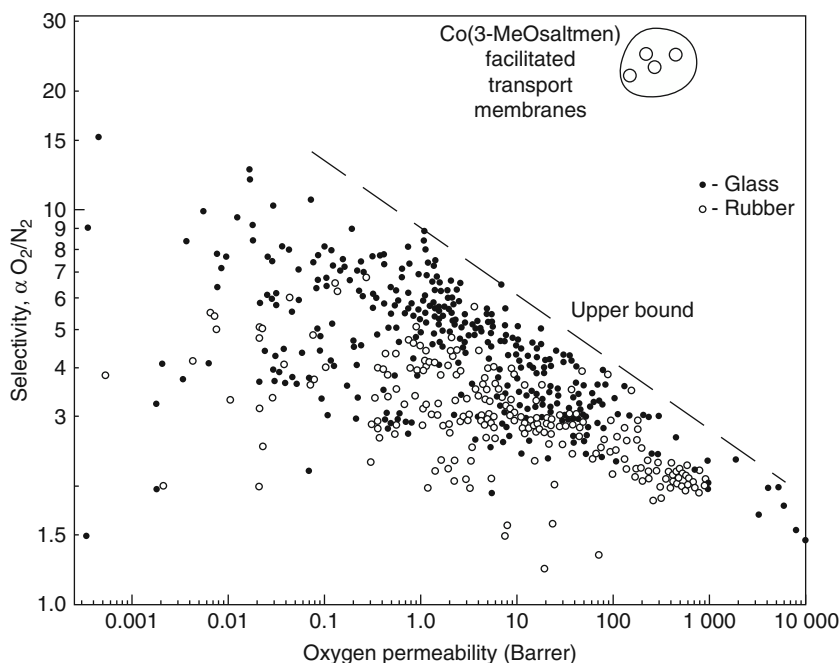


Figure 11.30 A Robeson plot of oxygen/nitrogen selectivity plotted against oxygen permeability for polymeric membranes [72] and Co(3-MeOsaltmen)-based facilitated transport membranes [71]

11.4 Conclusions and Future Directions

Carrier facilitated transport membranes have been the subject of serious study for more than 40 years, but no commercial process has resulted. These membranes are a popular topic with academic researchers, because spectacular separations can be achieved with simple laboratory equipment. Unfortunately, converting these laboratory results into practical processes requires the solution of a number of intractable technological problems.

Coupled transport with supported and emulsion liquid membranes has made very little real progress toward commercialization in the last 25 years. In addition, it is now apparent that only a few important separation problems exist for which coupled transport offers clear technical and economic advantages over conventional technology. Unless some completely unexpected breakthrough occurs, it is difficult to imagine that coupled transport will be used on a significant commercial scale within the next 10–20 years. The future prospects for coupled transport are, therefore, dim.

The prospects for facilitated transport membranes for gas separation are better because these membranes offer clear potential economic and technical advantages for a number of important separation problems. Nevertheless, the technical problems that must be solved to develop these membranes to an industrial scale are daunting. Industrial processes require high-performance membranes able to operate reliably without replacement for at least one and preferably several years. No current facilitated transport membrane

approaches this target. Development of industrial-scale facilitated transport membranes and systems requires access to membrane technology not generally available in universities, and a commitment to a long-term development program that few companies are willing to undertake.

References

1. Osterhout, W.J.V. (1935) How do electrolytes enter the cells? *Proc. Natl. Acad. Sci.*, **21**, 125.
2. Gliozzi, A. (1980) Carriers and channels in artificial and biological membranes, in *Bioenergetics and Thermodynamics* (ed. A. Braibanti), D. Reidel Publishing Co., New York, pp. 299–353.
3. Shean, G.M. and Sollner, K. (1966) Carrier mechanisms in the movement of ions across porous and liquid ion exchanger membranes. *Ann. N.Y. Acad. Sci.*, **137**, 759.
4. Kedem, O., Vofsi, D., and Bloch, R. (1963) Ion specific polymer membrane. *Nature*, **199**, 802.
5. Bloch, R. (1970) Hydrometallurgical separations by solvent membranes, in *Proceedings of Membrane Science and Technology Symposium* (ed. J.E. Flinn), Columbus Laboratories of Battelle Memorial Institute, and Plenum Press, New York, pp. 171–187.
6. Jagur-Grodzinski, J., Mariam, S., and Vofsi, D. (1973) The mechanism of a selective permeation of ions through solvent polymeric membranes. *Sep. Sci. Technol.*, **8**, 33.
7. Miyauchi, T. (1977) Liquid-liquid extraction process of metals. US Patent 4,051,230, Sep. 1977.
8. Largman, T. and Sifniades, S. (1978) Recovery of copper (II) from aqueous solutions by means of supported liquid membranes. *Hydrometallurgy*, **3**, 153.
9. Baker, R.W., Tuttle, M.E., Kelly, D.J., and Lonsdale, H.K. (1977) Coupled transport membranes: I. Copper separations. *J. Membr. Sci.*, **2**, 213.
10. Babcock, W.C., Baker, R.W., Kelly, D.J., and LaChapelle, E.D. (1980) Coupled transport membranes for uranium recovery, *Proceedings of ISEC'80*, University of Liege, Liege, Belgium, pp. 80–90.
11. Li, N.N. (1971) Permeation through liquid surfactant membranes. *AIChE J.*, **17**, 459.
12. Li, N.N. (1978) Facilitated transport through liquid membranes – an extended abstract. *J. Membr. Sci.*, **3**, 265.
13. Li, N.N., Cahn, R.P., Naden, D., and Lai, R.W.M. (1983) Liquid membrane processes for copper extraction. *Hydrometallurgy*, **9**, 277.
14. Matulevicius, E.S. and Li, N.N. (1975) Facilitated transport through liquid membranes. *Sep. Purif. Rev.*, **4**, 73.
15. Cussler, E.L. (1971) Membranes which pump. *AIChE J.*, **17**, 1300.
16. Reusch, C.F. and Cussler, E.L. (1973) Selective membrane transport. *AIChE J.*, **19**, 736.
17. Hayworth, H.C. (1981) A case in technology transfer. *Chemtech*, **11**, 342.
18. Ho, W.S.W., Li, N.N., Gu, Z., Marr, R.J. and Drexler, J. (1992) Emulsion liquid membranes, in *Membrane Handbook* (eds W.S.W. Ho and K.K. Sirkar), Van Nostrand Reinhold, New York, pp. 595–724.

19. Nymeyer, K., Visser, T., Assen, R., and Wessling, M. (2004) Super selective membranes in gas-liquid membrane contactors for olefin/paraffin separation. *J. Membr. Sci.*, **232**, 107.
20. Majumdar, S. and Sirkar, K.K. (1992) Hollow-fiber contained liquid membrane, in *Membrane Handbook* (eds W.S.W. Ho and K.K. Sirkar), Van Nostrand Reinhold, New York, p. 764.
21. Davis, J.C., Valus, R.J., Eshraghi, R., and Velikoff, A.E. (1993) Facilitated transport membrane hybrid systems for olefin purification. *Sep. Sci. Technol.*, **28** (1–3), 463.
22. Raghuraman, B. and Wiencek, J. (1993) Extraction with emulsion liquid membranes in a hollow-fiber contactor. *AIChE J.*, **39**, 1885.
23. Hu, S.Y. and Wiencek, J. (1998) Emulsion-liquid-membrane extraction of copper using a hollow-fiber contactor. *AIChE J.*, **44**, 570.
24. Fouad, E.A. and Bart, H.J. (2008) Emulsion liquid membrane extraction of zinc by a hollow-fiber contactor. *J. Membr. Sci.*, **307**, 156.
25. Zou, J., Huang, J., and Ho, W.S.W. (2008) Facilitated transport membranes for environmental, energy, and biochemical applications, in *Advanced Membrane Technology and Applications* (eds N.N. Li, A.G. Fane, W.S.W. Ho, and T. Matsuura), John Wiley & Sons, Inc., Hoboken, NJ, pp. 721–754.
26. Ho, W.S.W. (2002) Combined supported liquid membrane/strip dispersion process for the removal and recovery of metals. US Patent 6,350,419, Feb. 2002.
27. Vilt, M.E. and Ho, W.S.W. (2009) Supported liquid membranes with strip dispersion for the recovery of cephalexin. *J. Membr. Sci.*, **342**, 80.
28. Scholander, P.F. (1960) Oxygen transport through hemoglobin solutions. *Science*, **131**, 585.
29. Ward, W.J. III and Robb, W.L. (1967) Carbon dioxide-oxygen separation: facilitated transport of carbon dioxide across a liquid film. *Science*, **156**, 1481.
30. Ward, W.J. III (1970) Analytical and experimental studies of facilitated transport. *AIChE J.*, **16**, 405.
31. Kimura, S.G., Matson, S.L., and Ward, W.J. III (1979) Industrial applications of facilitated transport, in *Recent Developments in Separation Science* (eds N.N. Li, J.S. Schultz, P. Somasundaran, and J.S. Dranoff), CRC Press, West Palm Beach, FL, pp. 11–26.
32. Matson, S.L., Herrick, C.S., and Ward, W.J. III (1977) Progress on the selective removal of H₂S from gasified coal using an immobilized liquid membrane. *Ind. Eng. Chem. Process Des. Dev.*, **16**, 370.
33. Hughes, R.D., Mahoney, J.A., and Steigelmann, E.F. (1986) Olefin separation by facilitated transport membranes, in *Recent Developments in Separation Science* (eds N.N. Li and J.M. Calo), CRC Press, Boca Raton, FL, pp. 173–196.
34. Nishide, H., Kawakami, H., Suzuki, T., Axechi, Y., Seojima, Y., and Tsuchida, E. (1991) Effect of polymer matrix on the oxygen diffusion via a cobalt porphyrin fixed in a membrane. *Macromolecules*, **24**, 6306.
35. Suzuki, T., Yasuda, H., Nishide, H., Chen, X.-S., and Tsuchida, E. (1996) Electrochemical measurement of facilitated oxygen transport through a polymer membrane containing cobaltporphyrin as a fixed carrier. *J. Membr. Sci.*, **112**, 155.

36. Nishide, H., Kawakami, H., Sasame, Y., Ishiwate, K., and Tsuchida, E. (1992) Facilitated transport of molecular oxygen in cobaltporphyrin/poly(1-trimethylsilyl-1-propyne) membrane. *J. Poly. Sci. Part A: Polym. Chem.*, **30**, 77.
37. Peinemann, K.V., Shukla, S.K., and Schossig, M. (1990) Preparation and properties of highly selective inorganic/organic blend membranes for separation of reactive gases, *The 1990 International Congress on Membranes and Membrane Processes*. North American Membrane Society, Chicago, IL, pp. 792–794.
38. Ho, W.S.W. (1991) Polymeric membrane and process for separation of aliphatically unsaturated hydrocarbons. US Patent 5,062,866, Nov. 1991.
39. Pinnau, I., Toy, L.G., and Casillas, C.G. (1997) Olefin separation membrane and process. US Patent 5,670,051, Sep. 1997.
40. Noble, R.D. and Way, J.D. (1987) *Liquid Membranes*, ACS Symposium Series, Vol. **347**, American Chemical Society, Washington, DC.
41. Krull, F.F., Fritzmann, C., and Melin, T. (2008) Liquid membranes for gas/vapor separations. *J. Membr. Sci.*, **325**, 509.
42. Figoli, A., Sager, W.F.C., and Mulder, M.H.V. (2001) Facilitated oxygen transport in liquid membranes: review and new concepts. *J. Membr. Sci.*, **181**, 97.
43. Smith, K.A., Meldon, J.H., and Colton, C.K. (1973) An analysis of carrier-facilitated transport. *AICHE J.*, **19**, 102.
44. Schultz, J.S., Goddard, J.D., and Suchdeo, S.R. (1974) Facilitated transport via carrier-mediated diffusion in membranes: part I. Mechanistic aspects, experimental systems and characteristic regimes. *AICHE J.*, **20**, 417.
45. Baker, R.W. and Blume, I. (1990) Coupled transport membranes, in *Handbook of Industrial Membrane Technology* (ed. M.C. Porter), Noyes Publications, Park Ridge, NJ, pp. 511–558.
46. Babcock, W.C., Baker, R.W., Conrod, M.G., and Smith, K.L. (1981) Coupled transport membranes for removal of chromium from electroplating rinse solutions, *Chemistry in Water Reuse*, Ann Arbor Science Publishers, Ann Arbor, MI.
47. Babcock, W.C., Baker, R.W., LaChapelle, E.D., and Smith, K.L. (1980) Coupled transport membranes II: the mechanism of uranium transport with a tertiary amine. *J. Membr. Sci.*, **7**, 71.
48. Lamb, J.D., Brown, P.R., Christensen, J.J., Bradshaw, J.S., Garrick, D.G., and Izatt, R.M. (1983) Cation transport at 25°C from binary Na^+ - Mn^+ , Cs^+ - Mn^+ and Sr^{2+} - Mn^+ nitrate mixtures in a $\text{H}_2\text{O}-\text{CHCl}_3-\text{H}_2\text{O}$ liquid membrane system containing a series of macrocyclic carriers. *J. Membr. Sci.*, **13**, 89.
49. Izatt, R.M., Haws, R.M., Lamb, J.D., Dearden, D.V., Brown, P.R., McBride, Jr., D.W., and Christensen, J.J. (1984) Facilitated transport from ternary cation mixtures through water-chloroform-water membrane systems containing macrocyclic ligands. *J. Membr. Sci.*, **20**, 273.
50. Babcock, W.C., Baker, R.W., Kelly, D.J., LaChapelle, E.D., and Lonsdale, H.K. (1979) Coupled transport membranes for metal separations. Phase IV Final Report, US Bureau of Mines Technical Report, Springfield, VA, NTIS PC AO5/MF A01.
51. Neplenbroek, A.M., Bargeman, D., and Smolders, C.A. (1992) Supported liquid membranes: instability effects. *J. Membr. Sci.*, **67**, 121.
52. Neplenbroek, A.M., Bargeman, D., and Smolders, C.A. (1992) Mechanism of supported liquid membrane degradation: emulsion formation. *J. Membr. Sci.*, **67**, 133.

53. Zha, F.F., Fane, A.G., and Fell, C.J.D. (1995) Instability mechanisms of supported liquid membranes in phenol transport process. *J. Membr. Sci.*, **107**, 59.
54. Danesi, P.R., Reichley-Yinger, L., and Rickert, P.G. (1987) Lifetime of supported liquid membranes: the influence of interfacial properties, chemical composition and water transport on the long-term stability of the membranes. *J. Membr. Sci.*, **31**, 117.
55. Völkel, W., Halwachs, W., and Schügerl, K. (1980) Copper extraction by means of a liquid surfactant membrane process. *J. Membr. Sci.*, **6**, 19.
56. LeBlanc, O.H., Ward, W.J., Matson, S.L., and Kimura, S.G. Jr. (1980) Facilitated transport in ion-exchange membranes. *J. Membr. Sci.*, **6**, 339.
57. Rabago, R., Bryant, D.L., Koval, C.A., and Noble, R.D. (1996) Evidence for parallel pathways in the facilitated transport of alkenes through Ag⁺-exchanged Nafion films. *Ind. Eng. Chem. Res.*, **35**, 1090.
58. Pez, G.P. and Laciak, D.V. (1988) Ammonia separation using semipermeable membranes. US Patent 4,762,535, Aug. 1988.
59. Pez, G.P., Carlin, R.T., Laciak, D.V., and Sorensen, J.C. (1988) Method for gas separation. US Patent 4,761,164, Aug. 1988.
60. Quinn, R., Appleby, J.B., and Pez, G.P. (1995) New facilitated transport membranes for the separation of carbon dioxide from hydrogen and methane. *J. Membr. Sci.*, **107**, 139.
61. Laciak, D.V., Quinn, R., Pez, G.P., Appleby, J.B., and Puri, P.S. (1990) Selective permeation of ammonia and carbon dioxide by novel membranes. *Sep. Sci. Tech.*, **25**, 1295.
62. Deng, L., Kim, T.J., and Hägg, M.B. (2009) Facilitated transport of CO₂ in novel PVAm/PVA blend membrane. *J. Membr. Sci.*, **340**, 154.
63. Sandru, M., Haukebø, S.H., and Hägg, M.B. (2010) Composite hollow fiber membranes for CO₂ capture. *J. Membr. Sci.*, **346**, 172.
64. Pinna, I. and Toy, L.G. (2001) Solid polymer electrolyte composite membranes for olefin/paraffin separation. *J. Membr. Sci.*, **184**, 39.
65. Morisato, A., He, Z., Pinna, I., and Merkel, T.C. (2002) Transport properties of PA12-PTMO/AgBF₄ solid polymer electrolyte membranes for olefin/paraffin separation. *Desalination*, **145**, 347.
66. Hong, S.U., Kim, C.K., and Kang, Y.S. (2000) Measurement and analysis of propylene solubility in polymer electrolytes containing silver salts. *Macromolecules*, **33**, 7918.
67. White, K.M., Smith, B.D., Duggan, P.J., Sheahan, S.L., and Tyndall, E.M. (2001) Mechanism of facilitated saccharide transport through plasticized cellulose triacetate membranes. *J. Membr. Sci.*, **194**, 165.
68. Bessarabov, D.G., Sanderson, R.D., Jacobs, E.P., and Beckman, I.N. (1995) High-efficiency separation of an ethylene/ethane mixture by a large-scale liquid-membrane contactor containing flat-sheet nonporous polymeric gas-separation membranes and a selective flowing-liquid absorbent. *Ind. Eng. Chem. Res.*, **34**, 1769.
69. Teramoto, M., Matsuyama, H., Yamashiro, T., and Okamoto, S. (1989) Separation of ethylene from ethane by a flowing liquid membrane using silver nitrate as a carrier. *J. Membr. Sci.*, **45**, 115.

70. Bassett, R.J. and Schultz, J.S. (1970) Nonequilibrium facilitated diffusion of oxygen through membranes of aqueous cobaltodihistidine. *Biochim. Biophys. Acta*, **211**, 194.
71. Johnson, B.M., Baker, R.W., Matson, S.L., Smith, K.L., Roman, I.C., Tuttle, M.E., and Lonsdale, H.K. (1987) Liquid membranes for the production of oxygen-enriched air: II. Facilitated-transport membranes. *J. Membr. Sci.*, **31**, 31.
72. Robeson, L.M. (1991) Correlation of separation factor versus permeability for polymeric membranes. *J. Membr. Sci.*, **62**, 165.

12

Medical Applications of Membranes

12.1 Introduction

In this chapter, the use of membranes in medical devices is reviewed briefly. In terms of total membrane area produced, medical applications are equivalent to all industrial membrane applications combined. In terms of dollar value of the products, the market is far larger. In spite of this, little communication between these two membrane areas has occurred over the years. Medical and industrial membrane developers each have their own journals, societies, and meetings, and rarely look over the fence to see what the other is doing. This book cannot reverse 50 years of history, but every industrial membrane technologist should at least be aware of the main features of medical applications of membranes. Therefore, in this chapter, the three most important applications – hemodialysis (the artificial kidney), blood oxygenation (the artificial lung), and controlled release pharmaceuticals – are briefly reviewed.

12.2 Hemodialysis

The kidney is a key component of the body's waste disposal and acid–base regulation mechanisms. Each year approximately one person in ten thousand suffers irreversible kidney failure. Before 1960, this condition was universally fatal [1], but now a number of treatment methods can maintain these patients. Of these, hemodialysis is by far the most important, and approximately 1.5 million patients worldwide benefit from the process. Each patient is dialyzed two to three times per week with a dialyzer containing about 1 m^2 of membrane area. Economies of scale allow these devices to be produced for about US\$15 each; the devices are generally discarded after one or two uses. As a result, the market for dialyzers alone is more than US\$2 billion [2–4].

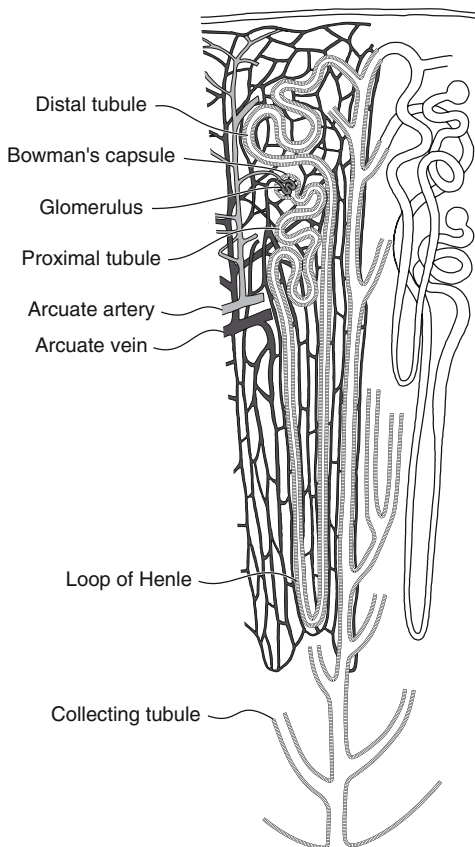


Figure 12.1 Schematic of a single nephron, the functional unit of the kidney. Microsolutes are filtered from blood cells in Bowman's capsules. As the filtrate passes toward the collection tubule, most of the microsolutes and water are reabsorbed by a type of facilitated transport process. The fluid finally entering the collecting tubule contains the nitrogenous wastes from the body and is excreted as urine. There are about 1 million nephrons in the normal kidney [1]

The operation of the human kidney simulated by hemodialyzers is illustrated in Figure 12.1. The process begins in the glomerulus, a network of tiny capillaries surrounding spaces called Bowman's capsules. Blood flowing through these capillaries is at a higher pressure than the fluid in Bowman's capsules, and the walls of the capillaries are finely microporous. As a result, water, salts, and other microsolutes in the blood are ultrafiltered into the capsule while blood cells stay behind. Each Bowman's capsule is connected by a relatively long, thin duct to the collecting tubule, ultimately forming urine, which is sent via the urethra to the bladder. The average kidney has approximately 1 million tubules and many Bowman's capsules are connected to each tubule. As the fluid that permeates into Bowman's capsules from the blood travels down the collection duct to the central tubule, more than 99% of the water and almost all of the

salts, sugars, and proteins are reabsorbed into the blood by a process similar to facilitated transport. The remaining concentrated fluid ultimately forms urine and is rich in urea and creatinine. This is the principal method by which these nitrogen-containing metabolites are discharged from the body. The acid–base balance of the body is also controlled by the bicarbonate level of urine, and many drugs and toxins are excreted from the body this way.

The first successful hemodialyzer was constructed by Kolf and Berk in The Netherlands in 1945 [5, 6]. Kolf's device used dialysis to remove urea and other waste products directly from blood. A flat cellophane (cellulose) tube formed the dialysis membrane; the tube was wound around a rotating drum immersed in a bath of saline. As blood was pumped through the tube, urea and other low molecular weight metabolites diffused across the membrane to the dialysate down a concentration gradient. The cellophane tubing did not allow diffusion of larger components in the blood such as proteins or blood cells. By maintaining the salt, potassium, and calcium levels in the dialysate solution at the same levels as in the blood, loss of these components from the blood was prevented.

Kolf's early devices were used for patients who had suffered acute kidney failure as a result of trauma or poisoning and needed dialysis only a few times. Such emergency treatment was the main application of hemodialysis until the early 1960s, because patients suffering from chronic kidney disease require dialysis two to three times per week for several years, which was not practical with these early devices. However, application of hemodialysis to this class of patient was made possible by improvements in the dialyzer design in the 1960s. The development of a plastic shunt that could be permanently fitted to the patient to allow easy access to their blood supply was also important. This shunt, developed by Scribner and coworkers [7], allowed dialysis without the need for surgery to connect the patient's blood vessels to the dialysis machine for each treatment.

Kolf's first tubular dialyzer, shown in Figure 12.2, required several liters of blood to prime the system, a major operational problem. In the 1950s, tubular dialyzers were

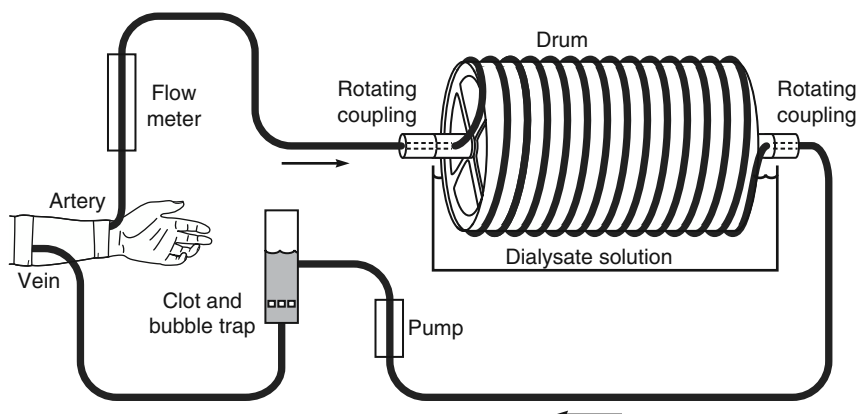


Figure 12.2 Schematic of an early tubular hemodialyzer based on the design of Kolf's original device. The device required several liters of blood to fill the tubing and minor surgery to connect to the patient. Nonetheless, it saved the lives of patients suffering from acute kidney failure [1]

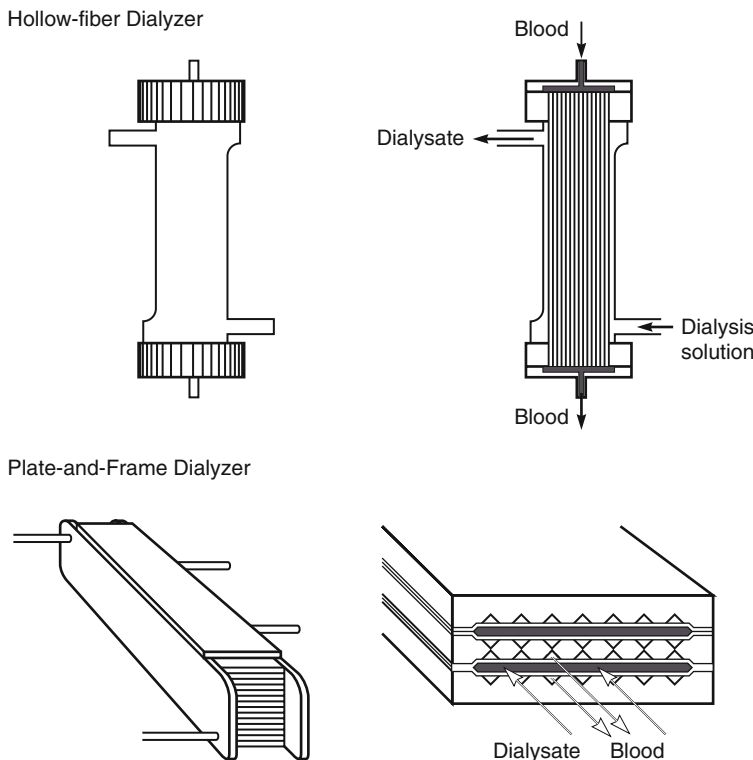


Figure 12.3 Schematic of hollow fiber and plate-and-frame dialyzers

replaced with coil (spiral) devices, also developed by Kolf and coworkers. This coil system was the basis for the first disposable dialyzer produced commercially in the early 1960s. The blood volume required to prime the device was still excessive, however, and during the 1960s the plate-and-frame and hollow fiber devices shown in Figure 12.3 were developed. In the US in 1975, about 65% of all dialyzers were coil, 20% hollow fiber systems, and 15% plate-and-frame. Within 10 years the coil dialyzer had essentially disappeared, and the market was divided two-thirds hollow fibers and one-third plate-and-frame. Hollow fiber dialyzers are now the only type used.

Hollow fiber dialyzers typically contain $1\text{--}2\text{ m}^2$ of membrane in the form of fibers 0.1–0.2 mm in diameter. A typical dialyzer module may contain several thousand fibers housed in a 2-in.-diameter tube, 1–2 feet long. Approximately 200 million hemodialysis procedures are performed annually worldwide. Because hollow fiber dialyzers are produced in such large numbers, prices are very low. Today a $1\text{--}2\text{ m}^2$ hollow fiber dialyzer sells for about US\$15, which is well below the module costs of any other membrane technology. These low costs have been achieved by the use of high speed machines able to spin several hundred fibers simultaneously around the clock. The entire spinning, cutting, module potting, and testing process is automated.

In a hollow fiber dialyzer the blood flows down the bore of the fiber, providing good fluid flow hydrodynamics. An advantage of the hollow fiber design is that only 60–100 ml of blood is required to fill the dialyzer. At the end of a dialysis procedure, hollow fiber dialyzers can also be easily drained, flushed with sterilizing agent, and reused. Dialyzer reuse was once widely practiced, in part for economic reasons, but currently, most dialyzers are discarded after a single use.

The regenerated cellulose membranes used in Kolf's first dialyzer were still in use in some dialyzers until the 1990s. Cellulose membranes are isotropic hydrogels generally about 10 µm thick and, although very water swollen, they have a high wet strength. The hydraulic permeability of cellulose is relatively low, and the membrane has a molecular weight cut-off of about 2000 Da. The permeability of cellulose hydrogel membranes compared to the calculated permeability of an aqueous film of equal thickness is shown in Figure 12.4.

Although cellulose was used successfully in hemodialyzers for many years, the ability of free hydroxyl groups on the membrane surface to activate the blood clotting process was a problem. When cellulose-based dialyzers are reused, the membrane's blood compatibility improves because a coating of protein has formed on the membrane surface. Beginning in the 1980s, synthetic polymers began to replace cellulose. Initially, these membrane materials were substituted cellulose derivatives, principally cellulose acetate, but now, polymers such as polyacrylonitrile, polysulfone, and poly(methyl methacrylate) are the most widely used materials. These synthetic fiber membranes are generally micro-porous with a finely microporous skin layer on the inside, the blood-contacting surface of the fiber. The hydraulic permeability of these fibers is up to 10 times that of cellulose membranes, and they can be tailored to achieve a range of molecular weight cutoffs by

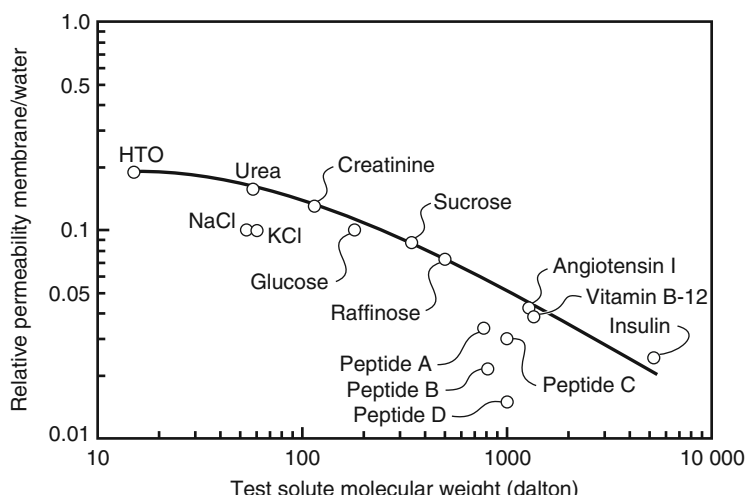


Figure 12.4 Solute permeability relative to the permeability of a film of water for various solutes in a regenerated cellulose membrane (Cuprophan 150). This type of membrane was widely used in hemodialysis devices until the 1980s

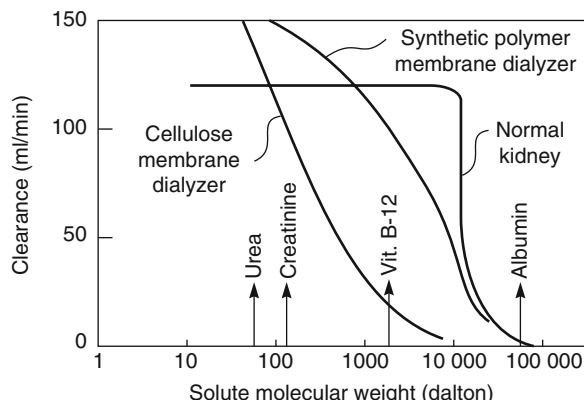


Figure 12.5 Clearance, a measure of membrane permeability, as a function of molecular weight for hemodialyzers and the normal kidney [8]

using different preparation procedures. The blood compatibility of the synthetic polymer membranes is good, and these membranes, particularly polysulfone (made hydrophilic by co-spinning with poly(vinyl pyrrolidone)), now have more than 80% of the current market.

An attractive feature of some of the new synthetic polymer membranes is their ability to remove some of the middle molecular weight metabolites in blood. This improvement in performance is illustrated by Figure 12.5. Cellulose membranes efficiently remove the major metabolites, urea and creatinine, from blood, but metabolites with molecular weights between 1000 and 10 000 are removed poorly. Patients on long-term dialysis are believed to accumulate these metabolites, which are associated with a number of health issues. The new synthetic polymer membranes appear to simulate the function of the normal kidney more closely.

12.3 Blood Oxygenators

Blood oxygenators are used during surgery when the patient's lungs cannot function normally. Pioneering work on these devices was carried out in the 1930s and 1940s by J.H. Gibbon [9, 10], leading to the first successful open heart surgery on a human patient in 1953. Gibbon's heart–lung machine used a small tower filled with stainless steel screens to contact blood with counter-flowing oxygen. Direct oxygenation of the blood was used in all such devices until the early 1980s. Screen oxygenators of the type devised by Gibbon were first replaced with a disk oxygenator, which consisted of 20–100 rotating disks in a closed cylinder containing 1–21 of blood. Later, bubble oxygenators were developed, in which blood was oxygenated in a packed plastic tower through which blood flowed. Because these direct-contact oxygenators required rather large volumes of blood to prime the device and, more importantly, damaged some of the blood components, they were used in only a few thousand operations per year in the 1980s. The introduction of indirect-contact membrane oxygenators resulted in significantly less blood damage and

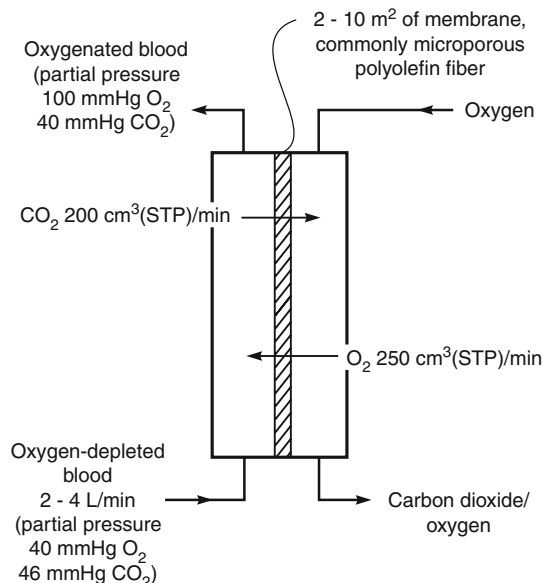


Figure 12.6 Flow schematic of a membrane blood oxygenator

lower blood priming volumes. The devices were rapidly accepted, and the total number of procedures performed following their introduction expanded rapidly. The first membrane oxygenators were introduced in 1980, and by 1985 they represented more than half of the oxygenators in use. This percentage had risen to 70% by 1990; now, only membrane oxygenators are used. Over the same period, the number of procedures using blood oxygenators has risen to more than 1 million per year worldwide. Each device costs around US\$1000, so the total annual market is about US\$1 billion.

The function of a membrane blood oxygenator is shown schematically in Figure 12.6. In the human lung, the total exchange membrane area between the blood capillaries and the air drawn in and out is about 80 m². The human lung membrane is estimated to be about 1 μm thick, and the total exchange capacity of the lung is far larger than is normally required. This allows people with impaired lung capacity to lead relatively normal lives. A successful heart-lung machine must deliver about 250 cm³(STP)/min oxygen and remove about 200 cm³(STP)/min carbon dioxide [11]. Because of the limited solubility of these gases in the blood, large blood flows through the device are required, typically 2–4 l/min, which is ~10 times the blood flow through a kidney dialyzer. The first membrane oxygenators used silicone rubber membranes, but now microporous polyolefin fibers are used. To maintain good mass transfer with minimal pressure drop through the device, blood is generally circulated on the outside of the fibers and high oxygen concentration, low carbon dioxide concentration gas is circulated down the lumen of the fibers. Concentration polarization in the blood-side liquid boundary layer significantly affects gas transport. Blood oxygenators used for short-term applications usually use microporous polyolefin fibers. In recent years, a number of clinicians have tried to use oxygenators for several days, or even weeks. In this work, silicone-coated membranes

are generally used to prevent wetting and liquid penetration of the fibers. An up-to-date review of blood oxygenators has been written by Wiese [12].

12.4 Plasma Fractionation

In recent years, membranes are being used to separate high molecular weight toxic components from blood in the treatment of a number of diseases. The procedure is called by several names, including plasma fractionation, therapeutic hemapheresis, therapeutic plasmapheresis, or therapeutic ampheresis. The general procedure is to produce cell-free blood (plasma) by continuous centrifugation or cross-flow filtration while returning the cells to the patient. The plasma produced is then filtered to remove very high molecular weight lipoproteins and triglycerides while passing albumin, β -globulins, IgG-globulin, and most other components with a molecular weight less than 300 000 Da. The filtered plasma is then returned to the patient.

An example of this type of double filtration set-up, taken from the review of Wiese [12] is shown in Figure 12.7. The first cross-flow plasma filtration membrane has a nominal pore size of $\sim 0.2 \mu\text{m}$. The second in-line (dead end) plasma fraction membrane

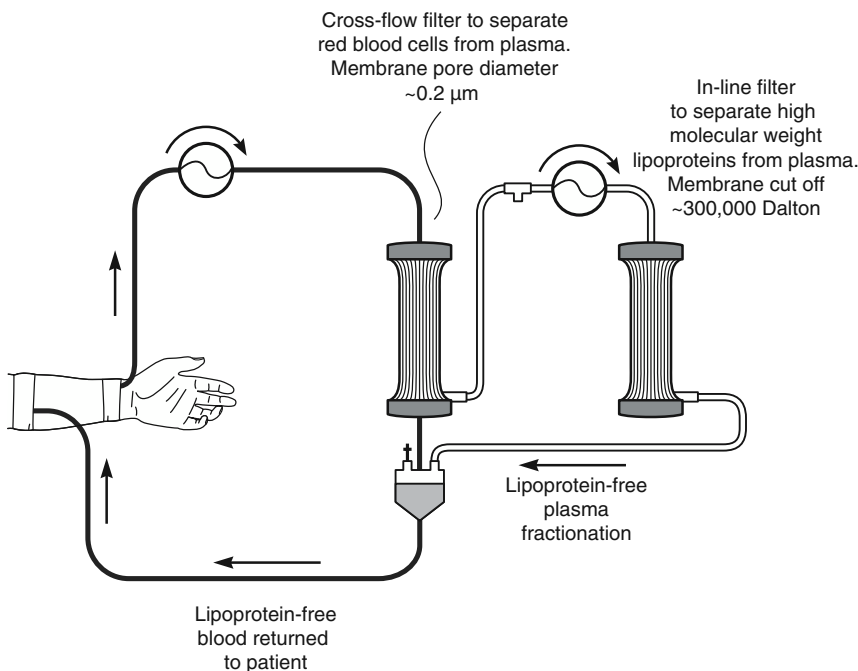


Figure 12.7 Double filtration used to remove high molecular weight lipoproteins and triglycerides in the treatment of myasthenia gravis, some forms of lupus and hypercholesterolemia [12]. The first membrane, with pore diameter of $\sim 0.2 \mu\text{m}$, separates blood cells from the plasma. The plasma permeate is then treated with a second tighter membrane (MW cutoff of 300 000), which removes high molecular weight lipoproteins. The twice-filtered plasma is then returned to the patient

has a molecular weight cut-off of about 300 000 Da. The use of these devices, while not commonplace, is growing. Currently, ~600 000 procedures per year are performed.

12.5 Controlled Drug Delivery

In controlled drug delivery systems, a membrane is used to moderate the rate of delivery of drug to the body. In some devices, the membrane controls permeation of the drug from a reservoir to achieve the drug delivery rate required. Other devices use the osmotic pressure produced by diffusion of water across a membrane to power miniature pumps. In yet other devices, the drug is impregnated into the membrane material, which then slowly dissolves or degrades in the body. Drug delivery is then controlled by a combination of diffusion and biodegradation.

The objective of all of these devices is to deliver a drug to the body at a rate predetermined by the design of the device and independent of the changing environment of the body. In conventional medications, only the total mass of drug delivered to a patient is controlled. In controlled drug delivery, both the mass and the rate at which the drug is delivered can be controlled, providing three important therapeutic benefits:

1. The drug is metered to the body slowly over a long period; therefore, the problem of overdosing and underdosing associated with conventional periodic medication is avoided.
2. The drug can often be given locally, ideally to the affected organ directly, rather than systemically as an injection or tablet. Localized delivery results in high concentrations of the drug at the site of action, but low concentrations and hence fewer side effects elsewhere.
3. As a consequence of metered, localized drug delivery, controlled release devices generally equal or improve the therapeutic effects of conventional medications, while using a fraction of the drug. Thus, the problems of drug-related side effects are correspondingly lower.

The concept of controlled delivery is not limited to drugs. Similar principles are used to control the delivery of agrochemicals, fertilizers, and pesticides, for example, and in many household products. However, most of the technology development in the past 30 years has focused on drug delivery; only this aspect of the topic is covered here.

Some of the benefits of a controlled release system are illustrated in Figure 12.8. The figure shows drug concentration at the site of drug action as a function of time. Conventional tablets or injections produce highly fluctuating concentration levels. After each drug dose, the drug concentration rises to a peak value and then declines. With drugs having a narrow therapeutic window, it is easy to produce excessively high drug concentrations, leading to drug-related side effects, or excessively low drug concentrations, leading to inadequate medications. The controlled release system meters the drug in at a constant rate so that the drug concentration is maintained at the optimum level for a prolonged period.

The origins of controlled release drug delivery can be traced to the 1950s. Rose and Nelson [13], for example, described the first miniature osmotic pump in 1955. A key early publication was the paper of Folkman and Long [14] in 1964, describing the use of

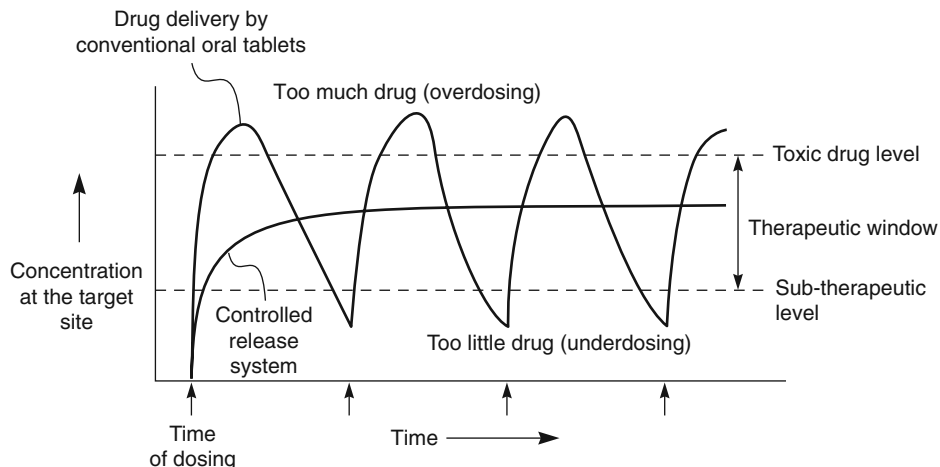


Figure 12.8 Drug concentrations at the target site for drug action achieved by repeated doses of a conventional medication (tablet, injection) and a single, long-lasting controlled release system

silicone rubber membranes to control the release of anesthetics and cardiovascular drugs. Concurrent discoveries in the field of hormone regulation of female fertility quickly led to the development of controlled release systems to release steroids for contraception [15, 16]. The founding of Alza Corporation by Alex Zaffaroni in the late 1960s gave the entire technology a decisive thrust. Alza was dedicated to developing novel controlled release drug delivery systems [17]. The products developed by Alza during the subsequent 25 years stimulated the entire pharmaceutical industry. The first pharmaceutical product in which the drug registration document specified both the total amount of drug in the device and the delivery rate was an Alza product, the Ocusert®, launched in 1974 [18]. This device, shown in Figure 12.9, consisted of a three-layer laminate with the drug sandwiched between two rate-controlling polymer membranes. The device is an ellipse about 1 mm thick and 1 cm in diameter. The device is placed in the cul de sac of the eye where it delivers the drug (pilocarpine) at a constant rate for seven days, after which it is removed and replaced. The Ocusert was a technical tour de force, although only a limited marketing success. Alza later developed a number of more widely used products, including multilayer transdermal patches designed to deliver drugs through the skin [19] and osmotic devices for oral drug delivery. Many imitators followed Alza's success, and an entire sub-industry has grown up that produces controlled release systems for a wide variety of drugs.

12.5.1 Membrane Diffusion-Controlled Systems

In membrane diffusion-controlled systems, a drug is released from a device by permeation from its interior reservoir to the surrounding medium. The rate of diffusion of the drug through the membrane governs its rate of release. The reservoir device illustrated in Figure 12.10 is the simplest diffusion-controlled system. An inert membrane encloses

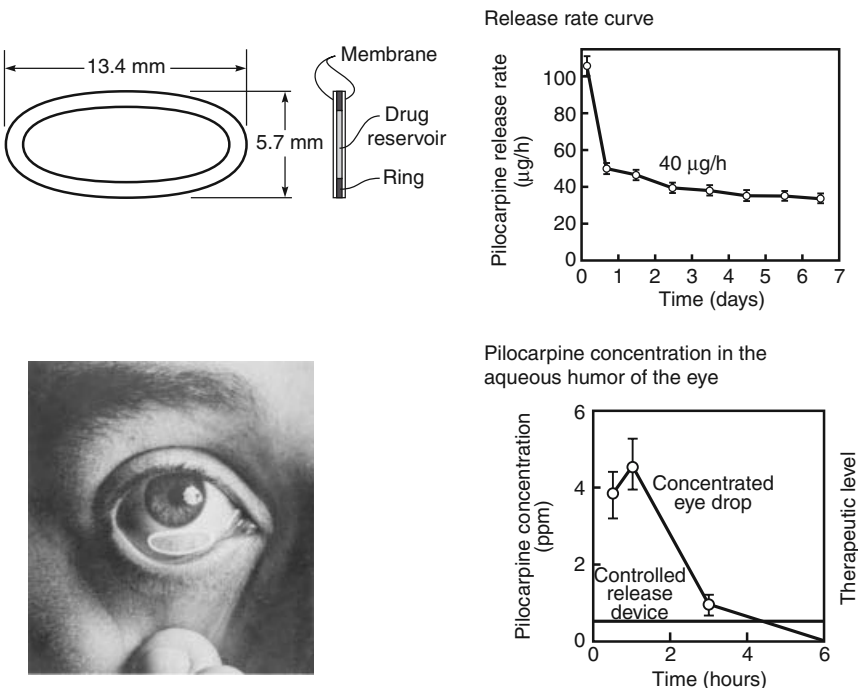


Figure 12.9 The Ocusert pilocarpine system is a thin multilayer membrane device. The central sandwich consists of a core containing the drug pilocarpine. The device is placed in the eye, where it releases the drug at a continuous rate for seven days. Devices with release rates of 20 or 40 µg/h are used. Controlled release of the drug eliminates the over- and underdosing observed with conventional eye drop formulations, which must be delivered every 4–6 h to maintain therapeutic levels of the drug in the eye tissue [18]

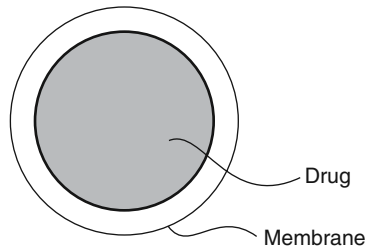


Figure 12.10 Reservoir device

the drug to be released; the drug diffuses through the membrane at a finite, controllable rate. If the concentration (or thermodynamic activity) of the material in equilibrium with the inner surface of the enclosing membrane is constant, then the concentration gradient, the driving force for diffusional release of the drug, is constant. This occurs when the inner reservoir contains a saturated solution of the material, providing a constant release

rate for as long as excess solid drug is maintained in the solution. This is called zero-order release. If, however, the active drug within the device is initially present as an unsaturated solution, its concentration falls as it is released. The release rate declines exponentially, producing a first-order release profile.

For a device containing a saturated solution of drug, and excess solid drug, Fick's law

$$J = -DK \frac{dc_s}{dx} \quad (12.1)$$

can be restated for a slab or sandwich geometry as

$$\frac{dM_t}{dt} = \frac{AJ}{\ell} = \frac{ADKc_s}{\ell} \quad (12.2)$$

where M_t is the mass of drug released at any time t , and hence dM_t/dt is the steady-state release rate at time t ; A is the total surface area of the device (edge effects being ignored); c_s is the saturation solubility of the drug in the reservoir layer; and J is the membrane-limiting flux.

The Ocusert system illustrated in Figure 12.9 is one example of a diffusion-controlled reservoir device [18]. Another is the steroid-releasing intrauterine device (IUD) shown in Figure 12.11 [20]. Inert IUDs of various shapes were widely used for birth control

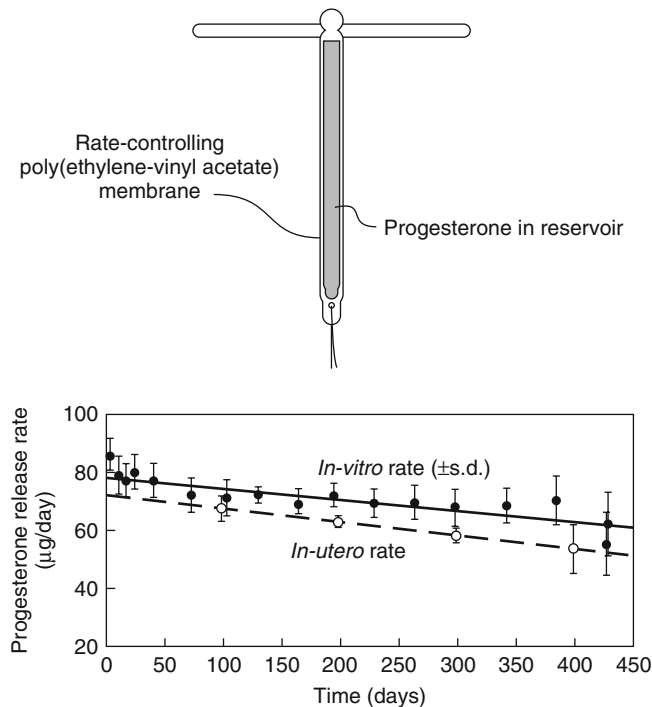


Figure 12.11 Progestasert® intrauterine device (IUD) designed to deliver progesterone for contraception at 65 μg/day for one year [20]

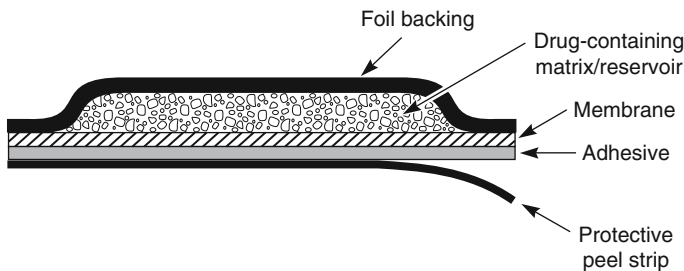


Figure 12.12 Schematic of a typical transdermal patch. Depending on the drug and the drug delivery rate to be achieved, these devices can vary from 3 to 30 cm² in area

in the 1950s and 1960s. The contraceptive effect of these IUDs was based on physical irritation of the uterus. Thus, the devices resulting in the lowest pregnancy rate were often associated with unacceptable levels of pain and bleeding, whereas more comfortable devices were associated with unacceptably high pregnancy rates. Researchers tried a large number of different IUD shapes in an attempt to produce a device that combined a low pregnancy rate with minimal pain and bleeding, but without real success.

Steroid-releasing IUDs, in which the contraceptive effect of the device comes largely from the steroid, offer a solution to the discomfort caused by inert IUDs. Such devices can use IUDs with a low pain and bleeding level as a platform for the steroid-releasing system. Scommegna *et al.* performed the first clinical trials to test this concept [16]. The commercial embodiment of these ideas is shown in Figure 12.11, together with the drug release rate curve [20]. Inspection of this curve shows an initial high drug release during the first 30–40 days, representing drug that has migrated into the polymer during storage of the device and which is released as an initial burst. Thereafter, the device maintains an almost constant drug release rate until it is exhausted at about 400 days. Later versions of this device were made that incorporated synthetic steroids that were more biologically active. These devices contained sufficient steroid to last two years or more.

A more familiar type of diffusion-controlled device is the transdermal patch shown in Figure 12.12. A variety of patch designs are used, but a typical patch has an area of 3–30 cm². The drug is contained in a liquid, gel, or polymer reservoir layer and a membrane is used to control delivery of drug to the skin. In some devices, the membrane is a separate layer; in others, the membrane may be the adhesive layer that sticks the device to the skin.

Human skin is a remarkably efficient barrier designed to keep “our insides in and the outsides out!” For this reason, transdermal delivery is limited to potent drugs that can produce the required effect when delivered at a few micrograms to milligrams per day. Only a handful of these potent drugs have been found that are able to penetrate the skin at a therapeutically useful rate; examples include scopolamine, nitroglycerin, nicotine, clonidine, fentanyl, estradiol, testosterone, lidocaine, and oxybutynin. Nonetheless, taken altogether the current US market for transdermal patches is over US\$3 billion per year.

Typically, a patch is designed to deliver a drug for about one week, after which it is removed and another patch is applied at a different site. Patch manufacturers often attribute the controlled release nature of the patch to membrane moderated drug delivery,

but in reality, drug delivery in many of these products is controlled more by the skin barrier than the device membrane.

Many attempts have been made to increase the number of drugs that can permeate the skin at a useful rate. Compounds such as DMSO (dimethyl sulfoxide), Azone (1-dodecylazacycloheptane-2-one), and alcohols have been used to enhance the permeability of the skin and so allow the drug to permeate, but success to date has been very limited [21]. Another approach has been to use an applied DC electric current to produce an increased flux of ionic drugs through the skin (iontophoresis), by application of short high voltage (100–1000 V) pulses of electricity to disrupt the skin and increase its permeability (electroporation). Neither of these approaches has become commercial [22].

There are two principal types of monolithic device. If the active agent is dissolved in the polymer medium, the device is called a *monolithic solution*. Examples of this type of device are pesticide-containing cat and dog collars to control ticks and fleas. Such devices are often used when the active agent is a liquid; some polymers (for example, poly(vinyl chloride)) can easily sorb up to 20% or more of these liquids. However, if the solubility of the active agent in the polymer medium is more limited, then only a portion of the agent is dissolved and the remainder is dispersed as small particles throughout the polymer. A device of this type is called a *monolithic dispersion*.

The kinetics of release from a monolithic solution system have been derived for a number of geometries by Crank [23]. For a slab geometry, the release kinetics can be expressed by either of two series, both given here for completeness

$$\frac{M_t}{M_0} = 1 - \sum_{n=0}^{\infty} \frac{8 \exp[-D(2n+1)^2\pi^2 t/\ell^2]}{(2n+1)^2\pi^2} \quad (12.3)$$

or

$$\frac{M_t}{M_0} = 4 \left(\frac{Dt}{\ell^2} \right)^{1/2} \left[\pi^{-1/2} + \sum_{n=0}^{\infty} (-1)^n \operatorname{erfc} \left(\frac{n\ell}{2\sqrt{Dt}} \right) \right] \quad (12.4)$$

where M_0 is the total amount of drug sorbed, M_t is the amount desorbed at time t , and ℓ is the thickness of the device.

Fortunately, these complex expressions reduce to two simple approximations, reliable to better than 1%, valid for different parts of the desorption curve. The early time approximation, which holds for the initial portion of the curve, derived from Equation 12.4, is

$$\frac{M_t}{M_0} = 4 \left(\frac{Dt}{\pi \ell^2} \right)^{1/2} \quad \text{for } 0 \leq \frac{M_t}{M_0} \leq 0.6 \quad (12.5)$$

The late time approximation, which holds for the final portion of the desorption curve, derived from Equation 12.3, is

$$\frac{M_t}{M_0} = 1 - \frac{8}{\pi^2} \exp \frac{-\pi^2 Dt}{\ell^2} \quad \text{for } 0.4 \leq \frac{M_t}{M_0} \leq 1.0 \quad (12.6)$$

These approximations are plotted in Figure 12.14, which illustrates their different regions of validity.

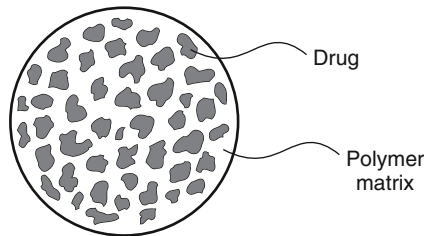


Figure 12.13 Monolithic device

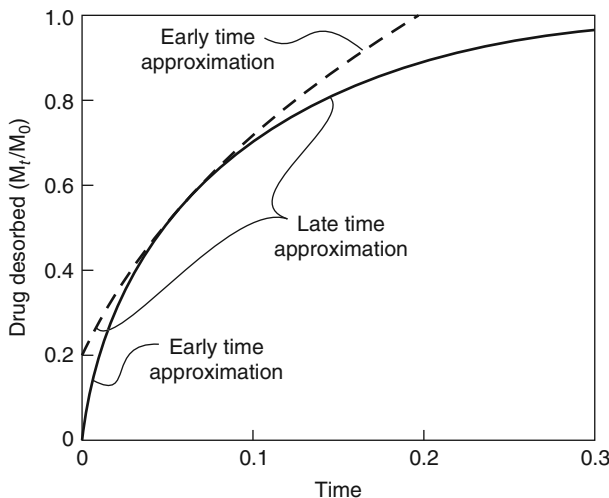


Figure 12.14 The fraction of agent desorbed from a slab as a function of time using the early time and late time approximations. The solid line shows the portion of the curve over which the approximations are valid ($D/l^2 = 1$) [24]

In general, the rate of release at any particular time is of more interest than the accumulated total release. This rate is easily obtained by differentiating Equations 12.5 and 12.6 to give

$$\frac{dM_t}{dt} = 2M_0 \left(\frac{D}{\pi \ell^2 t} \right)^{1/2} \quad (12.7)$$

for the early time approximation and

$$\frac{dM_t}{dt} = \frac{8DM_0}{\ell^2} \exp \left(\frac{-\pi^2 Dt}{\ell^2} \right) \quad (12.8)$$

for the late time approximation. These two approximations are plotted against time in Figure 12.15. Again, for simplicity, M_0 and D/ℓ^2 have been set at unity. The release

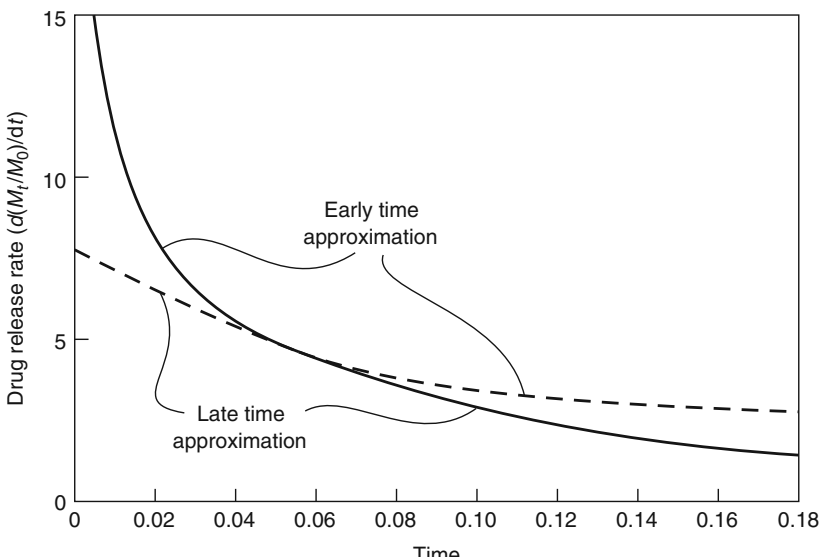


Figure 12.15 The release rate of drug initially dissolved in a slab as a function of time, using the early time and late time approximations. The solid line shows the portion of the curve over which the approximations are valid ($D/l^2 = 1$) [24]

rate falls off in proportion to $t^{-1/2}$ until 60% of the agent has been desorbed; thereafter, it decays exponentially.

The expressions (12.5–12.8) are also convenient ways of measuring diffusion coefficients in polymers. A permeant is contacted with a film of material of known geometry until equilibrium is reached. The film is then removed from the permeant solution, washed free of contaminants, and the rate of release of the permeant is measured. From the release curves, the diffusion coefficient and permeant sorption can be obtained.

A monolithic dispersion system consists of a dispersion of solid active drug in a rate-limiting polymer matrix. As with monolithic solution systems, the release rate varies with the geometry of the device; it also varies with drug loading. The starting point for release of drug from these systems can be described by a simple model due to Higuchi [25] and is shown schematically in Figure 12.16.

Higuchi's model assumes that solid drug in the surface layer of the device dissolves in the polymer matrix and diffuses from the device first. When the surface layer becomes exhausted of drug, the next layer begins to be depleted. Thus, the interface between the region containing dispersed drug and the region containing only dissolved drug moves into the interior as a front. The validity of Higuchi's model has been demonstrated experimentally numerous times by comparing the predicted release rate calculated from the model with the actual release rate. In addition, the movement of a dissolving front can be monitored directly by sectioning and examining monolithic devices that have been

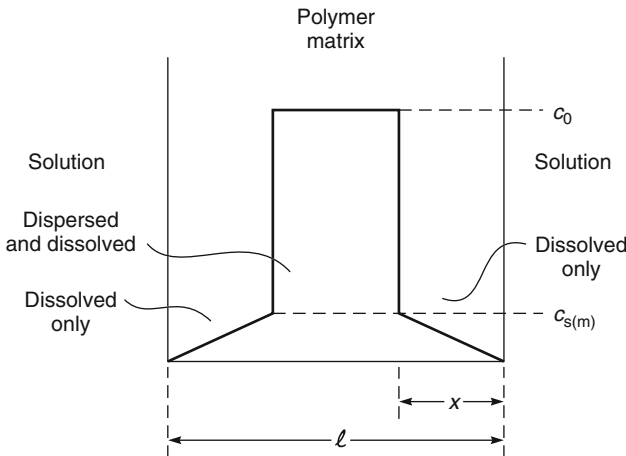


Figure 12.16 Schematic representation of a cross-section through a polymer matrix initially containing dispersed solid drug. The interface between the region containing dispersed drug and the region containing only dissolved drug has moved a distance x from the surface [25]

releasing agent for various lengths of time [26]. The proof of Higuchi is straightforward and leads to the equation

$$\begin{aligned} M_t &= A \left[DKt c_s (2c_0 - c_s) \right]^{1/2} \\ &\simeq (2DKt c_s c_0)^{1/2} \quad \text{for } c_0 \gg c_s \end{aligned} \quad (12.9)$$

The release rate at any time is then given by

$$\begin{aligned} \frac{dM_t}{dt} &= \frac{A}{2} \left[\frac{DKc_s}{t} (2c_0 - c_s) \right]^{1/2} \\ &\simeq \frac{A}{2} \left(\frac{DKc_s c_0}{t} \right)^{1/2} \quad \text{for } c_0 \gg c_s \end{aligned} \quad (12.10)$$

The Higuchi model is an approximate solution in that it assumes a “pseudosteady state,” in which the concentration profile from the dispersed drug front to the outer surface is linear. Paul and McSpadden [27] have shown that the correct expression can be written as

$$M_t = A \left[2DKt c_s (c_0 - Kc_s) \right]^{1/2} \quad (12.11)$$

which is almost identical to Equation 12.9 and reduces to it when $c_0 \gg c_s$. Clearly, the release rate is proportional to the square root of the loading; thus, it can be easily varied by incorporating more or less agent. Furthermore, although the release rate is by no means constant, the range of variation is narrower than would be the case if the agent

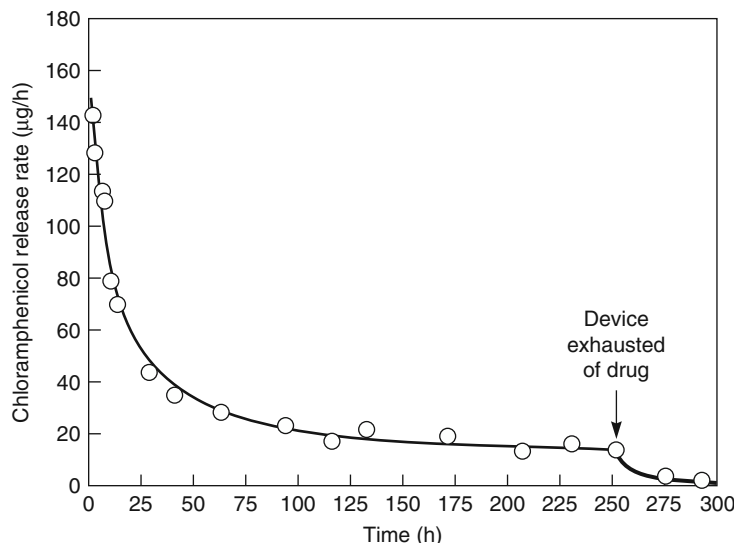


Figure 12.17 Release of the antibiotic drug chloramphenicol dispersed in a matrix of poly(ethylene-vinyl acetate). The solid line is calculated from Equation 12.10 [24]

were merely dissolved, rather than dispersed, in the matrix. An example of the release rate of the drug from an ethylene-vinyl acetate slab containing the dispersed antibiotic chloramphenicol is shown in Figure 12.17. The drug release rate decreases in proportion to the square root of time, in accordance with Equation 12.10.

12.5.2 Biodegradable Systems

The diffusion-controlled devices outlined so far are permanent, in that the membrane or matrix of the device remains implanted after its delivery role is completed. In some applications, particularly in the medical field, this is undesirable; such applications require a device that degrades during or subsequent to its delivery role.

Many polymer-based devices that slowly biodegrade when implanted in the body have been developed; the most important are based on polylactic acid, polyglycolic acid, and their copolymers. In principle, the release of an active agent can be programmed by dispersing the material within such polymers, with erosion of the polymer effecting release of the agent [28, 29]. One class of biodegradable polymers is *surface eroding*; the surface area of such polymers decreases with time as the conventionally cylindrical- or spherical-shaped device erodes. This results in a decreasing release rate unless the geometry of the device is appropriately manipulated or the device is designed to contain a higher concentration of the agent in the interior than in the surface layers. In a more common class of biodegradable polymer, the initial period of degradation occurs very slowly, after which the degradation rate increases rapidly. The bulk of the polymer then erodes over a comparatively short period. In the initial period of exposure to the body, the polymer chains are being cleaved but the molecular weight is still high, so the polymer's mechanical properties are not seriously affected. As chain cleavage continues,

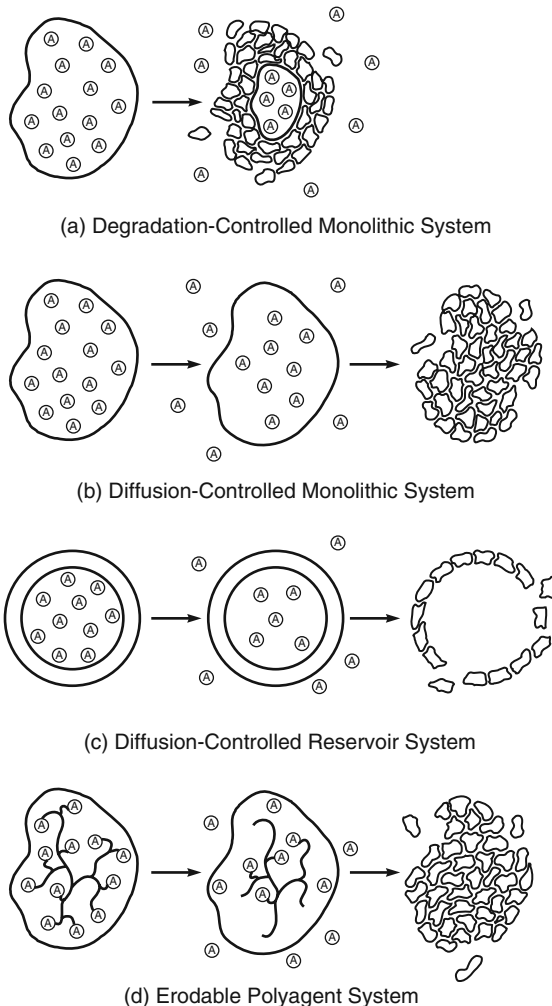


Figure 12.18 Methods of using biodegradable polymers in controlled release implantable devices to release the active agent, A. (a) Degradation-controlled monolithic system, (b) diffusion-controlled monolithic system, (c) diffusion-controlled reservoir system and (d) erodable polyagent system

a point is reached at which the polymer fragments become swollen or soluble in water. At this point, the polymer begins to dissolve. This type of polymer can be used to make reservoir or monolithic diffusion-controlled systems that degrade after their delivery role is over. A final category of polymer has the active agent covalently attached by a labile bond to the backbone of a matrix polymer. When placed at the site of action the labile bonds slowly degrade, releasing the active agent and forming a soluble polymer. The methods by which these concepts can be formulated into actual practical systems are illustrated in Figure 12.18.

12.5.3 Osmotic Systems

Osmotic effects are often a problem in diffusion-controlled systems because imbibition of water swells the device or dilutes the drug. However, several devices have been developed that actually use osmotic effects to control the release of drugs. These devices, called osmotic pumps, use the osmotic pressure developed by diffusion of water across a semipermeable membrane into a salt solution to push a solution of the active agent from the device. Osmotic pumps of various designs are widely applied in the pharmaceutical area, particularly in oral tablet formulations [30].

The forerunner of modern osmotic devices was the Rose–Nelson pump. Rose and Nelson were two Australian physiologists interested in the delivery of drugs to the gut of sheep and cattle [13]. Their pump, illustrated in Figure 12.19 consists of three chambers: a drug chamber, a salt chamber containing excess solid salt, and a water chamber. The salt and water chambers are separated by a rigid semipermeable membrane. The difference in osmotic pressure across the membrane moves water from the water chamber into the salt chamber. The volume of the salt chamber increases because of this water flow, which distends the latex diaphragm separating the salt and drug chambers, thereby pumping drug out of the device.

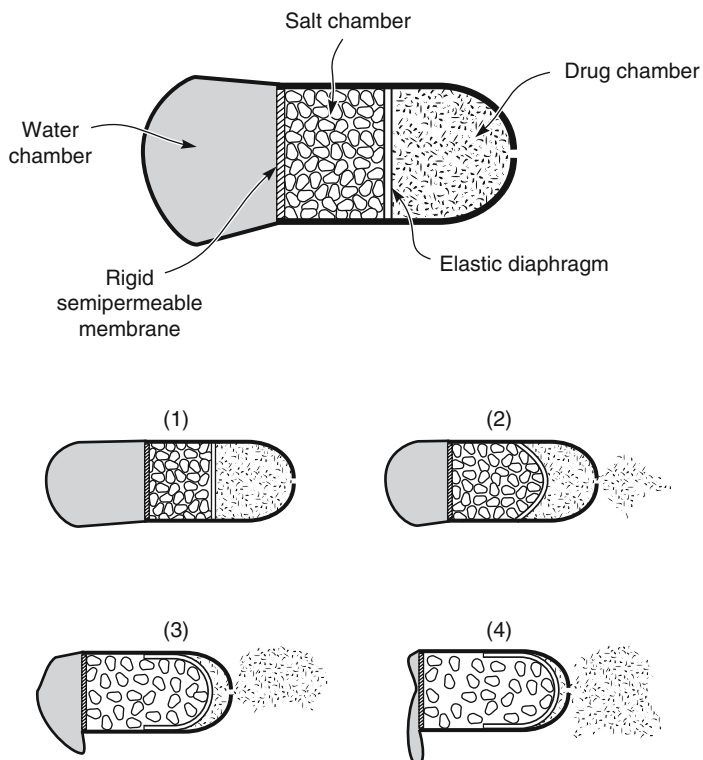


Figure 12.19 Principle of the three-chamber Rose–Nelson osmotic pump first described in 1955 [13]

The pumping rate of the Rose–Nelson pump is given by the equation

$$\frac{dM_t}{dt} = \frac{dV}{dt}c \quad (12.12)$$

where dM_t/dt is the drug release rate, dV/dt is the volume flow of water into the salt chamber, and c is the concentration of drug in the drug chamber. The osmotic water flow across a membrane is given by the equation

$$\frac{dV}{dt} = \frac{A\theta\Delta\pi}{\ell} \quad (12.13)$$

where dV/dt is a water flow across the membrane of area A , thickness ℓ , and osmotic permeability θ ($\text{cm}^3 \cdot \text{cm}/\text{cm}^2 \cdot \text{h} \cdot \text{atm}$), and $\Delta\pi$ is the osmotic pressure difference between the solutions on either side of the membrane. This equation is only strictly true for completely selective membranes – that is, membranes permeable to water but completely impermeable to the osmotic agent. However, this is a good approximation for most membranes. Substituting Equation 12.13 for the flux across the membrane gives

$$\frac{dM_t}{dt} = \frac{A\theta\Delta\pi c}{l} \quad (12.14)$$

The osmotic pressure of the saturated salt solution is high, on the order of tens of atmospheres, and the small pressure required to pump the suspension of active agent is insignificant in comparison. Therefore, the rate of water permeation across the semipermeable membrane remains constant as long as sufficient solid salt is present in the salt chamber to maintain a saturated solution and hence a constant osmotic pressure driving force.

The Higuchi–Leeper pump designs represent the first of a series of simplifications of the Rose–Nelson pump made by Alza Corporation beginning in the early 1970s. An example of one of these designs [31] is shown in Figure 12.20. The Higuchi–Leeper pump has no water chamber; the device is activated by water imbibed from the surrounding environment. This means that the drug-laden pump can be prepared and then stored for weeks or months prior to use. The pump is only activated when it is swallowed or implanted in the body. Higuchi–Leeper pumps contain a rigid housing, and the semipermeable membrane is supported on a perforated frame. This type of pump usually has a salt chamber containing a fluid solution with excess solid salt. The target application of this device was the delivery of antibiotics and growth hormones to cattle because repeated delivery of oral medications to animals is difficult. The problem is solved by these devices, which are designed to be swallowed by the cow and then to reside in the rumen, delivering a full course of medication over a period of days to weeks.

In the early 1970s, Theeuwes and Higuchi developed even simpler variants of the Rose–Nelson pump [32, 33]. One such device is illustrated in Figure 12.21. As with the Higuchi–Leeper pump, water to activate the osmotic action of the pump comes from the surrounding environment. The Theeuwes–Higuchi device, however, has no rigid housing – the membrane acts as the outer casing of the pump. This membrane is quite sturdy and is strong enough to withstand the pumping pressure developed inside the device. The device is loaded with the desired drug prior to use. When the device is

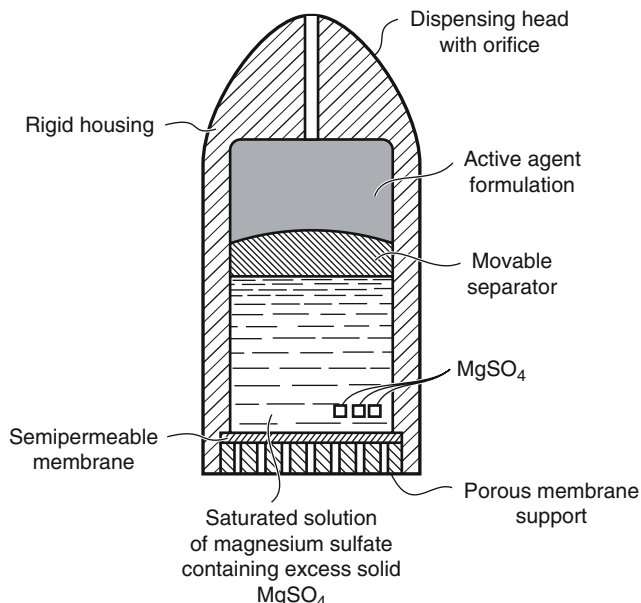


Figure 12.20 The Higuchi–Leeper osmotic pump design [28]. This device has no water chamber and can be stored in a sealed foil pouch indefinitely. However, once removed from the pouch and placed in an aqueous environment, for example, by an animal swallowing the device, the pumping action begins. The active agent is pumped at a constant rate according to Equation 12.14

placed in an aqueous environment, release of the drug follows a time course set by the salt used in the salt chamber and the permeability of the outer membrane casing.

The principal application of these small osmotic pumps has been as implantable controlled release delivery systems in experimental studies on the effect of continuous administration of drugs. The devices are made with volumes of 0.2–2 ml. Figure 12.21 shows one such device being implanted in a laboratory rat. The delivery pattern obtained with the device is constant and independent of the site of implantation, as shown by the data in Figure 12.22.

The development that made osmotic delivery a major method of achieving controlled drug release was the invention of the elementary osmotic pump by Theeuwes in 1974 [34]. The concept behind this invention is illustrated in Figure 12.23. The device is a further simplification of the Theeuwes–Higuchi pump, and eliminates the separate salt chamber by using the drug itself as the osmotic agent. The device is formed by compressing a drug having a suitable osmotic pressure into a tablet using a tabletting machine. The tablet is then coated with a semipermeable membrane, usually cellulose acetate, and a small hole is drilled through the membrane coating. When the tablet is placed in an aqueous environment, the osmotic pressure of the soluble drug inside the tablet draws water through the semipermeable coating, forming a saturated aqueous solution inside the device. The membrane does not expand, so the increase in volume caused by the imbibition of water raises the hydrostatic pressure inside the tablet slightly.

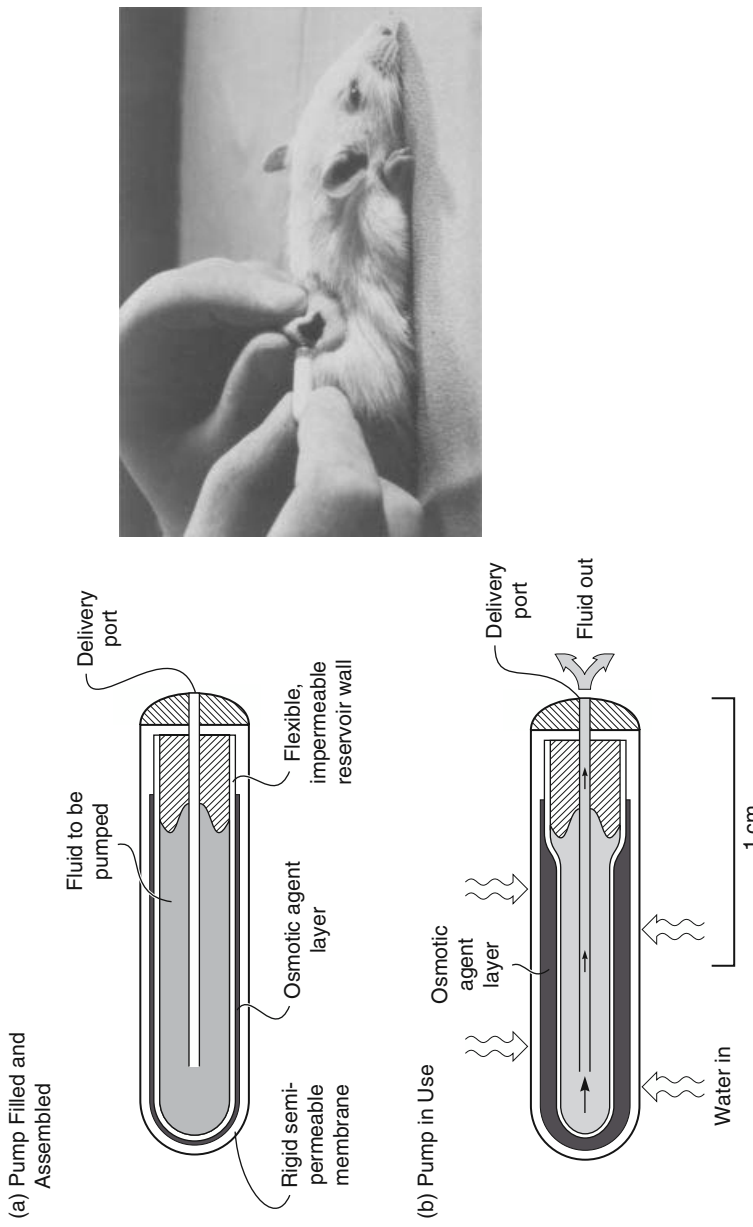


Figure 12.21 The Theeuwes-Higuchi osmotic pump has been widely used in drug delivery tests in laboratory animals. The device is small enough to be implanted under the skin of a rat and delivers up to 1000 µl of drug solution over a three to four day period [33].

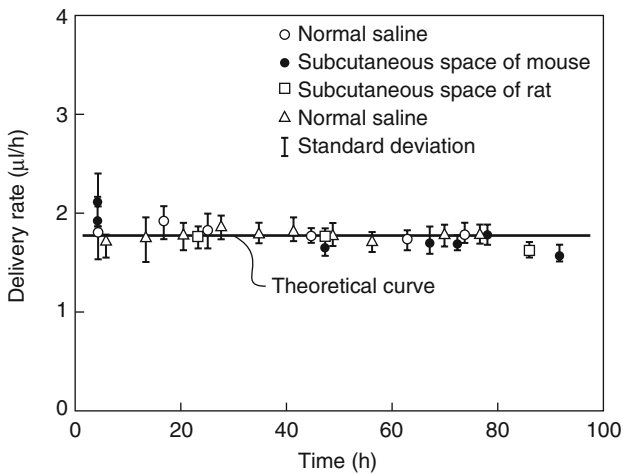


Figure 12.22 Drug delivery curves obtained with an implantable osmotic pump. Reprinted with permission from [33]. Copyright (1976) Springer Science + Business Media.

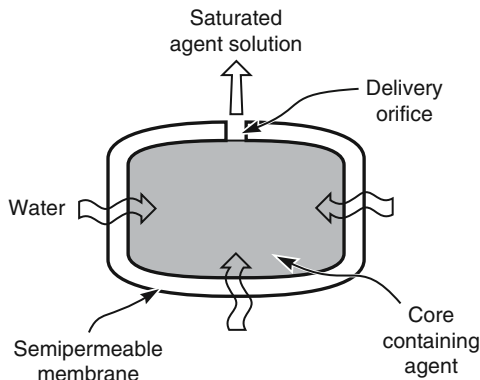
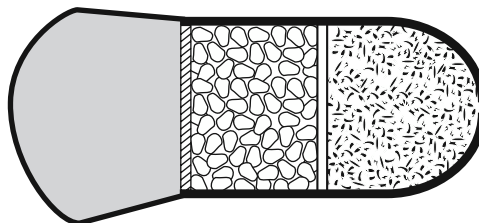


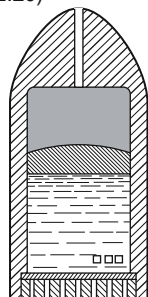
Figure 12.23 The Theeuwes elementary osmotic pump. Reprinted with permission from [34]. Copyright (1975) John Wiley and Sons Ltd.

This pressure is relieved by a flow of saturated drug solution out of the device through the small orifice. Thus, the tablet acts as a small chemical pump, in which water is drawn osmotically into the tablet through the membrane wall and then leaves as a saturated drug solution through the orifice. This process continues at a constant rate until all the solid drug inside the tablet has been dissolved and only a solution-filled shell remains. This residual dissolved drug continues to be delivered, but at a declining rate, until the osmotic pressures inside and outside the tablet are equal. The driving force that draws water into the device is the difference in osmotic pressure between the outside environment and a saturated drug solution. Therefore, the osmotic pressure of the dissolved drug solution has to be relatively high to overcome the osmotic pressure of the body, but for drugs with solubilities greater than 5–10 wt% these devices function very well. Later variations on

Rose-Nelson Pump
(Figure 12.19)



Higuchi-Leeper Pump
(Figure 12.20)



Higuchi-Theeuwes Pump
(Figure 12.21)



Theeuwes
Elementary
Osmotic
Pump
(Figure 12.23)

Scale: 1 cm

	Rose-Nelson pump	Higuchi-Leeper pump	Theeuwes-Higuchi pump	Theeuwes elementary osmotic pump
Approximate volume (cm ³)	80	35	3	< 1
Components	Rigid housing Water chamber Salt chamber Drug chamber Elastic diaphragm Membrane	Rigid housing Salt chamber Drug chamber Elastic diaphragm Membrane	Salt chamber Drug chamber Elastic diaphragm Membrane	Drug chamber Membrane
Number of components	6	5	4	2

Figure 12.24 The main types of osmotic pump drawn to scale

the simple osmotic tablet design have been made to overcome the solubility limitation. The elementary osmotic pump was developed by Alza under the name OROS®, and is commercially available for a number of drugs.

The four types of osmotic pumps described above are interesting examples of how true innovation is sometimes achieved by leaving things out. The first osmotic pump

produced by Rose and Nelson contained six critical components, had a volume of 80 cm³, and was little more than a research tool. In the early 1980s, Felix Theeuwes and others progressively simplified and refined the concept, leading in the end to the elementary osmotic pump, a device that looks almost trivially simple. It has been described as a tablet with a hole, but is, in fact, a truly elegant invention having a volume of less than 1 cm³, containing only two components, achieving almost constant drug delivery, and allowing manufacture on an enormous scale at minimal cost. Figure 12.24 shows examples of the four main types of osmotic pumps taken from the patent drawings. The pumps are drawn to scale to illustrate the progression that occurred as the design was simplified.

References

1. Merrill, J.P. (1961) The artificial kidney. *Sci. Am.*, **205**, 56.
2. Lysaght, J.P., Boggs, D.R., and Taimisto, M.H. (1986) Membranes in artificial organs, in *Synthetic Membranes* (ed. M.B. Chenoweth), Hardwood Academic Publishers, Chur, Switzerland, pp. 100–117.
3. Van Stowe, J.C. (1994) Hemodialysis apparatus, in *Handbook of Dialysis*, 2nd edn (eds J.T. Daugirdas and T.S. Ing), Lippincott-Raven Publishers, New York, pp. 59–78
4. Ofsthun, N.J., Karoor, S., and Suzuki, M. (2008) Hemodialysis membranes, in *Advanced Membrane Technology and Applications* (eds N.N. Li, A.G. Fane, W.S.W. Ho, and T. Matsuura), John Wiley & Sons, Inc., Hoboken, NJ, pp. 519–540.
5. Kolf, W.J. and Berk, H.T. (1944) The artificial kidney: a dialyzer with great area. *Acta. Med. Scand.*, **117**, 121.
6. Kolf, W.J. (1947) *New Ways of Treating Uremia: The Artificial Kidney, Peritoneal Lavage, Intestinal Lavage*, J and A Churchill, Ltd, London.
7. Quinton, W., Dilpard, D., and Scribner, B.H. (1960) Cannulation of blood vessels for prolonged hemodialysis. *Trans. Am. Soc. Artif. Inter. Organs*, **6**, 104.
8. M.L. Keen and F.A. Gotch (1991) Dialyzers and delivery systems, in *Introduction to Dialysis*, M.C. Cogan, P. Schoenfeld and F.A. Gotch (eds.), Churchill Livingston, New York, 1–7.
9. Gibbon, J.H. Jr. (1937) Artificial maintenance of circulation during experimental occlusions of pulmonary artery. *Arch. Surg. Chicago*, **34**, 1105.
10. Gibbon, J.H. Jr. (1954) Application of a mechanical heart and lung apparatus to cardiac surgery. *Minn. Med.*, **37**, 171.
11. Galletti, P.M. and Brecher, G.A. (1962) *Heart-Lung Bypass*, Grun and Stratton, New York.
12. Wiese, F. (2008) Membranes for artificial lungs in *Membranes for Life Sciences* (eds K.V. Peinemann and S.P. Nunes), Wiley-VCH Verlag GmbH, Weinheim, pp. 49–68.
13. Rose, S. and Nelson, J.F. (1955) A continuous long-term injector. *Aust. J. Exp. Biol.*, **33**, 415.
14. Folkman, J.M. and Long, D.M. (1964) The use of silicone rubber as a carrier for prolonged drug therapy. *J. Surg. Res.*, **4**, 139.

15. Croxatto, H.B., Diaz, S., Vera, R. Etchart, M. and Atria, P. (1969) Fertility control in women with a progestagen released in microquantities from subcutaneous capsules. *Am. Obstet. Gynecol.*, **105**, 1135.
16. Scommegna, A., Pandya, G.N., Christ, M., Lee, A.W. and Cohen, M.R. (1970) Intrauterine administration of progesterone by a slow releasing device. *Fert. Steril.*, **21**, 201.
17. Zaffaroni, A. (1981) Applications of polymers in rate-controlled drug delivery. *Polym. Sci. Tech.*, **14**, 293.
18. Sendelbeck, L., Moore, D., and Urquhart, J. (1975) Comparative distribution of pilocarpine in ocular tissues of the rabbit during administration of eyedrops or by membrane controlled delivery systems. *Am. J. Ophthalmol.*, **80**, 274.
19. Shaw, J. (1983) Development of transdermal therapeutic systems. *Drug Dev. Ind. Pharm.*, **9**, 579.
20. Pharriss, B.B., Erickson, R., Bashaw, J., Hoff, S., Place, V.A. and Zaffaroni, A. (1974) Progestasert: a uterine therapeutic system for long-term contraception. *Fert. Steril.*, **25**, 915.
21. Williams, A.C. and Barry, B.W. (2004) Penetration enhancers. *Adv. Drug Delivery Rev.*, **56**, 603–618.
22. Stamatialis, D.F. (2008) Drug delivery through skin: overcoming the ultimate biological membrane, in *Membranes for Life Sciences* (eds K.V. Peinemann and S.P. Nunes), Wiley-VCH Verlag GmbH, Weinheim, pp. 191–221.
23. Crank, J. (1956) *The Mathematics of Diffusion*, Oxford University Press, London.
24. Baker, R.W. (1987) *Controlled Release of Biologically Active Agents*, John Wiley & Sons, Inc., New York.
25. Higuchi, T. (1961) Rate of release of medicaments from ointment bases containing drugs in suspension. *J. Pharm. Sci.*, **50**, 874.
26. Roseman, T.J. and Higuchi, W.I. (1970) Release of medroxprogesterone acetate from a silicone polymer. *J. Pharm. Sci.*, **59**, 353.
27. Paul, D.R. and McSpadden, S.K. (1976) Diffusional release of a solute from a polymer matrix. *J. Membr. Sci.*, **1**, 33.
28. Heller, J. (1980) Controlled release of biologically active compounds from bioerodible polymers. *Biomaterials*, **1**, 51.
29. Pitt, C.G. and Schindler, A. (1980) The design of controlled drug delivery systems based on biodegradable polymers, in *Biodegradables and Delivery Systems for Contraception* (eds E.S.E. Hafez and W.A.A. van Os), MTP Press, Lancaster, pp. 17–46.
30. Santus, G. and Baker, R.W. (1995) Osmotic drug delivery: a review of the patent literature. *J. Controlled Release*, **35**, 1.
31. Higuchi, T. and Leeper, H.M. (1973) Improved osmotic dispenser employing magnesium sulfate and magnesium chloride. US Patent 3,760,804, Sep. 1973.
32. Theeuwes, F. and Higuchi, T. (1974) Osmotic dispensing agent for releasing beneficial agent. US Patent 3,845,770, Nov. 1974.
33. Theeuwes, F. and Yum, S.I. (1976) Principles of the design and operation of generic osmotic pumps for the delivery of semisolid or liquid drug formulations. *Ann. Biomed. Eng.*, **4**, 343.
34. Theeuwes, F. (1975) Elementary osmotic pump. *J. Pharm. Sci.*, **64**, 1987.

13

Other Membrane Processes

13.1 Introduction

Any book must leave something out, and this one has left out a good deal; it does not cover membranes used in packaging materials, sensors, ion-selective electrodes, battery separators, electrophoresis, affinity membranes, and thermal diffusion. In this final chapter, eight processes that come under the general title of “other” are briefly covered.

13.2 Dialysis

Dialysis was the first membrane process to be used on an industrial scale, with the development of the Cerini dialyzer in Italy [1, 2]. The production of rayon from cellulose expanded rapidly in the 1930s, resulting in a need for technology to recover sodium hydroxide from large volumes of hemicellulose/sodium hydroxide by-product solutions. The hemicellulose was of little value, but the 17–18 wt% sodium hydroxide, if separated, could be directly reused in the process. Hemicellulose has a much higher molecular weight than sodium hydroxide, so parchmentized woven fabric or impregnated cotton cloth made an adequate dialysis membrane. The Cerini dialyzer, illustrated in Figure 13.1, consisted of a large tank containing 50 membrane bags. Feed liquid passed through the tank while the dialysate solution passed countercurrently through each bag in parallel. The product dialysate solution typically contained 7.5–9.5% sodium hydroxide and was essentially free of hemicellulose. About 90% of the sodium hydroxide in the original feed solution was recovered. The economics of the process were very good, and the Cerini dialyzer was widely adopted. Later, improved membranes and improved dialyzer designs, mostly of the plate-and-frame type, were produced. A description of these early industrial dialyzers is given in Tuwiner’s book [3].

Dialysis was also used in the laboratory in the 1950s and 1960s, mainly to purify biological solutions or to fractionate macromolecules. A drawing of the laboratory dialyzer used by Craig and described in a series of papers in the 1960s is shown in Figure 13.2

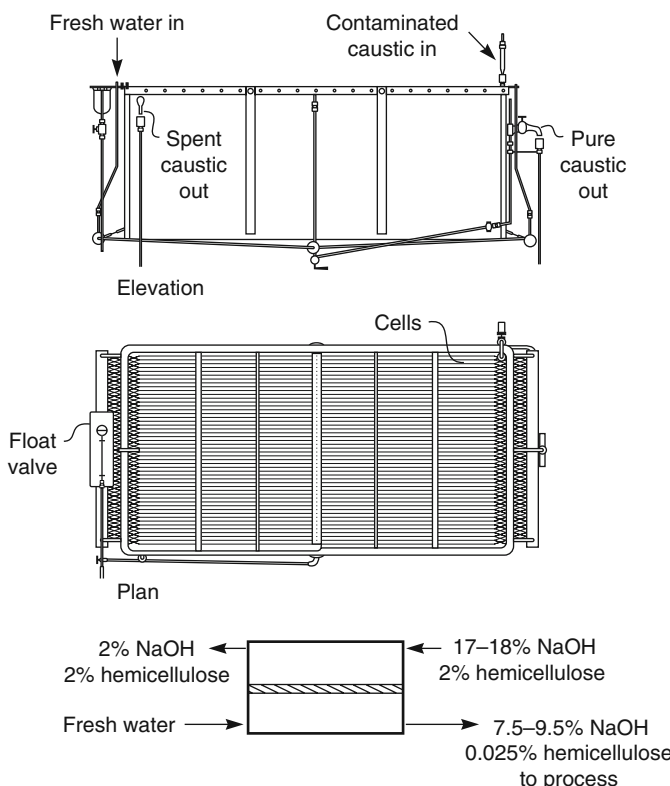


Figure 13.1 Elevation, plan drawing, and flow scheme of the Cerini dialyzer, the first successful industrial dialyzer used to recover sodium hydroxide from waste streams resulting from the production of rayon [2]

[4–6]. Until ultrafiltration membranes became available in the late 1960s, this device was the only way to separate many large-volume biological solutions.

The major current application of dialysis is the artificial kidney, and, as described in Chapter 12, more than 150 million of these devices are used annually. Apart from this one important application, dialysis has essentially been abandoned as a separation technique, because it relies on diffusion, which is usually unselective and inherently slow, to achieve a separation. Thus, most potential dialysis separations are better handled by ultrafiltration or electrodialysis, in which an outside force and more selective membranes provide better, faster separations. The only three exceptions – Donnan dialysis, diffusion dialysis, and piezodialysis – are described in the following sections.

13.3 Donnan Dialysis (Diffusion Dialysis)

One dialysis process for which the membrane does have sufficient selectivity to achieve useful separations is Donnan dialysis, sometimes called diffusion dialysis. If salt solutions

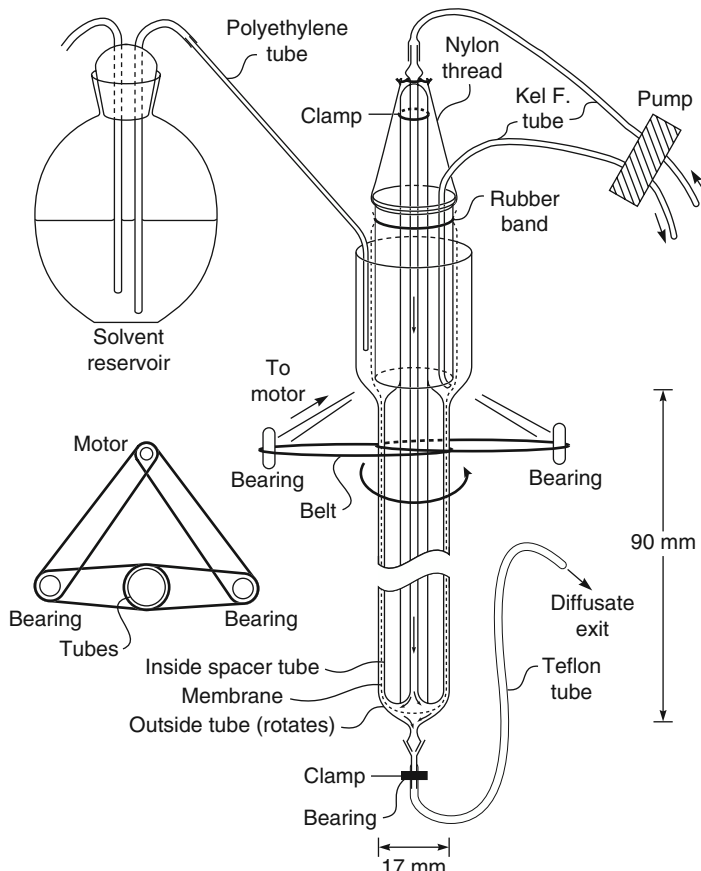


Figure 13.2 Schematic drawing of laboratory dialyzer developed by Craig [4] to separate low-molecular-weight impurities from biological solutions. This was the best method of performing this separation until ultrafiltration membranes became available in the late 1960s. The feed solution was circulated through the inside of the membrane tube; solvent solution was circulated on the outside. Boundary layer formation was overcome by rotating the outer shell with a small motor

are separated by a membrane permeable only to ions of one charge, such as a cation exchange membrane containing fixed negatively charged groups, then distribution of two different cations M^+ and N^+ across the membrane can be expressed by the Donnan expression

$$\frac{[M]_o}{[M]_\ell} = \frac{[N]_o}{[N]_\ell} \quad (13.1)$$

where $[M]_o$ and $[N]_o$ are the concentrations of the two ions in the feed solution, and $[M]_\ell$ and $[N]_\ell$ are the concentrations of the two ions in the product solution. The derivation of the expression is given in Chapter 10. This equation has the same form as Equation 11.10,

derived for coupled transport in Chapter 11, in which carrier selectivity transports ions across the membrane. The difference between coupled transport and Donnan dialysis lies in how the membrane performs the separation.

Donnan dialysis was first described as a separation technique in 1967 by Wallace [7, 8], who was interested in concentrating small amounts of radioactive metal ions. He used cation exchange membranes to treat a large volume of nearly neutral feed solution containing small amounts of metal salts such as uranyl nitrate $\text{UO}_2(\text{NO}_3)_2$. A small volume of 2M nitric acid was used as the receiving solution. Because the membrane contained fixed negative charges, negative ions from the surrounding solutions were essentially excluded from the membrane, and only hydrogen ions (H^+) and uranyl ions (UO_2^{2+}) could permeate the membrane. The very large difference in hydrogen ion concentration across the membrane meant that a large driving force was generated for hydrogen ions to diffuse to the dilute feed solution. To maintain electrical neutrality, an equal number of uranyl ions had to diffuse to the receiving solution. Wallace's apparatus and the results of one of his experiments are shown in Figure 13.3. In this experiment, 98% of the uranyl ions were stripped from the feed solution and concentrated 28-fold in the product nitric acid strip solution.

Like coupled transport, Donnan dialysis can concentrate metal ions many fold. The process is usually driven by an appropriate pH gradient. Because the membranes are normal cation or anion exchange membranes, the stability problems that plague the liquid membranes used in coupled transport are avoided. On the other hand, coupled transport uses carriers selective for one particular ion, excluding others. This property allows coupled transport membranes to selectively transport one particular ion across the membrane, both concentrating and separating the target ion from similar ions in the feed solution. Donnan dialysis membranes are essentially nonselective – all ions of the same charge in the feed solution are transported to the product solution at about the same rate.

Donnan dialysis can be made more selective if a complexing agent specific to one of the ions being transported across the membrane is added to the strip solution. For example, Huang *et al.* [9] used cation exchange membranes driven by sodium ions to transport copper and nickel ions across the membrane. Addition of complexing agents specific for nickel ions, such as oxalic acid or glycine, to the strip solution increased the selectivity of the membrane for nickel over copper dramatically. By removing nickel ions from the receiving solution, the complexing agent maintained a high driving force for nickel transport even when the copper ion concentration had reached an equilibrium level.

Although Donnan dialysis membranes can perform interesting separations, these membranes are a solution to few industrially important applications. Consequently, Donnan dialysis remains a solution in search of a problem.

The most important industrial application is the recovery of acids from spent metal pickling agents such as sulfuric acid, hydrochloric acid, or nitric–hydrofluoric acids [10–12]. These pickling acids remove scale from metal parts and over time become contaminated with iron, chromium, copper, nickel, zinc, and other heavy metals. Acid recovery by electrodialysis is possible but Donnan dialysis – a completely passive process – is often preferred because of its simplicity. The process utilizes the difference

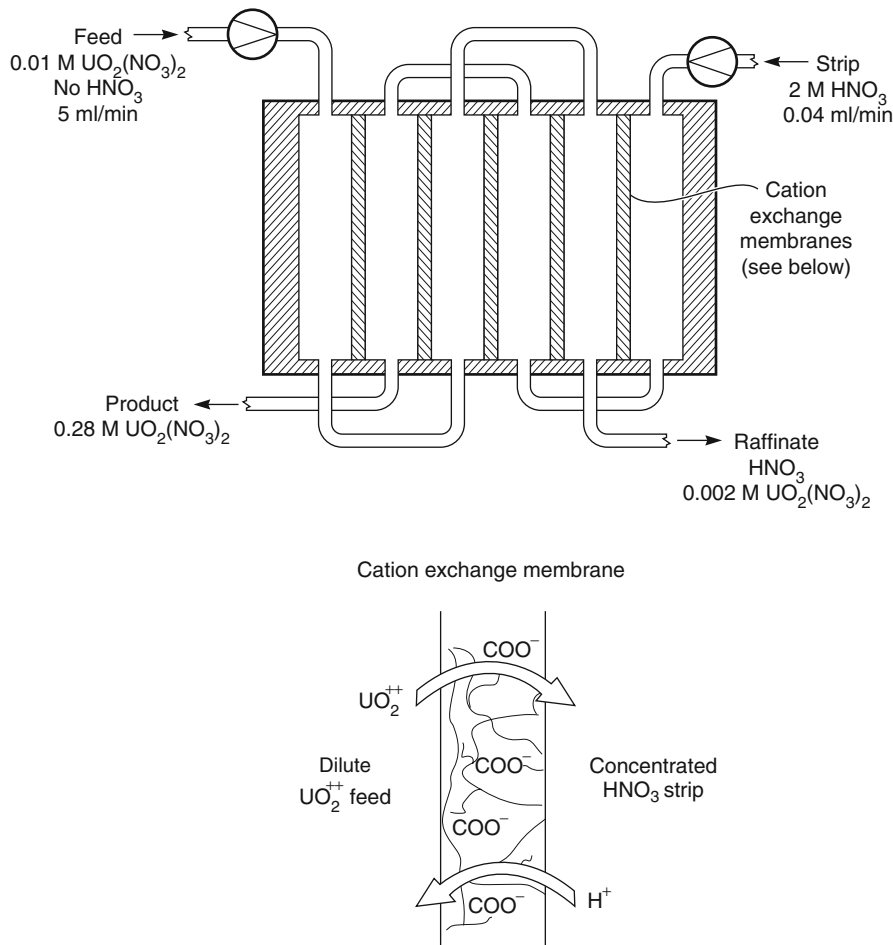


Figure 13.3 Illustration of a Donnan dialysis experiment to separate and concentrate uranyl nitrate, $\text{UO}_2(\text{NO}_3)_2$, using a cation exchange membrane with fixed positive charges. (After Wallace [7, 8])

in permeability of hydrogen ions and multivalent metal ions through anion exchange membranes. A flow schematic is shown in Figure 13.4. The feed solution, containing heavy metal salts and acid, flows countercurrently to water, from which it is separated by an anion exchange membrane. The membrane, which is freely permeable to anions, also preferentially permeates hydrogen ions over heavy metal cations. As a result, the acids in the feed solution, sulfuric acid in the example of Figure 13.4, are removed from the spent liquor and metal ions remain behind. Recovery of 70–80% acid, contaminated with only a small percentage of the metal ions, is possible.

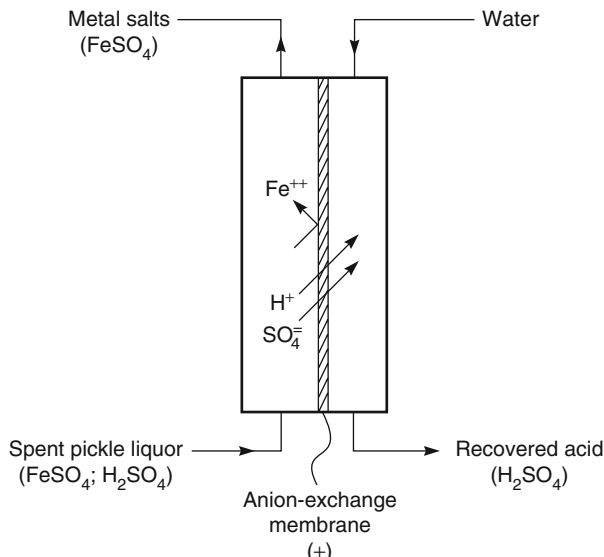


Figure 13.4 Schematic of a Donnan dialysis process to separate acids from heavy metal/acid mixtures

13.4 Charge Mosaic Membranes and Piezodialysis

Donnan dialysis, described in the previous section, is a type of ion exchange process. Ions of the same charge are redistributed across the membrane, but no net flow of salt from one side of the membrane to the other occurs. This is because ion exchange membranes are quite impermeable to salts. Although counter ions to the fixed charge groups in the membrane can easily permeate the membrane, ions with the same charge as the fixed charge groups are excluded and do not permeate. Sollner [13] proposed that, if ion exchange membranes consisting of separated small domains of anionic and cationic membranes could be made, they would be permeable to both anions and cations. These membranes are now called charge mosaic membranes; the concept is illustrated in Figure 13.5. Cations permeate the cationic membrane domain; anions permeate the anionic domain.

Charge mosaic membranes can preferentially permeate salts from water. This is because the principle of electroneutrality requires that the counter ion concentration inside the ion exchange regions be at least as great as the fixed charge density. Because the fixed charge density of ion exchange membranes is typically greater than 1 M, dilute counter ions present in the feed solution are concentrated 10- to 100-fold in the membrane phase. The large concentration gradient that forms in the membrane leads to high ion permeabilities. Water and neutral solutes are not concentrated in the membrane and permeate at low rates. When used as dialysis membranes, therefore, these charged mosaic membranes are permeable to salts but relatively impermeable to non-ionized solutes.

For charge mosaic membranes to work most efficiently, the cationic and anionic domains in the membrane must be close together to minimize charge separation effects [14–16]. The first charge mosaic membranes were made by distributing very small ion

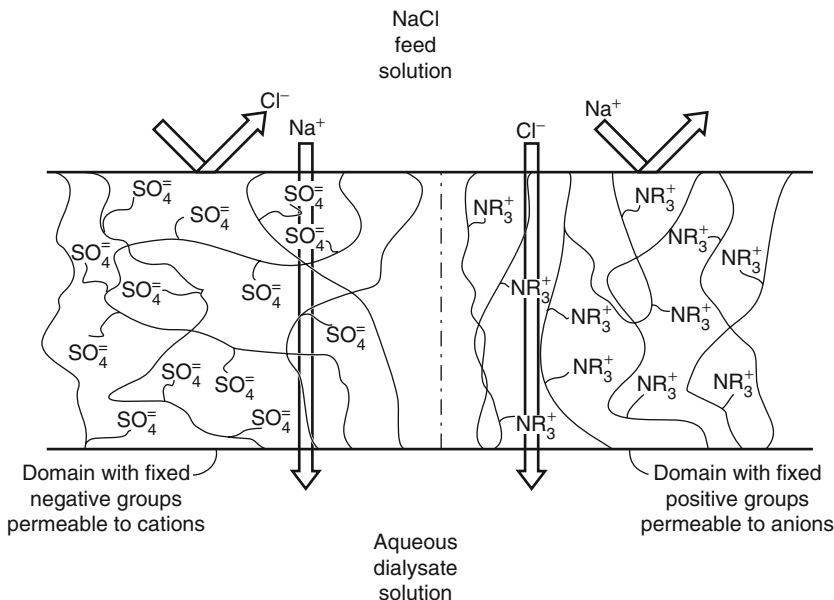


Figure 13.5 A charge mosaic membrane, consisting of separate finely dispersed domains, one domain containing fixed negative charges, the other containing fixed positive charges [13]

exchange beads in an impermeable support matrix of silicone rubber [17, 18]. A second approach, used by Platt and Schindler [19], was to use the mutual incompatibility of most polymers that occurs when a solution containing a mixture of two different polymers is evaporated. Figure 13.6 shows a photomicrograph of a film cast from poly(styrene-*co*-butadiene) and poly(2-vinyl pyridine-*co*-butadiene). The *co*-butadiene fraction makes these two polymers mutually soluble in tetrahydrofuran but, on evaporation of the solvent, a two-phase-domain structure extending completely through the membrane layer forms. Once formed, the poly(2-vinyl pyridine-*co*-butadiene) portion of the membrane is quaternized to form fixed positive groups, and the poly(styrene-*co*-butadiene) portion of the membrane is sulfonated to form fixed negative groups.

Miyaki and Fujimoto and coworkers [20, 21] have obtained an even finer distribution of fixed charge groups by casting films from multicomponent block copolymers such as poly(isoprene-*b*-styrene-*b*-butadiene-*b*-(4-vinyl benzyl)dimethylamine-*b*-isoprene). These films show a very regular domain structure with a 200–500 Å spacing. After casting the polymer film, the (4-vinyl benzyl)dimethylamine blocks were quaternized with methyl iodide vapor, and the styrene blocks were sulfonated with chlorosulfonic acid.

Using the block copolymer membranes described above, significant selectivities for electrolytes over non-electrolytes have been observed. Some data reported by Hirahara *et al.* [21] are shown in Table 13.1. The ionizable electrolytes were 100 times more permeable than non-ionized solutes such as glucose and sucrose, suggesting a number of potential applications in which deionization of mixed solutions is desirable. The permeabilities of salts in these membranes are also orders of magnitude higher than values

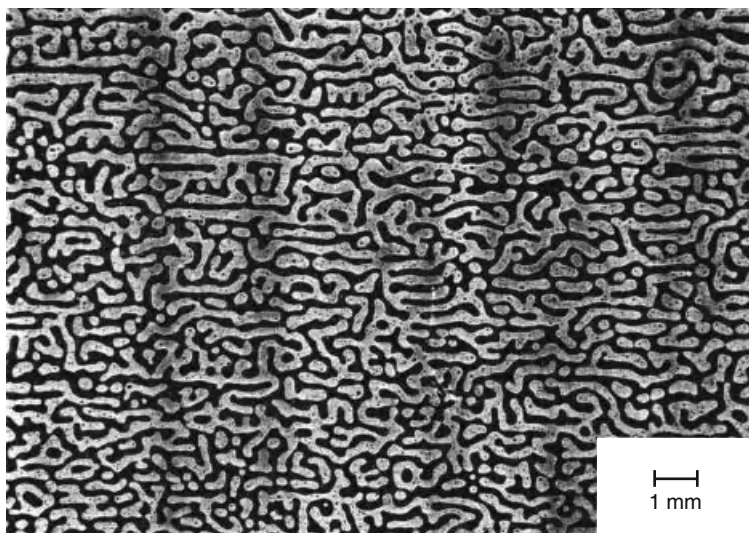


Figure 13.6 Film cast from a 1:2 mixture of poly(styrene-co-butadiene) and poly(2-vinyl pyridine-co-butadiene) with about 15 mol% butadiene content (10 wt% solution of the copolymers in tetrahydrofuran). Dark areas: poly(styrene-co-butadiene); light areas: poly(2-vinyl pyridine-co-butadiene). Reprinted with permission from [14]. Copyright (1971) Wiley-VCH.

Table 13.1 Solute flux measured in well-stirred dialysis cells at 25°C using 0.1 M feed solutions [21]

Solute	Flux (10^{-8} mol/cm 2 .s)
Sodium chloride	7.5
Potassium chloride	9
Hydrochloric acid	18
Sodium hydroxide	10
Glucose	0.08
Sucrose	0.04

Reprinted with permission from K. Hirahara, S.-I. Takahashi, M. Iwata, T. Fujimoto and Y. Miyaki, "Artificial membranes from multiblock copolymers (5)," *Ind. Eng. Chem. Prod. Res. Dev.*, **305**, 25. Copyright 1986, American Chemical Society and American Pharmaceutical Society.

measured for normal ion exchange membranes. In principle then, these membranes can be used in deionization processes, for example, to remove salts from sucrose solutions in the sugar industry.

A second potential application is pressure-driven desalination. When a pressure difference is applied across the membrane, the concentrated ionic groups in the ion exchange domains are swept through the membrane, producing a salt-enriched permeate on the low-pressure side. This process, usually called piezodialysis, has a number of conceptual

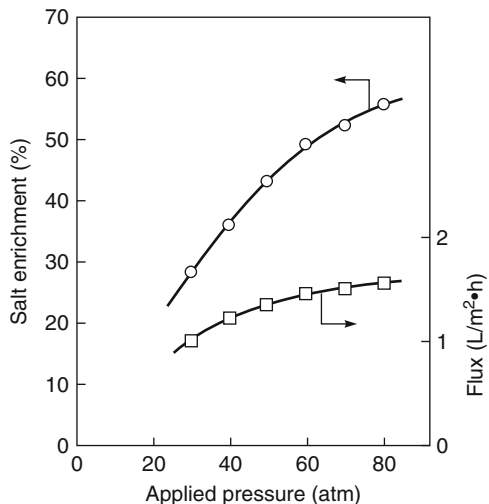


Figure 13.7 Piezodialysis of 0.02 M potassium chloride solution with block copolymer charge mosaic membranes [20]. Enrichment is calculated using the expression:

$$\text{enrichment} = 100 \left(\frac{\text{concentration permeate}}{\text{concentration feed}} - 1 \right)$$

advantages over the alternative, conventional reverse osmosis, because the minor component (salt), not the major component (water), permeates the membrane.

Charge mosaic membranes and piezodialysis continue to be the subject of sporadic research [22], but so far, this has met with little commercial interest. It was originally hoped that the flow of water and salt through charge mosaic membranes would be strongly coupled. If this were the case, the 100-fold enrichment of ions within the charged regions of the membrane would provide substantial enrichment of salt in the permeate solution. In practice, the enrichment obtained is relatively small, and the salt fluxes are low even at high pressures. The salt enrichment also decreases substantially as the salt concentration in the feed increases, limiting the potential applications of the process to desalination of low concentration solutions. Some results of piezodialysis experiments with block copolymer membranes and a potassium chloride solution are shown in Figure 13.7 [20].

13.5 Membrane Contactors and Membrane Distillation

In the membrane processes discussed elsewhere in this book, the membrane acts as a selective barrier, allowing relatively free passage of one component while retaining another. In membrane contactors, the membrane functions as an interface between two phases but does not control the rate of passage of permeants across the membrane. The use of a membrane as a contactor in a process to deoxygenate water is shown in Figure 13.8. Typically, the membrane used is a microporous hollow fiber that separates oxygen-containing water from a nitrogen sweep gas. Dissolved oxygen in the water

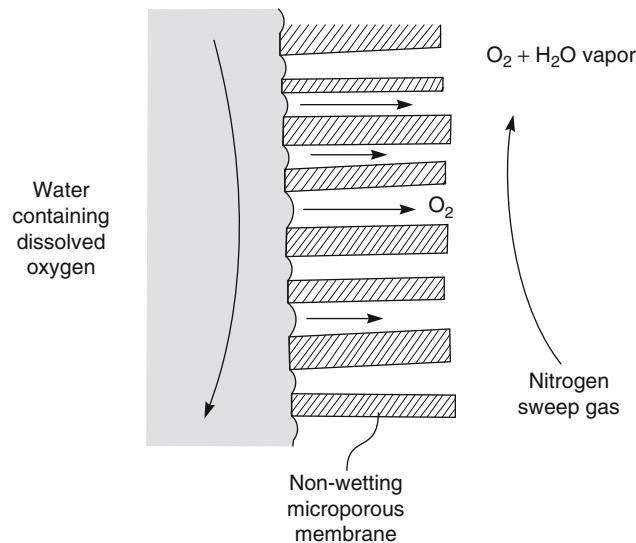


Figure 13.8 Application of a membrane contactor to remove dissolved oxygen from water

diffuses to the nitrogen sweep gas. Even though the dissolved oxygen concentration in the water is very low, its equilibrium partial pressure in the gas phase in contact with the water is high. This means that oxygen permeation through the membrane down the concentration gradient to the nitrogen sweep gas is high. The function of the membrane in this application is to provide a large surface area for contact between the water and the nitrogen sweep gas. The relative permeabilities of oxygen and water vapor through the membrane are not a factor; exactly the same separation could be achieved by running the water and nitrogen countercurrent to each other in a packed tower. However, as shown later, membrane contactors can offer useful advantages over packed towers.

Membrane contactors are often shell-and-tube devices containing microporous capillary hollow fiber membranes. The air-filled membrane pores are sufficiently small that capillary forces prevent direct mixing of the liquid phases on either side of the membrane. The membrane contactor shown in Figure 13.8 separates a liquid and a gas phase: this is a liquid/gas contactor. Membrane contactors can also be used to separate two immiscible liquids (liquid/liquid contactors) or two miscible liquids (usually called membrane distillation) [23]. Contactors can also be used to selectively absorb one component from a gas mixture into a liquid (gas/liquid contactors). The various types of membrane contactors that have been used are illustrated in Figure 13.9.

Contactors have a number of advantages compared to simple liquid/gas absorber/strippers or liquid/liquid extractors. Perhaps the most important advantage is high surface area per volume. The contact area of membrane contactors compared to traditional contactor columns is shown in Table 13.2. Membrane contactors provide 10-fold higher contactor areas than equivalent-sized towers. This makes membrane contactors small and light, sometimes an important advantage. Blood oxygenators, a type of gas/liquid contactor (discussed in Chapter 12), were not widely used for open heart surgery until the

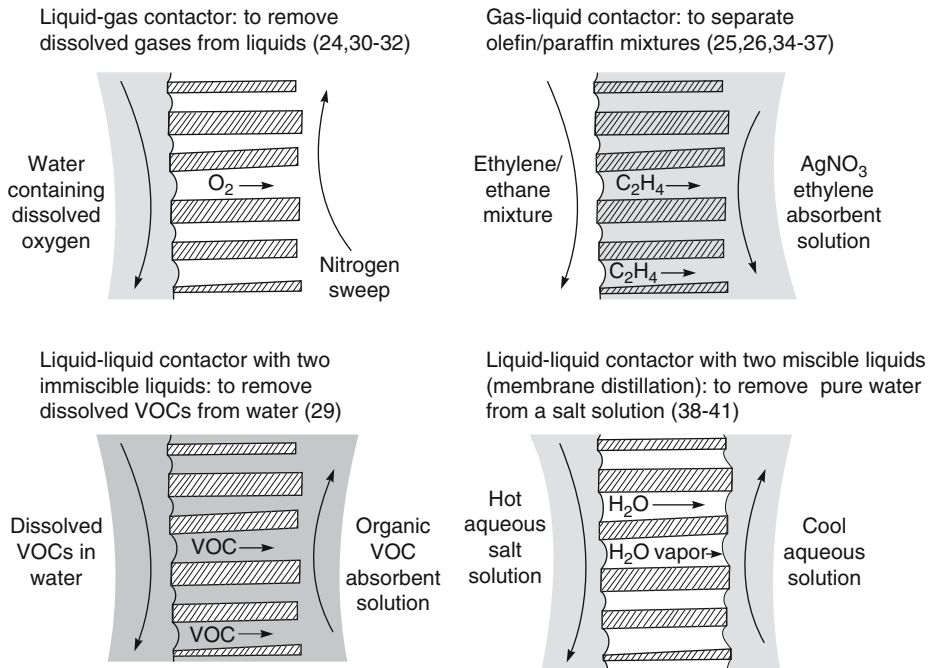


Figure 13.9 Examples of membrane contactors and their applications

Table 13.2 The contact area per unit volume of different devices used as contactors between two phases [25, 26]

Contactor	Surface area per volume (cm^2/cm^3)
Free dispersion columns	0.03–0.3
Packed/trayed columns	0.3–3
Mechanically agitated columns	2–5
Membranes	10–50

membrane blood oxygenator was developed, reducing the volume of blood required to operate the device to a manageable level. Similarly, the principal motivation to develop membrane contactors for offshore dehydration and carbon dioxide removal from natural gas is the reduction in weight and footprint possible. Kvaerner has shown that membrane contactors for this service have 1/4th of the footprint and 1/10th of the weight of conventional absorber/strippers with tray towers [24].

A second advantage of membrane contactors is the physical separation of the counter-flowing phases by the membrane. The membrane area between the two phases is then independent of their relative flow rates, so large flow ratio differences can be used without producing channeling, flooding, or poor phase contact, and maximum advantage can be taken of the ability of counter-flow to separate and concentrate the components crossing the membrane. This allows small volumes of high cost extractants to be used

Table 13.3 Details of Liqui-Cel® hollow fiber membrane contactor modules

Module dimensions

Diameter (cm)	Length (cm)	Number of fibers ($\times 1000$)	Membrane area (m^2)	Area/unit volume (cm^2/cm^3)
8	28	8	1.4	29
10	71	45	19	36
25	71	300	130	39

to treat large volumes of low value feed. Separation of the two phases also eliminates entrainment of one phase by the other, as well as foaming. Finally, unlike traditional contactors, fluids of equal density can be used for the two phases.

The main disadvantages of contactors are related to the nature of the membrane interface. The membrane acts as an additional barrier to transport between the two phases that can slow the rate of separation. Also, over time, the membranes can foul, reducing the permeation rate further, or develop leaks, allowing direct mixing of the two phases. These problems can be alleviated by overcoating the microporous film with a thin non-selective highly permeable layer – for example, silicone rubber – but this reduces the membrane permeance. Also, the membranes are necessarily thin (to maximize their permeation rate) and consequently cannot withstand large pressure differences across the membrane or exposure to harsh solvents and chemicals. In many industrial settings, this lack of robustness prohibits the use of membrane contactors.

Despite these caveats, the use of membrane contactors is growing rapidly. Positive reviews are given by Reed *et al.* [27], Qi and Cussler [25, 26], Gabelmann and Hwang [28], and Prasad and Sirkar [29].

Table 13.3 shows the dimensions of a series of industrial hollow fiber contactors produced by Hoechst Celanese under the trade name Liqui-Cel®. The contact area per unit volume (cm^2/cm^3) is between 25 and 40. This high surface-to-volume ratio is achieved by making the fluid space between the membranes small – in the case of Liqui-Cel devices, between 200 and 400 μm . This means that the fluids passed through these devices must be particulate-free to avoid rapid plugging with retained particulates.

13.5.1 Applications of Membrane Contactors

13.5.1.1 Liquid/Gas and Gas/Liquid Membrane Contactors

Delivery or removal of gases from liquids is currently the largest commercial application of membrane contactors. One example is blood oxygenators, described in Chapter 12. Industrial applications of similar devices include deoxygenation of ultrapure water for the electronics industry or boiler feed water [30] and the adjustment of carbonation levels in beverages [31, 32]. The performance of an industrial-scale oxygen removal system is shown in Figure 13.10. This unit consists of a 10-in.-diameter, rather short, capillary device containing about $135\ m^2$ of contactor area. The aqueous phase is circulated on the outer, shell-side of the fibers to avoid the excessive pressure required to circulate fluid at a high velocity down the fiber bore. The major resistance to mass transfer is in the liquid boundary on the outside of the fiber, so a baffled hollow fiber membrane

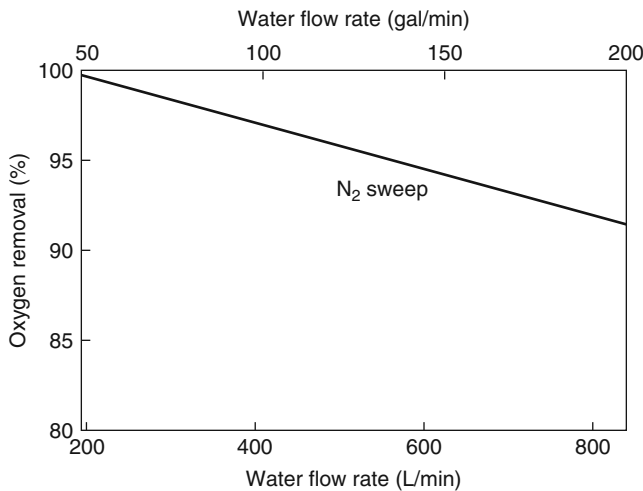


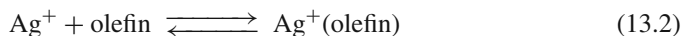
Figure 13.10 Oxygen removal from water with a 10-in.-diameter membrane contactor (135 m^2 membrane area) [30]

module design [33] is used to cause radial flow of the fluid across the membrane from a central fluid distribution tube. Nitrogen sweep gas flows down the inside of the fibers. This design produces good turbulent mixing in the contactor at moderate pressure drops.

In Europe, the TNO [34] and Kvaerner [24] are both developing contactors to remove water and carbon dioxide from natural gas. Glycol or amines are used as the absorbent fluid. The goal is to reduce the size and weight of the unit to allow use on offshore platforms, so oftentimes only the absorber, the largest piece of equipment in a traditional absorber/stripper, is replaced with a membrane contactor. Kvaerner has taken this technology to the pilot demonstration phase.

Another type of gas exchange process, developed to the pilot plant stage, is separation of gaseous olefin/paraffin mixtures by absorption of the olefin into silver nitrate solution. This process is related to the separation of olefin/paraffin mixtures by facilitated transport membranes, as described in Chapter 11. A membrane contactor provides a gas–liquid interface for gas absorption to take place; a flow schematic of the process is shown in Figure 13.11 [35, 36]. The olefin/paraffin gas mixture is circulated on the outside of a hollow fiber membrane contactor, while a 1–5 M silver nitrate solution is circulated countercurrently down the fiber bores. Hydrophilic hollow fiber membranes, which are wetted by the aqueous silver nitrate solution, are used.

The olefin fraction of the feed gas crosses the membrane and reacts reversibly with silver ions to form a soluble silver–olefin complex



The olefin-laden silver solution is then pumped to a flash tank, where the pressure is lowered and the temperature raised sufficiently to reverse the complexation reaction and liberate pure ethylene. The regenerated silver nitrate solution is returned to the contactor.

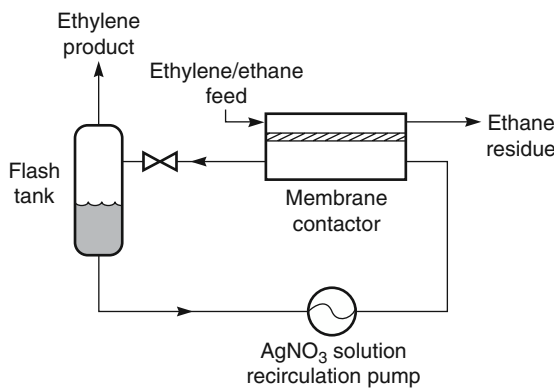


Figure 13.11 Flow schematic of the membrane contactor process developed by British Petroleum to separate ethylene/ethane mixtures by absorption into silver nitrate solution [35, 36]

In this process, the high cost of the silver nitrate carrier must be balanced against the cost of the membrane contactor. If the silver solution is circulated through the contactor at a very high rate, high fluxes are obtained, but the silver utilization calculated from the silver ion amount complexed in the contactor is low compared to the maximum possible complexation achievable under the condition of the test.

Absorption of olefin from olefin/paraffin mixtures has been scaled up to the pilot plant scale, and a number of successful trials were performed in the early 1990s. Separation factors of 200 or more were obtained, producing 99.7% pure ethylene. However, slow degradation of the silver nitrate solution is a problem, and a portion of the recirculating degraded silver nitrate solution must be continuously bled off and replaced with fresh solution. Boundary layer problems on the liquid side of the membrane are also a serious issue in these devices [25, 26].

To reduce the relatively large volume of silver nitrate solution held in the flash tank portion of the plant shown in Figure 13.11, Bessarabov *et al.* [37] have proposed using two membrane contactors in series, as shown in Figure 13.12. One contactor functions as an absorber, the other as a stripper. The first contactor removes ethylene from the pressurized feed gas into cold silver nitrate solution. The solution is then warmed and pumped to the second contactor where ethylene is desorbed from the silver nitrate solution into a low-pressure product ethylene gas stream. The regenerated silver nitrate solution is cooled and returned to the first contactor.

Bessarabov's devices use composite membranes consisting of a thin silicone rubber polymer layer coated onto a microporous poly(vinylidene fluoride) support layer. These membranes have high fluxes and minimal selectivities for the hydrocarbon gases, but the dense silicone layer provides a more positive barrier to bleed-through of liquid than do capillary effects with simple microporous membranes.

13.5.1.2 Liquid/Liquid Membrane Contactors (Membrane Distillation)

The most important application of liquid/liquid membrane contactors is membrane distillation, shown schematically in Figure 13.13. In this process, a warm, salt-containing

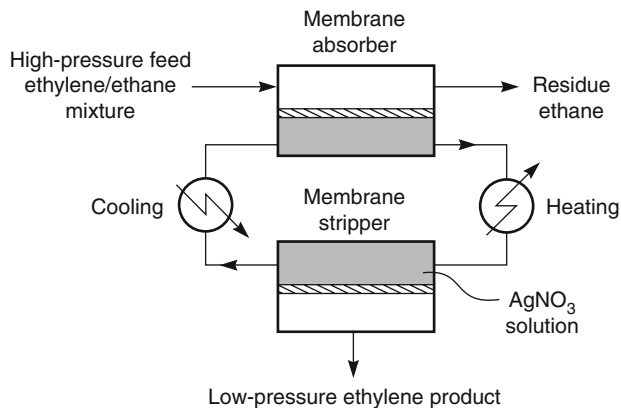


Figure 13.12 Flow schematic of process using two membrane contactors for the separation of ethylene/ethane mixtures proposed by Bessarabov *et al.* [37]

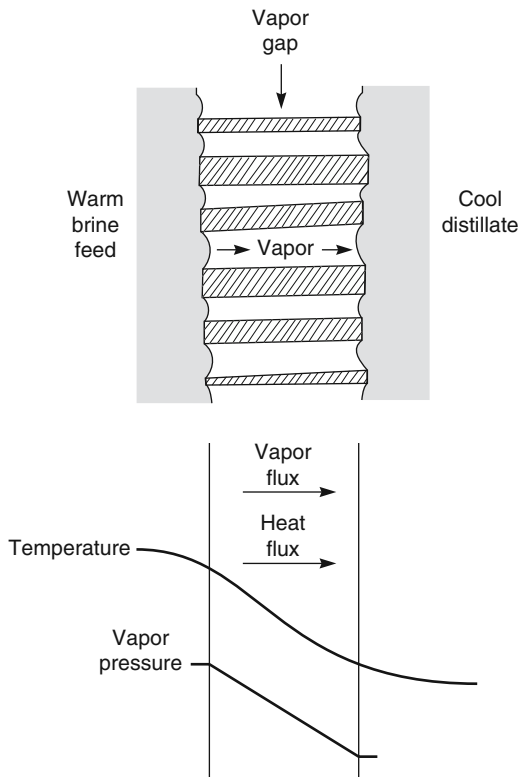


Figure 13.13 A schematic illustration of the membrane distillation process showing temperature and water vapor pressure gradients that drive the process

solution is maintained on one side of the membrane and a cool pure distillate on the other. The hydrophobic microporous membrane is not wetted by either solution and forms a vapor gap between the two solutions. Because the solutions are at different temperatures, their vapor pressures are different; as a result, water vapor diffuses across the membrane. The latent heat required to vaporize the water is removed from the feed solution, and is carried to the permeate solution when the vapor condenses. Consequently, the feed solution cools, and the permeate warms. In addition, simple conduction of heat through the membrane can occur, but in properly designed systems, this is usually small in comparison to the latent heat transport.

The water vapor flux is proportional to the vapor pressure difference between the warm feed and the cold permeate. Because of the exponential rise in vapor pressure with temperature, the flux increases sharply as the temperature difference across the membrane is increased. Dissolved salts in the feed solution decrease the vapor pressure driving force, but this effect is small unless the salt concentration is very high. Some typical results illustrating the dependence of flux on the temperature and vapor pressure difference across a membrane are shown in Figure 13.14.

Membrane distillation offers a number of advantages over alternative pressure-driven processes such as reverse osmosis. Because the process is driven by temperature gradients, low-grade waste heat can be used and expensive high-pressure pumps are not required. Membrane fluxes are comparable to reverse osmosis fluxes, so membrane areas

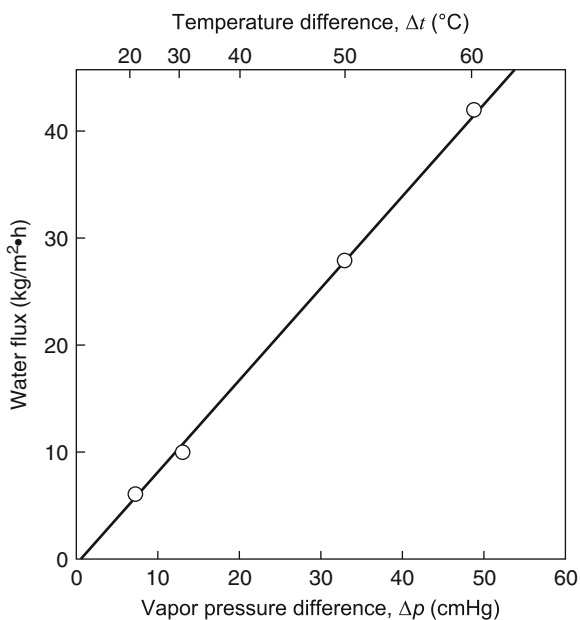


Figure 13.14 Water flux across a microporous membrane as a function of temperature and vapor pressure difference (distillate temperature: 18–38°C; feed solution temperature, 50–90°C). (Taken from the data of Schneider *et al.* [38])

are not excessive. Finally, the process is still effective with slightly reduced fluxes even for concentrated salt solutions. This is an advantage over reverse osmosis, in which the feed solution osmotic pressure places a practical limit on the concentration of a salt in the solution to be processed.

The principal application proposed for the technique is the separation of water from salt solutions. In the 1980s, a research group at Enka, then a division of Akzo, developed membrane distillation to the commercial scale using microporous polypropylene capillary membrane modules. The design and performance of their process are shown in Figure 13.15 [38]. In this device, the incoming salt solution is heated to close to 100°C and circulated on one side of the membrane. An approximately equal flow of cooler distillation solution is circulated countercurrently on the other side of the membrane. As water vapor passes from feed to permeate, the feed solution cools, while the permeate (distillate) solution warms by an equivalent amount. In the unit illustrated, the temperature of the brine solution cools from 100 to 58°C, and the distillate warms from 42 to 86°C. The warm permeate is run against the cooled incoming salt solution, recovering about half of the latent heat transported across the membrane. The remaining energy required is provided by the supplementary heater that warms the circulating brine solution to 100°C.

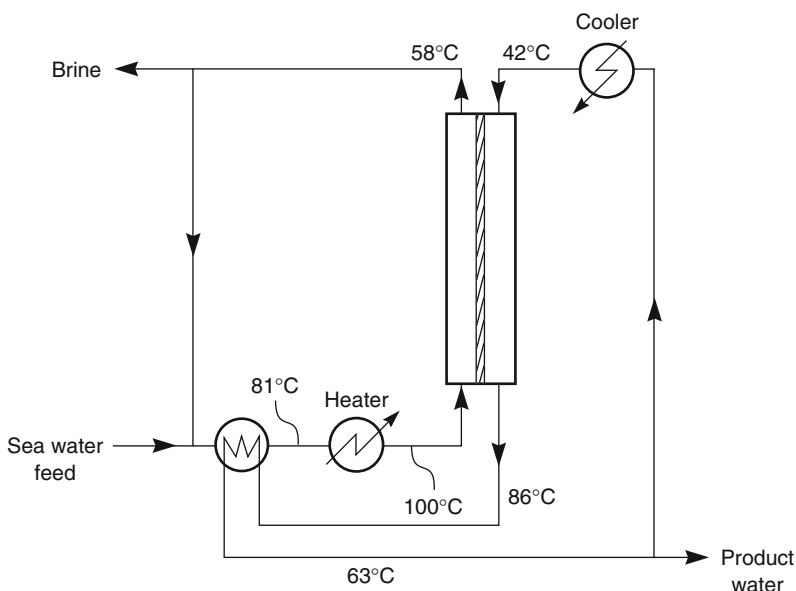


Figure 13.15 Flow scheme and performance data for a membrane distillation process for the production of water from salt solutions. Feed salt solution is heated to 100°C and passed countercurrent to cool distillate that enters at 42°C. The distillate product is almost salt-free. The distillate flux is almost constant up to salt concentrations as high as 20% NaCl. Reprinted with permission from [38]. Copyright (1988) Elsevier.

In this unit, about 8% of the water in the salt solution passes through the membrane each time the solution is circulated through the device. This means the salt solution is re-circulated several times before a fraction is removed as concentrated brine. The condensed distillate produced by the process is almost salt free. Essentially all the power to drive the process is provided as low-grade heat.

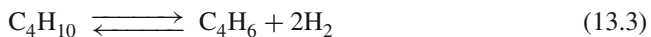
Despite the technical success of the device, a significant market did not develop. For large applications such as seawater desalination, for which the potential energy savings were important, the capillary membrane contactor modules were too expensive compared to low-cost, reliable reverse osmosis modules. For smaller applications on chemical process streams, the energy savings were not important, so cost and reliability compared to simple evaporation were an issue.

In recent years, there has been a revival of interest in the process. TNO has brought the technology to the small demonstration plant stage. More detailed discussions of the technology are found in a number of recent reviews [39–41].

13.6 Membrane Reactors

By the early 1980s, membrane technology had developed to the point at which a number of industrial groups began to consider using membranes to control the products of chemical reactions. Two properties of membranes are used; the first is the membrane as a contactor, as illustrated in Figure 13.16a. The membrane separates the reaction medium in one chamber from a second chamber containing a catalyst, enzymes, or a cell culture. This type of application has a long history in fermentation processes involving so-called bioreactors [42]. More recently, membrane reactors are being developed for conventional chemical separations [43]. As the reaction medium flows through the first chamber, membrane reactants diffuse through the membrane, react in the second chamber, and then diffuse back out to be collected as a product stream. The membrane provides a large exchange area between the catalytic material and the reaction medium but performs no separation function. In the example shown, the reactant is pectin, a high molecular weight polysaccharide present in citrus juice that causes an undesirable haze in the juice. Degradation of the pectin to galacturonic acid by the enzyme pectinase eliminates the haze [44].

The second type of membrane reactor, illustrated in Figure 13.16b, uses the separative properties of a membrane. In this example, the membrane shifts the equilibrium of a chemical reaction by selectively removing one of the components of the reaction. The example illustrated is the dehydrogenation reaction converting *n*-butane to butadiene and hydrogen



Removing hydrogen from the reaction chamber by permeation through the membrane causes the chemical equilibrium to shift to the right, and the conversion of butane to butadiene increases [45].

A third type of membrane reactor combines the functions of contactor and separator. An example of this combination membrane reactor is shown in Figure 13.16c, in which the membrane is a multilayer composite. The layer facing the organic feed stream is

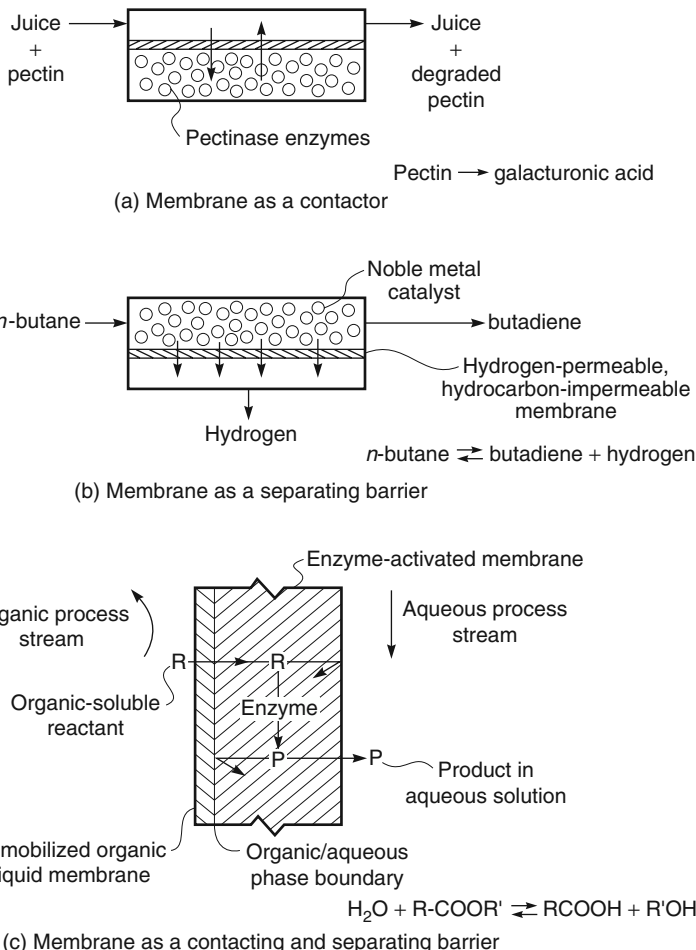


Figure 13.16 Examples of the three types of membrane reactor. (a) Membrane as a contactor, (b) membrane as a separating barrier and (c) membrane as a contacting and separating barrier

an immobilized organic liquid membrane; the layer facing the aqueous product solution contains an enzyme catalyst for the de-esterification reaction



Organic-soluble ester is brought to the reactor with the organic feed solution and freely permeates the immobilized organic liquid membrane to reach the catalyst enzyme. The ester is then hydrolyzed. The alcohol and acid products of hydrolysis are much more polar than the ester and, as such, are water soluble but relatively organic insoluble. These products diffuse to the aqueous permeate solution. The membrane provides both an active site for the reaction and separates the products of reaction from the feed [46].

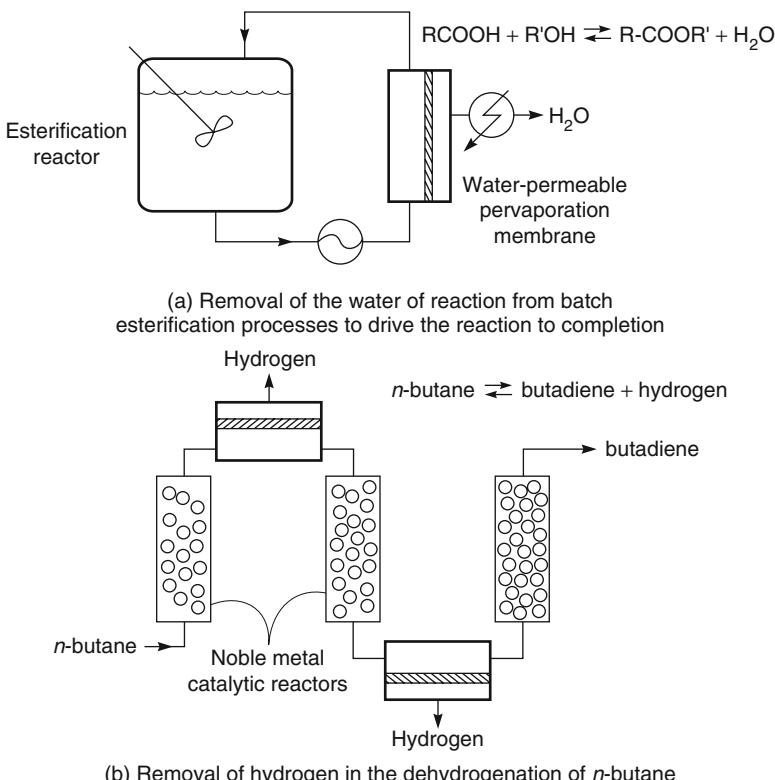


Figure 13.17 Examples of membrane reactors used to change the products of chemical reaction in which the membrane separation step is physically separated from the chemical reaction step. (a) Removal of the water of reaction from batch esterification processes to drive the reaction to completion and (b) removal of hydrogen in the dehydrogenation of n-butane

In the membrane reactor shown in Figure 13.16c, the chemical reaction and the separation step use the same membrane. However, in some processes it is desirable to separate reaction and separation into two distinct operations. If the net result of the process is to change the products of the chemical reaction, the process is still classified under the broad heading of membrane reactor. Two examples in which chemical reaction and separation are physically separated are shown in Figure 13.17. Figure 13.17a shows the use of a pervaporation membrane to shift the equilibrium of the de-esterification reaction [47, 48]. A portion of the organic solution in the esterification reactor is continuously circulated past the surface of a water-permeable membrane. Water produced in the esterification reaction is removed through the membrane. By removing the water, the reaction can be driven to completion.

Figure 13.17b shows the use of a hydrogen-permeable membrane to shift the equilibrium of the n-butane dehydrogenation reaction. The catalytic reactor is divided into steps, and a hydrogen-permeable membrane placed between each step. Because the hydrogen is removed from the reactor in two discrete steps, some inefficiency results, but separating the membrane separation step from the catalytic reactor allows the gas to be

cooled before being sent to the membrane separator. Polymeric membranes can then be used for the gas separation operation [45]. Such membranes can remove hydrogen very efficiently from the butane–butadiene/hydrogen mixture but cannot be used at the 400–500°C operating temperature of the catalytic reactor.

13.6.1 Applications of Membrane Reactors

Membrane reactors are being considered for many processes, and some are already being used on an industrial scale. A detailed description of this work is beyond the scope of this book; the three main application categories are described briefly below.

13.6.1.1 Cell Culture and Fermentation Processes

The traditional, and still the most common, fermentation process involves the addition of microbial cell cultures to the reaction medium in a batch reactor. This type of batch process is inherently slow, and microbial cells are lost with each batch of product. Recently there has been a great deal of interest in developing continuous fermentation processes using membrane bioreactors [42, 48–50]. Much of this work has concentrated on the production of ethanol or acetone/butanol by fermentation of low-grade food processing waste such as cheese whey, using a recycle membrane reactor design as shown in Figure 13.18. The principal advantages of the reactor are its continuous operation, the high cell densities that are maintained, and the lack of build-up of reaction products that inhibit the reaction.

Another type of microbiological reactor is the hollow fiber membrane bioreactor shown in Figure 13.19. In this device, the microbial cells are trapped on the shell side of a capillary hollow fiber module. The feed solution, containing substrate and the products of microbial reaction, is circulated down the bore of the fibers [51]. This device has proven useful in producing protein monoclonal antibodies from genetically engineered

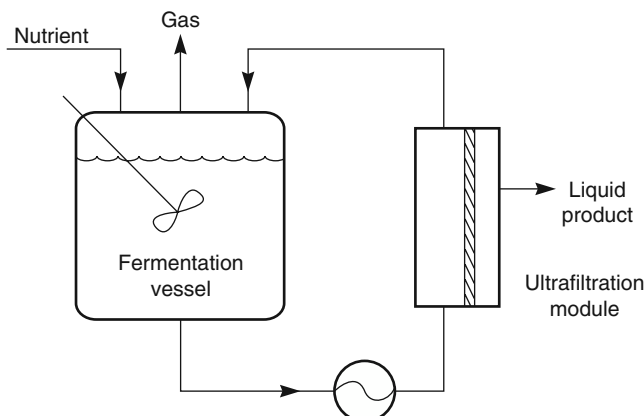


Figure 13.18 Continuous recycle fermenter membrane reactor. An ultrafiltration module removes the liquid products of fermentation as a clean product. This system is being developed for production of ethanol, acetone, and butanol by fermentation of food processing waste streams

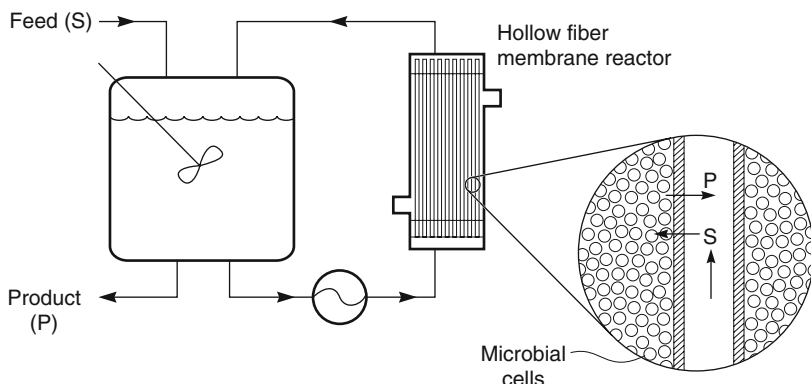


Figure 13.19 A hollow fiber membrane reactor. Nutrients (*S*) diffuse to the microbial cells on the shell side of the reactor and undergo reaction to form products (*P*) such as monoclonal antibodies Reprinted with permission from [14]. Copyright (1971) Elsevier Ltd.

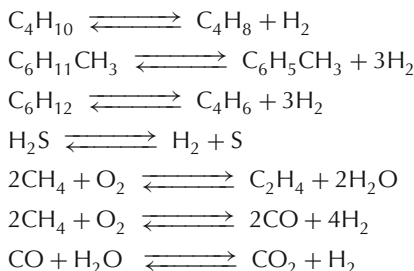
mammalian cells. Similar devices incorporating anaerobic microorganisms have been used to convert syngas (carbon monoxide and hydrogen) into ethanol [52]. By manipulating the molecular weight cut-off of the fiber, the flux of molecules of different molecular weights across the filter can be controlled. Very high cell densities can be achieved in these hollow fiber cartridges, which have been used to produce monoclonal antibodies.

13.6.1.2 Light Hydrocarbon Gas-Phase Catalytic Reactions

Several important refinery and chemical feedstock reactions appear to be good candidates for membrane reactor systems; some such reactions are listed in Table 13.4. Because of the high temperatures involved, developing the appropriate selective membranes is difficult, and this type of membrane reactor has not moved beyond the laboratory stage.

The first four reactions listed in Table 13.4 are dehydrogenation reactions in which one of the reaction products is hydrogen. By removing hydrogen, the reaction equilibrium

Table 13.4 Petrochemical reactions being considered as applications for membrane reactors



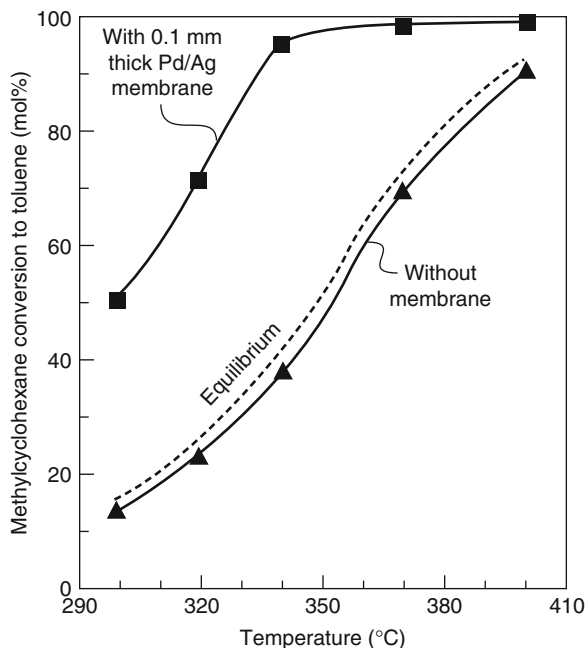
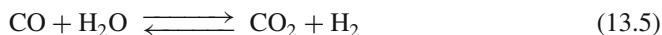


Figure 13.20 Methylcyclohexane conversion to toluene as a function of reactor temperature in a membrane and a nonmembrane reactor. Reprinted with permission from [53]. Copyright (1995) American Chemical Society.

can be driven to completion, increasing the degree of conversion of the dehydrogenated product significantly. An example of the improvement in conversion that is possible is shown in Figure 13.20 [53]. In this figure, the fractional conversion of methylcyclohexane to toluene in a simple tube reactor is compared to that in a reactor with hydrogen-permeable, palladium-silver-alloy walls. Without the membrane, the degree of conversion is limited to the equilibrium value of the reaction. By removing the hydrogen, higher degrees of conversion can be achieved. Figure 13.20 also illustrates the problem that has inhibited widespread use of membrane reactors – the high temperature of the reactions. The reactions listed in Table 13.4 are all normally performed at 300–500°C. These temperatures are far above the normal operating range of polymeric membranes, so hydrogen-permeable metal membranes, microporous carbon membranes, or ceramic membranes must be used. Unfortunately, current metal or ceramic membranes are too expensive and too unreliable to be used in a commercial process.

The most important potential application of hydrogen-permeable membrane reactors is the production of hydrogen by the water gas shift reaction



All plants producing hydrogen from coal or petroleum coke gasification or from reforming of natural gas use a catalytic shift reactor to convert CO in the gas to more hydrogen.

By removing the hydrogen, the reaction can be driven to completion and a pure hydrogen product gas stream produced. The U.S. Department of Energy has supported the development of palladium-based membranes for this separation for a number of years and the technology has reached bench/pilot-scale project stage. Tokyo Gas in Japan and a European Union-funded project have also operated similar units.

The most troublesome problem with these membrane reactors has been poisoning of the catalyst and membrane by trace components in the feed gas, in particular hydrogen sulfide, which can cause a catastrophic decrease in membrane flux within a few minutes of exposure. Most of today's palladium alloy membranes require H₂S levels of less than 1 ppm for long-term continuous operation. A discussion of the current status of palladium membranes is given in several recent articles and reviews [54, 55].

13.7 Ion-Conducting Membrane Reactors

Another membrane application that could become a business in the future is the use of ion-conducting membranes in membrane reactors. In the past 10 years, several hundred US patents have appeared on this topic, as well as many papers. The overall concept is to use ceramic membranes that conduct oxygen or hydrogen ions at high temperatures. Materials that can conduct both ions and electrons are called mixed-conducting matrices. Teraoka *et al.* published the first important papers describing these materials in the 1980s [56, 57]. Various complex metal oxide compositions, including some better known for their properties as superconductors, have mixed-conducting properties; recent efforts in the field focus on these materials. Examples are perovskites having the structure La_xA_{1-x}Co_yFe_{1-y}O_{3-z}, where A is barium, strontium, or calcium; x and y are 0–1; and the value of z makes the overall material charge neutral. Passage of oxygen ions and electrons is related to the defect structure of these materials; at temperatures of 800–1000°C, disks of these materials have shown extraordinary permeabilities to oxygen. Similar mixed-oxide membranes can also conduct protons [58].

Two large US consortia are working on the development of these membranes, one headed by Air Products [59–63] and the other by Praxair/BP [64–66]; there is also a BRITE (Basic Research in Industrial Technology for Europe) – funded European Group and others in Japan and China. If these groups are successful, the membranes could change the economic basis of the petrochemical industry. At the appropriately high operating temperatures, the membranes are perfectly selective for oxygen over nitrogen, and membranes with nominal oxygen permeabilities of 10 000 Barrer can be obtained. In principle, this means that a membrane 1 µm thick has a permeance of 10 000 × 10⁻⁶ cm³(STP)/cm²·s·cmHg. In practice, actual permeances are lower than this, because as the membranes become thinner, slow surface reaction kinetics become rate-controlling. Nonetheless, fluxes are high enough to make processes based on these membranes economically viable.

The most important applications, and a principal driving force behind the development of these membranes, are membrane reactor processes, such as the production of synthesis gas (syngas) by partial oxidation of methane or the oligomerization of methane to produce ethylene. Both processes are illustrated in Figure 13.21. In syngas production, oxygen

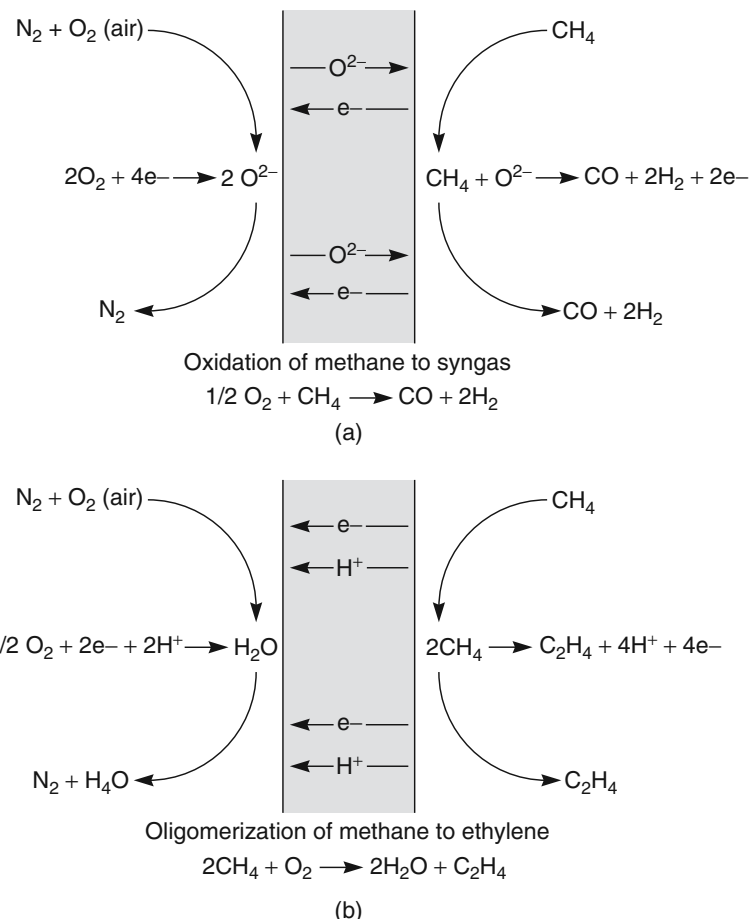


Figure 13.21 Use of ion-conducting ceramic membranes in a membrane reactor to produce (a) syngas ($CO + H_2$) and (b) ethylene

ions diffusing through the membrane react with methane to form carbon monoxide and hydrogen. This gas can then be used without further separation to form methanol or other petrochemicals. In ethylene production, methane is catalytically reacted to produce ethylene and hydrogen. The hydrogen permeates the membrane and then reacts with the oxygen in air to produce water. This second reaction produces the energy necessary to heat the process.

The membrane areas needed in these plants are not huge, but the technical challenges are substantial. Defect-free, anisotropic composite ceramic membranes with selective layers that are $1\text{--}5\ \mu\text{m}$ thick, able to operate continuously at $800\text{--}1000^\circ\text{C}$, nonpoisoning, nonfouling, and reasonable in cost are required – not impossible, but difficult. Prototypes of the type of reactor required are beginning to appear. Two module designs are shown in Figure 13.22 [67].

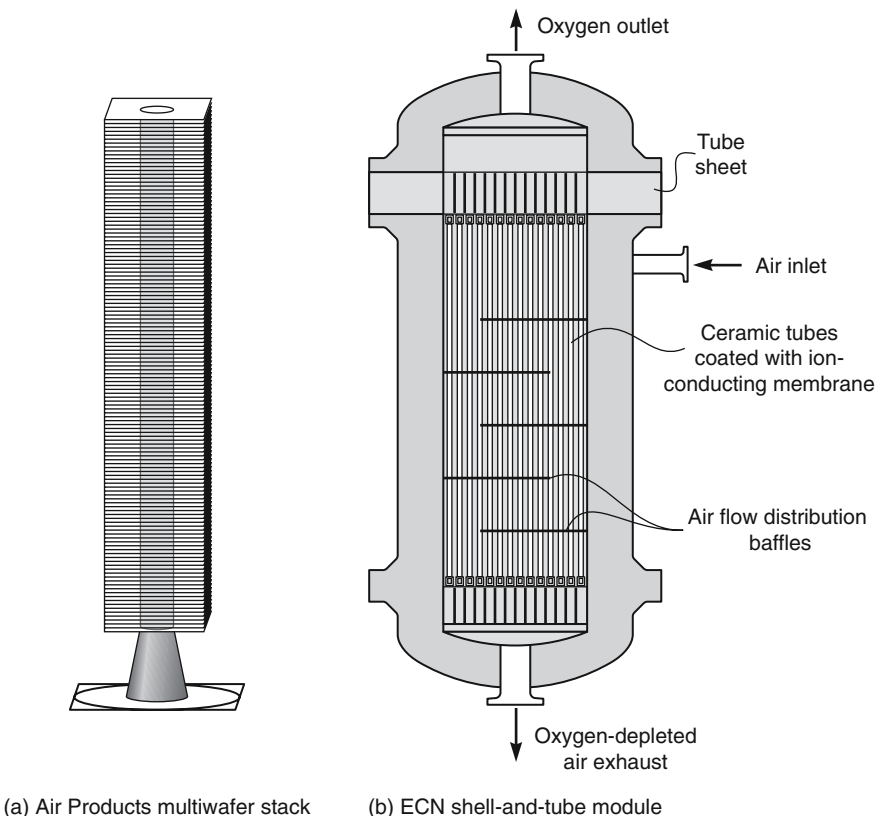


Figure 13.22 Two ceramic ion-conducting module designs. (a) The Air Products multi-wafer stack and (b) a tubular module design from ECN (The Netherlands). Reprinted with permission from [67]. Copyright (2006) Elsevier.

The most advanced design is the Air Products stacked wafer module. In this unit, porous wafers coated with the ion-conducting membrane are sealed to a hollow central ceramic product tube. In this way, only one seal between the ceramic tube and the enclosing pressure vessel shell must be made. This reduces the formation of leaks caused by differential thermal expansion at the membrane seals, which have caused many problems. Most of the other groups are developing shell-and-tube membrane modules, although hollow fiber ceramic fiber membranes have also been made [67, 68].

Other problems that have caused problems are poisoning of the membranes by some components of the feed gas (for example, carbon dioxide) which react with the perovskite membrane to form carbonates. Another operational issue is the narrow operating temperature window of the membranes. This is illustrated by the results of Shao *et al.* [69]. Below 850°C, the membranes are not stable because of the formation of structural changes in the perovskite, leading to formation of new non-permeable crystal phases. Much above 850°C, slow creep occurs and the membranes become mechanically unstable. The potential value of these devices is very large, but many problems remain to be solved.

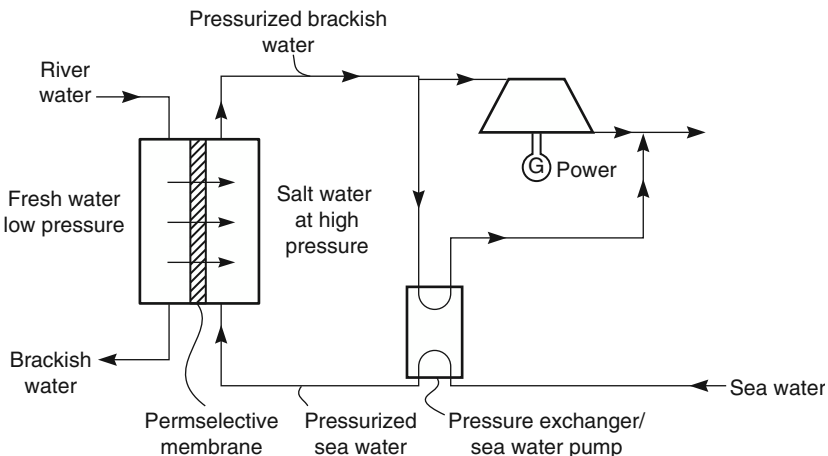


Figure 13.23 Flow scheme for pressure-retarded osmosis (PRO) to recover the energy of mixing usually lost when a river flows into the sea

13.8 Pressure-Retarded Osmosis (PRO) and Reverse Electrodialysis (RED)

A vast amount of energy is irreversibly dissipated when fresh river waters mix with the sea. In principle, this energy could be recovered by using a suitable osmotic membrane system to convert the osmotic pressure of seawater dilution into hydrostatic pressure to drive a turbine and generate electricity. Such a scheme was proposed by Norman [70] and independently by Jellinek [71] and Loeb [72]. The process experienced a brief vogue after the first oil shock in the mid-1970s, but later the process was largely abandoned. However, in the early 2000s, workers at SINTEF Norway [73] revived interest in the process. The SINTEF group brought a small demonstration plant on-line in 2011. However, the process still needs significant improvement before it becomes a commercially viable way of producing electricity and large-scale implementation becomes feasible.

The osmotic membrane flow scheme is illustrated in Figure 13.23. Loeb coined the term “pressure-retarded osmosis (PRO)” for this process. Low-pressure fresh water from a river is circulated on one side of a permselective membrane while seawater is circulated at a higher pressure on the permeate side of the membrane. Because of the osmotic pressure difference, a flow of water takes place from the low-pressure fresh water into the seawater. This flow will continue, provided the pressure of the salt-side solution is less than the osmotic pressure across the membrane. The pressurized salt solution is removed from the membrane cell. A portion of the high-pressure solution is sent to a pressure exchanger/seawater pump to provide the energy needed to pressurize the incoming seawater. The remaining solution is sent to a turbine to generate electricity. The water flux through the membrane is given by Equation 2.46 from Chapter 2, namely

$$J = A(\Delta\pi - \Delta p) \quad (13.6)$$

where A is the water permeation coefficient, $\Delta\pi$ is the osmotic pressure difference across the membrane, and Δp is the hydrostatic pressure difference across the membrane.¹

In PRO, the power that can be generated per unit membrane area is equal to the product of the water flux and the hydrostatic pressure of the salt solution. The maximum power per unit flux is therefore obtained at the maximum hydrostatic pressure under which PRO takes place, that is, the osmotic pressure difference, $\Delta\pi$. However, when Δp is close to $\Delta\pi$, the transmembrane water flux is very small, and a very large membrane area would be required, resulting in a high capital cost for the system. It is preferable, therefore, to operate PRO systems under conditions corresponding to the maximum power per unit membrane area, to minimize capital costs.

The power per unit membrane area, W , that can be generated in PRO is equal to the product of the water flux across the membrane and the hydrostatic pressure of the salt solution:

$$W = J_W \Delta p = A(\Delta\pi - \Delta p)\Delta p \quad (13.7)$$

By differentiating Equation 13.7 with respect to Δp , it can be shown that W reaches a maximum when $\Delta p = \Delta\pi/2$. Substituting this value for Δp in Equation 13.7 yields

$$W_{\max} = A\Delta\pi^2/4 \quad (13.8)$$

Equation 13.8 shows that the maximum power in a PRO system is directly proportional to the water permeability coefficient, A , and thus high flux membranes are preferred. The maximum power is also proportional to the square of the osmotic pressure difference. This arises because increasing the osmotic pressure of the salt solution increases both the optimum pressure at which the system operates (that is, $\Delta\pi/2$) and the water flux through the membrane at that pressure.

In calculating the maximum power per unit area using Equation 13.8, the osmotic pressure difference $\Delta\pi$ has been assumed to be constant at every point along the membrane. However, significant brine dilution has to be accepted in any real system. In optimized systems, the available osmotic pressure will be reduced by a significant factor (for example, 25%) if a factor of 2 dilution is accepted over the length of the membrane [73].

Concentration polarization is the major problem of PRO [73, 74]. The phenomenon is illustrated in Figure 13.24. External concentration polarization in the liquid boundary layers on either side of the membrane can be controlled in properly designed modules. However, even with very selective membranes, a small amount of salt will diffuse across the membrane. This salt becomes trapped in the porous support layer of the membrane. This salt can only escape by diffusing through the support layer, against a convective flow of water in the opposite direction, into the fresh water solution. Internal concentration polarization sharply reduces the effective osmotic pressure across the membrane and hence the fluxes obtained under PRO conditions. The phenomenon cannot be controlled by circulation of the fluids on either side of the membrane.

¹ This relationship is conventionally written $J_w = A(\Delta p - \Delta\pi)$. We have chosen the presentation shown so that the water flux in PRO is positive.

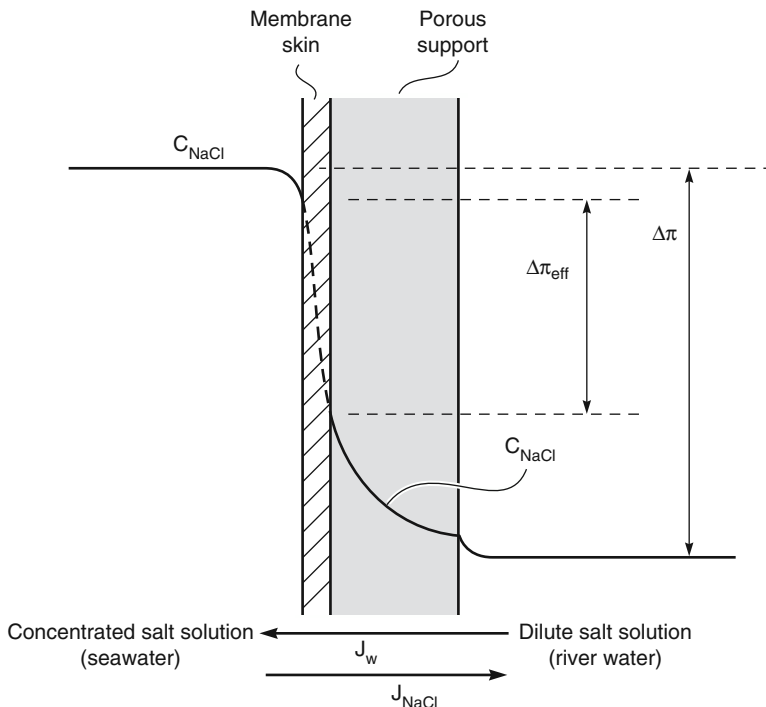


Figure 13.24 Diagram showing the salt concentration gradients that form in a composite membrane during pressure-retarded osmosis. Diffusion of small amounts of salt into the porous support layer significantly reduces the effective osmotic pressure $\Delta\pi_{\text{eff}}$ across the membrane

The problem of internal concentration polarization can be mitigated by producing membranes with extremely water-permeable and very selective skin layers supported on highly permeable porous substructures. The measure of performance of these membranes is usually taken to be the power produced ($J_w \cdot \Delta p$) per square meter of membrane. A membrane plant producing 5 W/m^2 could be economical in some locations. The best current membranes are in the range of $1\text{--}3 \text{ W/m}^2$ [73, 75, 76].

Reverse electrodialysis (RED) is a process related to PRO. In RED, the diffusion of ions from seawater to fresh water across the membrane in a normal electrodialysis stack is used to develop an electrical potential from which energy can be developed. The process was first proposed by Weinstein and Leitz [77]. A process flow scheme is shown in Figure 13.25. Like PRO, the RED process has been demonstrated in the laboratory, but major improvements in membrane performance and membrane cost are still required to make the process an economical method of making electricity.

The maximum voltage that can be generated by diffusion of seawater salt across the ion exchange membranes into the fresh water solution of a RED cell stack is $\sim 160 \text{ mV}$ per single cell pair, but the current would then be zero. For this reason, as in PRO, the stack is designed to operate at about half the maximum voltage, which is the point

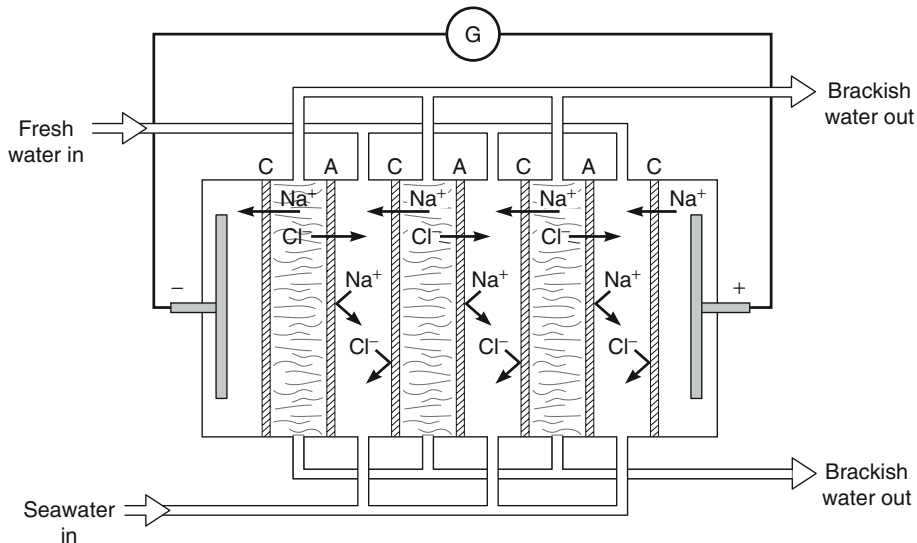


Figure 13.25 Flow schematic of a reverse electrodialysis (RED) stack. C is a cation exchange (fixed negative charge) membrane, A is an anion exchange (fixed positive charge) membrane. Diffusion of salt from the (concentrated) seawater cells into the (dilute) fresh water cells generates a voltage drop across the membrane stack electrodes

of maximum power production per membrane cell pair. In a practical device, several hundred cell pairs would be stacked together to produce a single large device and a useful cumulative voltage across the entire stack. The most active group developing RED technology is at the Wetsus Research Center in The Netherlands [78, 79].

Two membrane problems hindering development of the technology are leakage of co-ions across the membranes (that is, ions of the same charge as the fixed ion exchange groups), and osmotic transport of water from the fresh water cells to the seawater cells of the stack; better membranes are being made that may mitigate these problems [78]. However, concentration polarization at the membrane–solution interface remains a serious problem, because of differences between the very high permeance of ions in the membrane phase and the much lower permeance in the solution phase, particularly in the dilute fresh water channel. Creating turbulence in the solution by increasing the circulating velocity of the solutions can be used, but this uses a significant fraction of the power generated by the process [79]. A solution proposed by Dlugolecki *et al.* [80] is to make the netting material that forms the channel space between the membranes from ion-conductive materials, an idea suggested by the use of similar materials in electrodeionization systems described in Chapter 10. Use of these materials is claimed to triple the power density of RED stacks, bringing the power density to as much as 4 W/m^2 . This is approaching the power density required for economically viable processes.

13.9 Chiral Drug Separation

Many drugs are produced as racemic mixtures of two mirror image isomers. Often only one of these enantiomers has a beneficial pharmaceutical effect and the second enantiomer is much less active or, even worse, produces toxic side effects. For this reason many drugs must be resolved into their component enantiomers before being used. A number of techniques are available, but most are complex and costly. Resolution of racemic mixtures using stereoselective enzymatic reactions in a membrane bioreactor was pioneered by Sepracor and has been applied on an industrial scale for a number of important drugs [81, 82]. Several ingenious process schemes have been proposed, one of which is illustrated in Figure 13.26.

The process shown in Figure 13.26 uses the stereospecific, enzymatically-catalyzed hydrolysis of the ethyl ester of naproxen to the free acid to perform the chiral separation shown in Figure 13.27.

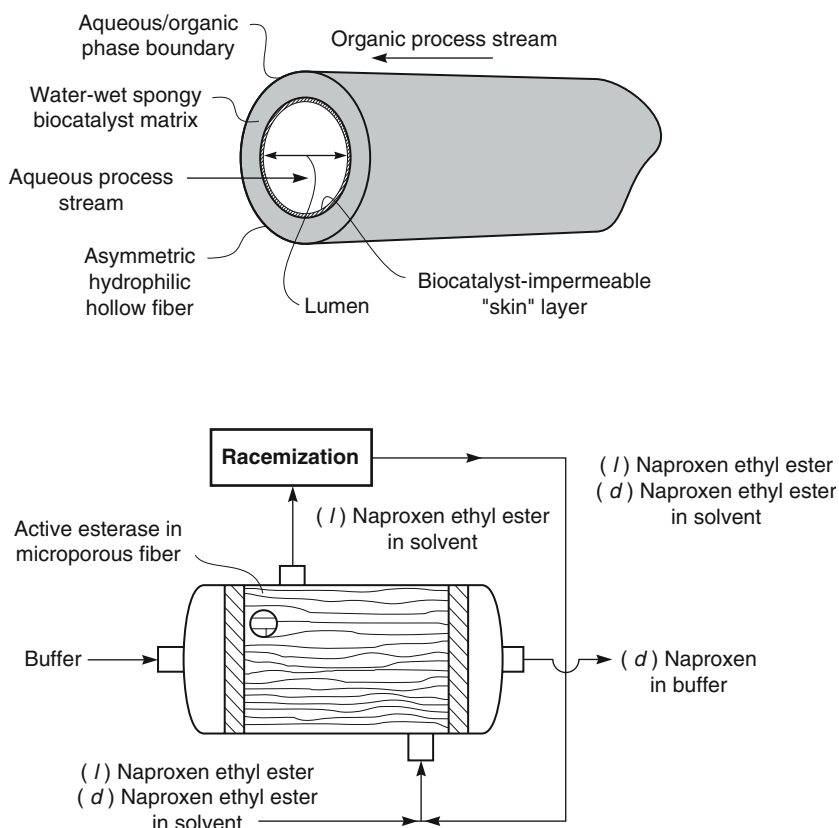


Figure 13.26 Application of a membrane bioreactor to separate chiral drug mixtures

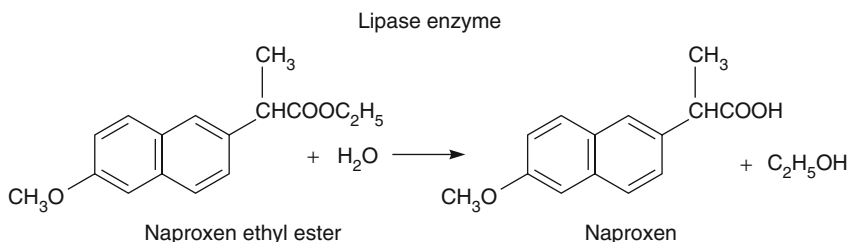


Figure 13.27 Chiral separation performed by the process shown in Figure 13.26

The lipase enzyme stereospecifically hydrolyzes the (+) isomer of naproxen ester. The enzyme is immobilized in the wall of an inside-skinned hollow fiber membrane. The racemic *d* and *l* naproxen ester mixture, dissolved in methyl isobutyl ketone, is introduced on the shell side of the fiber and an aqueous buffer solution is circulated through the fiber lumen. The lipase enzyme hydrolyzes the *d* form of naproxen ester, forming ethanol and naproxen *d*. Naproxen *d* is a carboxylic acid soluble in aqueous buffer but insoluble in methyl isobutyl ketone. Consequently, naproxen *d* is removed from the reactor with the buffer solution. The naproxen *l* ester remains in the methyl isobutyl ketone solution. This technique achieves an essentially complete separation of the *d* and *l* forms. In a clever final step, the naproxen *l* ester is racemized to a *d* and *l* racemic mixture and recirculated to the membrane reactor. In this way all of the original mixture is eventually converted to the pure, pharmaceutically active *d* form. This technology has been applied to the chiral resolution of a number of drugs. A full-scale plant for the chiral separation of diltiazem intermediates, developed by Tanabe/Sepracor engineers, contains 1440 m² of hollow fiber membrane and produces 75 tons/year of resolved diltiazem intermediate [81].

13.10 Conclusions and Future Directions

Of the processes described in this chapter, membrane contactors and membrane reactors have the greatest potential to develop into large-scale commercial processes. Both technologies are already used on a small scale in niche applications, and both are being developed for much larger and more important processes. Membrane contactors are currently most widely used to deaerate liquids, but the best long-term application may be in the natural gas industry to replace amine absorber/strippers to remove carbon dioxide and hydrogen sulfide. Similarly, membrane reactors are currently used only in a few specialized biotech applications. However, long-term, this type of device can be used in the petrochemical industry, with very different membranes, for dehydrogenation processes or the partial oxidation of methane. Such applications could be much more important, but the development of suitable membranes poses a number of very challenging technical problems.

References

1. Cerini, L. (1929) Apparatus for the purification of impure solutions of caustic soda and the like, on osmotic principles. US Patent 1,719,754, July 1929.
2. Cerini, L. (1931) Treatment of vegetable fibers of osmotic diaphragms. US Patent 1,815,761, July 1931.
3. Tuwiner, S.B. (1962) *Diffusion and Membrane Technology*, 1st edn, Reinhold Publishing Corporation, New York.
4. Chen, H.C., O'Neal, C.H., and Craig, L.C. (1971) Rapid laboratory dialysis for aminoacylation assay of tRNA. *Anal. Chem.*, **43** (8), 1017.
5. Craig, L.C. (1964) Differential dialysis. *Science*, **144**, 1093.
6. Craig, L.C. and Stewart, K. (1965) Dialysis. X. On thin film countercurrent dialysis. *Biochemistry*, **4** (12), 2717.
7. Wallace, R.M. (1967) Concentration and separation of ions by Donnan membrane equilibrium. *Ind. Eng. Chem. Process Des. Dev.*, **6**, 423.
8. Wallace, R.M. (1969) Concentration of ions using ion selective membranes, US Patent 3,454,490, July 1969.
9. Huang, T.C., Lin, Y.K., and Chen, C.Y. (1988) Selective separation of nickel and copper from a complexing solution by a cation-exchange membrane. *J. Membr. Sci.*, **37**, 131.
10. Oh, S.J., Moon, S.H., and Davis, T. (2000) Effects of metal ions on diffusion dialysis of inorganic acids. *J. Membr. Sci.*, **169**, 95.
11. Tongwen, X. and Weihua, Y. (2003) Industrial recovery of mixed acid ($\text{HF} + \text{HNO}_3$) from the titanium spent leaching solutions by diffusion dialysis with a new series of anion exchange membranes. *J. Membr. Sci.*, **220**, 89.
12. Strathmann, H. (2004) in *Ion-Exchange Membrane Separation Processes*, Membrane Science and Technology, Elsevier, Amsterdam.
13. Sollner, K. (1932) Über mosaik membranen. *Biochem Z.*, **244**, 370.
14. Leitz, F.B. (1976) in *Piezodialysis in Membrane Separation Processes* (ed. P. Meares), Elsevier Santi Publishing Company, Amsterdam, pp. 261–294.
15. Gardner, C.R., Weinstein, J.N., and Caplan, S.R. (1973) Transport properties of charge-mosaic membranes III. Piezodialysis. *Desalination*, **12**, 19.
16. Merten, U. (1966) Desalination by pressure osmosis. *Desalination*, **1**, 297.
17. Weinstein, J.N. and Caplan, S.R. (1970) Charge-mosaic membranes: dialytic separation of electrolytes from nonelectrolytes and amino acids. *Science*, **169**, 296.
18. Caplan, S.R. (1971) Transport in natural and synthetic membranes in membrane processes, in *Industry and Biomedicine* (ed. M. Bier), Plenum Press, New York, pp. 1–22.
19. Platt, K.L. and Schindler, A. (1971) Ionic membranes for water desalination. *Ang. Makromol. Chem.*, **19**, 135.
20. Ito, H., Toda, M., Ohkoshi, K., Iwata, M., Fujimoto, T., Miyaki, Y. and Kataoka, T. (1988) Artificial membranes from multiblock copolymers. 6. Water and salt transports through a charge-mosaic membrane. *Ind. Eng. Chem. Res.*, **27**, 983–987.

21. Hirahara, K., Takahashi, S., Iwata, M., Fujimoto, T. and Miyaki, Y. (1986) Artificial membranes from multiblock copolymers. 5. Transport behaviors of organic and inorganic solutes through a charge-mosaic membrane. *Ind. Eng. Chem. Prod. Res. Dev.*, **25**, 305–313.
22. Higa, M., Masuda, D., Kobayashi, E., Nishimura, M., Sugio, Y., Kusudou, T. and Fujiwara, N. (2008) Charge mosaic membranes prepared from laminated structures of PVA-based charged layers: 1. Preparation and transport properties of charges mosaic membranes. *J. Membr. Sci.*, **310**, 466.
23. D'elia, N.A., Dahuron, L., and Cussler, E.L. (1986) Liquid-liquid extractions with microporous hollow fibers. *J. Membr. Sci.*, **29**, 309.
24. Falk-Pedersen, O. and Dannstrom, H. (2001) Method for removing carbon dioxide from gases. US Patent 6,228,145, May 2001.
25. Qi, Z. and Cussler, E.L. (1985) Microporous hollow fibers for gas absorption: I. Mass transfer in the liquid. *J. Membr. Sci.*, **23**, 321.
26. Qi, Z. and Cussler, E.L. (1985) Microporous hollow fibers for gas absorption: II. Mass transfer across the membrane. *J. Membr. Sci.*, **23**, 333.
27. Reed, B.W., Semmens, M.J., and Cussler, E.L. (1995) Membrane contactors, in *Membrane Separation Technology: Principles and Applications* (eds R.D. Noble and S.A. Stern), Elsevier Science, Amsterdam, pp. 467–498.
28. Gabelman, A. and Hwang, S.T. (1999) Hollow fiber membrane contactors. *J. Membr. Sci.*, **159**, 61.
29. Prasad, R. and Sirkar, K.K. (1992) Membrane based solvent extraction, in *Membrane Handbook* (eds W.S.W. Ho and K.K. Sirkar), Van Nostrand Reinhold, New York, pp. 727–763.
30. Wiesler, F. and Sodaro, R. (1996) Degaeration: degasification of water using novel membrane technology. *Ultrapure Water*, **35**, 53.
31. Page, J.K.R. and Kalhod, D.G. (1996) Control of dissolved gases in liquids. US Patent 5,565,149, Oct. 1996.
32. Honda, K. and Yamashita, M. (1996) Method for deaerating liquid products. US Patent 5,522,917, June 1996.
33. Prasad, R., Runkle, C.J., and Shuey, H.F. (1994) Spiral-wound hollow fiber membrane fabric cartridges and modules having flow-directing baffles. US Patent 5,352,361, Oct. 1994.
34. Jansen, A.E., Feron, P.H.M., Hanemaajier, J.H., and Huisjes, P. (2002) Apparatus and method for performing membrane gas/liquid absorption at elevated pressure. US Patent 6,355,092, Mar. 2002.
35. Tsou, D.T., Blachman, M.W., and Davis, J.C. (1994) Silver-facilitated olefin/paraffin separation in a liquid membrane contactor system. *Ind. Eng. Chem. Res.*, **33**, 3209.
36. Valus, R.J., Eshraghi, R., Velikoff, A.E., and Davis, J.C. (1991) High pressure facilitated membranes for selective separation and process for the use thereof. US Patent 5,057,641, Oct. 1991.
37. Bessarabov, D.G., Sanderson, R.D., Jacobs, E.P., and Beckman, I.N. (1995) High-efficiency separation of an ethylene/ethane mixture by a large-scale liquid-membrane contactor containing flat-sheet nonporous polymeric gas-separation membranes and a selective flowing-liquid absorbent. *Ind. Eng. Chem. Res.*, **34**, 1769.

38. Schneider, K., Hölz, W., Wollbeck, R., and Ripperger, S. (1988) Membranes and modules for transmembrane distillation. *J. Membr. Sci.*, **39**, 25.
39. Lawson, K.W. and Lloyd, D.R. (1997) Membrane distillation. *J. Membr. Sci.*, **124**, 1.
40. El-Bourawi, M.S., Ding, Z., Ma, R., and Khayet, M. (2006) A framework for better understanding membrane distillation separation process. *J. Membr. Sci.*, **285**, 4.
41. Al-Obaidani, S., Curcio, E., Macedonio, F., Di Profio, G., Al-Hinai, H. and Drioli, E. (2008) Potential of membrane distillation in seawater desalination: thermal efficiency, sensitivity study and cost estimation. *J. Membr. Sci.*, **323**, 85.
42. Cheryan, M. (1998) *Ultrafiltration and Microfiltration Handbook*, Technomic Publishing, Co., Lancaster, PA, p. 445.
43. Kemmere, M.F. and Keurentjes, J.T.F. (2001) Industrial membrane reactors, in *Membrane Technology in the Chemical Industry* (eds S.P. Nunes and K.V. Peinemann), Wiley-VCH Verlag GmbH, Weinheim, pp. 191–221.
44. Shao, X., Fend, Y., Hu, S., and Govind, R. (1989) Pectin degradation in a spiral membrane reactor, in *Membrane Reactor Technology*, AIChE Symposium Series number 268, Vol. **85** (eds R. Govind and N. Itoh), AIChE, New York, pp. 85–92.
45. Rezac, M.E., Koros, W.J., and Miller, S.J. (1994) Membrane-assisted dehydrogenation of *n*-butane influence of membrane properties on system performance. *J. Membr. Sci.*, **93**, 193.
46. Matson, S.L. and Quinn, J.A. (1992) Membrane reactors, in *Membrane Handbook* (eds W.S.W. Ho and K.K. Sirkar), Van Nostrand Reinhold, New York, pp. 809–832.
47. Vane, L.M. (2005) A review of pervaporation for product recovery from biomass fermentation processes. *J. Chem. Technol. Biotechnol.*, **80**, 603.
48. Lipnizki, F., Hausmanns, S., Laufenberg, G., Field, R. and Kunz, B. (2000) Use of pervaporation bioreactor hybrid processes in biotechnology. *Chem. Eng. Technol.*, **27**, 569.
49. Cheryan, M. and Mehaia, M.A. (1986) Membrane bioreactors, in *Membrane Separations in Biotechnology* (ed. W.C. McGregor), Marcel Dekker, New York, pp. 255–302.
50. Lewandowicz, G., Bialas, W., Marczewski, B., and Szymanowska, D. (2011) Application of membrane distillation for ethanol recovery during fuel ethanol production. *J. Membr. Sci.*, **375**, 212.
51. Hu, W.S. and Dodge, T.C. (1985) Cultivation of mammalian cells in bioreactors. *Biotechnol. Prog.*, **1**, 209.
52. Hickey, R., Basu, R., Datta, R., and Tsai, S.P. (2011) Method of conversion of syngas using microorganism on hydrophobic membrane. US Patent 7,923,227, Apr. 2011.
53. Ali, J.K. and Rippin, D.W.T. (1995) Comparing mono-and bimetallic noble-metal catalysts in a catalytic membrane reactor for methylcyclohexane dehydrogenation. *Ind. Eng. Chem. Res.*, **34**, 722.
54. Bose, A.C. (ed.) (2009) *Inorganic Membranes for Energy and Environmental Applications*, Springer Science+Business Media, LLC, New York.
55. Liu, K., Song, C., and Subramani, V. (eds) (2010) *Hydrogen and Syngas Production and Purification Technologies*, John Wiley & Sons, Inc., Hoboken, NJ.

56. Teraoka, Y., Zhang, H., Furukawa, S., and Yamazoe, N. (1985) Oxygen permeation through perovskite-type oxides. *Chem. Lett.*, 1743.
57. Teraoka, Y., Nobunaga, T., and Yamazoe, N. (1988) The effect of cation substitution on the oxygen semipermeability of perovskite-type oxides. *Chem. Lett.*, 503.
58. Lin, Y. (2001) Microporous and dense inorganic membranes: current status and prospective. *Sep. Purif. Tech.*, **25**, 39.
59. Thorogood, R.M., Srinivasan, R., Yee, T.F., and Drake, M.P. (1993) Composite mixed conductor membranes for producing oxygen. US Patent 5,240,480, Aug. 1993.
60. Carolan, M.F., Dyer, P.N., Labar, J.M. Sr., and Thorogood, R.M. (1993) Process for restoring permeance of an oxygen-permeable ion transport membrane utilized to recover oxygen from an oxygen-containing gaseous mixture. US Patent 5,240,473, Aug. 1993.
61. Carolan, M.F., Dyer, P.N., Labar, J.M. Sr., and Thorogood, R.M. (1993) Process for recovering oxygen from gaseous mixtures containing water or carbon dioxide which process employs ion transport membranes. US Patent 5,261,932, Nov. 1993.
62. Carolan, M.F., Dyer, P.N., and Fine, S.M. (1993) Process for recovering oxygen from gaseous mixtures containing water or carbon dioxide which process employs barium-containing ion transport membranes. US Patent 5,269,822, Dec. 1993.
63. Kang, D., Srinivasan, R., Thorogood, R.M., and Foster, E.P. (1996) Integrated high temperature method for oxygen production. US Patent 5,516,359, May 1996.
64. Mazanec, T.J., Cable, T.L., Frye, J.G. Jr., and Kliewer, W.R. (1997) Solid-component membranes electrochemical reactor components electrochemical reactors use of membranes reactor components and reactor for oxidation reactions. US Patent 5,591,315, Jan. 1997.
65. Mazanec, T.J., Cable, T.L., Frye, J.G. Jr., and Kliewer, W.R. (1994) Solid multi-component membranes, electrochemical reactor components, electrochemical reactors and use of membranes, reactor components, and reactor for oxidation reactions. US Patent 5,306,411, April 1994.
66. Mazanec, T.J. and Cable, T.L. (1997) Oxygen permeable mixed conductor membranes. US Patent 5,648,304, July 1997.
67. Vente, J.F., Haije, W.G., Ijpelaan, R., and Rusting, F.T. (2006) On the full-scale module design of an air separation unit using mixed ionic electronic conducting membranes. *J. Membr. Sci.*, **278**, 66–71.
68. Tan, X., Wang, Z., Meng, B., Meng, X., and Li, K. (2010) Pilot-scale production of oxygen from air using perovskite hollow fibre membranes. *J. Membr. Sci.*, **352**, 189–196.
69. Shao, Z., Yang, W., Cong, Y., Dong, H., Tong, J. and Xiong, G. (2000) Investigation of the permeation behavior and stability of a $\text{Ba}_{0.5}\text{Sr}_{0.5}\text{Co}_{0.8}\text{Fe}_{0.2}\text{O}_3[\delta]$ oxygen membrane. *J. Membr. Sci.*, **172**, 177–188.
70. Norman, R.S. (1974) Water salination: a source of energy. *Science*, **186**, 350.
71. Jellinek, H.H. (1975) Osmotic work I. Energy production from osmosis on fresh water systems. *Kagaku Kogyo*, **19**, 87.
72. Loeb, S. (1976) Production of energy from concentrated brines by pressure-retarded osmosis: I. Preliminary technical and economic correlations. *J. Membr. Sci.*, **1**, 49–63.

73. Thorsen, T. and Holt, T. (2009) The potential for power production from salinity gradients by pressure retarded osmosis. *J. Membr. Sci.*, **335**, 103–110.
74. Lee, K.L., Baker, R.W., and Lonsdale, H.K. (1981) Membranes for power generation by pressure-retarded osmosis. *J. Membr. Sci.*, **8**, 141–171.
75. Post, J.W., Veerman, J., Hamelers, H.V.M., Euverink, G.J.W., Metz, S.J., Nijmeijer, K. and Buisman, C.J.N. (2007) Salinity-gradient power: evaluation of pressure-retarded osmosis and reverse electrodialysis. *J. Membr. Sci.*, **288**, 218–230.
76. Achilli, A., Cath, T.Y., and Childress, A.E. (2009) Power generation with pressure retarded osmosis: an experimental and theoretical investigation. *J. Membr. Sci.*, **343**, 42–52.
77. Weinstein, J.N. and Leitz, F.B. (1976) Electric power from differences in salinity: the dialytic battery. *Science*, **191**, 557.
78. Veerman, J., de Jong, R.M., Saakes, M., Metz, S.J. and Harmsen, G.J. (2009) Reverse electrodialysis: comparison of six commercial membrane pairs on the thermodynamic efficiency and power density. *J. Membr. Sci.*, **343**, 7–15.
79. Veerman, J., Saakes, M., Metz, S.J., and Harmsen, G.J. (2009) Reverse electrodialysis: performance of a stack with 50 cells on the mixing of sea and river water. *J. Membr. Sci.*, **327**, 136–144.
80. Dlugolecki, P., Dabrowska, J., Nijmeijer, K., and Wessling, M. (2010) Ion conductive spacers for increased power generation in reverse electrodialysis. *J. Membr. Sci.*, **347**, 101–107.
81. Lopez, J.L. and Matson, S.L. (1997) A multiphase/extractive enzyme membrane reactor for production of diltiazem chiral intermediate. *J. Membr. Sci.*, **125**, 189.
82. Matson, S.L. (1989) Method for resolution of stereoisomers in multiphase and extractive membrane reactors. US Patent 4,800,162, Jan. 1989.

Appendix

Table A1 Constants

Mathematical

$e = 2.71828$

$\ln 10 = 2.30259$

$\pi = 3.14159$

Gas law constant, R

1.987 cal/g-mol K

82.05 cm³ atm/g-mol K

8.314×10^7 g cm²/s² g-mol K

8.314×10^3 kg m²/s² kg-mol K

Standard acceleration of gravity

980.665 cm/s²

32.1740 ft/s²

Avogadro's number

6.023×10^{23} molecules/g-mol

Faraday's constant, F

9.652×10^4 abs-coulombs/g-equivalent

STP (standard temperature and pressure)

273.15 K and 1 atm pressure

Volume of 1 mol of ideal gas at STP = 22.41 l

Table A2 Conversion factors for weight and volume

Given a quantity in these units	Multiply by	To convert quantity to these units
Pounds	453.59	Grams
Kilograms	2.2046	Pounds
Ton, short (US)	2000	Pounds
Ton, long (UK)	2240	Pounds
Ton, metric	1000	Kilograms
Gallons (US)	3.7853	liters
Gallons (US)	231.00	Cubic inches
Gallons (US)	0.13368	Cubic feet
Cubic feet	28.316	liters
Cubic meters	264.17	Gallons (US)

Table A3 Conversion factors – other

Given a quantity in these units	Multiply by	To convert quantity to these units
Inches	2.54	Centimeters
Meters	39.37	Inches
Mils	25.4	Microns
Square meters	10.764	Square feet
Dynes	1	g cm/s
Centipoises	10^{-3}	kg/m·s

Table A4 Conversion factors for pressure

Given a quantity in these units	Atmosphere (atm)	mmHg (torr)	lb/in ² (psi)	kg/cm ²	kiloPascal (kPa)	Bar
Atmosphere (atm)	1	760	14.696	1.0332	101.325	1.01325
mmHg (torr)	1.3158×10^{-3}	1	1.9337×10^{-2}	1.3595×10^{-3}	0.13332	1.3332×10^{-3}
lb/in ² (psi)	6.8046×10^{-2}	51.715	1	7.0305×10^{-2}	6.8948	6.8948×10^{-2}
kg/cm ²	0.96787	735.58	14.224	1	98.069	0.98069
kiloPascal (kPa)	9.8692×10^{-3}	7.5008	0.14504	10.197×10^{-3}	1	0.01
Bar	0.98692	750.08	14.504	1.0197	100	1

Table A5 Conversion factors for energy

Given a quantity in these units	g cm ² /s ² (ergs)	kg m ² /s ² (joules)	Calories (cal)	British thermal units (Btu)	Horsepower. hour (hp·h)	Kilowatt hour (kWh)
g cm ² /s ² (ergs)	1	10^{-7}	2.3901×10^{-8}	9.4783×10^{-11}	3.7251×10^{-14}	2.7778×10^{-14}
kg m ² /s ² (joule)	10^7	1	2.3901×10^{-1}	9.4783×10^{-4}	3.7251×10^{-7}	2.7778×10^{-7}
Calories (cal)	4.1840×10^7	4.1840	1	3.9657×10^{-3}	1.5586×10^{-6}	1.1622×10^{-6}
British thermal units (Btu)	1.0550×10^{10}	1.0550×10^3	2.5216×10^2	1	3.9301×10^{-4}	2.9307×10^{-4}
Horsepower-hour (hp·h)	2.6845×10^{13}	2.6845×10^6	6.4162×10^5	2.5445×10^3	1	7.4570×10^{-1}
Kilowatt hour (kWh)	3.6000×10^{13}	3.6000×10^6	8.6042×10^5	8.4122×10^3	1.3410	1

Table A6 Conversion factors for liquid flux

Given a quantity in these units	$L/m^2 \text{ h}$ ($L\text{mh}$)	$gal (US)/ft^2 \text{ day}$ (gfd)	Multiply by value below to convert to corresponding units
$L/m^2 \text{ h}$ ($L\text{mh}$)	1	0.59	$cm^3/cm^2 \text{ s}$
$gal (US)/ft^2 \text{ day}$ (gfd)	1.70	1	2.78×10^{-5}
$cm^3/cm^2 \text{ s}$	3.60×10^4	2.12×10^4	4.72×10^{-5}
$cm^3/cm^2 \text{ min}$	600	353	1
$m^3/m^2 \text{ day}$	41.67	24.55	0.1667
$L/m^2 \text{ day}$	4.17×10^{-2}	2.46×10^{-2}	1.16×10^{-6}
			1.16×10^{-6}
			6.944×10^{-4}
			6.944×10^{-4}
			1×10^{-3}
			1

Table A7 Conversion factors for liquid permeance

Given a quantity in these units	$L/m^2 \text{ h bar}$	$L/m^2 \text{ h NegPa}$	Multiply by value below to convert to corresponding units
$L/m^2 \text{ h bar}$	1	10	2.777×10^{-9}
$L/m^2 \text{ h MegPa}$	0.1	1	2.777×10^{-10}
$L/m^2 \text{ s Pa}$	3.600×10^8	3.600×10^9	1
$gal (US)/ft^2 \text{ day psi}$	24.61	2.461×10^2	6.837×10^{-8}
$m^3/m^2 \text{ day bar}$	41.67	4.167×10^2	1.157×10^{-7}
			1.157×10^{-7}
			1
			1.693
			1

$m^3/m^2 \text{ day}$	$m^3/cm^2 \text{ min}$	$cm^3/cm^2 \text{ s}$	$gal (US)/ft^2 \text{ day}$ (gfd)	$L/m^2 \text{ day}$
		1.6667×10^{-3}	2.40×10^{-2}	24.0
		2.832×10^{-3}	4.07×10^{-2}	40.73
		60	864	8.64×10^5
		1	14.4	1.44×10^3
			1	10^3
			1×10^{-3}	1

Table A8 Conversion factors for gas flux

Given a quantity in these units	Multiply by value below to convert to corresponding units				
	$\text{cm}^3(\text{STP})/\text{cm}^2 \text{ s}$	$\text{L}(\text{STP})/\text{cm}^2 \text{ s}$	$\text{m}^3(\text{STP})/\text{m}^2 \text{ day}$	$\text{ft}^3(\text{STP})/\text{ft}^2 \text{ h}$	$\text{mol}/\text{m}^2 \text{ s}$
$\text{cm}^3(\text{STP})/\text{cm}^2 \text{ s}$	1	1×10^{-3}	864	118.1×10^5	0.4462
$\text{L}(\text{STP})/\text{cm}^2 \text{ s}$	1	8.64×10^5	1.181×10^5	0.4462×10^3	0.4462×10^9
$\text{m}^3(\text{STP})/\text{m}^2 \text{ day}$	1.157×10^{-3}	1.157×10^{-6}	0.1366	0.5162×10^{-3}	0.5162×10^{-7}
$\text{ft}^3(\text{STP})/\text{ft}^2 \text{ h}$	8.467×10^{-3}	8.467×10^{-6}	1	3.778×10^{-3}	3.778×10^{-7}
$\text{mol}/\text{m}^2 \text{ s}$	2.241	2.241×10^{-3}	1.936×10^3	2.647×10^2	1×10^{-4}
$\text{mol}/\text{cm}^2 \text{ s}$	2.241×10^4	22.41	1.936×10^7	2.647×10^6	1×10^4
$\mu\text{mol}/\text{m}^2 \text{ s}$	2.241×10^{-6}	2.241×10^{-9}	1.936×10^{-3}	2.647×10^{-4}	1×10^{-6}
					1

Table A9 Conversion factors for gas permeance

Given a quantity in these units	Multiply by value below to convert to corresponding units				
	$1 \times 10^{-6} \text{ cm}^3$ (STP)/ $\text{cm}^2 \text{ s}$	$\text{L (STP)}/$ $\text{m}^2 \text{ h bar}$	$\text{cm}^3(\text{STP})/$ $\text{cm}^2 \text{ min bar}$	$\text{mol}/\text{m}^2 \text{ s Pa}$	$\text{m}^3(\text{STP})/$ $\text{m}^2 \text{ s bar}$
1×10^{-6} $\text{cm}^3(\text{STP})/\text{cm}^2 \text{ s}$	1	2.700	4.501×10^{-3}	3.347×10^{-10}	7.501×10^{-7}
cmHg (gpu)					7.501×10^{-12}
$\text{L (STP)}/\text{m}^2 \text{ h bar}$	0.3703	1	1.666×10^{-3}	1.239×10^{-10}	2.778×10^{-7}
$\text{cm}^3(\text{STP})/\text{cm}^2$	0.2222×10^3	0.6000×10^3	1	0.7438×10^{-7}	1.666×10^{-4}
min bar					1.666×10^{-9}
$\text{mol}/\text{m}^2 \text{ s Pa}$	0.2988×10^{10}	0.8065×10^{10}	1.344×10^7	1	2.241×10^3
$\text{m}^3(\text{STP})/\text{m}^2 \text{ s bar}$	1.333×10^6	3.6000×10^6	6.000×10^3	4.462×10^{-4}	1×10^{-5}
$\text{m}^3(\text{STP})/\text{m}^2 \text{ s Pa}$	1.333×10^{11}	3.6000×10^{11}	6.000×10^8	44.62	1×10^5
$\text{mol}/\text{cm}^2 \text{ s kPa}$	2.988×10^{10}	8.065×10^{10}	1.344×10^8	10	2.241×10^4

A 1-μm-thick membrane having a permeability of 1 Barrer has a permeance of 1 gpu.

Table A10 Conversion factors for gas permeability

Given a quantity in these units	Multiply by value below to convert to corresponding units				
	$1 \times 10^{-10} \text{ cm}^3$ (STP) $\text{cm}/\text{cm}^2 \cdot \text{s} \cdot \text{cmHg}$ (Barber)	$\text{cm}^3(\text{STP}) \text{cm}/$ $\text{cm}^2 \cdot \text{s} \cdot \text{bar}$	$\text{mol} \cdot \text{m}^2 \cdot \text{s} \cdot \text{Pa}$	$\text{m}^3(\text{STP}) \text{m}/$ $\text{m}^2 \cdot \text{s} \cdot \text{Pa}$	$\text{mol} \frac{\text{cm}^3}{\text{cm}^2 \cdot \text{s}}$ Pa
1×10^{-10} $\text{cm}^3(\text{STP})$ $\text{cm}/\text{cm}^2 \cdot \text{s} \cdot \text{cmHg}$ (Barber)	1	7.501×10^{-9}	7.501×10^{-14}	3.347×10^{-16}	7.501×10^{-13}
$\text{cm}^3(\text{STP})$ s bar	1.333×10^8	1	1×10^{-5}	4.462×10^{-8}	1×10^{-4}
$\text{cm}^3(\text{STP}) \text{cm}/\text{cm}^2$ s Pa	1.333×10^{13}	1×10^5	1	4.462×10^{-3}	10
$\text{mol m}^2 \cdot \text{s} \cdot \text{Pa}$	2.988×10^{15}	2.241×10^7	224.1	1	2.241×10^3
$\text{m}^3(\text{STP}) \text{m}/\text{m}^2 \cdot \text{s}$ bar	1.333×10^{12}	1×10^4	0.1	4.462×10^{-4}	1×10^{-5}
$\text{m}^3(\text{STP}) \text{m}/\text{cm}^2 \cdot \text{s}$ Pa	1.333×10^{17}	1×10^9	1×10^4	4.462×10^{-5}	1×10^5
$\text{mol cm}/\text{cm}^2 \cdot \text{s kPa}$	2.988×10^{14}	2.241×10^6	22.41	0.1	224.1

Table A11 Vapor pressure of water and ice

Temp (°C)	Pressure (mmHg)								
-30	0.285	0	4.58	30	31.8	60	149	90	526
-29	0.317	1	4.93	31	33.7	61	156	91	546
-28	0.351	2	5.29	32	35.7	62	164	92	567
-27	0.389	3	5.69	33	37.7	63	171	93	589
-26	0.430	4	6.10	34	39.9	64	179	94	611
-25	0.476	5	6.54	35	41.2	65	188	95	634
-24	0.526	6	7.01	36	44.6	66	196	96	658
-23	0.580	7	7.51	37	47.1	67	205	97	682
-22	0.640	8	8.05	38	49.7	68	214	98	707
-21	0.705	9	8.61	39	52.4	69	224	99	733
-20	0.776	10	9.21	40	55.3	70	234	100	760
-19	0.854	11	9.84	41	58.3	71	244	101	788
-18	0.939	12	10.5	42	61.5	72	254	102	816
-17	1.03	13	11.2	43	64.8	73	266	103	845
-16	1.13	14	12.0	44	68.3	74	277	104	875
-15	1.24	15	12.8	45	71.9	75	289	105	906
-14	1.36	16	13.6	46	75.7	76	301	106	938
-13	1.49	17	14.5	47	79.6	77	314	107	971
-12	1.63	18	15.5	48	83.7	78	327	108	1004
-11	1.79	19	16.5	49	88.0	79	341	109	1039
-10	1.95	20	17.5	50	92.5	80	355	110	1075
-9	2.13	21	18.7	51	97.2	81	370	111	1111
-8	2.33	22	19.8	52	102	82	385	112	1149
-7	2.54	23	21.1	53	107	83	401	113	1187
-6	2.77	24	22.4	54	113	84	417	114	1228
-5	3.01	25	23.8	55	118	85	434	115	1267
-4	3.28	26	25.2	56	124	86	451	116	1310
-3	3.57	27	26.7	57	130	87	469	117	1353
-2	3.88	28	28.3	58	136	88	487	118	1397
-1	4.22	29	30.0	59	143	89	506	119	1443
0	4.58	30	31.8	60	149	90	526	120	1489

Table A12 Composition of air

Component	Concentration (vol%)	Concentration (wt%)
Nitrogen	78.09	75.52
Oxygen	20.95	23.15
Argon	0.933	1.28
Carbon dioxide	0.030	0.046
Neon	0.0018	0.0012
Helium	0.0005	0.00007
Krypton	0.0001	0.0003
Hydrogen	0.0005	0.00003
Xenon	0.000003	0.00004

Table A13 Typical osmotic pressures of solutions at 25°C

Compound	Concentration (mg/L)	Concentration (mol/L)	Osmotic pressure (psi)
NaCl	35 000	0.60	398
Seawater	32 000	—	340
NaCl	2 000	0.0342	22.8
Brackish water	2 000–5 000	—	15–40
NaHCO ₃	1 000	0.0119	12.8
Na ₂ SO ₄	1 000	0.00705	6.0
MgSO ₄	1 000	0.00831	3.6
MgCl ₂	1 000	0.0105	9.7
CaCl ₂	1 000	0.009	8.3
Sucrose	1 000	0.00292	1.05
Dextrose	1 000	0.0055	2.0

Table A14 Mean free path of gases (25°C, 1 bar)

Gas	λ (Å)
Argon	1017
Hydrogen	1775
Helium	2809
Nitrogen	947
Neon	2005
Oxygen	1039
UF ₆	279

Table A15 Estimated diameter of common gas molecules

Gas molecule	Kinetic diameter (Å)	Lennard-Jones diameter (Å)
Helium	2.60	2.55
Neon	2.75	2.82
Hydrogen	2.89	2.83
Nitrous oxide	3.17	3.49
Carbon dioxide	3.30	3.94
Acetylene	3.30	4.03
Argon	3.40	3.54
Oxygen	3.46	3.47
Nitrogen	3.64	3.80
Carbon monoxide	3.76	3.69
Methane	3.80	3.76
Ethylene	3.90	4.16
Propane	4.30	5.12
Propylene	4.50	4.68

Gas diameters can be determined as kinetic diameter based on molecular sieve measurements or estimated as Lennard-Jones diameters based on viscosity measurements. The absolute magnitude of the estimated diameters is not important, but the ratio of diameters can give a good estimate of the relative diffusion coefficients of different gas pairs (see Equation 8.4). On this basis the kinetic diameters do a better job of predicting the relative diffusion coefficients of carbon dioxide/methane (always greater than 1 and often as high as 5–10 in glassy polymers). However, the Lennard-Jones diameter does a better job of predicting the relative diffusion coefficients of propylene/propane (always greater than 1 and often as high as 5 in glassy polymers).

1 Å = 0.1 nm.

Table A16 Experimental diffusion coefficient of water in organic liquids at 20–25°C at infinite dilution

Liquid	Temperature (°C)	Viscosity	$\text{cm}^2/\text{s} \times 10^5$
Methanol	20	—	2.2
Ethanol	25	1.15	1.2
1-Propanol	20	—	0.5
2-Propanol	20	—	0.5
1-Butanol	25	2.60	0.56
Isobutanol	20	—	0.36
Benzyl alcohol	20	6.5	0.37
Ethylene glycol	25	—	0.24
Triethylene glycol	30	30	0.19
Propane-1,2-diol	20	56	0.075
2-Ethylhexane-1,3-diol	20	320	0.019
Glycerol	20	1500	0.008
Acetone	25	0.33	4.6
Furfuraldehyde	20	1.64	0.90
Ethyl acetate	20	0.47	3.20
Aniline	20	4.4	0.70
<i>n</i> -Hexadecane	20	3.45	3.8
<i>n</i> -Butyl acetate	25	0.67	2.9
<i>n</i> -Butyric acid	25	1.41	0.79
Toluene	25	0.55	6.2
Methylene chloride	25	0.41	6.5
1,1,1-Trichloroethylene	25	0.78	4.6
Trichloroethylene	25	0.55	8.8
1,1,2,2-Tetrachloroethane	25	1.63	3.8
2-Bromo-2-chloro-1,1, 1-trifluoroethane	25	0.61	8.9
Nitrobenzene	25	1.84	2.8
Pyridine	25	0.88	2.7

Source: F.P. Lees and P. Saram, *J. Chem. Eng. Data* **16**, 41 (1971).

Table A17 Diffusion coefficient of salts in water at 25°C at infinite dilution

Salt	Diffusion coefficient (cm ² /s × 10 ⁵)
NH ₄ Cl	1.99
BaCl ₂	1.39
CaCl ₂	1.34
Ca(NO ₃) ₂	1.10
CuSO ₄	0.63
LiCl	1.37
LiNO ₃	1.34
MgCl ₂	1.25
Mg(NO ₃) ₂	1.60
MgSO ₄	0.85
KCl	1.99
KNO ₃	1.89
K ₂ SO ₄	1.95
Glycerol	0.94
NaCl	0.61
NaNO ₃	1.57
Na ₂ SO ₄	1.23
Sucrose	0.52
Urea	1.38

Source: Data correlated by Sourirajan from various sources in *Reverse Osmosis*, Academic Press, New York (1970).

Table A18 Interdiffusion of gases and vapors into air at 20°C

Gas or vapor	Diffusion coefficient (cm ² /s)
O ₂ -Air	0.18
CO ₂ -Air	0.14
H ₂ -Air	0.61
H ₂ O-Air	0.22
n-Propyl alcohol	0.085
Ethyl acetate	0.072
Toluene	0.071
n-Octane	0.051

Source: Selected values from *International Critical Tables*, W.P. Boynton and W.H. Brattain.

Table A19 Interdiffusion of vapors into air, carbon dioxide or hydrogen

Gas/vapor	Diffusion coefficient (cm ² /s)		
	Air	CO ₂	H ₂
Oxygen	0.18	0.14	0.70
Water	0.22	0.14	0.75
Ethyl acetate	0.072	0.049	0.27
n-Propyl alcohol	0.085	0.058	0.32
Propyl butyrate	0.053	0.036	0.21

Index

- Air sparging 292–296
Anisotropic membranes 102–133
Artificial kidney 493–498
Artificial lung 498–500
- Back flushing 272–274, 295–299
Barrer, R.M. 325, 328
Batch systems 278–279
Bioreactors 296–299
Bipolar membranes 443–444
Blood oxygenators 498–500
Bondi method 61
Brackish water desalination 238–239, 438
Braid-supported fiber membranes 154–155
Bubble point 308–314
- Cadotte John 208, 216–220
Capillary condensation 83–86, 87–88
Carbon membranes 82–85, 145–147
Carrier facilitated transport 453–487
coupled transport applications 472–473
coupled transport characteristics 463–468
coupled transport theory 459–463
emulsion liquid membrane 469–471
facilitated transport applications 481–486
facilitated transport process design 476–478
facilitated transport theory 473–476
- Gliozzi’s biological model 455
hybrid emulsion-membrane contactors 458–459
supported liquid membranes 468–469
- Ceramic membranes 135–139, 337–338
Chlor-alkali processes 448–449
Chiral separations 551–552
Co-flow 197–199
Composite membranes (solution coated) 125–128, 336–337
Concentration polarization 179–197
boundary layer model 182–190, 257–275
gel layer model 262–269
in electrodialysis 428–435
in gases 196–197
in liquids 193–196
in pervaporation 191–195, 199, 203
in ultrafiltration 193–196, 261–264, 269–270, 275, 277–278
Peclet number 188–199
Wijmans plot 189, 194–195
Wilson plot 191–192
- Continuous column 348–349
Controlled drug delivery 501–518
biodegradable systems 510–511
diffusion-controlled systems 502–510
osmotic systems 512–518
Rose-Nelson osmotic pump 512–513, 517
- Theeuwes elementary osmotic pump 514–516

- Counter-flow 197–204
 Critical flux 264–267
 Cross-flow 197–202
- Darcy's law 24
 Depth filter 76–79, 305–307
 Dialysis 28–29, 521–526
 Cerini dialyzer 521–522
 charge mosaic membranes 526–529
 theory 28–29
 diffusion dialysis 521–523
 Donnan dialysis 522–526
 piezodialysis 526–529
- Diffusion coefficients 55–64
 diffusion of gases in polymers 53–59
 diffusion in liquids 56–58
- Donnan equation 421–424
 Donnan exclusion 222–225
 Dual sorption model 70–71
 Dynamically formed membranes 130–131
- Electrodialysis/ion exchange membranes 417–449
 bipolar membranes 430, 443–444
 Nafion membranes 425–428, 446–448
 ion exchange membranes 421–427
 theory 421–423
- Electrodialysis 428–444
 brackish water desalination 438
 Cowan-Brown plot 431–432
 current efficiency 433–435
 electrodeionization 442–443
 limiting current density 428–434
 overlimiting current 432–433
 salt from seawater 438–440
 system design 435–438
- Emulsion liquid membranes 469–471
 Expanded film membranes 102–103
- Facilitated transport, See Carrier facilitated transport
- Feed-and-bleed design 278–282
 Ferry model 75–76
- Ferry-Renkin equation 76
 Fick's law 25
 Flory-Huggins theory 64–69
 Frame-of-reference problem 91
 Flux paradox 269
 Free volume 61–64, 86–89
 Fuel cells 444–448
- Gas permeabilities 54, 332–333, 339, 350, 354
 Gas separation 325–375
 ceramic membranes 337–338
 continuous column 348–349
 metal membranes 337
 process design 339–348
 Robeson plot 329–334
 solution-diffusion model 40–44, 328–337
 sorption in polymers 64–71
 thermally rearranged/carbon membranes 338
 zeolite membranes 337
- Gas separation applications
 carbon dioxide/hydrogen 370–372
 carbon dioxide/hydrogen sulfide 361–365
 carbon dioxide/nitrogen 365–368, 370–372
 dehydration of air 369–370
 hydrogen separation 350–352
 natural gas dehydration 363–365
 natural gas dew point adjustment 365–366
 natural gas separations 359–368
 nitrogen removal from natural gas 365–368
 olefin separations 372, 483–485
 oxygen/nitrogen separations 352–359
 status 373–375
 vapor/gas separations 368–369
 vapor/vapor separations 372–373
- Gas solubility in liquids 67
 Gas solubility in polymers 64–71
 Gibbon, J.H. 471
 Glass (microporous) membranes 81–84, 148

- Glass transition temperature 61–63, 329–330, 332, 360
- Graham's Law of Diffusion 80–81, 325
- Graham, Thomas 79, 325
- Hemodialysis 493–498
- History of membrane technology 1–4
carrier facilitated transport 453–460
electrodialysis 417–420
gas separation 325–327
microfiltration 303–306
pervaporation 379–381
reverse osmosis 207–209
ultrafiltration 253–255
- Hollow-fiber membranes 148–155
braid-supported fiber membranes 153–155
double layer fibers 152–154
melt spinning 149–150
membrane recipes 152
solvent spinning 148–152
- Hollow-fiber modules (see membrane modules)
- Hyperfiltration 35–40, 245–246
- Interfacial polymerization membranes 121–125, 217–29
- Ion-conducting membranes reactors 544–546
- Ion exchange membranes 423–428
fuel cells 444–448
- Isotropic membranes 98–102
dense membranes 98–100
microporous membranes 100–102
- Knudsen diffusion 79–86
- Kolf kidney 495
- Liquid membranes (see carrier facilitated transport)
- Loeb-Sourirajan membranes 102–116
- Log reduction value (LRV) 309
- Lube oil separation 245–246
- Maxwell model of permeability 142
- Maxwell-Stefan equation 90–91
- Melt extruded film 99–100
- Membrane bioreactors 297–299
- Membrane cleaning 236, 271–274
- Membrane contactors 529–538
- Membrane defects 132–133, 335–337
- Membrane distillation 529–538
- Membrane fouling 231–236, 257–274, 292–295
- Membrane modules 154–167
hollow fiber 162–165
plate-and-frame 155–157, 276–277
spiral-wound 158–161, 167, 275–276
tubular 157–158, 276
vibrating 165–167
module selection 167–169
- Membrane preparation 97–154
anisotropic membranes 102–133
carbon membranes 145–147
ceramic membranes 135–139
dynamically formed 130–131
expanded film membranes 102–103
formation by absorption of water vapor 120–122
formation by solvent evaporation 119–120
formation by thermal gelation 116–118
glass (microporous) membranes 148
interfacial composite membranes 121–125, 217–219
ion exchange membranes 423–428
Loeb-Sourirajan membranes 102–116
melt extruded film 99–100
metal membranes 134–135, 337
mixed-matrix membranes 141–145, 338
- Nafion membranes 425–428, 446–448
- nucleation track membranes 100–102
- plasma polymerization 128–130
- slip cast ceramic membranes 135–137
- sol gel ceramic membranes 137–139
- solution cast membranes 98–99
- zeolite membranes 139–141
- Membrane porosity 72–74
- Membrane pressure gradients 22–27

- Membrane reactors 538–546
 applications 541–545
 bioreactors 297–299, 541–542
 gas-phase catalytic reactions
 542–544, 544–6
 gas ion-conducting 544–546
- Membrane surface treatment 131–132
- Membrane tortuosity 72–74
- Metal membranes 134–135, 337
- Microfiltration 303–323
 applications 320–323
 bacterial challenge test 306–310
 bubble test 310–314
 cross-flow filtration 275–292,
 304–305, 316–321
 depth filters 73–79, 304–305,
 316–320
 inline filtration 316–322
 latex challenge test 309–310
 log reduction value (LRV) 309
 membranes 305–306
 pleated cartridge 313–317
 prefilters 316–319
 sterile filtration 322–323
 ultrapure water 241–243, 323
- Microporous membranes 73–89,
 100–102
- Mixed-matrix membranes 141–145, 338
- Molecular dynamics simulations 18–22
- Molecular radius 21, 75–77
- Molecular sieving (of gases) 81–83
- Multistep-multistage processes 280–282,
 289–293, 345–349
- Municipal water treatment 296–299
- Nafion 425–428, 446–448
- Nanofiltration 222–225, 244–245
- Nucleation track membranes 73,
 100–101
- Office of Saline Water (OSW) 2
- Osmotic pressure 25–27, 31–35,
 210–211, 240–241
- Palladium membranes 134–135, 337
- Percolation threshold 142–144
- Pervaporation 379–412
 theory 44–49, 381–390
 applications 400–412
 GFT Membrane Systems 397
 membrane materials 389–395
 modules 395–398
 process design 398–400
 organic/organic separations 409–412
 organics from water 406–409
 solvent dehydration 401–406
- Phase diagrams 112–116
- Phase separation membranes 104–112
- Piezodialysis 526–529
- Plasma fractionation 500–501
- Plasma polymerization membranes
 129–130
- Plate-and-frame modules (see membrane
 modules)
- Poiseuille flow 80, 303
- Polymers with intrinsic microporosity
 (PIMS) 18, 86–89
- Poly (1-trimethylsilyl-1-propyne)
 [PTMSP] 86–89
- Pore flow membranes 72–90
- Pore flow model 16–18, 23–24, 72–90
- Pressure-retarded osmosis (PRO) 199,
 547–549
- Pressure ratio 339–343
- Recycle designs 347–349
- Rejection coefficient 37, 210, 221–222
- Reverse electrodialysis (RED) 549–550
- Reverse osmosis 207–247
 applications 237–246
 brackish water desalination 221–222,
 238–239
- cellulosic membranes 39, 213–216
- furfuryl alcohol membranes 219–220
- hyperfiltration 224–227, 245–246
- interfacial composite 124–125,
 217–219
- Jeddah plant 208, 218
- membrane cleaning 236
- membrane fouling 231–236
- membrane selectivity 227–230
- modules 228–231

- nanofiltration membrane 222–224,
 244–245
 noncellulosic membranes 216–217
 PEC-1000 membrane 220, 229–230
 seawater desalination 221–222,
 240–241
 silt density index 233–234
 theory 31–40, 208–212
 ultrapure water 241–243
 wastewater treatment 242–244
 Robeson plot 329–334, 486
- Salt permeability constant 37, 209
 Screen filter 75–76, 305–307
 Seawater desalination 221–222,
 240–241
 Slip cast ceramic membranes 135–139
 Sol gel ceramic membranes 135–139
 Solution cast membranes 98–99
 Solution-diffusion model 18–53
 Solvent dewaxing 245–246
 Sorption coefficients in polymers 64–71
 Spin coating 130–131
 Spiral-wound modules (see membrane
 modules)
 Stokes-Einstein equation 56–58
 Submerged membrane modules 293–299
 Structure-permeability correlations
 53–71
 Surface diffusion 82–86
 Sweep modules 197–204, 348–349,
 369–370
- Template leaching 102–104
 Thermally rearranged/microporous
 carbon membranes 145–147
 Track etch membranes (see nucleation
 track) 100–102, 306–307
 Transdermal patch 13, 505–506
 Tubular membranes (see membrane
 modules)
- Ultrafiltration 253–299
 applications 282–292
 biotechnology applications
 289–293
 cheese production 284–286
 electrocoat paint 283–284
 fruit juice 286–287
 batch operation 278
 concentration polarization 261–271
 constant flux operation 257–261
 constant pressure operation 257–261,
 278–282
 critical flux 264–267
 critical pressure 264
 feed-and-bleed operation 278–283
 gel layer model, formation 262–269
 membrane characterization 72,
 254–257
 membrane cleaning 271–274
 membrane fouling 257–261,
 271–274
 membrane modules 274–277
 membranes 274
 oil-water emulsions 287–288
 PVA recovery 288–290
 system design 278–282,
 293–296
 submerged membrane modules
 293–296
 membrane bioreactors 297–299
 Ultrapure water 241–243
- Vibrating membrane modules
 165–166
- Water permeability constant 36–37
 Wijmans plot 194–196
- Zaffaroni Alex 3, 502
 Zeolite membranes 139–141, 337–338